University of East Anglia

School of Pharmacy

Design and synthesis of novel classes of HDACs and KMTs inhibitors

by

Remy Thomas Narozny

Supervisor: Prof. A. Ganesan

Second Supervisor: Prof. Mark Searcey

Thesis for the degree of Doctor of Philosophy

November 2018

"Your genetics is not your destiny."

George McDonald Church

Abstract

For long, scientists thought that our body was driven only by our genetic code that we inherited at birth. However, this determinism was shattered entirely and proven as false in the second half of the 21st century with the discovery of epigenetics. Instead, cells turn genes on and off using reversible chemical marks. With the tremendous progression of epigenetic science, it is now believed that we have a certain power over the expression of our genetic traits. Over the years, these epigenetic modifications were found to be at the core of how diseases alter healthy cells, and environmental factors and lifestyle were identified as top influencers. Epigenetic dysregulation has been observed in every major domain of medicine, with a reported implication in cancer development, neurodegenerative pathologies, diabetes, infectious disease and even obesity. Substantially, an epigenetic component is expected to be involved in every human disease. Hence, the modulation of these epigenetics mechanisms has emerged as a therapeutic strategy. Histone deacetylases (HDAC) are silencing epigenetic markers involved in the mediation of the acetylation system. Aberrant HDAC activities have been associated with the development of a broad range of pathologies, and HDAC inhibition is highly regarded as a potential therapeutic target. This approach became successful with the approval by the FDA of several epidrugs. However, they present undesired side effects. Lack of selectivity was identified as a principal suspect and, therefore, the development of novel compounds that would target more selectively the epigenetics enzymes represent a major axis of research for future pharmacological applications.

Accordingly, this work focus on designing new classes of HDAC inhibitors. A variety of structures, build around the use of amino acids, were explored and potential inhibitors were produced with different cores. These series were then evaluated in enzymatic inhibition assays on HDAC and in cell growth inhibition assays on leukaemia cell lines. Additionally, we were also involved in the international consortium A-ParaDDisE that aimed to develop epigenetic modulators as drug candidates against the main parasitic diseases: malaria, schistosomiasis, leishmaniasis and Chagas disease. This collaboration resulted in the identification of critical targets for the different parasites and the development of testing methods to move compounds toward clinical development. The antischistosomal effect of some of our inhibitors was, thus, evaluated. Finally, a side project was carried at the University of Salerno in Italy in a short-term scientific mission that aimed to develop a new class of SETD8 methyltransferase inhibitors.

Acknowledgements

I must first acknowledge my supervisor Prof. Ganesan who offered me this fantastic opportunity to develop a research project. Thanks, Prof. Ganesan for the stimulating discussions, suggestions and guidance during this PhD work and for the numerous opportunities to attend conferences that highly contributed to my development as a researcher. I especially thank you for the support, over these four years, not only on the project but also on the pursuit of my career.

I also thank my second supervisor Prof. Mark Searcey for his support during this project and his help in grant applications.

I want to thank Prof. Gianluca Sbardella, from the University of Salerno in Italy, for hosting a research visit for three months. I would also like to thank the member of his group for their warm welcome and their help during this mission and in particular Dr Ciro Milite for his support on this part of my PhD work.

Sincere thanks also to Prof. Manfred Jung (University of Freiburg, Germany), Prof. Laurent Bischoff (University of Rouen Normandy, France), Prof. Wolfgang Sippl (Institute of Pharmacy at the Martin-Luther University of Halle-Wittenberg, Germany) and Dr Maria Teresa Borrello (INSERM U1068 Cellular Stress Group, Cancer Research Center of Marseille, France) who contributed to this thesis by operating the biology testing and the molecular docking.

I thank the University of East Anglia and the A-ParaDDisE consortium for funding this research project. I would also like to thank the COST action Epichembio for financially supporting my short-term scientific mission at the University of Salerno in Italy.

In addition, I express my gratitude to the previous and current members of Prof. Ganesan research group and particularly Teresa Borrello, Carys Thomas, Adam Lee, Mohammed Aldholmi and Philip Schuler for the friendly working environment, the enriching conversation, and the support over these four years. Many thanks as well the undergraduate student who contributed to this project: Alex Chan, Angus Yuen, Faustin Falissard, Karolina Sliwa and Ludmilla Sturm.

I am incredibly grateful to my colleagues and friends Mahmoud, Quim, Sara and Hui for their support and all the great deal of time spent together. Thanks, Andrew and Ryan, for your help in the lab, the great football games and the shared drinks. Thank you, Elise, for the cheerful atmosphere and enthusiasm you created in the office, and for being a fantastic geeky friend who always shares my over-excitement for movies, series, comics and more importantly cakes. Thanks to the 2015 survivors group Serena, Valeria, Noe and Liao for our dinners and talks. Thanks, Sarah for all the good moments (although I lost auditory acuity). Thank you Mar and Gerard for the cuckoo times, barbecue, Christmas dinner and all the laughs. Silvia, Foodie, thanks for your

support, our discussions, our laughs and your trust. I'm sure you will be there soon. Finally, thank you Lucka for our long runs and endless debate about life, dreams, science, Mars; thanks for the gif talks, the cinematic exchanges, the crazy snaps and your support.

With a special mention to my flat 5 family: Bianca, Martina, Bela, Rodrigo, Carter and Pedro. It was fantastic to join your flat when I arrived in Norwich, and I genuinely enjoyed our time there. What a cracking place to live! I hope we will meet again.

Enfin, je dédie cette thèse à ma famille, sans qui rien n'aurait été possible. Même si vous ne compreniez pas toujours ce que je voulais faire ni où j'allais, merci de m'avoir toujours soutenu malgré tous les déménagements, les expatriations, et les longues absences. Je n'aurais jamais accompli ce rêve sans vous.

Contents

List of Figures

List of Scheme

List of Tables

Abbreviations

3'UTR	3'-untranslated region
53BP1	Tumor suppressor p53 binding-protein 1
5mC	5-methylcytosine
α-Syn	α-synucleic
δ	Chemical shift
γH2AX	Histone H2AX phosphorylated at serine 139
μW	Microwave
A or Ala	Alanine
AA	Amino acid
Aβ	β-amyloid
ABL	Abelson murine leukaemia viral oncogene homolog
Ac_2O	Acetic anhydride
AcOH	Acetic acid
AD	Alzheimer's disease
ADP	Adenosine diphosphate
ALS	Amyotrophic lateral sclerosis
ALTRA	All-trans retinoic acid
AML	Acute myeloid leukaemia
AML1	Acute myeloid leukaemia protein 1
AMP	Adenosine monophosphate
A-ParaDDisE	Anti-parasitic drug discovery in epigenetics
APL	Acute promyelocytic leukaemia
ART	ADP-ribosyltransferase
ATP	Adenosine triphosphate
BBB	Blood-brain barrier
BC	Before Christ
Bcl	B-cell lymphoma
Bcl-xl	B-cell lymphoma-extra large
BDNF	Brain-derived neurotrophic factor
BET	Bromo domain and extra-terminal
BFL	Bcl-2-modifying factor
BID	BH3 interacting-domain death agonist
BIM	Bcl-2-like protein 11

BMF	Bcl-2-related protein A1
Bn	Benzyl
Boc	tert-butoxycarbonyl
BRD	Bromodomain-containing protein
BSA	Bovine serum albumin
C or Cys	Cysteine
c-FLIP	Caspase 8-like inhibitory protein
Calc	Calculated
CARM1	Coactivator-associated arginine methyltransferase 1
CBP	CREB-binding protein
Cbz	Benzyl chloroformate
CD71	Transferrin receptor protein 1
CDI	Carbodiimidazole
CDK	Cyclin-dependent kinase
CDKN1	Cyclin-dependent kinase inhibitor 1
CML	Chronic myelomonocytic leukaemia
ConfGen	A conformational search method
COST	European cooperation in science & technology
CpG	Cytosine-phosphate-Guanidine
CQ	Chloroquine
CREB	cAMP response element-binding protein
CTL	Cytotoxic T-cell
CTP	Cytidine triphosphate
CuAAC	Copper-catalyzed azide-alkyne cycloaddition
Cy_2NMe	*N*-Methyldicyclohexylamine
D or Asp	Aspartic acid
d	day
DAC	Dependant protein deacetylases
DCM	Dichloromethane
DEAD	Diethyl azodicarboxylate
DIAD	Diisopropyl azodicarboxylate
DIBAl-H	Diisobutylaluminium hydride
DIPEA	diisopropylethylamine
DMF	Dimethylformafide
DMSO	Dimethyl sulfoxide

DNA	Deoxyribonucleic acid
DNMT	DNA methyltransferase
DOT1L	Disruptor of telomeric silencing 1-like
dppf	Bis(diphenylphosphino)ferrocene
DTT	DL-Dithiothreitol
EDC	*N*-Ethyl-*N*′-(3-dimethylaminopropyl)carbodiimide hydrochloride
EGFR	Epidermal growth factor receptor
EHMT1	Euchromatic histone-lysine *N*-methyltransferase 1
Enz	Enzyme
EpiChemBio	Epigenetic chemical biology – COST action 1406
Eq	Equivalent
ERK2	Mitogen-activated protein kinase
ESI	Electrospray ionisation
Et_2O	Diethyl ether
Et_3N	Triethylamine
EtOAc	Ethyl acetate
EtOH	Ethanol
EZH2	Enhancer of zeste homolog 2
F or Phe	Phenylalanine
FAD	Flavin adenine dinucleotide
FDA	Food and Drug Administration
Fmoc	Fluorenylmethyloxycarbonyl
FOXO	Forkhead box protein
FRDA	Friedreich's ataxia
FXS	Fragile X syndrome
GATA	Erythroid transcription factor
GLP	Glucagon-like peptide
GSK3b	Glycogen synthase kinase 3-b
H or His	Histidine
h	hour
H3K4	Histone 3 lysine 4
H3K4me1	Histone 3 lysine 4 mono-methylated
H3K4me2	Histone 3 lysine 4 di-methylated
H3K9	Histone 3 lysine 9

H3K27	Histone 3 lysine 27
H3K27me3	Histone 3 lysine 27 tri-methylated
H4K20	Histone 4 lysine 20
H4K20me1	Histone 4 lysine 20 mono-methylated
HAT	Histone acetyltransferase
HATU	Hexafluorophosphate azabenzotriazole tetramethyl uronium
HBTU	Hexafluorophosphate benzotriazole tetramethyl uranium
HD	Huntington's disease
HDAC	Histone deacetylase
HDACi	Histone deacetylase inhibitor
HDLP	Histone deacetylase-like protein
HDR	Homology-directed repair
HER2	Human epidermal growth factor receptor 2
hHDAC	Human histone deacetylase
HME	Histone modifying enzyme
HMGCR	3-hydroxy-3-methylglutaryl coenzyme A reductase
HMT	Histone methyltransferase
HOBt	Hydroxybenzotriazole
HPLC	High performance liquid chromatography
Htn-Q150	Polyglutamine human huntingtin protein fragment
Htt	Huntingtin protein
IC_{50}	Half maximal inhibitory concentration
IMDPH	Inosine monophosphate dehydrogenase
IUGR	Intrauterine growth restriction
JAK	Janus kinase
JmjC	JumonjiC
K or Lys	Lysine
K_D	Binding constant
KDM	Lysine demethylase
K_i	Inhibition constant
KMT	Lysine methyltransferase
L or Leu	Leucine
LCMS	Liquid chromatography-mass-spectrometry
LigPrep	Ligand preparation program
LSD1	Lysine Specific demethylase 1

LSD2	Lysine Specific demethylase 2
M or Met	Methionine
MCE	Microfluidic capillary electrophoresis
MDM2	Murine double minute 2
MDS	Myelodysplastic syndrome
Me	Methyl
MeCN	Acetonitrile
MeOH	Methanol
MHC	Major histocompatibility complex
Mhtt	Mutant huntingtin protein
MICA	MHC class I polypeptide-related sequence A
MICB	MHC class I polypeptide-related sequence B
min	minute
miRNA	MicroRNA
MLL1	Myeloid/lymphoid or mixed-lineage leukaemia 1
MM-GB/SA	Method to estimate ligand-binding affinities
MOA	Mechanism of action
MOE	Molecular operating environment
MPP^+	1-methyl-4-phenylpyridinium
mRNA	Messenger RNA
MsCl	Mesyl chloride
MTOC	Microtubule organizing centre
mTOR	Mechanistic target of rapamycin
NAD^+	Nicotinamide adenine dinucleotide
ND	Neurogenerative diseases
NHEJ	Non-homologous end joining
NK	Natural killer
NKG2D	Natural killer cell protein group 2D
Nle	Norleucine
NMC	NUT midline carcinoma
NMM	*N*-methylmorpholine
NMR	Nuclear magnetic resonance
NTDs	Neglected tropical diseases
OPLS	Optimized potential for liquid simulations
P or Pro	Proline

p53K382me1	p53 lysine382 mono-methylated
PCNA	Proliferating cell nuclear antigen
PD	Parkinson's disease
PDB	Protein data bank
Pd/C	Palladium on charcoal
$Pd(dba)_2$	Bis(dibenzylideneacetone)palladium(0)
PDGFR	Platelet-derived growth factor receptor
$Pd(OAc)_2$	Palladium acetate
PfHDAC	Plasmodium falciparum histone deacetylase
PfSir	Plasmodium falciparum sirtuin
PI3K	Phosphatidylinositol 3-kinase
PKC	Protein kinase C
PLK	Polo-like kinase
PML	Promyelocytic leukaemia protein
PolyQ	Polyglutamine
PPARγ	Peroxisome proliferator-activated receptor γ
PPh_3	Triphenylphosphine
pRb	Retinoblastoma protein
PRC2	Polycomb repressor complex 2
PRMT	Arginine methyltransferase
PROPKA tool	p*K*a calculation software
PUMA	p53 upregulated modulator of apoptosis
PyBOP	benzotriazol-1-yl-oxytripyrrolidinophosphonium hexafluorophosphate
Q or Gln	Glutamine
R or Arg	Arginine
RARα	Retinoic acid receptor α
RMSD	Root-mean-square deviation
RNA	Ribonucleic acid
RNAi	RNA interference
ROS	Reactive oxygen species
Rpd3	Reduced potassium dependency 3
rt	Room temperature
RXR	Retinoid X receptor
SA-βGal	Senescence-associated β-galactosidase

SAHA	Suberoylanilide hydroxamic acid
SAM	*S*-adenosyl methionine
SE14	Serine-glutamate tetradecapeptide
sec	second
SET	Su(var)3-9, Enhancer-of-zeste and Trithorax
SETD	SET-domain containing
siRNA	Small interfering RNA
Sirt	Sirtuin
SMA	Spinal muscular atrophy
SmHDAC	*Schistosoma mansoni* histone deacetylase
SMYD	SET and MYND-domain containing protein
SNP	Single-nucleotide polymorphism
SNpc	Substanctia nigra pars compacta
T3P	Propane phosphonic acid anhydride
TbDAC	*Trypanosoma brucei* histone deacetylase
TBDMS	Tris-buffered saline, 0.1% Tween 20
TBS-T	tert-butyldimethylsilyl
tBuOH	tert-butanol
TcDAC	*Trypanosoma cruzi* histone deacetylase
TCEP	Tris(2-carboxyethyl)phosphine
Tf_2O	Triflic anhydride
TFA	Trifluoroacetic acid
TfN_3	Trifluoromethanesulfonyl azide
THF	Tetrahydrofuran
TIPS	Triisopropylsilane
TLC	Thin layer chromatography
TMSOH	Trimethylsilanol
TMSOTf	Trimethylsilyl triflate
TRDMT1	tRNA aspartic acid methyltransferase
Tris HCl	Tris(hydroxymethyl)aminomethane hydrochloride
Trt	Trityl
TsCl	Tosyl chloride
Tween-20	Polysorbate 20
VDR	Vitamin D receptor
VEGFR	Vascular endothelial growth factor receptor

VSG	Variant surface glycoprotein
WHO	World health organization
Xphos	2-Dicyclohexylphosphino-2′,4′,6′-triisopropylbiphenyl
Y or Tyr	Tyrosine
ZBG	Zinc binding group
ZnF	Zinc finger protein

Chapter 1. Introduction

1. Epigenetics

Heredity. This notion has been a long-term question mark in scientific history. Indeed the Greek philosopher Aristotle was already interested in inheritance in 350 BC.[1,2] Although the observation that living organisms inherit traits from their parents has been used since prehistory to enhance crop plants and animals through selective breeding the processes remained an enigma for centuries. In his book "*On the origin of species"* Darwin introduced the concept of natural selection as a long-term mechanism of adaptation of an organism to its environment. In a population, slight variations between individuals were affecting the survival capability. Accordingly, individuals more suited to a specific environment were more likely to survive and more likely to reproduce and pass down their heritable traits to the next generations.

The twentieth century started with a revolution when Bateson coined the word genetics (from the Greek word *genesis*-byγένεσις, "origin") following the work of Mendel and Hugo de Vries that laid the foundation of genes.[3] Although genetics was unable to understand the physical reality of heredity, it provided an accurate depiction of the laws involved and of its outcome. The field then experienced a significant gain in interest and met several breakthroughs with the discovery of the nucleus being the repository of genetic information in eukaryotes, the identification of the DNA as genetic material,[4] and the determination of the DNA structure.[5]

These advances gave us a better understanding of the previously described natural selection. Differences in the DNA sequence induced variation between individuals and the selection was influenced by the inherited genes.

Nevertheless, these theories were unable to explain the adaptation of an organism during its lifetime. For example, complex organisms such as humans or animals originate from a single fertilized egg. Over the development of the embryo to adulthood, this cell will multiply, and the newly formed stem cells will differentiate and acquire specific biological functions. However, the adaptive alterations occurring during this process are ignored by the natural selection theories.

Scientists, therefore, became interested in the relationship between DNA and the production of proteins. Their work led to the discovery of the genetic code, the set of rules used by living cells to translate information encoded within the genetic material into proteins. Genes on the DNA are first transcribed into RNA and then translated to proteins. This two-step sequence, DNA making RNA and RNA producing proteins was called *the central dogma of molecular biology* by Crick.[6] But the mechanisms involved had yet to be understood. Additionally, those mechanisms were

responsible for the phenotypic differentiation of cells and, therefore, represented their adaptation to experience. As the genotype was unaltered the question of inheritance of these mechanisms rapidly came up.

"We certainly need to remember that between genotype and phenotype, and connecting them to each other, there lies a whole complex of developmental processes. It is convenient to have a name for this complex: epigenotype seems suitable."

Waddington, 1942.[7]

These interrogations, coupled to the introduction of the notion of epigenotype by Waddington, laid the foundation of a new field of study called epigenetics (from the Greek word *epi*-επι, "upon") defined as the study of heritable changes in phenotype that occur without modification of the DNA sequence.

Over the last 25 years, considerable progress has been made in the field, and epigenetics mechanisms were identified to occur on the chromatin, the physiological form of genetic material. In response to environmental signals, enzymes known as chromatin-modifying enzymes can activate a range of epigenetic modifications, tagging the DNA, which can then be passed down to the next generation.[8] These tags, which do not modify the genotype sequence, are the core machinery in the control of gene expression. Chemically altering histone tails, cytosine, and non-coding RNAs, these epigenetic marks modulate the gene expression by profoundly affecting the state of compaction of chromatin.

To date, epigenetic dysregulation had been linked to most major diseases such as cancer, neurodegenerative diseases and diabetes.[9–11] However contrary to genome mutation, epigenetic marks are reversible. Thus, epigenetic modulators have considerable potential as therapeutic agents, and interest in the field has been steadily growing for years.

2. Chromatin

History of chromatin started around 1880 when Flemming coined the term. Histones, one of the components of chromatin, were discovered shortly after in 1884.[12] Over the first half of the twentieth-century, genetic researchers mainly focused on the discovery of the genetic material carrier, and little was done to understand chromatin further. The period between 1973 and 1975 witnessed a groundbreaking series of publications which identified a subunit model in chromatin.[13–16] This subunit, called nucleosome, was then successfully crystallized and observed by X-ray in 1984,[17] and then in 1997 at higher resolution,[18] by Richmond.

The nucleosome represents the first high-order of DNA packaging in eukaryotes. Each nucleosome is composed of 146 base pairs of DNA forming a superhelix around a histone core.

This core consists of a pair of four histones (H2A, H2B, H3, and H4) organized as an octamer structure (Figure 1.1) which is further stabilized by a fifth histone (H1) playing the role of the linker.

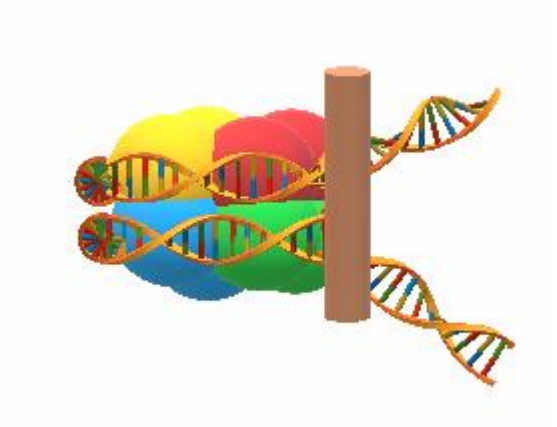

Figure 1.1: Schematic view of the nucleosome.
H2A dimer is shown in yellow, H2B in red, H3 in blue, H4 in green and H1 in brown. Adapted from Biochemistry (4th Edition).[19]

Inside the cell, chromatins are divided into two categories. Indeed, in 1928, long before it was understood, Heitz had observed two states of chromatin. He called euchromatin the form which was expressing genes and heterochromatin the mode which was transcriptionally inactive.[20,21] This distinction is the core of modern epigenetics. As previously mentioned, epigenetic mechanisms, that affect the state of the chromatin, regulate gene expression. Heterochromatin is a condensed conformation in which the DNA, tightly wrapped around the histone core, is not accessible to transcription factors. As shown in the X-ray structure (Figure 1.2), the histones are packed inside the structure of the nucleosome. Meanwhile, histone tails are easily accessible to chromatin-modifying enzymes. Chemical alterations of the histones impact the interaction with DNA and loosen the structure. As a result, this decondensed structure becomes more accessible to transcription factors. Thus, genes are expressed in euchromatin. Representation of both states is shown below (Figure 1.3).

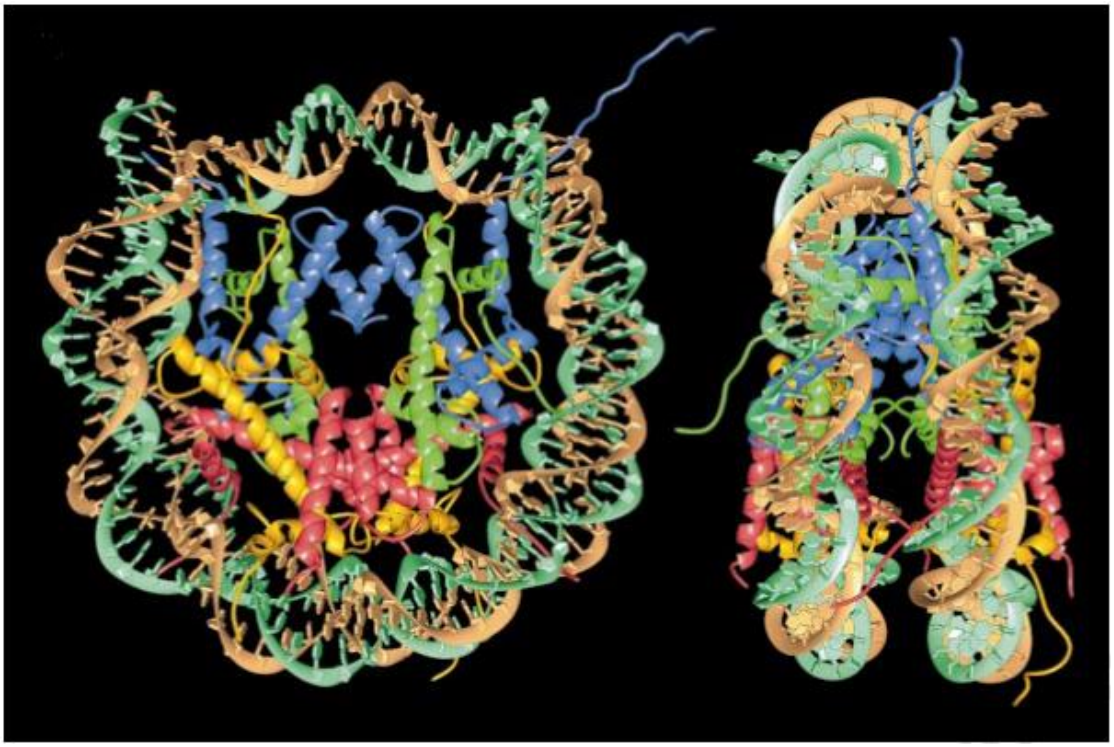

Figure 1.2: High-resolution structure of nucleosome.
DNA double brand are shown in brown and turquoise. Histone protein main chains are shown as ribbon (H3: blue; H4: green; H2A: yellow; H2B: red). Taken from Luger et al.[18]

Current research in epigenetics focuses on the study of these histone post-translational modifications. Additionally, a second significant reaction affecting the state of chromatin, and thus the expression of genes, was observed with DNA methylation.

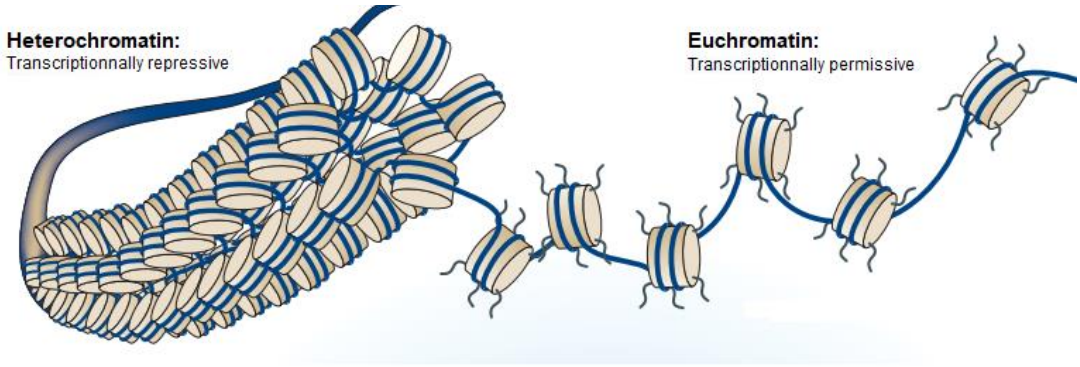

Figure 1.3: Packaged nucleosome representation (heterochromatin) and bead on string representation (euchromatin).
The blue strands represent the DNA, nucleosome are beige cylinders, and histone tails are black lines. Taken from Arrowsmith et al.[22]

3. Epigenetic modulators: DNA methylation and histone post-translation modifications

Modern epigenetic research is mainly focusing on two categories of mechanism.

3.1 DNA methylation

The first class consists of markers targeting the DNA. By definition, epigenetics modifications cannot alter the DNA sequence, but the genome is still a cog in the highly dynamic machinery. Hotchkiss detected chemically modified DNA bases in 1948.[23] This modified nucleotide turned out to be 5-methylcytosine (5mC) resulting from methylation of the DNA. The occurrence of this altered base was observed in a wide range of organisms, and in particular, it was reported that 2 to 7 per cent of cytosine on mammalian DNA was converted to 5mC.[24] In the mid-1970s, Holliday and Pugh suggested that 5mC was involved in the process of gene regulation during development,[25] and this role was later confirmed.[26]

Over the following years, numerous studies led to a better understanding of the DNA methylation. In the DNA, all cytosines are not equal in front of this epigenetic mark. Indeed, the cytosine-phosphate-guanidine (CpG) dinucleotide was found to be a hotspot for DNA methylation with around 70 % of CpG region being methylated.[27,28]

Catalysed by a class of enzyme called DNA methyltransferase (DNMTs), cytosine of the CpG regions reacts with *S*-adenosyl methionine (SAM) acting as a methyl donor (Scheme 1.1). This interaction promotes the introduction of a methyl group on the 5th position of the cytosine to form 5mC (**1-4**).

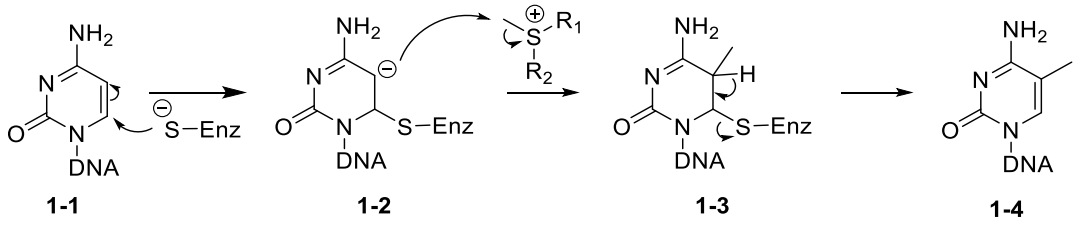

Scheme 1.1: DNA methylation mechanism.

DNMTs have been widely studied and well characterized. In mammals, DNMTs consist of three enzymes namely DNMT1, DNMT3A, and DNMT3B. Historically, a fourth enzyme named DNMT2 had been identified, but later evidence revealed that the protein didn't methylate DNA but RNA.[29] Therefore, it was renamed TRDMT1 (tRNA aspartic acid methyltransferase 1).

DNMT1 is the most abundant DNMT in adult cells,[30] and acts as a *maintenance* methylase. During DNA replication, the epigenetic alterations are not copied to the newly synthesized strand. DNMT1 recognizes and binds to the CpG site of this hemi-methylated DNA, only bearing methylation on the parent strand, to reproduce the cytosine methylation motif on the new stand. The role of the DNMT is, therefore, to maintain the epigenetic profile through mitosis and promotes the inheritance of DNA methylation pattern.[31]

DNMT3a and DNMT3b are *de novo* DNA methyltransferases showing an equal affinity for hemi-methylated and non-methylated DNA.[32] The role of DNMT3 enzymes is to initiate the methylation process of DNA that occurs after embryo implantation. Both DNMT3a and DMNT3b are crucial for early development, and the inactivation was reported to cause early embryonic lethality.[33,34] The DNMT3 group also includes a catalytically inactive member, DNMT3L. However, DNMT3L has an essential role as a booster of activity during development. Binding to the catalytic domain of DNMT3a or DNMT3b enzymes, it increases their catalytic activity 15-fold.[35]

However, it is important noting that the opposition *maintenance*/*de novo* function of these enzymes is not absolute. Mounting evidence suggests that DNMT1 may also be required as *de novo* methylation of the genome,[36,37] while a DNMT3 class can fill the role of *maintenance* methylation during DNA replication.[38,39] In particular, human cancer cells lacking DNMT1 have shown only a 20 percent reduction in methylation of CpG sites.[40]

Heterochromatin is frequently rich in methylated regions, thus preventing the binding of transcription factors to gene promoters and repressing gene expression. On the other hand, euchromatin is impoverished in methylated CpG region, and genes are accessible to transcriptional mechanism.[34,41,42]

Over the years, a variety of diseases have been linked to aberrant DNA methylation activity either by hypomethylation or hypermethylation.[43–45] DNMT inhibitors are, therefore, interesting therapeutic agents and this approach successfully led to the discovery of 5-azacytidine (vidaza®) and 5-aza-20-deoxycytidine (decitabine®) which were approved by the Food and Drug Administration (FDA) for the treatment of myelodysplastic syndromes (MDS) and chronic myelomonocytic leukaemia (CML).[46] The development of new classes of DNMT inhibitor is currently a significant axis of research in the field.

3.2 Histone post-translational modifications

In the mid-1960s, Allfrey published results of his work on histone methylation and acetylation.[47] Although post-translational modifications of protein had been reported a few years earlier with phosphorylation[48] and acetylation,[49] this pioneering work laid the foundation of the model proposing that histone modifications could affect the accessibility to DNA and regulate the gene expression.[50]

In the following years, several histone modifications affecting the gene expression, such as acetylation, methylation, phosphorylation, ubiquitination, and glycosylation, were discovered.[51]

These reactions are catalyzed by histone modifying enzymes (HMEs) and occur on the N-terminal histone tails (Figure 1.4).

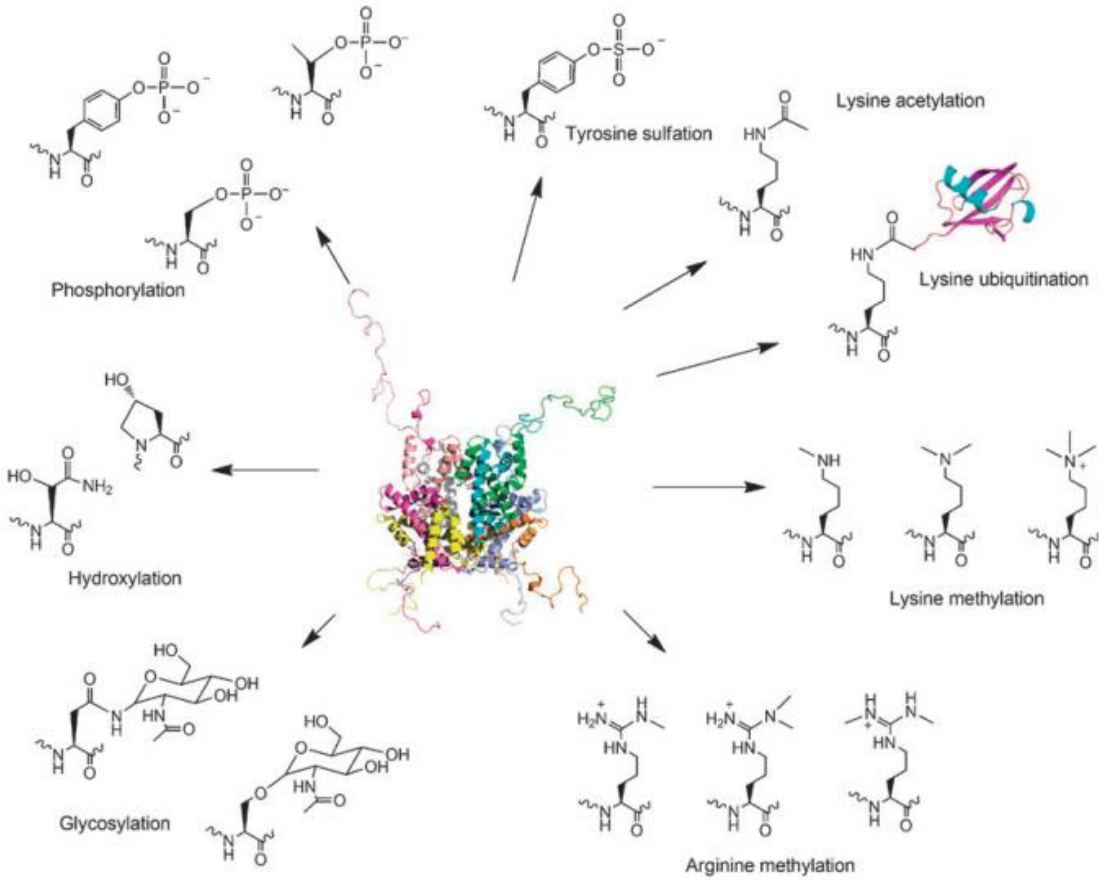

Figure 1.4: Overview of post-translational modification of protein.
Taken from Liu et al.[52]

HMEs were divided into three categories depending on their function: writers, readers, and erasers (Figure 1.5).

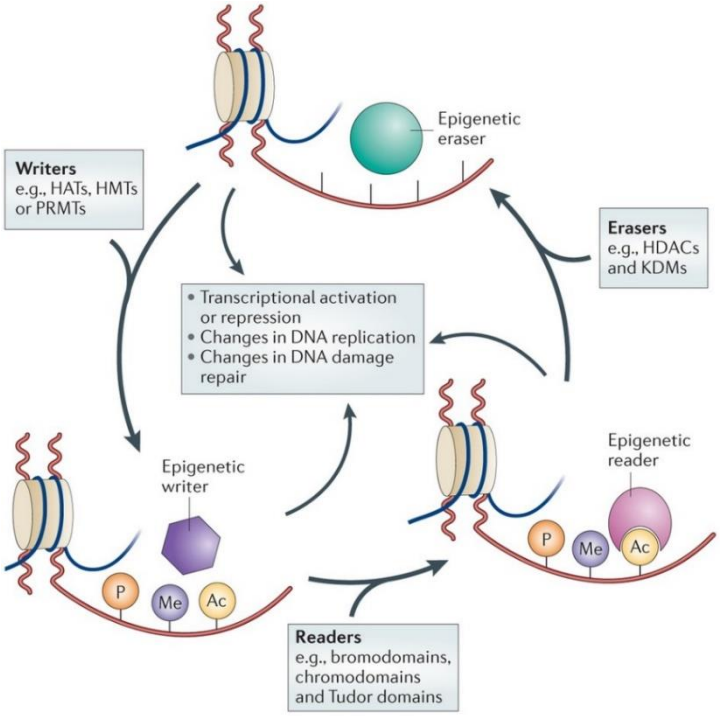

Figure 1.5: Epigenetic writers, erasers, readers.
Taken from Falkenberg et al.[53]

3.2.i Epigenetic writers

Writers represent the enzymes which can introduce an epigenetic mark on the histone tails.

Histone acetyltransferases (HATs) were first isolated in 1996.[54] These enzymes can interact with a histone lysine side chain on H2A, H2B, H3 and H4.[9,51] Positively charged lysine side chains have a strong affinity for negatively charged DNA, and their interaction is involved in the high order of compaction of heterochromatin. HATs are responsible for the transfer of acetyl group on the lysine amino group and convert it into a neutral amide group. The loss of charge disrupts the interaction with DNA which leads to the formation of the transcriptionally active euchromatin and the expression of affected genes. Additionally, HATs were also reported to promote the acetylation of non-histone protein such as p53.[55]

Another important class of enzyme was reported in 2000 with the isolation of the first human histone methyltransferase (HMT).[56] Similarly to the DNMTs, the methylation process involves the SAM co-factor as a methyl donor.[57]

This subclass of HME can interact with the N-terminal lysine side chain of histone but also on arginine, and the HMTs are able to transfer up to three methyl group to a lysine. However, their effect on the state of compaction of the chromatin and the gene expression is subtle. Indeed contrary to acetylated lysine, methylation of the amino group does not remove the charge and

only affects the steric hindrance. Although this could suggest that a higher degree of methylation induces a higher disruption of the interaction with DNA the relation between lysine methylation and gene transcription was shown to be more complicated. The change of conformation between euchromatin and heterochromatin, and by extension the activation or deactivation of gene transcription, is not only dependent of the degree of methylation (mono, di- or tri-methylated) but is also conditioned by the position of the epigenetic mark. For instance, mono, di- and tri-methylated H3K4 are found in the active site of transcription.[58] On the other hand di- and tri-methylated H3K9 and H3K27 are marks for heterochromatin and gene silencers, but H3K9 monomethylation is linked with gene expression.[58–61] Thus methylations could be both activating and repressing marks.

3.2.ii Epigenetic readers

Reader enzymes represent the second leading category of HMEs. This class recognizes histone modifications introduced by writer enzymes and specifically bind to the epigenetic marks. Thus, their action mediates the DNA transcription. For example, chromodomains and Tudor domains showed a high affinity for the site of lysine methylation while bromodomains bind to acetylated lysine.[62] Historically, reader enzymes have been less studied than writers and erasers. Bromodomains, notably, have been highly investigated since their identification in 1992,[63,64] and their recognition as specific acetylated lysine binders in 1999.[65] Protein containing bromodomains, in particular, those from the bromodomain and extra-terminal (BET) family, are currently regarded as compelling therapeutic agents in oncology,[66,67] and selective and potent inhibitors are under investigation.[68,69]

3.2.iii Epigenetic erasers

The erasers are the last category of HMEs. Conversely to writers enzymes, erasers describe the proteins responsible for the removal of the epigenetic marks. These enzymes are crucial in the gene transcription machinery and confer the reversible nature to epigenetic mechanisms. Current research on erasers mainly focuses on two class of erasers: the lysine demethylase (KDM) and the histone deacetylase (HDAC).

Lysine demethylase

The first class is the lysine demethylase which recognizes mono, di- and trimethylated lysine residue on H3 and H4 and alters the order of methylation. From the discovery of methylated histone in the early 1960s, and even after the isolation of the first KMT in the late 1990s,[56] the demethylation process remained a question mark in the field. Whether enzymes, capable of catalyzing the removal of methylation mark, existed or not was an important debate in the

scientific community. For several years a dogma was that histone methylation, contrary to other epigenetic marks, was irreversible and that the removal could only occur by histone exchange.[70] It was only in 2004 that Shi reported, in a groundbreaking study, the identification of Lysine-specific demethylase (LSD1).[71] This enzyme was found to catalyze the specific post-translational demethylation of H3K4me1/me2. However, LSD1 was not able to interact with the trimethylated lysine residue on H3K4.[72] Recently a second demethylase LSD2 has also been reported to interact with H3K4me1/me2.[73]

In 2004, the second subfamily of KDM, containing a JumonjiC (JmjC) domain, was identified.[74] So far about 30 members of the JmjC domain-containing proteins have been identified and classified in five subgroups (KDM2/7, KDM3, KDM4, KDM5, and KDM6).[72,75] Contrary to the LSD1/2 family of demethylase, JmjC domain-containing proteins can promote the demethylation of mono, di- and tri-methylated marks.[72] This difference is due to their mechanism (Figure 1.6). Indeed, the demethylation process occurs through successive oxidative steps converting the methyl group firstly to a hydroxymethyl and then to formaldehyde. However while the LSD1/2 family uses flavin adenine dinucleotide (FAD) redox cofactor, JmjC domain-containing proteins are Fe(II) and 2-oxoglutarate dependant.[75]

Alteration of the KDMs activity has been linked to a variety of diseases in oncology, in particular, in leukaemia and in neurology.[9,75–77] Therefore, the development of KDM inhibitors as therapeutic agents is of growing importance.[78–80]

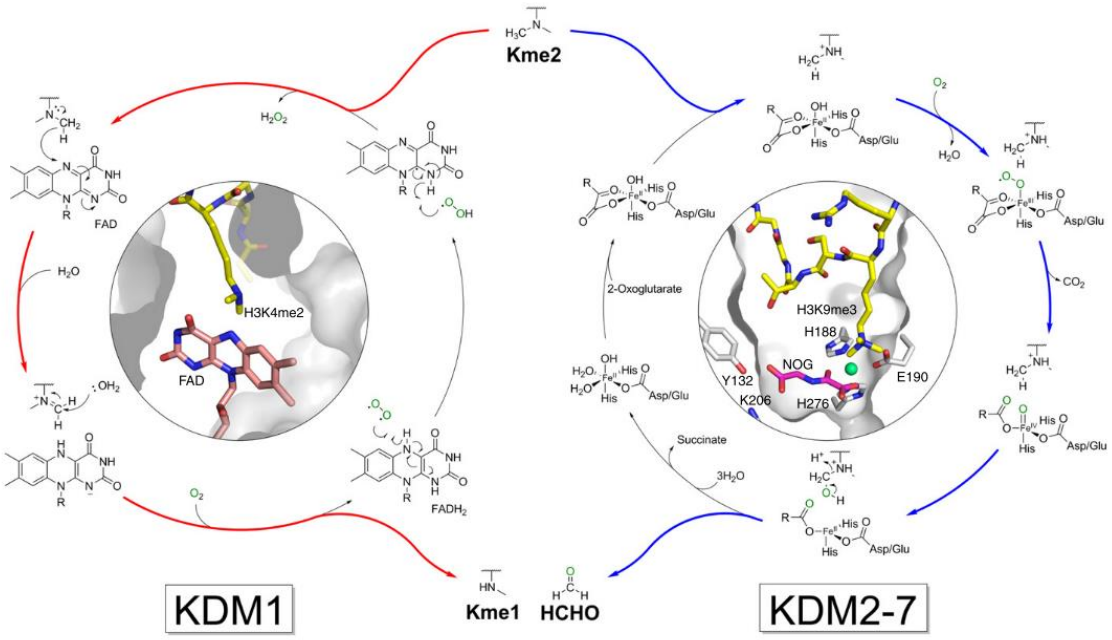

Figure 1.6: Lysine demethylation mechanism catalyzed by LSD1 (KDM1) and JmjC family (KDM2-7).

Taken from Thinnes et al.[75]

Histone deacetylase

Histone deacetylases are the second leading class of erasers. These enzymes promote the formation of the heterochromatin by catalyzing the removal of acetyl group on lysine side chains and restoring the positive charge on the histone tails. Thus, histone deacetylases have a silencing role in the control of gene expression (Figure 1.7).

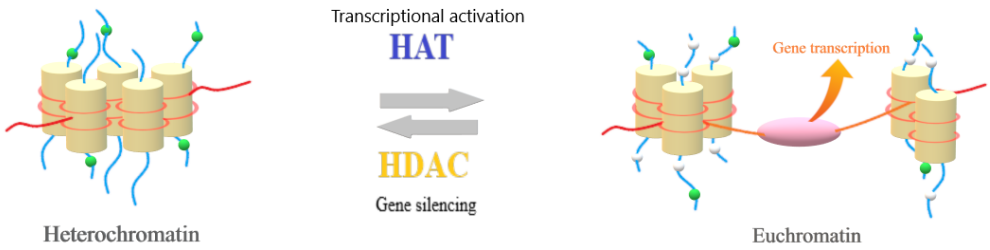

Figure 1.7: Effect of acetylation mark on chromatin state.

Histone octamers are shown as a yellow cylinder, histone tails as the blue line, DNA strand as a red line, acetyl marks as white beads and others epigenetic marks as green beads. Adapted from Verdin et al.[50]

Although Inoue had reported enzymatic deacetylation of histone,[81] the study of histone deacetylation had a breakthrough in the 1990s when Taunton published the isolation of the first histone deacetylase named HDAC1.[82] In the following years, several histone deacetylases were reported, and to date, 18 different enzymes have been identified.[50,83]

These enzymes were named in order of discovery and were divided into classes depending on their similarity of sequence (Table 1.1). Class I shares sequence similarity with the yeast Rpd3 protein and is made of HDAC1, HDAC2, HDAC3, and HDAC8. Class II proteins, composed of HDAC4, HDAC5, HDAC6, HDAC7, HDAC9, and HDAC10, have sequences analogues to yeast Hda1 protein. Class III is similar to the yeast Sir2 protein and consists of seven Sirtuin enzymes called Sirt1-7. Finally, HDAC11 constitutes the class IV due to its resemblance to both classes I and II deacetylase. In addition to this classification, histone deacetylase enzymes are divided into two superfamilies: the histone deacetylase family (class I, II and IV) and the Sir2 regulator family (class III).

Family	Class	Subclass	Protein
Histone deacetylase	Class I		HDAC1, HDAC2, HDAC3, HDAC8
	Class II	Class IIa	HDAC4, HDAC5, HDAC7, HDAC9
		Class IIb	HDAC6, HDAC10
	Class IV		HDAC11
Sir2 regulator	Class III	I	Sirt1, Sirt2, Sirt3
		II	Sirt4
		III	Sirt5
		IV	Sirt6, Sirt7

Table 1.1: HDAC classification.

The most significant difference between these two families is the mechanism of deacetylation.

On the one hand, sirtuins catalyze the removal of acetyl marks on lysine side chain in a nicotinamide adenine dinucleotide (NAD^+) dependant reaction (Figure 1.8).[83,84]

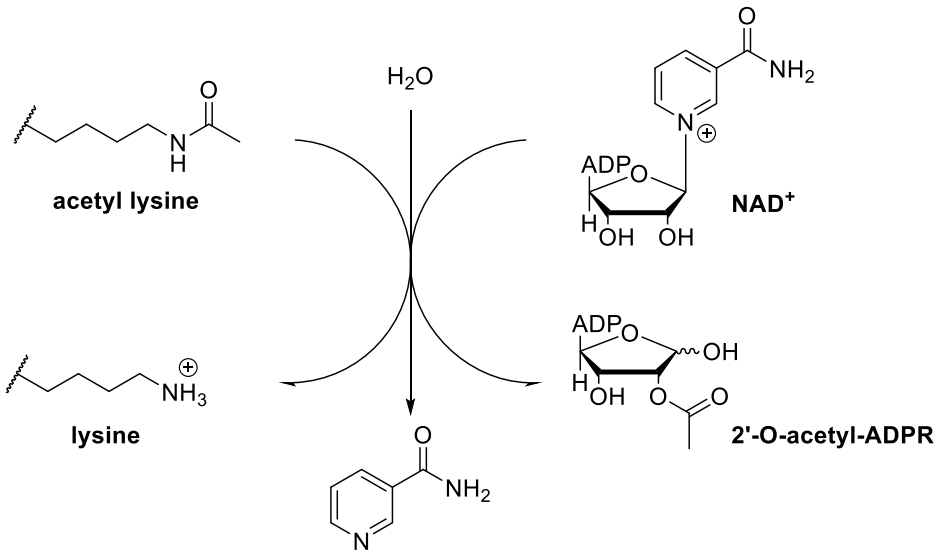

Figure 1.8: Lysine deacetylation by Sirtuin family.

Sirtuins are localized in different sections of the cell with Sirt1 and Sirt2 found in both the nucleus and the cytoplasm, Sirt3 in the nucleus and the mitochondria, Sirt4 and Sirt5 found exclusively in the mitochondria, and Sirt6 and Sirt7 present only in the nucleus (Figure 1.9).[85] Except for Sirt4 and Sirt5, histone substrates and biological roles were identified for every other enzyme.[9,50,55] Additionally Sirt1 was also reported to have deacetylase activity on non-histone protein such as p53.[86] The therapeutic potential of the Sirtuin family has been evaluated for several pathologies,[87] but modulators are mainly considered as promising agents in the treatment of type 2 diabetes,[88] and age-related diseases.[89–91]

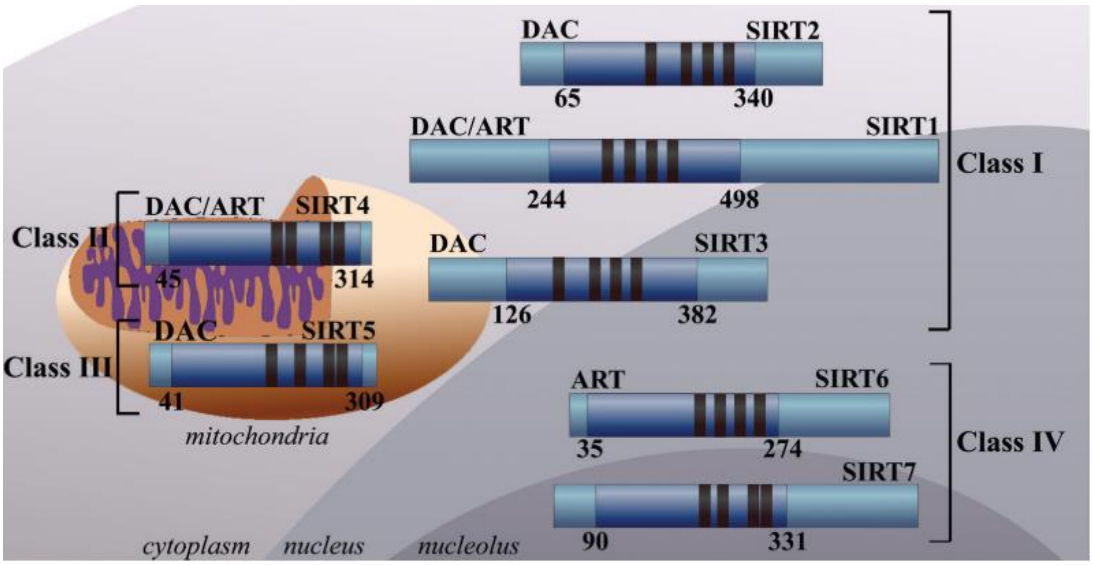

Figure 1.9: Schematic representation of the Sirtuin histone deacetylases.
The subcellular localization, dependent protein deacetylases (DAC) or ADP-ribosyltransferases (ART) binding domains (dark blue) and zinc-binding domains (black) are depicted. Taken from Karagiannis et al.[85]

On the other hand, the HDAC family catalyzes the deacetylation of lysine in a metal-dependent manner. Finnin proposed the mechanism of the reaction in 1999 based on the crystal structure of the *A. aeolicus* HDAC homolog.[92] This histone deacetylase-like protein (HDLP) shared a sequence homology to human HDAC1 and revealed the nature of the catalytic core of the enzyme. The catalytic pocket of the HDACs contains a Zn^{2+} cation and a water molecule both involved in the deacetylation mechanism (Scheme 1.2). In the first place, the zinc ion is chelated to the water and the surrounding amino acid residues, two aspartic acids (D168, D258) and a histidine (H170). Then in the presence of acetylated lysine, the zinc atom binds to the carbonyl group, and this interaction brings together the lysine side chain and the water molecule. The carbonyl, polarized by the presence of the zinc, then undergoes a nucleophilic attack by the water molecule, whose nucleophilic character has been enhanced by a close-by histidine residue (H131), to form a tetrahedral intermediate stabilized by hydrogen bonding to a tyrosine (Y297). Finally, the breaking of the carbon-nitrogen bond releases the lysine, which is then protonated by reaction with H132.

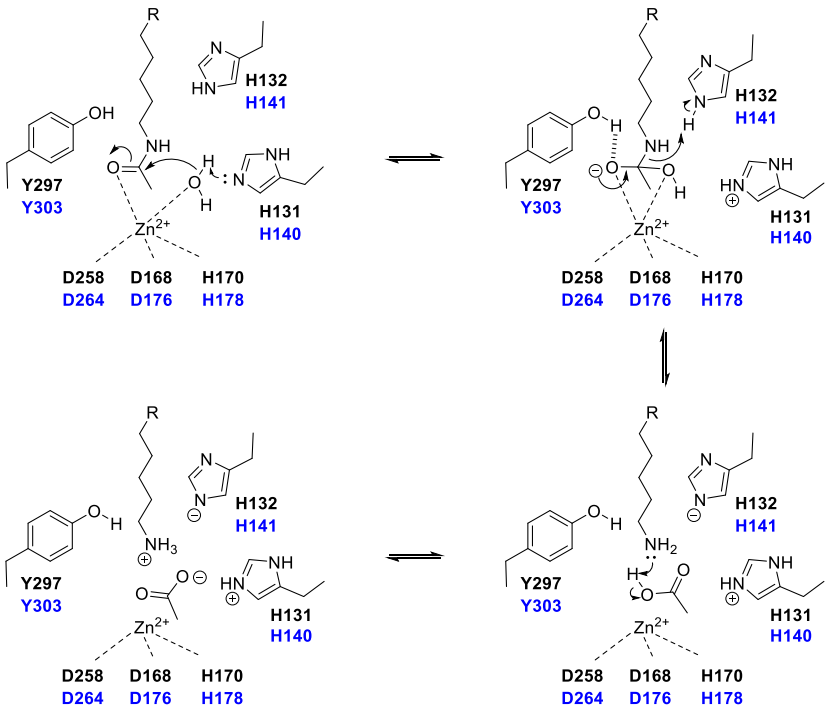

Scheme 1.2: Proposed mechanism of lysine deacetylation.
HDLP residues are labelled in black and their HDAC1 counterpart in blue.

Similarly to the Sirtuin family, HDACs can be found in different sections of the cell and were linked to various functions (Figure 1.10). Class I are exclusively found inside the nucleus and are involved in cellular proliferation and survival.[93] Class IIa can move between the nucleus and the cytoplasm and is mainly linked to tissue-specific roles.[94,95] Class IIb contains cytoplasmic proteins

playing an essential role in cell growth, migration and survival.[96–98] Finally, HDAC11 shuttles between the nucleus and the cytoplasm and has been linked to the regulation of immune function.[99]

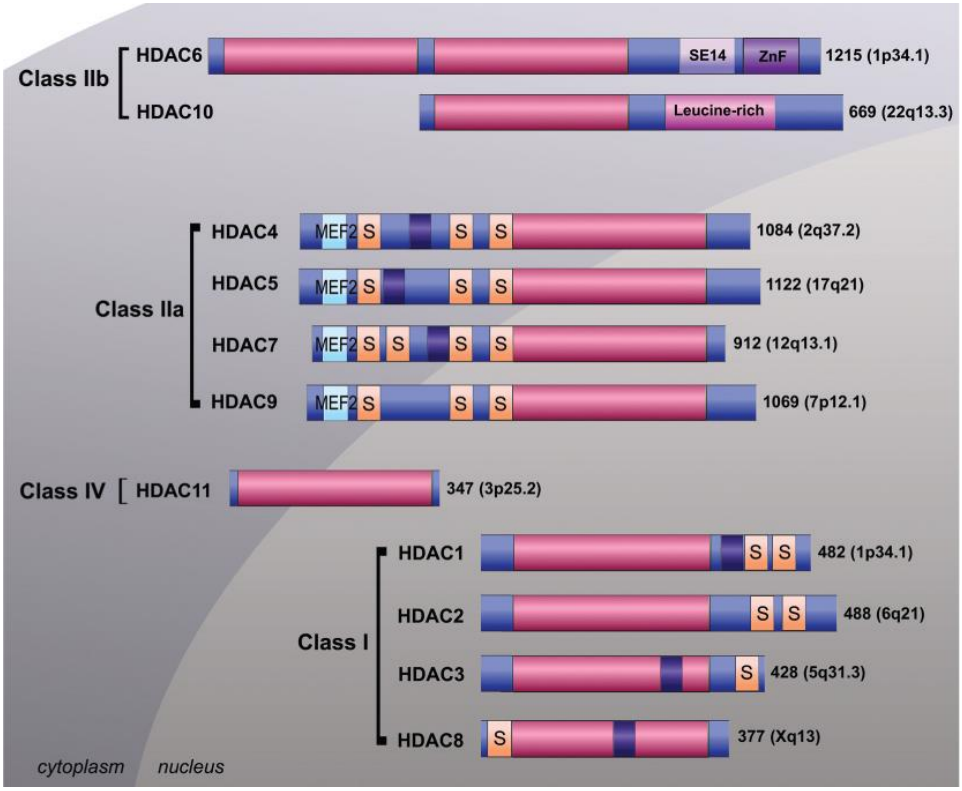

Figure 1.10: Schematic representation of metal-dependent HDAC enzymes and their subcellular localization.

***The deacetylase catalytic domain (pink), nuclear localization signal (purple), myocyte enhancer factor 2 binding domain (light blue), and serine binding motif (orange) are shown. SE14 (serine-glutamate tetradecapeptide) and ZnF (zinc finger protein) binding domain, as well as leucine-rich domain, are also depicted. Taken from Karagiannis et al.*[85]**

With the discovery of the mechanism, and following the publication of potent HDAC inhibitors in the late 1990s,[100–102] a general pharmacophore of HDAC inhibitors (HDACi) was identified (Figure 1.11). Typical HDACi are made up of three distinct regions:

- A cap region or surface recognition domain interacting with the enzyme rim
- A zinc-binding group (ZBG) or warhead which chelates to the zinc in the active site
- A linker connecting the cap and the ZBG and fitting in the enzyme channel

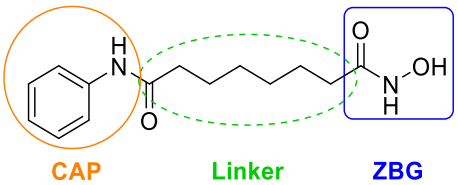

Figure 1.11: Domain of HDACi pharmacophore shown on vorinostat (Zolinza®).

Abnormal HDACs activities have been linked to several diseases and HDAC inhibitors are considered as remarkable therapeutic targets especially in cancer and neurodegenerative diseases.[9,53,94,95] In 2006, vorinostat (Zolinza®) became the first HDAC inhibitor approved by the FDA for the treatment of cutaneous T-cell lymphoma. This success boosted the field, and a variety of inhibitor structures and zinc binding group have been studied.[103–105] The development of more potent and selective HDAC inhibitors, and their investigation as therapeutic agents is currently an expanding field of broad interest.

Chapter 2. HDACs and SETD8 inhibitors: overview and perspective.

1. SETD8 inhibition

1.1 Introduction

As mentioned in the first chapter, lysine methylation on histone proteins is a major post-translational modification and is a main actor in the regulation of the chromatin compaction and the gene expression. Besides, depending on the degree of methylation and its location, histone lysine methylation is correlated with either activation or repression of genes. Most KMTs contain the SET (Su(var), Enhancer of zeste, Trithorax) domain , and evidence suggests that the catalysis could follow a specific pathway, known as a sequential bi-bi kinetic mechanism, in which the association of the substrate and the release of the product occur randomly.[106–108]

SETD8 (also known as Pr-SET7, SET8, or KMT5A) is a member of the SET domain-containing family with a growing popularity rating (Figure 2.1). Indeed, SETD8 maps to chromosome 12 and is identified as the sole histone methyltransferase in mammals that is capable of the mono-methylation of histone H4 lysine 20 (H4K20me1). This modification is involved in a range of biological processes such as DNA replication, DNA damage repair and heterochromatin formation.[109,110] SETD8 is a nucleosome-specific methyltransferase,[111] and important studies have been investigating its precise role in gene expression.

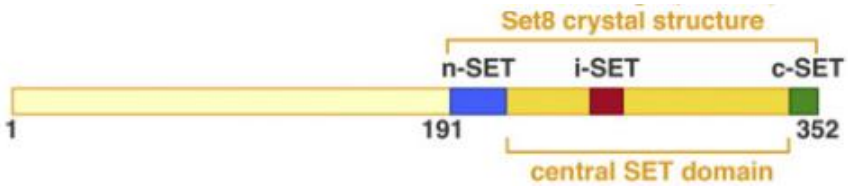

Figure 2.1: SETD8 protein catalytic SET domain.
Taken from Girish et al. [112]

1.2 Therapeutics applications

SETD8 has been identified as a key player in oncology and overexpression of SETD8 was measured in different types of tumours such as bladder cancer, non-small cell and small cell lung carcinoma, and leukaemia.[106]

MicroRNAs (miRNAs) are a cluster of non-encoding single-stranded RNA molecules of 20–24 nucleotides. These molecules function to silence gene expression by binding to complementary recognition sequences of the 3'-untranslated region (3'UTR) of target miRNAs, leading to either miRNA degradation or translation inhibition.[113,114] There is increasing evidence suggesting that single-nucleotide polymorphisms (SNPs) in the 3'UTR of SETD8 targeted by miRNA alter the

gene expression and thereby affect an individual's cancer risk. To begin with, a polymorphism at the miR-502 binding site in the 3'UTR of SETD8 has been associated with breast cancer,[115] epithelial ovarian cancer,[116] small-cell lung cancer,[117] and hepatocellular carcinoma.[118] Moreover, a significant increase in SETD8 levels was noted in samples of bladder and pancreatic cancers, myelogenous leukaemia, hepatocellular carcinoma and non-small cell lung carcinoma.[119] Moreover, several miRNAs, such as miR-127-3p and miR-382 were reported to target SETD8 in osteosarcoma cell,[120] gliomas,[121] and non-small cell lung cancer,[122] and inhibit tumour progression. Finally, miR-7 was shown to not only decrease the invasive potential of breast cancer but also to affect the sensitivity to DNA damage.[123]

DNA damage response is a signalling pathway activated by DNA double-strand breaks. The presence of the lesion is first recognised by sensor proteins which then initiate a cascade of reactions via a range of protein-protein interactions and post-translational modifications.[106,124] Then, the chromatin relaxes to allow waves of DNA damage repair proteins to flank the lesion and operate. The interaction between histone modifications, such as histone H4 lysine K20 methylation, and specific reader domains which are able to distinguish the site and degree of methylation plays a key role in the recruitment of DNA damage repair proteins.[125] One of the first responses is the phosphorylation of a variety of proteins and, among them, the spreading of histone H2AX at serine 139 (γH2AX) marks acts as an anchor for larger proteins.[126] These interactions can be detected by immunofluorescence and γH2AX is, therefore, a hallmark of DNA damage. The reduction of SETD8 activity has been negatively correlated to the formation of γH2AX and led to increased sensitivity to DNA damage due to defects during DNA replication or mitosis and to an increased genomic instability.[126–128] Afterwards, the 53BP1 protein is recruited for the recognition of the DNA damage site. This protein contains a tandem tudor domain specifically binding to mono- and di-methylated lysine in H4K20 but not to unmethylated or trimethylated H4K20.[129] It was demonstrated that the recruitment process of 53BP1 required a prompt increase of H4K20me1 on the sites of the DNA double-strand breaks and that SETD8 activity was, therefore, crucial in the DNA damage response.[128,130]

In addition to H4K20, SETD8 is also involved in the methylation of other proteins. In particular, the methylation of the proliferating cell nuclear antigen (PCNA) was found to be not only responsible for the recruitment of SETD8 on the DNA double-strand breaks sites in the DNA damage response,[128] but also play a role in human carcinogenesis.[119]

SETD8 also regulates the tumour suppressor protein p53. The transcription factor p53 is a DNA sequence-specific transcriptional regulator that responds to various cellular stresses and controls the expression of numerous genes. Its activity was reported to highly affect cell-cycle arrest,

apoptosis, senescence or DNA damage response.[131,132] The p53 protein is involved in multiple interactions with activators, repressors, and transcriptional components to express or silence the transcription of targeted genes but p53 also prevents DNA damage and limits its spreading by controlling the cell cycle. As a result of its high importance for cell survival, an exquisite control mechanism has evolved to enable a fast response but prevent an inappropriate activation. In order to be transcriptionally active, and thus recruit co-factors, the p53 protein has the ability to recognise and bind specific DNA sequences.[131,132] The p53 pathway is directly regulated by the activity of SETD8. Indeed, the monomethylation of p53 on lysine 382 (p53K382me1) by the SETD8 methyltransferase suppresses the p53-dependent transcription activation.[133] Under normal conditions, a high level of p53K382me1 could block the p53 pathway by preventing its acetylation. During the DNA damage response, a decrease in p53K382me1 levels was observed thus suggesting that SETD8 could be downregulated.[133] This is correlated with recent research of neural crest-derived tumours.[134] Indeed, SETD8 methyltransferase is overexpressed in numerous cancer cells including neuroblastoma.[119] Accordingly, the p53 pathway is highly inhibited by the important level of p53K382me1 (Figure 2.2). As a result, the study showed that inhibition of SETD8 induced p53-dependent cell death in neuroblastoma.[134] Alongside its effect on p53 methylation, SETD8 also indirectly affects the p53 pathway by methylation of Numb. This protein exists in multiple isoforms in mammals and plays a key role in cell division.[135] The Numb protein was shown to interacts with several proteins,[136] and in particular, the formation of a complex with p53 and the E3 ubiquitin ligase MDM2 was observed.[137] As a result of this interaction, Numb promotes apoptosis in a p53-dependent manner. However, the interaction of Numb with SETD8 leads to the methylation of the protein on the K158 and the K163 residues. This methylation adversely affects the binding with p53 and prevents the promotion of apoptosis. Moreover, this disruption results in increased ubiquitination and degradation of p53.[137]

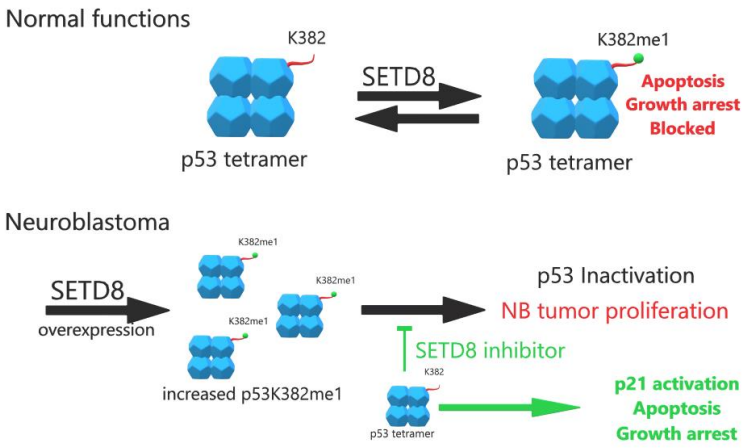

Figure 2.2: Model of SETD8 normal functions and role in neuroblastoma.
Re-drawn from Veschi et al.[134]

Although SETD8 has been mainly studied for its links to oncology, it has also been linked to other pathologies.[106]

SETD8 was reported to be expressed at a higher level in $CD71^+$ erythroid precursors compared to other cell types.[138] This result suggested that SETD8 could have Erythroid-cell-specific functions. In a study to identify the role of the SETD8/H40K20me1 pathway in erythroid cells, the downregulation of SETD8 was shown to impair the erythroid maturation.[139] Erythroid maturation is characterized by haemoglobin accumulation, changes in cell surface marker expression, and a progressive decrease in cell and nuclear size that culminate in enucleation.[140] Malik and coworkers recently reported that the knockout of SETD8 didn't alter the proliferation and the morphology of self-renewing cells, but resulted in a slower haemoglobin accumulation, larger mean cell area, incomplete nuclear condensation, and lower rates of enucleation.[141] The study also established that SETD8 functions as a transcriptional repressor of the erythroid cell and identified a link between the activity of the SETD8 methyltransferase and the expression of the transcription factors GATA-2. Later, another study provided evidence that SETD8 is also a context-dependent GATA-1 corepressor in erythroid cells.[142] These results led to the hypothesis that SETD8 controls erythroid cell maturation and function physiologically. More recent studies confirmed that the methyltransferase SETD8 is essential for the maturation and the survival of erythroid cells.[141,143] Interestingly, these studies suggest that the crucial role for SETD8 in erythroid proliferation and survival doesn't regulate the expression of the anti-apoptotic protein Bcl-xL and is independent of the p53 pathway. Besides, they also demonstrated that the Gata2 repressor function of SETD8 only occurs in the early stages of maturation as SETD8 downregulation only affected proerythroblasts but not the more mature basophilic erythroblast in which the gene is silenced. Therefore, the SETD8 methyltransferase could be required for the initiation of Gata2 but not its maintenance.[143]

In addition, the monomethylation of H4K20 was shown to regulate cell differentiation in adipogenesis.[144] Adipocyte differentiation is controlled by a cascade of transcription factors, and among them, peroxisome proliferator-activated receptor γ (PPARγ) is considered as a key regulator of adipogenesis. PPARγ is a member of the nuclear receptor superfamily and is present in two isoforms PPARγ1, and PPARγ2. Recent studies have shown that PPARγ upregulates SETD8 during adipogenesis.[144] Reciprocally, it was also demonstrated that SETD8 monomethylation of H4K20 was required to enhance the transcription of PPARγ. Furthermore adipogenesis was also promoted by an increase of H4K20me1 marks on PPARγ proteins following the activation of the receptor.[144,145] Finally, H4K20me1 levels increase robustly toward the end of adipocyte differentiation while the knockout of SETD8 suppressed adipogenesis.[144,145]

Intrauterine growth restriction (IUGR) occurs when a foetus fails to reach full growth potential in utero and sets up neurodevelopmental deterioration and long-term neurological damages. Those are correlated with a smaller hippocampus, the brain region involved in the formation of memory, as well as modification in brain connectivity. The PPARγ pathway was shown to be involved in hippocampal repair and plasticity,[146] and its activation improves cognitive function in neurodegenerative disorders.[147–149] As a result of the reported link between PPARγ and SETD8, Ke and coworkers studied the possible relationship with IUGR.[147] The study demonstrated that IUGR induces a reduction of the levels of PPARγ, SETD8 and H4K20me1 in juvenile rat hippocampus. Besides, IUGR also downregulates the Wnt signalling pathway, which plays a crucial role in a range of biological and pathophysiological processes including CNS development.[150,151] For instance, the Wnt3a gene is essential for the normal growth of the hippocampus, and it regulates the expansion of the caudomedial cortex, from which the hippocampus develops. Moreover, Axin2, another Wnt signalling target gene, is essential for myelination and remyelination in brain development. Interestingly, the Wnt signalling was proved to be mediated by the H4K20 monomethylation by SETD8.[152] Therefore, IUGR could result from a stream of reaction with a reduced PPARγ associated with a downregulated SETD8 and H4K20me1 abundance. The downregulation of H4K20me1 could then be associated with a reduced expression of Wnt signalling genes Wnt3a and Axin2.

Finally, SETD8 is also required for the maintenance of adult skin and mediates Myc-induced epidermal differentiation.[153] Indeed, knockout of SETD8 in c-Myc-overexpressing skin resulted in a loss of proliferation, impaired differentiation and caused apoptosis. The loss of differentiation is due to the disappearance of the transcription factor p63, a critical H4K20me1-mediated regulator required for epidermal stratification and differentiation,[154] in the SETD8-depleted skin.[153] On the other hand, the loss of proliferation is likely due to the overexpression of p53 in the SETD8-depleted skin which results in increased apoptosis in the epidermis.[153]

1.3 SETD8 inhibitors

Methyltransferase SETD8 plays a critical role in a wide range of biological processes and could be an attractive target for a variety of pathologies such as oncology, neurological disorder or treatment of obesity. Therefore, the development of selective SETD8 inhibitors would provide new chemical probes to investigate the role of SETD8 further, but would also offer a lead structure for the development of therapeutic agents.

The first report about SETD8 inhibitors occurred in 2007,[155] and since then only a limited number of inhibitors have been reported.[156] Besides, only a fraction of them was showing a degree of selectivity against other methyltransferases.

1.3.i Dye-like compound: H acid and thymolphthalein

In the first publication, two classes of molecules were identified as potent SETD8 inhibitors (Figure 2.3).[155] The first compound corresponded to H-acid **2-1**, the 4-amino-5-hydroxynaphthalene-2,7-disulfonic acid. Derivatives of aminonaphthol have been extensively used as intermediates in the development of dyes, but they also emerged as synthetic intermediates in the development of biologically active compounds in the pharmaceutical industry.[156,157] The second inhibitor was the thymolphthalein **2-2**, which is a dye commonly used as an indicator in the acid-base titration. Use of these molecules as inhibitors first originated from studies on the inhibition of the arginine methyltransferase PRMT1.[158,159] These compounds were then screened against SETD8, H3K9-specific methyltransferase G9a, and the H3K4-specific methyltransferase SETD7 which are all SET-domain containing KMTs.[155,156] The assay revealed that both **2-1** and **2-2** exerted an influence on SETD8 but had no inhibition activity on the non-nucleosomal methyltransferase G9a and SETD7 (Table 2.1). In a cell assay on the human cervical carcinoma HeLa cells, the very low lipophilicity of **2-1** likely induced a low cellular uptake and no inhibition effect was observed on the cell proliferation, even at a high concentration of 500 µM. On the contrary, thymolphthalein **2-2** had a concentration-dependent effect on cell viability and showed a selective downregulation of the methylation mark H4K20me1 but not of H3K27me3.[155]

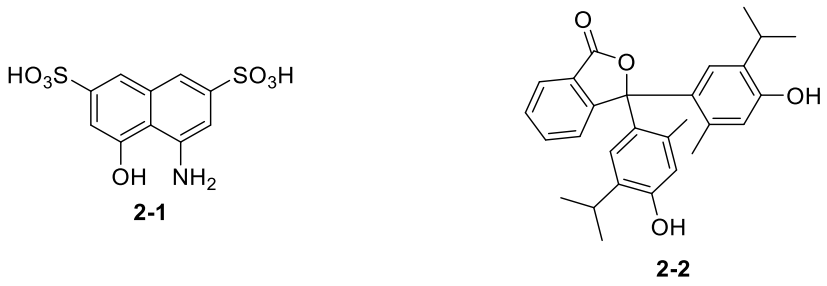

Figure 2.3: Structure of the dye-like SETD8 inhibitors 2-1 and 2-2.

Compound	Methyltransferase	IC_{50} (µM)
	SETD8	3.8
2-1	G9a	> 500
	SETD7	> 1380
	SETD8	9.0
2-2	G9a	> 1450
	SETD7	> 1450

Table 2.1: Inhibition by 2-1 and 2-2 of a panel of methyltransferases.[155]

1.3.ii EBI compounds

A couple of years later, three novel classes of SETD8 inhibitor were reported.[160] Using computational tools, Kodama et al. performed a virtual screening based on the crystal structure of SETD8 (PDB ID: 1ZKK). They generated over 3550 molecules which were predicted to bind to the enzyme according to their *in silico* methodology.[160] They then submitted 161 commercially available compounds to *in vitro* enzymatic inhibition assay. They identified three molecules EBI-099 **2-3**, EBI-435 **2-4** and EBI-455 **2-5** (Figure 2.4) with a strong inhibitory effect on SETD8. Besides, **2-3** was shown to downregulate the methylation activity of SETD8 but had no impact on G9a.[156,160]

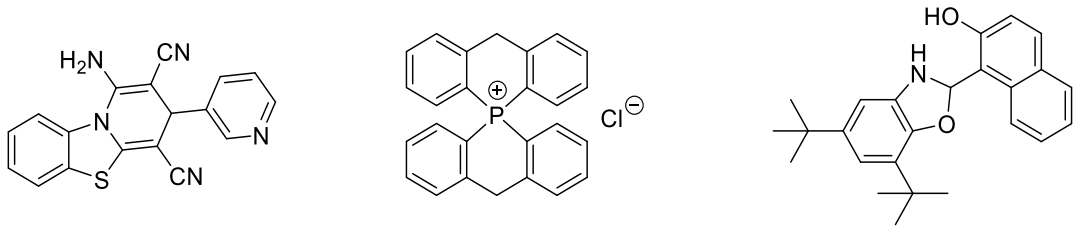

EBI-099 (2-3) | **EBI-435 (2-4)** | **EBI-455 (2-5)**

Figure 2.4: Structure of the EBI classes of SETD8 inhibitors.

1.3.iii MC compounds

In 2012, bis(bromo- and dibromomethoxyphenol) derivatives were reported to inhibit SETD8.[161] These compounds originated from a series of simplified analogues of AMI-5, which had been published as potent inhibitors of both protein arginine methyltransferase (PRMT) and histone lysine methyltransferase.[162] In this study, they had identified a structure, analogous to dibenzylideneacetone, which behaved as multiple epigenetic ligands inhibiting at the same time all the tested PRMT, HAT, and SIRT enzymes, as well as the methyltransferase SET7 (Figure 2.5). Interestingly, the number of bromine substituents on both phenyl rings had a significant impact on the inhibition of the acetylation-linked enzyme. Indeed, **2-6** and **2-7**, which are both carrying a 3,5-dibromo-4-hydroxyphenyl, were active on every epigenetic target while **2-8** was potent on methyltransferase enzyme PRMT, CARM1 and SET7, but inactive on HAT and SIRT.

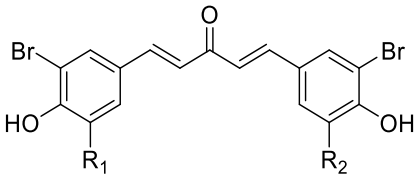

2-6: R_1 = Br, R_2 = Br
2-7: R_1 = H, R_2 = Br
2-8: R_1 = H, R_2 = H

Figure 2.5: Structure of dibenzylideneacetone derivative 2-6 to 2-8.

Those compounds were then evaluated against three lysine methyltransferases, SET7, G9a and SETD8. They all displayed inhibitory effect on each methyltransferase in the range 4.3-62.5 µM.[161]

Modification of the scaffold to introduce a methoxy group in place of the hydroxy led to the successful synthesis of selective inhibitors (Figure 2.6).[161]

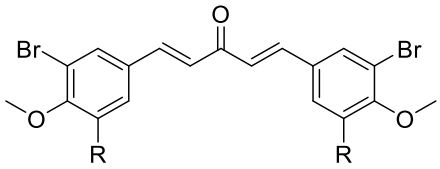

MC1947 (2-9): R = H
MC1946 (2-10): R = Br

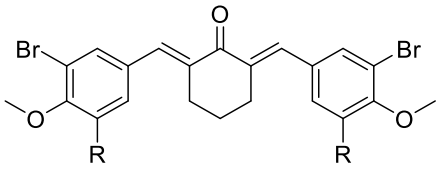

MC2569 (2-11): R = H
MC1948 (2-12): R = Br

Figure 2.6: Structure of the MC compounds.

These four compounds displayed micromolar activity on SETD8 but had no inhibition effect on both G9a and SET7 (Table 2.2). Besides, they were also tested against the multiprotein polycomb repressor complex 2 (PRC2), the active component of methyltransferase EZH2. Interestingly both **2-9** and **2-11** were active on EZH2 whereas both **2-10** and **2-12**, which feature bromine instead of hydrogen, were also selective against EZH2.

Compound	SETD8	G9a	SET7	EZH2
	IC_{50} (µM) or % inhibition at 75 µM			
2-9	9.0 ± 0.4	> 250	> 250	74.9 ± 4.0
2-10	3.3 ± 0.2	> 250	> 250	8.7 %
2-11	10.2 ± 0.5	> 250	> 250	313.8 ± 15.0
2-12	2.6 ± 0.1	> 250	164.4 ± 11.0	6.2 %

Table 2.2: Inhibitory activities of MC compound on SETD8, G9a, SET7 and EZH2.[161]

The results were confirmed by assessing H4K20me1 levels in Western blot analyses of leukaemia U937 cells after 24h treatment with the compounds at 50 µM. Furthermore, **2-9** also induced cell death and U937 differentiation.[161]

1.3.iv Nahuoic acid A

Isolated from cultures of *Streptomyces sp.* obtained from marine sediment collected in Papua New Guinea, nahuoic acid A was identified in 2013 as a selective SAM- competitive SETD8 inhibitor *in vitro*, following a screen of a library of marine organism extracts and pure marine natural products (Figure 2.7).[163]

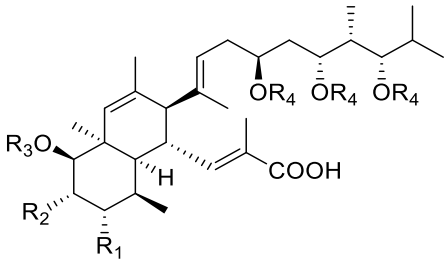

Nahuoic acid A (2-13): R_1=OH, R_2=H, R_3=H, R_4=H
Nahuoic acid B (2-14): R_1=H, R_2=OH, R_3=H, R_4=H
Nahuoic acid C (2-15): R_1=OH, R_2=OH, R_3=H, R_4=H

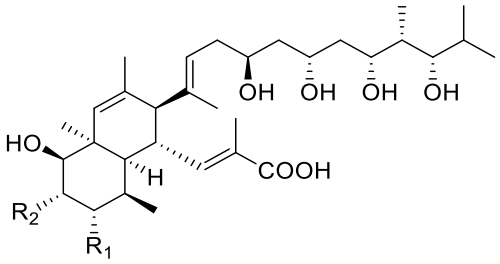

Nahuoic acid D (2-16): R_1=OH, R_2=H
Nahuoic acid E (2-17): R_1=H, R_2=OH

Figure 2.7: Structure of Nahuoic acid 2-13 to 2-17.

The authors reported that nahuoic acid A inhibited SETD8 with a micromolar IC_{50} (Table 2.3: Inhibitory activities of nahuoic acids on SETD8.[164]) but had no significant activity against other methyltransferases such as G9a, EHMT1, SETD7, SUV39H2, SUV420H1, SUV420H2, DOT1L, PRMT3, and PRMT5 and MLL complexes (Figure 2.8). Moreover, they demonstrated that **2-13** was a noncompetitive inhibitor with respect to the binding of the peptide substrate but instead competed with SAM binding with a *K*i value of 2 µM.[163]

Compound	SETD8
	IC_{50} (µM)
2-13	8
2-14	27
2-15	41
2-16	76
2-17	13

Table 2.3: Inhibitory activities of nahuoic acids on SETD8.[164]

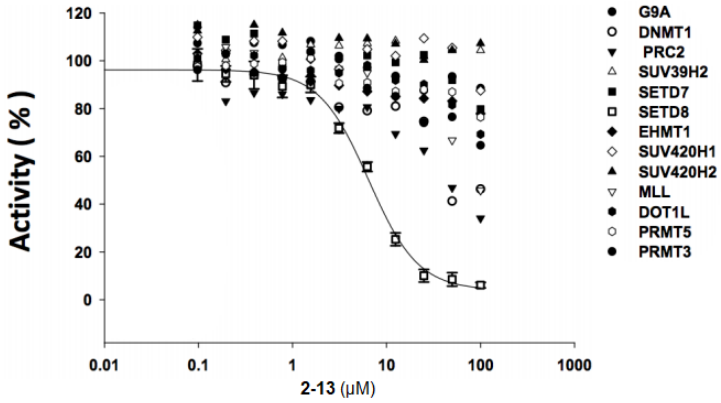

Figure 2.8: Activity of nahuoic acid A (2-13) on SETD8 and 12 other methyltransferases.
Adapted from Williams and al.[163]

Following these results, they isolated nahuoic acid B-E and showed they were also exerting an inhibitory effect on SETD8.[164] Moreover, they demonstrated that nahuoic acid A inhibited proliferation of several cancer cell lines *in vitro* with modest potencies. Finally, **2-13** showed selective inhibition of SETD8 in U2OS osteosarcoma cells.[164]

Interestingly, these compounds are the only reported SAM competitive selective SETD8 inhibitors.[164]

1.3.v UNC and MS compound

Jin and coworkers reported in 2009 the discovery of potent and selective G9a inhibitors based on 2,4-diaminoquinazoline.[165] Following up from this study, they demonstrated that 2,4-diaminoquinazolines are selective, substrate-competitive inhibitors of the lysine methyltransferases G9a and GLP.[156,166] Next, they screened their library of quinazoline-based inhibitors against SETD8. From over 150 compounds, they identified UNC0379 (**2-18**) as the most potent inhibitors of the series (Figure 2.9).[166]

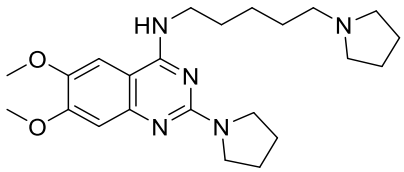

UNC0379 (2-18)

Figure 2.9: Structure of UNC0379 (2-18).

The result of the screening, a radioactive biochemical assay that measures the transfer of the tritiated methyl group from ^{3}H-SAM to a peptide substrate catalysed by SETD8, was then confirmed in an orthogonal biochemical assay, microfluidic capillary electrophoresis (MCE)

assay. Next, they performed mechanism of action (MOA) studies to determine whether the inhibition was due to competition with the substrate or with the SAM co-factor. In a series of assays, they demonstrated that the IC_{50} was proportional to the histone H4 substrate concentration while the variation of the SAM concentration had no effect on the inhibition. Therefore, they determined that compound **2-18** is competitive with the substrate and noncompetitive with the SAM co-factor.[166] Moreover, inhibition assay on a panel of enzymes showed that UNC0379 **2-18** was selective for SETD8 over 15 other methyltransferases, including G9a and GLP (Figure 2.10).

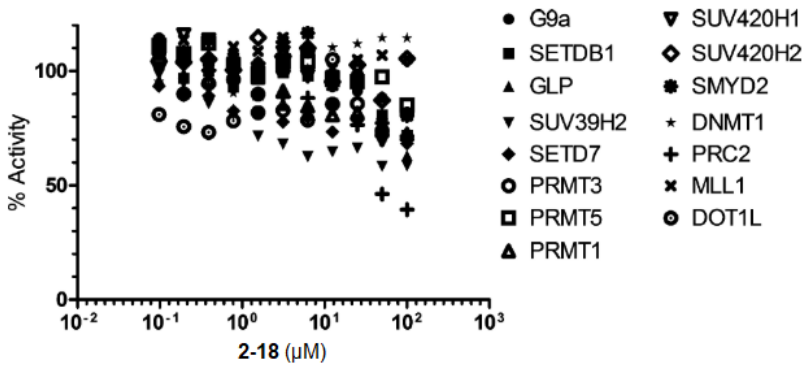

Figure 2.10: Activity of 2-18 on 15 methyltransferases.
Adapted from Ma et al.[166]

They then synthesised a series of analogues and studied the SAR of the quinazoline scaffold.[166,167] First, they focused on the modification of the C2-substituent (Table 2.4). This position was found to be mainly intolerant to modification. Indeed, most adjustments resulted in a significant loss of potency. In particular, an extension of the ring (**2-19**, **2-20**) and substitution of the pyrrolidine by chlorine (**2-21**), phenyl (**2-22**) or aniline (**2-23**) led to inactive compounds. The replacement by a dimethylamino group (**2-24**) was the only modification that maintained similar activity. Importantly, disubstitution of the amino group seemed to be required for proper inhibition (**2-25**, **2-26**).

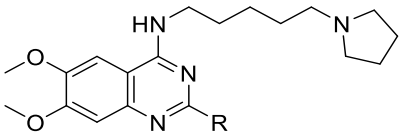

Compound	R	SETD8 IC_{50} (µM)
2-18	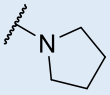	7.3 ± 1.0
2-19	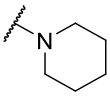	94 ± 18
2-20	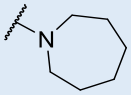	> 250
2-21		> 250
2-22	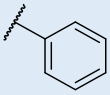	> 250
2-23	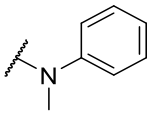	> 250
2-24		9.2 ± 1.2
2-25	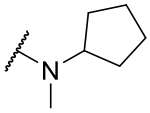	37.0 ± 9.3
2-26	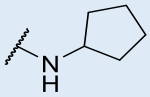	> 250

Table 2.4: SAR of the C2-position of 2-18.[166,167]

Then, they studied the substituent on the C4-position. This position was shown to be much more tolerant to modification. The ring size of the terminal cyclic amino group did not have a significant impact on SETD8 potency with both cyclic (**2-27**) and acyclic (**2-28**) amino groups maintaining a similar activity. The length of the alkyl chain had more impact on the potency (**2-29**, **2-30**) and the 5-carbon linker was the optimum. Introducing amide in the chain (**2-31**) also reduced the activity of the compound. Finally, *N*-methyl analogue (**2-32**) was drastically less potent than **2-18**, suggesting that the hydrogen of the secondary amine could serve as a hydrogen bond donor.

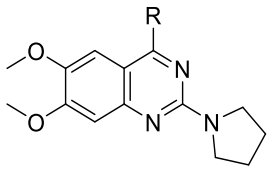

Compound	R	SETD8 IC_{50} (µM)
2-18	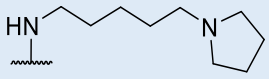	7.3 ± 1.0
2-27	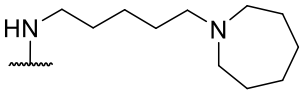	7.9 ± 1.2
2-28	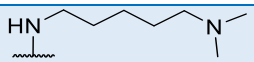	7.9 ± 1.4
2-29	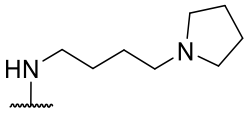	43 ± 13
2-30	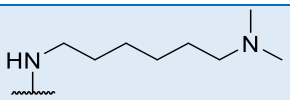	26 ± 5
2-31	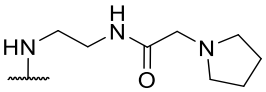	63 ± 19
2-32	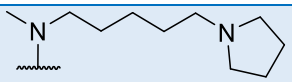	> 250

Table 2.5: SAR of the C4-position of 2-18.[166,167]

Finally, the authors looked at the methoxy substituents on C6 and C7 (Table 2.6). Replacement by hydrogens led to an important drop of potency, in particular at the C6 position that led to inactive compounds (**2-33**, **2-34**). At the C6 position, the methoxy and ethoxy (**2-35**) groups were preferred, and a larger group (**2-36**) or a less electron-donating group (**2-37**) was disfavoured. At the C7 position, modifications were more tolerated, and diverse groups could be introduced without affecting the potency (**3-38**, **3-39**, **3-40**).

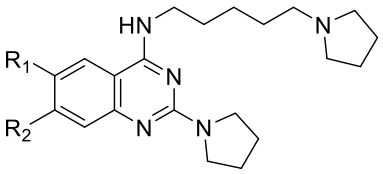

Compound	R_1	R_2	SETD8 IC_{50} (µM)
2-18	MeO-	MeO-	7.3 ± 1.0
2-33	H-	MeO-	> 250
2-34	MeO-	H-	52 ± 11
2-35	EtO-	MeO-	9.5 ± 0.9
2-36	iPrO-	MeO-	61 ± 12
2-37	Cl-	MeO-	46 ± 11
2-38	MeO-	EtO-	11 ± 1
2-39	MeO-	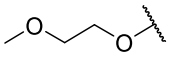	8 ± 0.8
2-40	MeO-	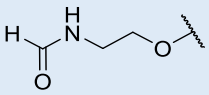	8.7 ± 0.4

Table 2.6: SAR of the C6 and C7 positions of 2-18.[166,167]

Recently, two new compounds were reported.[168] MS2177 (**2-41**) directly followed the previous SAR by introducing an aminoethyl group on the C7 position (Figure 2.11). This compound was shown to be more potent than **2-18** in a scintillation proximity assay (Table 2.7). Besides, isothermal titration colourimetry (ITC) confirmed the binding to SETD8 with a binding constant much lower than that of **2-18**. Similarly to **2-18**, competition assay confirmed that **2-41** was competitive with the H4 substrate and noncompetitive with SAM co-factor.[168]

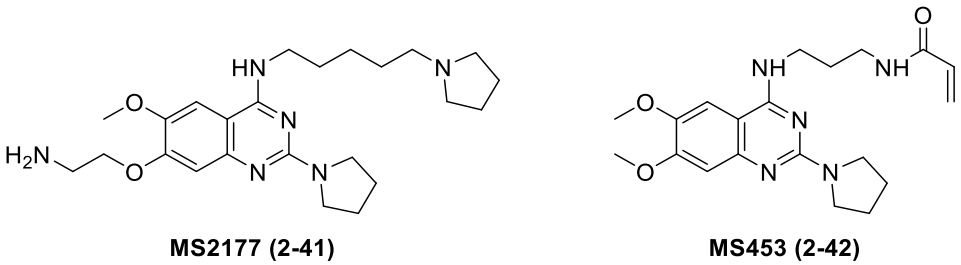

Figure 2.11: Structure of MS compounds.

Compound	SETD8 IC_{50} (µM)	K_D (µM)
2-18	7.3	1.3
2-41	1.9	18

Table 2.7: Activity of MS2177 (2-41) and 2-18 on SETD8 and binding constant K_D.[168]

Crystal structure of **2-41** in complex with SETD8 was then obtained and used to design a new inhibitor. Indeed, the 4-(pentylpyrrolidine) group of **2-41** appeared to be close to a cysteine residue, and the authors decided to modify the structure to benefit from this interaction. The alkyl chain was therefore modified to introduce an electrophile group, and MS453 (**2-42**) was synthesised.[168] This compound was reported to be a covalent inhibitor of SETD8 with a nanomolar IC_{50} in a scintillation proximity assay after five hours of incubation (Table 2.8).

Compound	SETD8 IC_{50}	
	1 h of incubation	5 h of incubation
2-42	6.90 µM	804 nM

Table 2.8: Activity of MS453 (2-42) on SETD8.[168]

Finally, **2-42** was shown to selectively inhibit SETD8 over 28 other methyltransferases (Figure 2.12).

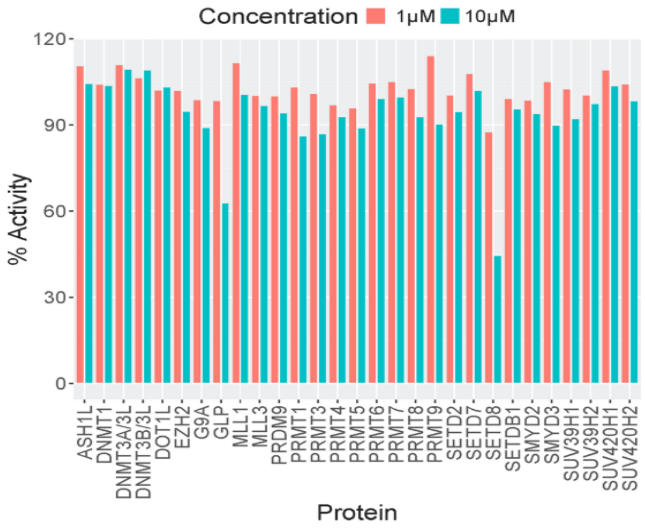

Figure 2.12: Activity of MS453 (2-42) on 29 methyltransferases.
Taken from Butler et al.[168]

1.3.vi SPS8I compound and derivatives.

In 2012, Luo and coworkers formulated a radioactivity-based scintillation proximity imaging assay in a high throughput screening format to identify new protein methyltransferase inhibitors.[169] A few years later, they identified three structures selectively inhibiting SETD8 after screening over 5000 commercially available compounds on the KMTs.[170] These compounds were called SPS8I1-3, for Small-molecule Pool of SETD8 Inhibitor and are displayed in Figure 2.13.

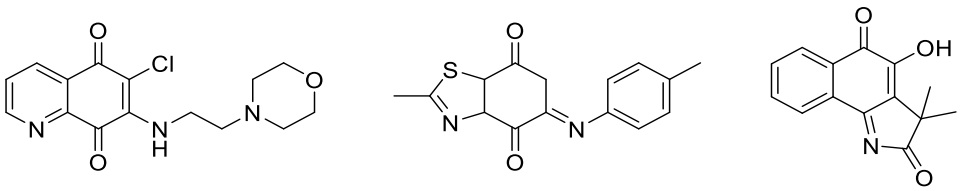

Figure 2.13: Structure of SPSI8 compounds.

The three compounds were evaluated against a panel of six lysine methyltransferases. SPS8I1 (**2-43**) and SPS8I3 (**2-45**) were not active against GLP, SETD7, but inhibited all the other methyltransferases with IC_{50} values in the low micromolar or submicromolar range, whereas SPS8I2 (**2-44**) also inhibited GLP (Table 2.9).

Compound	SETD2	GLP	G9a	SETD8	SMYD2	SETD7
	IC_{50} (µM)					
2-43	1.5 ± 0.2	> 100	6.5 ± 0.4	0.21 ± 0.02	0.5 ± 0.2	> 100
2-44	2.3 ± 0.2	4.7 ± 0.3	3.1 ± 0.2	0.5 ± 0.2	2.0 ± 0.2	> 100
2-45	1.0 ± 0.7	> 100	3.2 ± 0.1	0.7 ± 0.2	3 ± 1	> 100

Table 2.9: Activity of SPSI81-3 on lysine methyltransferases.[170]

Interestingly, studies of the MOA revealed that those three compounds inhibited SETD8 differently. Indeed, **2-43** was found to be substrate dependent, **2-44** was neither substrate nor SAM-dependent, and **2-45** was both substrate and SAM dependent.[170]

Additionally, all three inhibitors contained a Michael-acceptor quinoid motif that could react with active cysteine residues in accordance to the covalent interaction observed in MS453 (**2-42**). Thus, the authors performed further mechanistic studies and showed that SPS8I1–3 inhibited SETD8 through an irreversible slow-onset process. They then identified that both **2-43** and **2-44** specifically interacted with the C270 of SETD8, whereas **2-45** targeted cysteine residues in a nonspecific manner.[170]

A series of quinones inhibiting SETD8 with an IC_{50} value below 5 µM was then patented by the same authors.[171] Besides, these compounds also inhibited other KMTs (SETD2, SETDB1, GLP, G9a, SMYD2, SMYD3, MLL1, and SETD7) and PRMTs (PRMT1, PRMT3, CARM1, PRMT8) in the low micromolar range.

1.3.vii Peptide-based inhibitors.

Although SETD8 inhibitor development has mostly been based on the use of small molecules, a different approach was reported in 2016 with the first inhibitors based on a peptide.[172] Working on the development of substrate competitive SETD8 inhibitors, the authors used a combination of docking studies and synthesis to study the SAR of the H4 peptide. They focused on the residues 16-23 of the H4 peptide (Figure 2.14) and used molecular modelling to investigate the binding potential of mutants in which the lysine K20, methylated by SETD8, had been replaced by a set of natural and unnatural amino acids.

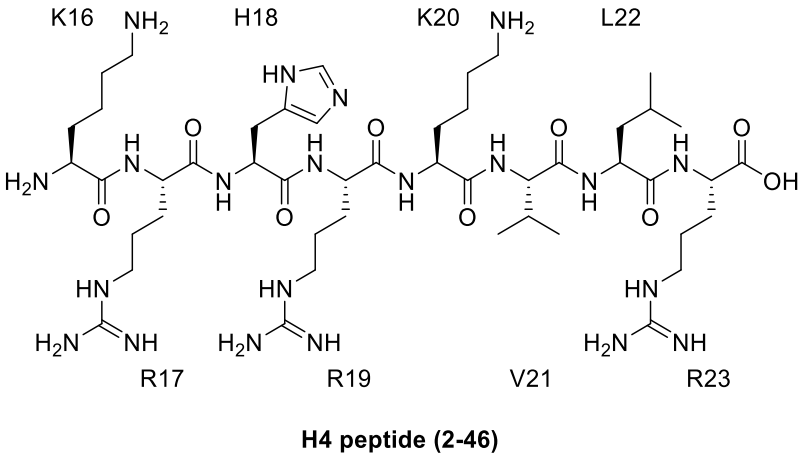

Figure 2.14: Structure of the (16 - 23) area of H4 peptide (2-46).

Then, they synthesised a set of compounds and evaluated their binding constant by isothermal titration calorimetry (Table 2.10).

Compound	Side chain	K_D (μM)
2-46	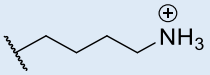	46.60 ± 2.80
2-47	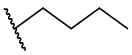	0.14 ± 0.01
2-48	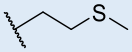	1.26 ± 0.05
2-49	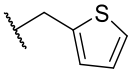	1.58 ± 0.10
2-50	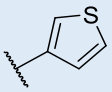	6.70 ± 0.50

Table 2.10: ITC binding of the native H4 (2-46) and K20 substituted mutant peptides.[172]

Next, they decided to modify the H4 peptide further and substitute other amino acid residues. The norleucine peptide **2-47**, which offered the best binding, was modified alternatively on its arginine R17 residue and leucine L22 residue.[172]

Replacement of R17 with shorter, hydrophobic, and sulfur-containing residues targeting the cysteine residues and hydrophobic pockets near the entrance of the pocket, resulted in a significant reduction of the binding (Table 2.11).

Compound	Side chain	K_D (μM)
2-47	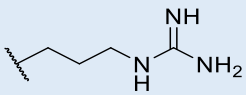	0.14 ± 0.01
2-51	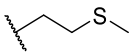	14.80 ± 2.00
2-52	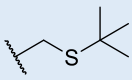	3.04 ± 0.38
2-53	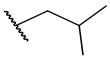	5.57 ± 0.36
2-54	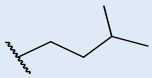	1.84 ± 0.14

Table 2.11: ITC binding of the Nle H4 (2-47) and R17 substituted mutant peptides.[172]

On the other hand, L22 sits in a mostly hydrophobic pocket with some charge on the periphery. This position was more tolerant to substitution by larger hydrophobic groups (Table 2.12). However, with the exception of β-cyclohexylalanine, modifications of L22 resulted in slightly less potent compounds.

Compound	Side chain	K_D (μM)
2-47	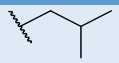	0.14 ± 0.01
2-55	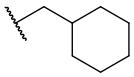	0.12 ± 0.01
2-56	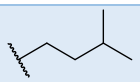	0.21 ± 0.01
2-57	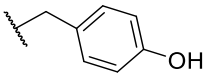	0.32 ± 0.02
2-58	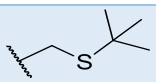	0.58 ± 0.01
2-59	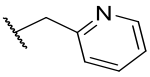	0.80 ± 0.04

Table 2.12: ITC binding of the Nle H4 (2-47) and L22 substituted mutant peptides.[172]

The norleucine substituted peptide (**2-47**) was then tested as a SETD8 substrate competitive inhibitor against the H4 peptide in the presence of SAM. It was found to have a *K*i of 50 nM and an IC_{50} of 0.33 μM.[172] Finally, assays on a panel of 32 methyltransferases revealed that the peptide **2-47** demonstrated some selectivity (Figure 2.15).

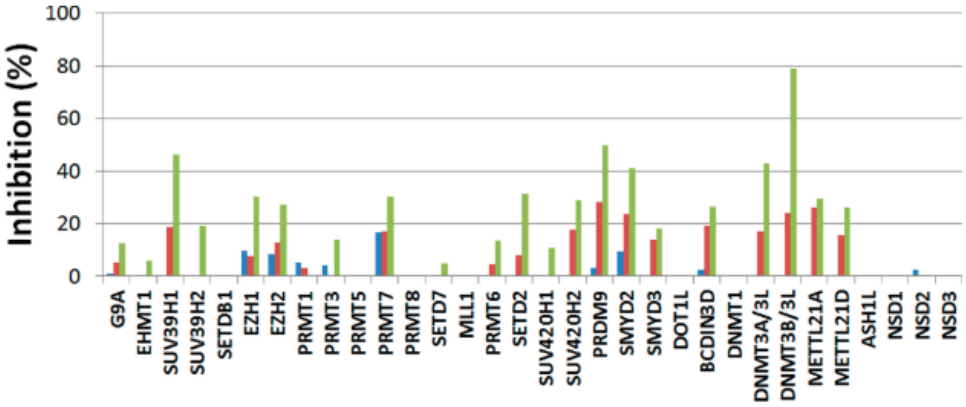

Figure 2.15: Inhibition of 32 methyltransferases by Nle H4 peptide (2-47).
Taken from Judge et al.[172]

1.4 Summary

SETD8 was identified as the only mammalian methyltransferase responsible for the monomethylation of lysine K20 on histone H4. H4K20me1 is a methyl mark critical for the genomic integrity of eukaryotic cells, and SETD8, therefore, plays a crucial role in the regulation of transcriptional activity. In addition, this unique methyltransferase also interacts with non-histone proteins such as p53 and PCNA. Over the last decades, its action on different substrates, and H4K20 in particular has been linked to a wide range of biological processes. Moreover, a dysregulation of the SETD8 activity has been linked to several pathologies including cancer, neurological disorders, and obesity. Nonetheless, the functions of the protein, and its effect in both normal and altered cells, are not fully understood yet. Thus, the development of new chemical tools is required to pursue the investigation of the biological role. Over the past decades, SETD8 inhibitors emerged as potential therapeutic agents and their development has experienced a steadily growing interest. As a result, significant progress has been made in medicinal chemistry, assay development, structural biology and high-throughput screening. These advances successfully led to the development of different classes of SETD8 inhibitors, but a limited number have been reported so far. Moreover, only a fraction of them is showing a degree of selectivity and/or cellular activity. The development of more potent and more selective SETD8 inhibitors is of great importance and the recent identification of the binding to the nucleosome,[112] as well as the resolution of the crystal structure of SETD8 in complex with inhibitors,[168,172] could pave the way for new generation of inhibitors.

2. HDAC inhibition

2.1 Introduction

Lysine acetylation is the most studied epigenetic post-translational modification. In histones, lysine acetylation decreases their affinity for DNA and relaxes the nucleosome to enable the gene transcription. Conversely, HDACs act as gene repressors by removing histone acetylation marks and prevent the recognition by bromodomains. In addition, more than 50 non-histone proteins have been identified as a substrate for one of the HDACs.[173] HDACs have a regulatory role in cell development, cell proliferation, cell migration and cell death. Therefore, HDAC inhibitors (HDACi) have vast potential as therapeutic agents in the treatment of a range of pathologies.

2.2 Therapeutic applications

2.2.i Therapeutic applications targeting human HDACs

Oncology

HDAC inhibitors have been thoroughly studied as anticancer agents. In many cancers, an increased level of expression of HDAC had been observed,[174] and treatment with HDAC inhibitors had a significant impact.[53]

Induced apoptosis

Cell death is one of the most studied anticancer effects of HDAC inhibitors.[175,176] Treatment with HDACi induces tumour cell death with all the characteristics of apoptosis, and the therapeutic efficacy has been observed in preclinical models.[176–179] Their therapeutic potential comes from their ability to induce apoptosis in tumour cells selectively. Indeed *in vitro* studies have shown that transformed cells could be 10-fold more sensitive to HDACi than normal cells.[180] Notwithstanding, as a result of the numerous biological effects of HDACi-induced cell death is likely mediated by multiple molecular pathways in all cell types. Indeed, both the intrinsic and extrinsic apoptotic pathways have been shown to be involved. Moreover, there is growing evidence that the effect of HDACi can be cell-type dependent.[175,176]

The intrinsic pathway was reported to be critical for the potent apoptotic effect of HDACi, and its activation resulted from overexpression and an upregulation of the activity of proapoptotic BH3-only genes such as Bim, Bid, Bmf, Noxa and Puma.[181] In addition, it was reported that over 4200 genes responded differently to treatment with an HDACi between normal and transformed cells,[182] and the authors identified a tumour-cell-selective pro-apoptotic gene-expression signature with the BCL2 family genes. In cancer cells, upregulation of the proapoptotic gene BMF was observed after treatment with HDACi while the prosurvival gene BCL2A1 encoding BFL-1 was downregulated.[182] Moreover, the upregulation and downregulation of the BCL2 family, induced by treatment with HDACi, were also reported in a variety of cancer cell lines such as chronic lymphocyte leukaemia,[183] breast and brain cancer,[184] hepatocellular carcinoma,[185] and other haematological malignancies.[186] Besides, the altered expression of the apoptotic genes Bmf, Bim, Puma and Noxa, was proved to be linked to the histone hyperacetylation of the gene promoters induced by the treatment with HDACi.[175,187–189] Finally, HDACi also indirectly regulate the expression of proapoptosis and antiapoptosis genes by mediating the expression of micro-RNAs,[190–192] and the activity of transcription factors such as E2F1,[193] p53,[194] and Sp1.[195]

Activation of the extrinsic pathway also plays an important role in HDACi-induced apoptosis.[181] Firstly, HDACi can repress the expression of c-FLIP, an endogenous inhibitor of caspase-8 that

inhibits the activation of the extrinsic apoptosis pathway.[196] Secondly, HDACi enhance the sensitivity of malignant cells to death receptors ligands and increase the expression of death receptors.[197] In addition, the induction of death receptors has been demonstrated to be tumour cell-selective,[179] and the restriction of these two pathways reduced the efficacy of HDACi in preclinical studies.[177,179,198]

A third mechanism of the HDACi-induced cell death has been identified with the generation of reactive oxygen species (ROS), and pre-incubation with antioxidants have been shown to protect the HDACi-induced cell death.[199,200] Moreover, the increase in ROS levels precedes changes in mitochondrial membrane potential, the release of cytochrome c, and subsequent tumour cell death.[201,202] It has recently been proposed that the regulation of ROS might underpin the tumour-selective killing activity of these agents.[180,200]

Finally, HDACi-induced cell death can also occur through the accumulation of DNA damage.[203] In the first place, HDACi treatment downregulated critical proteins involved in the DNA damage response and required for DNA damage sensing, homology-directed repair (HDR) and nonhomologous end joining (NHEJ).[203–205] In addition, HDACi were shown to induce DNA damage which could be repaired in normal cells but not in transformed cells.[206] Furthermore, HDACi treatment was shown to induce hyperacetylation of Ku70 in prostate cancer cells, thus reducing Ku70 DNA binding and increasing the sensitivity to DNA-damaging agents.[206] Finally, the slowed down DNA replication in cancer cells, induced by HDACi, and the previously described accumulation of ROS species can also cause DNA damage.[207,208]

Cell cycle arrest

In the first place, HDAC inhibitors can induce cell cycle arrest at the G1/S cell cycle checkpoint and the G2/M boundary.[175] Treatment with HDACi is associated with p53-independent induction of CDKN1A transcription. This gene, located on chromosome 6 in human, is encoding the p21 WAF1/CIP1 protein, a cyclin-dependent kinase CDK inhibitor acting as a regulator of cell cycle progression at G1 and S phase.[209] In addition, treatment with HDAC inhibitors was also shown to upregulate other CDK inhibitors.[175] Two genes involved in DNA synthesis, CTP synthase and thymidylate synthetase, are transcriptionally repressed by HDAC inhibitors.[210] Loss of these enzymes would have a similar effect to antimetabolite treatment that blocks S-phase progression, thereby also contributing to the G1/S arrest.[174]

Treatment with HDAC inhibitors also induces downregulation of cyclin D and cyclin A genes and contributes to the loss of CDK2 and CDK4 kinase activities and hypophosphorylation of pRb.[174,175] Therefore, HDAC inhibition blocks the activation of G2/M regulatory complexes and leads to G2/M arrest.[211]

Finally, a biological hierarchy has been established between the different processes and evidence suggested that apoptosis induced by the treatment with HDAC inhibitor is dominant over the G1/S arrest, which itself is dominant over the G2/M arrest.[175]

Differentiation

Induced differentiation is another critical effect of HDAC inhibitors. Oncogenic fusion proteins, such as PML-RARα and AML1-ETO, are known to initiate tumorigenesis by inhibiting cellular differentiation.[212] In acute promyelocytic leukaemia (APL), a PML-RARα-driven acute myeloid leukaemia, HDAC inhibition can induce a differentiation-mediated antitumor response.[53] Indeed, treatment of APL by HDAC inhibitors showed a therapeutic effect in a mouse model by reversing the myeloid differentiation block caused by the repression of RARα genes.[175,213] The treatment enhanced the sensitivity to retinoic acid in APL cells and restored the sensitivity in resistant APL lines.[214] As a result, a sequential HDAC inhibitor/all-trans retinoic acid (ALTRA) treatment was shown to reprogram differentiation in refractory and high-risk AML in clinical trials.[215]

In addition, HDAC inhibitors induce differentiation of AML1-ETO-driven AML cells both *in vitro* and *in vivo* in a mouse model.[216] This differentiation co-occurred with tumour cell arrest coupled with an increase in the promyeloid differentiation genes PU-1, GATA-2, SCL, and C/EBPa.[216]

A similar effect was observed in the treatment of NUT midline carcinoma (NMC), a malignant pediatric tumour driven by the BRD4-NUT oncogenic fusion protein.[217] Squamous cell differentiation was restored *in vitro* after treatment with HDAC inhibitor and resulted in cancer cell growth inhibition and increased survival of mice suffering from NMC.[217] Furthermore, treatment with the FDA-approved HDAC inhibitor vorinostat of a patient with NMC showed antitumor response by positron emission tomography.[217] Similar response was observed in the xenografted tumour from the same patient, providing preclinical and clinical evidence for HDAC inhibitor therapy for NMC.[217]

More broadly, HDAC inhibitors have been shown to induce differentiation of primary sarcoma cell lines,[218] human hepatoma cells,[219] small cell lung cancer cells,[220] and breast cancer.[221]

Senescence

In addition to the previously described increased expression of p21 WAF1/CIP1, treatment of cancer cell lines with HDAC inhibitors induces cell senescence and staining of associated biomarkers such as senescence-associated β-galactosidase (SA-βGal).[222] HDACi-induced senescence was shown to be linked to a downregulation of the polycomb repressor of cytokinesis 1 (PRC1) component Bmi1.[175,223] Moreover, the PRC2 component and senescence inhibitor

protein EZH2 was also downregulated. Interestingly, these reduced levels of expression were not due to a direct effect of HDAC inhibition on these proteins. Instead, they resulted from the upregulation of miR-31, a transcriptional target of histone deacetylase inhibitors.[223]

Autophagy

Autophagy was observed in cancer cells after treatment with HDAC inhibitors.[224–226] However, the exact role of autophagy in the mediation of HDACi therapeutic effect has not been elucidated yet. In an *in vitro* study of hepatocellular carcinoma cell lines, HDACi-induced cell death was shown to require autophagy.[227] On the other hand, in glioblastoma cell lines, inhibition of autophagy greatly increased HDACi-induced apoptosis.[228] Although these results seem to suggest that the effect of autophagy on HDACi-induced apoptosis could be tumour cell line-dependant, opposing observations were also obtained within a single cancer cell line. In U937 cells, activation of autophagy increased the sensitivity to vorinostat-induced apoptosis. Meanwhile, U937 cells with acquired resistance to vorinostat possessed a high level of autophagy, and its inhibition restored the sensitivity of the cells to vorinostat.[229] These results indicate that autophagy can switch from a proapoptotic signal to a prosurvival function.

The link between HDAC inhibition and the activation of an autophagic response is not fully understood, but several pathways have been identified. HDACi where shown to induce autophagy in cells through inhibition of mechanistic target of rapamycin (mTOR) pathway.[227] In addition, a recent study demonstrated that HDACi-induced autophagy was also dependent on the forkhead box proteins (FOXO) pathway.[230] Finally, the previously described increased vorinostat-induced apoptosis, following autophagy inhibition, was shown to be linked to ubiquitinated protein accumulation.[231]

Immunomodulatory effects

There is growing evidence that HDACi can enhance immunogenicity either by directly affecting malignant cells to make them more attractive immune targets, or by altering immune cell activity.[175] HDACi were showed to upregulate the expression of major histocompatibility complex MHC class I and II molecules and the antigen-processing machinery.[232–234] Moreover, HDACi were reported to induce the expression of MHC class I related molecules MICA and MICB on the surface of tumour cells.[235,236] Those molecules bind to the activating immunoreceptor NKG2D (natural killer cell protein group 2D) on the surface of natural killer (NK) cells, γδ T cells and CD8 T cells. Therefore, HDACi can increase the NK cell cytotoxicity by activating the NKG2D signalling pathways.[235,237] HDACi can also induce immunogenic tumour cell death and lead to enhanced tumour clearance by CTL killing and dendritic cell phagocytosis.[233,238] Besides, it was established that an intact immune system was critical for an

HDACi-induced anticancer response against solid and haematological tumours.[239,240] The *in vivo* antitumor effects and antitumor immunity was also shown to be enhanced by immune-stimulating antibodies increasing CTL activity.[238]

Despite these results, it was also reported that HDACi treatment, and in particular, the knockdown of some class I HDAC isoforms, could downregulate the expression of B7-H6, an NK-cell activating ligand, and therefore decrease NK cell activation and tumour cell killing.[241]

Conclusion

HDACi are exciting new anticancer agents that induce tumour-cell death, cycle-arrest, differentiation, senescence, autophagy and immunogenicity (Figure 2.16). If the therapeutic potential of HDAC inhibitors in oncology has been established, the molecular processes underlying the effects of HDACi remain to be fully elucidated. To this end, the development of more potent and more isoform selective HDACi represents a high-profile topic.

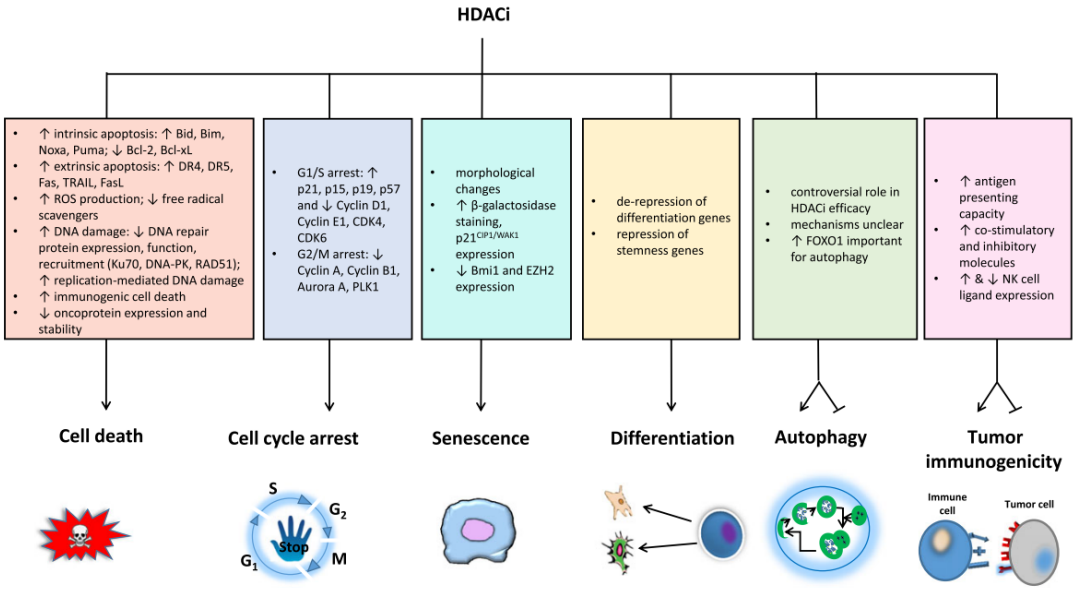

Figure 2.16: Overview of biological response to HDACi treatment in cancer cells.
Taken from Newbold et al.[175]

Neurodegenerative diseases

Histone deacetylases represent emerging therapeutic targets in the context of neurodegeneration. Indeed, pharmacologic inhibition of HDACs activities in the nervous system has shown beneficial effects in several preclinical models of neurological disorders.[95]

Huntington's disease

Huntington's disease (HD) is a dominantly inherited neurodegenerative disorder characterized by progressive impairment in cognitive and motor functions. HD is caused by a mutation encoding an abnormal expansion of a trinucleotide (CAG)-encoded polyglutamine repeats in the huntingtin protein (htt). Increasing evidence suggests that mutant htt (mhtt) disrupts the normal transcriptional regulation of susceptible neurons but the mechanisms by which mhtt causes neuronal dysfunction and death remains unclear.[95] Global reduction of the levels of histone acetylation was first identified in neurons,[242] and since then the link between hypoacetylation and neurodegeneration has been well established.[243,244]

In a *Drosophila* model of HD, treatment with vorinostat managed to stop the progressive neuronal photoreceptor degeneration and reduced the mortality rate of the flies.[245] Moreover, inhibition of reduced potassium dependency 3 (Rpd3, orthologue to human class I HDAC), as well as the orthologue of human SIRT1-3, led to neuroprotection effect.

To evaluate the hypothesis that expanded polyglutamine (polyQ) domains could interfere with the transcriptional regulation, RNA interference (RNAi) was used in *C. elegans* neurons expressing an expanded polyQ human htt fragment (Htn-Q150).[246] This study revealed that knockdown of had-3 (orthologue to human HDAC3) suppressed Htn-Q150 toxicity while the repression of others HDACs resulted in increased toxicity. These results suggest that, in *C. elegans*, HDAC3 acts as an antagonist of the polyQ toxicity pathway.

In R6/2 mouse model, the most widely used mouse model for HD, treatment with HDACi resulted in increased level of acetylation, protection against 3-nitropropionic acid neurotoxicity, improved motor performance, delayed of the onset of the neuropathological development, and extended survival in a dose-dependent manner.[247] Besides, one of the primary challenge in the treatment of neurological diseases is to cross the blood-brain barrier (BBB). Complexation of vorinostat with cyclodextrin was proved to increase the brain permeability and significantly improved the efficacy of the drug in the R6/2 mouse model.[248]

In addition to the alteration of the transcription and the deregulation of the acetylation level, HD toxicity also results from a defect in microtubule-based transport.[249] HDAC6 was reported to be a microtubule α-tubulin deacetylase.[250] Therefore, its inhibition resulted in an increase of α-tubulin acetylation and enhanced vesicular transport of brain-derived neurotrophic factor (BDNF).[249]

HD pathology is also associated with impaired cognitive functions and motor deficits. HdhQ7/Q111 transgenic HD mice display cognitive deficits, which are associated with reduced

hippocampal expression of the CREB-binding protein (CBP), decreased levels of histone H3 acetylation, and lower expression of CREB/CBP target genes related to memory. Treatment with HDACi resulted in enhanced transcription of selective CREB/CBP target genes and a significant improvement of recognition memory.[251]

In addition to these *in vitro* and *in vivo* studies, the effects of HDAC inhibition on HD were also evaluated in clinical trials. HDACi treatment in myoclonic hyperkinesias in HD patients showed beneficial effect both as monotherapy,[252] and in combination with haloperidol, a typical antipsychotic.[253] These studies reported an improvement of motor performance and an attenuation of the aggressiveness in the patients.[254] As a follow-up, several HDACi are now undergoing clinical trials.[255]

Alzheimer's disease

Alzheimer's disease (AD) is one of the most severe age-related neurodegenerative disorder affecting the cortex and hippocampus, respectively the learning and memory centres in the brain. The disease is characterized by abnormal phosphorylation levels of the tau protein, leading to the formation of neurofibrillary tangles. In addition, the accumulation of β-amyloid (Aβ) neurotic plaques induces a neuroinflammatory response by promoting the release of proinflammatory mediators that perpetuate reactive gliosis, disrupt the Wnt pathway and cause oxidative stress.[85,256] This cascade of reactions enhance the neuropathological damages and lead to neuronal death.

HDACs, especially HDAC2 and HDAC6, have been associated with AD. In mice, overexpression of HDAC2 demonstrated an adverse effect on brain functions and resulted in reduced synaptic plasticity and damaged memory formation.[257] Conversely, a deficiency in HDAC2 resulted in the improvement of the same functions, thus demonstrating a crucial modulating activity of HDAC2 in synaptic plasticity, learning and memory.[257] Regarding HDAC6, several studies revealed its implication in neurodegenerative diseases.[258] Brains of AD patients expressed a higher level of HDAC6, and the tau protein was found to bind to HDAC6 both *in vitro* and in human brain tissues.[259] This protein also acts as an HDAC6 inhibitor,[260] and treatment with more potent HDACi resulted in a lower level of tau phosphorylation which may decrease neurofibrillary tangle formation in AD.[261] Besides, AD displays deregulation of mitochondrial transport, and HDA6 has been shown to play a crucial role in its mediation through an association with glycogen synthase kinase-3b GSK3b.[262]

Treatment with HDACi has been shown to improve contextual memory in a mouse model and inhibited the production of Aβ in cells.[263] HDACi treatment have demonstrated beneficial effects upon AD pathology and memory performance with no signs of toxicity in AD transgenic mouse models.[264–267] Increased synaptic plasticity, improved learning and memory, attenuation of spatial

memory deficits, and repressed apoptosis in stressed neuronal systems all resulted from the restoration of acetylation of histone H4 and the clearance of Aβ accumulation after HDACi treatment,[85,265,268,269] Moreover, inhibition of HDAC6, by treatment with selective HDAC6 inhibitors or siRNA, was shown to promote neurite extension or protect neurons from oxidative stress.[259,270]

However, as we mentioned earlier, HDACi have cell-specific effects and are well-known for their potential to induce cell death and cell-cycle arrest in cancer cells, but similar effects have been observed in neuronal cells.[271]

As a result, the development of more selective or isoform-specific inhibitors could be a crucial requirement for the treatment of AD.

Parkinson's disease

Parkinson's disease (PD) is one of the most devastating neurodegenerative diseases. The two typical hallmarks of PD are a progressive loss of dopaminergic neurons from the substantia nigra pars compacta (SNpc), and the presence of aggregates of α-synuclein (α-Syn), called Lewy bodies, that are expressed in many regions of the central and peripheral nervous systems.[95] Although the exact mechanisms of neurodegeneration are not fully elucidated yet, the abnormal level of Lewy bodies in PD, as well as the misfolding and oligomerization of α-Syn, were shown to be key contributing factors to the development of PD.[272–274]

It has been demonstrated that HDAC6 is localized in brain sections of PD patients and regulates the formation of aggregates in the response of misfolded protein stress.[97]

In cell culture, HDAC6 activated the formation of aggresomes containing the polyubiquitinated mutant DJ-1, a protein involved in the early stages of PD.[275] Furthermore, HDAC6 also improved the transport of DJ-1 to the microtubule organizing centre (MTOC).[275]

Several studies have shown that HDACi treatment of cellular models displayed neuroprotective effects.[276] Besides, class IIa selective HDACi were reported to promote the growth of neural processes and protect both dopaminergic and sympathetic neurons from MPP^+-induced cytotoxicity.[277]

Summary

In addition to their potential as anticancer agents, HDAC inhibitors could be at the forefront in the development of new therapies for neurodegenerative diseases (ND). Most ND remain incurables, and several clinical trials have experienced a gruesome fate. As an illustration, 244 compounds entered a clinical trial in the Alzheimer's disease pipeline between 2002 and 2012,

and analysis revealed a failure rate of 99.6%.[278] HDAC inhibition represents a new approach for ND, and has shown promising results for the treatment of Huntington's disease, Parkinson's disease and Alzheimer's disease. Furthermore, HDAC has also been linked to other ND such as amyotrophic lateral sclerosis (ALS), spinal muscular atrophy (SMA), ischemic stroke, Friedreich's ataxia (FRDA), and fragile X syndrome (FXS).[95,279] However, some side effects were also observed with pan-inhibitors, so the development of more selective or isoform-specific inhibitors are therefore required.

Conclusion

HDAC inhibitors have been extensively studied in cancer and neuropathology, and their therapeutic potential has been well established. Nevertheless, over the last few years, a broader scope of pathology has been investigated. Among others, HDAC inhibitors have been studied in diabetes,[280] obesity,[281] cardiac hypertrophy,[282] autism,[283] alcohol use disorder,[284,285] and a range of fibrosis.[286–288]

In this respect, the use of HDACi is a highly promising therapeutic strategy, and the key to the use of HDACi as therapeutic tools lie in the development of isoform-specific inhibitors to investigate further the roles of HDAC isoforms in the pathology of diseases.

2.2.ii Therapeutic applications targeting non-human HDACs

While research on HDACs was mainly focused on the human enzymes, HDAC are also expressed in other species. Although mutations are observed between human and non-human HDACs, they also present a significant rate of homology which can vary with species. Besides, those HDAC orthologues can show similarities in function and can be used as a model, as we mentioned earlier with the *Drosophila* flies.

As we saw, HDACs are involved in a wide range of biological processes and the disruption of their level of expression profoundly affect the cells, leading to the development of important diseases. As a result, the idea arose to use epigenetic modulators as a therapy against parasitic diseases to disrupt the epigenetic machinery of the parasites.

A-ParaDDisE project

Following up with this idea, a collaborative project called A-ParaDDisE, for Anti-Parasitic Drug Discovery in Epigenetics, was funded by the European Union. This collaboration involved international universities and research centres from Australia, Brazil, France, Germany, Italy, Sweden, and the UK. It aimed to investigate the therapeutic potential of epigenetic modulators against several Neglected Tropical Diseases (NTDs) in particular, malaria, Chagas disease, leishmaniasis and schistosomiasis.

These diseases, mainly affecting the population of developing countries, infect over one billion people altogether, cause hundreds of thousand deaths every year and represent a major economic burden. Besides, treatments for all these diseases face drug resistance due to the lack of alternative drugs. Prolonged dosing schedules and low drug availability are further issues of the current therapies. The development of new drugs is, therefore, a priority.

The strategy of this collaboration was to target enzymes and proteins in the different parasites. More specifically those involved in the modification of histones via acetylation/deacetylation and methylation/demethylation.

The project was structured around several units, each dedicated to a specific aspect of the drug discovery pipeline and the high complementarity between the different research groups allowed going through the complete process of the development (Figure 2.17). The various stages included the identification of histone modifying enzyme in the parasites and their characterization as potential targets, the production of recombinant proteins of the selected targets, the development of related biological assays, the generation of crystal structure and X-ray analysis to enable modelling and virtual screening, the set-up of high-throughput screening, the synthesis of optimized modulators, and finally the realisation of *in vitro* and *in vivo* pharmacological and toxicological studies.

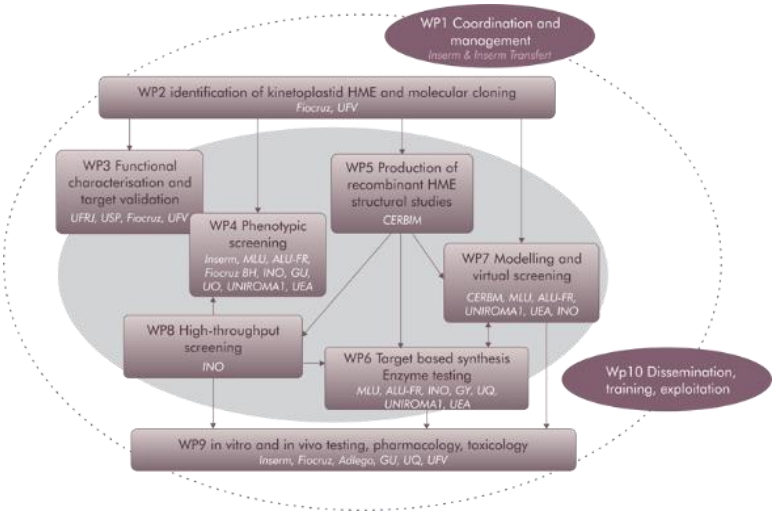

Figure 2.17: Organization chart of the A-ParaDDisE project.
Research groups were affiliated with different units of specific functions. Taken from A-ParaDDise website.[289]

Plasmodium HDACs

Malaria is a mosquito-borne infectious disease caused by six *Plasmodium* species. To date, it represents one of the most critical diseases with an estimated 216 million cases of malaria in 2016 and 445 000 casualties.[290] The prevention and the treatment mainly focus on mosquito control

and chemotherapy but *Plasmodium falciparum*, the principal malarial protozoan parasite, has become increasingly resistant to chloroquine (CQ) and artemisinin, the best drugs available.[291,292]

In *Plasmodium falciparum*, five genes were identified to encode HDACs. Two genes (PfSir2A and PfSir2B) were class III human HDAC orthologues while the other three encoded proteins similar to human class I (PfHDAC1) or class II (PfHDAC2 and PfHDAC3) HDACs.[293–295] Like its human homologue, PfHDAC1 is localized in the nucleus, and a study of its level of expression at several stages of development revealed that PfHDAC1 is functionally essential for the parasite in both mosquito vector and human host.[296] The functional roles of PfHDAC1 have not been fully elucidated, but treatment with HDACi affected the parasite's survival. HDACi caused altered histone acetylation pattern in *Plasmodium falciparum* and inhibited *P. falciparum* growth in erythrocytes at both the early and late stages of the parasite's life cycle.[297,298] In addition, PfHDAC2 was reported to be a global silencer of virulence gene expression and to play a role in *P. falciparum* transcriptional controls by regulating the frequency of switching from the asexual cycle to sexual development.[294]

As a consequence, HDACs represent interesting targets in *Plasmodium falciparum*, and the development of potent and selective inhibitors is investigated as therapeutic agents.[298–300]

Leishmanial HDACs

Leishmaniasis is an infectious disease caused by 20 species of *Leishmania* and is transmitted by sandfly bites. The prevalence of the disease is difficult to determine but the WHO estimates that 4 to 12 million people are currently affected while 200 million people live in areas where the disease is common. Moreover, about 2 million new cases and 25000 deaths occur every year.[301,302]

In *Leishmania*, four class I/II HDACs orthologues were identified as well as three genes encoding for the SIRT class of deacetylases.[293] As with *Plasmodium*, the functional roles of class I/II HDACs in *Leishmania donovani* have not been fully elucidated, but a transient up-regulation was observed during the promastigote-to-amastigote differentiation.[303]

Over the past few years, several HDACi have been tested *in vitro* and *in vivo* against the *Leishmania* parasite to evaluate the therapeutic potential.[304–306] Treatment with HDACi was shown to affect the parasite survival. Besides, in order to assess the role of class I and class II HDACs, *L. donovani* amastigote and promastigote forms were treated with selective human HDAC6 and selective hHDAC8 inhibitors.[306] In promastigotes, lower cytotoxicity was observed after treatment with hDAC8 inhibitors than with hHDAC6 inhibitors. In amastigotes, the cytotoxic activity of the hHDAC6-selective inhibitors was found to be 2-fold lower than that of its effect on the promastigote stage while hHDAC8-selective inhibitors had no cytotoxic effect.[306]

These results suggest that the antileishmanial activity observed after treatment with HDACi is mainly due to the inhibition of the HDAC6-like activity of *L. donovani*, especially in the amastigote form. Targeting the protozoan HDAC6 with isoform-selective inhibitors could, therefore, represent a therapeutic strategy for leishmaniasis.

Trypanosoma HDACS

Trypanosoma brucei is the parasite responsible for African Trypanosoma, also known as sleeping sickness, and is transmitted by an insect vector belonging to different species of tsetse fly. The disease is present in sub-Saharan Africa with a population of 70 million in the high-risk region and, in 2015, it was estimated that about 11000 people were infected with 2500 new cases of infections.[301] Besides, the diseases cause 3500 deaths yearly.

T.brucei possesses four HDAC orthologues (TbDAC1-4), of which two share similar sequence identity with human class I HDAC (TbDAC1 and TbDAC2), while the other two have higher homology with class II HDAC (TbDAC3 and TbDAC4).[293,307,308] In addition, both TbDAC2 and TbDAC4 have been reported to be localized in the cytoplasm and appear not to be required for viability, while TbDAC1 and TbDAC3 are nucleus-localized and play a critical role for the parasite survival.[307]

Following host infection, *T. brucei* evades the mammalian host's immune response by periodically changing its variant surface glycoprotein (VSG) coat.[309] It was then reported that TbDAC1 antagonizes telomeric silencing in bloodstream-form cells, and that TbDAC3 is required for VSG silencing in both bloodstream and insect-stage cells.[310]

The use of antitrypanosomal HDAC inhibitors has not been extensively studied yet, but treatment with four HDACi, clinically approved for the treatment of cancer, was shown to have an antitrypanosomal effect on the bloodstream form of *T. brucei*.[311] However, those compounds induced higher cytotoxicity on mammalian cells than on the parasites. Those results were also observed with other class of HDACi, with potent cytotoxicity on *T. brucei* but a lack of selectivity which could induce severe side effects.[312,313] Those results suggest that HDACi-based therapies represent an attractive strategy against *Trypanosoma,* but more selective compounds have to be developed. To this end, further studies are required to identify specificities of the TbDACs structures that could be exploited.

T.cruzi is another species of *Trypanosoma* and is responsible for the American Trypanosoma, also called Chagas disease. This infectious disease affects 6.6 million people in Central America and South America and is guilty for 8000 deaths every year.[301] The genome of *T. cruzi* has been successfully sequenced,[314] and four HDAC orthologues have been identified. However, little has

been done to investigate the modulation of HMEs in *T. cruzi*. This represented an essential objective of the A-ParaDDisE project. In gene knockout studies, TcDAC1 and TcDAC2 were found to be critical to the parasite survival.[315] The consortium evaluated TcDAC2 as a priority therapeutic target. Consequently, the enzyme has been produced in quantity and in an enzymatically active form. An HTS-compatible assay has been developed, and diffracting crystals have been produced.[315] However, no potent inhibitors of TcDAC2 have been reported so far. Therefore, the development of TcDAC2i is a challenging new field of study that could pave the way to a new therapeutic strategy for the Chagas disease.

Schistosoma HDACs

Schistosomiasis, also called bilharzia, is an acute and parasitic disease caused by several species of parasitic worms *Schistosoma*. Member of the NTDs, schistosomiasis is the most devastating parasitic disease after malaria with over 250 million people infected worldwide and a number of people in need of preventive chemotherapy globally estimated at 208 million, of which 112 million are school-aged children.[301]

The infection was reported in 78 countries and is endemic in 52 of them with a moderate to high risk of transmission. In particular, the parasite is widespread in poor countries of tropical and sub-tropical areas.

The process of transmission and the life cycle of the Schistosoma has been fully established (Figure 2.18).[316] Eggs of the parasite are found in contaminated water sources of infected areas. Hatching releases miracidia, the primary form of the parasite, which infects an intermediate host. Inside, miracidia evolve through successive generation to produce a larval form called cercariae. This new form is able to survive without the host and is released in the water. Cercariae represent the infective form of the parasite toward humans. In these regions with limited resources, river and lake have considerable importance, and people frequently use them to swim, fish or as drinking sources. Upon contact with the human, cercariae are able to penetrate the human skin and infect healthy people. During the penetration, cercariae lose their tails to become schistosomula. This new form can then migrate via the blood system and reach the intestine or the liver. There, schistosomula mature to give birth to adult worms, which are unable to relocate in blood vessels and, therefore, are trapped in the organ's tissues. Over their 3 to 30 years lifespan, mature worms mate and produce eggs. A part of them penetrates blood vessels and is passed out of the body in the faeces or urine, regenerating the cycle. However, the adult worms and the rest of the eggs remain trapped inside the different tissues, causing immune reactions and damages to organs.

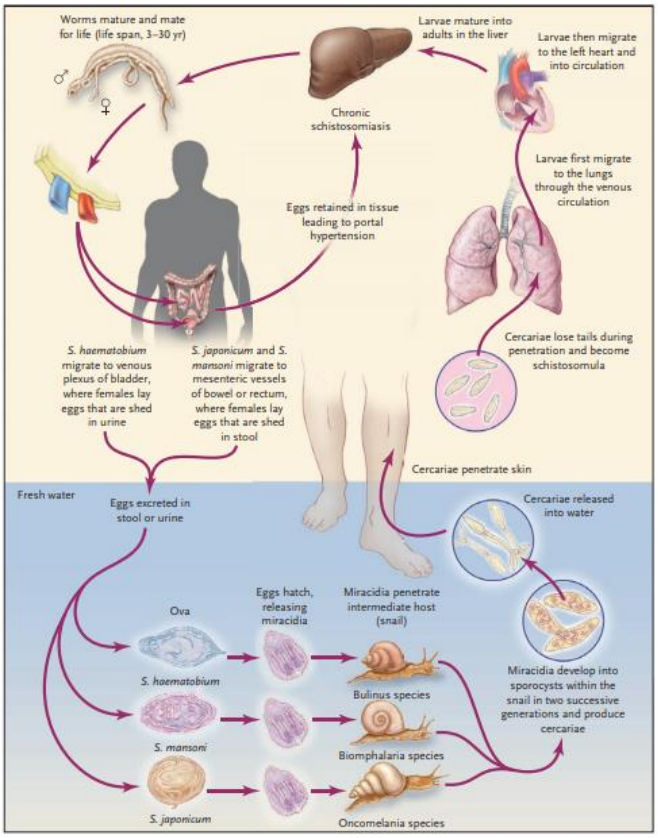

Figure 2.18: Life cycle of the Schistosoma.
Taken from King.[316]

The WHO strategy to control the expansion of the disease mainly focus on preventive chemotherapy of the at-risk population and the improvement of the access to safe water sources.[317]

This strategy rests on the massive use of praziquantel (Figure 2.19), a safe and low-cost treatment. This drug is effective at single-dose against all forms of schistosomiasis and is used for an early and late stage of the infection. Therefore, it is registered on the WHO Model List of Essential Medicines.

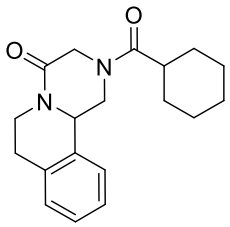

Figure 2.19: Structure of Praziquantel

However, a significant limitation of this strategy is the limited availability of the drug. According to WHO, only 13% of people requiring treatment were reached globally in 2013.[317] Moreover, although the treatment with praziquantel is efficient, it does not prevent reinfection and constant access to the drug is therefore required in high-risk areas.

In addition, one of the biggest problems is the lack of alternative drugs. Indeed, praziquantel is the only treatment available, and after decades of use some resistance emerged in different areas of the world.[318–320]

With such a critical prevalence and incidence, coupled to the low availability of the drug, the spreading of the praziquantel-resistant parasite would have a dramatic effect and could annihilate decades of progress in the control of the disease. Therefore, the need for new drug targets and the development of new therapies is crucial.

Schistosomiasis was a primary target of the A-ParaDDisE consortium. Several class I HDAC orthologues were isolated in the *Schistosoma mansoni* species and were identified as SmHDAC1, SmHDAC3 and SmHDA8.[321] Furthermore, the authors quantified the level of expression of these SmHDAC at every stage of life (Figure 2.20A). Those three SmHDAC were expressed at every stage of life, but the level of expression was dependent on the form of the parasite. In particular, their level of expression was significantly higher in miracidia, the form resulting from egg hatching. Moreover, the comparison of their relative expression revealed that SmHDAC8 was the most expressed SmHDAC at every stage of life (Figure 2.20B). These results suggested that SmHDAC8 could have a vital role in the parasite and, therefore, its inhibition could have interesting antischistosomal effects.

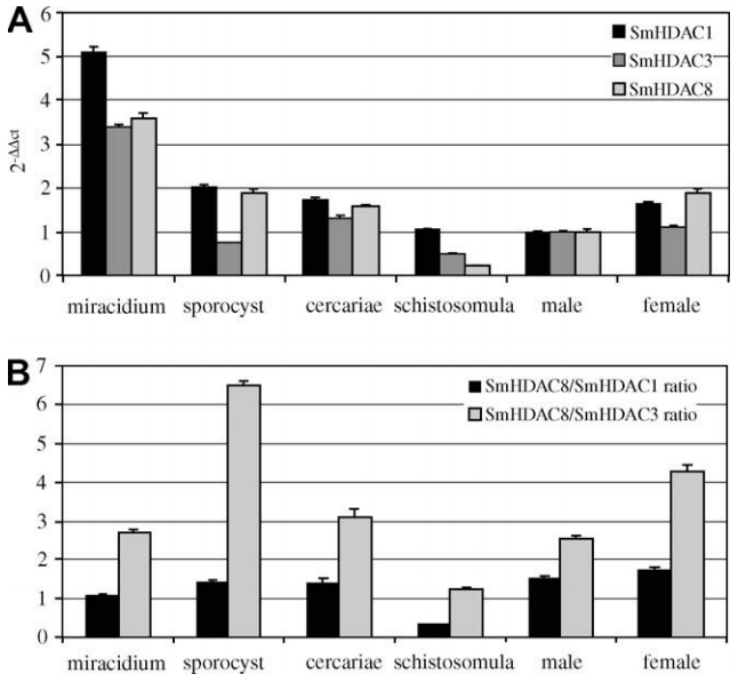

Figure 2.20: Quantification of transcripts of SmHDAC1, 3 and 8 at different *S. mansoni* life-cycle stages.

(A) SmHDAC1, SmHDAC3 and SmHDAC8 mRNA were measured by quantitative real-time PCR. S. mansoni α-tubulin was used as a reference gene. Results are expressed as the $2^{-\Delta\Delta}$Ct ratio compared to the expression in male worms taken arbitrarily as the baseline. (B) Relative expression of SmHDAC8 compared respectively to SmHDAC1 (black bars) and SmHDAC3 (grey bars). Taken from Oger et al.[321]

Following up, another study was designed to evaluate the importance of SmHDAC8 in the development of the parasite.[322] Using RNA interference, the transcription level of SmHDAC8 was downregulated by 50% in schistosomula and no effect on the integrity, mortality, and motility was observed. The natural level of expression of SmHDAC8 in schistosomula being significantly lower than in other life forms, the impact of the downregulation was expected to be stronger on adult worms. Consequently, the mutated schistosomula were used to infect mice. After 35 days, mice infected with SmHDAC8 knocked-down parasites showed an overall 50% reduction in the number of recovered adult worms compared to control in three independent experiments (Figure 2.21A). In addition, the tissue egg burden was reduced by 45%, again compared to the control (Figure 2.21B). These experiments confirmed that SmHDAC8 is required for infection of the definitive host and plays a significant role in parasite homeostasis.

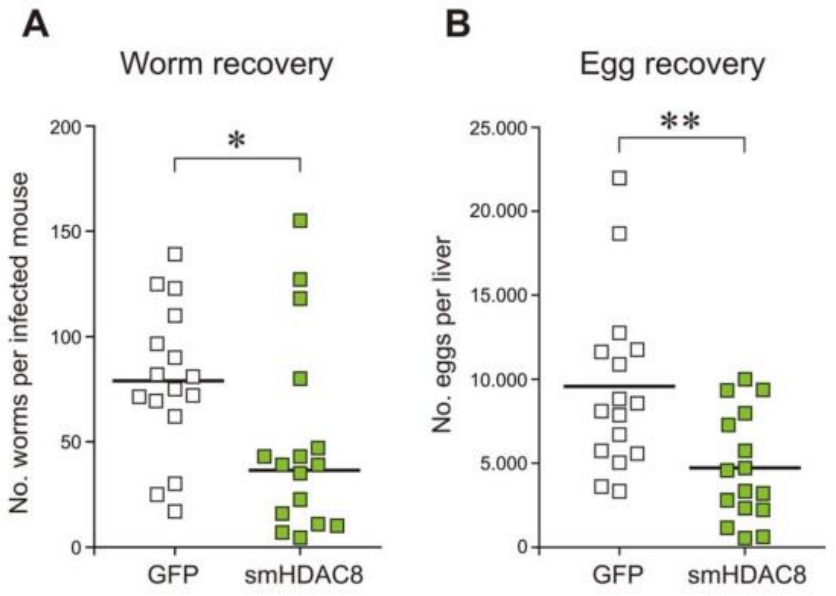

Figure 2.21: Infection of mice with SmHDAC8 knocked-down parasites for 35 days.
(A) Average number of worms is decreased by 50%. (B) The number of recovered eggs from the livers of infected mice is decreased. Taken from Marek et al.[322]

As a result of these studies, SmHDAC8 inhibition was shown to have a high impact, and the development of potent SmHDAC8 inhibitors could offer a new strategy for the development of a therapeutic agent against schistosomiasis.

One of the earliest studies of HDACi efficacy revealed that treatment with non-selective HDACi inhibited the class I SmHDAC in every form of the life-cycle.[323] In addition, HDACi were shown to induce a dose-dependent increase of mortality in schistosomula via an apoptosis mechanism.[323] Similar results were observed using other HDACi.[324,325] Interestingly, treatment with HDACi shows important toxicity against schistosomula while praziquantel is mainly potent on adult

worms.[326] Therefore, therapies based on HDACi could be a great alternative to praziquantel in the early stages of the infection and for preventive treatment.

However, there are several challenges to overcome in order to develop drugs based on SmHDAC inhibition. Indeed, if the use of HDACi was shown to be effective, those inhibitors were usually more active on hHDAC than on the parasite.[322–325] Such inhibitors present a risk of cross-reactivity which could cause off-target effects. In order to minimize these potential side-effects, specific SmHDAC inhibitors have to be developed.

To this end, the crystal structure of SmHDAC8 was solved and analysed to find differences with the hHDACs that could be exploited to afford selectivity.[322] It is important to note that, although the enzyme was crystalized without inhibitors, analysis of the structure revealed an L-tartrate molecule provided by the crystallization buffer, which was bound in the SmHDAC8 active site where it coordinated the catalytic zinc ion.

Comparison of the active sites of hHDAC8 and SmHDAC8 highlighted several significant differences (Figure 2.22).[322]

First, the M274 of the human enzyme is replaced by H292 in SmHDAC8. This modification diminishes the hydrophobic character of the pocket that usually accommodates the aliphatic chain of the acetylated lysine.

Secondly, a change in conformation was observed between the SmHDAC8 Y341 and the hHDAC8 Y306. Indeed, the hydroxyl group of Y306 is turned towards the zinc ion, where it interacts with the warhead of the inhibitors. On the other hand, Y341 side chain points towards the rim of the catalytic pocket.

The third and most exciting difference is the conformation of the SmHDAC8 F151 compared to the hHDAC8 F152. In the parasite enzyme, F151 is turned away from the catalytic pocket and is inserted into a smaller hydrophobic pocket formed by loops that surround the active site. On the other hand, F152 is turned towards the active site, adopting a flipped-in conformation in all inhibitor- and substrate-bound hHDAC8 structures reported in the Protein Data Bank (PDB). Moreover, careful inspection of the hHDAC8 structure revealed that F152 could not adopt a flipped-out conformation because of the presence of the L31 side chain that is locked in this conformation by the surrounding residues.

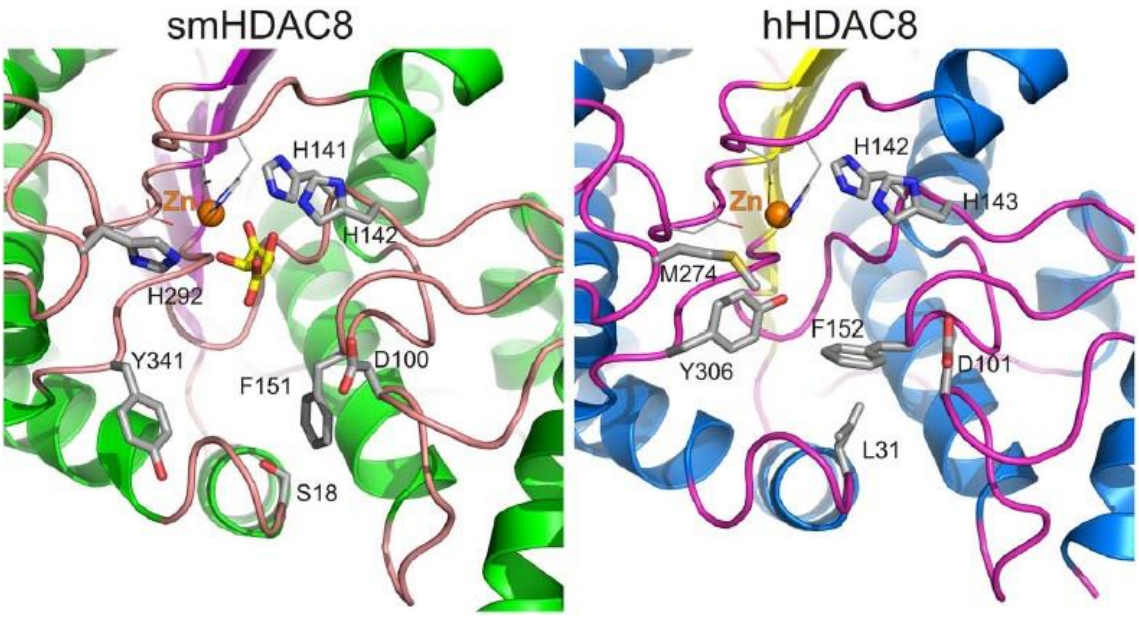

Figure 2.22: Ribbon representation of the active sites of (A) SmHDAC8 in complex L-tartrate from the buffer, (B) hHDAC8 (PDB 1T67).
Adapted from Marek et al.[322]

Interestingly, this phenylalanine is conserved in every hHDAC, and an investigation of the available crystallized enzyme structures revealed that, due to surrounding amino acid residues, the flipped-in conformation is also conserved (Figure 2.23).[322]

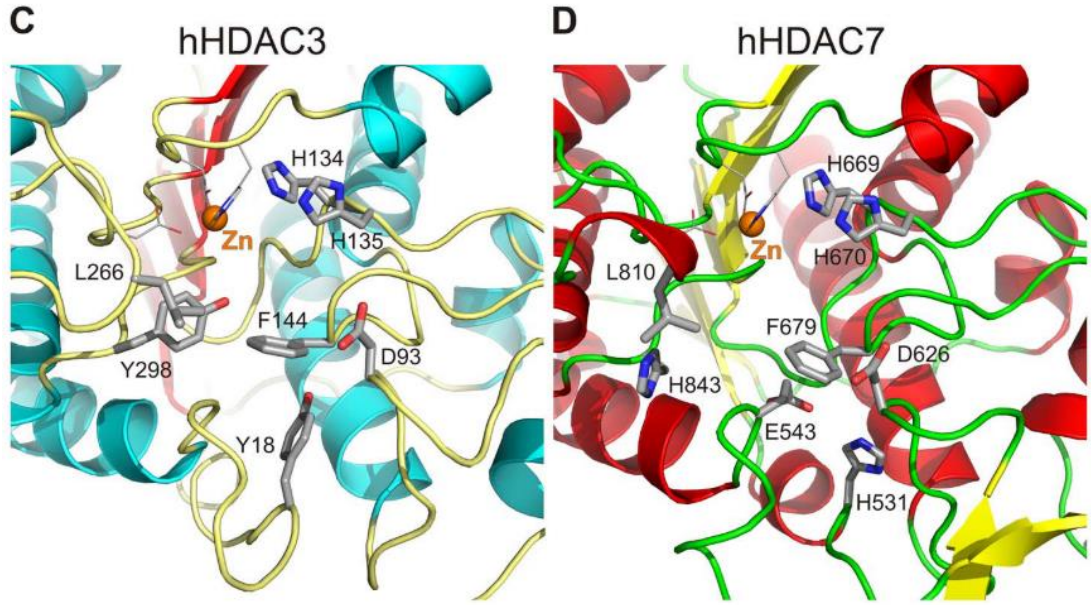

Figure 2.23: Ribbon representation of the active sites of (C) hHDAC3 (PDB 4A69) (D) hHDAC7 (PDB 3COY).
Adapted from Marek et al.[322]

Finally, hDAC8 and SmHDAC8 were co-crystallized in complex with two non-selective inhibitors to observe the impact of the structural differences on the binding.[322]

In complexes with SAHA, the conformation of the phenylalanine was conserved in both enzymes. As expected, the differences in conformation affected the rim of the enzymes and induced modification of the binding (Figure 2.24A and B).

Unexpectedly, in the case of the inhibitor M344, both HDAC8 displayed a flipped-in conformation (Figure 2.24C and D). In hHDAC8, the binding was similar to that of vorinostat. On the other hand, in SmHDAC8 the inhibitors adopted a completely different binding. However, despite the flipped-in conformation, the binding of M344 with both enzymes was not comparable. These findings clearly demonstrate that SmHDAC8 F151 is flexible and can adopt both flipped-out and flipped-in conformations. This is likely due to the presence of the amide group on M344, which can interact with D100 through hydrogen bonding. Therefore, F151 could adopt the most suitable conformation in order to optimize the bonding.

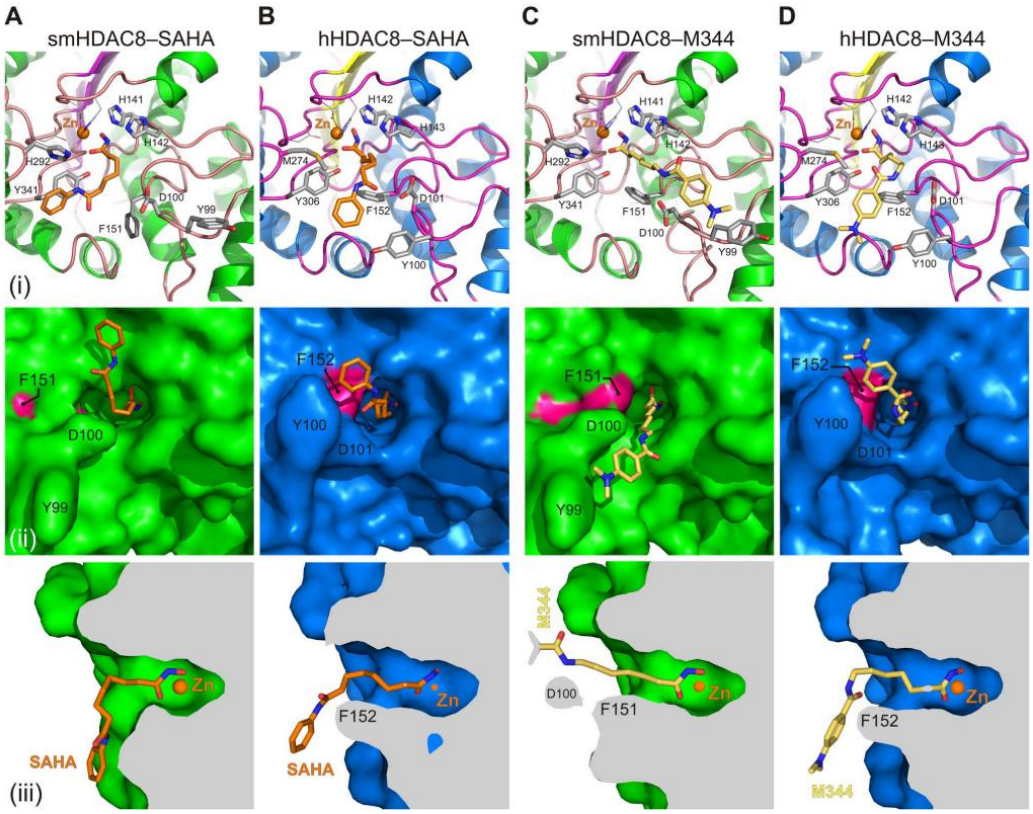

Figure 2.24: Close-up view of the active sites of the (A) SmHDAC8/SAHA, (B) hHDAC8/SAHA (PDB 1T69), (C) SmHDAC8/M344, (D) hHDAC8/M344 (PDB 1T67)
Complexes are shown as ribbon and sticks (i), surface view (ii), and side cut surface view (iii). Taken from Marek et al.[322]

In conclusion, inhibition of SmHDAC8 is a potent target for the development of antischistosomal activity, but selective inhibitors are likely to be required to avoid side-effects. Structural

differences between the catalytic site of SmHDAC8 and those of hHDACs have been identified. In particular, the phenylalanine flipped-in/flipped-out conformation difference modifies the shape of the enzyme rim and highly affect the binding of inhibitors. The development of inhibitors specifically targeting those differences could, therefore, be the key to future therapies.

2.3 HDAC inhibitors

Following the approval by FDA of some HDACi in mid-2000, the development of new classes has experienced steady growth over the last decade. Based on the structure of the natural substrate and these first inhibitors, a pharmacophore containing three elements was established (Figure 2.25).

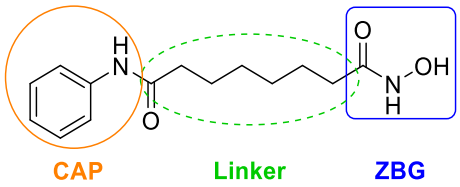

Figure 2.25: Typical HDACi pharmacophore.

First, the zinc-binding group (ZBG) is a polar functional group that form monodentate or bidentate coordination to the zinc cation. The second element is the linker that substitutes the lysine side chain of the natural substrate. The linker has to accommodate the narrow channel of the enzyme and is usually a linear moiety. The last part is the cap that is localized at the rim of the protein and is involved in side interactions with the enzyme.

Over the years, a variety of structure has been synthesized. Several functional groups were found to be potent ZBG, and important diversity of cap group was explored to develop selective HDACi.

2.3.i Hydroxamic acid HDAC inhibitors

The first hydroxamic acid-based HDACi reported was the natural product trichostatin A **2-60** (Figure 2.26).[327] A few years later, suberoylanilide hydroxamic acid (SAHA, **2-61**) was also reported as a potent non-selective HDACi.[101,102] SAHA later became the first HDAC inhibitor to enter clinical trials under the name of vorinostat and received FDA approval for the treatment of cutaneous T-cell lymphoma.[328].

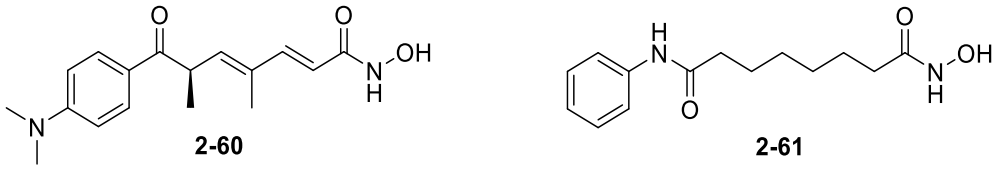

Figure 2.26: Structure of trichostatin A (2-60) and SAHA (2-61).

The strong affinity for metal ions coupled to the success of vorinostat has made hydroxamic acid a favourite choice of ZBG in the development of HDACi. Afterwards, several inhibitors derived from vorinostat were developed and joined clinical trials. In particular, belinostat (Belodaq™, **2-62**) and panobinostat (Farydak™, **2-63**) were successful candidates (Figure 2.27).[329,330]

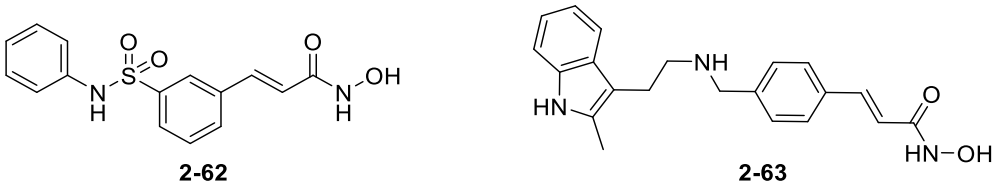

Figure 2.27: Structure of belinostat (2-62) and panobinostat (2-63).

These drugs are pan-inhibitors and potently inhibit class I HDAC, with the exception of HDAC8, class IIb and class IV HDAC (Table 2.13). However, they display no inhibition activity on HDAC4 and HDAC7.

It is worth noting that differences in assay methodology and enzyme preparation are frequent in HDAc inhibition. Therefore, the absolute IC_{50} values of HDAC inhibitors should not be directly compared between publications.

Class	Isoform	Vorinostat IC_{50} (nM)	Belinostat IC_{50} (nM)	Panobinostat IC_{50} (nM)
Class I	HDAC1	76	18	3
	HDAC2	360	34	13
	HDAC3	58	21	2
	HDAC8	>1000	160	280
Class IIa	HDAC4	>1000	>1000	200
	HDAC5	160	76	8
	HDAC7	>1000	600	530
	HDAC9	78	44	6
Class IIb	HDAC6	27	15	11
	HDAC10	88	31	2
Class IV	HDAC11	110	44	3

Table 2.13: The IC_{50} values of approved HDAC inhibitors against individual isoforms.[330]

Notably, those second-generation of inhibitors both displayed a cinnamoyl group on the linker that can also be found in two other clinical candidates, pracinostat (**2-64**) and resminostat (**2-65**).[331,332] Besides cinnamoyl linker, several rigid linkers were investigated, and some inhibitors

became clinical candidates (Figure 2.28). For example, a benzyl was used in givinostat (**2-66**),[333] and abexinostat (**2-67**),[334]while a pyrimidine linker is employed in quisinostat (**2-68**),[335] and CHR-3996 (**2-69**).[336]

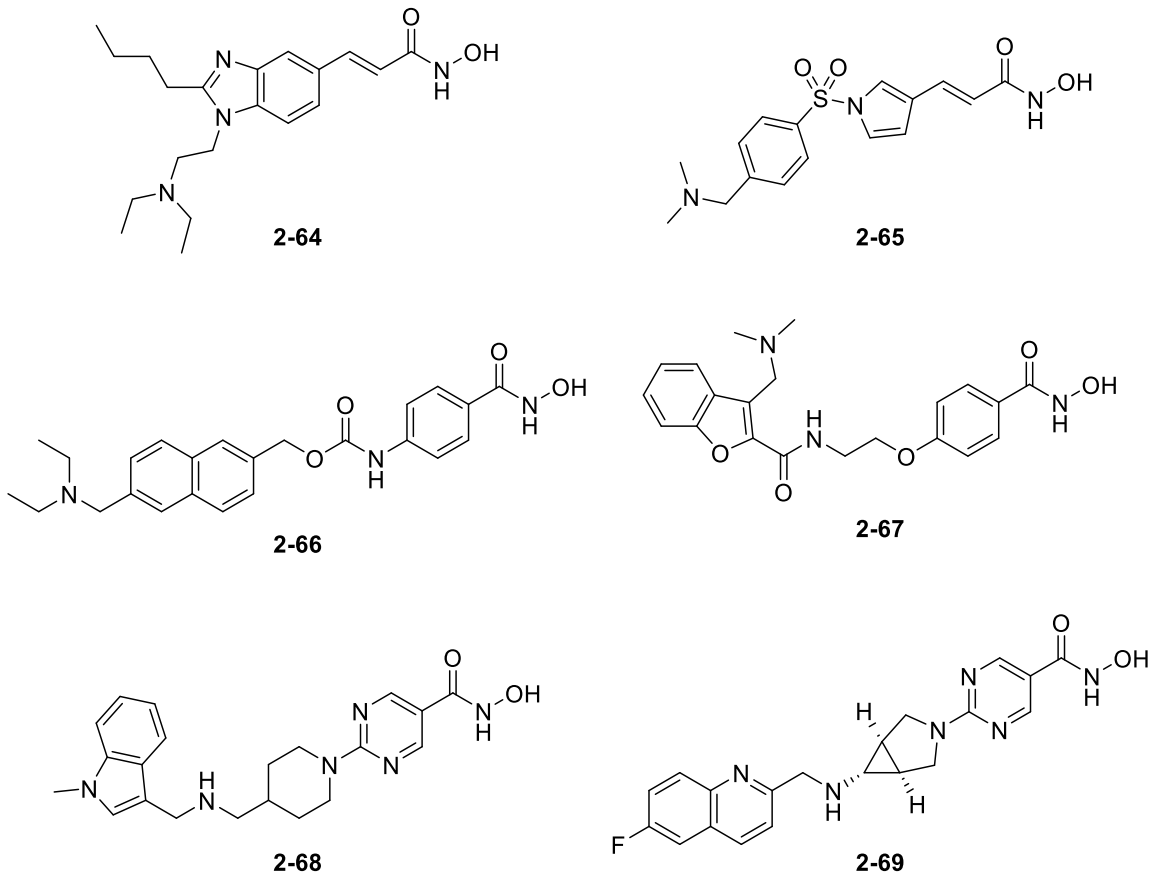

Figure 2.28: Structure of clinical candidate with rigid linkers.

Some of these compounds were shown to be highly potent against the different HDACs and displayed some selectivity (Table 2.13).

Class	Isoform	2-64 IC_{50} (nM)	2-68 IC_{50} (nM)	2-69 IC_{50} (nM)
Class I	HDAC1	49	0.1	3
	HDAC2	96	0.3	4
	HDAC3	43	4.9	7
	HDAC8	140	4.3	ND
Class IIa	HDAC4	56	0.6	ND
	HDAC5	47	3.7	200
	HDAC7	137	119	ND
	HDAC9	70	32.1	ND
Class IIb	HDAC6	>1000	76.8	2100
	HDAC10	40	0.5	ND
Class IV	HDAC11	93	0.4	ND

Figure 2.29: IC_{50} values of HDAC inhibitors 2-64, 2-68 and 2-69 against individual isoforms.[331,335,336]

Although those clinical candidates are promising compounds, current research is focusing on the development of more selective inhibitors.

One fundamental approach toward hydroxamic acid HDAC6-selective inhibitors was the introduction of new cap groups such as tricyclic carbazole, pyrrolidinone, or benzimidazole (Figure 2.30). Tubastatin A (**2-70**), was developed via structure-based design and homology modelling. Tubastatin A displayed HDAC6 inhibitory activity and 50 to 2000-fold selectivity versus other HDAC isoforms.[337] The selectivity was further increased in a second-generation by the same group.[338] Inhibitors derived from a tricycle poly hydro acridine (**2-71**) were reported to have a nanomolar activity on HDAC6 and a 100-fold selectivity against all the other HDACs.[339] A novel class of 3-aminopyrrolidinone-based hydroxamic acid (**2-72**) inhibitors was reported to have a nanomolar IC_{50} on HDAC6, a 10-fold selectivity against HDAC8 and over 4000-fold against HDAC1–3 isoforms.[340] Besides, scientists from Dana-Farber Cancer Institute reported a series of new selective HDAC6 inhibitors based on substituted benzimidazole heterocycles (**2-73**) with inhibitory activity in picomolar concentration range against HDAC6 and micromolar activity against other HDACs.[341] Selective HDAC6 inhibition was also achieved with cycloheptane-fused tetrahydrobenzothiazepines (**2-74**) with a 100-fold selectivity against HDAC8 and up to 1000-fold on other HDACS.[342]

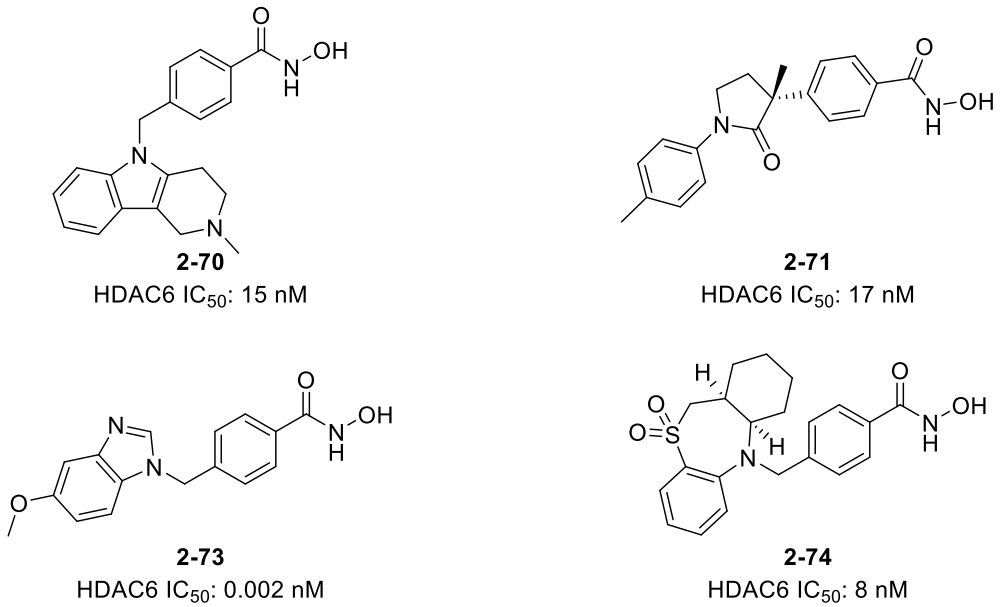

Figure 2.30: Examples of HDAC6 selective hydroxamic acid inhibitors.

Drug discovery efforts, directed toward hydroxamic acid derivatives able to interact with the unique subpocket of HDAC8, resulted in resulted in the discovery of indole derivative PCI-34051 (**2-75**).[343] This compound was reported to inhibit HDAC8 with a *K*i value of 10 nM and 200-fold selectivity over HDAC1–3, 6, and 10. Selective HDAC8 inhibitors could be produced using click chemistry (**2-76**) and resulted in an HDAC8 inhibition activity in the nanomolar range, a 35-fold selectivity against HDAC6 and over 500-fold selectivity against HDAC1/2/4.[344] Recently, a significant advancement in the development of potent and selective HDAC8 inhibitors was reported. Triazolyl-benzohydroxamic acid compound **2-77** was reported to inhibit HDAC8 with a subnanomolar IC_{50}, over 1000-fold selectivity over HDAC6 and significantly greater selectivity for all other HDACs.[345] To date, this compound is both the most potent and most selective HDAC8 inhibitor reported.

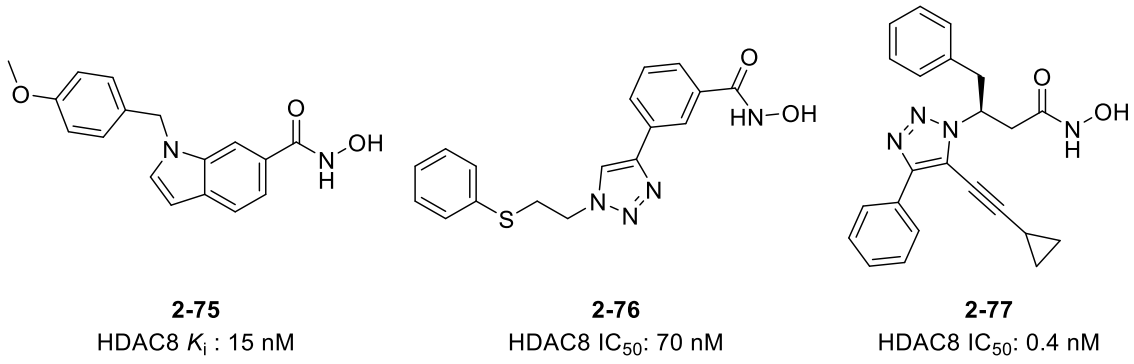

Figure 2.31: Examples of HDAC8 selective hydroxamic acid inhibitors.

Hydroxamic acids have proved to be a major ZBG for the development of HDACi, and both potent and selective inhibitors based on hydroxamic acids have been synthesised.

However, hydroxamic acids also have limitations. In particular, use of hydroxamic acid precipitates drug clearance through glucuronidation, and can also form mutagenic metabolites via Lossen-type rearrangements.[346] As a result, alternative ZBG have also been investigated.

2.3.ii Benzamide

Beside hydroxamic acids, benzamide is also able to coordinate in a bidentate fashion to the zinc cation through the amine and the carbonyl oxygen. Several HDAC inhibitors using benzamide as ZBG also became successful candidates (Figure 2.32). Two examples in clinical development are entinostat (**2-78**), which was in Phase I clinical trials for the treatment of metastatic melanoma,[347,348] and mocetinostat (**2-79**) in clinical trials for the treatment of myelogenous leukaemia and advanced solid tumours .[349–351] In addition, an example containing a pyridine capping group and an *N*-(2-amino-fluorophenyl)-benzamide unit had remarkable results and advanced to clinical trial. Indeed, tucidinostat (**2-80,** Epidaza™), was approved in China for the treatment of relapsed or refractory peripheral T-cell lymphoma.[352] It also displays anticancer activity in colon, lung, breast, pancreatic and liver solid tumour cells, and in myeloid leukaemia cells.[353,354]

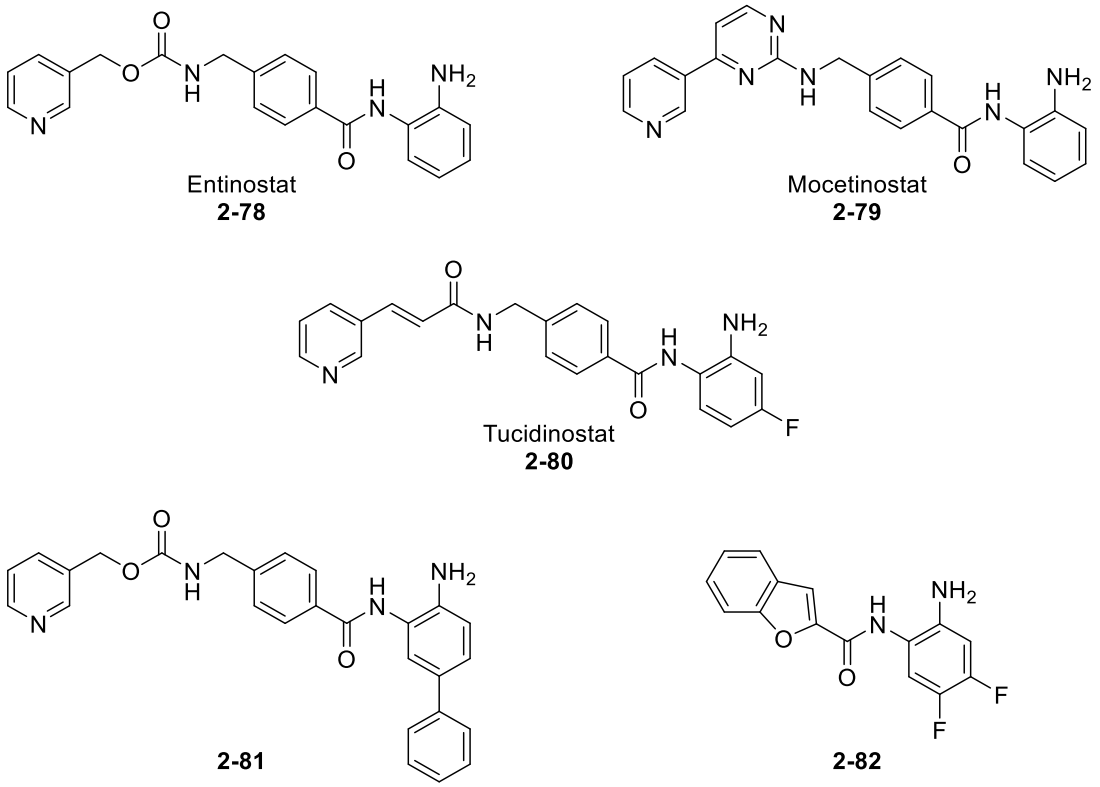

Figure 2.32: Examples of benzamide HDAC inhibitors.

These clinical candidates benzamide are primarily class I HDAC isoform selective (Table 2.14). However, it is important to note that HDAC8 is usually poorly inhibited. The lack of inhibition of HDAC8 is attributed to structural differences at the bottom of the active site tunnel and in particular, the substitution of leucine residue by tryptophan in HDAC8 which prevents the binding of the bulky 2-aminoanilide moiety.[103,355] Furthermore, class II HDACs are characterised by a restricted space of the corresponding region at the bottom of the active site, which also prevents the binding of the bulky ZBG.[103]

Besides, by taking advantage of the structural differences between the class I HDAC isoforms, more selective compounds could be produced with **2-81** being a selective inhibitor of HDAC1 and HDAC2.[356] Conversely, analogue **2-82** displays high activity on HDAC3 but low potency on the other class I HDACs.[357]

Class	Isoform	Entinostat IC_{50} (nM)	Tucidinostat IC_{50} (nM)	2-81 IC_{50} (nM)	2-82 IC_{50} (nM)
Class I	HDAC1	260	100	10	5800
	HDAC2	310	160	72	7900
	HDAC3	500	70	6180	170
	HDAC8	>1000	730	>20000	ND
Class IIa	HDAC4	>1000	>1000	>50000	ND
	HDAC5	>1000	>1000	>50000	ND
	HDAC7	>1000	>1000	>50000	ND
	HDAC9	>1000	>1000	ND	ND
Class IIb	HDAC6	>1000	>1000	>50000	ND
	HDAC10	250	80	ND	ND
Class IV	HDAC11	650	430	ND	ND

Table 2.14: IC_{50} values of benzamide HDAC inhibitors against individual isoforms.[354,356,357]

2.3.iii Mercaptoacetamides and α-mercaptoketone

Kozikowski and coworkers looked for alternative functional groups that could display similarities with the hydroxamic acids. They identified mercaptoacetamide as a suitable ZBG and synthesised a series of compounds derived from vorinostat, such as **2-83**, which presented HDAC inhibition activity in a submicromolar range of concentration (Figure 2.33).[358] This compound was shown to be mainly potent on HDAC6 with a 34-fold selectivity against HDAC1 and over 60-fold selectivity against HDAC2, HDAC8 and HDAC10 (Table 2.15).[359] The second generation of inhibitors was synthesised by introducing an isoxazole as a capping group and reversing the amide.[360] Compound **2-84** was shown to selectively inhibit HDAC6 with a nanomolar activity and over 22-fold selectivity against HDAC1, HDAC2, HDAC3, HDAC4 and HDAC5. Besides, the authors also investigated the impact of chiral mercaptoacetamides. Introduction of a methyl led to two enantiomers **2-85**. This chiral centre was shown to have a high impact on the inhibition profile as (*S*)-**2-85** was mostly inactive on every HDAC while the enantiomer (*R*)-**2-85** retained its activity on HDAC6 but with much higher selectivity. Interestingly, introducing two methyls led to inactive compounds. Using a similar approach, the α-mercaptoketone vorinostat analogue **2-86** was synthesised and was more active in HDAC inhibition compared to vorinostat.[361]

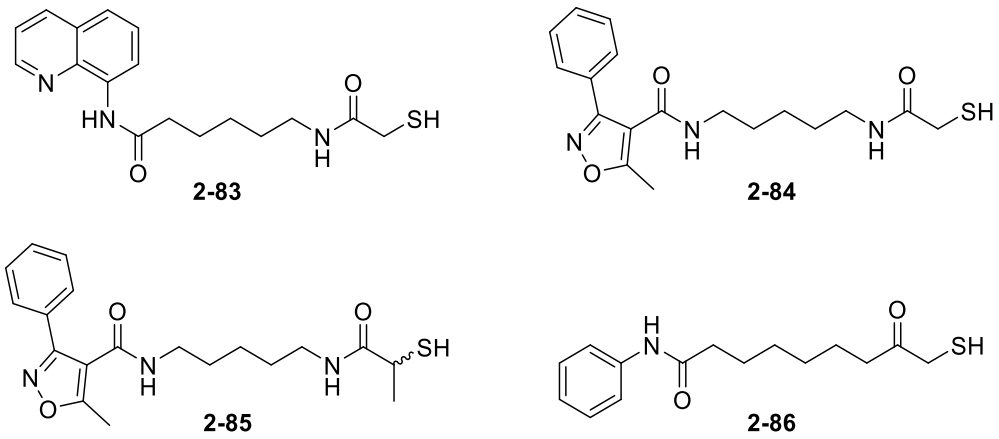

Figure 2.33: Examples of mercaptoacetamide and α-mercaptoketone HDAC inhibitors.

Class	Isoform	2-83 IC_{50} (nM)	2-84 IC_{50} (nM)	(*S*)-2-85 IC_{50} (nM)	(*R*)-2-85 IC_{50} (nM)
Class I	HDAC1	3220	5700	>30000	>30000
	HDAC2	7380	28000	>30000	>30000
	HDAC3	ND	14000	6180	15000
	HDAC8	6120	ND	ND	ND
Class IIa	HDAC4	ND	10000	>30000	>30000
	HDAC5	ND	15000	>30000	>30000
Class IIb	HDAC6	95	260	>30000	280
	HDAC10	10700	ND	ND	ND

Table 2.15: IC_{50} values of mercaptoacetamide HDAC inhibitors against individual isoforms.[359,360]

2.3.iv Cyclic-peptide analogues

Cyclic peptide moieties are the most complex capping groups of all HDAC inhibitors. In 1998, the natural product FK228 (**2-87**), a bicyclic depsipeptide isolated from the bacteria *Chromobacterium violaceum*, was identified by Yoshida and coworkers as an HDAC inhibitor (Figure 2.34).[362] Over the last decade, several other bacterial natural product such as largazole (**2-88**) and thailandepsin A (**2-89**) were discovered and identified as HDACi.[363–365]

Although these compounds don't have apparent ZBG, Yoshida et al. showed that the zinc coordination resulted from the disulfide bridge reduction, releasing a thiol sidechain that can interact with the metal.[366] This rather weak ZBG benefits from a sizeable macrocyclic cap that offer better binding to the enzyme surface than the phenyl ring present in hydroxamic acid inhibitors such as vorinostat.[367] Those natural products are a highly potent class I HDAC

inhibitors and moderate HDAC6 inhibitors. FK228 was later approved for the treatment of cutaneous T-cell lymphoma as romidepsin (Istodax™).[368]

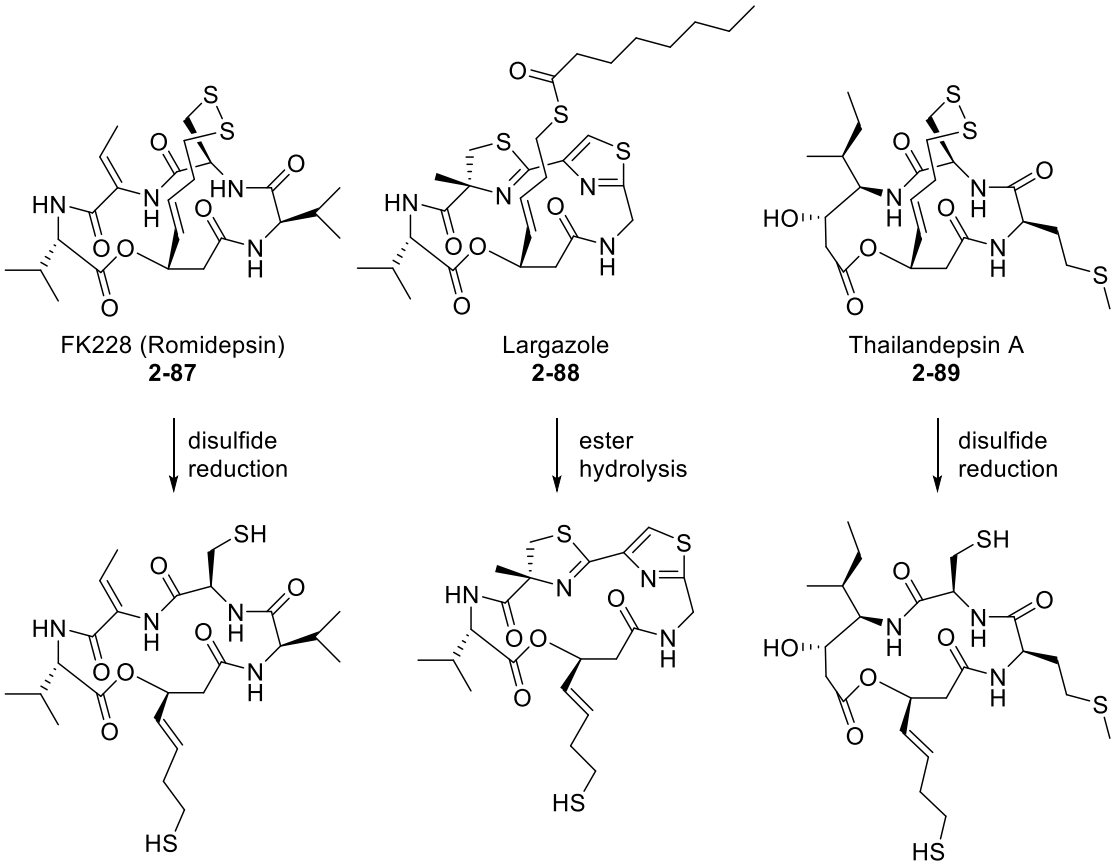

Figure 2.34: Examples of depsipeptide natural product HDAC inhibitors.

Class	Isoform	Romidepsin IC_{50} (nM)	Largazole IC_{50} (nM)	Thailandepsin A IC_{50} (nM)
Class I	HDAC1	0.8	0.4	14
	HDAC2	1.0	0.9	3.5
	HDAC3	1.3	0.7	4.8
	HDAC8	26	100	>1000
Class IIa	HDAC4	470	>1000	>1000
	HDAC5	>1000	>1000	ND
	HDAC7	>1000	>1000	>1000
	HDAC9	>1000	>1000	>1000
Class IIb	HDAC6	330	42	380
	HDAC10	0.9	0.5	ND
Class IV	HDAC11	0.3	>1000	ND

Table 2.16: IC_{50} values of the active forms of depsipeptide HDAC inhibitors against individual isoforms.[367]

Following the successful total synthesis of largazole, numerous research groups reported derivatives with variations in potency and selectivity. Those analogues mainly explored the role of the amino side chains in the cyclic peptides. The 4-methylthiazoline residue has hydrophobic interactions with the side chains F150 of the HDAC1, and these interactions may be crucial for HDAC class I isoform selectivity of largazole.[103] Therefore, several groups focused on the alteration of the methyl group of the 4-methylthiazoline moiety at the C7 position to increase these interactions. A series of new largazole derivatives with different substituents at the C7 position was reported (**2-90a-c**) with low nanomolar inhibition activity on HDAC1.[369] Alternatively, the residue was replaced in a romidepsin-largazole hybrid (**2-91**),[370] and in bipyridyl analogue (**2-92**).[371] Finally, the ring was also expanded with the introduction of a β-alanine (**2-93**).[372]

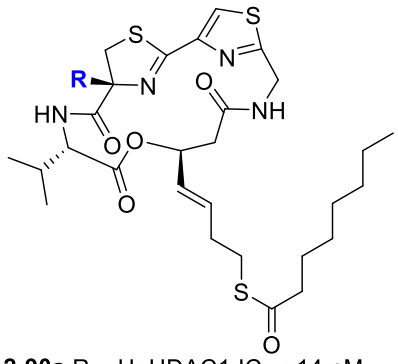

2-90a R = H; HDAC1 IC_{50}: 14 nM
2-90b R = Et; HDAC1 IC_{50}: 160 nM
2-90c R = Bn; HDAC1 IC_{50}: 5 nM

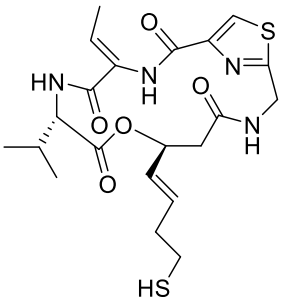

2-91
HDAC1 IC_{50}: 3 nM

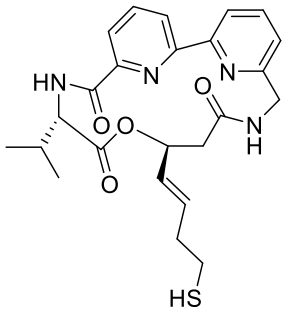

2-92
HDAC1 IC_{50}: 21 nM

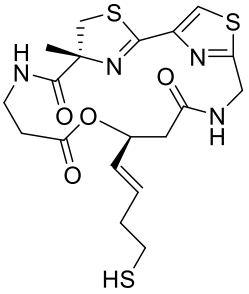

2-93
HeLa HDAC IC_{50}: 3 nM

Figure 2.35: Examples of synthetic depsipeptide HDAC inhibitors.

2.3.v Multitarget compound

Combination therapy, the use of multiple drugs to treat a single disease, is commonly used for the treatment of aggressive diseases such as cancer or AIDS. Nonetheless, the use of a single drug that modulates several targets might be therapeutically advantageous over the use of drugs in combination. Polypharmacology refers to the ability of drugs to interact simultaneously and specifically with multiple targets. In cancer research, the design and synthesis of new molecules that simultaneously modulate multiple oncogenic targets are of current interest.[373]

Multitarget drugs offer several advantages compared to combination therapy with more predictable pharmacokinetic (PK) and pharmacodynamic (PD) relationship of the drug, lower toxicity, and greater efficacy against advanced-stage diseases.[374] Besides, it can produce a better synergy as one motif might improve the bioavailability of the second entity, leading to the simultaneous presence of the chemical entities in multiple tissues.[373]

HDAC inhibition activity is mainly due to the presence of strong ZBG, and the simple pharmacophore of HDACs was shown to tolerate a large variety of cap groups. As this region interacts with the enzyme surface, the idea emerged to use a second pharmacophore as cap group.

In other words, the introduction of an alkyl linker, bearing a potent ZBG, on a biologically active compound could potentially confer some additional HDAC inhibition effect to the molecule.

This approach has gained significant interest over the last decades, and several multitarget drugs have been reported.[373,375]

To begin with, the dual inhibition of protein kinases and HDACs has become the most popular choice for epigenetic multitarget drugs (Figure 2.36). Introduction of hydroxamic acid (**2-94**) or benzamide (**2-95**) on the approved ABL kinase inhibitor imatinib (**2-96**) successfully led to potent dual-target inhibitors. Both compounds were micromolar inhibitors of the ABL, PDGFR-β and VEGF-R2 kinases. Besides, they featured antiproliferative activity HeLa and K562 cell lines in the micromolar range.[376] Interestingly, no difference in activity was observed between the wild-type ABL and the imatinib-resistant mutant T315I. Similarly, the substitution of an ether group on the approved kinase inhibitor erlotinib (**2-97**) by a heptanoic hydroxamic acid led to nanomolar inhibitors (**2-98**) of HDACs, EGFR and HER2.[377] This compound became a promising Phase I clinical candidate against intermediate or high-risk head and neck squamous cell carcinoma.[378] Several series were then reported, both for hydroxamic acid and benzamide, with a more rigid linker,[379] substitutions of the quinazoline,[380] or attachment of the zinc binding group onto the aryl ring of erlotinib rather than the quinazoline moiety.[381]

In addition to protein kinases, the dual inhibition of HDACs and phosphatidylinositol 3-kinase (PI3K) was also investigated. This led to the candidate CUDC-907 (**2-99**), a potent nanomolar dual HDAC and pan-PI3K inhibitor which was effective in cell lines and a tumour xenograft model.[382] The compound is currently in phase I clinical trials for lymphoma and solid tumours.

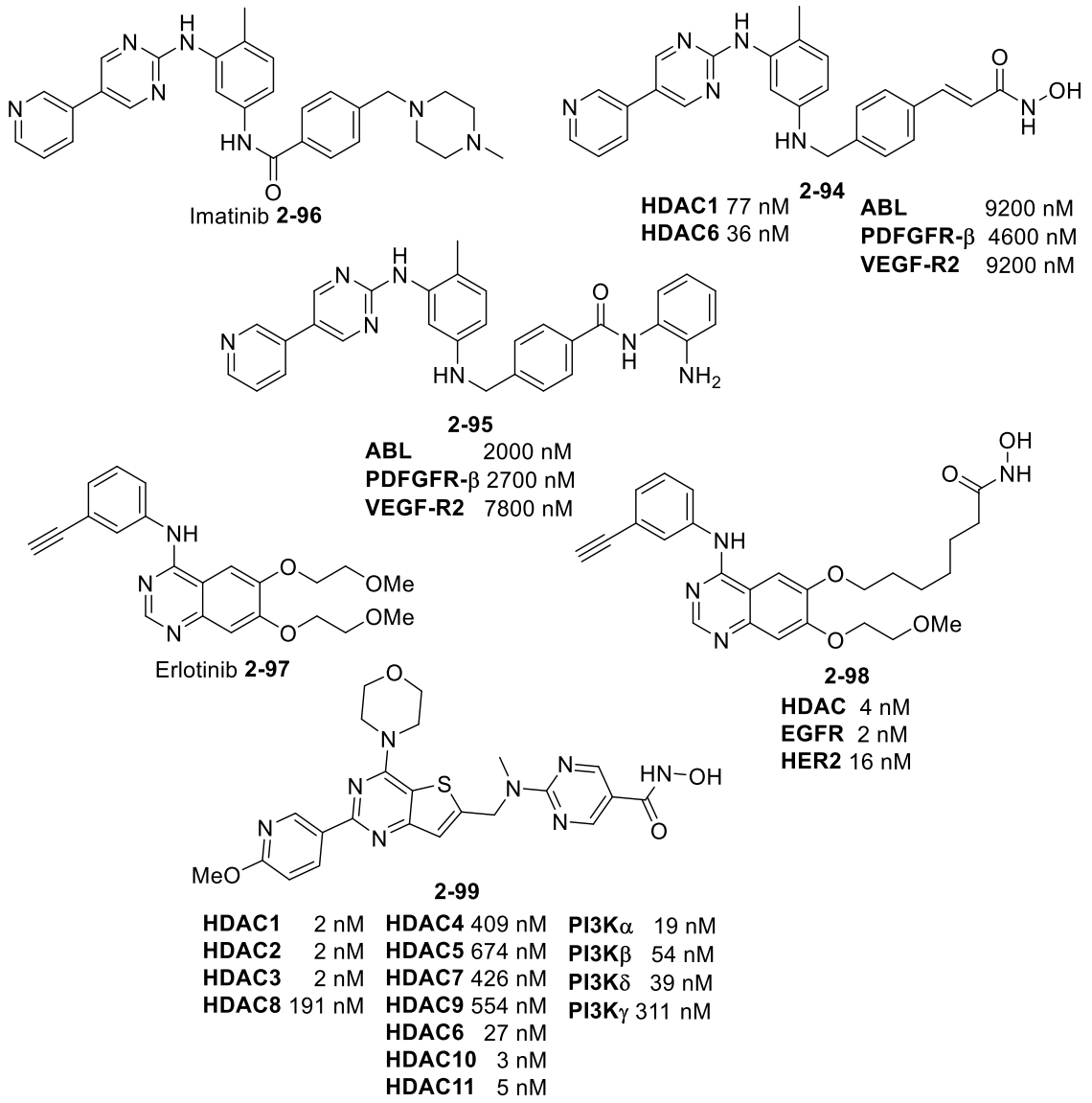

Figure 2.36: Example of dual HDAC and kinase inhibitors.
IC_{50} values are indicated.[375]

In addition to these compounds, various dual inhibitors of HDACs and non-kinase enzymes have been synthesized (Figure 2.37).[373,375] Compound **2-100** was developed as HDAC-inosine monophosphate dehydrogenase (IMDPH) dual inhibitor for the treatment of chronic myelogenous leukaemia.[383] The statin inhibitors of 3-hydroxy-3-methylglutaryl coenzyme A reductase (HMGCR) lovastatin have a beneficial effect in cancer and, coupled with a hydroxamic acid, lovastatin derivative **2-101** inhibited both HDAC and HMGCR and was active in colitis-associated colorectal cancer in a mouse model.[384] Epigenetic response was also coupled to receptor ligand to bind to the nuclear vitamin D receptor (VDR) (**2-102**),[385] or the retinoid X (RXR) (**2-103**).[386] Finally, this approach can also be used for dual epigenetic targets like a dual active HDAC-bromodomain and extra-terminal (BET) inhibitor (**2-104**).[387]

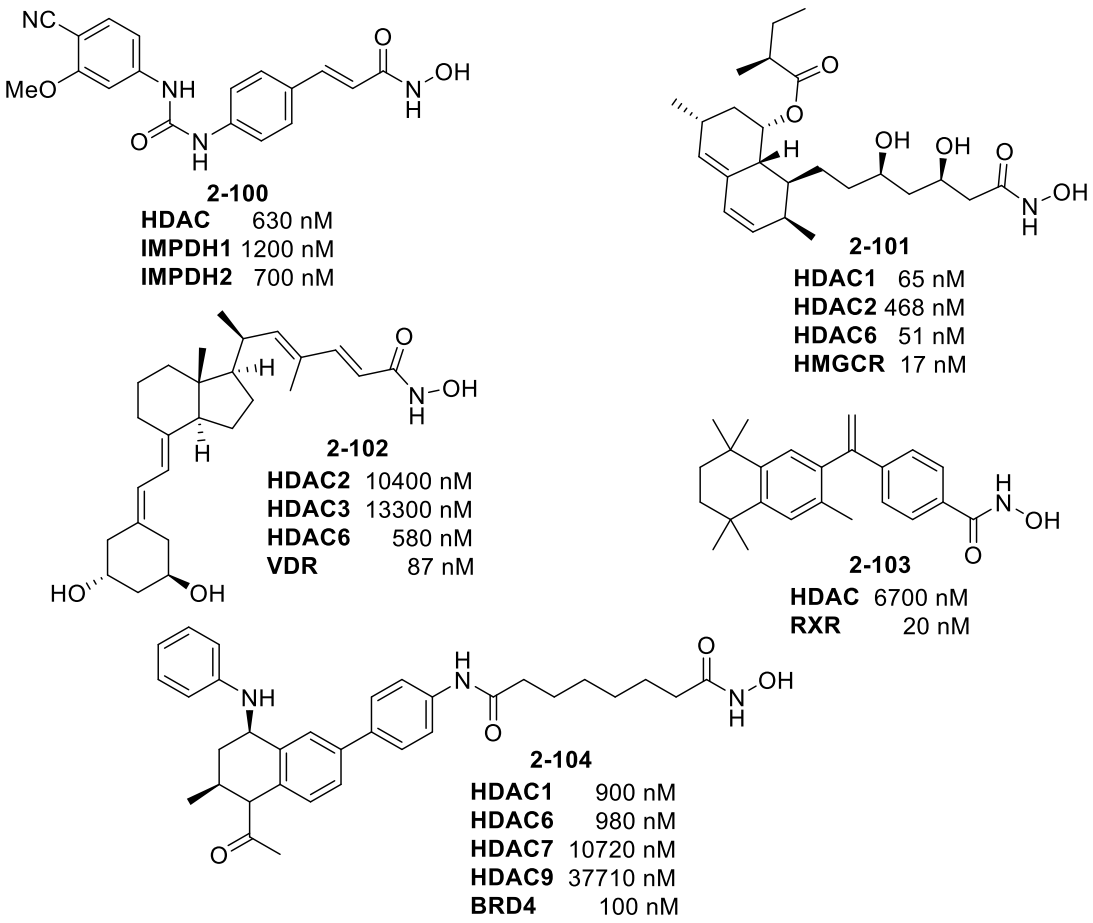

Figure 2.37: Example of dual inhibitors of HDAC and non-kinase enzyme.
IC_{50} values are indicated.[375]

To sum up, the HDAC pharmacophore was shown to be highly versatile, and potent HDAC inhibition can be obtained as long as a strong ZBG and a linker are available. Multitarget drugs are promising and offer significant advantages over the more common combination therapy. To date, HDAC inhibition has been combined with the following targets: ABL, EGFR, HER2, JAK, PDGFR, P13K, PLK, PKC and VEGFR kinases; inosine-5'-monophosphate dehydrogenase; HMG-CoA reductase; phosphodiesterase type 5; DNA cross-linking; DNA alkylation; topoisomerase; vitamin D receptor; retinoid X receptor; estrogen receptor; tubulin; and RAS localization.[375] In addition, it is possible to inhibit two epigenetic targets simultaneously by dual inhibition of HDACs and DNA methyltransferases, sirtuins, Jumonji C demethylases and bromodomains.[375] Therefore, the multitarget approach has excellent and exciting future prospects for the development of more efficient drug with reduced side-effects.

2.4 SmHDAC8 inhibitors

Over the last few years, and following the identification of SmHDAC8 as a potential target against schistosomiasis, several academic groups have investigated the development of selective inhibitors.

As part of their study on the crystal structure of SmHDAC, Marek and coworkers also performed a virtual screening to search for inhibitor scaffolds that would fit into the enlarged catalytic pocket of SmHDAC8.[322] They identified several linker-less aromatic hydroxamate derivatives, which fitted in the enzyme channel and had little interaction with the enzyme rim but where predicted to be highly potent inhibitors (Figure 2.38). Those compounds **2-105**, **2-106** and **2-107** were then tested on SmHDA8 as well as on a panel of hHDACs. These novel inhibitors showed similar activity on SmHDAC8 as the two references, vorinostat and M344, with an IC_{50} of 2-4 µM.[322] On hHDACs, those inhibitors were more selective than the reference compounds with a 3-7 fold selectivity against hHDAC1 and hHDAC3. However, they were not selective against hHDAC6 and hHDAC8 and featured higher potency on these HDAC than on SmHDAC8. Although the selectivity remained a potential issue, those compounds were a significant improvement to the reference pan-HDACi. Besides, treatment of schistosomula with **2-107** was shown to induce 100% mortality at 50 µM within 3 days and induced apoptosis even at 10 µM. Treatment of worm pairs caused a complete separation of male and female couples within 3 days at 50 µM and 5 days at 20 µM.[322]

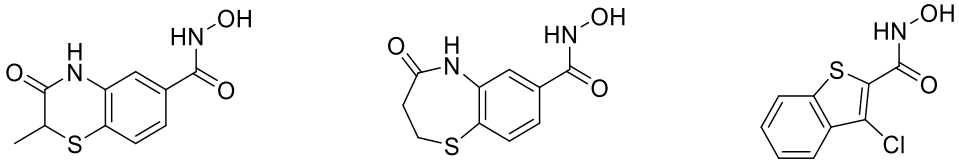

Figure 2.38: Structure of SmHDAC8 inhibitors 2-105, 2-106 and 2-107.[322]

Recently, a series of 3-aminobenzohydroxamate derivatives was reported (Figure 2.39).[325] The inhibitors were evaluated for their inhibitory activity against SmHDAC8, hHDAC1, hHDAC6, and hHDAC8. In *in vitro* assay, 27 compounds, like **2-108**, exhibited a nanomolar inhibition activity and demonstrated high selectivity for SmHDAC8 over the major human HDAC isoforms HDAC1 and HDAC6 (Table 2.17). Some compounds, such as **2-109** and **2-110**, were also reported to have a preference for SmHDAC8 over hHDAC8. Furthermore, SmHDA8 was crystallized in complex with **2-109**, and docking studies revealed the formation of a hydrogen bond between the amide and H292 in SmHDAC8. As mentioned earlier, in hHDAC8 this histidine is replaced by M274 and, therefore, cannot form a similar bond. In addition, the difference of

conformation of the phenylalanine residue was observed with F151 adopting a flipped-out conformation in SmHDAC8 while the corresponding F152, F150 and F620 took a flipped-in conformation in hHDAC8, hHDAC1 and hHDAC6 respectively.[325] This could partly explain the observed selectivity.

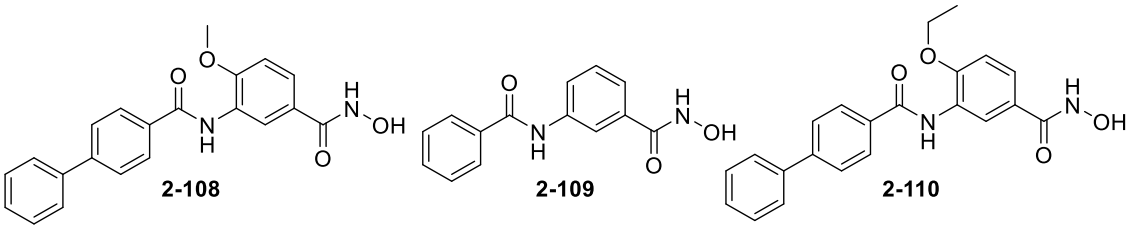

Figure 2.39: Example of 3-aminobenzohydroxamate inhibitors of SmHDAC8.

In phenotypic assays, **2-109** had a moderate effect on the viability of the schistosomula at 10 µM and 20 µM.[325] On the other hand, both **2-108** and **2-110** showed significant dose-dependent toxicity. Treatment of worm pairs with **2-110** caused 90% separation of male and female pairs within 5 days at 20 µM, and a corresponding reduction in egg laying by these worm pairs was also induced, reaching 80% for the 20 µM dose.

Compound	SmHDAC8 IC_{50} (nM)	hHDAC8 IC_{50} (nM)	hHDAC1 IC_{50} (nM)	hHDAC6 IC_{50} (nM)	% viability 20µM
2-108	75	26	6300	390	33.4
2-109	468	582	34000	3000	75.6
2-110	92	149	2800	600	35.8

Table 2.17: IC_{50} values for 3-aminobenzohydroxamate derivatives. The results of toxicity assay on schistosomula are also shown.[325]

Inspired by these results, a series of isophthalic acid-based HDAC inhibitors were reported in 2017 (Figure 2.40).[388] Compound **2-111** and **2-112** were the most promising compound and were more potent on SmHDAC8 than on hHDAC1, hHDAC6 and hHDAC8 (Table 2.18). However, in similar phenotypic assays, **2-111** showed moderate toxicity toward schistosomula at 20 µM in a dose-independent fashion. **2-112** showed a dose-dependent effect but was only slightly active. Moreover, none of them significantly affected adult worm pairing during 5 days of culture *in vitro*.

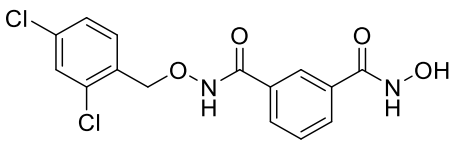

2-111

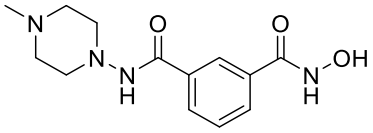

2-112

Figure 2.40: Structure of isophthalic acid SmHDAC8 inhibitors.

Compound	SmHDAC8 IC_{50} (nM)	hHDAC8 IC_{50} (nM)	hHDAC1 IC_{50} (nM)	hHDAC6 IC_{50} (nM)	% viability 20 µM
2-111	400	630	> 10000	5120	75
2-112	750	1310	> 10000	7110	79

Table 2.18: IC_{50} values for isophthalic acid derivatives. The results of toxicity assay on schistosomula are also shown.[388]

Finally, a novel class of inhibitor was recently identified by structure-based virtual screening, and a series of *N*-(2,5-dioxopyrrolidin-3-yl)-n-alkylhydroxamate was reported (Figure 2.41).[389] Compound **2-113** was the most potent inhibitor of SmHDAC8 and was slightly selective against hHDAC1 and hHDAC6 but was more active on hHDAC8. Removal of the chlorine (**2-114**) highly impacted the potency, while the extension of the alkyl chain (**2-115**) reduced the activity on SmHDAC8 and hHDAC8 but increased hHDAC6 inhibitory activity making it the favourite target. Furthermore, **2-113** induced dose-dependent apoptosis in the infective larval stage of *S. mansoni*, affecting 67 % of the larvae after 3 days at a dose of 100 µM. This is comparable to the effect achieved with the pan-HDAC inhibitor vorinostat (43% at 100 µM).[389]

Although this class of inhibitor was found to be less potent and less selective than those previously reported, this series offers an interesting new perspective. So far, hydroxamic acid has been used as a terminal moiety while the cap group was linked through the carbonyl. This scaffold reversed the use of hydroxamic acid with a cap linked directly to the nitrogen of the ZBG. Besides, the crystal structure of SmHDAC8 in complex with **2-113** revealed that the n-pentyl moiety is buried beneath the zinc cation in the SmHDAC8 foot-pocket , where it makes non-polar contacts with SmHDAC8 residues F21, T140 and C152.[389] This specificity could be further explored with the introduction of different cap groups providing more interaction with the enzyme rim and could lead to new class of more potent SmHDAC8 inhibitors.

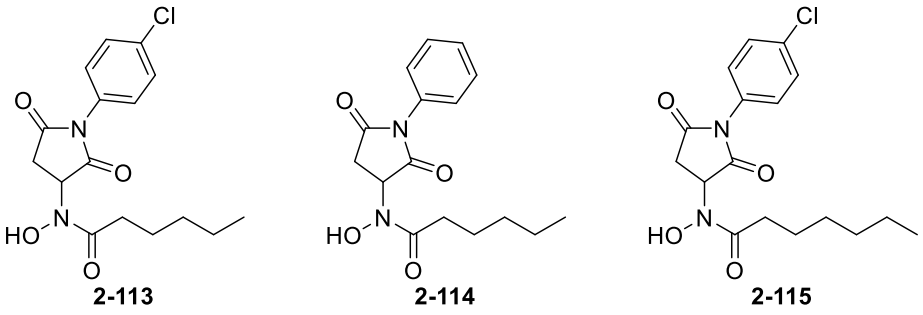

Figure 2.41: Structure and IC_{50} value of *N*-(2,5-dioxopyrrolidin-3-yl)-*n*-alkylhydroxamate inhibitors.[389]

In conclusion, several classes of inhibitor were reported to have strong inhibitory activity on SmHDAC8. Besides, they induced apoptosis in schistosomula and were able to affect the pairing of adult worms. Those inhibitors also reported selectivity against hHDACs, in particular, hHDAC1 and hHDAC6. Although some compounds were also selective against hHDAC8, most are still more active on hHDAC8 than on the parasite.

However, it has been reported that hHDAC8 inhibition showed only limited effects on many cell types.[390] In addition, HDAC8 inhibitor had the most limited impact on the human acetylome among a panel of selective inhibitors of HDACs.[325] Cytotoxicity studies of the different SmHDAC8 inhibitors have also shown a relatively low effect on cell proliferation, indicating that the inhibition of human HDAC8 does not result in intrinsic toxicity.

Hence, although future investigation could lead to new classes of SmHDAC8 inhibitor with greater selectivity on hHDAC8, it is believed that high selectivity against other class I and class II HDAC, especially hHDAC1 and hHDAC6, will be more important for a potential therapeutic setting.

2.5 Summary

HDACs are a class of enzymes involved in a wide range of biological processes, and deregulation of their activity has been linked to a large panel of pathology. Therefore, their inhibition was regarded as an attractive strategy for the development of new therapies. The discovery of several non-selective HDAC inhibitors confirmed their therapeutic potential, and a decade ago, FDA approved the first inhibitors. This became the launching ramp for the development of new classes of HDACi, and a variety of compounds were reported. More selective inhibitors helped to better investigate the role of the different class and isoform of HDACs and to identify new functions.

The field has experienced steady growth in popularity over the last decade, and it will, without doubt, lead to exciting findings in the coming years. To this end, current research mainly aims to develop highly selective compounds targeting a limited number of HDAC isoforms.

Chapter 3. Synthesis of new classes of HDAC inhibitors

1. Introduction

The central part of this thesis is focused on the synthesis of new classes of HDAC inhibitors. As we saw in the previous chapter, a large variety of structures has been investigated, and structure-activity relationship studies of HDAC inhibitors demonstrated that important variations on the scaffold are tolerated. Several series of compounds were reported with diverse structures playing the role of the cap group without compromising biological activity. To investigate further this flexibility of skeleton, we designed several scaffolds that could lead to the development of new classes of HDAC inhibitors. Synthetic pathways for these structures were established, and examples of compounds were synthesised in order to evaluate their potency and selectivity on HDAC inhibition.

2. Synthetic approach

As a starting point in our search of new scaffolds, we identified a series of specific features. First, we decided to focus on the synthesis of low molecular weight compounds with limited numbers of H-bond donors and acceptors. Those factors comply with the rule-of-five, also known as Lipinski's rules. Published by Lipinski,[391] these rules depict a set of molecular properties that are of importance in pharmacokinetics for oral bioavailability. Although there are multiple successful exceptions in drug development, these rules are still commonly used as a general guideline in drug discovery to increase the chances of developing a lead-compound with appealing pharmacokinetics properties.

Secondly introducing a centre of chirality was also of higher importance. Indeed, a chiral centre in the scaffold would secure a non-flat topology. As the enzyme rim is made of numerous chiral amino acids, this trait in the inhibitors could create isoform-dependent interactions and, therefore, provide a selectivity.

A third factor was the accessibility of commercial building blocks with high diversity.

Finally, we opted for the sole use of hydroxamic acid as zinc binding group. Thus, it was crucial to have at our disposal a carbonyl precursor or to have the ability to introduce one, to form the hydroxamic acid.

Based on these factors, amino acids emerged as an essential class of building block that fulfilled all the above criteria. To begin with, they naturally possess a chiral centre, allowing the investigation of enantiomeric effects, and they can also be easily coupled to synthesise molecules

with several chiral centres. Secondly, they have a high diversity with a variety of H-bond acceptor/donor side chains, acid/base properties and a range of lipophilicity. Moreover, their C-terminal carbonyl group, either a carboxylic acid or an ester can be converted to hydroxamic acid. Finally, they are commercially available with a variety of N-terminal, C-terminal and side chain protective groups hence being able to adapt to diverse synthetic pathways.

As results, we decided to design and develop new classes of HDAC inhibitors build around the use of amino acids.

2.1 First scaffold: imidazole-based inhibitors

The imidazo-ketopiperazine structure appeared as an interesting scaffold.

The first engaging trait of the structure was the similarity with 2,5-diketopiperazines (Figure 3.1), a privileged scaffold in drug discovery.[392,393] Ganesan group has been interested in diketopiperazine for years, and several libraries of compounds were produced by solid-phase synthesis and reported in the literature.[394–396]

Another influential factor was the presence of two chiral centres in the structure of imidazo-ketopiperazine. Schematically, this scaffold is a fusion between a diketopiperazine, which derived from the cyclization of a dipeptide, and an imidazole. For that reason, the configuration of the stereo-centres originate from the amino acid starting materials and can thus be controlled efficiently.

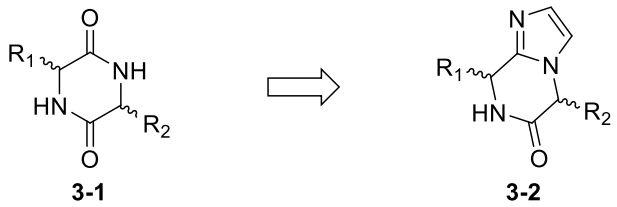

3-1 **3-2**

Figure 3.1: Structure of 2,5-diketopiperazine (3-1) and imidazo-ketopiperazine (3-2).

The synthesis of an imidazo-ketopiperazine has been reported by Bischoff and coworkers in 2010.[397] Based on conditions developed by Hopkins,[398] imidazole **3-4** was synthesised by intramolecular cyclization of the *N*-glycinyl thioamide substituted dipeptides **3-3** (Scheme 3.1). The N-terminal protection of **3-4** was removed in acidic conditions and then neutralized to generate a free amine. The spontaneous intramolecular reaction of the deprotected intermediate resulted in the second cyclization to afford the imidazo-ketopiperazine **3-5**.

We foresaw that the imidazo-ketopiperazine core could serve as a capping group in a new class of HDAC inhibitor. In addition, a linker, and by extension the zinc-binding group, could be introduced on the scaffold through the reactivity of the formed thiol.

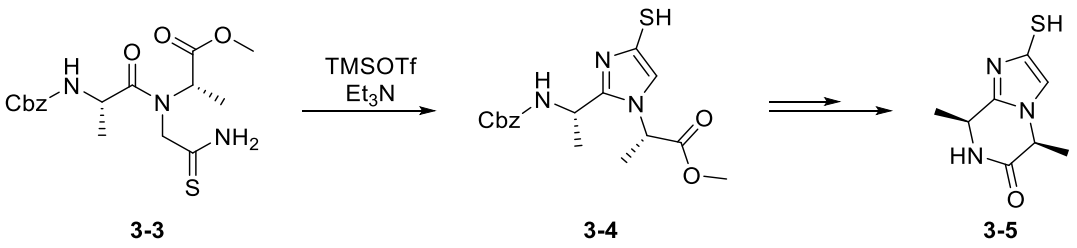

Scheme 3.1: Synthetic pathway to imidazo-ketopiperazine.

Bertrand Lecointre, a PhD student in Bischoff group, started the investigation of this scaffold as part of a visiting mission in Ganesan group prior to my arrival. He developed a first synthetic route featuring an L-Phe-L-Ala analogue of **3-3** and successfully synthesised a series of inhibitors.[399] My PhD work followed on from his preliminary results, and my first assignment consisted of optimising the developed synthetic pathway by introducing improvements in this sequence. This would then be applied to the synthesis of known inhibitors as well as new analogues with this scaffold.

In a one-pot sequence of three reactions (Scheme 3.2), L-Ala methyl ester **3-6** was initially alkylated by reaction with iodoacetamide in the presence of DIPEA to give the glycidyl amide **3-7**. Following addition of Cbz-L-Phe-OH, propane phosphonic acid anhydride (T3P) was used as a coupling agent to form the dipeptide **3-8** by condensation. In the same pot, the solvent was removed by evaporation and the residue redissolved in 1,2-dimethoxyethane. Then, treatment with Lawesson's reagent resulted in a selective thionation, and the thioamide **3-9** was isolated in a 44% overall yield over the three reactions.

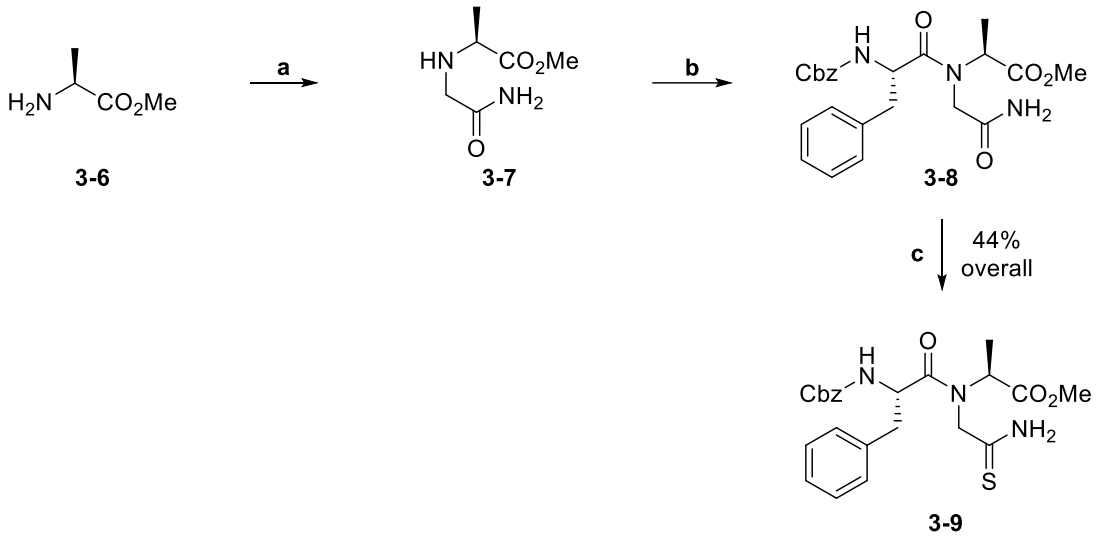

Reagents & Conditions: a. Iodoacetamide (1.2 eq), DIPEA (2.5 eq), MeCN, rt, 6 h; **b.** Cbz-L-Phe-OH (2.5 eq), T3P (4.5 eq), DIPEA (4.5 eq), rt, 16 h; **c.** Lawesson's reagent (0.6 eq), DME, rt, 6 h

Scheme 3.2: Synthesis of the dipeptide thioamide L-Phe-L-Ala.

In this sequence, T3P was preferred to more common coupling reagent based on carbodiimide, uronium or phosphonium such as EDC, HATU or PyBOP. Although these traditional classes of reagents have been extensively used in peptide synthesis, T3P displays several exciting properties and is becoming a prominent reagent.[400] Among other assets, T3P is highly soluble in organic solvent, non-hazardous and promotes the amide bond formation in mild conditions. More importantly, it was identified as a first choice coupling reagent to avoid epimerization,[401] and the by-product of the reaction can be easily removed by aqueous work-up.

The mechanism of the reaction is detailed below (Scheme 3.3). At first, carboxylic acid **3-10** is deprotonated, and the resulting carboxylate attacks the cyclic phosphonic acid anhydride T3P **3-11**. The activated carboxylic acid **3-12** then undergoes a nucleophilic attack of the amine to form the desired peptide bond, releasing at the same time the phosphonate by-product **3-13**. Finally, the amide **3-14** is deprotonated to afford the desired product **3-15**.

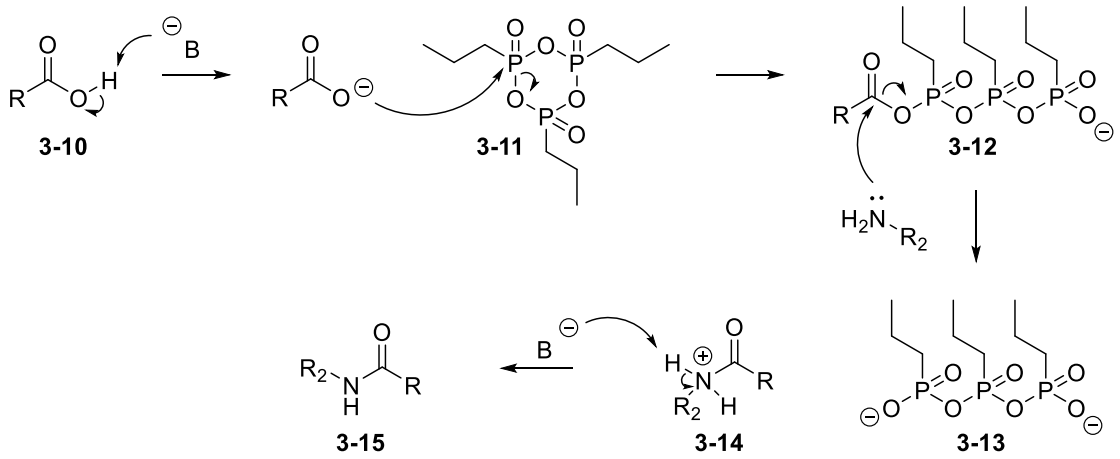

Scheme 3.3: T3P coupling mechanism.

In a second one-pot sequence of four reactions (Scheme 3.4), thioamide **3-9** was treated with trimethylsilyl triflate and Et_3N. After completion, the volatiles were evaporated, and the residue was kept at reflux in toluene. This resulted in the dehydrative cyclization of thioamide **3-9**, affording the disulfide **3-16**. Next, the disulfide bond was reduced with DL-dithiothreitol, and the regenerated thiol then performed a nucleophilic substitution on ω-halo-esters **3-17** leading to the formation of thioether **3-18**.

The structure of vorinostat motivated the initial choice of a 7-carbon alkyl chain as mimicking its linker, in size and functionality, it should favour the synthesis of an active compound.

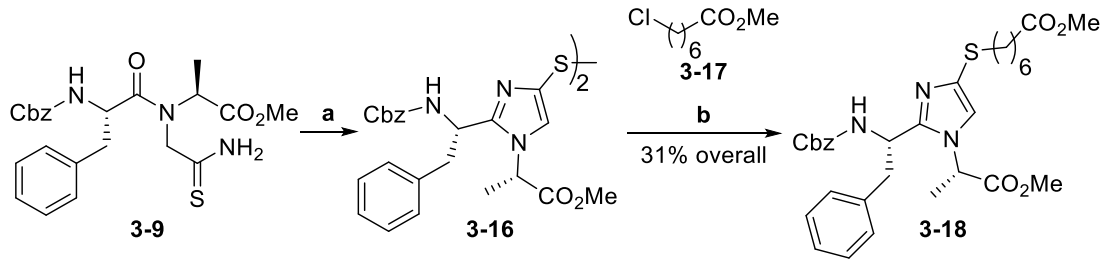

Reagents & Conditions: a. i) TMSOTf (5 eq), Et_3N (8 eq), Toluene/DCM 9/1, -78 °C -> rt, 6 h; ii) Toluene, reflux, 16 h; **b.** i) DTT (4 eq) , DCM, rt, 16 h; ii) **3-17**(1.4 eq), NaI (4.2 eq), Et_3N (2.5 eq), rt, 1h

Scheme 3.4: Synthesis of thioester 3-18 from thioamide 3-9.

The mechanism of the cyclization was reported by Bischoff (Scheme 3.5).[397] In the first step, the L-Phe-L-Ala peptidic carbonyl of **3-9** was activated by reaction with trimethylsilyl triflate. Secondly, intramolecular nucleophilic attack, by the thioamide, led to the cyclisation of **3-19** and to the formation of a more stable intermediate **3-20**. Finally, reflux in toluene eliminated TMSOH and to the imidazole ring. In addition, the reaction being carried out in the presence of air, the

thiol intermediate **3-21** was oxidized by O_2 and reacted with a second molecule to create a more stable disulfide bridge and form the dimer **3-16**.

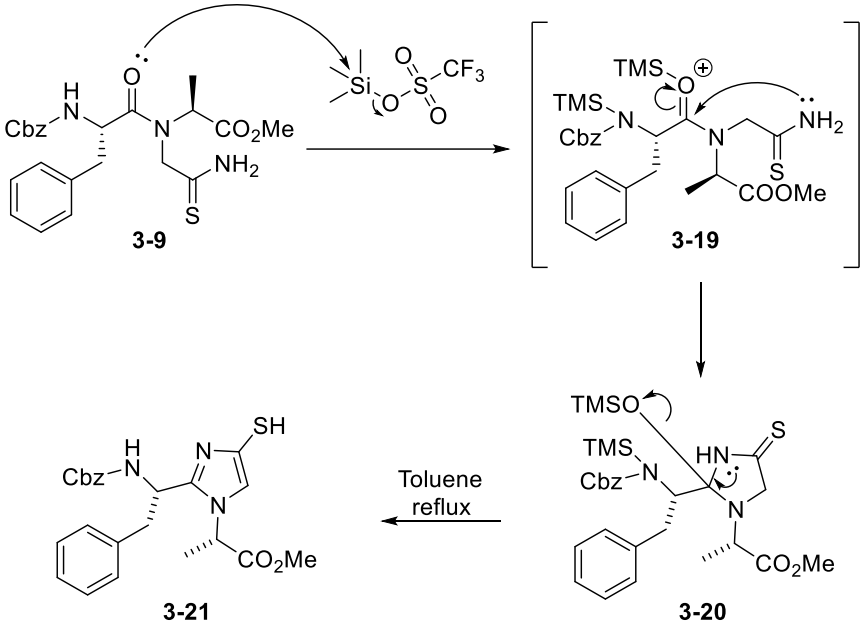

Scheme 3.5: Mechanism of the imidazole cyclization.

Removal of the N-terminal Cbz protecting group of **3-18** in strongly acidic conditions resulted in the protonated amine, which was then neutralized with $NaHCO_3$ to afford the free amine (Scheme 3.6). The amine then spontaneously cyclized through nucleophilic attack on the methyl ester to afford the imidazo-ketopiperazine **3-22**. The ester side chain was then hydrolysed to provide the carboxylic acid. In the last step, we tried to couple the carboxylic acid with *O*-(tert-butyldimethylsilyl) hydroxylamine, but no desired product was recovered after purification.

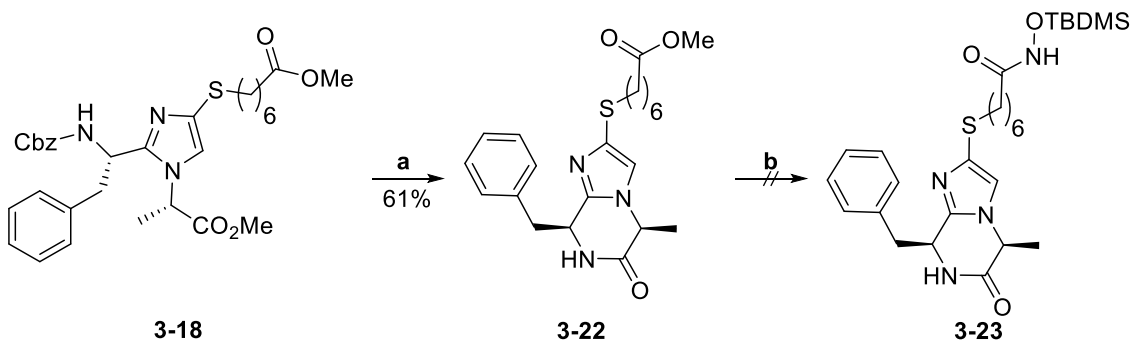

3-18 3-22 3-23

Reagents & Conditions: a. i) anisole (8 eq), HBr (33% in AcOH) (15 eq), rt, 2.5 h; ii) $NaHCO_3$ (1M), rt, 30 min; **b.** i) HCl (6M), THF, rt, 6h; ii) PyBOP (1.2 eq), DIPEA (2.2 eq), $NH_2OTBDMS$ (1.2 eq), MeCN, rt, 6 h

Scheme 3.6: Attempt to synthesise 3-23.

Despite an unfortunate attempt, we managed to familiarize with the general route previously developed. From there, several new ideas arise to modify the synthetic pathway and to optimize it.

One of the solutions was to look at the first steps of the sequence. On the one hand, the ability to run one-pot reaction was highly beneficial. This process removed the need for isolation and purification of intermediate compounds, thus speeded up the synthesis. On the other hand, successive reactions could lead to lower yield, increased number of side products and were more difficult to monitor due to the presence of numerous chemical entities.

Therefore, we decided to check if we could improve the overall yield of formation of thioamide **3-9** by cutting the one-pot three reactions sequence. However, although we could have run each reaction separately, we decided only to isolate the glycidyl amide intermediate **3-8**. This decision was a compromise between our will to improve the yield and the convenience of the one-pot sequence. Additionally, isolation of highly polar intermediate **3-7** would have been difficult and could have lessened the yield.

This modification resulted in a significant improvement of the overall yield (Table 3.1).

Entry	Overall yield
One-pot 3 reactions sequence	44%
Isolation of intermediate **3-8** followed by conversion to **3-9**	89%

Table 3.1: Comparison of synthetic methods to form thioamide 3-9.

This led us to also reconsider the second one-pot sequence. Indeed, we noticed that the divergence between analogues only occurred over the last step of the sequence. Therefore, we decided to split again the sequence into separated reactions to isolate the disulphide **3-16**, which is the last common intermediate. Accordingly, we were able to synthesise and isolate **3-16** in 62% yield.

Turning to the developed route, we realised that this synthetic pathway could also be used to form a linear analogue derived from our imidazo-ketopiperazine. Using the intermediate **3-18**, we could skip the ring closure steps and directly convert the ester to hydroxamic acid to synthesise **3-25** (Scheme 3.7).

This "open" version of the imidazole-based scaffold had more flexibility in the cap part of the molecule compare to the "closed" imidazo-ketopiperazine. As a result, the interactions between the inhibitors and the enzyme rim could be profoundly affected. This could lead to a different profile of activity, and the assessment of the evolution in potency and selectivity between these two structures could then be of great interest for further optimisation of the scaffolds.

However, to comply with this new objective, some adaptations of the synthesis were required. Indeed, the presence of two methyl esters on the intermediate **3-18** would render the conversion to hydroxamic acid more difficult. It was likely that getting a proper selectivity between the methyl ester on the side chain and the second from the L-alanine would have been challenging, and several side products would have been formed. Hence, methyl ester on the side chain had to be avoided.

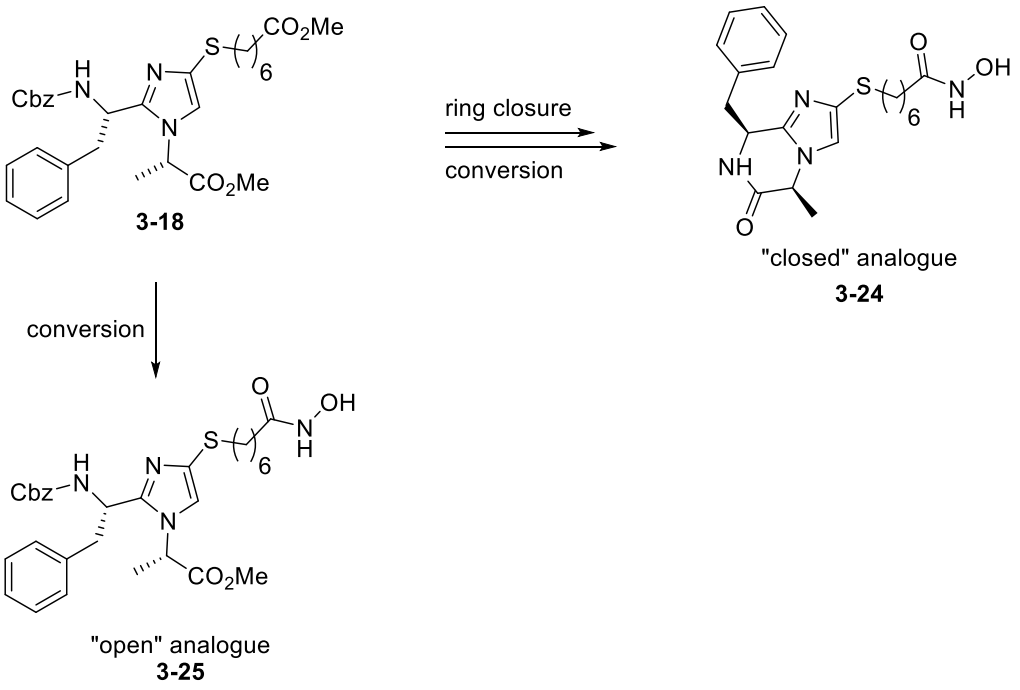

Scheme 3.7: Modification of the synthetic pathway to "open" and "closed" analogues.

Taking this idea a step further, and combining it with the other modifications we envisaged led us to perform the ring closure, and so formation of the imidazo-ketopiperazine, from the disulfide **3-16**, giving us a new synthetic pathway (Scheme 3.8). Starting from the isolated disulfide **3-16**, N-terminal Cbz protective group was removed under strongly acidic condition followed by neutralisation with $NaHCO_3$ (1M) to afford the imidazo-ketopiperazine disulfide **3-26**.

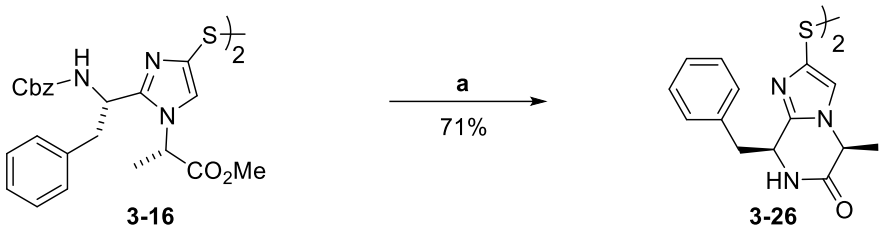

Reagents & Conditions: a. i) anisole (8 eq), HBr (33% in AcOH) (15 eq), rt, 2.5 h; ii) $NaHCO_3$ (1M), rt, 30 min

Scheme 3.8: Synthesis of disulfide 3-26.

2.1.i Spotlight on "closed" analogue

Focusing on the imidazo-ketopiperazine scaffold, the disulfide intermediate **3-26** was reduced to thiol with tris(2-carboxyethyl)phosphine (TCEP) followed by the addition of ω-bromo-esters in the presence of Et_3N to give the alkylated imidazo-ketopiperazine ethyl ester **3-27** (Scheme 3.9).

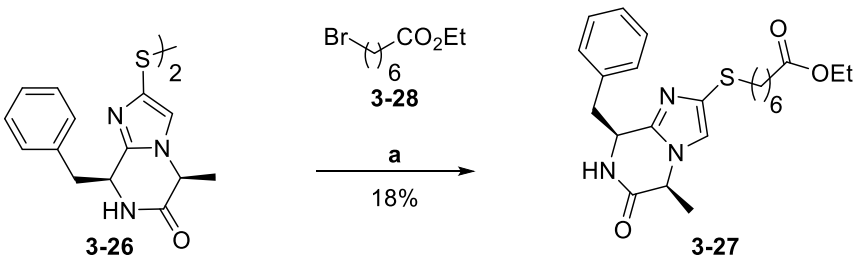

Reagents & Conditions: a. i) TCEP (3 eq), Et_3N (3 eq), MeOH/THF/H_2O, rt, 16 h ; ii) **3-28** (3 eq), Et_3N (3 eq), DCM, rt, 6 h

Scheme 3.9: Synthesis of ethyl ester 3-27.

TCEP is a powerful reducing reagent commonly used in biochemistry to break disulfide bonds in a protein, and it offers several advantages compared to DTT. First, it is odourless and highly soluble in water. Moreover, despite having different reactivity, both reagents could react during the alkylation step leading to the formation of side products. Thanks to its high solubility in water, TCEP can be removed from the reaction mixture with a quick extraction before adding the halide reagent to prevent the side reaction. However, as shown by the mechanism (Scheme 3.10) water is required in the reaction mixture for the reduction of the disulfide, and a mix of solvents has to be used. Therefore, either DTT or TCEP was used as reducing agent depending on the solubility of the reactants.

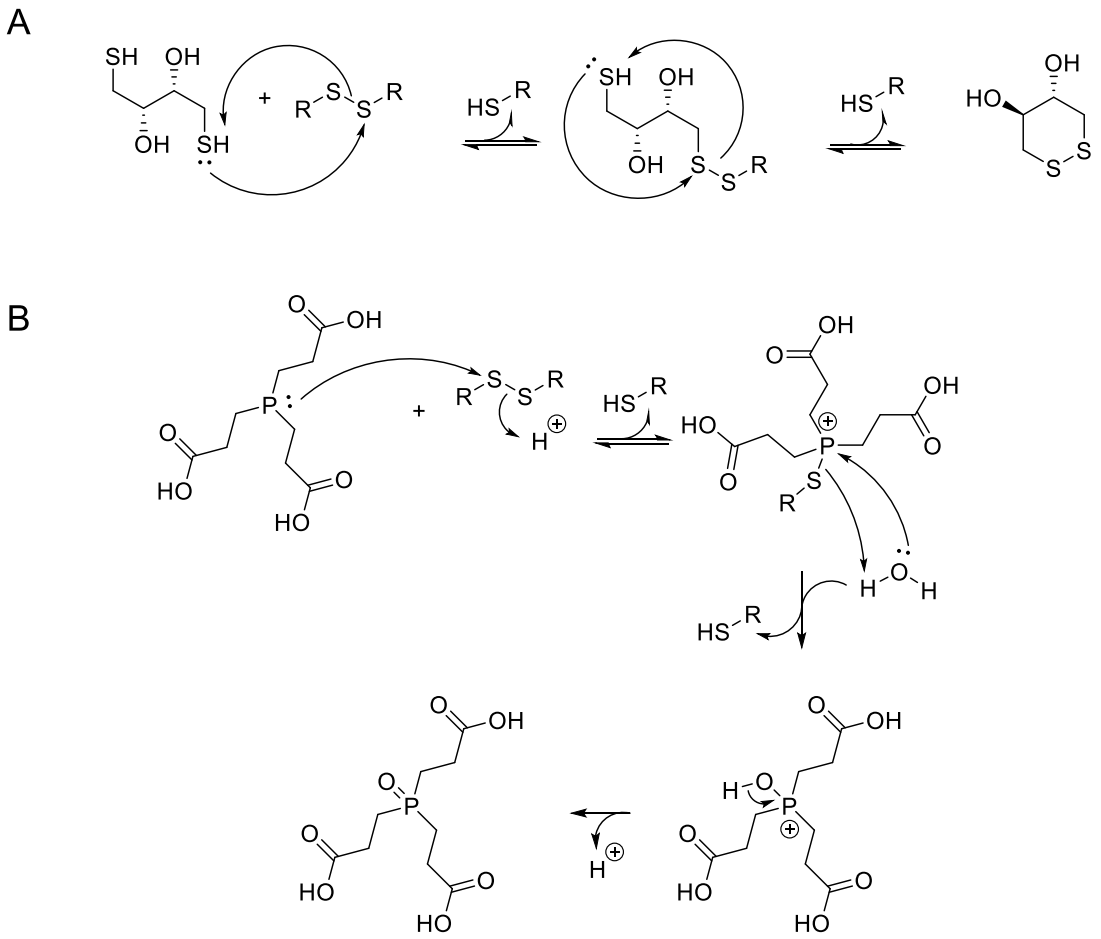

Scheme 3.10: Mechanism of disulfide reduction by DTT (A) and TCEP (B).

In the last step, the ethyl ester **3-27** reacted with hydroxylamine, in the presence of a catalytic amount of potassium cyanide, to give the final compound **3-28** (Scheme 3.11) in 29% yield. Although the conversion of ester to hydroxamic acid could occur without it, the addition of a catalytic amount of potassium cyanide in the reaction was reported to favour and accelerate the reaction by cyanide catalysed nucleophilic displacement.[402]

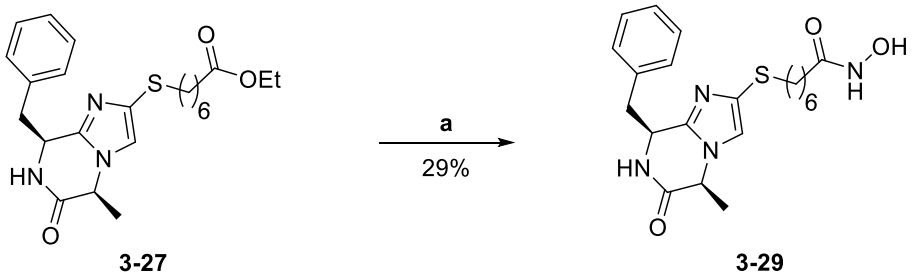

3-27 **3-29**

Reagents & Conditions: **a.** KCN (0.2 eq), aq. NH_2OH/MeOH/THF 0.5/1/1, rt, 16 h

Scheme 3.11: Synthesis of final compound 3-29.

Following the synthesis of this compound, we decided to modify the linker length and make analogues with six and eight carbons. Bertrand Lecointre had previously studied the impact of the linker size, and six to eight carbons chain were shown to be the most suitable lengths.[399] Furthermore, in accordance with our will to optimise the synthesis, we decided to introduce side chains that were already containing the hydroxamic acid.

Ethyl 7-bromoheptanoate **3-28** was hydrolysed to the corresponding carboxylic acid **3-31** with lithium hydroxide in 96% yield as reported in the literature,[403] and then converted to hydroxamic acid **3-34** in 62% yield following activation with CDI (Scheme 3.12).[404] Similarly, commercially available 6-bromohexanoic acid **3-30** and 8-bromooctannoic acid **3-32** were activated and converted to afford the hydroxamic acids **3-33** and **3-35** in 79% and 84% yields respectively.

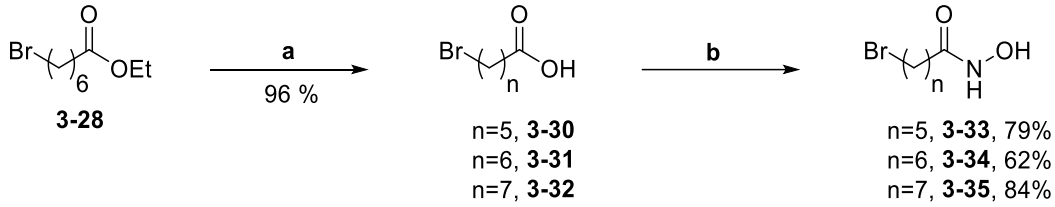

Reagents & Condition: a. $LiOH.H_2O$ (1.3 eq), THF/EtOH/H_2O 1/1/1, rt, 3 h; **b.** CDI (1.5 eq), $NH_2OH.HCl$ (2 eq), THF, rt, 16 h

Scheme 3.12: Synthesis of alkyl linkers.

After that, disulfide **3-26** was reduced, with either TCEP or DTT, and the regenerated thiol was then alkylated, by hydroxamic acids **3-33** and **3-35**, to provide the final compounds **3-36** and **3-37**, respectively in 60% and 51% yield (Scheme 3.13).

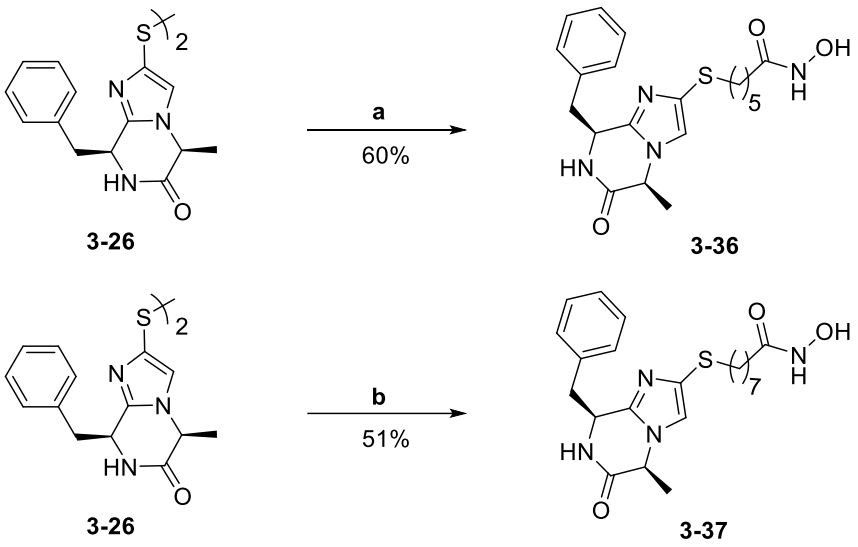

Reagents & Conditions: a: i) TCEP (3 eq), MeOH/THF/H_2O, rt, 16 h; ii) **3-33** (3 eq), DIPEA (3 eq), $CHCl_3$, rt, 16 h; **b.** i) DTT (8 eq) , Et_3N (2.5 eq) , DCM, rt, 16 h; ii) **3-35** (2.4 eq), Et_3N (5 eq), rt, 4 h

Scheme 3.13: Synthesis of compounds 3-36 and 3-37.

Those three compounds had been synthesised and evaluated on HDAC enzymatic assay as part of Bertrand Lecointre work.[399] However, this modified synthesis is more convergent and reduced the number of steps. As a result, the yield of the synthesis was greatly improved with a 36% to 43% yield from disulfide **3-16** to **3-37** and **3-36**, respectively, compared to 3% to 11% with the previous synthetic pathway.

2.1.ii Spotlight on "open" analogue

In respect to the previously developed synthesis, and to evaluate the impact of the cap group, we then focused on the formation of analogues with a non-cyclized imidazole core.

Starting from isolated disulfide **3-16**, and following its reduction to thiol with either DTT or TCEP, the imidazole core was coupled with the 6-, 7- and 8-carbon alkyl side chains **3-33**, **3-34** and **3-35** to retrieve respectively the final compounds **3-38**, **3-39** and **3-40** (Scheme 3.14).

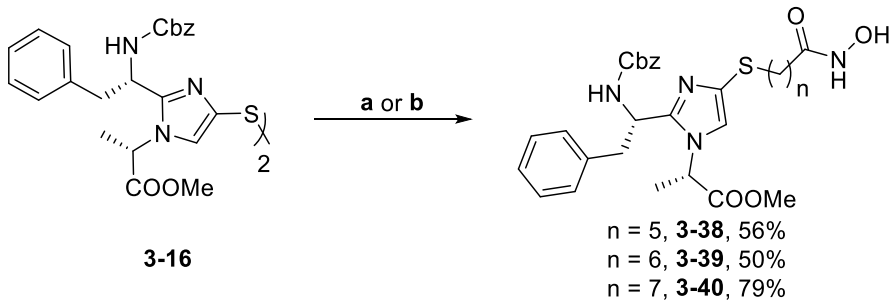

3-16

Reagents & Conditions: a. i) TCEP (3 eq), MeOH/THF/H_2O, rt, 16 h; ii) **3-34** (4 eq), DIPEA (4 eq), $CHCl_3$, rt, 16 h; **b.** i) DTT (8 eq) , Et_3N (5 eq) , DCM, rt, 16 h; ii) **3-33** or **3-35** (2.4 eq), rt, 6 h

Scheme 3.14: Synthesis of "open" analogues 3-38 to 3-40.

With regard to this synthesis, we decided to change the nature of the linker. On the one hand, alkyl linkers offer great flexibility and can adapt to the enzyme channel to optimise the interaction with the zinc cation, resulting in high potency. On the other hand, this plasticity flattens the impact of amino acid differences between HDAC isoforms and thus can hamper the selectivity. Therefore, we decided to introduce a bulkier and less flexible spacer containing a benzyl ring.

Starting with the preparation of the linker, 4-(bromomethyl)benzoic acid was activated with thionyl chloride and converted to hydroxamic acid **3-41** in 90% yield (Scheme 3.15), in agreement with reported procedures.[405,406] The 4-(bromomethyl)-*N*-hydroxybenzamide linker **3-41** was then coupled with the disulfide **3-16,** following its reduction with DTT, to afford the final compound **3-42** in 24% yield.

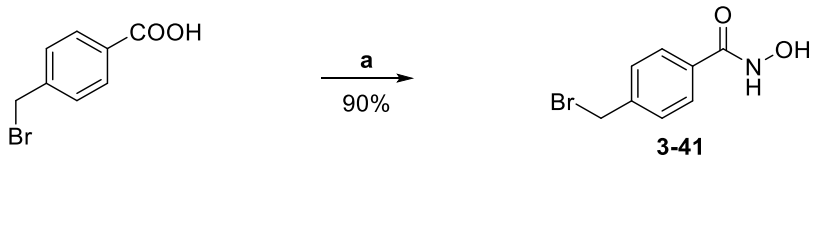

3-41

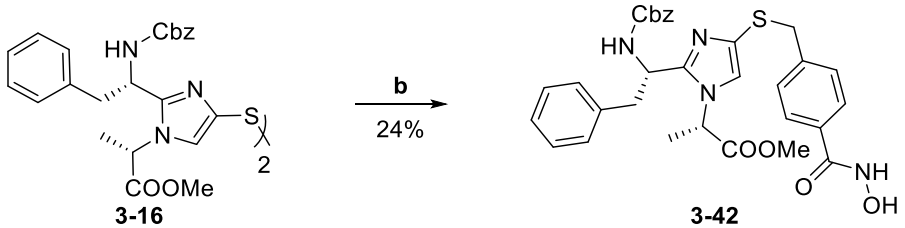

3-16 3-42

Reagents & Conditions: a. i) $SOCl_2$, reflux, 4.5 h; ii) $NH_2OH.HCl$ (2.2 eq), NaOH (2M), Et_2O, rt, 30 min; **b.** i) DTT (8 eq) , Et_3N (4 eq) , DCM, rt, 16 h; ii) **3-41** (10 eq), rt, 6 h

Scheme 3.15: Synthesis of linker 3-41 and compound 3-42.

Wishing to keep investigating rigid and bulky linkers, we decided to turn to cinnamic acid derivatives. This choice of linker derived from the structure of the two HDAC inhibitors panobinostat and belinostat, approved by FDA and both containing a cinnamic group as a linker (Figure 3.2).

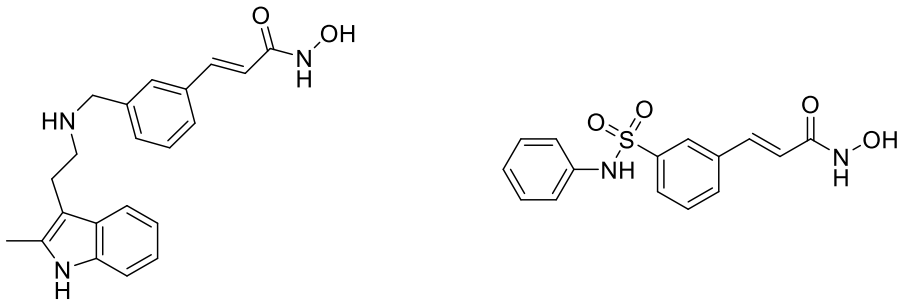

Figure 3.2: Structure of panobinostat and belinostat.

Based on the large-scale synthetic route of belinostat published by Reisch and coworkers,[407] a first pathway was investigated (Scheme 3.16).

Disulfide **3-16** was reduced to thiol by DTT, and coupled with 1-bromo-3-(bromomethyl)benzene **3-43** to afford the thioether intermediate **3-44** in 69% yield. The following step consisted of a palladium-catalysed coupling reaction with tert-butyl acrylate to synthesise **3-45**. Several conditions were tested (Table 3.2)[408,409] but none showed a positive outcome, and only starting material was recovered.

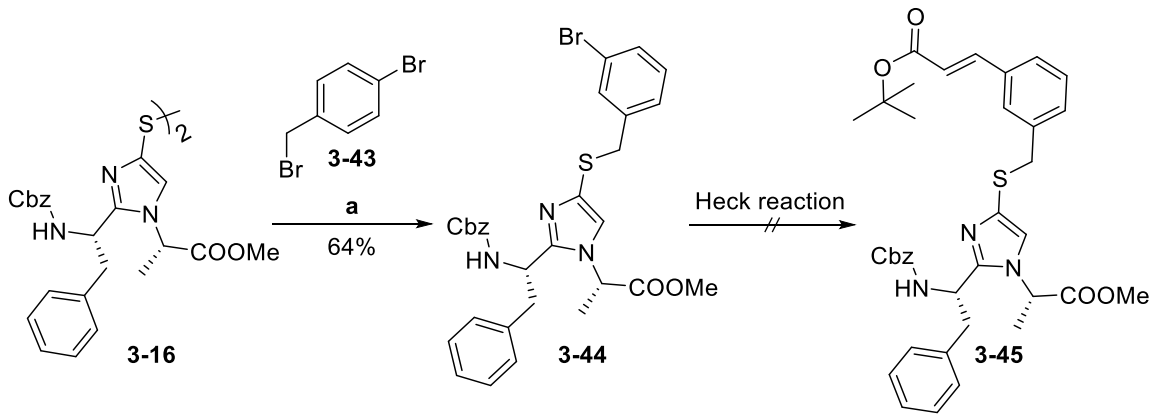

Reagents & Conditions: a. i) DTT (8 eq) ,DCM, rt, 16 h; ii) **3-43** (2.4 eq), Et_3N (5 eq), rt, 3 h

Scheme 3.16: Attempt to make cinnamic analogue 3-45.

Entry	Conditions	Yield
1	Et_3N (5 eq), t-Butylacrylate (1.2 eq), PPh_3 (0.5 eq), $Pd(OAc)_2$ (0.5 eq), DMF, 80 °C, 16 h	Starting material
2	Et_3N (1.7 eq), t-Butylacrylate (1.2 eq), PPh_3 (0.5 eq), $Pd(OAc)_2$ (0.5 eq), K_2CO_3 (1 eq), DMF, 80 °C, 16 h	Starting material
3	Et_3N (1.7 eq), t-Butylacrylate (1.2 eq), PPh_3 (0.5 eq), *$Pd(OAc)_2$ (0.5 eq), $NaHCO_3$ (1 eq), DMF, 80 °C, 16 h	Starting material
4	Et_3N (1.7 eq), t-Butylacrylate (1.2 eq), PPh_3 (0.5 eq), *$Pd(OAc)_2$ (0.5 eq), K_2CO_3 (1 eq), DMF, 80 °C, 16 h	Starting material
	*another batch of $Pd(OAc)_2$ was used	

Table 3.2: Heck reaction conditions.

In order to understand these results, we turned to the Heck reaction mechanism (Scheme 3.17). The first step of Heck reaction is an oxidative addition which inserts the palladium(0) in the aryl bromide bond to give the palladium(II) intermediate **3-46**. In a second step, the palladium(II) forms a π–complex **3-47** with the alkene bond, followed by a syn-addition of aryl and palladium(II) to afford **3-48**. The complex then undergoes an internal rotation to the trans-isomer **3-49,** and a β-hydride elimination step leads to the complex **3-50**. Finally, the complex releases the desired alkene **3-51** and palladium(0) is regenerated by reductive elimination of **3-52**.

As only starting materials were recovered in our reactions, it suggests that one of the steps in the catalytic cycle could be blocked or tremendously slowed down, thus preventing the required high catalytic turnover.

The first difference between our compound and belinostat is the absence of electro-withdrawing group on the aryl ring which is known to accelerate the reaction.[410] However, although this factor may have some influence, the mixture was kept at a high temperature overnight and should have overcome a lower rate of reaction. Moreover, aryl bromide remains a common substrate for Heck reactions, which was successfully reported with a large variety of substituents.

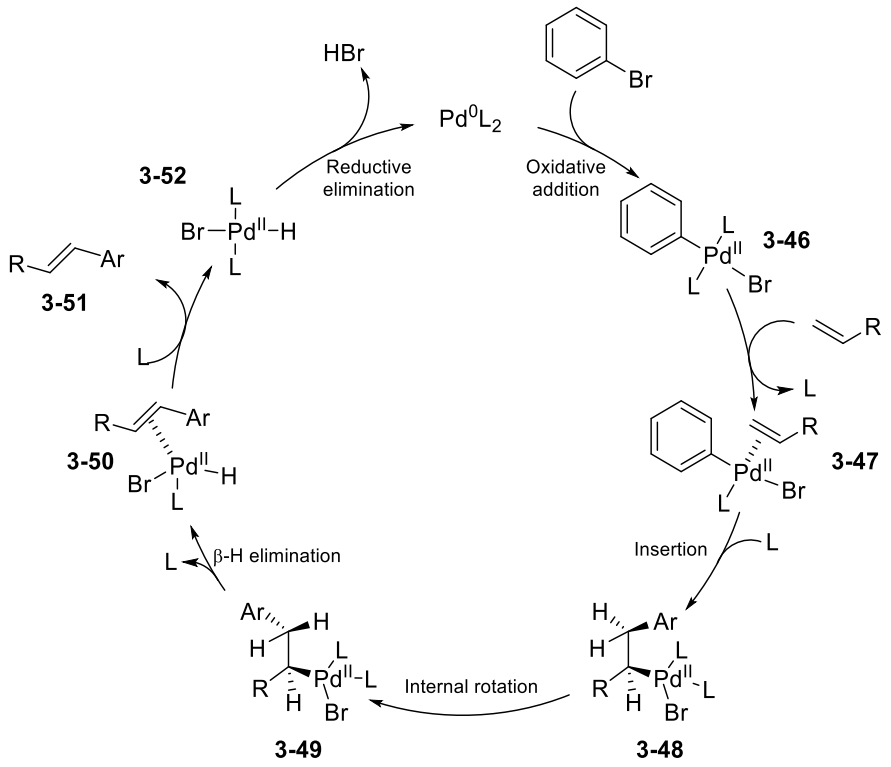

Scheme 3.17: Heck mechanism.[411]

We then checked the literature to find examples of Heck coupling between acrylate ester and (bromobenzyl)(methyl)sulfane derivative to have a better comparison of structure but none were found. The closest and only similar reaction involved a sulfone instead of sulfane (Scheme 3.18).[412] Interestingly the reaction was reported to last three days at 100 °C. As low reactivity was also observed, a side effect inherent to the structure could be affecting the cycle turn-over.

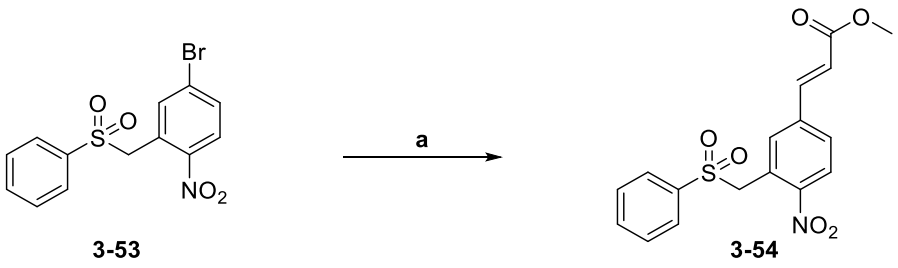

Reagents & Conditions: a. methyl acrylate (2 eq), DIPA (1.75 eq), PPh_3 (0.04 eq), $Pd(OAc)_2$ (0.02 eq), DMF, 100°C, 3 d

Scheme 3.18: Heck reaction example between sulfone 3-53 and methyl acrylate.

A hypothesis was a side interaction between palladium and sulfane/sulfone, hampering proper catalysis. To check this hypothesis, we went back to the literature and extended the search to any Heck reaction on this kind of structure. Once more only minimal material was found (Scheme

3.19).[413] In the only example, the product **3-56** was obtained at only 12% yield under microwave irradiation, suggesting once again low reactivity of the structure in Heck couplings.

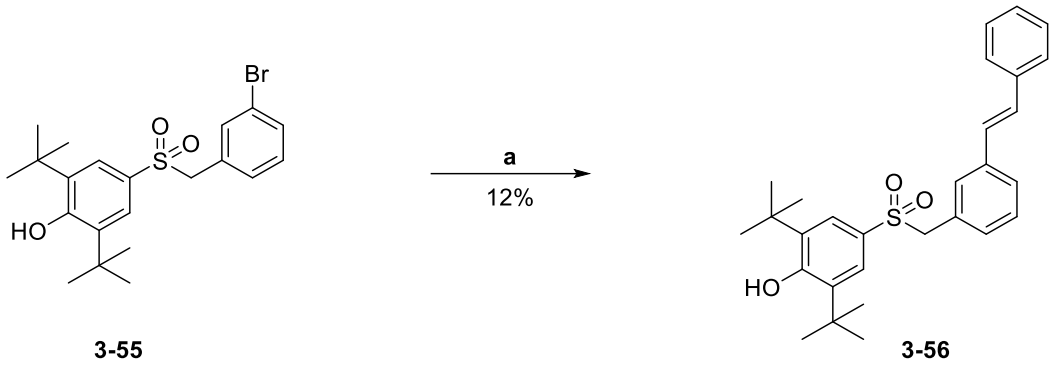

3-55 **3-56**

Reagents & Conditions: a. $Pd_2(dba)_3$ (0.02 eq), $Pd(P(t\text{-Butyl})_3)_2$ (0.04 eq), Cy_2NMe (1.14 eq), styrene (1.14 eq), THF, rt, 3 d or μW (110 °C, 300 sec)

Scheme 3.19: Heck reaction example on sulfone 3-55.

Interestingly, when the search was extended to any coupling reaction catalysed by palladium, several examples of Suzuki reaction were found with both sulfone and sulfane derivatives.[414,415,416] However, the Suzuki coupling mechanism differs from the Heck reaction (Scheme 3.20). Thus, we examined the different steps to find a potential explanation in the divergent reactivity.

Although oxidative additions are similar in both cycles, the introduction of the vinyl group is distinct. In Heck reaction, the vinyl directly interacts with the palladium and undergoes a migratory insertion. On the other hand, in Suzuki reaction the vinyl is initially bonded to a boron nucleus, forming a boronic ester **3-57**. After reaction with a base to build **3-58**, the reactive species then goes through a transmetalation step with the palladium(II) complex **3-59**. This step results in **3-61**, as trans and cis isomers, that then undergoes reductive elimination to regenerate palladium(0) and releases the desired compound **3-62**. To my knowledge, the mechanism of this transmetalation has not been fully elucidated yet, but a different insertion process of the vinyl could affect the reaction speed.

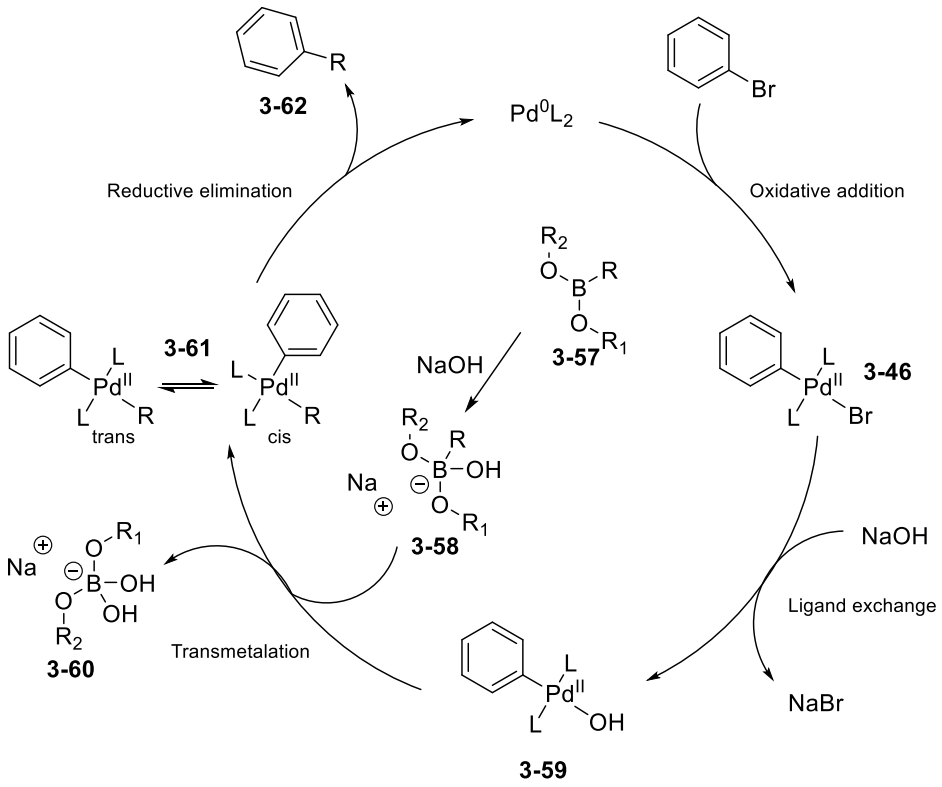

Scheme 3.20: Suzuki coupling mechanism.[417]

Moreover, a key step in the Heck reaction mechanism is the internal rotation allowing the syn β-H elimination and the formation of the alkene bond. Meanwhile, in Suzuki reaction, this step is not necessary as the double bond is not affected by the transmetalation. The hypothetic interaction between the palladium and the sulfane/sulfone after the migratory insertion of the acrylate could, therefore, impede the internal rotation and highly hamper the catalytic cycle.

In spite of these hypotheses, no further work was done to study this reaction, and we decided to change the synthetic route (Scheme 3.21).

Disulfide **3-16** was reduced with DTT, and the newly formed thiol coupled with 4-(bromomethyl)benzaldehyde **3-63**, which resulted from the reduction of 3-(bromomethyl) benzonitrile with DIBAl-H,[418] to give the benzaldehyde **3-64** in 54% yield. Afterwards, Knoevenagel condensation with malonic acid[419] in pyridine led to the successful procurement of cinnamic acid derivative **3-65** in 97% yield. However, attempts to couple *O*-tritylhydroxylamine with EDC/HOBt/NMM[420] was unsuccessful, and no product was recovered.

Although we are confident that the last step could be successful under other conditions, due to the time constraints and the lack of starting material the reaction couldn't be repeated and will be part of future work.

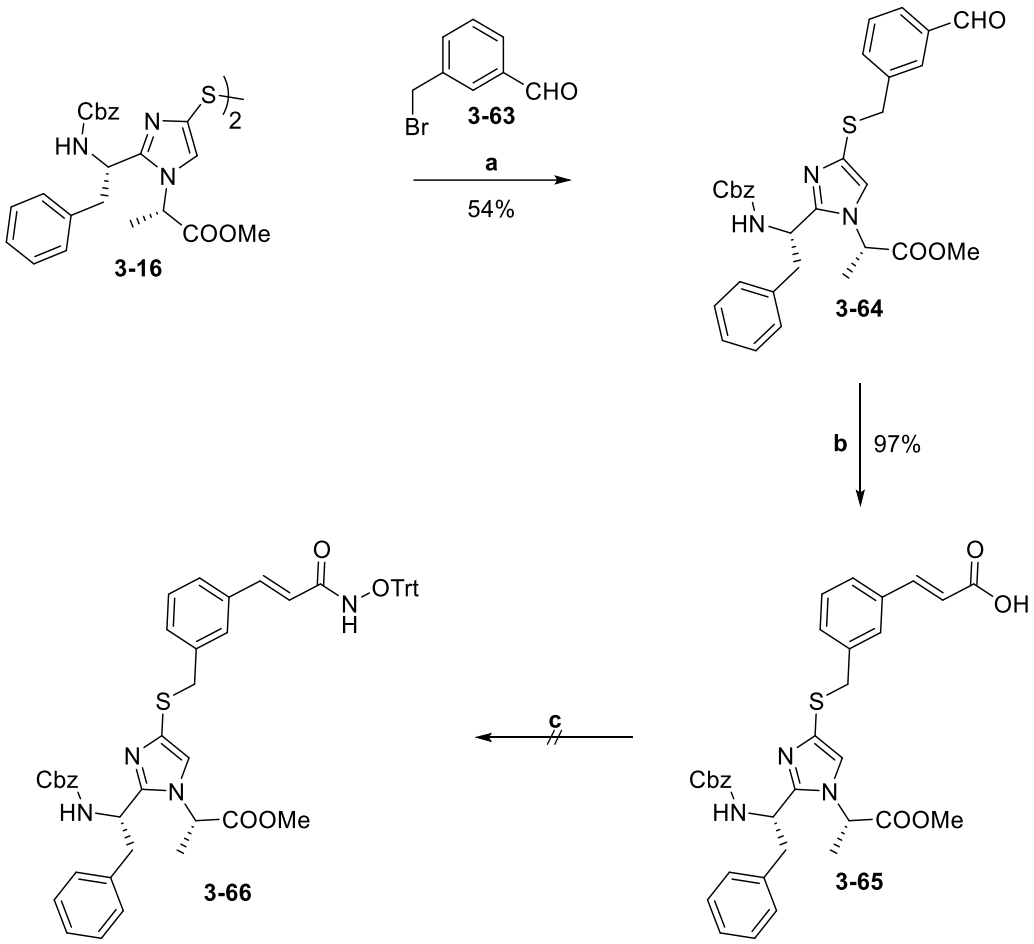

Reagents & Conditions: a. i) DTT (4 eq), Et_3N (2.5 eq), DCM, rt, 16 h; ii) **3-63** (2 eq), rt, 6 h; **b.** malonic acid (3 eq), piperidine (0.5 eq), pyridine, 100 °C, 2 h; **c.** EDC (1.3 eq), HOBt (1.3 eq), NH_2OTrt (1.5 eq), NMM (1.5 eq), THF, rt, 16 h

Scheme 3.21: Alternative route to cinnamic hydroxamate compound 3-66.

2.2 Second Scaffold: From Lysine to Aspartic acid

A common and straightforward idea to design a class of inhibitors is to use the structure of the natural substrate. Several studies have been made to take advantage of the substrate acetyllysine side chain in a peptidomimetic approach. This strategy led to the discovery of the aminosuberoyl hydroxamic acid class of inhibitors, and extensive work has been done to investigate cyclic and linear peptide and non-peptide cap groups.[421–424]

In contrast with these studies, little work has been done to investigate the use of amino acids with non-alkyl sidechains. In 2004, Fairlie published the results of a new class of HDACi, derived from cysteine, as antitumor agent.[425] This led us to consider the synthesis of a new class derived from a different amino acid.

Several parameters were used to select a candidate. Firstly, we needed easy accessibility from a commercial source, so we opted in favour of natural amino acids. Secondly, the high reactivity of the sidechain was required to be able to introduce a hydroxamic acid as zinc binding group. Finally, we wanted to maintain a five-atom length, between the main chain and the carbonyl, to mimic the acetylated lysine. The above factors led us to choose aspartic acid as the core of the scaffold, and to couple it to β-alanine on the side chain to introduce the hydroxamic acid (Scheme 3.22).

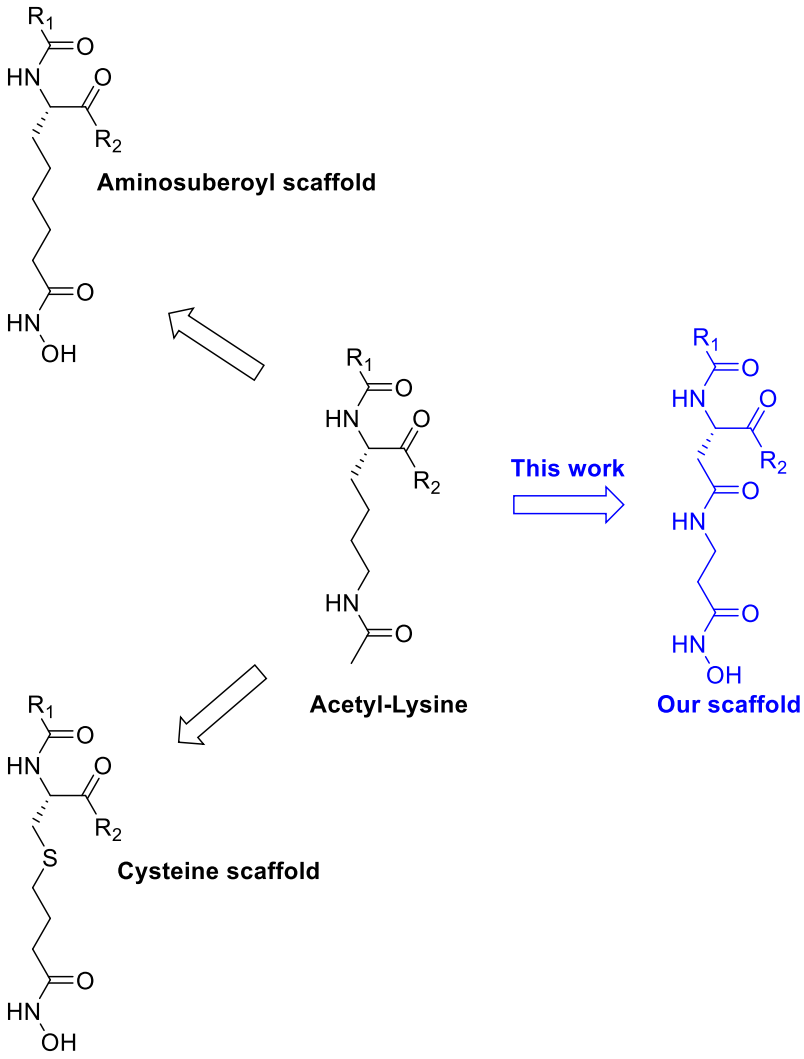

Scheme 3.22: Overview of our scaffold and reported related structure.

Our first synthetic approach consisted of a solid phase synthesis commonly used in peptide synthesis. The principle consists in using polymer beads as a support for the reaction. This resin is usually made of polystyrene with a small percentage (1-2%) of a second polymer bearing a specific reactive group. Depending on the nature of these groups different resins can be obtained, and their reactivity thus conditions the choice of resin.

In peptide synthesis, the first step consists in attaching an N-protected amino acid to the polymer by its C-terminal side to give **3-67** (Scheme 3.23). As the polymer bead is insoluble in the solvent, the reaction mixture can be filtered, and the resin washed several times with a small amount of solvent to remove any traces of reagents. In the same manner, washing is consistently done following every step. Secondly, the N-protection is removed to give a free amine **3-68,** which can then be coupled to a second amino-acid bearing the same N-protection to synthesise a dipeptide **3-69**. To avoid the formation of side products, this step is usually followed by a capping reaction to convert the potential remaining free amines, which were not successfully coupled, to unreactive species such as acetyl amide group. The rest of the synthesis will then consist in repeating the sequence deprotection/coupling/capping until the desired peptide sequence **3-70** is synthesised. In the last step, the peptide is cleaved from the resin, and the desired peptide **3-71** is recovered.

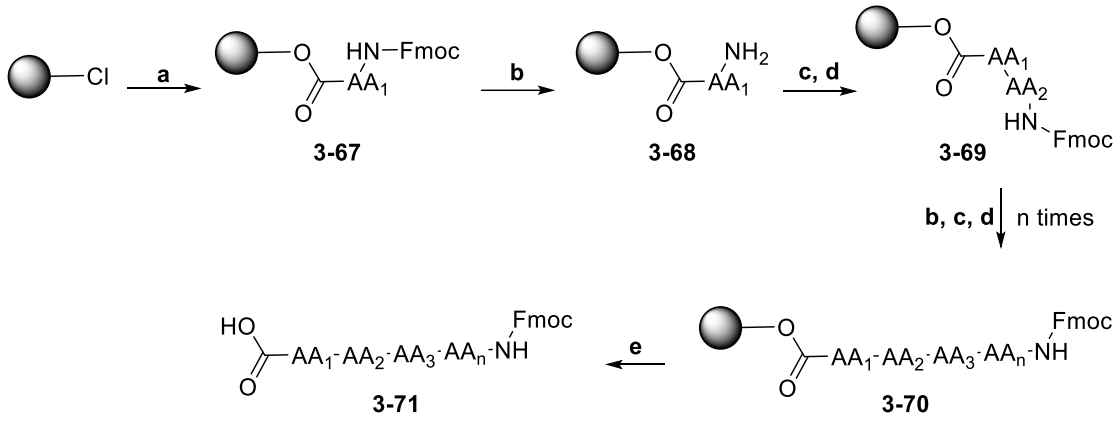

Reagents: a. Fmoc-NH-AA_1-OH, DIPEA, DMF; **b.** piperidine, DMF; **c.** Fmoc-AA_n-OH, HATU, DIPEA, DMF; **d.** Ac_2O, piperidine; **e.** TFA, DMF

Scheme 3.23: General Solid Phase Peptide Synthesis using a Fmoc strategy.

This type of synthesis offers several advantages over solution phase synthesis. As mentioned, no purification is needed after coupling as washing remove unreacted reagents and resulting by-products. Moreover, there is a repetition of simple steps. Therefore the synthetic process can be automated, and long peptide sequences can be obtained rapidly. On the other hand, the success of intermediary steps is difficult to control. Additionally, resins have a limited loading permitted (usually 0.8-1.8 mmol/g). In extended peptide synthesis of high molecular weight this limitation has a low impact but for the small molecules more significant amount of resin is required, and the synthesis can be more expensive than solution phase.

Turning to our synthesis, we decided to use a hydroxylamine resin and attach it to the side chain to directly obtain the desired hydroxamic acid after cleavage (Scheme 3.24).

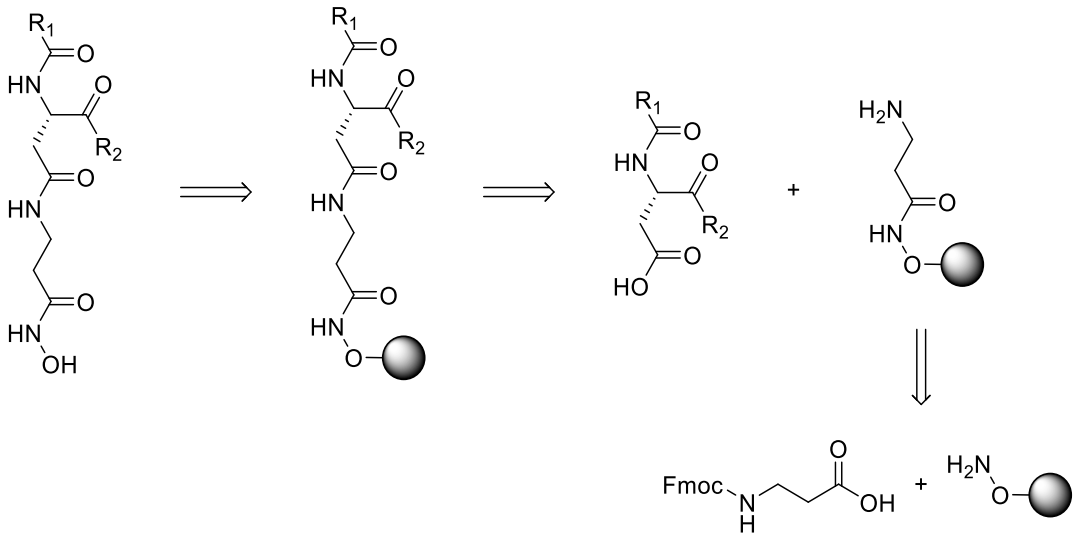

Scheme 3.24: Retrosynthesis of the Aspartic acid scaffold.

Firstly, we had to prepare the resin we were going to use. Our idea was to use a Fmoc strategy, meaning the N-terminal part of the intermediate would be Fmoc protected. As Fmoc protecting group are removed in basic conditions (Scheme 3.25) this approach required to use a resin which would be stable in these conditions and could be selectively cleaved in the last stage of the synthesis.

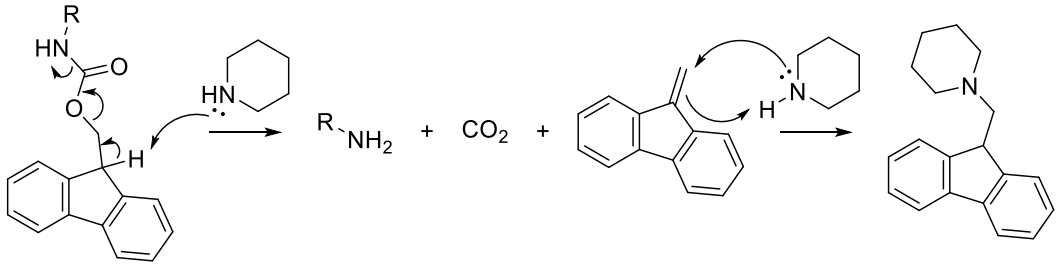

Scheme 3.25: Mechanism of Fmoc deprotection with piperidine.

We chose a 2-chlorotrityl chloride polymer which could be rapidly cleaved by TFA in DCM and presented a high loading (1.3 mmol/g). Following a reported procedure,[426] hydroxylamine was protected using Fmoc chloride in the presence of a carbonate base in 86% yield. Then 2-chlorotrityl chloride polystyrene resin **3-73** was swelled in DCM. Afterwards, Fmoc protected hydroxylamine **3-72,** and DIPEA were added, and the mixture was shaken for 48 hours to form a

Fmoc-hydroxylamine resin **3-74**. The resin was finally capped by washing with MeOH to eliminate unreacted chloride.

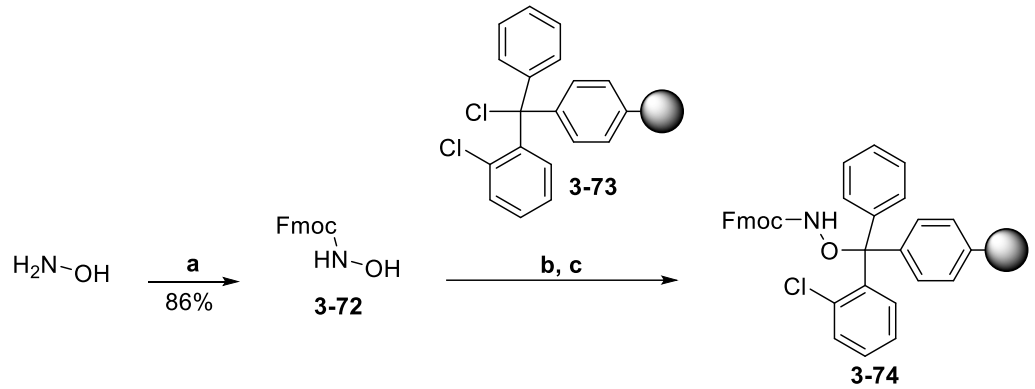

Reagents & Conditions: a. Fmoc-Cl (1 eq), $NaHCO_3$ (2.2 eq), EtOAc, rt, 4 h; **b.** 2-Chlorotrityl chloride polystirene resin **3-73**, DIPEA (2 eq), DCM, rt, 48 h; **c.** MeOH, rt, 15 min

Scheme 3.26: Preparation of Fmoc-hydroxylamine resin 3-74.

In parallel, we worked on the aspartic acid synthons (Scheme 3.27). Starting from Fmoc-L-Asp(OtBu)-OH, activation by HATU followed by addition of benzylamine led to the amide **3-75** in 98% yield. The tert-butyl ester was then rapidly hydrolysed with TFA to afford carboxylic acid **3-76** in 98% yield.

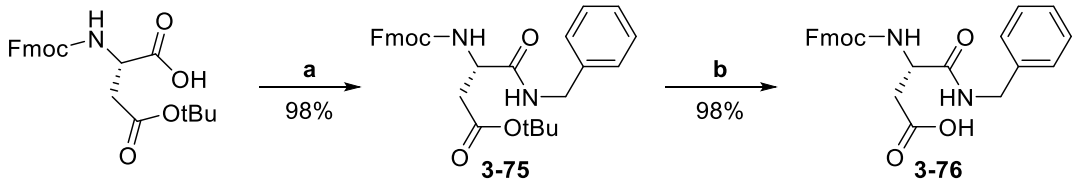

Reagents & Conditions: a. Benzylamine (1.1 eq), HATU (1.1 eq), DIPEA (4 eq), DCM, rt, 4 h; **b.** TFA, DCM, rt, 2 h

Scheme 3.27: Synthesis of 3-76.

This paragraph presents the results obtained by Ludmilla Sturm and Karolina Sliwa, two undergraduate students that I supervised during their placement in Ganesan group. The resin **3-74** was first deprotected with piperidine in DMF, and then coupled to Fmoc-β-Alanine with HBTU and HOBt additive to get **3-77 (**Scheme 3.28**)**. To improve the coupling, this step was repeated before reacting with acetic anhydride to cap the potentially remaining free amine. Then the resin was once again deprotected, coupled twice with aspartic acid **3-76**, still with HBTU and HOBt, and capped to get **3-78**. Following the same sequence, reaction with cinnamoyl chloride led to dipeptide **3-79.** Finally, the resin was cleaved with TFA. However, residue from the cleavage was a mixture, and after purification by flash chromatography, no desired compound was recovered.

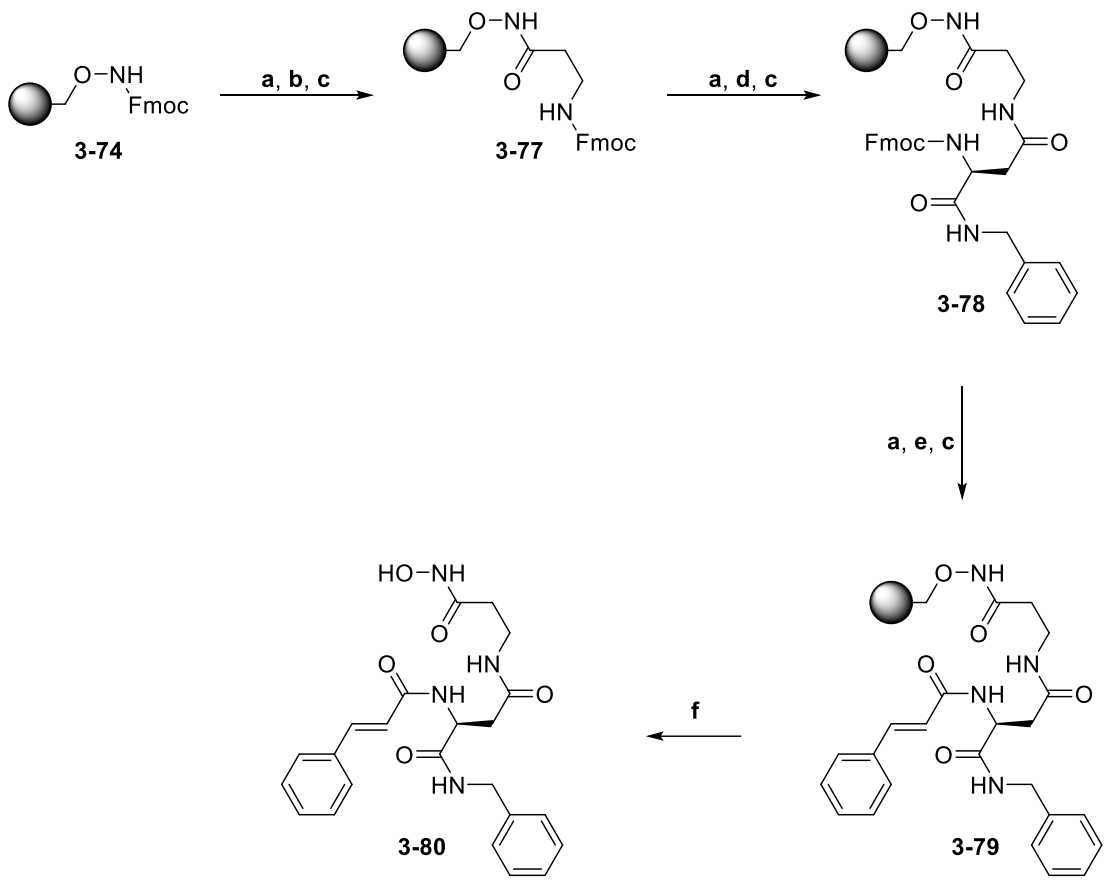

Reagents & Conditions: a. Piperidine, DMF, rt, 20 min; **b.** Fmoc-β-Ala-OH (3 eq), HBTU (3 eq), HOBt (3 eq), DIPEA (6 eq), DMF, rt, 4 h; **c.** Ac_2O / pyridine 1:9, rt, 20 min; **d. 3-76** (3 eq), HBTU (3 eq), HOBt (3 eq), DIPEA (6 eq), DMF, rt, 4 h; **e.** cinnamoyl chloride (3 eq), DIPEA (4 eq), DMF, rt, 16 h; **f.** TFA, DCM, rt, 2 h

Scheme 3.28: Solid phase synthesis of 3-80.

As mentioned earlier, one of the difficulties of solid phase synthesis is to monitor the success of each step. Qualitative methods were developed to check the coupling reaction, and in particular, the Kaiser test became the most commonly used procedure. At the end of a coupling step, a small number of beads was recovered, washed with solvent and placed in a test tube. Then a drop of three solutions were added: 5% (wt/vol) ninhydrin in ethanol, phenol (80% wt/vol) in ethanol and 2% (vol/vol) aqueous KCN (0.001 M) in pyridine. The tube was then heated at 100 °C for 5 minutes. Incomplete coupling resulted in the blue colouration of the polymer beads while complete coupling showed no change of colour. This difference is due to the reaction between ninhydrin and primary amine (Scheme 3.29). Ninhydrin firstly loses water molecule to form the ketone **3-81** which then undergoes nucleophilic substitution with a primary amine to give a Schiff base **3-82**. Isomerisation to **3-83** followed by hydrolysis led to the amine **3-85** which then reacted

with a second molecule of **3-81** to afford the imine **3-86** also known as Ruhemann's purple. The observation of blue colour in the Kaiser test thus indicates the formation of **3-86** and, by extension, confirms the presence of remaining free amine.

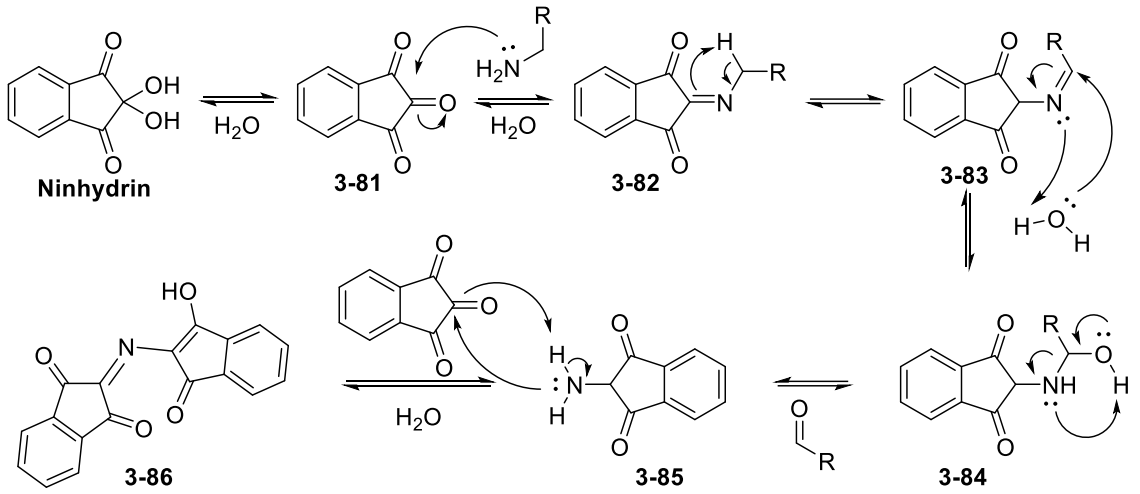

Scheme 3.29: Kaiser test mechanism.

Although this procedure was used in our synthesis, it is only a qualitative test that monitors the coupling step. Insufficient loading during the synthesis of the resin, incomplete Fmoc deprotection, and defective capping can all be reasons for reduced yield and formation of a side product. An alternative for monitoring the synthesis would be to take a sample of the resin after each coupling, cleave it and analyse the residue by LCMS. However, this approach wasn't practical due to a technical issue on our instrument. Besides, as only a limited amount of material can be loaded on the resin, it is usually necessary to optimise each step to ensure almost quantitative coupling. After a few attempts that gave unsatisfactory and irregular results, we opted for another approach.

Since parallel work was already involving solution phase reactions, we decided to switch to a full solution synthesis. Moreover, one drawback of this pathway was the early formation of amide **3-75** from aspartic acid. This position was important as it could also be used as a diverging step in the elaboration of the future library. Thus, we decided to modify the synthetic route to perform this reaction at a later stage.

Starting from the same Fmoc-L-Asp(OtBu)-OH, we opted to convert the C-terminal carboxylic acid to allyl ester. The allyl group was chosen as a protecting group of the carboxylic acid to be selectively deprotected on a later stage of the synthesis in orthogonal conditions to basic Fmoc deprotection and acidic tert-butyl cleavage. Compound **3-87** was isolated in 97% yield after reaction with allyl bromide (Scheme 3.30).

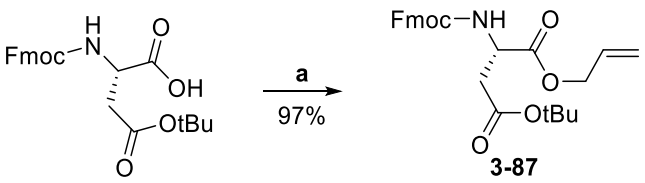

Reagents & Conditions: a. Allyl bromide (10 eq), DIPEA (2 eq), reflux, 1 h

Scheme 3.30: Synthesis of allyl ester 3-87.

Similarly to the previous route, tert-butyl ester on the side chain was then hydrolysed with TFA to afford **3-88** in 79% yield (Scheme 3.31). The newly synthesised carboxylic acid side chain was then coupled with β-alanine ethyl ester with HATU and DIPEA to get compound **4-89** in 81% yield.

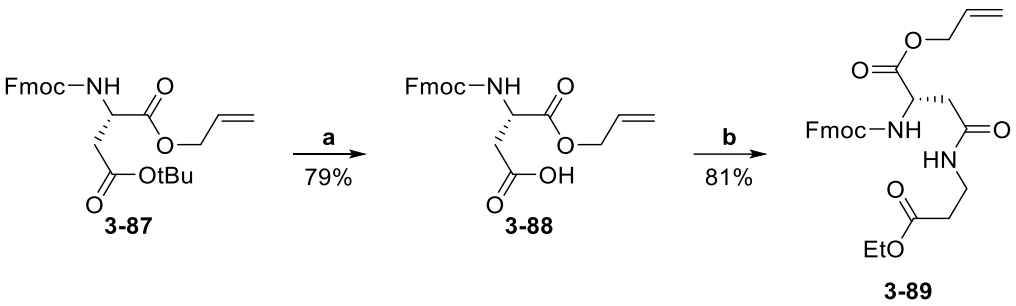

Reagents & Conditions: a. TFA (10 eq), DCM, rt, 2 h; **b.** HATU (1.1 eq), DIPEA (4 eq), β-Ala-OEt.HCl (1.1 eq), DCM, rt, 4 h

Scheme 3.31: Synthesis of 3-89.

The rest of the synthesis, until **3-94**, was investigated with the help of Angus Yuen, another undergraduate student that I supervised during his research project in the Ganesan group. The allyl group was firstly removed with palladium(0). This reaction could be carried in mild conditions with $Pd(Ph_3)_4$ as a source of palladium, and additional phenylsilane is acting as a scavenger of the reaction.[427] Free carboxylic acid **3-90** was obtained in 58% yield and then coupled to benzylamine to give **3-91** in 76% yield (Scheme 3.32).

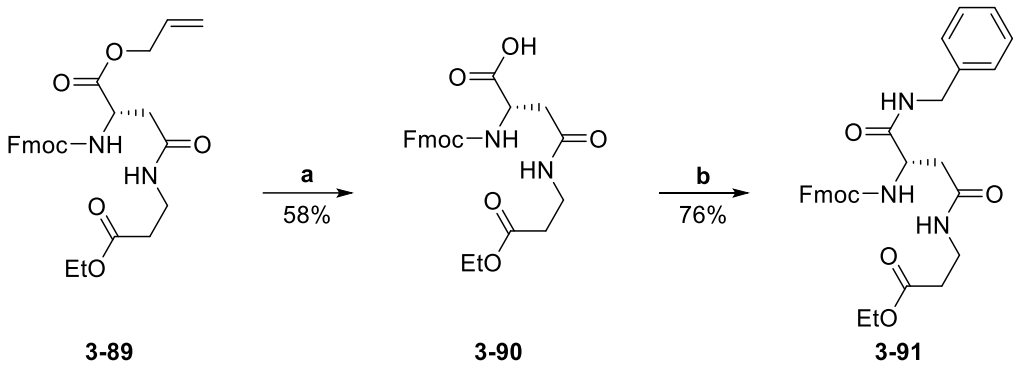

Reagents & Conditions: a. Phenylsilane (1 eq), $Pd(PPh_3)_4$ (0.05 eq), DCM, rt, 16 h: **b.** EDC (1.2 eq), $HOBt.H_2O$ (1.2 eq), DIPEA (1.1 eq), Benzylamine (1.1 eq), DCM, rt, 16 h

Scheme 3.32. Synthesis of 3-91.

Following this step, the N-terminal Fmoc protecting group was cleaved with diethylamine to give the free amine **3-92** in 44% yield (Scheme 3.33). Then reaction with cinnamoyl chloride, in the presence of Et_3N, led to the isolation of cinnamyl compound **3-93** in 26% yield.

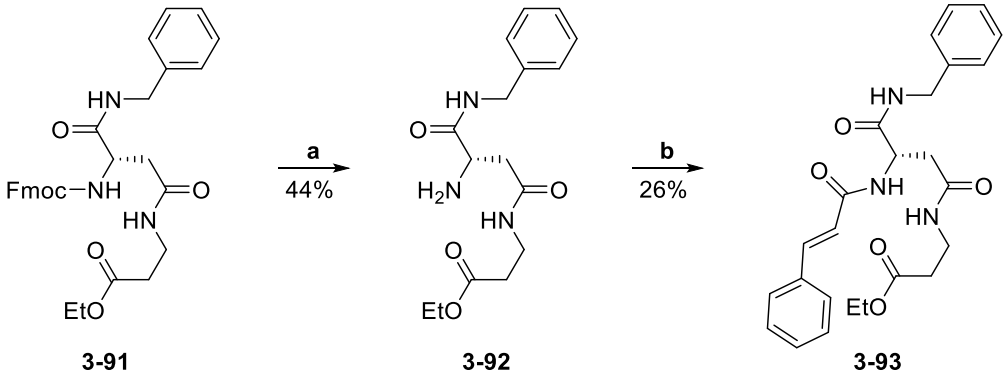

Reagents & Conditions: a. Diethylamine (22 eq), DCM, rt, 16 h; **b.** Cinnamoyl chloride (1 eq), Et_3N (5 eq), DCM, rt, 1h

Scheme 3.33: Synthesis of 3-93.

In the last step, we tried to convert the ethyl ester to hydroxamic acid with hydroxylamine and a catalytic amount of potassium cyanide (Scheme 3.34). However, this reaction did not work as expected. After several hours of reaction, a TLC control showed a mixture of starting material and a second product. As the reaction was made on a small scale, we tried to push the reaction toward completion. Keeping the stirring longer showed no apparent evolution so more reagent was added to the mixture and the reaction mixture was left stirring overnight. New monitoring by TLC indicated the formation of several new compounds and no desired compound was isolated.

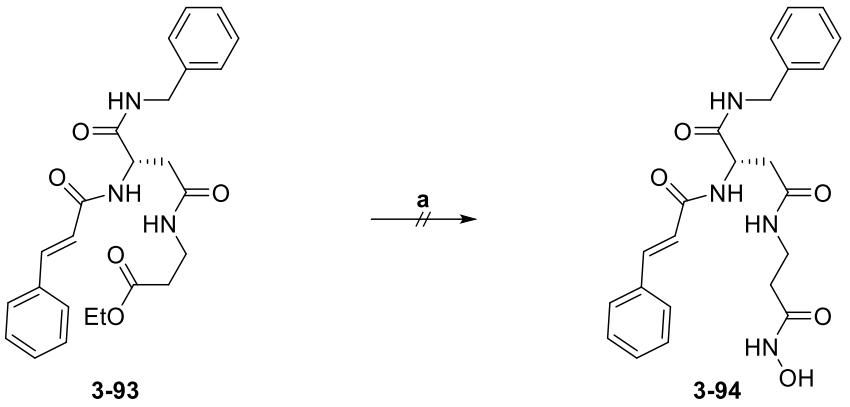

3-93 **3-94**

Reagents & Conditions: a. KCN (0.5 eq), aqueous NH_2OH/THF/MeOH 0.5:1:1, rt, 16 h

Scheme 3.34: Attempt to synthesise 3-94.

Due to the lack of remaining intermediate **3-93** and time constraints, the reaction could not be repeated. Despite this unsuccessful last step conversion, we still believe that this synthetic route is viable with proper optimisation of the reaction conditions.

Although this could prove to be fruitful, we looked for a potential alternative. Firstly, we could opt for an indirect conversion with a primary ethyl ester hydrolysis followed by activation of carboxylic acid and reaction with hydroxylamine. Naturally, the main drawback of this adjustment would be to add a step to the synthesis.

Another possibility would be to switch the steps in order to introduce the hydroxamic acid earlier in the synthesis such as on intermediate **3-91**. Notwithstanding optimisation of reactions may be needed. Indeed, hydroxylamine is a weak base, and Chang and coworkers[428] reported that Fmoc deprotection of amino acid could be slowly achieved .

Alternatively, the most interesting modification could be to directly couple a β-alanine hydroxamic acid with the intermediate **3-88**. This side chain was successfully synthesised starting from commercially available Boc-β-alanine (Scheme 3.35). According to a published procedure,[429] the free carboxylic acid was first activated with CDI and a solution of hydroxylamine was added to give the Boc-β-alanine hydroxamic acid **3-95**. Low yield of the reaction could be due to the high solubility of the product in aqueous solution, and the reaction would need optimisation.

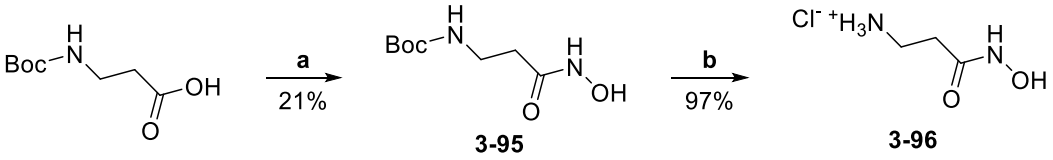

Reagents & Conditions: a. CDI (1 eq), $NH_2OH.HCl$ (1 eq), THF, rt, 16 h; **b.** HCl 1M in EtOAc, rt, 16 h

Scheme 3.35: Synthesis of β-alanine hydroxamic acid 3-96.

By using ^1H NMR a shifting of proton signal on the α-position from carbonyl confirmed the successful conversion from carboxylic acid to hydroxamic acid (Figure 3.3).

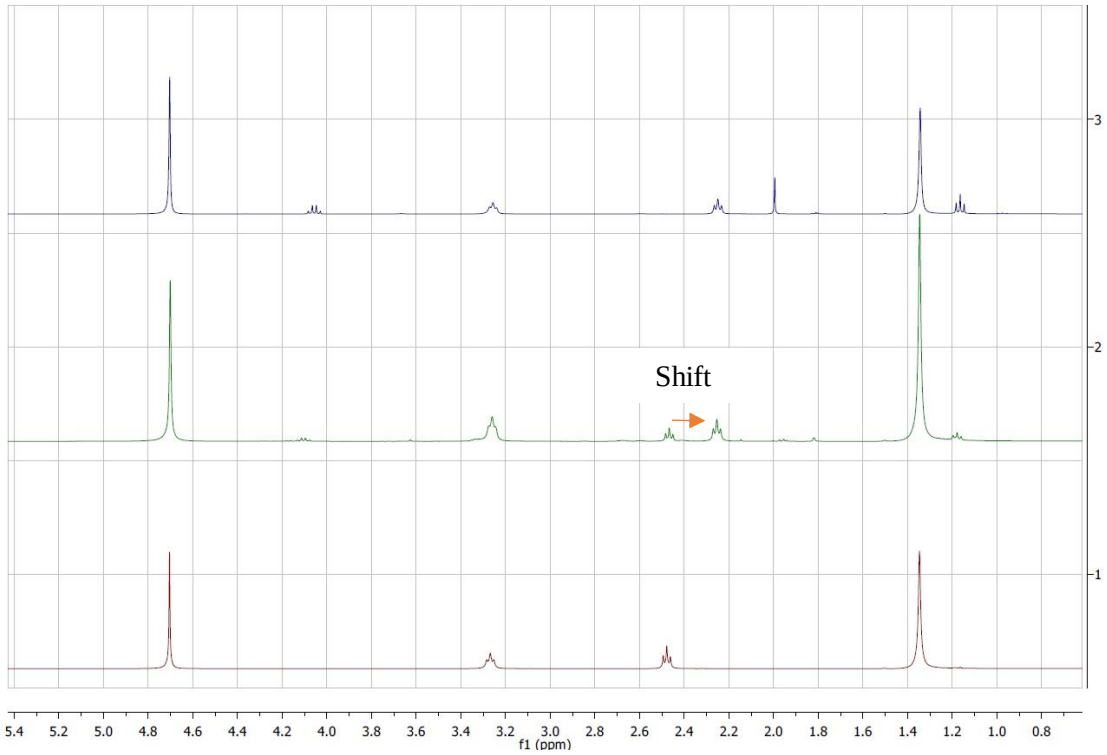

Figure 3.3: ^1H NMR spectrum of formation of Boc-β-Ala-NH_2OH 3-95.
Starting material (red), incomplete reaction (green), product 3-105 (blue)

In the second step, the *N*-(tert-butoxycarbonyl) group of **3-95** was cleaved under acidic conditions using a solution of HCl in EtOAc to give the β-alanine hydroxamic acid hydrochloric salt **3-96** in 97% yield.

2.3 Third scaffold: triazole-based inhibitors

The copper-catalyzed azide-alkyne cycloaddition, also known as 1,4-CuAAC or click chemistry is a powerful reaction developed by Sharpless and Fokin,[430] which allows the formation of a

triazole from azide and alkyne (Scheme 3.36). Improving the 1,3-dipolar cycloaddition previously developed by Huisgen,[431] this process has enormous scope and has been extensively used.

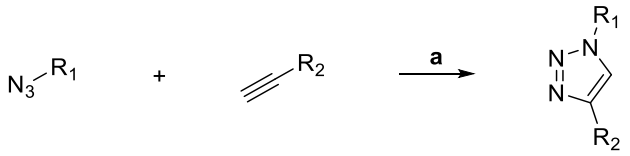

Reagents & Conditions: a. Cu(II), sodium ascorbate, tBuOH/H_2O, rt

Scheme 3.36: General 1,4-CuAAC reaction.

The main advantage of this reaction, besides compatibility with most functional groups, is the fast synthesis of a regioselective 1,4-triazole in mild conditions. This selectivity is explained by the mechanism of the reaction. Nonetheless, it is worth noting that several mechanisms can be found in the literature.

A standard version refers to the one proposed by Sharpless and Fokin and involves mono-nuclear copper(I) intermediate (Scheme 3.37). In a first step, the interaction between the copper and the acetylene leads to the formation of copper(I) acetylide **3-97**. Then, coordination between the copper and the azide forms the intermediate **3-98**, which undergoes intramolecular cyclization to give a 6-membered copper-containing compound **3-99**. The cycle then proceeds via internal rearrangement to form the triazole **3-100** and is finally protonated to afford the 1,4-disubstituted triazole **3-101**.

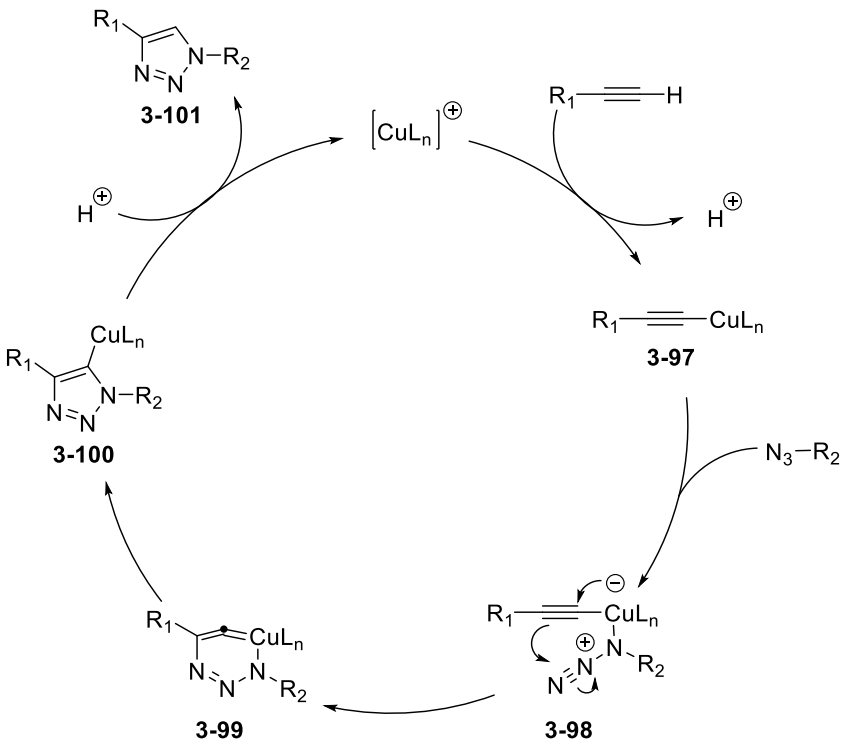

Scheme 3.37: CuAAC mechanism proposed by Sharpless and Fokin.[430]

Although this mechanism can still be found, Fokin and coworkers proposed an alternative version in 2013 that was more consistent with the latest results.[432] Using several sources of copper, with different isotopic composition, they showed that dinuclear copper(I) intermediate had to be involved to fit their experimental results and the mechanism was then modified as shown below (Scheme 3.38). Notably, the previously proposed 6-membered ring intermediate **3-99** was replaced by a new transitional compound **3-105** involving two copper atoms.

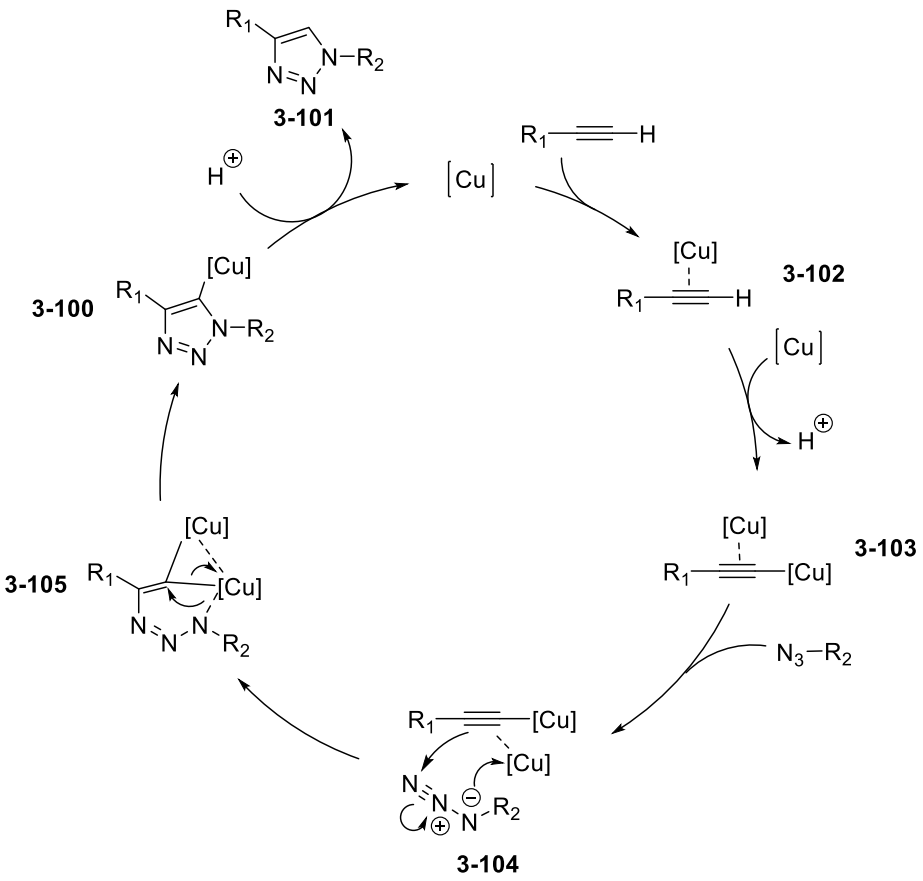

Scheme 3.38: CuAAC mechanism revised by Fokin.[432]

To the author's knowledge, the most recent studies showed that both mechanisms are actually involved in the CuAAC reaction (Scheme 3.39). Indeed, Bertrand reported in 2015 the successful isolation of key intermediates **3-97** and **3-100** (R_1 = phenyl, R_2 = benzyl, L = cyclic (alkyl)(amino)carbenes) showing that mononuclear copper catalysis was happening.[433] Additionally, intermediates **3-106** and **3-107** were isolated (X = TfO), proving the reaction was also proceeding through the dinuclear copper cycle. However, the latter catalytic cycle was kinetically favoured and therefore matched with Fokin's results.

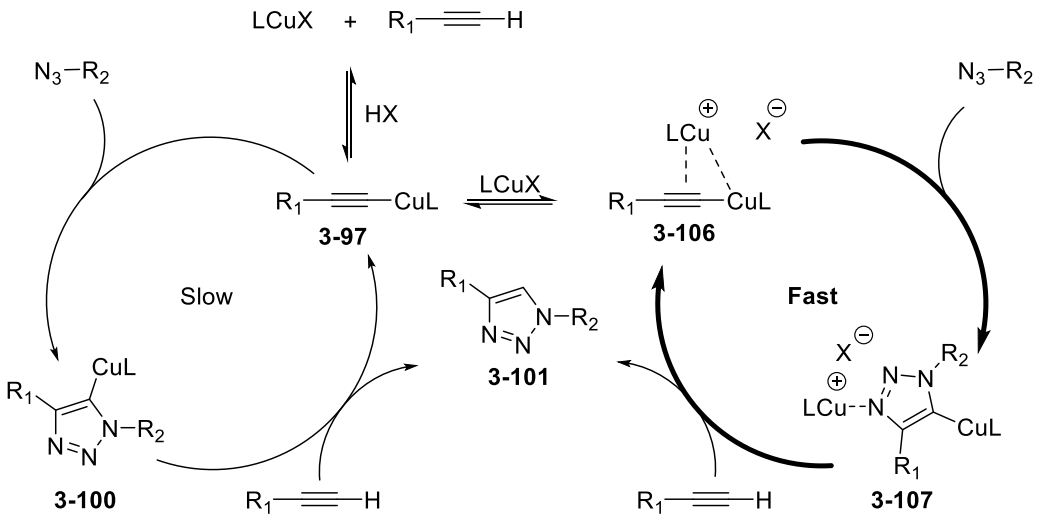

Scheme 3.39: CuAAC mechanism revised by Bertrand.[433]

With a simple and efficient method to synthesise triazoles with regioselective control, medicinal chemists naturally became interested in taking benefits of this reaction. In the field of HDAC inhibitors, several groups studied the possibility to design dual target compounds. Indeed, by introducing an acetylene or azide group on the extremity of a molecule of interest, biologically active and potent against any target, it became possible to quickly couple this compound with a chain bearing a hydroxamic acid to add a potential effect on HDAC. This strategy was successfully applied to conjugate HDAC inhibition with a variety of targets such as topoisomerase,[434,435] antibiotics,[436] cyclooxygenase,[437] protein kinase,[438] or estrogen receptor modulators.[439]

Although exciting results were obtained, this approach generally considered triazole as a linker between a complex compound and a simple alkyl zinc binding group. In comparison, limited work has been done to design, specifically, HDAC inhibitors and exploit the powerful potential of click chemistry to make a library combining triazole and hydroxamic acid. Thus, we became interested in designing a scaffold based on the triazole.

First and foremost, the synthetic route was depending on the position of the zinc binding group on the triazole. Indeed, linkage to the nitrogen on the 1st position of the triazole would require a precursor bearing the azide group (Scheme 3.40). Conversely, linkage to the carbon on 4th position would need an acetylene group, thus completely changing the synthesis of the precursor.

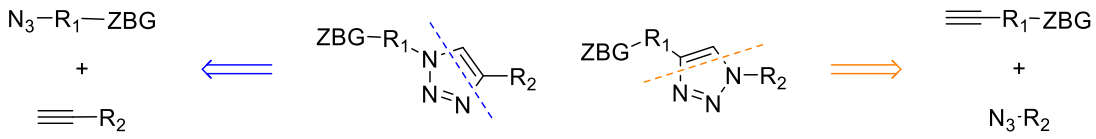

Scheme 3.40: Two possible 1,4-triazole configurations.

Our choice inclined toward the first option with an azide precursor. Several factors motivated this decision. To begin with, the latter option has been more investigated. In particular, several inhibitors were successfully discovered by Wang,[440–442] Jiang,[443] and Suzuki.[344,444,445] Thus, we decided that exploring the other configuration would be of more significant interest. In the second place, Suzuki also showed that reversing the triazole from a C4-bonded zinc binding group to an N1-bonded was slightly improving the potency against HDAC8 but greatly enhancing the selectivity toward class I and class II HDACs (Figure 3.4).[446] Moreover, a library of N-bonded triazole-based HDAC inhibitors was reported to have antimalarial and antileishmanial activity.[305] This work was of particular interest to us as the parasitic diseases were one of the targets at the origin of this project.

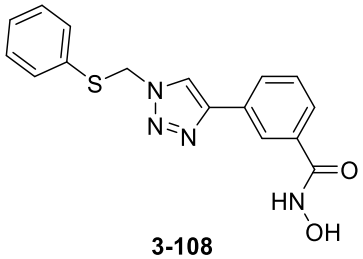

3-108

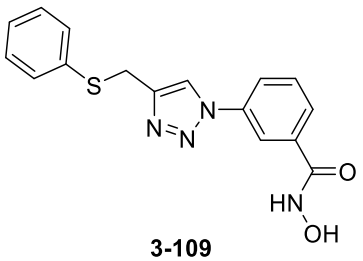

3-109

Compound	IC_{50} (μM)					
	HDAC1	HDAC2	HDAC3	HDAC8	HDAC4	HDAC6
3-108	38	>100	68	0.070	44	2.4
3-109	>100	>100	>100	0.053	>100	2.2

Figure 3.4: Reported HDAC inhibition of C-bonded and N-bonded triazole.[446]

In accordance with the global chemistry of this thesis, we desired to use amino acids in our designed structure, as they are commercially available with a source of chirality and can be converted to hydroxamic acid.

Combining these ideas, we designed our scaffold and a first general synthetic route in which an amino acid would be converted to azide to form the triazole and then the hydroxamic acid (Scheme 3.41).

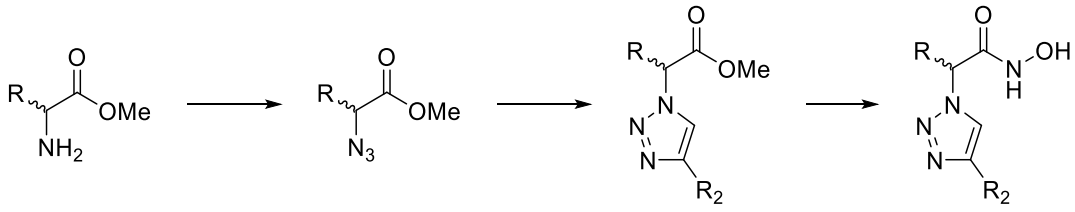

Scheme 3.41: General synthetic pathway to triazole compounds.

In the literature, only one example of the closely related structure was found (Scheme 3.42). Indeed, a series based on a 1,4,5-trisubstituted triazole had been patented in 2014.[447] This library, with an alkyne on the 5th position, was reported to inhibit HDAC8 selectively.

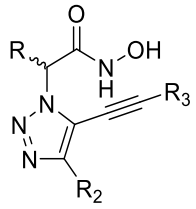

Scheme 3.42: Patented structure of 1,4,5-trisubstituted triazole HDAC inhibitors.[447]

Although limited data were published, one crucial piece of information was extracted from this patent. To build their SAR four different amino-acid were used on the 1st position of the triazole. Natural phenylalanine, tryptophan and valine, as well as the non-natural phenyl glycine, were investigated, and the authors suggested that best results were obtained with phenylalanine.

These results, also limited, validated our decision to investigate this scaffold. Moreover, we decided to use phenylalanine as a starting material. Finally, this also led us to consider a future modification of the structure to study a 1,4,5-trisubstituted triazole.

Turning our attention to the synthesis, the first step consisted in converting the commercial L-phenylalanine methyl ester to the corresponding azide-phenylalanine methyl ester. In 1972 Cavender and coworkers published the first method to convert alkyl amine to alkyl azide using trifluoromethanesulfonyl azide (TfN_3).[448] This method presented two main drawbacks. Firstly, the preparation of triflyl azide from sodium azide and triflic anhydride required a biphasic mixture of water and DCM, but triflic anhydride tends to be hydrolysed. Thus, a large excess of reagent was necessary. Secondly, the use of DCM, containing the freshly formed TfN_3, could face a solubility problem with primary amine during the azide transfer. Additionally, it is important to note that isolated triflic azide, as many azide salts, is known to be energetic materials that are sensitive to shock and friction and potentially explosive.[449] Therefore, they have to be kept in solution.

The Wong group improved this method by using a mixture of H_2O/MeOH/DCM as a solvent for the diazo transfer reaction and by adding a metal catalyst such as copper(II) sulfate or zinc(II) chloride.[450,451] Interestingly the reaction with chiral amine occurs with retention of configuration. The mechanism was proposed by Wong and has been recently confirmed (Scheme 3.43).[452] In the first step, copper(II) interacts with the amine to give **3-110**. Nucleophilic attack of the amine on the electrophilic terminal nitrogen of the azide leads to the formation of the tetrazene **3-111** which then cyclized to a more stable five-member copper containing complex **3-112**. Internal rearrangement then releases the product of diazo transfer **3-113** and copper-imido complex **3-114**.

Finally, complex **3-110** is regenerated. As the C-N bond from the primary amine remains intact during the diazo transfer cycle, the reaction is not subject to epimerization.

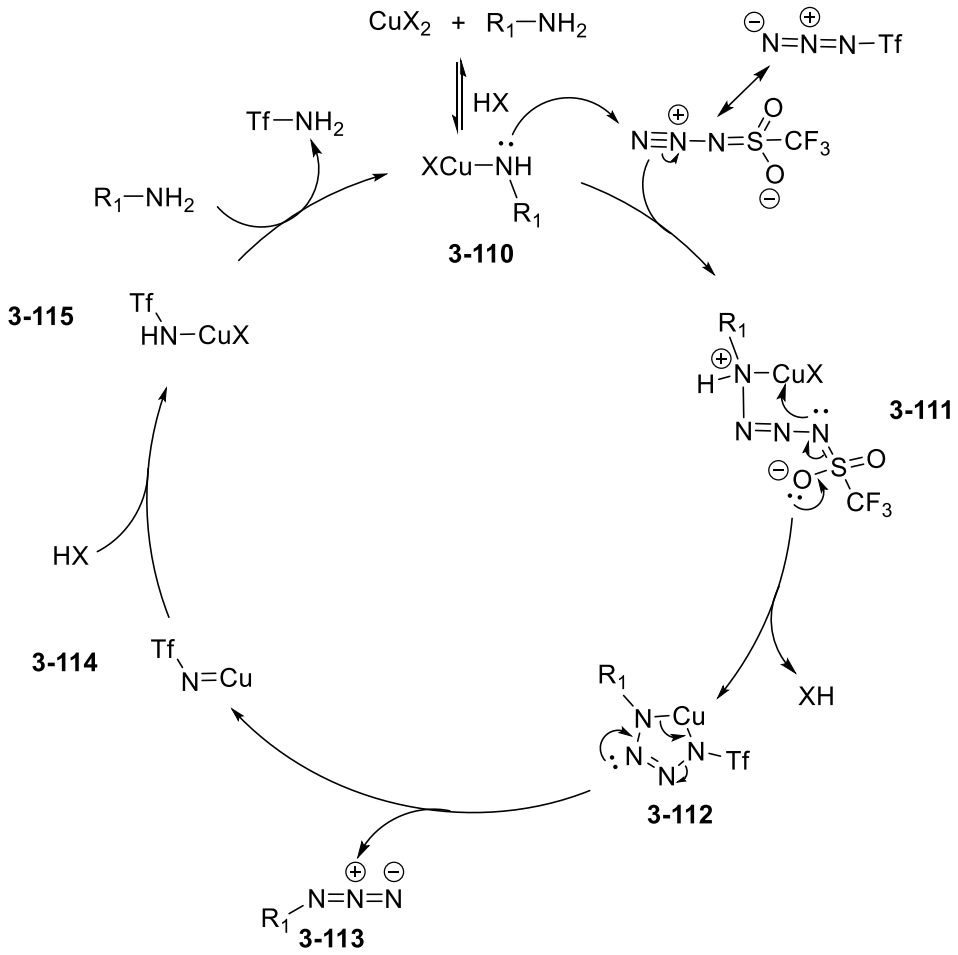

Scheme 3.43: Plausible mechanism of copper-catalysed diazo transfer reaction.[452]

Based on this work, Yan and coworkers further optimised the reaction by switching to a single solvent of reaction, with either acetonitrile or pyridine, thus preventing hydrolysis of triflic anhydride, reducing the amount of reagent needed and avoiding solubility issues.[453]

2.3.i Focus on 1,4-disubstituted triazole

With this established methodology, we could focus on the synthesis. Accordingly, triflic azide was prepared by reaction of sodium azide and triflic anhydride at 0 °C in acetonitrile for two hours (Scheme 3.44). The freshly prepared solution was then added to L-phenylalanine methyl ester, in the presence of Et_3N and a catalytic amount of $CuSO_4$, to form the corresponding azide **3-116** in 50% yield. Following this step, reaction with phenylacetylene under CuAAC conditions led to the formation of the triazole **3-117** in 98% yield.

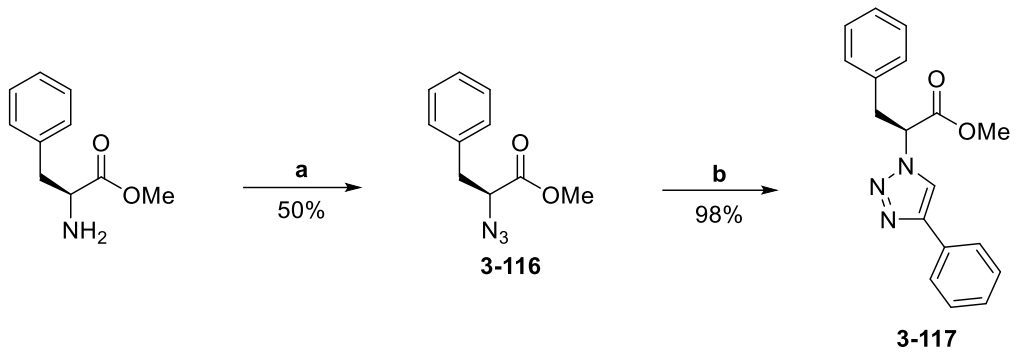

Reagents & Conditions: a. NaN_3 (1.4 eq), Tf_2O (1.2 eq), $CuSO_4$ (0.01 eq), Et_3N (2 eq), MeCN, 0°C -> rt, 16 h; **b.** Phenylacetylene (1.2 eq), $CuSO_4.5\ H_2O$ (0.01 eq), sodium ascorbate (0.1 eq), H_2O/t-BuOH 2:1, rt, 16 h

Scheme 3.44: Synthesis of 1,4 disubstituted triazole 3-117.

Subsequently, the methyl ester was hydrolysed to carboxylic acid **3-118** with hydrochloric acid at 70 °C in 97% yield, followed by activation with CDI and conversion to hydroxamic acid **3-119 (**Scheme 3.45**)**.

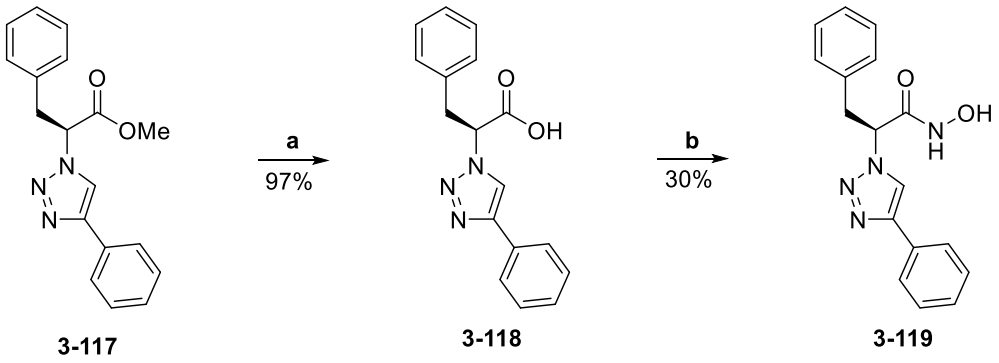

Reagents & Conditions: a. HCl (6M), 70 °C, 16 h; **b.** CDI (1.2 eq), $NH_2OH.HCl$ (2 eq), THF, rt, 2 d

Scheme 3.45: Synthesis of 3-119.

This synthetic pathway successfully led to the procurement of the final compound **3-119**. However, the last step was incomplete even after two days, and the purification was difficult. Thus, we decided to change the order of the steps and introduce a protected hydroxamic acid earlier in the synthesis. We also decided to start the synthesis directly from unprotected L-phenylalanine to avoid the additional hydrolysis.

Consequently, L-phenylalanine was converted to azido-L-phenylalanine under the same conditions in 79% yield (Scheme 3.46).

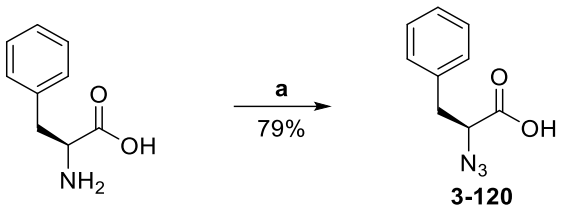

3-120

Reagents & Conditions: a. NaN_3 (1.4 eq), Tf_2O (1.2 eq), $CuSO_4$ (0.01 eq), Et_3N (2 eq), MeCN, 0°C -> rt, 16 h

Scheme 3.46: Synthesis of azido-L-Phe-OH 3-120.

Alternatively, synthesis of some α-azido acids had been recently reported using different conditions.[454] We decided to compare the methods (Table 3.3), but similar results were obtained. Importantly the control of the temperature during the preparation of the triflyl azide was found to be crucial for the reaction. When the temperature was not properly maintained at 0 °C during the addition of triflic anhydride on sodium azide or during the reaction, decomposition was observed with the reaction mixture turning dark brown, and resulted in low yield or unsuccessful amine-azide conversion.

Try	Methods	
	TfN_3 1.2 eq, $CuSO_4$ 1% eq, Et_3N 2 eq, MeCN	TfN_3 1.2 eq, $CuSO_4$•$5H_2O$ 1% eq, K_2CO_3 2.7 eq, MeOH/MeCN/H_2O 5/2/1
Try 1	77%	81%
Try 2	79%	70%
Try 3		87%

Table 3.3: Isolated yield of diazo transfer reaction in two conditions.

Intermediate **3-120** was activated with CDI and then coupled with *O*-benzylhydroxyl amine to give **3-121** in 71% yield. Then, the azide underwent the CuAAC reaction to afford 1,4-disubstituted triazole (Scheme 3.47).

Several groups were introduced to the 4th position. Firstly, we decided to evaluate the impact of the substituent on the phenyl ring and analogues were synthesised with a modification on the para position. The hydrogen on the para position was respectively substituted by fluorine (**3-122)**, highly electronegative atom of similar size, a methoxy group (**3-123)** possessing an electron-donating mesomeric effect and a trifluoromethyl group having an electron-withdrawing effect (**3-124**). Secondly, we also decided to look at the role of the aromatic ring in the structure. We chose to substitute it with a smaller non-aromatic cycle and synthesised the cyclopropyl analogue **3-**

125. This part was explored with the help of Alex Chan, an undergraduate student that I supervised during his research project in the Ganesan group, who synthesised compound **3-122**, **3-123** and **3-124**.

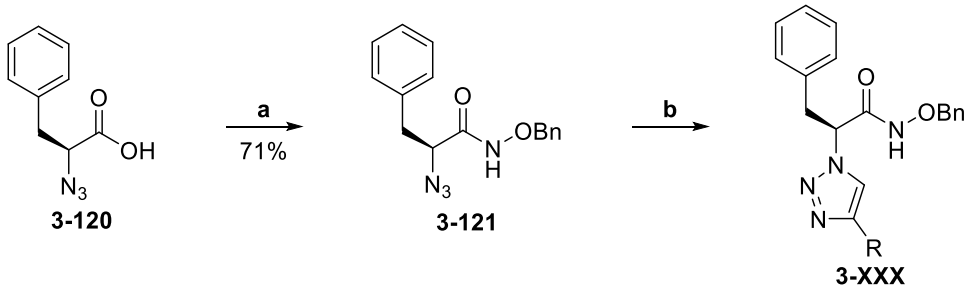

Reagents & Conditions: a. CDI (1.2 eq), $NH_2OBn.HCl$ (2 eq), THF, rt, 16 h; **b.** $CuSO_4.5\ H_2O$ (0.01 eq), sodium ascorbate (0.1 eq), acetylene (1.2 eq), H_2O/t-BuOH 2:1, rt, 16 h

R group	Compound	Yield
4-fluorophenyl	**3-122**	65%
4-methoxyphenyl	**3-123**	76%
4-(trifluoromethyl)phenyl	**3-124**	64%
cyclopropyl	**3-125**	59%

Scheme 3.47: Synthesis of 1,4 disubstituted triazole compound.

The final step of the synthesis consisted of the *O*-benzyl deprotection to obtain the free hydroxamic acid. A typical procedure involves the use of palladium on charcoal under hydrogen atmosphere to reduce the oxygen-carbon bond. However, this hydrogenation turned out to be substrate dependent, and the method was unsatisfying (Scheme 3.48). Indeed, the cyclopropyl analogue was only partially reduced after 16 hours of reaction while the other compounds were not reacting. In our opinion, the primary explanation for the unsuccessful reduction came from the conditions of reaction that involved low and uncontrolled pressure of hydrogen in the flask. Due to the lack of a hydrogenation lab and specific equipment, it was impossible to perform the reaction at higher pressure safely, so we looked for another deprotective method. Our choice inclined toward the use of boron trichloride commonly used method for ether debenzylation which had also been reported to be successful for *O*-benzyl hydroxamic acid deprotection.[455,456]

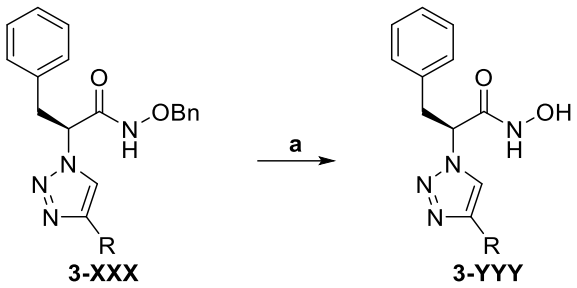

Reagents & Conditions: a. H_2 (1 atm), Pd/C (0.01 eq), MeOH, rt, 16 h

R group	Compound	Product	Yield
4-fluorophenyl	**3-122**	**3-126**	-
4-methoxyphenyl	**3-123**	**3-127**	-
4-(trifluoromethyl)phenyl	**3-124**	**3-128**	-
cyclopropyl	**3-125**	**3-129**	35%

Scheme 3.48: Hydrogenation of protected triazole.

A proposed mechanism frequently found in the literature is shown below (Scheme 3.49). In a first step interaction between the lone pair of the oxygen and the boron forms the zwitterion **3-130**. Halide migration releases benzyl halide and forms the dibromo(organo)borane **3-131**. Over aqueous workup, the intermediate is then hydrolysed to afford the hydroxyl group. However, recent computational studies suggest that this mechanism, and especially the migration of halogen, is too thermodynamically unfavourable to occur, and a bimolecular pathway is likely involved with an interaction between two molecules of complex **3-130**.[457,458]

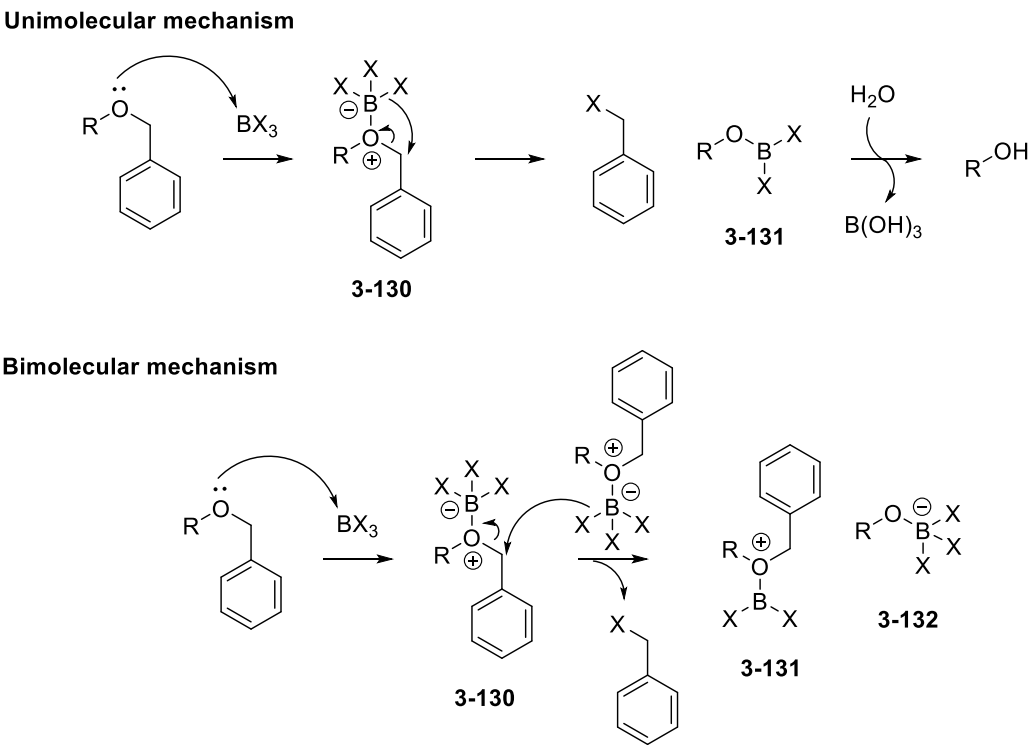

Scheme 3.49: Proposed unimolecular and bimolecular mechanism for BX_3-ether cleavage.[458]

Ergo, slow addition of BCl_3 at -78 °C in DCM proved to be a fast and successful method for the deprotection of our triazoles (Scheme 3.50). Compounds **3-126**, **3-127** and **3-128** were also synthesised by Alex Chan.

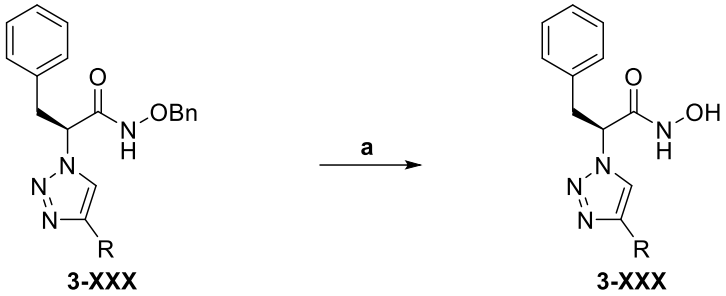

Reagents & Conditions: a. BCl_3 (1 M in DCM, 3 eq), DCM, -78 °C, 45 min

R group	Compound	Product	Yield
4-fluorophenyl	**3-122**	**3-126**	53%
4-methoxyphenyl	**3-123**	**3-127**	53%
4-(trifluoromethyl)phenyl	**3-124**	**3-128**	58%
cyclopropyl	**3-125**	**3-129**	49%

Scheme 3.50: Deprotection of triazole with BCl_3 to get final compounds.

Alternatively, we also tried to form the triazole in the presence of non-protected hydroxamic acid. Azide-L-Phe-NH_2OBn intermediate **3-121** was deprotected using BCl_3 in 89% yield, and the resulting azido-phenylalanine hydroxamic acid **3-133** was put in reaction with phenylacetylene under CuAAC conditions, but no reaction was observed (Scheme 3.51).

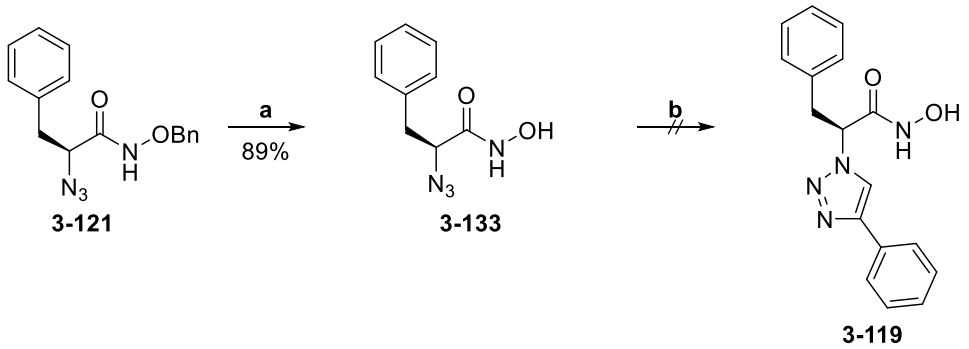

Reagents & Conditions: a. BCl_3 (1 M in DCM, 3 eq), DCM, -78 °C, 45 min; **b.** $CuSO_4$.5 H_2O (0.01 eq), sodium ascorbate (0.1 eq), phenylacetylene (1.2 eq), H_2O/t-BuOH 2:1, rt, 16 h

Scheme 3.51: Attempt to form triazole from unprotected hydroxamic acid 3-133.

Checking the literature, we found no example of a similar reaction. Although we didn't explore further this pathway, we tried to understand what could prevent the reaction as click chemistry is usually very versatile and reliable. An explanation could come from the high affinity of hydroxamic acid for metal. Indeed, interaction with the copper catalyst could block the catalytic cycle necessary for the CuAAC reaction. Moreover, such coordination could be favoured by the possibility to form a stabilised 6-member ring due to the presence of the azide group (Figure 3.5). Meanwhile, protected hydroxamic acid could adequately react in the click reaction as the presence of the benzyl would decrease the nucleophilicity of the oxygen and impose steric hindrance that could prevent the interaction with the copper.

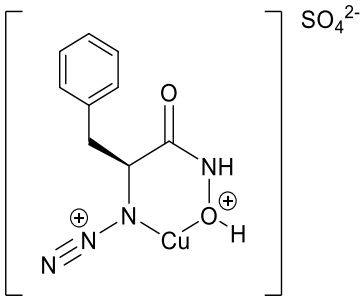

Figure 3.5: Structure of potential copper interaction with 3-133.

2.3.ii Focus on 1,4,5-trisubstituted triazole

Following this first generation of compounds, we decided to investigate a second generation based on 1,4,5-trisubstituted triazole. Several synthetic pathways could be used to form a trisubstituted triazole. A first possibility would be to use a disubstituted alkyne to react with the azide. However, this method has numerous drawbacks. In the CuAAC reaction, region selectivity and rate of reaction depend on the formation of the complex between the copper and the highly reacting terminal alkynyl. However, internal alkynes are less reactive, and the regioselectivity is more challenging to control. Thus, this method was not considered.

A second method would be to introduce the substitution on the 5th position directly from our 1,4-disubstituted triazoles. The main advantage of this method would be to directly use the previously established synthetic route as it would simply add a diverging step. However, this required a C-H activation on the 5th position of the triazole which tends to be difficult. Progress has been made over the last decade to activate this bond with copper or palladium, but these methods usually require high temperature or microwave irradiation.[459,460] More recently, Wei and coworkers reported a one-pot strategy to synthesise trisubstituted triazole, in mild conditions, from azido compound, a terminal alkyne, and an aryl halide by using a mixture of copper and palladium as a catalyst.[461] To explain the higher reactivity achieved with their method, they proposed the following mechanism (Scheme 3.52). The reaction starts with a copper catalytic cycle similar to the CuAAC reaction to form a 1,4 disubstituted triazole-copper complex **3-100**. In parallel, in a second catalytic cycle, oxidative addition of aryl halide on palladium(0) affords **3-134**. Then, complex **3-100** undergoes a transmetalation with the aryl halide-palladium complex **3-134** to get an aryl-palladium-triazole complex **3-136** and regenerate the copper halide. Reductive elimination then renews palladium(0) species and leads to the formation of the desired 1,4,5-trisubstituted triazole **3-137**. Notably, two side products can be produced during the reaction. Complex **3-100** can be protonated to afford the 1,4-disubstituted triazole **3-101** of the CuAAc reaction. Additionally transmetalation between palladium(II) complex **3-134** and copper(I) acetylide **3-97** can form the internal alkyne **3-135**.

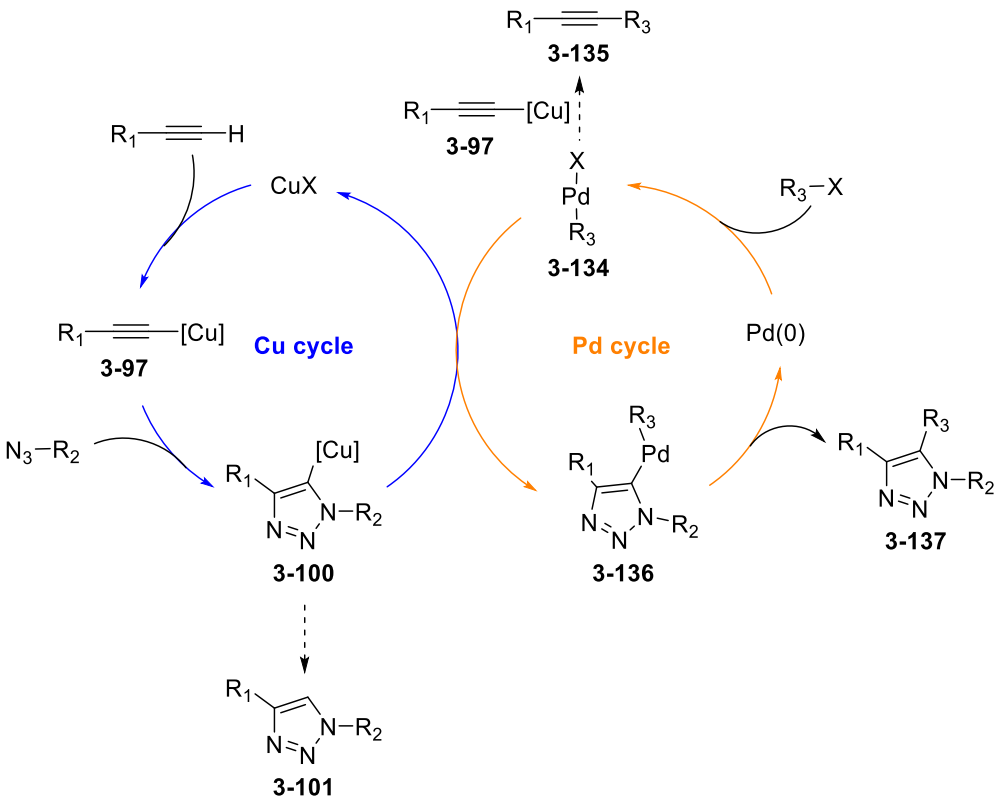

Scheme 3.52: Mechanism of Cu/Pd catalysed triazole formation.[461]

This method was interesting as a large variety of terminal alkyne, and an aryl halide, are commercially available. Therefore, a broad scope of substituents on both 4th and 5th position of the triazole could be explored.

We decided to try the method and set up the reaction between azide-L-phenylalanine methyl ester **3-116**, phenylacetylene, and bromobenzene in the presence of palladium(0) and copper(I) (Scheme 3.53). However, only the 1,4-disubstituted triazole was recovered. This suggested that the transmetalation step did not work, due to either kinetic or potential issues with the palladium. The reaction was repeated with a second batch of palladium, but similar results were observed.

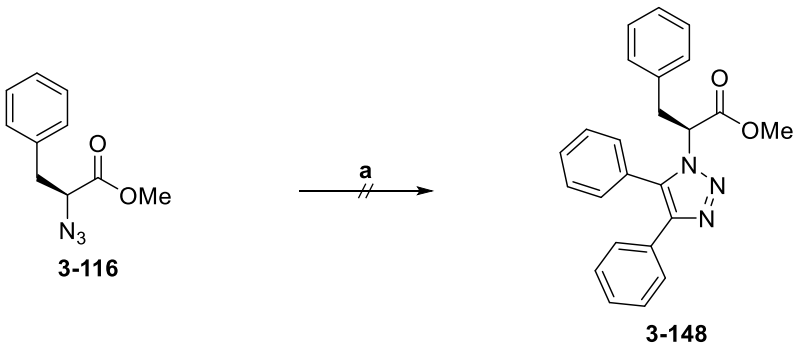

Reagents & Conditions: a. Bromobenzene (1.5 eq), phenylacetylene (1.5 eq), $Pd(dba)_3$ (0.025 eq), K_2CO_3 (2 eq), CuCl (1 eq), XPhos (0.1 eq), DMF, 70 °C, 16 h

Scheme 3.53: Attempt to form 1,4,5-trisubstituted triazole 3-138.

Thus, we decided to reproduce one of the published compounds. Following a reported procedure,[462] we synthetized benzyl azide **3-139** from benzyl bromide and sodium azide in 86% yield (Scheme 3.54) and then carried out its reaction with phenylacetylene and bromobenzene.

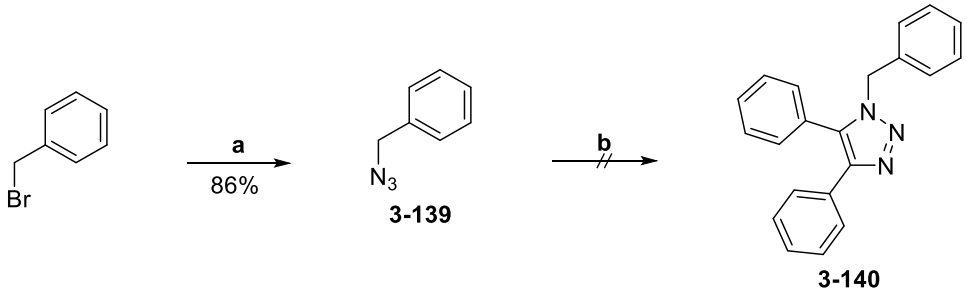

Reagents & Conditions: a. NaN_3 (2 eq), H_2O/Acetone 1:6, rt, 16 h; **b.** Bromobenzene (1.5 eq), phenylacetylene (1.5 eq), $Pd(dba)_3$ (0.025 eq), K_2CO_3 (2 eq), CuCl (1 eq), XPhos (0.1 eq), DMF, 70 °C, 16 h

Scheme 3.54: Attempt to synthesise 3-140.

As showed in the following NMR spectrum, once again only disubstituted triazole was obtained (Figure 3.6).

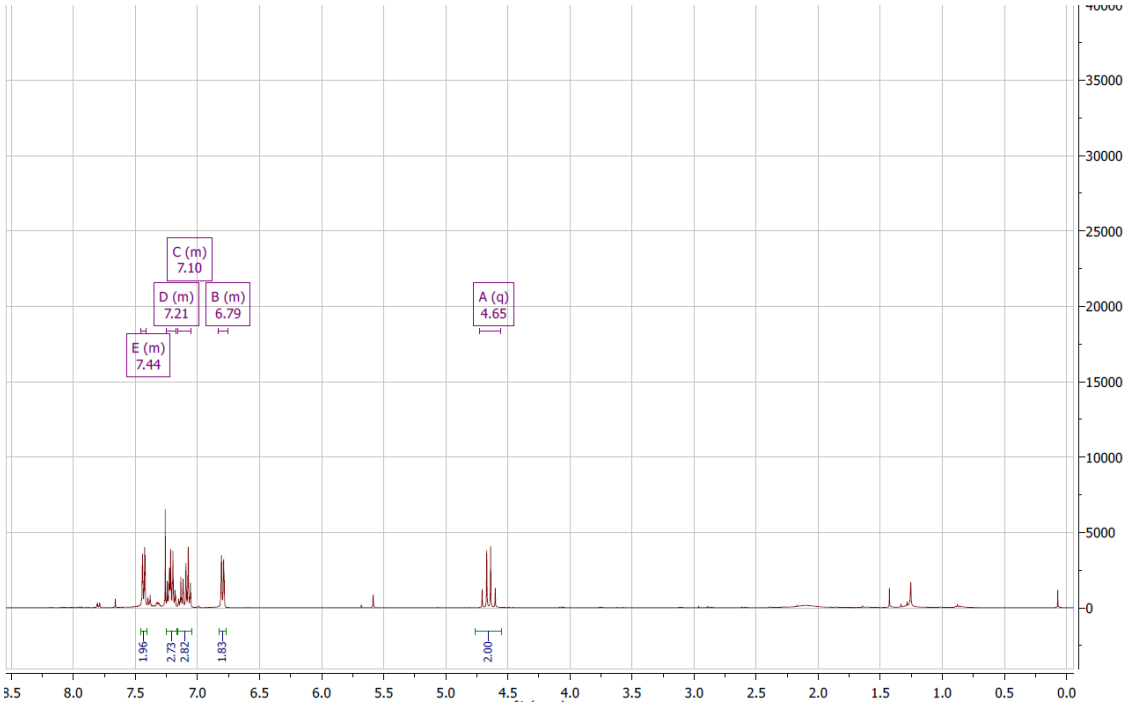

Figure 3.6: ^{1}H NMR spectrum of the recovered compound from 3-140 synthesis.

It was unclear to us why the transmetalation with the palladium cycle seemed to be problematic but facing unsuccessful, yet consistent, results we decided to look for an alternative pathway.

Instead of forming a precursor to our desired triazole **3-137** containing either hydrogen on the 5th position or a transition metal, a third possibility would be to synthesise an intermediate containing iodine on the same position (Scheme 3.55). This intermediate **3-141** would be stable and isolable and the C-I bond, much more reactive than a C-H bond, could then be used in the palladium-catalysed coupling reaction.

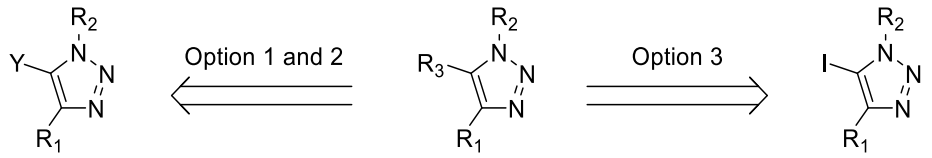

Scheme 3.55: Tri-substituted triazole precursors.

This procedure was also reported by Sharpless and Vokin,[463] and consists of a cycloaddition of organic azide and 1-iodoalkyne catalysed by copper(I). Similar to the CuAAC mechanism, two mechanisms are plausible and likely to coexist (**Scheme 3.56**). In a first catalytic cycle copper(I) interacts with the iodoalkyne to afford acetylide complex **3-97**. Following the previously described mechanism copper-triazole complex **3-100** is formed and final copper exchange

through σ-bond metathesis, with a second molecule of iodoalkyne, regenerates **3-97** and releases the 5-iodotriazole **3-141**. Alternatively, alike the dinuclear CuAAC cycle, iodoalkyne is activated by π-complexation with copper and then proceeds to a 6-member cyclization **3-143**. Final interaction with iodoalkyne affords **3-141** and regenerates **3-142**.

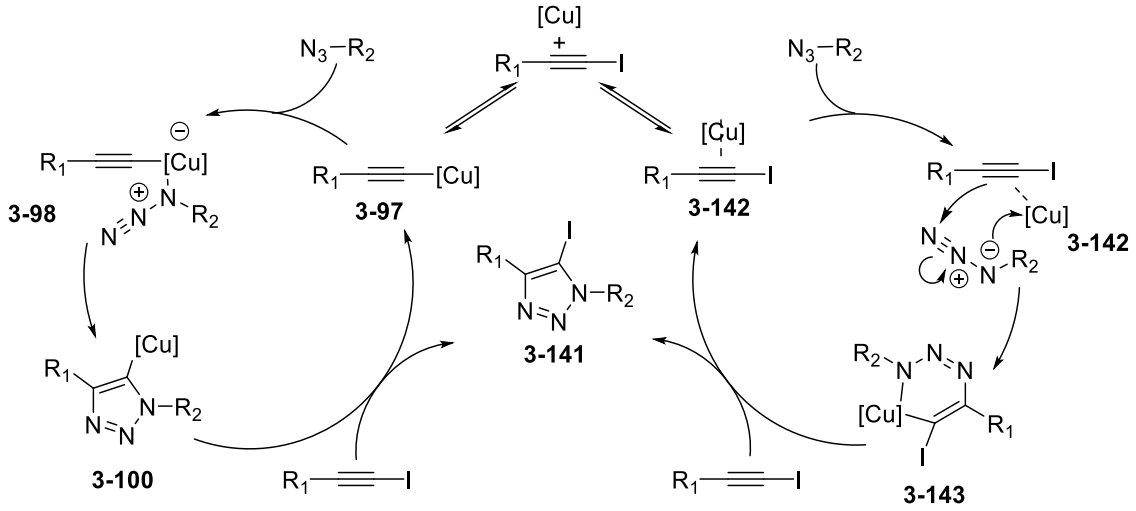

Scheme 3.56: Mechanism of formation of 5-iodotriazole.[463]

The intermediate iodo-triazole **3-141** was reported to be reactive under a variety of coupling conditions such as Heck, Suzuki and Sonogashira.[464–466] Although this method offered a vast scope of reaction and was of great potential, the rationale behind the investigation of the previous pathway was due to the previously mentioned trisubstituted triazole patent.[447] Indeed, their synthetic route was based on this procedure, and we wanted to get a maximum of distance between our work and theirs. Importantly the patented structure contains an alkynyl group on the 5th position. Therefore, despite using a similar intermediate, we could still diverge from the patent by avoiding the Sonogashira reaction and focus on another coupling.

Our interest in trisubstituted triazole, as well as our decision to switch to this synthetic pathway, was soon supported by an eminent publication. Indeed, simultaneously to our work, the authors of the patent disclosed the biological results of their scaffold.[467] Several crucial factors were highlighted by their SAR studies (Scheme 3.57). First of all, the (*S*)-stereochemistry of the initial amino acid seemed to be essential for potency, as switching to (*R*)-configuration resulted in a loss of activity. Secondly, the group on the 4th position had limited impact on the potency, and the position was therefore tolerant to modifications. On the other hand, the size of the group attached to the alkynyl had a great effect on the activity, and groups bigger than phenyl should be avoided. Finally, the alkynyl group was crucial for the scaffold as a reduction to alkene and alkane led from sub-nanomolar HDAC8 activity to inactive compounds.

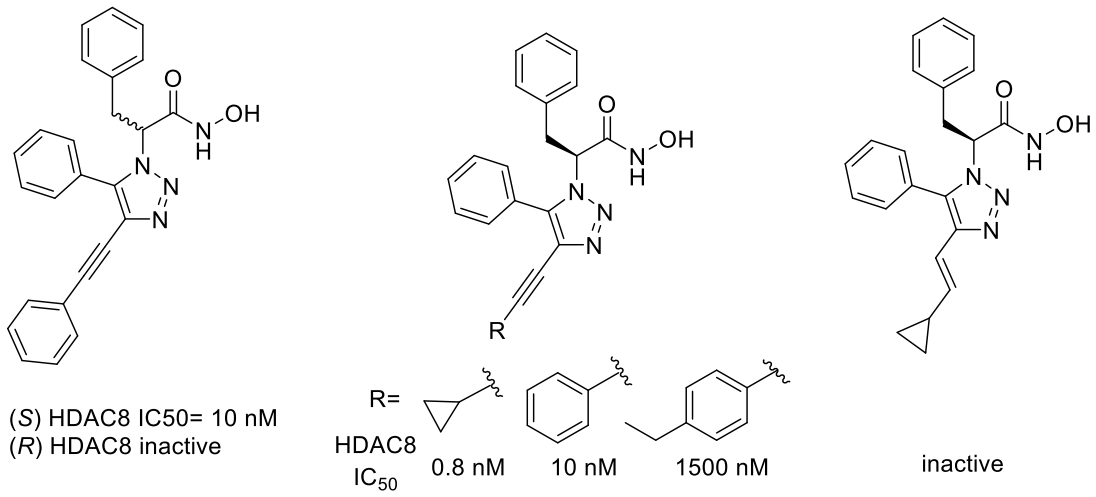

Scheme 3.57: Selection of important SAR of 5-alkynyl trisubstituted triazole scaffold.[467]

This last information profoundly influenced the design of our molecule. To our understanding, the alkynyl fits in an enzyme groove and acts as a linker to place the R group in a hydrophobic pocket. Increasing the size of the group tends to decrease the potency likely because of a hindrance with the pocket size. Moreover, reduction of the linker changes the direction in which the R group is pointing. Thus, fitting in the hydrophobic pocket becomes impossible, and the disturbance results in a loss of potency.

Consequently, to substitute the alkynyl linker of this patented scaffold, we looked for a small and flat structure that could keep a comparable alignment, in the continuity of the triazole bond, to bring a hydrophobic group in the enzyme's pocket. We reckoned that an aromatic ring could match those factors and opt for a 2,5-disubstituted thiophene linker.

Turning our attention to the synthesis and following Sharpless procedure,[463] *N*-iodomorpholine hydrogen iodine salt **3-144** was synthesised in 88% yield by reaction of iodine on morpholine (Scheme 3.58). Phenylacetylene was then treated with copper(I) iodine and *N*-iodomorpholine to give 1-iodo-phenylacetylene **3-145** in 98% yield. Similarly, 1-fluoro-4-(iodoethynyl)benzene **3-146** was synthesised in 70% yield.

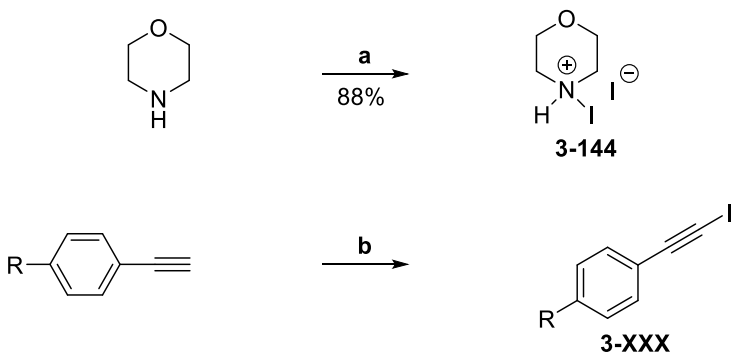

Reagents & Conditions: a. I_2 (1 eq), MeOH, rt, 1 h; **b.** CuI (0.05 eq), **3-144** (1.1 eq), THF, rt, 1 h

R group	Compound number	Yield
H	**3-145**	98%
F	**3-146**	70%

Scheme 3.58: Synthesis of Iodoalkyne.

Following the synthesis of these compounds, we could focus on the formation of the triazole. In the same Sharpless publication, 1,4,5-trisubstituted triazoles were successfully prepared in a two-steps one-pot synthesis. 5-Iodotriazoles were primarily formed by copper(I) catalysis. Then, in a Suzuki-Miyaura coupling, palladium(0) and boronic acid were added to afford the desired 1,4,5-trisubstituted triazole. This procedure was interesting as several thiophene boronic acids are commercially available and one-pot reaction speeds up the synthesis.

Accordingly, azide intermediate **3-121** underwent copper catalysed cyclisation by reaction with iodoalkyne and copper(I) iodide in the presence of triethylamine. Following consumption of starting material, monitored by TLC, palladium(0) acetate, thiophene-2-boronic acid, and excess of trimethylamine were added (Scheme 3.59). Several couplings were attempted, but each reaction resulted in the isolation of the corresponding 1,4-disubstituted triazole, and no desired compounds were obtained.

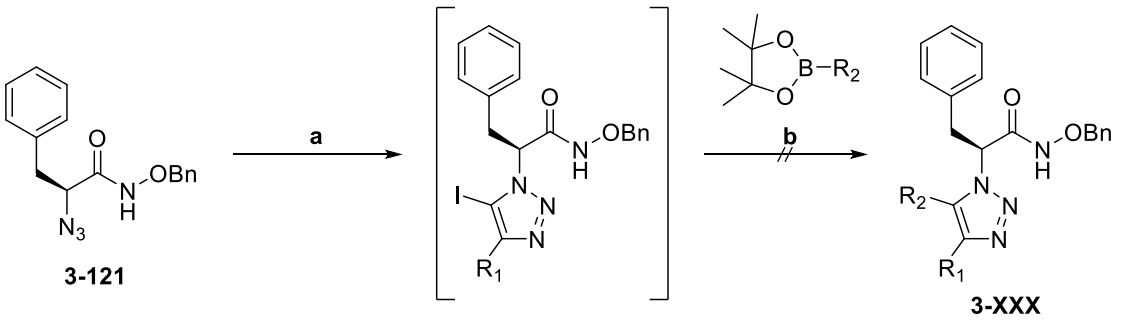

Reagents & Conditions: a. CuI (0.05 eq), **3-144** or **3-146** (1 eq), Et_3N (2 eq), THF, rt, 2 h; **b.** $Pd(OAc)_2$ (0.01 eq), Et_3N (1 eq), Boronic ester (2 eq), THF, 65 °C, 16 h

R1	R2	Product number	Isolated Compound
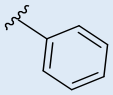	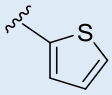	**3-147**	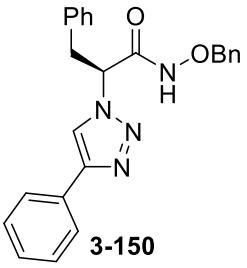 **3-150**
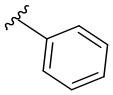	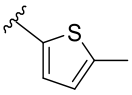	**3-148**	
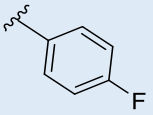	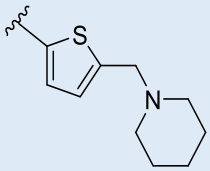	**3-149**	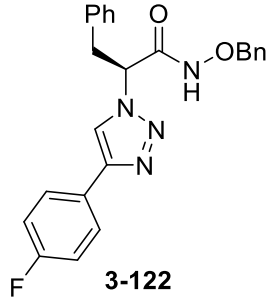 **3-122**

Scheme 3.59: Attempt of synthesis of 5-thiophenyl triazole.

These results were surprising, and the formation of the disubstituted triazole could come from reductive dehalogenation of the 5-iodotriazole intermediate, which has been shown to occur in the presence of copper salt.[468]

Consequently, we decided to opt in favour of a distinct two-step synthesis and to isolate the intermediate 5-iodotriazole. This would not only allow us a proper control of the formation of this crucial intermediate but would also remove the copper salt from the media. Following the same procedure, 5-iodotriazole were synthesised and successfully isolated (Scheme 3.60).

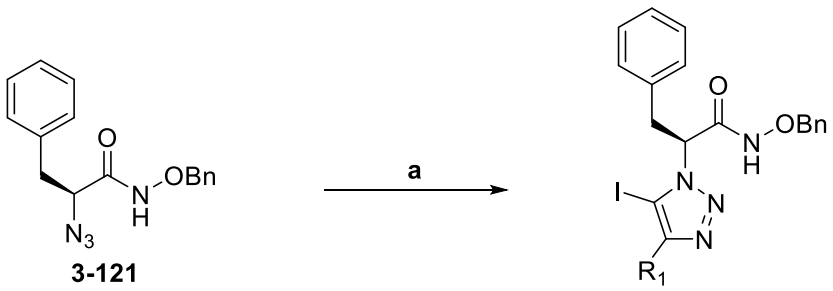

3-121 **3-XXX**

Reagents & Conditions: a. CuI (0.05 eq), **3-145** or **3-146** (1 eq), Et_3N (2 eq), THF, rt, 2 h

R_1 group	Compound number	Yield
Phenyl	**3-151**	64%
4-Fluorophenyl	**3-152**	34%

Scheme 3.60: Synthesis of 5-iodotriazole.

Subsequently, Suzuki couplings were tried again (Scheme 3.61). This was investigated with the help of Faustin Falissard, a visiting undergraduate student that I supervised, who performed the reaction in entry 4-6. Once more, several conditions were used,[465,466,469] but no desired products were obtained. Instead, mixtures of starting material and 1,4-disubstituted triazole were recovered.

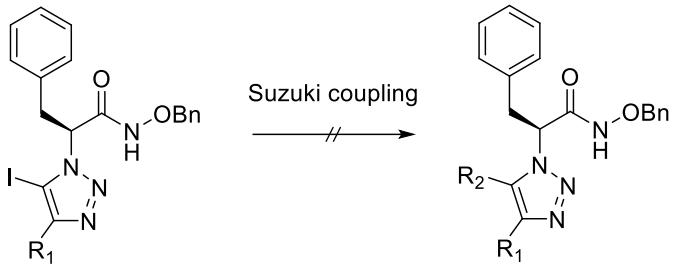

Entry	R1	Organoborane	Coupling conditions
1	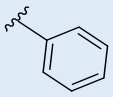	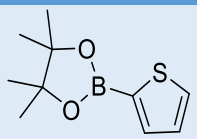	$PdCl_2(PPh_3)_2$ 0.04 eq, K_2CO_3 1 eq, Organoborane 1.5 eq, THF, 70 °C, 16 h
2	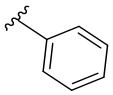	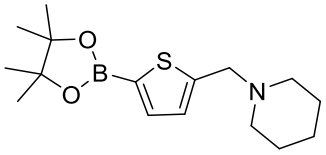	$Pd(OAc)_2$ 0.04 eq, Et_3N 1 eq, Organoborane 1.5 eq, THF, 65 °C, 16 h
3	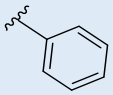	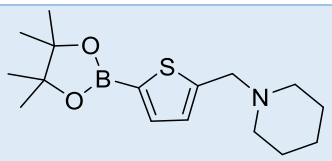	$PdCl_2(PPh_3)_2$ 0.04 eq, KOH 2 eq, Organoborane 1.5 eq, THF, 75 °C, 16 h
4	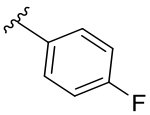	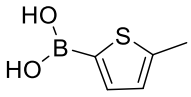	$Pd(PPh_3)_4$ 0.05 eq, K_3PO_4 2 eq, Organoborane 2 eq, Dioxane, 90 °C, 16 h
5	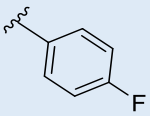	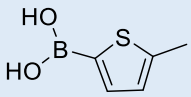	$Pd(OAc)_2$ 0.04 eq, K_3PO_4 5 eq, Organoborane 2 eq, DMF, 100 °C, 16 h
6	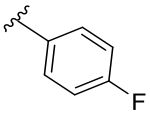	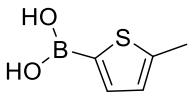	$PdCl_2(PPh_3)_2$ 0.04 eq, KOH 2 eq, Organoborane 1.5 eq, THF, 60 °C, 16 h

Scheme 3.61: Suzuki coupling conditions.

We could then conclude that the results of the one-pot sequence were not solely due to the presence of copper salt in the reaction mixture. Another example of reductive dehalogenation with palladium catalyst has also been reported.[470] According to the authors, this could be due to steric hindrance at the 1st and 4th position of the triazole. This could indeed prevent the transmetalation process with the boronic acid. As a result, the palladium catalytic cycle would be blocked in the oxidative addition intermediate state. The cycle would, therefore, proceed to a β-H elimination/reductive elimination, with a ligand being the source of the β-H atom, to form the dehalogenated 1,4-disubstituted triazole.

Future optimisation of conditions of reaction could potentially overcome this issue. Alternatively, as the 4th position seems tolerant to a variety of substitute, reduction of the size of the group on the 4th position could also help the reaction. Those will be part of future work for this scaffold.

2.4 Scaffold 4: hydantoin-based inhibitors

Hydantoins, or glycolylureas, are interesting heterocyclic structures, which have been successfully used in drug development, and currently, form an important class of anticonvulsant.

In regards to their achievement, we became interested in the structure and its use in the development of HDAC inhibitors. Besides, hydantoin structure can be seen as a non-classical isoterism of the diketopiperazine derivative scaffold and the triazole scaffold previously described. Introduced by Langmuir in 1919,[471] and later extended by Friedman,[472] the concept of bioisoterism refers to the replacement of a group in a molecule by another group of similar electronic or steric arrangement. As shown below (Scheme 3.62) hydantoin does share similarities with both diketopiperazines and, to some extent, triazoles.

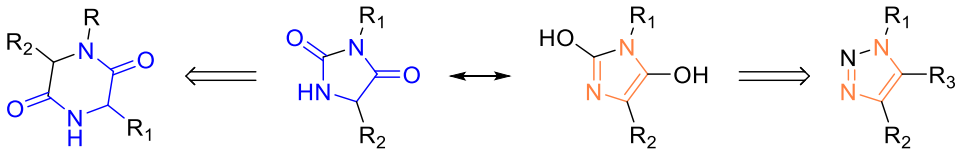

Scheme 3.62: Hydantoin isoterism.

Checking the literature, we found that several hydantoins bearing hydroxamic acid as zinc binding group had been reported as matrix metalloproteinase inhibitors.[473–476] Surprisingly this structure has not been investigated for HDAC inhibition. Besides only one publication reported the use of a hydantoin, in virtual screening, on *Schistosoma mansoni* HDAC8 inhibition.[324] This validated our decision to explore hydantoin-based structures as HDAC inhibitors.

Over the years, several synthetic pathways were developed to synthesise hydantoins,[477] but two are historical of great interest. The 1st method was reported by Urech in 1873.[478] Mixing an amino acid and potassium cyanate (Scheme 3.63), the amine proceeds to a nucleophilic attack on the cyanate to form an intermediate carbamide **3-153**. Internal condensation of the urea and the carboxylic acid then leads to the formation of the cyclic intermediate **3-155**. Finally, loss of water affords hydantoin **3-156**.

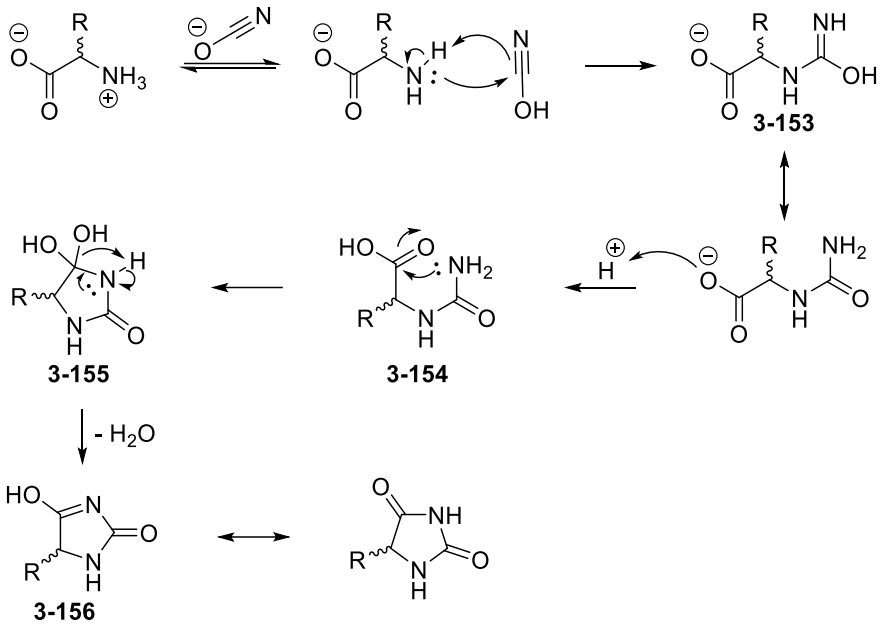

Scheme 3.63: Urech hydantoin synthesis.

The second method is known as the Bucherer-Bergs reaction and consists in the reaction between a carbonyl, potassium cyanide and ammonium carbonate (Scheme 3.64).[479] In a first step, cyanohydrin **3-157** is formed by the nucleophilic addition of cyanide on the carbonyl. Nucleophilic substitution, by reaction with ammonium ion, then leads to the formation of an aminonitrile intermediate **3-158**. Next, nucleophilic addition on carbon dioxide leads to cyano-carbamic acid **3-159**, which then undergoes an intermolecular cyclization to 5-imino-oxazolidin-2-one **3-160**. Subsequently, rearrangement briefly opens the cycle to form an isocyanate **3-161**, which spontaneously cyclises to afford the hydantoin. **3-162**.

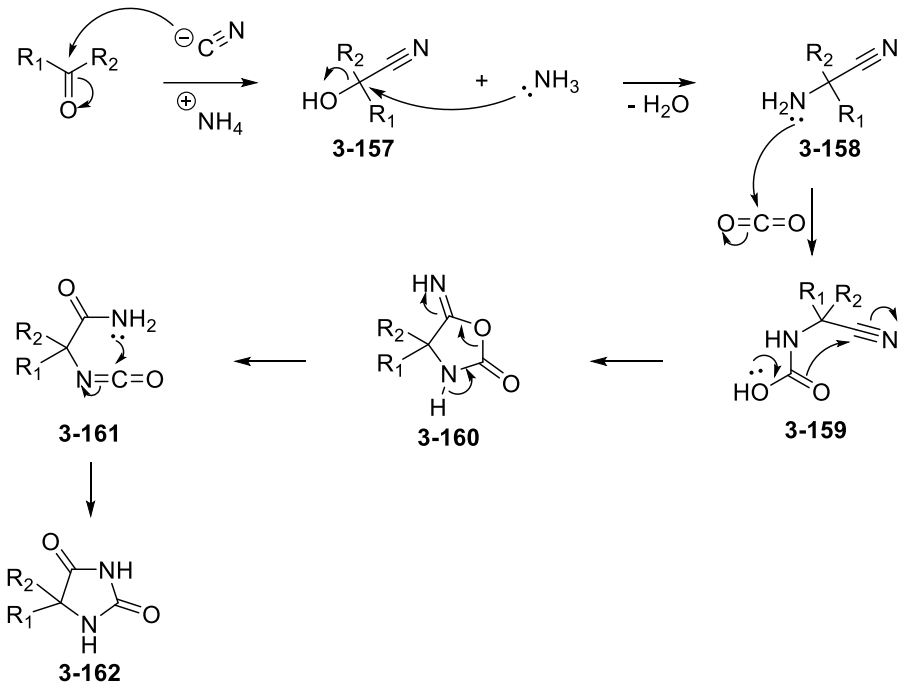

Scheme 3.64: Bucherer-Bergs reaction.

As previously mentioned, hydantoin was seen as a bioisostere of triazole. Thus, our main objective was to develop a class of inhibitors analogue to the triazole scaffold. Accordingly, we wanted to keep an amino acid core, especially phenylalanine, on the hydroxamic acid part of the molecule. Thus, we chose to form the hydantoin from the amine end of phenylalanine. Although the previously described synthetic pathways have been successfully used in the past, a more recent publication became of great interest to us. Liu and coworkers published in 2014 a new method for the synthesis of 3,5-disubstituted or 3,5,5′- trisubstituted chiral hydantoins from Boc-protected dipeptides (Scheme 3.65).[480] Activation of the peptide bond with triflic anhydride leads to the formation of an intermediate salt **3-163** that then undergoes an intramolecular cyclisation to release both triflic acid and intermediate **3-164**. Two possible mechanisms are then likely to afford the hydantoin **3-167**. In a first pathway, the tert-butyl protecting group is then expelled to form an oxazolidone **3-165**, which then goes through Mumm rearrangement to give **3-167**. Alternatively, a second pathway forces ring opening to give the isocyanate **3-166** that then cyclizes to hydantoin.

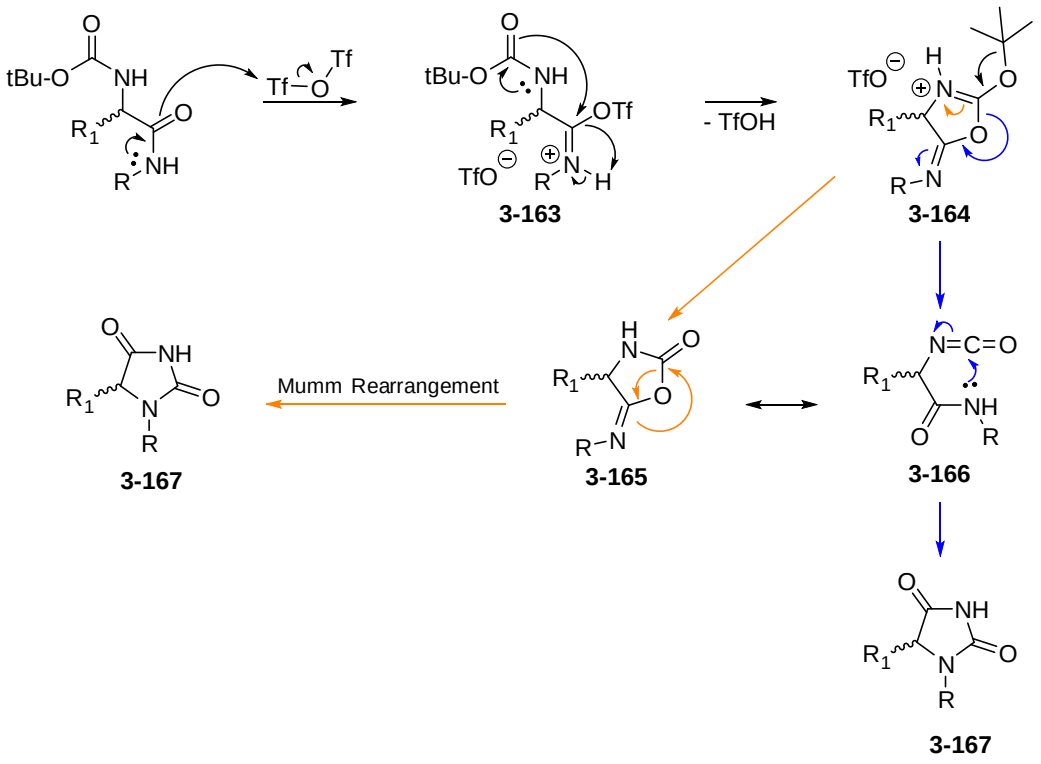

Scheme 3.65: Synthesis of hydantoin from Boc-dipeptide.[480]

This procedure fitted perfectly with our will to build the hydantoin structure from amino acids. Moreover, it also easily introduces a second chiral centre in the molecule, in the 5th position.

We decided to introduce a protected hydroxamic acid prior to the hydantoin formation. Thus, starting from Boc-protected L-phenylalanine, we used CDI to activate the carboxylic acid and converted it to *O*-benzylhydroxamic acid **3-168** in 86% yield (Scheme 3.66). Boc-protection was then hydrolysed in acidic conditions, and the free amine **3-169** was obtained in 99% yield.

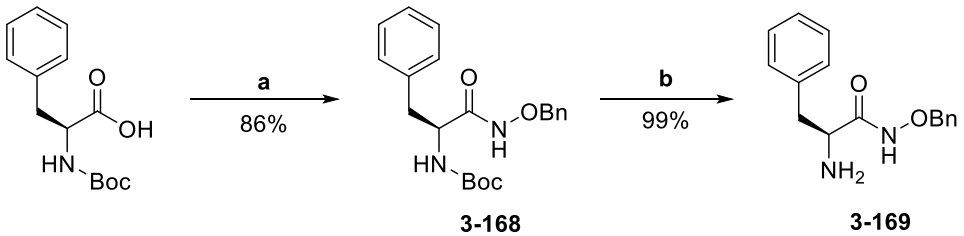

Reagents & Conditions: a. CDI (1.5 eq), $NH_2OBn.HCl$ (2 eq), THF, rt,16 h; **b.** TFA (10 eq), DCM, rt, 3 h

Scheme 3.66: Synthesis of NH_2-L-Phe-NHOBn 3-169.

Amine **3-169** was then coupled to several Boc-protected amino acids to form the corresponding dipeptides using EDC/HOBt or HBTU (Scheme 3.67).

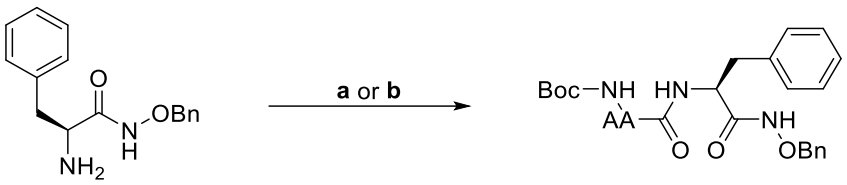

3-169 3-XXX

Reagents & Conditions: a. Boc-AA-OH (1 eq), EDC (1.1 eq), HOBt (1.1 eq), NMM (3.3 eq), DMF, rt, 16 h; **b.** Boc-AA-OH (1.2 eq), HBTU (1.2 eq), DIPEA (3.5 eq), DCM, rt, 16 h

Boc-AA-OH	Compound number	Product	Yield
Boc-L-Phe-OH	**3-170**	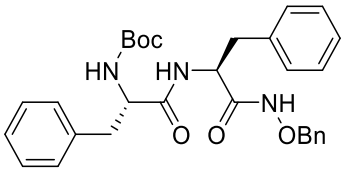	63%
Boc-L-Pro-OH	**3-171**	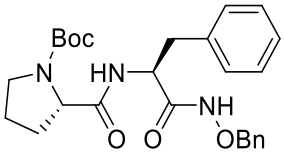	35%
Boc-β-Ala-OH	**3-172**	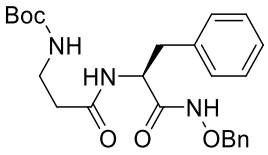	18%

Scheme 3.67: Synthesis of Boc-dipeptide-*O*-benzyl hydroxamic acid.

Following this synthesis, we applied the previous protocol for the cyclisation. The dipeptide was dissolved in dry acetonitrile and a base, either pyridine or 2,6-lutidine was added followed by dropwise addition at 0 °C of triflic anhydride (Scheme 3.68). The reaction mixture was then stirred at room temperature. Colour change of the reaction mixture was observed, and the reaction progression, checked by TLC, showed no remaining starting materials after two hours. However, no desired products were recovered after workup and purification by flash chromatography. Instead, NMR showed that only starting material was recovered.

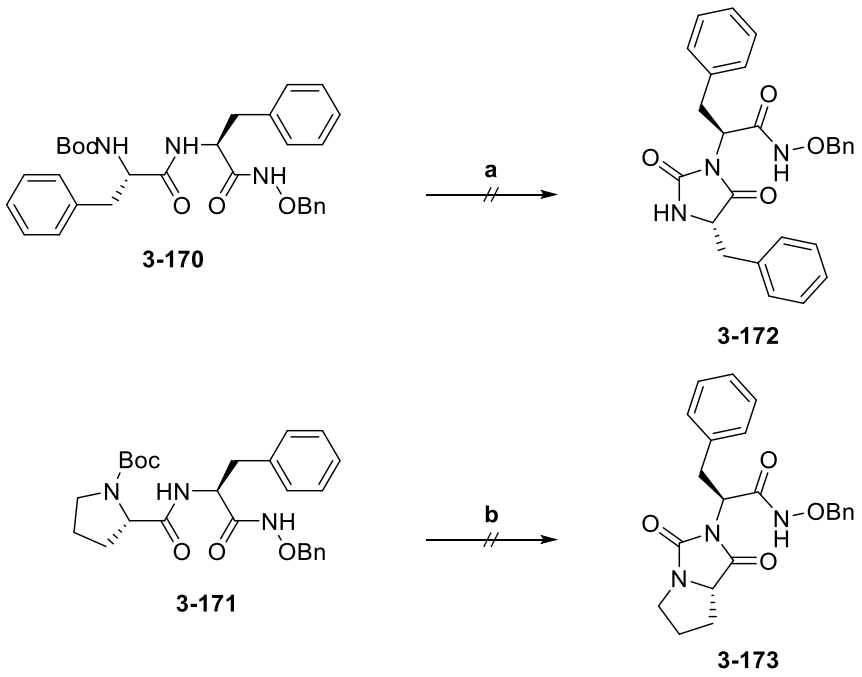

Reagents & Conditions: a. Tf_2O (1.5 eq), pyridine (3 eq), MeCN, rt, 2 h or 16 h;
b. Tf_2O (2 eq), 2,6-lutidine (4 eq), MeCN, rt, 16 h

Scheme 3.68: Attempt of hydantoin cyclization.

We thought that it could be due to a kinetic issue. A rapid reaction with triflic anhydride and activation of amide bond could explain the visual changes we observed, but the ring closure could then be slower than expected, and aqueous workup could quench the activated intermediate to give back the starting material. Thus, we repeated the reaction and let the mixture stir overnight, instead of two hours, but we obtained the same result.

Another potential explanation could be a competition between the amide and the hydroxamic acid during the activation step (Scheme 3.69). The reaction between the triflic anhydride and the hydroxamic acid, instead of amide, would prevent the formation of the hydantoin. Besides, only starting material was recovered and no apparent side product was formed. Applying the same intramolecular pathway to activated hydroxamic acid would give a complex 8-membered ring. This structure has not been reported, and its formation under these conditions is therefore unlikely.

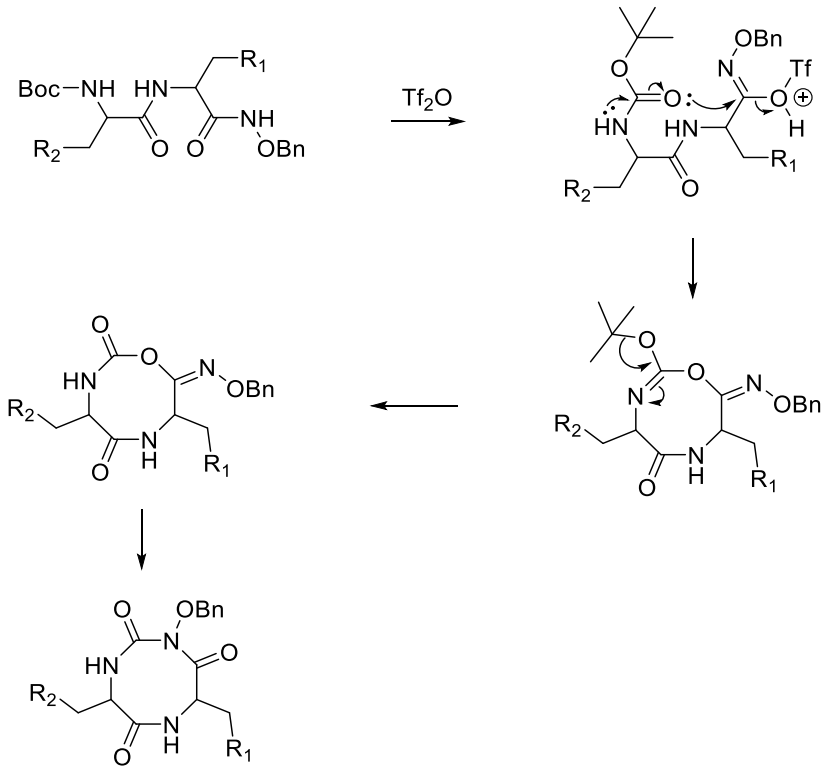

Scheme 3.69: Activation of hydroxamic acid and resulting cyclisation.

Consequently, we decided to change the synthetic route. In the first part, we would synthesise methyl ester dipeptide, and then form the hydantoins. Subsequently, they would be converted to hydroxamic acid. Dipeptides were synthesised by coupling L-phenylalanine methyl ester with Boc-protected amino-acid (Scheme 3.70).

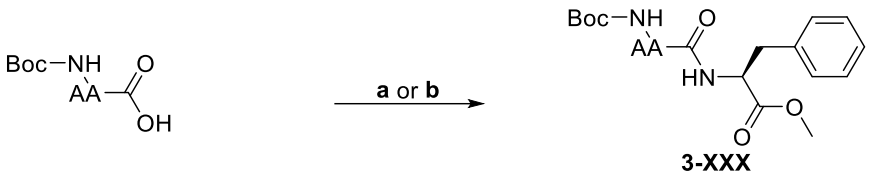

Reagents & Conditions: a. H-L-Phe-OMe (1.2 eq), EDC (1.2 eq), HOBt (1.2 eq), DIPEA (2.5 eq), DCM, rt, 16 h; **b.** H-L-Phe-OMe (1.1 eq), HATU (1.1 eq), DIPEA (4 eq), DCM, rt, 2 h

Boc-AA-OH	Product	Compound number	Yield
Boc-L-Ala-OH	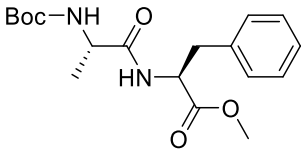	**3-174**	68%
Boc-L-Phe-OH	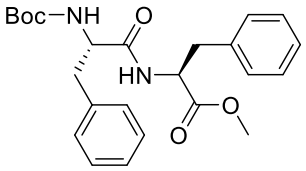	**3-175**	65%
Boc-D-Phe-OH	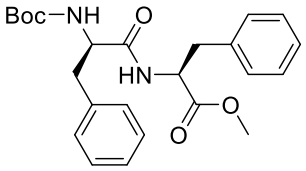	**3-176**	95%
Boc-L-Tyr(OBn)-OH	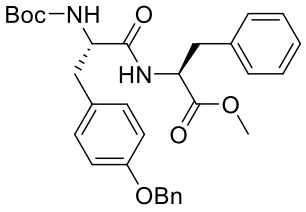	**3-177**	82%

Scheme 3.70: Synthesis of Boc-dipeptide methyl ester.

The triflic anhydride and pyridine procedure was then applied to these dipeptides. By contrast with *O*-benzylhydroxamic acid dipeptide, hydantoins were successfully formed and isolated under the same conditions (Scheme 3.71).

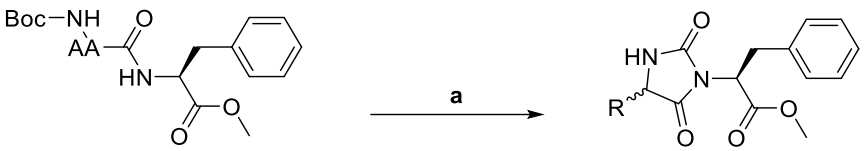

Reagents & Conditions: a. Tf_2O (1.5 eq), pyridine (3 eq), MeCN, rt, 2 h

Starting material	Product	Compound number	Yield
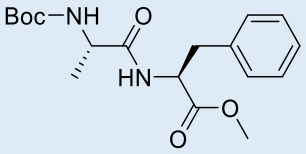	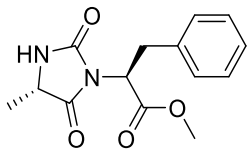	**3-178**	54%
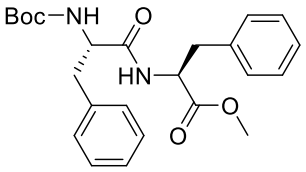	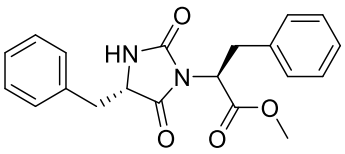	**3-179**	73%
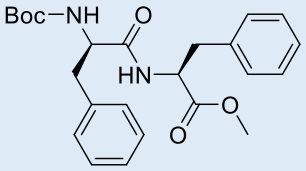	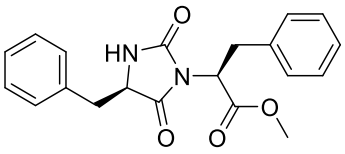	**3-180**	98%
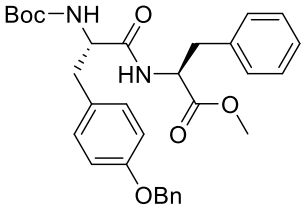	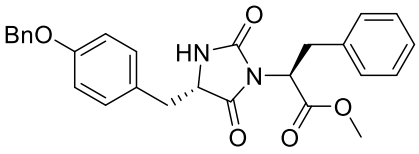	**3-181**	67%

Scheme 3.71: Synthesis of hydantoin methyl ester.

We then decided to convert these compounds to hydroxamic acid by direct nucleophilic substitution with hydroxylamine in methanol (Scheme 3.72). However, it turned out that solubility in methanol was low, and no reaction was observed. The reaction was repeated, and a second solvent was added to increase the solubility, but similar results were obtained by addition of THF and acetonitrile.

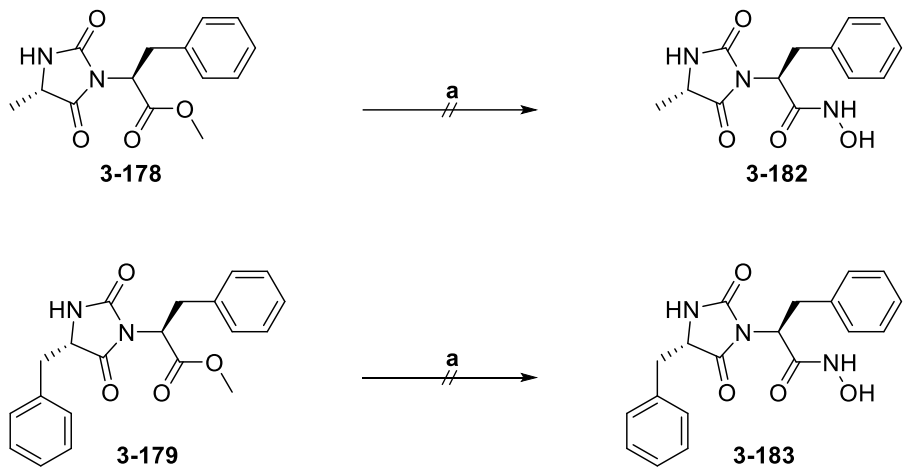

Reagents & Conditions: a. $NH_2OH.HCl$ (20 eq), KOH (20 eq), MeOH, rt, 16 h

Scheme 3.72: Attempt of direct conversion of hydantoin methyl ester to hydroxamic acid.

Thus, we decided to firstly form a carboxylic acid and then convert it to hydroxamic acid. Hydantoin methyl esters were hydrolysed using HCl in dioxane at 80 °C (Scheme 3.73).

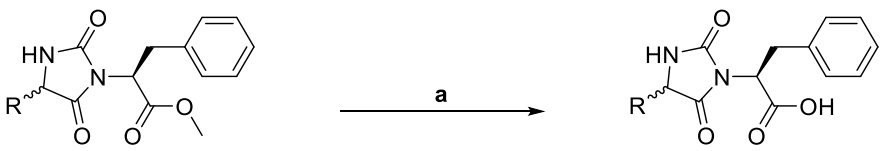

Reagents & Conditions: a. HCl (6M; 20 eq), Dioxane, 80 °C, 16 h

Starting material	Product	Compound number	Yield
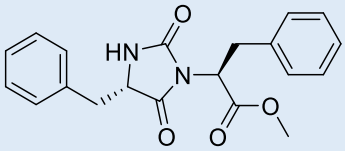	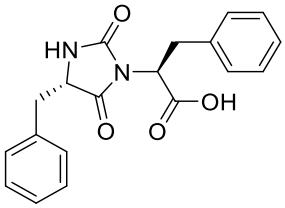	**3-184**	85%
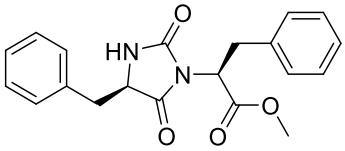	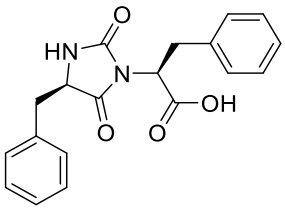	**3-185**	98%
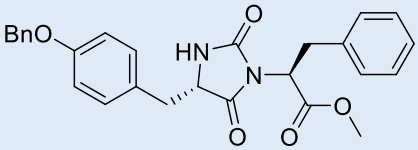	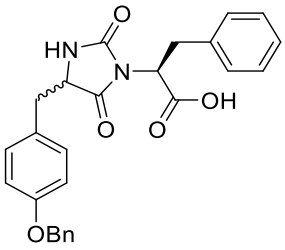	**3-186**	82%

Scheme 3.73: Hydrolysis of methyl ester

Importantly, the ^{1}H NMR spectrum of **3-186** showed a split signal of one of the CH_2 in the 3.1-2.4 ppm region (Figure 3.7). Moreover, the signal from the four aromatic protons of the tyrosine was also split. Based on these observations we concluded that epimerization had occurred on the tyrosine.

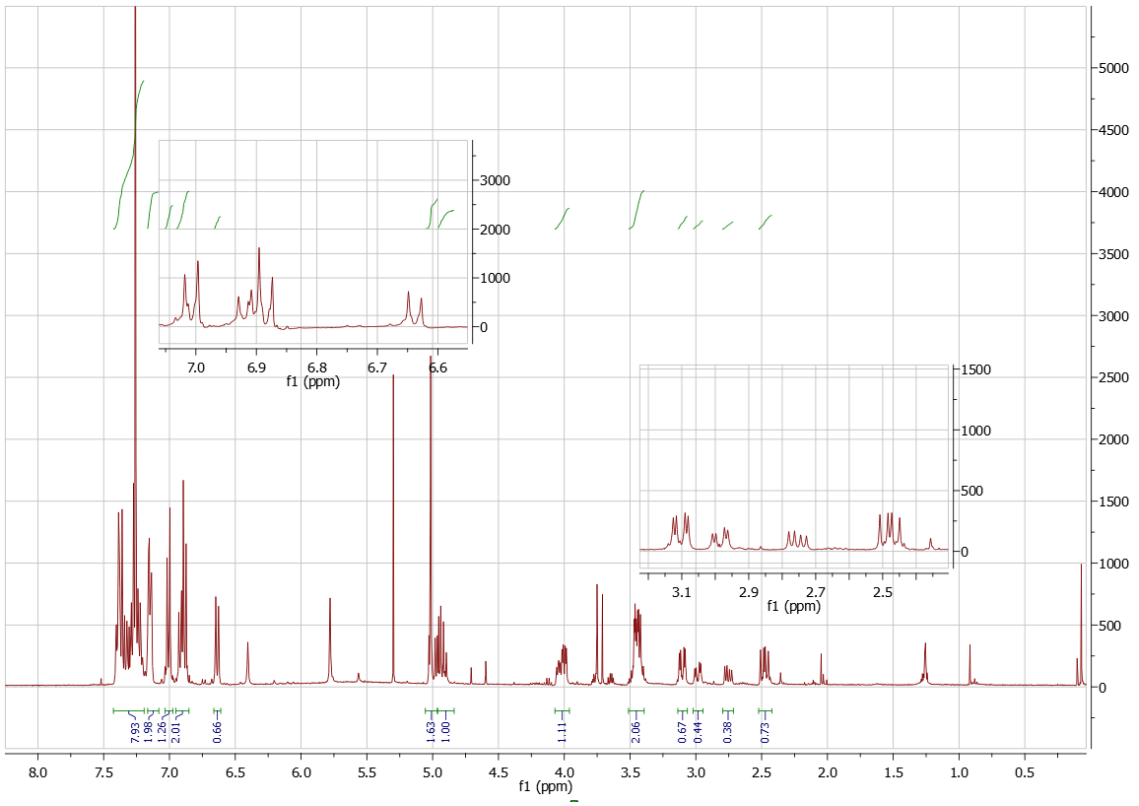

Figure 3.7: ^{1}H NMR spectrum of 3-186.

In a subsequent step, the newly formed carboxylic acids were activated with CDI and converted to hydroxamic acid. We decided to investigate the use of different sources of protected hydroxylamine.

Firstly, we used *O*-benzylhydroxylamine on **3-186**. Thus, both protecting groups would be removed simultaneously in a final step. Surprisingly, two compounds were isolated (Scheme 3.74). The first one corresponded to the desired product **3-187** and was the major product. However, the second compound only displayed 14 aromatic protons and 2 CH_2 protons from an *O*-benzyl group in the ^{1}H NMR spectrum (Figure 3.8). Our first thought was to consider it as remaining starting material, but a combination of ^{13}C NMR, 2D NMR (COSY, HSQC, HMBC, in Appendix) and mass-spectrometry revealed the successful introduction of the protected hydroxylamine but the loss of tyrosine protection.

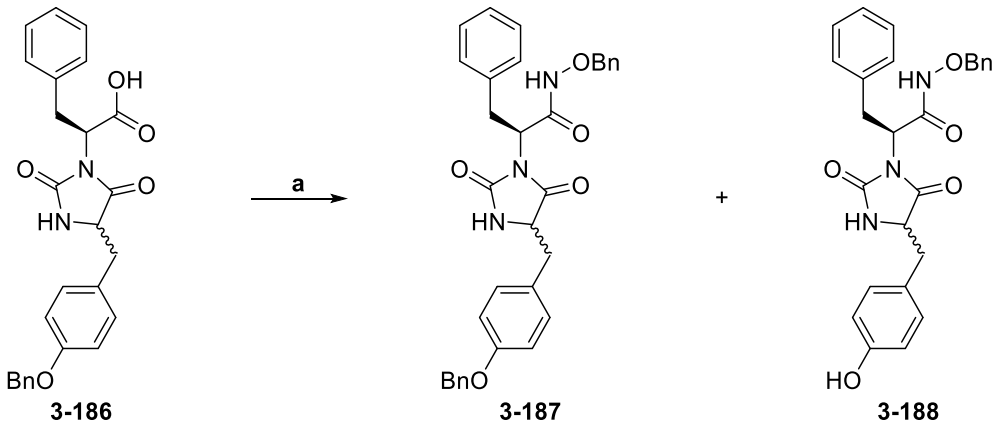

3-186 **3-187** **3-188**

Reagents & Conditions: a. CDI (1.5 eq), $NH_2OBn.HCl$ (2 eq), THF, rt, 16 h

Scheme 3.74: Formation of 3-187 and 3-188.

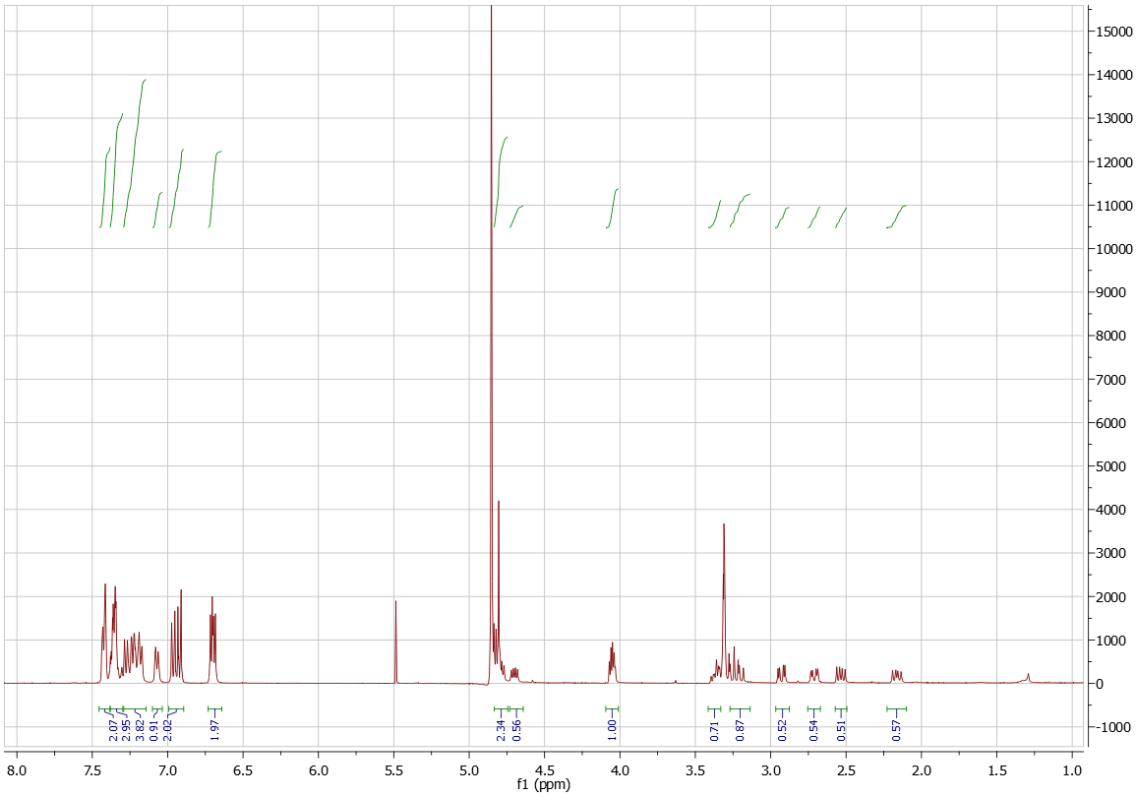

Figure 3.8: ^{1}H NMR spectrum of the second compound isolated with 3-187.

Compound **3-187** then reacted with BCl_3 at low temperature over 4 hours, and the reaction was purified after completion. Analysis of the isolated product revealed that only the protection of the hydroxamic acid had been removed, while the tyrosine remained intact. Therefore, it corresponded to the final product **3-189**.

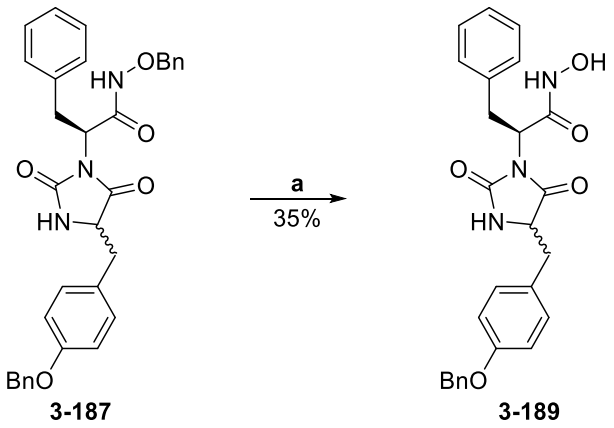

3-187 **3-189**

Reagents & Conditions: a. BCl_3 (5.5 eq, 1M in DCM), THF, 0 °C, 4 h

Scheme 3.75: Synthesis of the final compound 3-189.

Finally, we used TBDMS-protected hydroxylamine on **3-185** (Scheme 3.76**)**. However, we observed some deprotection during the purification, and the free hydroxylamine **3-190** was directly isolated.

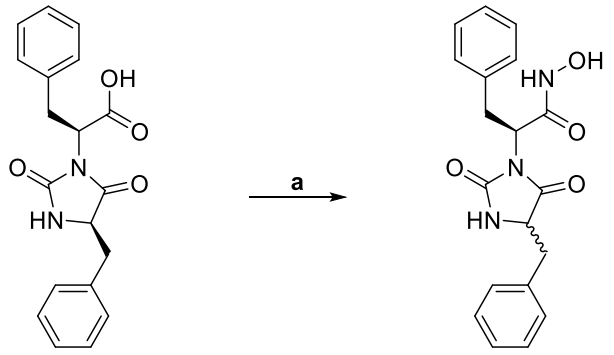

3-185 **3-190**

Reagents & Conditions: a. CDI (1 eq), $NH_2OTBDMS$ (1 eq), THF, rt, 16 h

Scheme 3.76: Synthesis of compound 3-190.

2.5 Scaffold 5: Praziquantel – HDACi hybrid

In chapter 2, we discussed the enormous potential of multitarget drugs. One of the main advantages of this approach is to prevent the development of resistance and the loss of potency of a therapy. Besides, we also mentioned that, among the epigenetic mechanisms, HDAC inhibition had been the preferential target in the development of dual inhibitors. Thus, we sought to develop a molecule with such properties.

Turning more specifically to our project, one of our main objectives was to work on schistosomiasis.

On the one hand, HDAC inhibition with vorinostat was showed to be efficient against Schistosoma worms with a therapeutic effect leading to the reduction of the infectivity and an increase in mortality induced by the inhibitor.

On the other hand, we have the commercially available drug praziquantel at our disposal, which is highly efficient in the treatment of the infection but started to experience drug resistance from the parasite. Thus, the idea to combine both compounds to create a potential dual-target molecule naturally emerged.

Looking at the structure of the two drugs, we decided to connect them using the shared amide bond (Scheme 3.77). The fused tricyclic part from praziquantel would be used as the cap group while the hydroxamic acid alkyl chain from vorinostat would play the role of linker and zinc binding group.

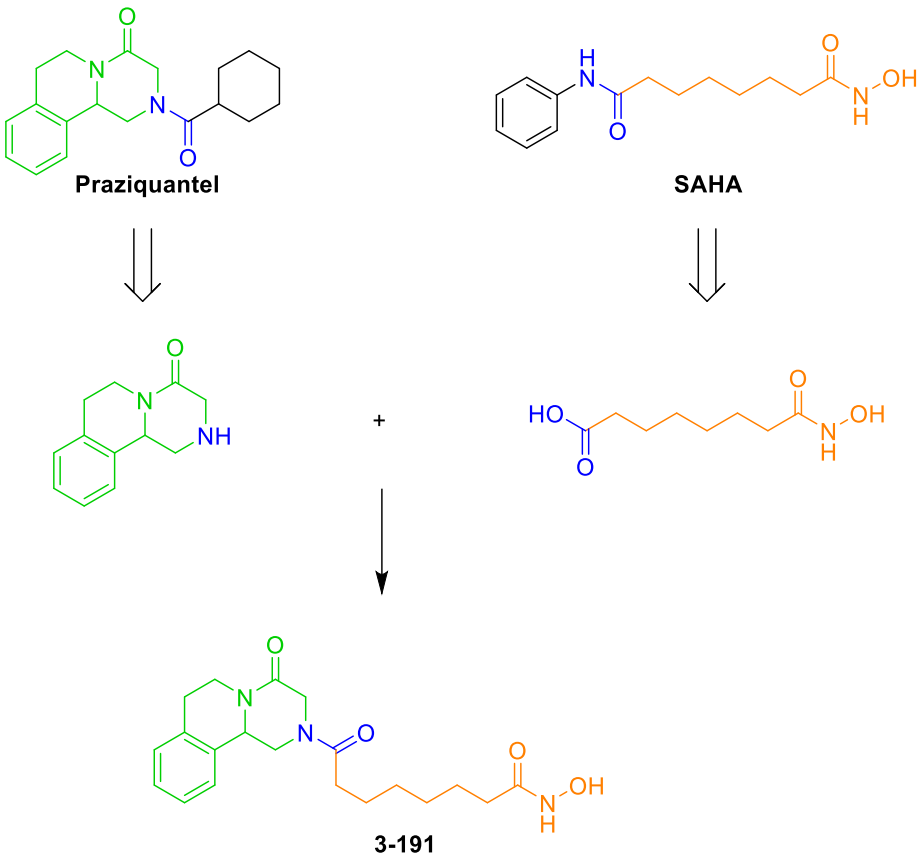

Scheme 3.77: Design of a potential multitarget compound.

Regarding the synthesis of this praziquantel-vorinostat hybrid, it started with the synthesis of the praziquanamine intermediate. Following a reported procedure,[481] chloroacetyl chloride **3-192**

reacted through nucleophilic substitution with phenethylamine in the presence of $NaHCO_3$ to give the chloroacetamide **3-193** in 86% yield (Scheme 3.78).

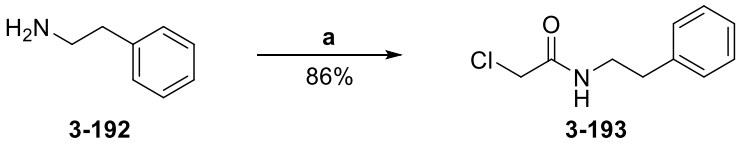

3-192 **3-193**

Reagents & Conditions: a. Chloroacetyl chloride (1.2 eq),$NaHCO_3$ (1 eq), DCM, rt, 4 h

Scheme 3.78: Synthesis of chloroacetamide 3-193.

The intermediate **3-193** then reacted with amino-acetaldehyde dimethyl acetal, in a novel nucleophilic substitution, to give the dimethyl acetal **3-194**. Without isolation, the addition of sulfuric acid triggered the cyclisation to form the praziquanamine **3-195** in 41% overall yield after two steps.

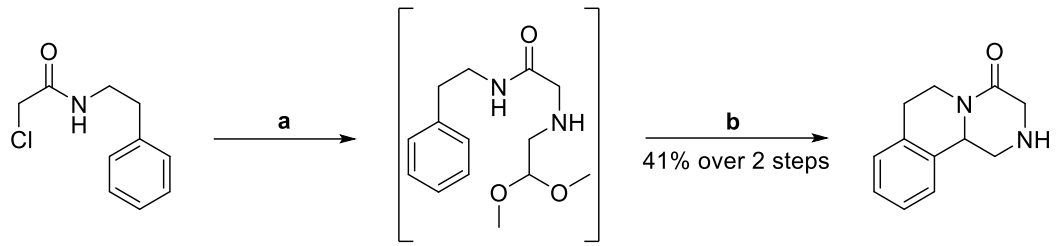

3-193 **3-194** **3-195**

Reagents & Conditions: a. Dimethoxyethylamine (2 eq), toluene, reflux, 2 h; **b.** H_2SO_4 (4.5 eq), rt, 3 h

Scheme 3.79: Synthesis of praziquanamine 3-195.

The reaction of cyclisation was based on the method published by Pictet and Spengler in 1911.[482] In a successive two steps sequence, methyl-acetals are activated by the acidic condition, then substituted by nucleophilic attack of the nitrogen to form an iminium ion **3-197**. Then a stepwise internal cyclisation with loss of aromaticity led to the formation of intermediate **3-201**. A final deprotonation step restores the aromaticity and results in the substituted tetrahydroisoquinoline **3-195**. The cyclisation to form the 1,2,3,4-tetraisoquinoline derivative corresponds to a 6–endo-trig reaction and is favoured according to Baldwin's rules.[483] However, Pictet-Spengler reaction is usually tricky when a non-substituted phenyl is involved, and superacids or high temperature are generally used to force the reaction.[484] Nonetheless, in this case, the presence of the acyl group on the reacting nitrogen leads to the formation of an *N*-acyliminium ion intermediate **3-200** more electrophilic than a simple iminium ion and more sensitive to cyclisation.[485] The reaction could, therefore, be done at room temperature.

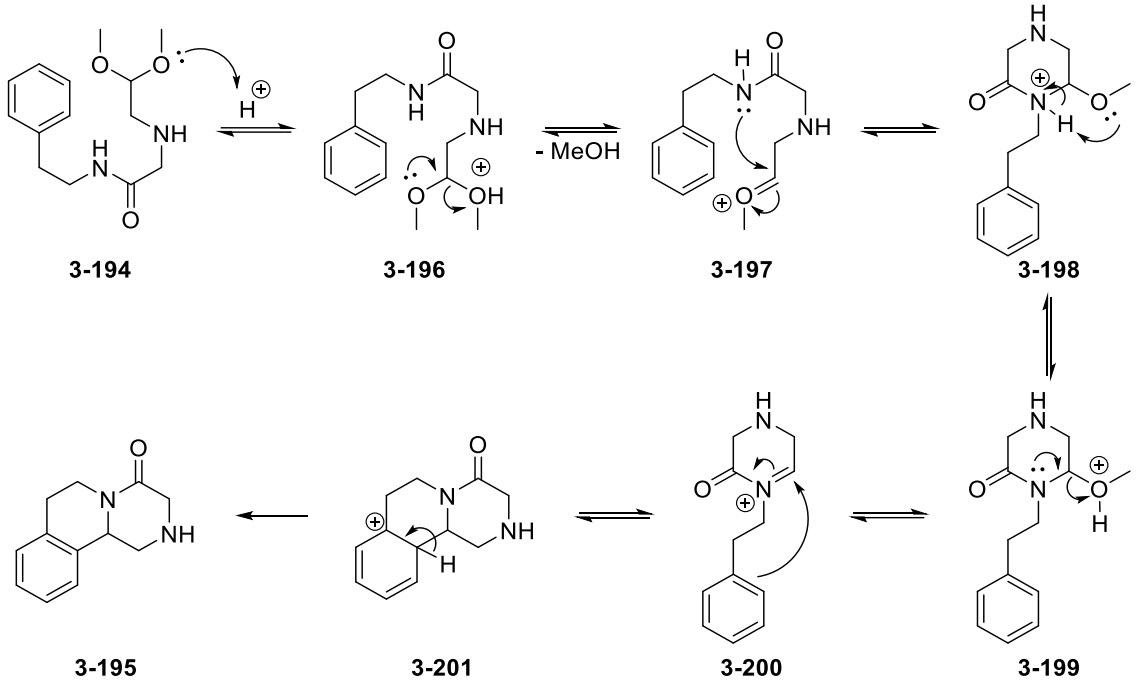

Scheme 3.80. Pictet-Spengler reaction mechanism.

Praziquanamine **3-195** then reacted with methyl 8-chloro-8-oxooctanoate by nucleophilic substitution to form a methyl ester precursor **3-202** in 88% yield (Scheme 3.81). It was later converted to hydroxamic acid using hydroxylamine, potassium hydroxide, and potassium cyanate to give the final compound **3-191** in 19% yield.

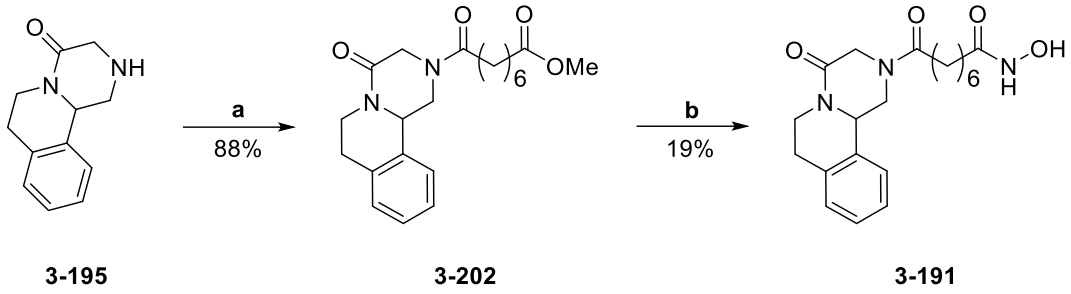

Reagents & Conditions: a. Methyl 8-chloro-8-oxooctanoate (1.2 eq), DIPEA (2 eq), THF, rt, 1 h; **b.** KCN (0.05 eq), NH_2OH (50% aq.)/THF/MeOH 0.5/1/1, rt, 24 h

Scheme 3.81: Synthesis of hybrid compound 3-191.

Alternatively, the *O*-benzylhydroxamic acid linker could be prepared in a two-step reaction. Methyl 8-chloro-8-oxooctanoate was dissolved in THF and reacted with *O*-benzylhydroxylamine hydrochloride and DIPEA to afford compound **3-203** in 83% yield. The methyl ester was then hydrolyzed to carboxylic acid **3-204** with lithium hydroxide in 88% yield.

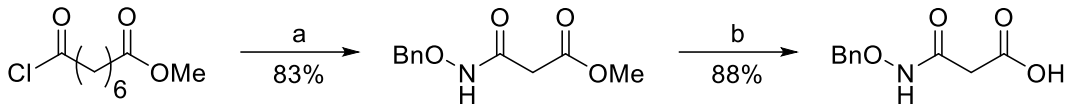

3-203 **3-204**

Reagents & Conditions: a. NH_2OH HCl (1.5 eq), DIPEA (3 eq), THF, rt, 16 h; **b.** LiOH (3.9 eq), H_2O, rt, 16 h

Scheme 3.82: Synthesis of linker 3-204.

2.6 Scaffold 6: 4-amino-2-hydroxybutanoic acid derivative

As mentioned in chapter 2, a crystal structure of SmHDAC8 without inhibitor has been reported, but a closer look at the catalytic site revealed the presence of an L-tartrate from the buffer.[322]

Carboxylic acids are rather weak zinc binding groups because of their monodentate interaction with the metal. However, the presence of a hydroxyl group on the α-position could be seen as a structure derived from a hydroxamic acid (Figure 3.9). Based on the crystal structure,[322] interactions are expected between this hydroxyl group and the zinc atom. Thus α-hydroxyl carboxylic acid is a bidentate zinc binding group, and to our knowledge, HDAC inhibitors based on this structure have not been reported.

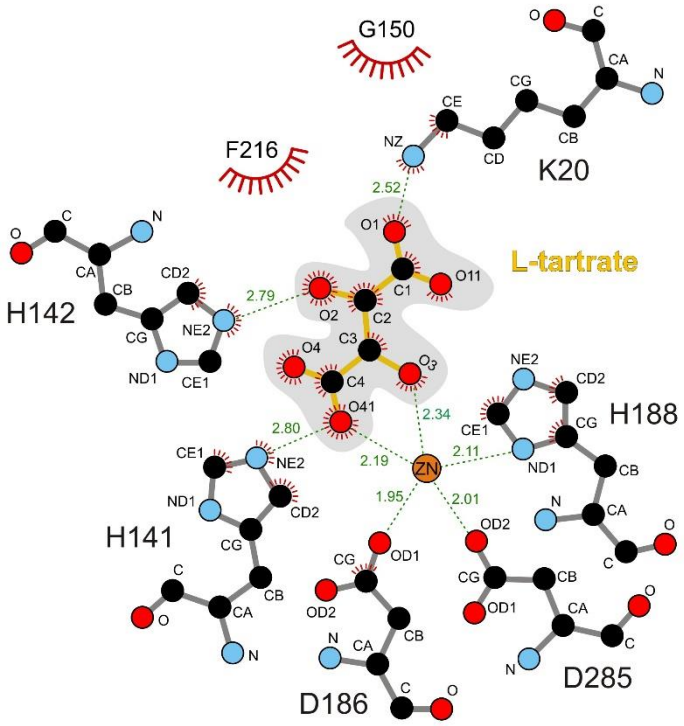

Figure 3.9: View of the interaction of L-tartrate with SmHDAC8 catalytic zinc ion.
Taken from Marek et al.[322]

Moreover, it is worth noting that additional hydrogen bonds were observed. Indeed, the β-hydroxyl group is forming a hydrogen bond with a close-by histidine H142, while the second carbonyl is bonding to a neighbouring lysine K20. These additional interactions could also be investigated.

This structure piqued our curiosity, and we started investigating. However, we decided only to synthesise a couple of compounds to evaluate their potential interest as HDAC inhibitors and keep these structures as part of future work.

The α-hydroxyl-carboxylic acid compounds were obtained by nucleophilic substitution of (2*S*)-4-amino-2-hydroxybutanoic acid on acyl chloride at room temperature (Scheme 3.83). The nature of the acyl chlorides was chosen to get a small aromatic cap group and a linker chain of 6-7 atoms.

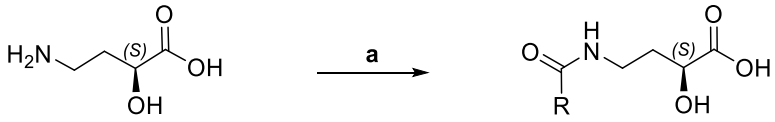

3-XXX

Reagents & Conditions: a. RCOCl (1 eq), NaOH (1 eq, 1M aq.), rt, 16 h

Acyl Chloride	Product	Compound number	Yield
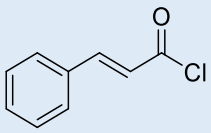	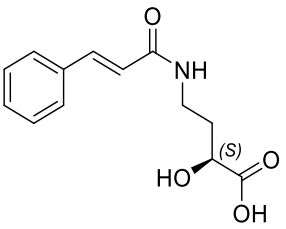	**3-205**	54%
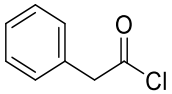	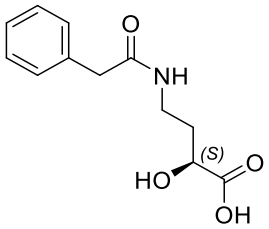	**3-206**	55%

Scheme 3.83: Synthesis of 2-hydroxybutanoic derived compound 3-205 and 3-206.

3. Biological evaluation

Now that potential inhibitors had been synthesised, we were ready to evaluate their inhibitory activity on HDAC.

3.1 Principle of the inhibition assays

3.1.i HDAC enzymatic inhibition assay

The compounds were first evaluated using an enzymatic assay following a previously described procedure.[486]

In this two-step assay, the fluorogenic substrate, which comprises a sequence with an acetylated lysine, is incubated with human recombinant HDAC. Then, the substrate is treated with a lysine developer solution that releases a fluorophore from the substrate. The light emission, resulting from the excitation of the fluorophore, can then be quantified with a fluorescence reader.

The developer consists of an enzyme called trypsin, which cleaves the peptide chain at the lysine residue. In the assay, the fluorophore is initially linked to the acetylated substrate in an inactive form (Figure 3.10). After incubation, and deacetylation by the HDAC, the trypsin recognises the free lysine and cleaves the peptide, releasing an activated dye. Then using a specific wavelength, the dye is excited, and the fluorimeter measures the resulting emission at a precise wavelength.

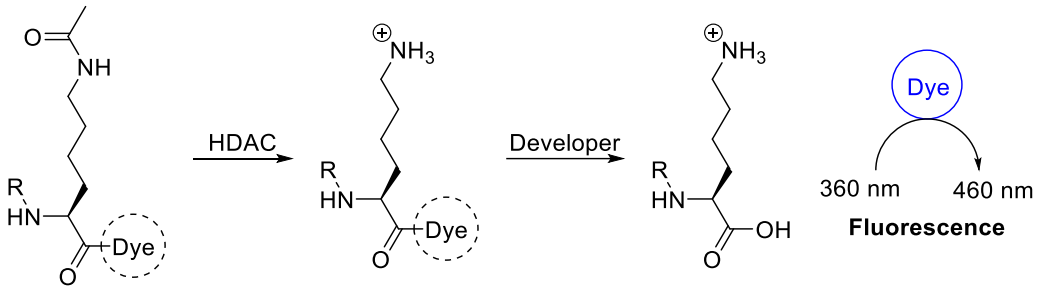

Figure 3.10: Principle of the fluorogenic HDAC assay.

In the evaluation of the inhibition potency of a compound, the inhibitor is added during the first step of the assay. The inhibition of the HDAC activity results in a reduced amount of deacetylated substrate. Thus, after treatment with the developer, a smaller number of active dyes are released in the mixture, and the fluorescence measured by the fluorimeter decreases accordingly in a dose-dependent manner.

The compounds activity was measured at different concentration in a dose-response experiment in order to determine the half maximal inhibitory concentration (IC_{50}). To this end, six to seven

concentration points for each compound were evaluated, and the resulting percentage of activity was fitted in a sigmoid dose-response curve.

An example of the sigmoidal dose-response curves obtained with the enzymatic evaluation is shown in Figure 3.11.

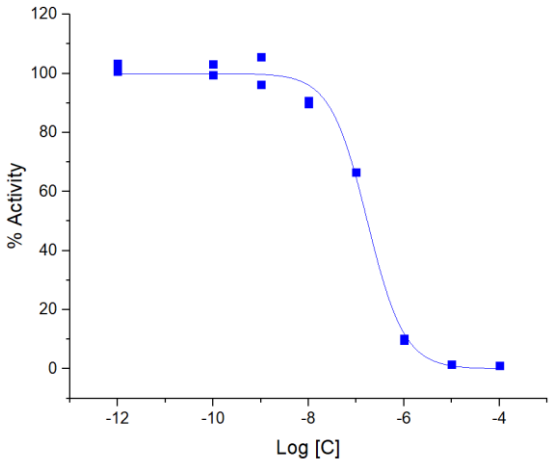

Figure 3.11: Dose-response curves showing the effects of compound 3-40 on HDAC6 enzymatic activity (n = 2).
The X-axis is in logarithm of concentration (Molar); the Y-axis is the % of activity relative to 100% activity (HDAC6 + substrate, no inhibitor).

Using similar assays, several compounds were also tested on other human HDACs as well as parasite HDACs.

To determine the enzymatic activity of our compounds, we collaborated with the groups of Prof. M. Jung from the University of Freiburg in Germany and Prof. L. Bischoff from the Rouen Normandy University in France who performed the enzymatic assays. In addition, both Prof. M. Jung and Prof. L. Bischoff performed SmHDAC8 inhibition assays, and Prof. M. Jung carried out TcDAC2 inhibition assay.

3.1.ii Cell viability assay

In addition to the HDAC enzymatic assay, and in order to determine if the activity could be translated to pharmacological effects in cells, several compounds were tested in three AML cellular models, namely MV4-11, U937 and THP-1 cell lines.

The CellTiter-Glo® Luminescent Cell Viability Assay is a method that detects the presence of metabolically active cells in culture based on quantitation of the ATP present. This assay is based on the established proportionality between the amount of ATP and the number of cells in the culture.[487]

The homogeneous assay procedure involves adding a single reagent (CellTiter-Glo® Reagent) directly to the cells after incubation with the HDAC inhibitors. The reagent then induces the cell lysis, and the action of the Ultra-Glo™ Recombinant Luciferase generates a stable luminescent signal proportional to the amount of ATP present in the culture. The luciferase reaction for this assay requires the presence of Mg^{2+} and oxygen to produce bioluminescence and is shown in Figure 3.12.

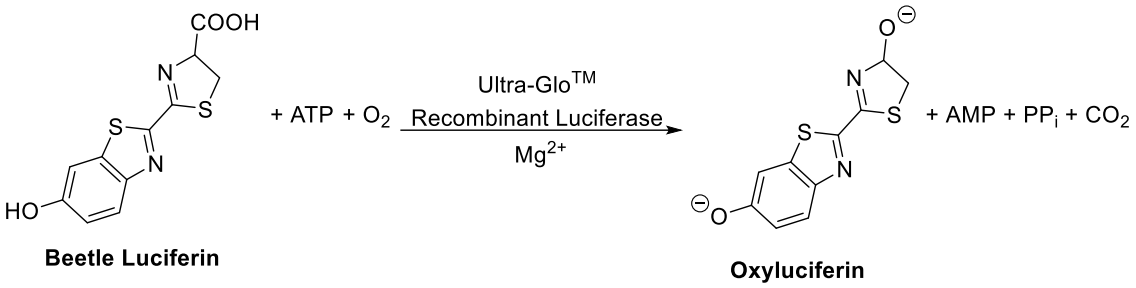

Figure 3.12: CellTiter-Glo® reaction.
***Adapted from manufacturer manual*.** [488]

To evaluate the antitumor effect of our compounds, we collaborated with Dr M. T. Borrello from the French INSERM U1068 Cellular Stress Group in Marseille who carried out the cell viability assay. In addition, Dr M. T. Borello also performed western blot analysis.

3.2 Results and discussion

3.2.i Imidazole-based scaffold

"Closed" analogue

As previously mentioned, Bertrand Lecointre had first investigated the imidazo-ketopiperazine scaffold prior to my arrival. In addition, compound **3-29**, **3-36** and **3-37** had been evaluated in the enzymatic assay on HDAC1, HDAC6 and HDAC8.[399] The results of these assays are integrated into this section as part of the general evaluation of the scaffold. On the other hands, further biological evaluations were done using the compounds that were synthesised in chapter 3. The molecular docking studies and the cell assays therefore fully result from this PhD work.

The initial investigation of the inhibition activity focused on HDAC6, and the results are shown in Table 3.4.

Compound	IC_{50} (nM) (n = 1)
3-29	74
3-36	1945
3-37	333

Table 3.4: Activity of 3-29, 3-36 and 3-37 in enzymatic inhibition assay on HDAC6.[399]

The first conclusion from these results is the confirmation that the linker size has a substantial impact on the activity. A closer look at the imidazo-ketopiperazine scaffold with an alkyl linker of respectively five carbons (**3-36**), six carbons (**3-29**) and seven carbons (**3-37**) reveals an optimum size of linker. Indeed **3-29**, which shares a similar linker with vorinostat, is the most potent inhibitor of HDAC6.

A likely explanation of the observed SAR comes from a balance between strong hydroxamic acid chelation to the zinc ion in the active site of the HDAC and proper interaction of the cap group with the enzyme rim.

In the case of the optimum linker size (**3-29**), the high activity results from the best combination of strong chelation to the zinc atom and enzyme rim interaction.

Regarding the seven carbon linker (**3-37**), we observe a reduced activity. Yet still, the compound presents an interesting sub-micromolar inhibition. We hypothesise that the interaction between the zinc binding group and the active site is poorly affected by the extension of the linker. However, the elongation of the alkyl chain could disrupt the interaction with the rim, thus lowering the activity.

On the other hand, with a short linker (**3-36**), we observe an important loss of potency. As mentioned before the role of the linker is not only to allow the zinc binding group to reach the active site of the enzyme but also to favour the interaction with the rim. Accordingly, we identified two potential explanations for this reduced activity. On the one hand, it could be due to a weaker interaction between the hydroxamic acid and the zinc ion. A five-carbon alkyl chain could be too short to adequately fulfil its duty as a linker and fail to enable proper chelation. The hydroxamic acid being unable to reach the active site, the measured activity would therefore mainly result from the cap-enzyme rim interaction. On the other hand, the zinc-binding could be the predominant interaction due to the strong affinity between the hydroxamic acid and the zinc cation. In this case, the linker could partially drag the cap group into the enzyme channel and disturb its interaction with the rim.

The activity of the imidazo-ketopiperazine compounds was also evaluated against other isoforms of HDAC (Table 3.5).

Compound	HDAC1 IC_{50} (nM)	HDAC8 IC_{50} (µM)
3-29	879	0.97
3-36	4493	N/A
3-37	826	2.81

Table 3.5: Activity of compound 3-29, 3-36 and 3-37 against HDAC1/8 (n = 1).[399]

We were glad to observe that the compounds were all potent HDAC1 inhibitors with a micromolar or submicromolar IC_{50}. However, they all presented a lower inhibition effect than against HDAC6. Similar to the preliminary observation, the less potent compound corresponded to the shortest linker, while the two other compounds shared a nanomolar activity. In contrast, a more significant difference was observed against HDAC8 with **3-29** maintaining a submicromolar IC_{50} while the potency of **3-37** dropped to over 2.5 micromolar IC_{50}.

Following these preliminaries results obtained by Bertrand Lecointre, we tried to understand the evolution of the activity between the different isoforms of HDAC.

We decided to model docking of the inhibitors into the enzyme active site. Figure 3.13 shows the results of these docking studies that were operated by Prof. W. Sippl from the Martin-Luther University of Halle-Wittenberg in Germany.

In the first place, we examined the interaction of **3-29** (Figure 3.13A) and **3-37 (**Figure 3.13B) with HDAC6. As expected, we observe bidentate chelation of the hydroxamic acid with the zinc cation for both compounds. Moreover, a stabilising hydrogen bonding is predicted between the aspartic acid residue D497 of the enzyme and the amido part of the imidazo-ketopiperazine for both compounds. In addition, two hydrogen bonds are predicted, in the catalytic site, between the hydroxamic acid and the histidines H610 and H611. On the other hand, the observed difference in potency between **3-29** and **3-37** could be due to the orientation of the cap group on the rim. Indeed, the docking of **3-29** forecast that the benzyl on the imidazo-ketopiperazine fits in a hydrophobic pocket created by the proline P501 and the leucine L749 residues. Meanwhile, the extended linker of **3-37** is predicted to force the phenyl out of the pocket and flip the cap group to the opposite orientation, thus slightly destabilising the interaction compared to **3-29**.

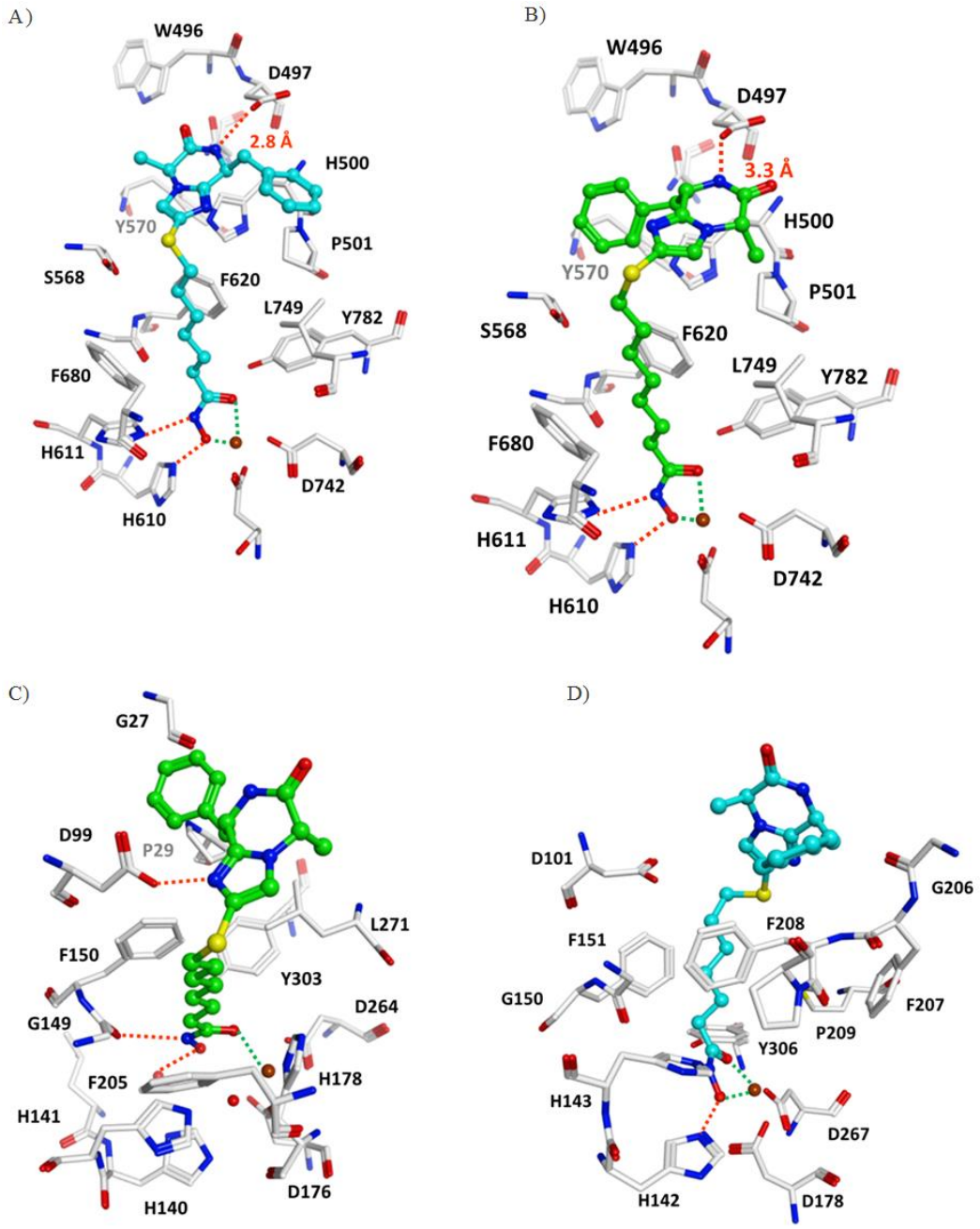

Figure 3.13: Molecular docking of compounds (A) 3-29 and (B) 3-37 in the HDAC6 active site (PDB ID: 5EDU). Docking (C) of 3-37 in the HDAC1 active site (PDB ID: 5ICN) and (D) of 3-29 in the HDAC8 active site (PDB ID: 2V5X) are also shown.

Hydrogen bonds are shown as orange coloured dashed lines, coordination between the hydroxamic acid and the zinc ion (coloured brown) is shown as green coloured dashed lines. Conserved water molecules in the active site are shown as red spheres. Figure supplied by Prof. Sippl.

Then we turned our attention to the docking of **3-37** with HDAC1 (Figure 3.13C). Surprisingly, the chelation with the zinc cation is predicted to be only monodentate. However, the hydroxamic acid is still involved in two hydrogen bonds in the catalytic site. Besides, the imidazo-ketopiperazine is still expected to interact with a surrounding amino acid residue, but with the

aspartic acid D99. These predictions are consistent with the experimental results. The loss of potency compared to HDAC6 inhibition would, therefore, result from weaker chelation to the metal while the multiple hydrogen bonds would help to maintain a submicromolar activity. Additionally, the imidazo-ketopiperazine would be now binding to the enzyme through its imidazole ring. This interaction could block the cap group in a single position and explain that **3-29** and **3-37** shares similar IC_{50} values.

Finally, we looked at the docking between **3-29** and HDAC8 (Figure 3.13D). In this case, the compound is once again chelated bidentately to the metal, but only one hydrogen bond is predicted. More importantly, the imidazo-ketopiperazine end of the molecule is sticking out of the enzyme pocket and is more exposed to the solvent than on the other isoforms. The only predicted interaction with the amino acid residues of the enzyme is between the phenylalanine F208 and the benzyl side chain of the scaffold. The relatively similar activity of **3-29** on HDAC8 compare to HDAC1 could, therefore, be due to the recovery of stronger chelation which could compensate the reduction of side interactions with the enzyme. However, the extended alkyl chain of **3-37** could expose the compound even more to the solvent and prevent the interaction with F208, thus explaining the significant drop in potency.

To sum up, the short linker of **3-36** impairs its activity against both HDAC1 and HDAC6, thus limiting its interest. On the other hand, both compounds **3-29** and **3-37** show significant activity on HDAC1, HDAC6 and HDAC8 and offer a noteworthy selectivity (Table 3.6).

Compound	HDAC1/HDAC6	HDAC8/HDAC6
3-29	11,9	13,1
3-36	2,3	N/A
3-37	2,5	8,4

Table 3.6: Selectivity of compound 3-29, 3-36 and 3-37 between HDAC1/6 and HDAC8/6.

As our most interesting inhibitor **3-29** was displaying a selectivity between the HDAC isoforms, we decided to evaluate its inhibitory effect against all 11 human HDACs. The French CRO Cerep performed these assays, and the results are shown in Table 3.7.

It is important to note that the tests were performed with some differences in the assay conditions. Therefore, the values are not directly comparable to the previously described activity.

In this assay, compound **3-29** showed substantial inhibition of HDAC6/8 and a more limited activity against HDAC1. Conversely, only little inhibition was observed on the others HDACs. Consequently, this compound has a remarkable degree of isoform selectivity with a 13-fold

degree of selectivity between the two preferential targets HDAC6 and HDAC8. Moreover, the inhibitor is 45-fold less active against HDAC1 and has minimal activity (IC_{50}>10 μM) on the other HDACs isoforms. This compound, therefore, presents a higher selectivity than ricolinostat (Table 3.8), a selective HDAC6 inhibitor currently in clinical candidate against multiple myeloma and metastatic breast cancer.[489,490]

class I isoforms		class IIa isoforms		class IIb or IV isoforms	
HDAC1	57%, IC_{50}: 7.3 μM	**HDAC4**	4%	**HDAC6**	99%, IC_{50}: 160 nM
HDAC2	32%	**HDAC5**	23%	**HDAC10**	44%
HDAC3	38%	**HDAC7**	9%	**HDAC11**	10%
HDAC8	90% IC_{50}: 2.1 μM	**HDAC9**	1%		

Table 3.7: Percentage inhibition of individual HDAC isoforms by 3-29.
Values are the mean of two measurements. The assay was performed with a test concentration of 10 μM. IC_{50} values were determined for HDAC1, HDAC6 and HDAC8.

Class	Isoform	Potency (fold) / HDAC6	
		3-29	**ricolinostat**
Class I	HDAC1	45	12
	HDAC2	> 62	10
	HDAC3	> 62	11
	HDAC8	13	21

Table 3.8: Selectivity of HDAC6 inhibitors 3-29 and ricolinostat against class I HDAC.[489]

Following the evaluation of these compounds on the enzymatic isoforms of HDAC, we decided to move to further studies and evaluate their activity on the cellular assay for the growth inhibition of cancer cell lines (Table 3.9). Each test was performed in triplicate with an incubation time of 72 and 96 hours.

Compound	Cell line	IC_{50} (µM, n = 3) 72 h	IC_{50} (µM, n = 3) 96 h
	MV4-11	4.50 ± 0.25	6.75 ± 0.40
3-29	THP-1	10.4 ± 0.32	9.01 ± 0.30
	U937	0.90 ± 0.23	0.46 ± 0.72
	MV4-11	>25	>25
3-36	THP-1	>25	>25
	U937	>25	>25
	MV4-11	1.66 ± 0.18	2.60 ± 0.71
3-37	THP-1	1.72 ± 0.20	1.70 ± 0.60
	U937	0.14 ± 0.02	0.31 ± 0.19

Table 3.9: Cell growth inhibition by compounds 3-29, 3-36 and 3-37 in MV4-11, THP-1 and U937 cell lines.

In agreement with the results of the enzymatic assay, no activity was observed with **3-36** as an inhibitor. By contrast, we were pleased to detect a micromolar inhibition with both **3-29** and **3-37**. Interestingly, those compounds were active on every cell line and, in particular, the U397 lymphoma cell line was highly responsive to the treatment with the inhibitors. However, contrary to the enzymatic assay conclusions, the optimum linker size for this assay corresponded to the seven carbon alkyl chain of **3-37**. In our opinion, this doesn't result from the intrinsic activity on the HDAC but rather from a better cellular penetration due to the increase of lipophilicity.

We then decided to do a western blot of the U937 cells following treatment with **3-37**. This analysis revealed a dose-dependent effect on histone H3 and tubulin acetylation level (Figure 3.14). This suggests that compound **3-37** is active on class I and class II HDAC isoforms.

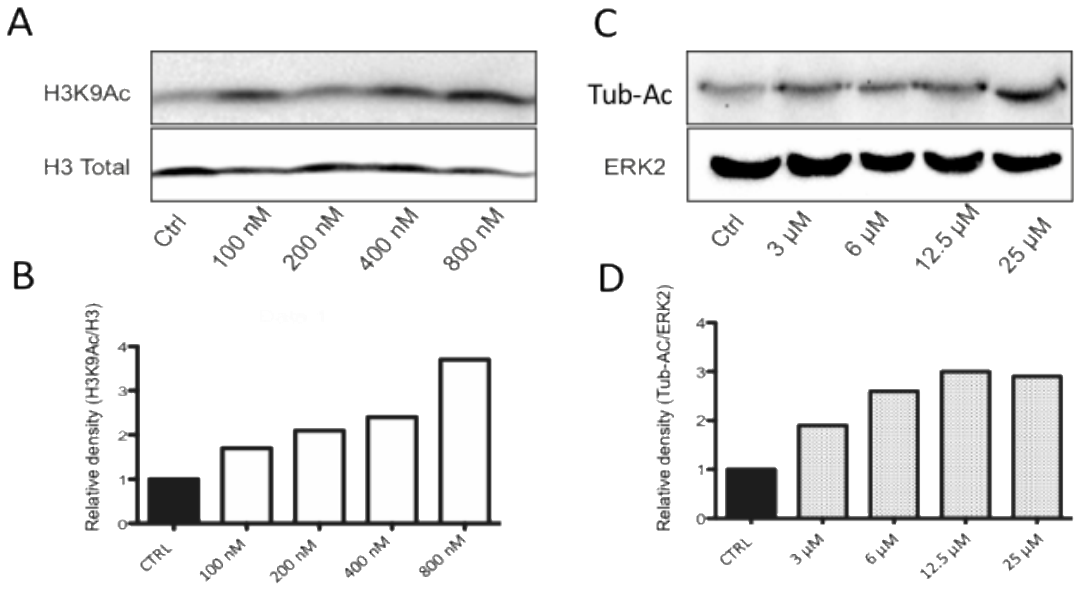

Figure 3.14: Western blot analysis of acetylated H3K9 (A) and acetylated Tubulin (C) and their relative loading controls (H3 total and ERK2), after treatment of U937 cells with HDAC inhibitor 3-37.

Western blot signals were quantified by densitometry using Image Lab 6.0 (BIORAD) and signal intensities plotted against the loading controls (B and D plots).

Finally, we decided to investigate whether these compounds could inhibit HDAC in a *Schistosoma mansoni* parasite. Their activity was evaluated in an enzymatic inhibition assay on SmHDAC8 (Table 3.10). The reported IC_{50} corresponds to the mean value of two experiments in a dose-response assay.

Compound	SmHDAC8 IC_{50} (µM)	SmHDAC8/hHDAC8
3-29	2.20 ± 0.33	2.27
3-37	0.61 ± 0.03	0.22

Table 3.10: Enzymatic inhibition of SmHDAC8 by 3-29 and 3-37 and their selectivity between SmHDAC8 and hHDAC8. (n = 2)

Once more, both compounds show a micromolar to submicromolar inhibition. A pleasing observation was to find out that, contrary to the results obtained in the human HDAC8 enzymatic assay, compound **3-37** turned out to be a highly active inhibitor of SmHDAC8. Even more importantly, **3-37** is 4.5-fold more active against the parasite HDAC8 than on its human analogue. This selectivity toward the *Schistosoma mansoni* HDAC8, which is not observed with **3-29**, could have a significant impact on the development of more selective inhibitors.

To sum up, **3-29** and **3-37** are of particular interest as HDAC inhibitors. These two compounds showed micromolar to submicromolar activity against different cancer cell line in the cell growth inhibition assay. Their effect was shown to affect the histone H3 and the α-tubulin acetylation level in a western blot. This analysis is consistent with the enzymatic assay on the different HDAC which revealed a selective inhibition of HDAC1, HDAC8 and HDAC6 with the latter being the most potent target. This selectivity was also predicted in docking studies which correlated with the experimental observation. Moreover, although **3-29** corresponded to the most exciting compound in enzymatic inhibition assay against human HDAC, both in terms of potency and selectivity, the extension of the linker to **3-37** offered better results in cell assays, in all likelihood by increasing the cellular uptake. Finally, those compounds are not only potent inhibitors in human but also showed a significant effect on the *Schistosoma mansoni* HDAC8. Besides, **3-37** also featured notable properties regarding the selectivity with a higher potency on the parasite HDAC8 than on its human equivalent.

The results of this class of inhibitor on human HDAC and leukaemia cells were recently published in the Royal Society Philosophical Transaction B journal.[491]

"Open" analogue

We then turned our attention to compounds **3-38** and **3-40** which are the "open" analogue of respectively **3-36** and **3-37** and evaluated their activity on HDAC6 (Table 3.11). With this structure, we observed an improvement of the activity. In particular, we found a significant difference of potency between the five-carbon linker of **3-38** compared to its analogue **3-36**. Following the previous hypotheses on the effect of a short linker, the enhanced potency could result from the higher flexibility of the cap group. The strong interaction between the hydroxamic acid warhead and the zinc cation could drag the imidazole end in the enzyme channel, but the higher degree of freedom of the non-cyclized amino acids could still ensure proper interaction with the rim. Additionally, the presence of the Cbz-group could offer more possibilities of interactions with the surrounding amino acids through hydrogen bonding or π-stacking, thus increasing the potency.

Compound	IC_{50} (nM)
3-38	226 (n = 2)
3-40	172 (n = 2)

Table 3.11: Enzymatic inhibition of 3-38 and 3-40 on HDAC6.

We then decided to evaluate these compounds against the *Schistosoma mansoni* HDAC8 and the *Trypanosoma cruzi* HDAC2 (TcDAC2). The percentage of inhibition was measured using two concentration of inhibitors (Table 3.12).

Compound	Concentration (µM)	SmHDAC8 %Inhibition	TcDAC2 %Inhibition	
3-38	25	86.5	51.7	
	5	26.2	37.8	
3-40	25	69.5	80.2	TcDAC2
	5	41.5	56.6	IC_{50}: 5.4 µM

Table 3.12: Percentage of inhibition of 3-38 and 3-40 on SmHDAC8 and TcDAC2 at different concentration.

Unfortunately, only limited inhibition was observed on the parasite HDACs, so the compounds were not submitted to a more detail dose-response assay to determine their IC_{50}. However, an exception was made for compound **3-40** on TcDAC2, and an IC_{50} of 5.4 µM was determined. This value usually corresponds to moderate activity in HDAC enzymatic assays and the compound would not be considered as a first-class inhibitor. However, no TcDAC2 inhibitors have been reported in the literature so far. This compound is, therefore, an exciting hit, and future optimisation of the structure could lead to one of the first class of TcDAC2 inhibitors.

With limited effects on the parasites, we turned our attention to the activity against cancer cells, and the compounds were submitted for cell growth inhibition assay. The tests were done in triplicate with an incubation time of 72 hours and 96 hours (Table 3.13).

Compound	Cell line	IC_{50} (µM, n = 3) 72 h	IC_{50} (µM, n = 3) 96 h
	MV4-11	> 25	> 25
3-38	THP-1	3.25 ± 0.18	3.24 ± 0.41
	U937	0.41 ± 0.19	0.33 ± 0.10
	MV4-11	> 25	> 25
3-40	THP-1	8.45 ± 0.47	5.05 ± 0.07
	U937	2.71 ± 0.54	1.80 ± 0.60

Table 3.13: Cell growth inhibition by compounds 3-38 and 3-40 in MV4-11, THP-1 and U937 cell lines.

The first conclusion from these assays is to observe a selectivity between the cell lines. Contrary to their imidazo-ketopiperazine analogues, which are either active on every cell lines or totally inactive, these compounds express a cell growth inhibition only on THP-1 and U937 leukaemia cell lines. More biological studies would be required to fully understand the difference in activity. Nevertheless, we identified potential explanations. The imidazo-ketopiperazine compounds showed a selective inhibition against HDAC1/6/8. However, this scaffold could have a different profile of inhibition against the HDAC isoforms. Depending on the influence of each HDAC in

the cell growth of the different cell lines, the response to treatment with these inhibitors would thus be divergent. Additionally, as mentioned in the first two chapters, HDACs are also interacting with non-histone proteins, such as p53, and the three cell lines used in the assay are not equal regarding their p53 status. Indeed, MV4-11 has a wild-type status while THP-1 and U937 are mutated as most AML cells.[492] This was shown to affect the antiproliferative activity of MV4-11 compared to another cell line when treated with HDAC inhibitors.[493,494]

The second conclusion from this assay comes from the effect of the linker length. In agreement with the enzymatic results, this scaffold is more tolerant to the number of atoms in the alkyl chain. Indeed, when a five-carbon linker in **3-36** led to a completely inactive compound in cells, the same linker in **3-38** turned out to be preferential in this scaffold and led to an active compound both on THP-1 and U937. On the other hand, the extension of the linker to a seven-carbon alkyl chain in **3-40** resulted in a loss of potency. This could be due to the high lipophilicity of the compound (logP = 5.95, calculated with MarvinSketch 18.19).

To sum up, keeping the imidazole scaffold uncyclized had several effects on the properties as HDAC inhibitors. Both **3-38** and **3-40** are potent HDAC6 inhibitors in the enzymatic assay, and the difference in the linker length had limited impact on the activity. In cancer cells, the issue with short linkers was overcome, and nanomolar activity on U937 cell line was observed. Moreover, this structure is more selective than the imidazo-ketopiperazine scaffold, with strong activity on U937, moderate on THP-1 and low activity on MV4-11. Finally, the compounds have limited potency on SmHDAC8, but **3-40** was identified as an exciting hit on TcDAC2.

3.2.ii Triazole-based scaffold

The scaffold was first tested on enzymatic inhibition assay. Compound **3-119** and **3-130** were tested on HDAC6 in duplicate (Table 3.14).

Compound	IC_{50} (µM)
3-119	>20
3-130	15.5

Table 3.14: Enzymatic inhibition of HDAC6 by 3-119 and 3-130. (n = 2).

Although substituting the phenyl on the 4th position of the triazole (**3-119**) to a cyclopropyl (**3-130**) slightly improved the potency, those compounds displayed low activity on HDAC6.

We then decided to evaluate the inhibition properties of **3-119** on SmHDAC8 and TcDAC2 (Table 3.15). Again, low activity was observed.

Compound	Concentration (µM)	SmHDAC8 %Inhibition	TcDAC2 %Inhibition
3-119	25	51.6	36.4
	5	37.0	36.1

Table 3.15: Percentage of inhibition of 3-119 on SmHDAC8 and TcDAC2 at different concentration.

Despite these disappointing preliminary results, we decided to submit the different compounds of the scaffold to the cell growth inhibition assay (Table 3.16). Indeed, the compounds could still be potent on other HDAC isoforms and present antitumor effect.

Compound	Cell line	IC_{50} (µM, n = 3) 72 h	IC_{50} (µM, n = 3) 96 h
3-119	MV4-11	> 25	> 25
	THP-1	> 25	> 25
	U937	> 25	> 25
3-127	MV4-11	> 25	> 25
	THP-1	> 25	> 25
	U937	1.50 ± 0.70	0.70 ± 0.08
3-128	MV4-11	> 25	> 25
	THP-1	> 25	> 25
	U937	> 25	> 25
3-129	MV4-11	> 25	> 25
	THP-1	24.3 ± 1.42	23.2 ± 0.78
	U937	10.7 ± 0.15	9.04 ± 0.27
3-130	MV4-11	> 25	> 25
	THP-1	> 25	> 25
	U937	> 25	> 25

Table 3.16: Cell growth inhibition of triazole-based compound in MV4-11, THP-1 and U937 cell lines.

These assays mainly led to no significant activity on cancer cell growth. Nevertheless, two compounds displayed potent activity on the U937 leukaemia cell line. Interestingly, they both featured fluorine group on the 4th position of the triazole with **3-127** bearing a 4-fluorophenyl and **3-129** bearing a 4-(trifluoromethyl)phenyl.

The high electronegativity and the small size of the fluorine could explain these results. Indeed, both fluorine and trifluoromethyl groups are electron withdrawing groups, and the electron-poor benzyl ring could be involved in side interactions with the surrounding amino-acid residues. Additionally, due to its high electronegativity, fluorine is able to interact with hydrogens. The scientific community is still wrangling to determine if this kind of interaction should be considered as hydrogen bond, but weak interactions have been reported and could be

involved.[495,496] Besides, this interaction is weaker with a CF_3 group than with fluorine, and that would be consistent with the reduction in activity observed between **3-127** and **3-129**. Nevertheless, a more in-depth investigation will be required to establish and understand the SAR.

3.2.iii Praziquantel – HDACi hybrid

As this scaffold was explicitly designed as a potential anti-parasitic agent, the compound was only tested in the enzymatic inhibition assay against SmHDAC8 (Table 3.17). We were pleased to observe a strong inhibition on the parasite, and this preliminary result validated the possibility of forming potent HDAC inhibitor derived from praziquantel. This compound is currently evaluated in phenotype assay on schistosomula and adult worms.

Compound	SmHDAC8 IC_{50} (nM)
3-192	768 ± 126

Table 3.17: Enzymatic inhibition of SmHDAC8 by 3-192.

3.2.iv 4-amino-2-hydroxybutanoic acid scaffold

Following the synthesis of 4-amino-2-hydroxybutanoic compounds, **3-205** was submitted to enzymatic inhibition assay against HDAC6 and to the cancer cell growth inhibition assay (Table 3.18). Unfortunately, the compound showed weak inhibition in the enzymatic assay and no measurable effect in cancer cells.

Compound	HDAC6 IC_{50} (µM)	Leukaemia Cell line	IC_{50} (µM, n = 3) 72 h	IC_{50} (µM, n = 3) 96 h
3-205	> 20	MV4-11	> 25	> 25
		THP-1	> 25	> 25
		U937	> 25	> 25

Table 3.18: Evaluation of 3-205 activity in the enzymatic assay on HDAC6 and cancer cell growth inhibition assay.

Chapter 4. Development of a new class of SETD8 inhibitor.

1. Introduction

This chapter will present the results of a three-month project completed at the University of Salerno in Italy. As a member of the COST action Epichembio, the first European chemical biology network focused on epigenetics, I enrolled in a short-term scientific mission to develop a novel class of inhibitors of lysine methyltransferase SETD8 in the group of Prof. G. Sbardella.

2. Synthetic approach

Following the publication by Ma[166] and Butler[168] of potent and selective SETD8 inhibitors, we were interested in the development, and the evaluation, of a new class of compound, derived from their reported quinazoline. Our approach consisted in switching the core of the molecule from a fused bicyclic structure to a phenylpyrimidine (Scheme 4.1).

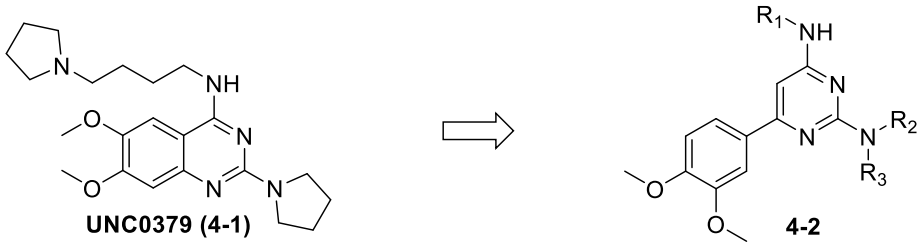

Scheme 4.1: From published quinazoline 4-1 to phenylpyrimidine scaffold 4-2.

Methoxy groups were shown to have great importance for the structure-activity in particular in the 6th position of the quinazoline.[167] Thus we decided to maintain these groups on the phenyl part of our scaffold. On the other hand, substituents on the 2nd and 4th position were more tolerant to modulation. Therefore, we decided to use them as points of diversity and to explore several variations on these positions.

The synthesis started with 2,4,6-trichloropyrimidine which was successfully coupled to 3,4-dimethoxyphenylboronic acid under Suzuki conditions (Scheme 4.2) in 74% yield. This reaction was reported to be highly regioselective,[497,498] and no formation of 2-phenylpyrimidine side product was observed.

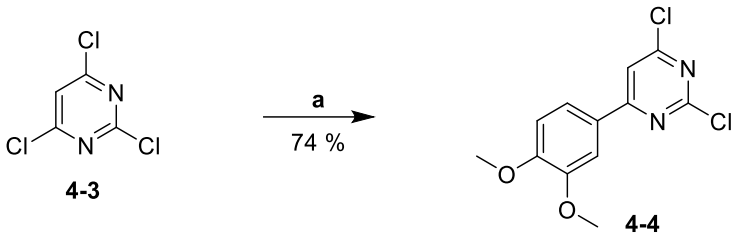

Reagents & Conditions: a. 3,4-dimethoxyphenylboronic acid (1.1 eq), Cs_2CO_3 (3 eq), $Pd(dppf)Cl_2 \cdot DCM$ (0.1 eq), Dioxane/H_2O 2:1, μW (80 °C, 300 W, 30 min)

Scheme 4.2: Formation of 3,4-dimethoxyphenylpyrimidine 4-4 by Suzuki coupling.

The second step of the synthesis consisted of a reaction of amination at C4 of the pyrimidine. Direct nucleophilic displacement of 2,4-dichloropyrimidine with neutral nitrogen nucleophiles has been successfully reported,[499,500] but those conditions led to low regioselectivity, and a mixture of 2-substituted and 4-substituted pyrimidine was formed. Higher regioselectivity can be achieved by using LiHMDS and palladium catalyst,[501] but we opted in favour of the first method. Although the formation of regioisomers is usually undesired and tends to be avoided, the rationale behind this decision was to consider this reaction as an additional diverging step to expand our library. This lack of selectivity would allow not only to study the effect of various substituents on the pyrimidine core but also the impact of their positioning.

In a first synthetic attempt, we decided to introduce a 3-dimethylamino-1-propylamine on the heterocycle. This reagent was commercially available, and the quinazoline SAR reported good potency with dimethylamino alkyl chain at the 4th position. Therefore, we considered it an interesting first choice of reagent to establish the synthesis.

Amination of the 2,4-dichloropyrimidine **4-4** was successfully achieved in 63% yield by reaction with 3-dimethylamino-1-propylamine (Scheme 4.3). The crude was purified by flash chromatography on aluminium oxide with hexane and ethyl acetate, and both 4-substituted pyrimidine **4-5** and 2-substituted pyrimidine **4-6** were isolated in a 53:47 ratio respectively.

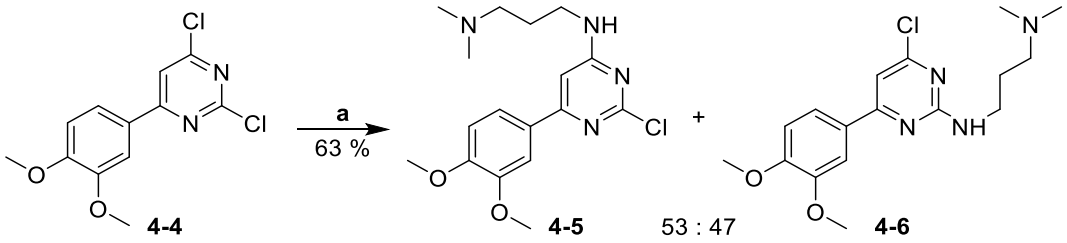

Reagents & Conditions: a. 3-dimethylamino-1-propylamine (3 eq), THF, μW (80 °C, 300 W, 30 min)

Scheme 4.3: Synthesis of regioisomers 4-5 and 4-6.

Identification of the corresponding structure of the two regioisomers was achieved by NMR spectroscopy. In ^{1}H NMR spectra, the chemical shift of the hydrogen at C5 was profoundly impacted by the nature of the substituent at C4. Chlorine is an electronegative atom with an electron withdrawing effect on the aromatic ring that results in a deshielding effect on the proton in ortho-position. Amino groups, on the other hand, have a positive mesomeric effect on the pyrimidine which increases the electron density of the ring and has a shielding effect on the proton. This difference was observed with a chemical shift for the proton on the 5th position of 6.51 ppm in **4-5** and 6.91 ppm in **4-6** (Scheme 4.4). Similar characteristics were reported in the literature,[501] and the regioselectivity had been confirmed by 2D NMR on a related structure before my arrival in the research group.

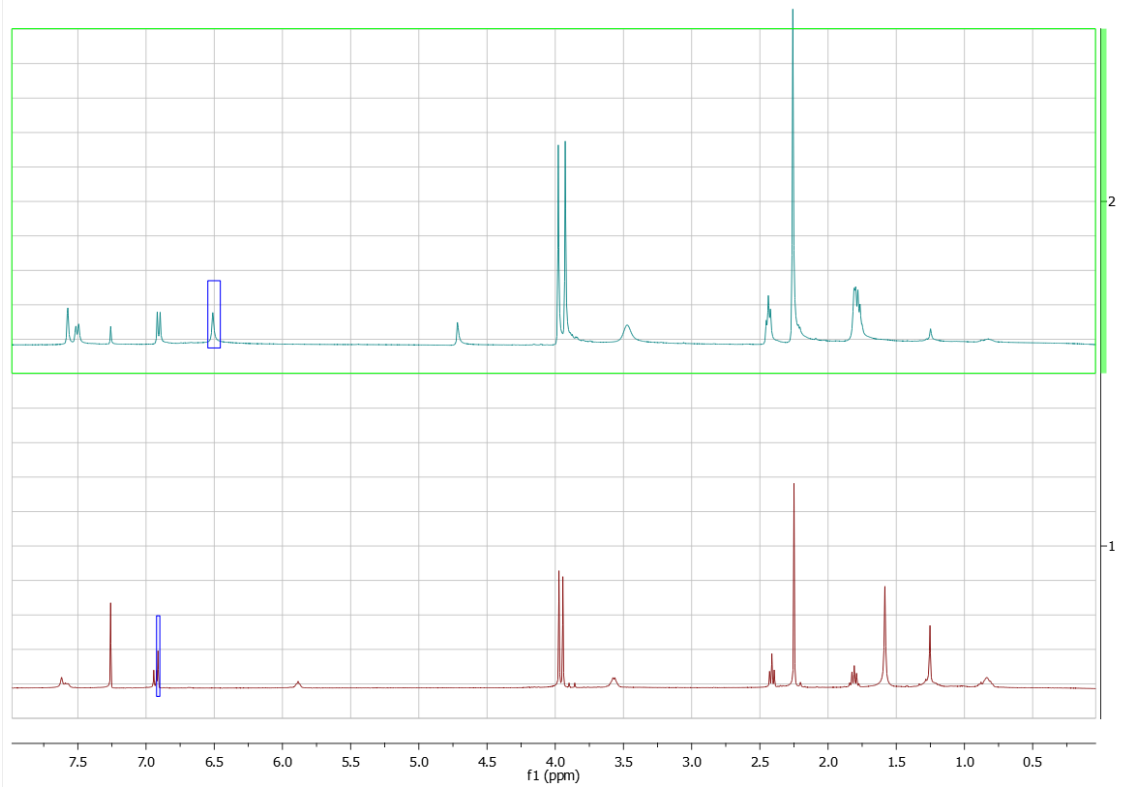

Scheme 4.4: Chemical shift difference in ^{1}H NMR of 4-5 (up) and 4-6 (down).

In the final step, the second amination reaction was carried out on both regioisomers with pyrrolidine (Scheme 4.5). The resulting compounds **4-7** and **4-8** were isolated in 44% and 68% yield respectively.

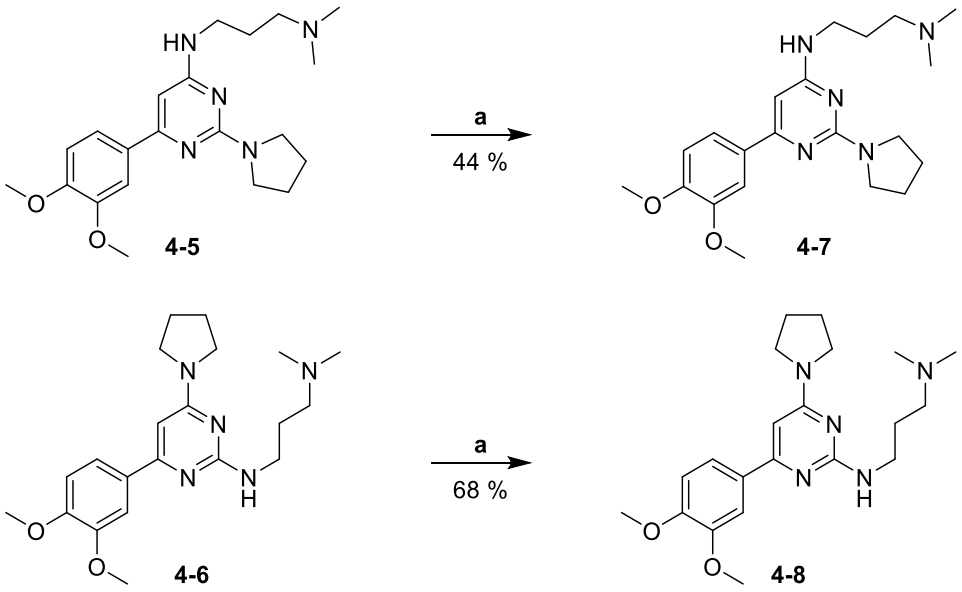

Reagents & Conditions: a. pyrrolidine (10 eq), THF, μW (120 °C, 300 W, 30 min)

Scheme 4.5: Synthesis of final compounds 4-7 and 4-8.

Following the setup of the synthetic pathway, we identified three axes of diversity to explore in order to build an original series of compounds.

First of all the length of the alkyl side chain could be modified. The reported SAR of **UNC0379** (**4-1**) focused on a terminal amino group linked to the quinazoline by a 5 or 6-member chain. We decided to investigate the impact of the linker by synthesising analogues using either a 3-carbon chain, as we did previously, or 5-carbon chain which was used in the **UNC0379** series.

The second point of interest was the nature of the amino groups. Modification of the pyrrolidine on the 2nd position resulted in a loss of potency of the compound in most examples of the SAR, so we decided to keep this structure in our analogues. On the other hand, the terminal amino group of the side chain was more tolerant to substitution. We chose to study the effect of such modification and to make analogues bearing either *N*, *N*-dimethylamino or pyrrolidinyl groups on the side chain end.

Finally, we turned our attention to the methoxy groups. Although we had chosen not to alter their nature as they seemed of importance for the potency, we decided to modify their position on the phenyl ring to probe the effect on inhibition. We opted in favour of two combinations: a meta,-para disubstituted phenyl and ortho,-meta disubstituted phenyl. A summary of the planned modifications is shown below (Scheme 4.6).

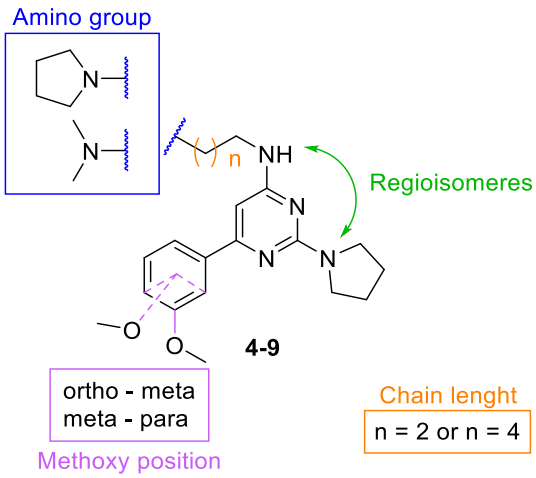

Scheme 4.6: Overview of scheduled changes in the series.

Regarding the synthesis of these analogues, most modifications directly fitted in the established pathway. Accordingly, Suzuki coupling of 2,4,6-trichloropyrimidine with 2,3-dimethoxyphenyl boronic acid successfully afforded **4-10** in 73% yield (Scheme 4.7).

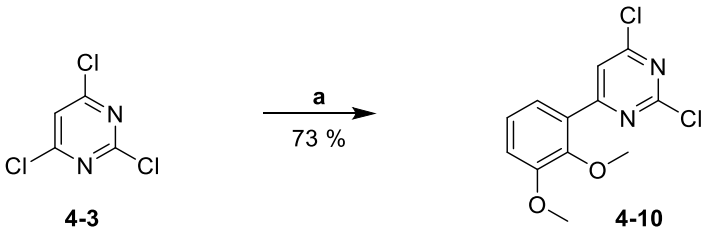

Reagents & Conditions: a. 2,3-dimethoxyphenylboronic acid (1.1 eq), Cs_2CO_3 (3 eq), $Pd(dppf)Cl_2 \cdot DCM$ (0.1 eq), Dioxane/H_2O 2:1, μW (80 °C, 300 W, 30 min)

Scheme 4.7: Formation of 2,3-dimethoxyphenylpyrimidine 4-10 by Suzuki coupling.

Similarly to the first synthesis, the next reaction was an amination step. However, some of the desired amino side chains were either not commercially available or too expensive to be considered. Thus we decided to modify this part of the synthetic pathway by a two-step route. Amination would first be performed with a terminal hydroxyl moiety on the alkyl chain, and in a second reaction, the alcohol would be converted to the desired amine. Although this alternative added one more step to the synthesis, the possibility to introduce any amine on the side chain was an attractive asset.

Meta,-para substituted compound **4-4** reacted with 5-amino-1-pentanol under microwave heating to afford in 72% yield the regioisomers **4-11** and **4-12** in a 65:35 ratio (Scheme 4.8). Similarly, ortho,-meta substituted compound **4-10** gave **4-13** and **4-14** in 87% yield in a 72:28 proportion.

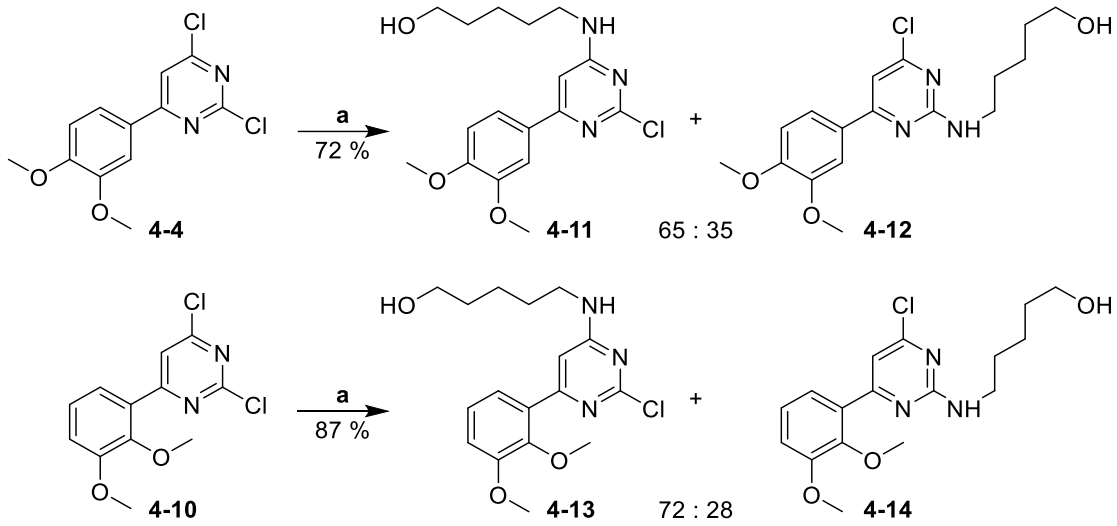

Reagents & Conditions: a. 5-amino -1-pentanol (3 eq), THF, μW (80 °C, 300 W, 30 min)

Scheme 4.8: Synthesis of isomers 4-11 to 4-14.

These compounds then reacted with pyrrolidine in the same conditions as previously described to afford the corresponding 2-(1-pyrrolidinyl)-pyrimidine (Scheme 4.9) and 4-(1-pyrrolidinyl)-pyrimidine (Scheme 4.10)

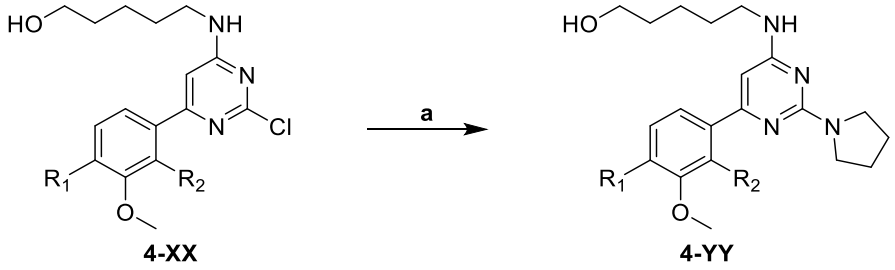

Reagents & Conditions: a. pyrrolidine (10 eq), THF, μW (120 °C, 300 W, 30 min)

R_1	R_2	4-XX	4-YY	Yield
OMe	H	**4-11**	**4-15**	68%
H	OMe	**4-13**	**4-16**	87%

Scheme 4.9: Synthesis of 2-pyrrolidinyl-pyrimidine intermediates 4-15 and 4-16.

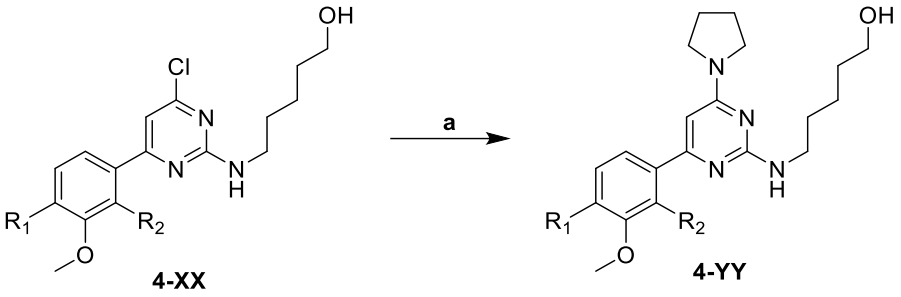

Reagents & Conditions: a. pyrrolidine (10 eq), THF, μW (120 °C, 300 W, 30 min)

R_1	R_2	4-XX	4-YY	Yield
OMe	H	**4-12**	**4-17**	96%
H	OMe	**4-14**	**4-18**	89%

Scheme 4.10: Synthesis of 4-pyrrolidinyl-pyrimidine intermediate 4-17 and 4-18.

A first option for the conversion of alcohol to amine was to use a Mistunobu reaction. Reported in 1967,[502] this reaction converted an alcohol to an ester using triphenylphosphine and diethyl azodicarboxylate (DEAD) to activate the corresponding carboxylic acid **4-20** (Scheme 4.11). This reaction was extensively studied, and similar results were reported with a variety of nucleophiles substituting the carboxylic acid.[503]

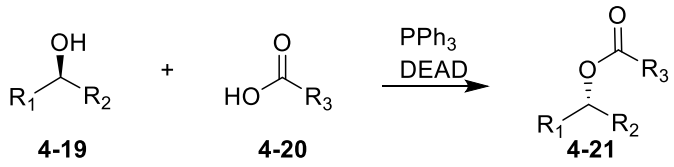

Scheme 4.11: Mitsunobu reaction.

We decided to try the reaction and substitute the alcohol with dimethylamine. However one of the requirements of the reaction is the presence of an acidic proton. As shown in the mechanism (Scheme 4.12), the betaine intermediate **4-22** catches a proton to form **4-23**. This step which requires a nucleophile with a p*K*a lower than 15 is a limitation in the scope of the reaction and usually prevents the use of amine.

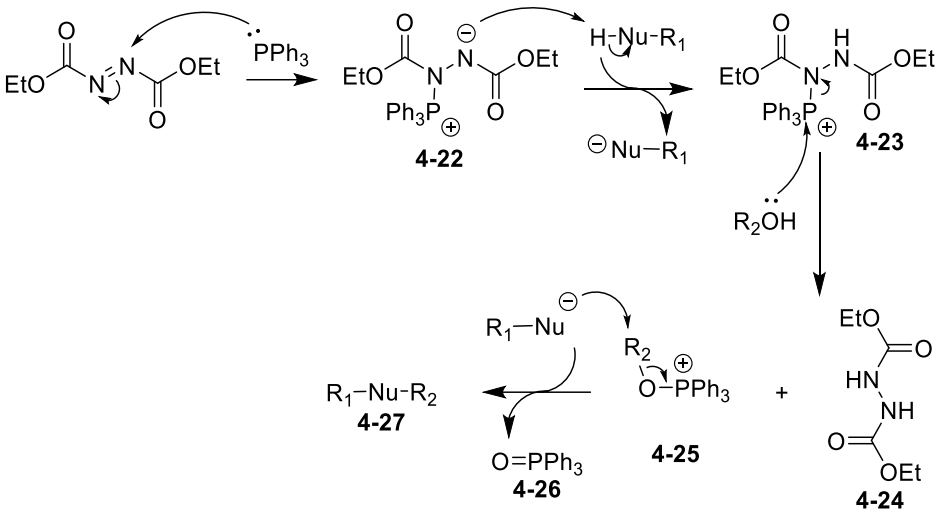

Scheme 4.12: Mistunobu reaction mechanism.

In 1995 Fukuyama reported a practical method for the preparation of secondary amine with Mitsunobu reaction[504] by using sulfonyl group to increase the acidity of the amine. This reaction became of great importance and is now known as the Fukuyama-Mitsunobu reaction.

However, a Mitsunobu reaction between an alcohol and dimethylamine was successfully reported by Laclef.[505] In this example, the acidic proton was not provided by the dimethylamine but by an adjacent sulfinamide on the molecule. We thus performed the reaction with dimethylamine hydrochloride as a pronucleophile, but no reaction was observed and only starting material was recovered (Scheme 4.13). We, therefore, decided to use an alternative pathway. Interestingly, in the weeks that followed the end of this project, Huang reported a novel protocol successfully using amine as a nucleophile in the Mitsunobu reaction.[506]

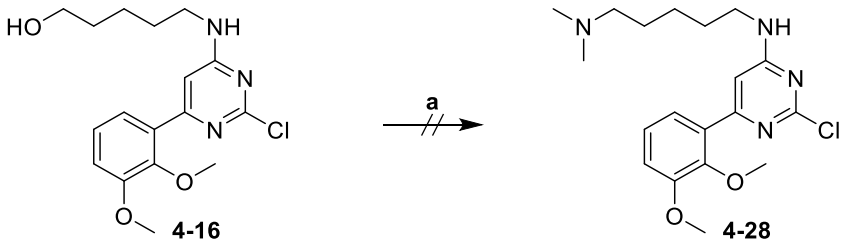

Reagents & Conditions: a. Dimethylamine hydrochloride (3 eq), PPh_3 (1.5 eq), DIAD (1.6 eq), THF, rt, 16h

Scheme 4.13: Attempt of Mistunobu reaction to form 4-28.

We opted in favour of a more common two-step sequence. The alcohol was first activated by reaction with a sulfonyl chloride to form a better nucleofuge which then reacted by nucleophilic substitution with dimethylamine to afford the desired compound. In the first instance, both tosyl

chloride and mesyl chloride were used. Both methods successfully provided the desired compounds, but higher yields were obtained with the latter sulfonyl chloride. Activation of the terminal alcohol with mesyl chloride followed by substitution with basic amine was therefore used as a preferred method. Several final compounds were then synthesised from 2-pyrrolidinyl-pyrimidine (Scheme 4.14), and 4-pyrrolidinyl-pyrimidine (Scheme 4.15) intermediates using dimethylamine and pyrrolidine.

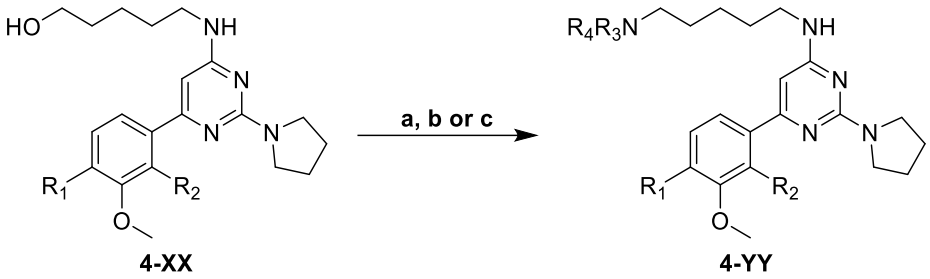

4-XX 4-YY

Reagents & Conditions: a. MsCl (1.1 eq), Et_3N (1.2 eq), DCM, 0°C, 3 h; **b.** Dimethylamine hydrocloride (20 eq), Et_3N (20 eq) THF, μW (120 °C, 300W, 1 h); **c.** pyrrolidine (10 eq), THF, 80 °C, 16 h

R_1	R_2	4-XX	NR_3R_4	4-YY	Yield
OMe	H	**4-15**	Pyrrolidine	**4-29**	51%
H	OMe	**4-16**	Dimethylamine	**4-30**	20%
H	OMe	**4-16**	Pyrrolidine	**4-31**	62%

Scheme 4.14: Synthesis of 2-pyrrolidinyl-pyrimidine final compounds 4-29 to 4-31.

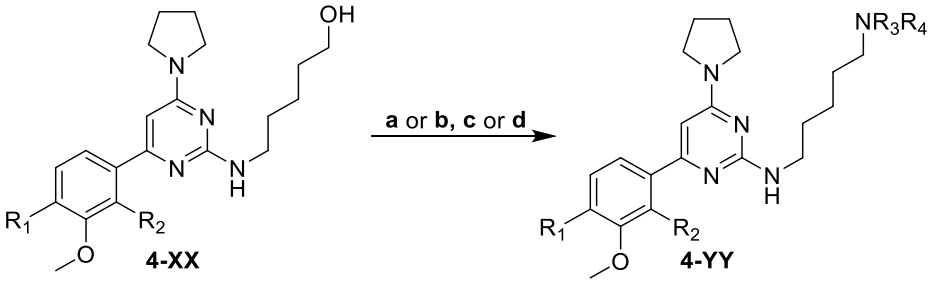

4-XX 4-YY

Reagents & Conditions: a. TsCl (1.8 eq), pyridine (3 eq), DCM, 0°C, 2 h; **b.** MsCl (1.1 eq), Et_3N (1.2 eq), DCM, 0°C, 3 h; **c.** Dimethylamine (20 eq, 2M in MeOH), THF, 80 °C, 16 h; **d.** pyrrolidine (20 eq), THF, rt, 16 h

R_1	R_2	4-XX	NR_3R_4	4-YY	Yield
OMe	H	**4-17**	Dimethylamine	**4-32**	44%
H	OMe	**4-18**	Dimethylamine	**4-33**	19%
H	OMe	**4-18**	Pyrrolidine	**4-34**	21%

Scheme 4.15: Synthesis of 4-pyrrolidinyl-pyrimidine final compounds 4-32 to 4-34.

Following the successful synthesis of these compounds, we turned our attention to the formation of analogues with a shorter alkyl side chain. Starting from previously synthesised intermediate **4-4** and **4-10**, reaction with 3-amino-1-propanol under microwave irradiation led to the isolation of four new isomers (Scheme 4.16).

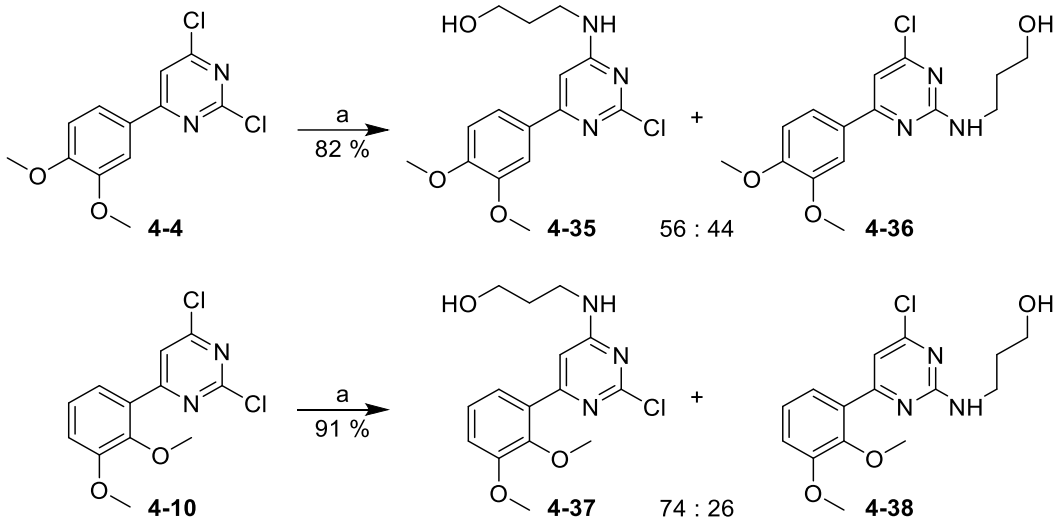

Reagents & Conditions: a. 3-amino -1-pentanol (3 eq), THF, μW (80 °C, 300 W, 30 min)

Scheme 4.16: Synthesis of intermediate 4-35 to 4-38.

These intermediates then reacted with pyrrolidine under microwave irradiation to afford the corresponding 2-(1-pyrrolidinyl)-pyrimidine (Scheme 4.17) and 4-(1-pyrrolidinyl)-pyrimidine (Scheme 4.18).

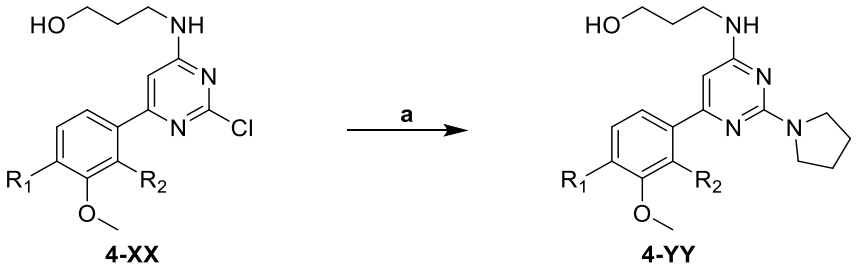

Reagents & Conditions: a. pyrrolidine (10 eq), THF, μW (120 °C, 300 W, 30 min)

R_1	R_2	4-XX	4-YY	Yield
OMe	H	**4-35**	**4-39**	73%
H	OMe	**4-37**	**4-40**	79%

Scheme 4.17: Synthesis of 2-pyrrolidinyl-pyrimidine intermediate 4-39 and 4-40.

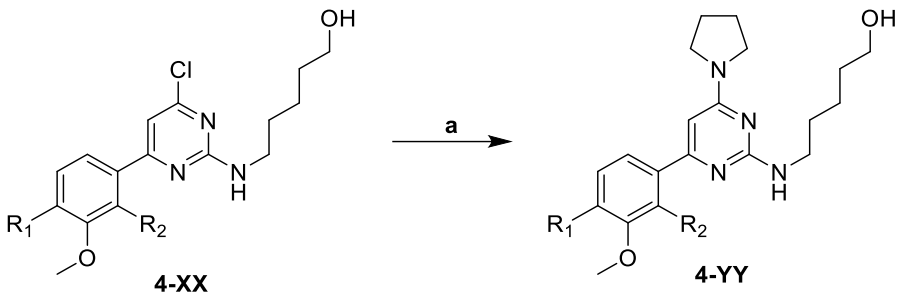

Reagents & Conditions: a. pyrrolidine (10 eq), THF, μW (120 °C, 300 W, 30 min)

R_1	R_2	4-XX	4-YY	Yield
OMe	H	**4-36**	**4-41**	89%
H	OMe	**4-38**	**4-42**	93%

Scheme 4.18: Synthesis of 2-pyrrolidinyl-pyrimidine intermediate 4-41 and 4-42.

Finally, several final compounds were synthesised using mesyl chloride activation from lastly formed 2-pyrrolidinyl-pyrimidine intermediate (Scheme 4.19) and 4-pyrrolidinyl-pyrimidine (Scheme 4.20).

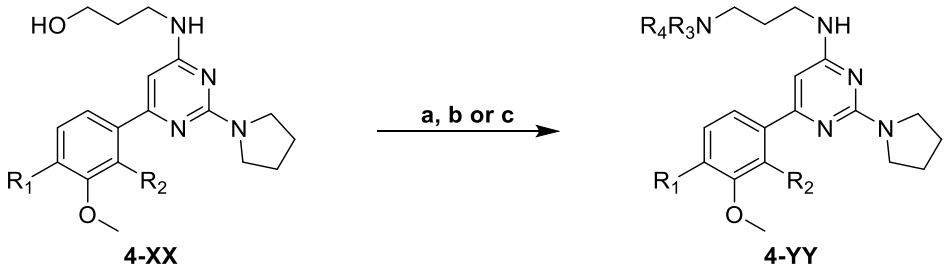

Reagents & Conditions: a. MsCl (1.1 eq), Et_3N (1.2 eq), DCM, 0°C, 3 h; **b.** Dimethylamine (20 eq, 2M in THF), THF, 80 °C, 16 h; **c.** pyrrolidine (10 eq), THF, 80 °C, 16 h

R_1	R_2	4-XX	NR_3R_4	4-YY	Yield
OMe	H	**4-39**	Pyrrolidine	**4-43**	61%
H	OMe	**4-40**	Dimethylamine	**4-44**	45%
H	OMe	**4-40**	Pyrrolidine	**4-45**	67%

Scheme 4.19: Synthesis of 2-pyrrolidinyl-pyrimidine final compounds 4-43 to 4-45.

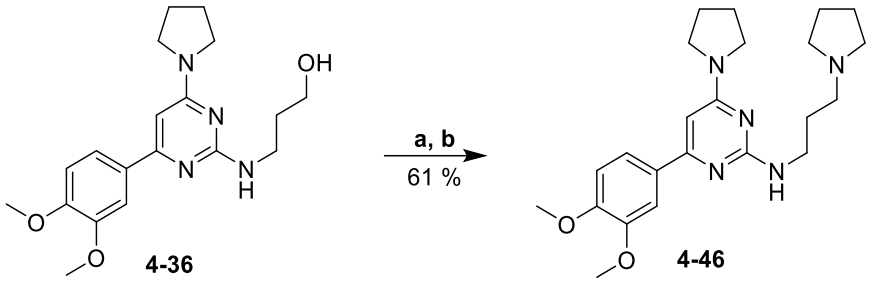

Reagents & Conditions: a. MsCl (1.1 eq), Et_3N (1.2 eq), DCM, 0°C, 3 h; **b.** pyrrolidine (20 eq), THF, 80 °C, 16 h

Scheme 4.20: Synthesis of 4-pyrrolidinyl-pyrimidine final compound 4-46

Due to time constraints, some analogues were not synthesised, but during this project, a total of 12 analogues of a new series were produced as potential SETD8 inhibitors. An overview of the final compounds is shown below (Figure 4.1).

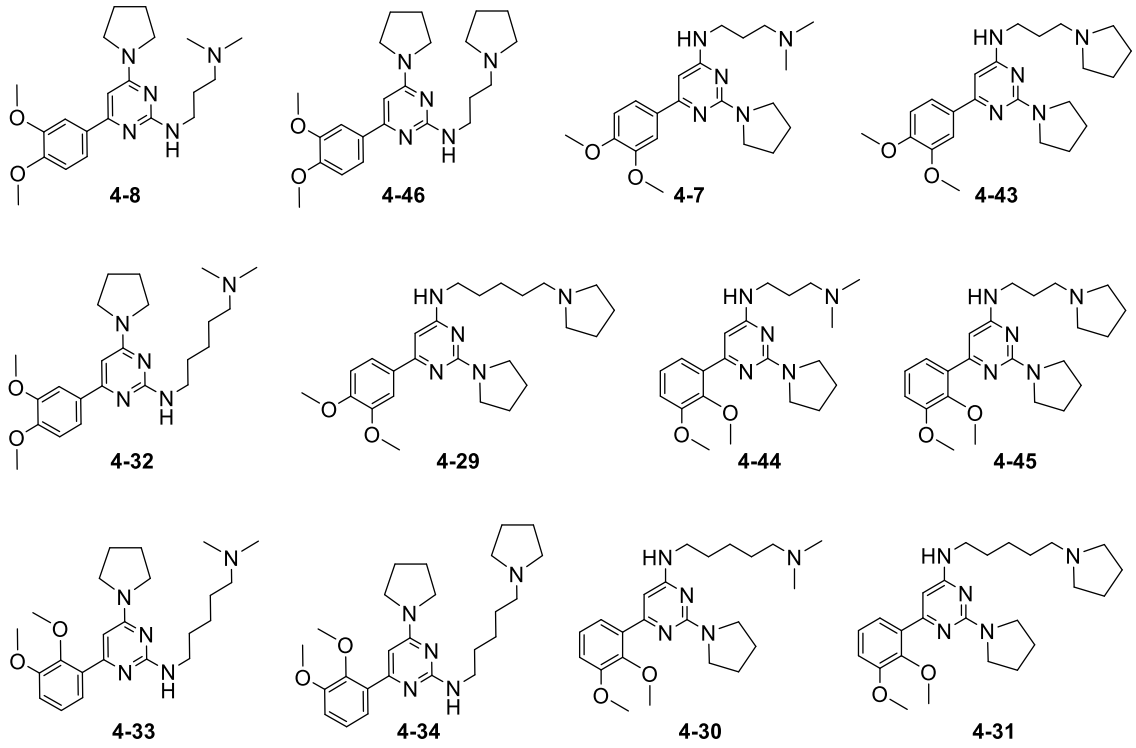

Figure 4.1: Overview of synthesised compounds.

3. Biological evaluation

3.1 Principle of the SETD8 inhibition assay

Sbardella group developed the methyltransferase inhibition assay by adapting the general conditions of the AlphaLisa homogeneous proximity immunoassays provided by PerkinElmer.

The assay relies on the Alpha technology, which is a bead-based assay taking advantage of antibody specificity (Figure 4.2).

The assay is a multi-step procedure. In the first instance, the target is incubated with AlphaLISA anti-analyte conjugated acceptor beads and biotinylated antibodies. As a result, the target is captured between the biotinylated antibodies and the acceptor beads. In a second step, the streptavidin donor beads are added. Following an incubation time, the donor beads couple to the biotinylated antibody ends, creating a structure in which the target is linked to both the acceptor and the donor beads. Finally, a laser emitting at specific wavelengths excites the donor beads. This excitation causes the release of singlet oxygen that then transfers the excitation to the acceptor beads in a cascade reaction. As a result, the acceptor beads radiate at a specific wavelength that can then be detected and quantified.

This type of assay offers excellent versatility. Moreover, as the released singlet oxygen can only reach the acceptor beads that are coupled to the donor beads, the Alpha technology has a high sensitivity.

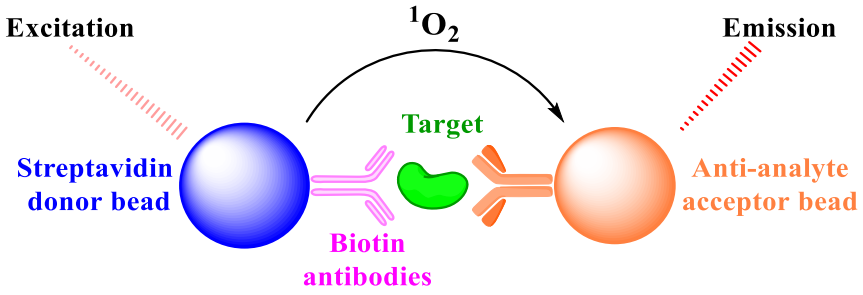

Figure 4.2: Principle of the AlphaLISA assay.
Adapted from the manufacturer manual.[507]

To turn specifically to the SETD8 assay, the human recombinant SETD8 was first incubated with the potential inhibitor followed by the addition of histone H4 and SAM. After incubation, anti-monomethyl-histone H4 lysine 20 (H4K20me1) AlphaLISA acceptor beads and the biotinylated anti-H4 antibodies were added, and the mixture was incubated. Finally, streptavidin donor beads were added, incubated in the dark, and the resulting signals were measured with a plate reader (excitation at 680 nm and emission at 615 nm).

3.2 Results and discussion

Several compounds were profiled in the SETD8 inhibition assay. They were tested by the Sbardella group at a single dose of 100 µM and compared to the activity resulting from the treatment with UNC0379 at a concentration of 5 µM. The results are shown in Figure 4.3, which

displays the observed percentage of activity for each compound. These results are the mean of triplicate experiments.

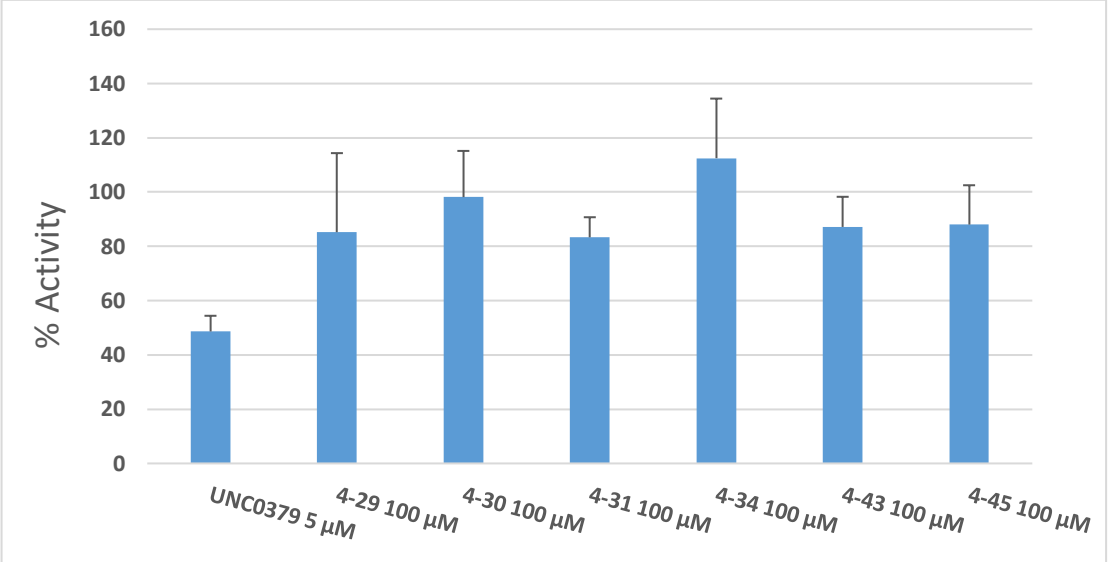

Figure 4.3: Percentage of activity of SETD8 measured after treatment with a fixed dose of inhibitors in the AlphaLisa assay. (n = 3)

We were disappointed to discover that the designed scaffold led to poor inhibition of SETD8 even at a high concentration of 100 µM.

It is still unclear why our modification resulted in such a significant loss of potency. Wishing to find an explanation we looked at the reported crystal structure of SETD8 in complex with MS2177, an analogue of UNC0379 (Figure 4.4).[168]

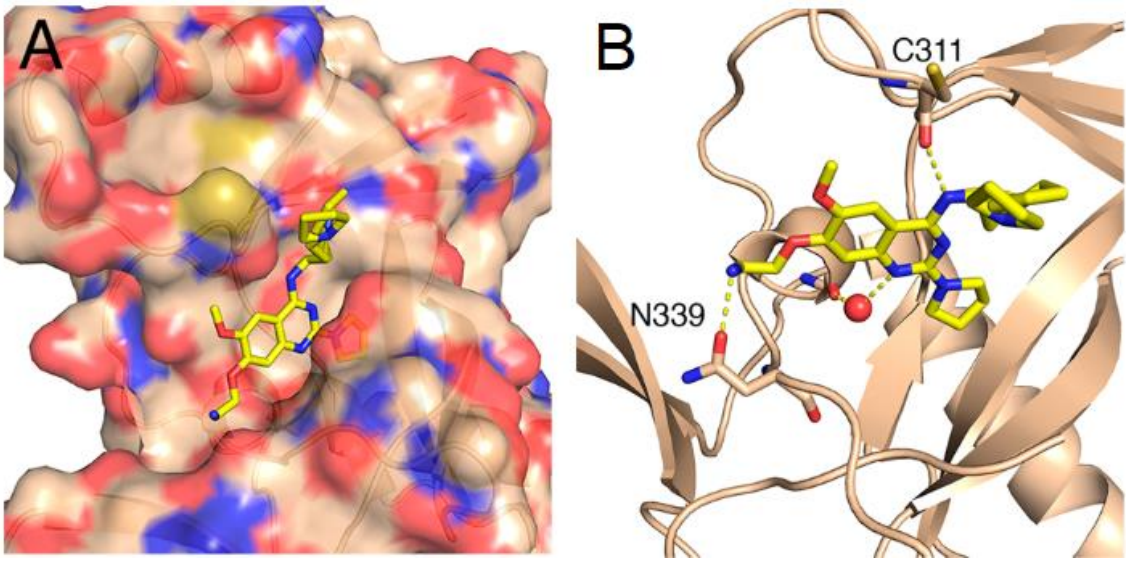

Figure 4.4: X-ray crystal structure of MS2177 in complex with SETD8. (A) MS2177 bound to SETD8. (B) Polar interactions between MS2177 and SETD8 are shown.
Adapted from Butler et al.[168]

Two crucial interactions between the enzyme and the quinazoline core of the molecule were observed. A primary hydrogen bond is formed between the N1 of the compound and a water molecule, and a second hydrogen bond is detected between the cysteine C311 and the amino group on the C4 position. Although our scaffold also possesses a similar structure, which could still be involved in hydrogen bonding, our modification deeply affected the flatness of the scaffold. Consequently, the pyrimidine part of our molecules could be forced to adopt a different position to prevent a collision between the phenyl ring and the enzyme, thus making the hydrogen bond formation impossible.

Conclusion

The primary objective of this thesis was to develop several new classes of inhibitors of the histone deacetylases class of enzyme and to evaluate their potential as anticancer agents. HDACs activity has been extensively linked to cancer development, and selective inhibitors are expected to become leading therapeutic agents in the coming years.

Additionally, HDAC inhibitors could be of great interest for the development of new antiparasitic therapies. This thesis was partially funded by the A-ParaDDisE project, an international collaboration which aimed to develop new classes of epigenetic modulators to target four of the most important Neglected Tropical Diseases: malaria, leishmaniasis, schistosomiasis and Chagas disease. Those infectious diseases collectively infect more than one billion people, mainly in developing countries, and cause hundreds of thousands of deaths annually. The appearance of drug resistance and the lack of alternative therapies raise the spectre of a potential worldwide crisis in the future and could annihilate decades of progress in the control of these diseases.

During this thesis, we designed and developed the synthetic route of different new classes of HDAC inhibitors bearing a hydroxamic acid as a zinc-binding group.

A first scaffold was based on the imidazo-ketopiperazine. Several compounds were synthesized and evaluated against different targets. In enzymatic assay against human HDAC, the length of the linker was found to play a critical role for the potency of the inhibitor. Both compounds **3-29** and **3-37** were potent against three HDAC isoforms: HDAC1, HDAC6 and HDAC8 with a micromolar to submicromolar IC_{50} in enzymatic inhibition assay. Following these results, the inhibition profile of **3-29** was evaluated against every HDAC isoforms. This compound was found to be selective for HDAC1/6/8 isoforms. Then, these compounds were tested in cancer-cells growth inhibition assays, and **3-29** and **3-37** displayed a micromolar activity on three different leukaemia cell lines: MV4-11, THP-1 and U937. Finally, a western blot analysis of **3-37** on U937 revealed a significant effect both on histone H3 and α-tubulin acetylation. These results indicated an inhibition activity against class I and class II HDACs and were consistent with selective inhibition of HDAC1/6/8. Compounds **3-29** and **3-37** were also tested on SmHDAC8 to evaluate their potential in the development of new treatment against schistosomiasis. Both compounds featured micromolar to nanomolar IC_{50} values in enzymatic inhibition of the parasite HDAC. Besides, a limitation of the HDACi-based antischistosomal strategy often lies behind a lack of selectivity against hHDAC8. On the other hand, **3-37** was 4.5-fold more active against SmHDA8 than hHDAC8. This scaffold represents an interesting new class of HDAC inhibitors, and these results were recently published.[491]

Following the synthesis of this scaffold, the synthetic plan was modified to create a second scaffold based on imidazole, and several compounds were synthesized. This scaffold was more tolerant towards the size of the linker and **3-38,** and **3-40** showed nanomolar activity on hHDAC6. These compounds were also highly active in cancer cell growth inhibition assay and displayed a selectivity between the different cancer cell lines. On the other hand, they only had a limited effect on SmHDAC8. However, **3-40** was found to have a 5 µM IC_{50} on *Trypanosoma cruzi* TcDAC2. To date, no inhibitors have been reported against TcDAC2. Therefore **3-40** represents an exciting hit and this scaffold could lead to one of the first class of TcDAC2 inhibitors.

Thirdly, we investigated a scaffold derived from aspartic acid. A general synthetic pathway was established, but optimization is still required.

Then we explored the use of a triazole core. A series of 1,4-disubstituted triazoles were synthesized. Two compounds, **3-127** and **3-129** selectively inhibited cancer-cell growth in the U937 cell line with a micromolar IC_{50} while the other analogues were inactive on the different cell lines. Next, attempts were made to introduce a thiophene group on the 5^{th} position of the triazole. Several approaches were investigated to obtain 1,4,5-trisubstituted triazoles, but they were unsuccessful and will require further investigation.

Next, we designed a new class based on hydantoins. The synthetic pathway was established, and several compounds were synthesized, but their activity has not been evaluated yet.

Based on the structure of praziquantel, the only drug available for the treatment of schistosomiasis, we aimed to design a dual-target compound. Introducing a hydroxamic acid on the core of the molecule, we synthesized the first praziquantel-HDAC hybrid **3-192**. This compound was found to express a nanomolar inhibition activity on SmHDAC8 and is currently evaluated in toxicity studies against schistosomula and adult worm. This approach carries great potential, and we have high expectation for this scaffold's future.

Finally, the discovery of an L-tartaric acid binding to the zinc cation in the crystal structure of SmHDAC8 led us to explore a scaffold based on 4-amino-2-hydroxybutanoic acid. However, almost no activity was observed against HDAC6 or in cell assays against THP-1, MV4-11 and U937.

In addition to the work on HDAC inhibitors, I enrolled in a short-term scientific mission, which was funded by the COST action Epichembio. This side project, which took place at the University of Salerno in Italy in the group of Prof. Sbardella, aimed to develop a new class of inhibitors against SETD8, the only known methyltransferase capable of monomethylation of H4K20. Derived from selective SETD8 inhibitors recently reported, we designed a new scaffold and

synthesised a series of compounds. However, only low inhibition was observed on SETD8 in an enzymatic assay.

Overall, this thesis provides the synthetic pathway of several new classes of epigenetic inhibitors for the prevention of cancer. Diverse scaffolds displayed cytotoxic activity on leukaemia cell lines and were showed to be potent and selective hHDAC inhibitors. Promising effect were also observed on parasitic targets with micromolar to nanomolar SmHDAC8 inhibition activity and up to 4.5-fold selectivity over hHDAC8. Furthermore, this project led to the identification of a micromolar hit on TcDAC2, a *Trypanosoma cruzi* HDAC without any inhibitor so far. As a result, each scaffold could become the topic of a future research project to establish their stucture-activity relationship and to design second generation inhibitors with therapeutic applications not only for cancer treatment benefits, but also for Schistosomiasis and Chagas disease, two parasitic diseases which are currently impacting over 250M people. Our novel classes of compounds may move us a step closer to treating these dreadful conditions.

Future work

This project explored different classes of molecules and offers a range of evolution for each of them.

4. Imidazole-based scaffold

Both the "open" imidazole scaffold and the "closed" imidazo-diketopiperazine were shown to be valuable classes of HDAC inhibitors. Further biological studies are needed, as some compounds have not been tested yet. In particular, it will be interesting to evaluate the imidazo-diketopiperazine compounds on TcDAC2. Moreover, the substitution of the alkyl linker for a benzyl in **3-42** could have a great impact in terms of potency and selectivity and has yet to be evaluated.

Regarding the SAR perspectives, they mainly focus on two axes. The first one concerns the nature of the linker. In addition to bulky and rigid groups such as benzyl, we could introduce groups likely to form hydrogen bonding in the enzyme channel. For example, the disulfide could be alkylated with a short halo-acid, deprotected, and then coupled with the synthesized β-alanine hydroxamic acid **3-96** (Scheme 6.1). Similarly, this approach could be used to make compounds derived from a 4-amino-2-hydroxybutanoic acid, either as free carboxylic acid or as hydroxamic acid, thus combining two of the scaffolds explored.

The second main modification would be on the nature of the amino acids. Using hydrogen bond acceptor/donor residues, like a tyrosine instead of the phenylalanine, would explore the possibilities to form side interactions with the enzyme rim.

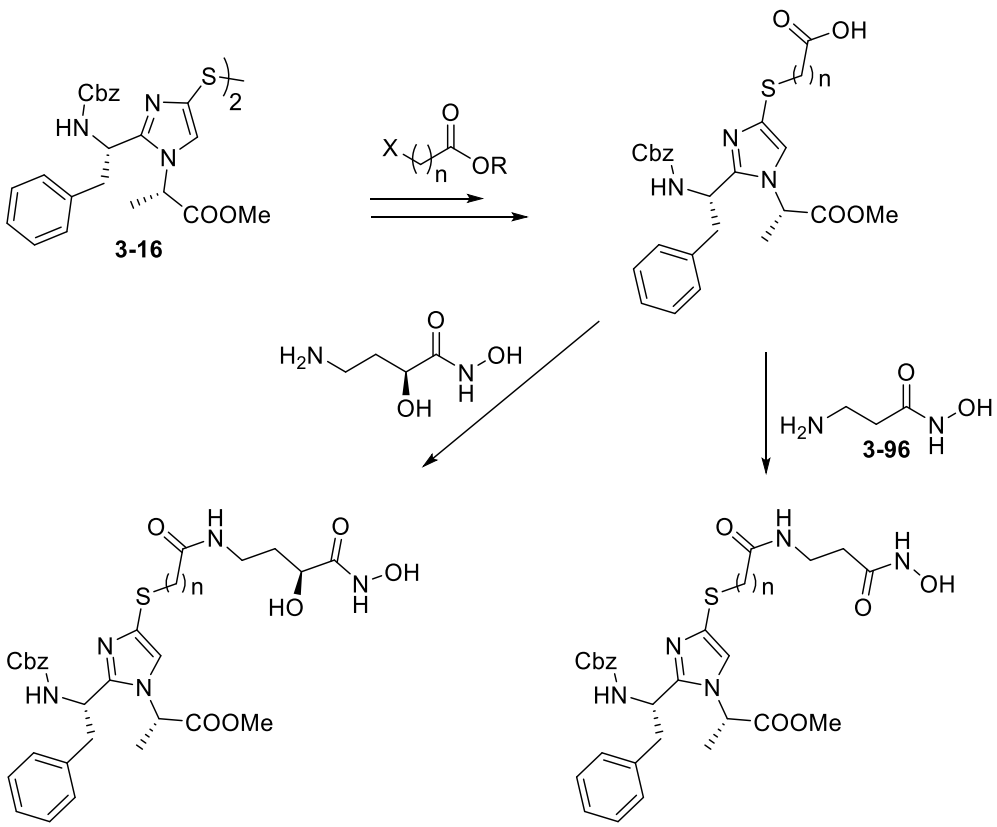

Scheme 6.1: Example of alternative linkers.

5. Aspartic acid-based scaffold

This scaffold still requires some optimization, in particular for the last step and introduction of hydroxamic acid. Then, a vast diversity can be explored both on the C-terminal and on N-terminal moieties of aspartic acid. These could include cyclic and non-cyclic aliphatic, electron-rich and electron-poor aromatic rings. In addition, this derived aspartic hydroxamate could be introduced into the cyclic-peptide or cyclic depsipeptide classes of HDACi.

6. Triazole-based scaffold

A couple of synthesized triazoles showed promising results in cancer cells with a specific cell growth inhibition of U937. Docking studies could help to understand the specific role of the fluorine substituents on the phenyl and offer new insights to design analogues. In addition, the introduction of thiophene or similar heterocycles on the 5th position of the triazole has to be investigated further. As steric hindrance was identified as a possible explanation of the unsuccessful attempts to synthesise these analogues, replacement of the phenyl on the 4th position by smaller or more flexible group could become beneficial.

7. Hydantoin-based scaffold

Several compounds have been synthesised and still have to be tested against the different targets. Based on these results, future work will focus on building a SAR around the use of natural and non-natural amino acids on both N1 and C3 positions.

8. Praziquantel-HDACi hybrid

We have high expectation for this compound, or more generally for this strategic approach, toward the development of new therapeutic agents for schistosomiasis. If the potency is confirmed in the phenotype assay, further investigation will be needed to certify a dual mechanism of action and determine their individual impact. To this end, the methyl ester precursor is also tested.

9. Pyrimidine series

The pyrimidine series turned out to be mostly inactive on SETD8. As the activity of the original quinazoline was shown to be mainly due to the formation of hydrogen bonding from the pyrimidine part of the molecule, further investigation of the SAR of our series could lead to more potent inhibitors. In particular, the replacement of the phenyl by smaller aromatic rings or more flexible aliphatic groups could offer better interactions with the surrounding residues and restore the inhibitory potential of the scaffold.

Chapter 5. Experimental

1. General procedures for Chemistry

All chemicals and solvents were purchased from appropriate suppliers including Sigma Aldrich, Fluorochem, Alfa Aesar, and Novabiochem. All anhydrous solvents were purchased as Aldrich®sure/seal bottles. All solvents were reagent grade. TLC was used to monitor the reaction and performed on aluminum-backed silica gel coated plates (Merck DC, Alufolien Kieselgel 60 F254) with spots visualized by UV-light (λ 254 nm) or stained with dyes (potassium permanganate solution, phosphomolybdic acid stain, Hanessian's Stain or ninhydrin), followed by heating. Product concentration after reactions and extractions involved the use of a rotary evaporator operating at reduced pressure and the term *in vacuo* refers to the solvent concentration at reduced pressure. Products were normally purified by column flash chromatography using TELOS® flash silica cartridge or by reverse-phase flash chromatography using RediSep Rf Gold® Reversed-phase C18 column. NMR spectra were recorded on a 400 MHz Brüker *Utrashield plus* spectrometer at 400 MHz for ^{1}H NMR and 100 MHz for ^{13}C NMR. Spectral data were reprocessed with MestReNova. The spectra were calibrated to the residual deuterated solvent peak ($CDCl_3$, CD_3OD, DMSO-d6, D_2O) according to literature.[508] The chemical shifts are reported in δ (ppm) units followed by brackets containing spectra details in this order: multiplicity (s: singlet, d: doublet, t: triplet, q: quartet, quint: quintuplet, m: multiplet, dd: double doublet, dt: doublet of triplet, dq: doublet of quadruplet, td: triplet of doublet, qd: quadruplet of doublet, br: broad, ABq: 2nd order quadruplet), coupling constants (reported in Hz), number of protons (from integration). ^{13}C NMR were reported with chemical shifts. Mass spectra were recorded with a Shimadzu LCMS 2010EV or Agilent technology 6210 LC/MS Time-of-Flight using Milli-Q water and HPLC grade acetonitrile (0.01% TFA). Infrared spectroscopic analysis was performed by ATR-FTIR (attenuated total reflectance-Fourier-transform infrared spectroscopy) on a Perkin-Elmer Spectrum 400 FTIR spectrometer. Selected IR spectroscopic peaks were reported in wavenumbers (cm^{-1}).

2. General procedure for Biological assays

2.1 HDACs enzyme inhibition assays

HDACs inhibition was tested *in vitro* by Prof. M. Jung from the University of Freiburg in Germany and Prof. L. Bischoff from the Rouen Normandy University in France using biochemical assays as previously described.[325,486]

2.2 Cell growth inhibition assays

Dr Maria T. Borrello from INSERM U1068 Cellular Stress Group, Cancer Research Center of Marseille in France performed the cell inhibition assays.

AML cell lines THP-1, MV4-11 and U937 were obtained from the DMSZ (German Collection of Microorganisms and Cell Cultures) and European Collection of Cell Cultures. They were authenticated by DNA-fingerprinting. The cell lines were used at low passage number for a maximum of 6 months post-resuscitation and tested regularly for mycoplasma infection.

Cells lines were cultured in RPMI 1640 medium (GIBCO) supplemented with 10% Foetal Calf Serum (FCS, GIBCO) and 5% of 2 mM L-glutamine. Cells were grown at 37 ˚C with 5% CO_2, and cell density was maintained at 25×104 cells/mL. For the assay, cells were plated in a 96-well clear bottomed microtitre plate at a density of 2.5×104 cells/well for U937 and 5×104 cells/well for THP-1 and MV4-11. Inhibitor stock solutions (20 mM in DMSO) were dissolved in cell media at the appropriate concentration, and 10 µL of each concentration incubated with the cells for 72 h or 96 h. Cell viability was then measured using CellTiter-Blue® (Promega, Southampton, UK) and normalised to the vehicle control (DMSO) and a dose-response curve determined with GraphPad 6 using a non-linear regression model.

2.3 H3K9Ac and AcTubulin Western Blotting

Dr M. T. Borrello from INSERM U1068 Cellular Stress Group, Cancer Research Center of Marseille in France performed the western blots.

Antibodies for immunoblotting were purchased from Cell Signalling (anti-Acetylated-α- (Lys40) tubulin #9725) or Abcam (anti-H3 #ab100938, Goat anti-Rabbit IgG (HRP) #ab97080, and ERK2 #ab32081). The antibodies from Cell Signalling were diluted to 1:1000 in 3% bovine serum albumin (BSA) dissolved in TBS-T (w/v); the antibodies from Abcam were diluted 1:5000 (primary) or 1:10000 (secondary) in 3% BSA dissolved in TBS-T solution.

Blotting procedures were performed as previously described.[509]

2.4 SETD8 inhibition

Prof. G. Sbardella from the University of Salerno in Italy performed the SETD8 inhibition assays.

Methyltransferase activity assays were operated by taking advantage of AlphaLisa homogeneous proximity immunoassays developed by us by adapting the general conditions described by PerkinElmer. The assays were performed in white opaque OptiPlate-384 (PerkinElmer, # 6007299) at room temperature (22 °C) in a final volume of 25 µL using the following buffer: Tris-

HCl 50 mM pH 8.8, NaCl 50 mM, MgCl 2 5 mM, DTT 1 mM, BSA 0.01%. The compounds were dissolved in DMSO and diluted in assay buffer, keeping constant the concentration of DMSO (1%) in each well. In each assay, the 100% activity (positive control) was reached using the vehicle (DMSO) while the 0% activity (negative control) was obtained without the protein. For each incubation step, the OptiPlate was sealed with protective foil to prevent evaporation and contamination.

Briefly, 2.5 µL of human recombinant SETD8 (expressed in house) (final concentration 1 µM) were first incubated with 5 µL of each compound for 30 min, then 2.5 µL of a mixture of Histone H4 (Active Motif, # 31223) (final concentration 150 nM) and of SAM (Sigma, # A7007) (final concentration 200 µM) were added. The reaction was incubated for 60 min then it was stopped by the addition of 5 µL of High Salt Buffer (50 mM Tris-HCl pH 7.4, 0.1% Tween-20, 1 M NaCl, 0.3% poly-L-lysine). After an incubation of 15 min, 5 µL of a mixture of anti-methyl-histone H4 lysine 20 (H4K20me1) AlphaLISA acceptor beads (PerkinElmer, # AL145) (final concentration 20 µg/mL) diluted in Epigenetic Buffer (PerkinElmer, # AL008) and the biotinylated anti-H4 antibody (PerkinElmer, # AL146) (final concentration 1 nM) were added in each well in subdued light. After an incubation of 60 min, 5 µL of streptavidin donor beads (PerkinElmer, # 6760002) diluted in Epigenetic Buffer were added in each well (final concentration 20 µg/mL) in subdued light. After incubation, in the dark, for 30 min at room temperature, signals were read in an Alpha mode with a PerkinElmer EnSight II multimode plate reader (excitation at 680 nm and emission at 615 nm).

3. Molecular docking

Molecular docking was done by Pr. W. Sippl at the Institute of Pharmacy at the Martin-Luther University of Halle-Wittenberg in Germany.

MOE1 (version 2012.10, Chemical Computing Group, Montreal, Canada)[510] was used to generate the molecular structures of all inhibitors under study. The inhibitor structures were subsequently prepared for docking using the LigPrep tool[511] as implemented in Schrödinger's software, where all possible tautomeric forms were generated, and energy minimized using the OPLS force field. Conformers of the prepared ligands were calculated with ConfGen using the default settings.

The crystal structure of human HDAC1 (PDB ID 5ICN), HDAC6 (Catalytic Domain CD2, PDB ID 5EDU), HDAC8 (PDB ID 2V5X) in complex with hydroxamic acid-based inhibitors were retrieved from the Protein Data Bank (PDB; www.rcsb.org).[512] All water molecules were deleted except the two water molecules occupying the catalytic pocket, which were kept in the docking step. The protein structure was subsequently prepared with Schrödinger's Protein Preparation

Wizard[513]: Hydrogen atoms were added, and the H-bond network was subsequently optimized. The protonation states at pH 7.0 were predicted using the PROPKA tool in Schrödinger. The structures were finally subjected to a restrained energy minimization step using the OPLS2005 force field (RMSD of the atom displacement for terminating the minimization was 0.3 Å).

The receptor grid preparation for the docking procedure was carried out by assigning the co-crystallized ligand as the centroid of the grid box. The generated 3D conformers were docked into the receptor model using Glide[514] (Schrödinger Inc., New York, USA) in the Standard Precision mode. A total of 20 poses per ligand conformer were included in the post-docking minimization step, and a maximum of two docking poses was output for each ligand conformer.

In a previous study, Sippl group found that rescoring the docking poses by using an MM-GB/SA protocol resulted in a significant correlation between calculated interaction energies and in vitro inhibition data.[388,515] Therefore, the same protocol was applied to the compounds under study. To calculate the binding free energy, they used the AMBER12EHT force field implemented in the MOE2012.10 program together with the continuum solvation model GB/SA. The experimentally observed geometries of the zinc-hydroxamic acid complexes were best reproduced using this setup. Partial charges were fixed using the MOE Protonate3D tool according to the used force-field followed by a short minimization. To estimate the binding free energy a minimizing of the protein-ligand complexes derived from the docking was carried out. During complex minimization the heavy atoms of the protein were tethered with a deviation of 0.5 Å (force constant (3/2) kT / $(0.5)^2$). The complex showing the lowest binding free energy was chosen for each inhibitor and HDAC isoform. Using this docking and rescoring protocol the experimentally derived structures of the cocrystallized inhibitors of HDAC6 (PDB ID 5EDU), and HDAC8 (PDB 2V5X) could be reproduced with an RMSD value below 1.00 Å.

4. Synthetic procedures.

4.1 Imidazole-based scaffold

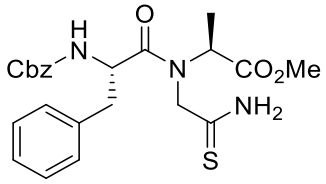

3-9

Methyl *N*-(2-amino-2-thioxoethyl)-*N*-(((benzyloxy)carbonyl)-L-phenylalanyl)-L-alaninate

To L-Ala-OMe.HCl (2.0 g, 14.33 mmol, 1 eq) in dry MeCN (20 mL) under argon atmosphere and at 0 °C was added iodoacetamide (3.18 g, 17.19 mmol, 1.2 eq) and dry DIPEA (6.3 mL, 35.82 mmol, 2.5 eq). The reaction mixture was warmed up to room temperature and stirred 6 h. The reaction mixture was cooled to 0 °C then Z-L-Phe-OH (6.43 g, 21.49 mmol, 2.5 eq) and dry DIPEA (11.2 mL, 14.33 mmol, 4.5 eq) were added. T3P (50% in EtOAc, 12.8 mL, 21.49 mmol, 1.5 eq) was then added dropwise. The reaction mixture was stirred at 0 °C for 30 min, warmed up to room temperature, and stirred for 16 h. The reaction mixture was then diluted with water (140 mL) and extracted with EtOAc (2 x 200 mL). Combined organic layers were washed with a saturated solution of $NaHCO_3$ (150 mL), then brine (150 mL). The organic layer was then dried over $MgSO_4$, filtered and evaporated under reduced pressure to afford a sticky oil. This crude compound was then dissolved in a mixture of dry DME (110 mL) under argon atmosphere. At 0 °C was added Lawesson's reagent (2.28 g, 5.64 mmol, 0.6 eq) in one portion. The reaction mixture was warmed up to room temperature and stirred for 6 h. The reaction mixture was then diluted with EtOAc (200 mL) and washed with a saturated solution of $NaHCO_3$ (150 mL). The aqueous layer was back-extracted with EtOAc (3 x 150 mL). The combined organic layer was washed with brine (200 mL), dried over $MgSO_4$, filtered and evaporated. The residue was then purified by flash chromatography (gradient Hexane/EtOAc) to afford the desired compound (2.86 g, 44% yield). ^{1}H NMR (400 MHz, $CDCl_3$) δ 9.24 (s, 1H), 7.28 – 7.21 (m, 8H), 7.15 – 7.10 (m, 2H), 5.44 (s, 1H), 5.05 – 4.89 (m, 3H), 4.48 (q, *J* = 7.4 Hz, 1H), 4.11 – 4.02 (m, 2H), 3.65 (s, 3H), 2.99 – 2.82 (m, 2H), 1.32 (d, *J* = 7.1 Hz, 3H). ^{13}C NMR (101 MHz, $CDCl_3$) δ 201.75, 172.70, 172.47, 156.10, 135.94, 135.07, 129.52, 128.94, 128.58, 128.28, 128.02, 127.63, 67.22, 56.81, 56.56, 52.81, 52.75, 38.61, 13.86. IR (cm^{-1}): 3306, 2989, 2902, 1716, 1661, 1526, 1496, 1454, 1255, 1226, 1066, 1049, 749, 700. MS(ESI+): Calc for $[C_{23}H_{27}N_3O_5S+H]^+$ 458.175; Found 458.171

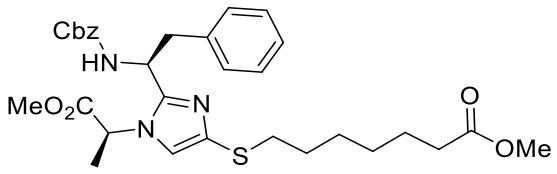

3-18

Methyl 7-((2-((*S*)-1-(((benzyloxy)carbonyl)amino)-2-phenylethyl)-1-((*S*)-1-methoxy-1-oxopropan-2-yl)-1*H*-imidazol-4-yl)thio)heptanoate

To a solution of intermediate **3-9** (1.2 g, 2.62 mmol, 1 eq) in dry toluene (9 mL) and dry DCM (1 mL) under argon atmosphere and at -78 °C were added dry Et_3N (2.8 mL, 20.98 mmol, 8 eq) and TMSOTf (2.37 mL, 13.11 mmol, 5 eq) dropwise. The mixture was then allowed to warm up to room temperature and stirred 16 h. MeOH (5 mL) was then added, and the reaction mixture was stirred 15 min at room temperature. Volatiles were evaporated under reduce pressure. The residue was dissolved in toluene (20 mL) and the reaction mixture was heated at reflux for 3 h. After completion, toluene was evaporated under reduce pressure. The residue was dissolved in dry DCM (20mL) under argon atmosphere and DTT (1.62 g, 10.49 mmol, 4 eq) was added. The reaction mixture was stirred for 16 h at room temperature. In a separated flask, 7-chloroheptanoate (0.63 mL, 3.67 mmol, 1.4 eq) was added to a solution of NaI (1.65 g, 11.02 mmol, 4.2 eq) in acetone (10 mL) and the mixture was kept at reflux 16 h. Et_2O (20 mL) was added to the acetone solution and the mixture was washed twice with a solution of $Na_2S_2O_3$ (2 M, 2 x 30 mL). The organic layer was dried over $MgSO_4$ and the solution was added to the main reaction's flask. Then Et_3N (0.89 mL, 6.56 mmol, 2.5 eq) was added and the reaction mixture was stirred at room temperature for 1 h. Afterwards 5 mL of a saturated solution of Na_2CO_3 was added, stirring was continued for 15 min, and then the aqueous layer was extracted with EtOAC (3 x 20 mL). The combined organic layers were dried on $MgSO_4$ and concentrated *in vacuo*. The crude was purified by flash chromatography on silica (gradient Hexane/EtOAC) to lead to the desired product (480 mg, 31% yield). ^{1}H NMR (400 MHz, $CDCl_3$) δ 7.37 – 7.27 (m, 5H), 7.22 – 7.15 (m, 3H), 7.05 – 6.98 (m, 2H), 6.85 (s, 1H), 5.74 (d, *J* = 8.6 Hz, 1H), 5.12 – 5.03 (m, 2H), 4.95 (td, *J* = 9.3, 5.5 Hz, 1H), 4.38 (q, *J* = 7.2 Hz, 1H), 3.64 (s, 3H), 3.59 (s, 3H), 3.31 (dd, *J* = 12.7, 5.3 Hz, 1H), 3.19 (dd, *J* = 12.7, 9.8 Hz, 1H), 2.87 – 2.73 (m, 2H), 2.29 (t, *J* = 7.5 Hz, 2H), 1.66 – 1.56 (m, 4H), 1.47 – 1.38 (m, 2H), 1.37 – 1.28 (m, 2H), 1.11 (d, *J* = 7.2 Hz, 3H). ^{13}C NMR (101 MHz, $CDCl_3$) δ 174.29, 170.31, 155.63, 148.08, 137.00, 136.51, 132.74, 129.57, 128.65, 128.62, 128.19, 128.02, 126.98, 119.63, 66.91, 53.07, 52.93, 51.58, 49.14, 42.53, 35.47, 34.10, 29.44, 28.82, 28.30, 24.91, 17.61. IR (cm^{-1}): 3334, 2930, 1714, 1524, 1455, 1244, 1163, 1030. MS(ESI+): Calc for $[C_{31}H_{39}N_3O_6S+H]^+$ 581.256, Found 582.653

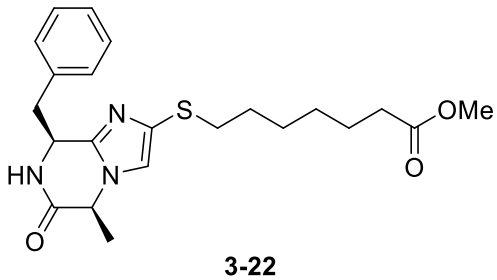

3-22

Methyl 7-(((5*S*,8*S*)-8-benzyl-5-methyl-6-oxo-5,6,7,8-tetrahydroimidazo[1,2-*a*] pyrazin-2-yl)thio)heptanoate

To a solution of **3-18** (480 mg, 0.83 mmol, 1 eq) in dry DCM (5 mL) under argon atmosphere, anisole (0.7 mL, 2.48 mmol, 8 eq) was added. The reaction mixture was cooled at 0 °C and a solution of HBr (33 % in AcOH, 2.24 mL, 12.38 mmol, 15 eq) was added dropwise. The reaction mixture was allowed to warm up at room temperature, and stirred for 2.5 h. Then the volatiles were removed under reduce pressure. The residual oil was dissolved in the minimum amount of dichloromethane and Et_2O (10 mL) was added. The residual solid was filtered and washed three times with Et_2O to give a solid. The intermediate salt (360 mg) was dissolved in water (5 mL) and a solution of $NaHCO_3$ (1 M) was added until pH = 8. The reaction mixture was stirred at room temperature for 30 min and extracted with DCM (3 x 10 mL). The organic was then washed with brine, dried over $MgSO_4$ and evaporated *in vacuo* to afford the desired compound. (210 mg, 61%). ^{1}H NMR (400 MHz, $CDCl_3$) δ 7.26 – 7.18 (m, 3H), 7.06 – 6.94 (m, 3H), 6.79 (s, 1H), 5.09 – 5.00 (m, 1H), 4.46 (qd, *J* = 7.0, 1.3 Hz, 1H), 3.65 (s, 3H), 3.28 (d, *J* = 4.8 Hz, 2H), 2.91 – 2.80 (m, 2H), 2.30 (t, *J* = 7.5 Hz, 2H), 1.69 – 1.56 (m, 4H), 1.49 – 1.39 (m, 2H), 1.38 – 1.29 (m, 2H), 1.00 (d, *J* = 7.1 Hz, 3H). ^{13}C NMR (101 MHz, $CDCl_3$) δ 174.29, 168.28, 141.07, 135.24, 135.13, 130.25, 128.76, 127.50, 118.77, 53.33, 52.76, 51.60, 43.13, 35.43, 34.09, 29.55, 28.83, 28.37, 24.92, 19.99. IR (cm^{-1}): 2930, 1700, 1436, 1410. MS(ESI+): Calc for $[C_{22}H_{29}N_3O_3S+H]^+$ 416.201; Found 416.631

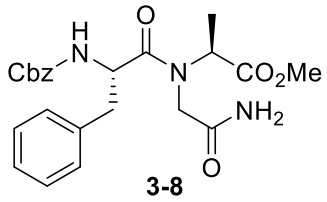

3-8

Methyl *N*-(2-amino-2-oxoethyl)-*N*-(((benzyloxy)carbonyl)-L-phenylalanyl)-L-alaninate

To L-Ala-OMe.HCl (12 g, 85.97 mmol, 1 eq) in dry MeCN (60 mL), under argon atmosphere and at 0 °C, was added iodoacetamide (19.1 g, 103.17 mmol, 1.2 eq) and dry DIPEA (37.5 mL, 214.93 mmol, 2.5 eq). The reaction mixture was warmed up to room temperature and stirred 20 h. The

reaction mixture was cooled to 0 °C then Z-L-Phe-OH (38.5 g, 128.96 mmol, 1.5 eq) and dry DIPEA (60 mL, 343.89 mmol, 4 eq) were added. T3P (50% in EtOAC, 76.8 mL, 128.96 mmol, 1.5 eq) was then added dropwise. The reaction mixture was stirred at 0 °C for 30 min, warmed up to room temperature and stirred for 16 h. Water (100 mL) was added and the aqueous layer was extracted with EtOAc (4 x 150 mL). The combined organic layer were washed with saturated $NaHCO_3$ (100 mL), then with brine (100 mL), dried over $MgSO_4$, filtered and concentrated under reduce pressure. The crude material was purified by flash chromatography on silica (gradient DCM/MeOH) to afford **3-8** (37.05 g, 98%). ^{1}H NMR (400 MHz, $CDCl_3$) δ 7.35 – 7.27 (m, 7H), 7.24 – 7.15 (m, 3H), 5.87 (s, 1H), 5.59 (d, *J* = 7.7 Hz, 1H), 5.11 – 4.99 (m, 3H), 4.63 (q, *J* = 7.4 Hz, 1H), 4.22 (q, *J* = 7.1 Hz, 1H), 3.72 (s, 3H), 3.87 – 3.57 (m, 5H), 3.04 (dd, *J* = 13.9, 7.3 Hz, 1H), 2.96 (dd, *J* = 13.4, 6.8 Hz, 1H), 1.39 (d, *J* = 7.2 Hz, 3H). ^{13}C NMR (101 MHz, $CDCl_3$) δ 172.54, 172.27, 171.05, 156.08, 136.15, 135.44, 129.59, 128.95, 128.64, 128.31, 128.10, 127.57, 67.19, 56.59, 52.78, 49.85, 47.60, 38.90, 13.91. IR (cm^{-1}): 3315, 2970, 1732, 1673, 1264, 1216. MS(ESI+): Calc for $[C_{23}H_{27}N_3O_6\text{-}Na]^+$ 464.180; Found 464.662

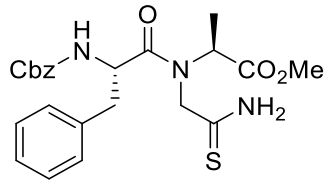

3-9

Methyl *N*-(2-amino-2-thioxoethyl)-*N*-(((benzyloxy)carbonyl)-L-phenylalanyl)-L-alaninate

To a solution of **3-8** (14.04 g, 13.36 mmol, 1 eq) in dry DCM (55 mL) under argon atmosphere was added Lawesson's reagent (3.24 g, 8.02 mmol, 0.6 eq) in one portion. The reaction mixture was warmed up to room temperature and stirred for 16 h. The DCM was evaporated and EtOAC (50 mL) was added to the residue. The solution was washed with a saturated solution of $NaHCO_3$ (3 x 50 mL). Organic layer was washed with brine (50 mL), dried over $MgSO_4$, filtered and evaporated. The residue was then purified by flash chromatography (gradient Hexane/EtOAc) to afford the desired compound (5.50 g, 90% yield). ^{1}H NMR (400 MHz, $CDCl_3$) δ 9.24 (s, 1H), 7.28 – 7.21 (m, 8H), 7.15 – 7.10 (m, 2H), 5.44 (s, 1H), 5.05 – 4.89 (m, 3H), 4.48 (q, *J* = 7.4 Hz, 1H), 4.11 – 4.02 (m, 2H), 3.65 (s, 3H), 2.99 – 2.82 (m, 2H), 1.32 (d, *J* = 7.1 Hz, 3H). ^{13}C NMR (101 MHz, $CDCl_3$) δ 201.75, 172.70, 172.47, 156.10, 135.94, 135.07, 129.52, 128.94, 128.58, 128.28, 128.02, 127.63, 67.22, 56.81, 56.56, 52.81, 52.75, 38.61, 13.86. IR (cm^{-1}): 3306, 2989, 2902, 1716, 1661, 1526, 1496, 1454, 1255, 1226, 1066, 1049, 749, 700. MS(ESI+): Calc for $[C_{23}H_{27}N_3O_5S+H]^+$ 458.175; Found 458.171.

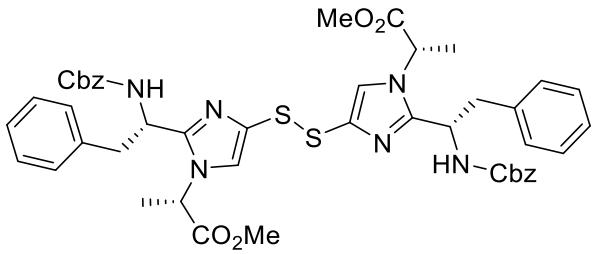

3-16

Dimethyl 2,2'-(disulfanediylbis(2-((*S*)-1-(((benzyloxy)carbonyl)amino)-2-phenylethyl)-1*H*-imidazole-4,1-diyl))(2*S*,2'*S*)-dipropionate

To **3-9** (6.0 g, 13,11 mmol, 1 eq) in dry toluene (30 mL) and dry DCM (3 mL) under argon atmosphere and at -78 °C were added dry DIPEA (18.3 mL, 104.91 mmol, 8 eq) and TMSOTf (11.9 mL, 104.91 mmol, 5 eq) dropwise. The mixture was then allowed to warm up to room temperature and stirred 16 h. MeOH (30 mL) was then added and the reaction mixture was stirred 20 min at room temperature. Volatiles were evaporated under reduce pressure and the residue heated at reflux in toluene for 3 h. After completion, toluene was evaporated under reduce pressure. The residue was dissolved in EtOAc (20 mL) and a white precipitate appeared. After filtration, the filtrate was purified by flash chromatography (gradient Hexane/EtOAc) leading to the desired compound (3.57 g, 62%). ^{1}H NMR (400 MHz, $CDCl_3$) δ 7.35 – 7.27 (m, 10H), 7.22 – 7.14 (m, 6H), 7.07 – 7.01 (m, 6H), 5.84 (d, *J* = 8.0 Hz, 2H), 5.05 (q, *J* = 12.4 Hz, 4H), 4.96 (td, *J* = 9.1, 6.2 Hz, 2H), 4.45 (q, *J* = 7.0 Hz, 2H), 3.54 (s, 6H), 3.33 (dd, *J* = 12.8, 5.7 Hz, 2H), 3.23 (dd, *J* = 12.6, 9.7 Hz, 2H), 1.12 (d, *J* = 7.2 Hz, 6H). ^{13}C NMR (101 MHz, $CDCl_3$) δ 170.47, 155.77, 148.69, 136.92, 136.44, 133.79, 129.59, 128.68, 128.58, 128.14, 127.95, 126.95, 123.09, 66.89, 53.19, 52.81, 49.06, 42.30, 17.40. IR (cm^{-1}): 3325, 2989, 2901, 1746, 1709, 1528, 1497, 1454, 1255, 1232, 1077, 1050, 750, 701. MS(ESI+): Calc for $[C_{46}H_{48}N_6O_8S_2+H]^+$ 877.305, Found 877.341

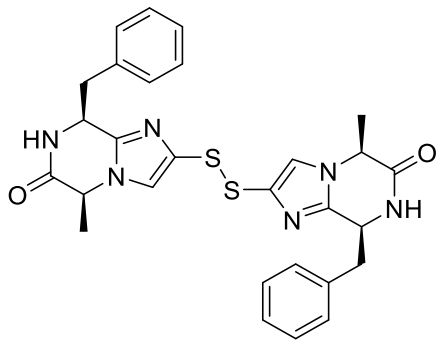

3-26

(5*S*,5'*S*,8*S*,8'*S*)-2,2'-Disulfanediylbis(8-benzyl-5-methyl-7,8-dihydroimidazo[1,2-*a*]pyrazin-6(5*H*)-one)

To **3-16** (2.0 g, 2.28 mmol, 1 eq) in dry DCM (20 mL) at 0 °C and under argon atmosphere was added anisole (3.72 mL, 34.21 mmol, 15 eq) and HBr (33% in AcOH, 12.39 mL, 68.41 mmol, 30 eq). The reaction mixture was then stirred at room temperature for 2 h. Volatiles were removed by evaporation under reduced pressure and the residue was dissolved in a minimum of DCM. Et_2O was added, leading to the formation of a precipitate recovered by filtration. The solid was then dissolved in water (5 mL) and an aqueous solution of $NaHCO_3$ (2 M) was added until pH = 8. The reaction mixture was stirred at room temperature 1 h. DCM (5 mL) was added and the reaction mixture was stirred vigorously for 16 h. The layers were separated and the aqueous layer was extracted with DCM (5 mL). Combined organic layer was washed with brine, filtered and evaporated to afford the desired compound (886 mg, 71%). ^{1}H NMR (400 MHz, $CDCl_3$) δ 7.23 – 7.11 (m, 3H), 7.02 (s, 1H), 6.94 (d, *J* = 6.5 Hz, 2H), 5.04 (s, 1H), 4.46 (q, *J* = 7.0 Hz, 1H), 3.35 (dd, *J* = 13.7, 5.5 Hz, 1H), 3.22 (dd, *J* = 13.7, 3.6 Hz, 1H), 0.91 (d, *J* = 7.1 Hz, 3H). ^{13}C NMR (101 MHz, $CDCl_3$) δ 168.00, 142.32, 136.52, 135.33, 130.41, 128.57, 127.22, 121.64, 53.43, 52.24, 43.10, 20.06. IR (cm^{-1}) 3060, 2930, 1670, 1452, 1356, 1298, 743, 700, 655, 607. MS(ESI+): Calc for $[C_{28}H_{28}N_6O_2S_2+H]^+$ 545.179; Found 545.203

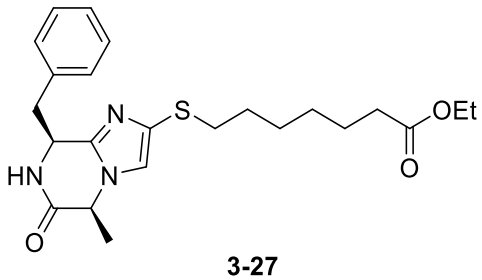

3-27

Ethyl 7-(((5*S*,8*S*)-8-benzyl-5-methyl-6-oxo-5,6,7,8-tetrahydroimidazo[1,2-*a*]pyrazin-2-yl)thio)heptanoate

TCEP.HCl (355.0 mg, 1.24 mmol, 3 eq) was added in Milli-Q water (10 mL). Then aqueous NaOH (1M) was added until pH = 5. The solution was then added to intermediate **3-26** (225.0 mg, 0.41 mmol, 1 eq) in a mixture of THF (5 mL) and MeOH (3 mL) and the reaction mixture was stirred at room temperature for 16 h. Volatiles were evaporated and the aqueous was extracted with $CHCl_3$ (2 x 10 mL). Combined organic layer was dried over $MgSO_4$, filtered and evaporated. The crude was dissolved in dry DCM (5 mL) under nitrogen atmosphere. Ethyl 7-bromoheptanoate (241 μL, 1.23 mmol, 3 eq) and Et_3N (172 μL, 1.23 mmol, 3 eq) were added. The reaction mixture was stirred at room temperature for 6 h. The solvent was evaporated and the residue purified by flash chromatography (gradient DCM/MeOH) to afford the desired product (63 mg, 18%). ^{1}H NMR (400 MHz, $CDCl_3$) δ 7.24 – 7.21 (m, 3H), 7.02 – 6.98 (m, 2H), 6.79 (s, 1H), 5.06 – 5.02 (m, 1H), 4.46 (qd, *J* = 7.1, 1.4 Hz, 1H), 4.11 (q, *J* = 7.1 Hz, 2H), 3.30 – 3.24 (m, 2H), 2.91 – 2.77 (m, 2H), 2.28 (t, *J* = 7.5 Hz, 2H), 1.68 – 1.58 (m, 4H), 1.49 – 1.39 (m, 2H), 1.39 – 1.29 (m, 2H), 1.24 (t, *J* = 7.1 Hz, 4H), 1.01 (d, *J* = 7.1 Hz, 3H). ^{13}C NMR (101 MHz, $CDCl_3$) δ 173.82, 168.57, 141.02, 135.12, 134.95, 130.31, 128.51, 127.30, 118.77, 60.26, 53.14, 52.54, 42.83, 35.39, 34.29, 29.45, 28.74, 28.29, 24.87, 19.85, 14.29. IR (cm^{-1}) 3318, 2928, 1717, 1212, 1028. MS(ESI+): Calc for $[C_{23}H_{31}N_3O_3S+H]^+$ 430.216; Found 430.690

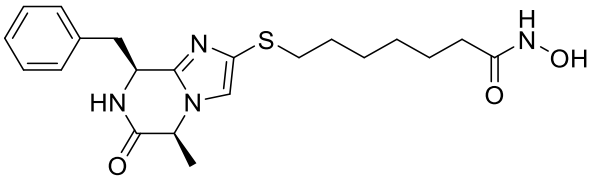

3-29

7-(((5*S*,8*S*)-8-benzyl-5-methyl-6-oxo-5,6,7,8-tetrahydroimidazo[1,2-*a*]pyrazin-2-yl)thio)-*N*-hydroxyheptanamide

To the ethyl ester intermediate **3-27** (63 mg, 0.15 mmol, 1 eq) in a mixture of MeOH/THF (2.4 mL, 1:1) was added KCN (1.9 mg, 0.03 mmol, 0.2 eq) followed by an aqueous solution of NH_2OH (50%, 0.6 mL). The reaction mixture was stirred at room temperature for 2 days. The solvents

were evaporated and the residue purified by reverse phase flash chromatography (gradient water/MeCN-0.05% TFA) to afford the desired compound as an oil (18 mg, 29%). ^{1}H NMR (400 MHz, D_2O) δ 7.52 (d, *J* = 7.6 Hz, 1H), 7.38 – 7.29 (m, 3H), 6.98 – 6.86 (m, 2H), 5.57 – 5.50 (m, 1H), 4.76 – 4.70 (m, 1H), 3.37 – 3.29 (m, 2H), 3.01 – 2.85 (m, 2H), 2.16 (t, *J* = 7.3 Hz, 2H), 1.65 – 1.53 (m, 4H), 1.52 – 1.41 (m, 2H), 1.37 – 1.27 (m, 2H), 0.70 (d, *J* = 7.2 Hz, 3H). ^{13}C NMR (101 MHz, D_2O) δ 173.31, 168.22, 140.55, 133.07, 129.93, 129.13, 128.27, 127.43, 123.09, 53.73, 50.37, 40.96, 35.31, 32.19, 28.30, 27.52, 26.74, 24.71, 17.94. IR (cm^{-1}) 3151, 2927, 2851, 1668, 1455, 1200, 1133, 701. MS(ESI+): Calc for $[C_{21}H_{28}N_4O_3S+H]^+$ 417.196; Found 417.302

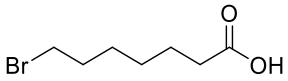

3-31

7-Bromoheptanoic acid

To a solution of ethyl 7-bromoheptanoate (3.0 g, 12.65 mmol, 1 eq) in a mixture of THF/H_2O/EtOH 1:1:1 (30 mL), LiOH (0.39 g, 16.45 mmol, 1.3 eq) was added. The reaction mixture was stirred at room temperature for 3 h. The solvent was removed *in vacuo*, and the residue was dissolved in DCM (10 mL). The reaction mixture was acidified with HCl (4 M) and stirred 10 min at room temperature. The organic layer was separated, washed with brine (3 x10 mL), dried over $MgSO_4$ filtered, and concentrated *in vacuo*. The crude was submitted to the next step without additional purification (2.55 g, 96% yield). ^{1}H NMR (400 MHz, $CDCl_3$) δ 3.40 (t, *J* = 6.8 Hz, 2H), 2.36 (t, *J* = 7.4 Hz, 2H), 1.90 – 1.81 (m, 2H), 1.65 (quint, *J* = 7.5 Hz, 2H), 1.51 – 1.42 (m, 2H), 1.42 – 1.33 (m, 2H). ^{13}C NMR (101 MHz, $CDCl_3$) δ 180.31, 34.04, 33.84, 32.62, 28.26, 27.89, 24.53. Consistent with reported analysis.[516]

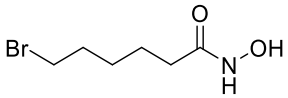

3-33

6-Bromo-*N*-hydroxyhexanamide

To 6-bromohexanoic acid (3.0 g, 15.38 mmol, 1 eq) in dry THF (25 mL) under nitrogen atmosphere was added CDI (3.74 g, 23.07 mmol, 1.5 eq) and the reaction mixture was stirred at room temperature 1 h. Hydroxylamine hydrochloride (2.14 g, 30.76 mmol, 2 eq) was added and the reaction mixture was stirred at room temperature for 16 h. The reaction was stopped by addition of $KHSO_4$ 5% (30 mL) and the THF was evaporated. The aqueous solution was extracted with EtOAc (3 x20 mL) and the combined organic layer was washed with brine, dried over $MgSO_4$, filtered and evaporated. The crude was purified by flash chromatography (gradient

DCM/MeOH) to afford the desired compound (2.56 g, 79%). ^{1}H NMR (400 MHz, $CDCl_3$) δ 8.75 (br, 1H), 3.40 (t, *J* = 6.7 Hz, 2H), 2.17 (t, *J* = 7.3 Hz, 2H), 1.92 – 1.82 (m, 2H), 1.67 (quint, *J* = 7.5 Hz, 2H), 1.53 – 1.42 (m, 2H). ^{13}C NMR (101 MHz, $CDCl_3$) δ 171.66, 33.67, 32.85, 32.40, 27.69, 24.61. IR (cm^{-1}) 3205, 3048, 2921, 2863, 1622, 1545, 1462, 1061, 644. MS(ESI+): Calc for $[C_6H_{12}BrNO_2+H]^+$ 210.013, Found 209.923

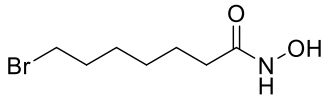

3-34

7-Bromo-*N*-hydroxyheptanamide

To **3-31** (2.5 g, 11.96 mmol, 1 eq) in dry THF (20 mL) under nitrogen atmosphere was added CDI (2.91 g, 17.94 mmol, 1.5 eq) and the reaction mixture was stirred at room temperature 1 h. Hydroxylamine hydrochloride (1.66 g, 23.91 mmol, 2 eq) was added and the reaction mixture was stirred at room temperature for 16 h. The reaction was stopped by addition of $KHSO_4$ 5% (30 mL) and the THF was evaporated. The aqueous solution was extracted with EtOAc (3 x 20 mL) and the combined organic layer was washed with brine, dried over $MgSO_4$, filtered and evaporated. The crude was purified by flash chromatography (gradient DCM/MeOH) to afford the desired compound (1.67 g, 62%). ^{1}H NMR (400 MHz, $CDCl_3$) δ 8.41 (s, 1H), 3.40 (t, *J* = 6.7 Hz, 2H), 2.16 (t, *J* = 7.4 Hz, 2H), 1.91 – 1.79 (m, 2H), 1.66 (quint, *J* = 7.5 Hz, 2H), 1.50 – 1.41 (m, 2H), 1.41 – 1.30 (m, 2H). ^{13}C NMR (101 MHz, $CDCl_3$) δ 172.05, 33.99, 32.89, 32.57, 28.25, 27.82, 25.32. IR (cm^{-1}): 3167, 2930, 2856, 1622, 1465, 972. MS(ESI+): Calc for $[C_7H_{14}BrNO_2+H]^+$ 224.029; Found 223.990

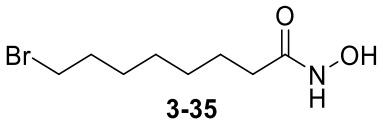

3-35

8-Bromo-*N*-hydroxyoctanamide

To 8-bromooctannoic acid (3.0 g, 13.45 mmol, 1 eq) in dry THF (22 mL) under nitrogen atmosphere was added CDI (3.27 g, 20.17 mmol, 1.5 eq) and the reaction mixture was stirred at room temperature 1 h. Hydroxylamine hydrochlorine (1.87 g, 26.89 mmol, 2 eq) was added and the reaction mixture was stirred at room temperature 16 h. The reaction was stopped by addition of $KHSO_4$ 5% (30 mL) and the THF was evaporated. The aqueous solution was extracted with EtOAc (3 x 20 mL) and the combined organic layer was washed with brine, dried over $MgSO_4$, filtered and evaporated. The crude was purified by flash chromatography (gradient DCM/MeOH) to afford the desired compound as an orange solid (2.70 g, 84%). ^{1}H NMR (400 MHz, $CDCl_3$) δ

8.69 (br, 1H), 3.40 (t, *J* = 6.8 Hz, 2H), 2.14 (t, *J* = 7.5 Hz, 2H), 1.91 – 1.78 (m, 2H), 1.68 – 1.58 (m, 2H), 1.47 – 1.37 (m, 2H), 1.37 – 1.28 (m, 4H). ^{13}C NMR (101 MHz, $CDCl_3$) δ 171.91, 34.15, 33.15, 32.87, 29.10, 28.60, 28.15, 25.45. IR (cm^{-1}) 3270, 2929, 2911, 2844, 1661, 1620, 1560, 1424, 1068, 724, 642. MS(ESI+): Calc for $[C_8H_{16}BrNO_2+H]^+$ 238.044, Found 237.992

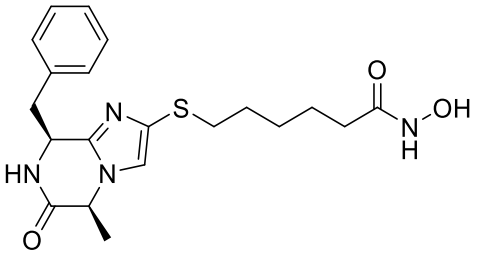

3-36

6-(((5*S*,8*S*)-8-Benzyl-5-methyl-6-oxo-5,6,7,8-tetrahydroimidazo[1,2-*a*]pyrazin-2-yl)thio)-*N*-hydroxyhexanamide

TCEP.HCl (157.9 mg, 0.551 mmol, 3 eq) was added in Milli-Q water (10 mL). Then aqueous NaOH (1M) was added until pH = 5. The solution was then added to intermediate **3-26** (100.0 mg, 0.18 mmol, 1 eq) in MeOH (6 mL) and the reaction mixture was stirred at room temperature for 16 h. Volatiles were evaporated and the aqueous was extracted with $CHCl_3$ (2 x 10 mL). Combined organic layer was dried over $MgSO_4$, filtered and evaporated. The crude was dissolved in $CHCl_3$ (5 mL) under nitrogen atmosphere. Compound **3-33** (115.8 mg, 0.551 mmol, 3 eq) and DIPEA (96.2 μL, 0.551mmol, 3 eq) were added. The reaction mixture was stirred at room temperature for 16 h. The solvent was evaporated and the residue purified by reverse phase flash chromatography (gradient water/MeCN-0.05% TFA) to afford the desired compound (44 mg, 60%). ^{1}H NMR (400 MHz, MeOD) δ 7.35 (s, 1H), 7.17 – 7.13 (m, 3H), 6.84 – 6.76 (m, 2H), 5.21 (td, *J* = 3.8, 1.7 Hz, 1H), 4.51 (qd, *J* = 7.2, 1.7 Hz, 1H), 3.25 – 3.22 (m, 1H), 3.13 (dd, *J* = 14.0, 4.1 Hz, 1H), 2.87 – 2.76 (m, 2H), 2.01 (t, *J* = 7.1 Hz, 2H), 1.63 – 1.51 (m, 4H), 1.40 (q, *J* = 7.4 Hz, 2H), 0.61 (d, *J* = 7.2 Hz, 3H). IR (cm^{-1}): 3067, 2934, 1661, 1455, 1182, 720. ^{13}C NMR (101 MHz, MeOD) δ 171.36, 166.53, 141.48, 133.81, 129.94, 128.56, 127.63, 122.36, 53.76, 50.72, 41.06, 35.22, 32.07, 28.67, 27.16, 24.69, 17.90. MS(ESI+): Calc for $[C_{20}H_{26}N_4O_3S+H]^+$ 403.180; Found 403.114

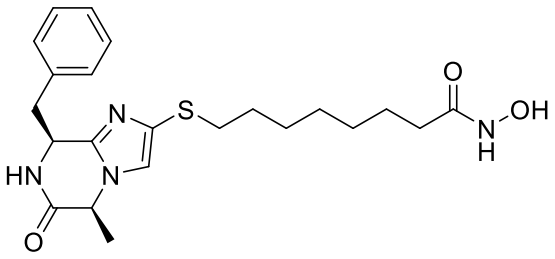

3-37

8-(((5*S*,8*S*)-8-Benzyl-5-methyl-6-oxo-5,6,7,8-tetrahydroimidazo[1,2-*a*]pyrazin-2-yl)thio)-*N*-hydroxyoctanamide

To intermediate **3-26** (100 mg, 0.18 mmol, 1 eq) in DCM (2 mL) and toluene (0.25 mL) was added DTT (227 mg, 1.47 mmol, 8 eq). The mixture was stirred 16 h at room temperature. Compound **3-35** (105 mg, 0.44 mmol, 2.4 eq) and Et_3N (124 µL, 0.92 mmol, 5 eq) were added and the reaction mixture was stirred 4 h at room temperature. The reaction mixture was diluted with EtOAc (20 mL) and washed with saturated solution $NaHCO_3$ (2 x 10 mL), brine (10 mL). Organic layer was then dried over $MgSO_4$, filtered and evaporated. Residue was purified by flash chromatography (gradient DCM/MeOH) to afford the desired compound as an oil (40 mg, 51%). ^{1}H NMR (400 MHz, MeOD) δ 7.31 (s, 1H), 7.24 – 7.16 (m, 3H), 6.91 – 6.85 (m, 2H), 5.22 (td, *J* = 3.8, 1.7 Hz, 1H), 4.56 (qd, *J* = 7.1, 1.6 Hz, 1H), 3.34 (m, 1H), 3.19 (dd, *J* = 13.9, 4.0 Hz, 1H), 2.96 – 2.81 (m, 2H), 2.08 (t, *J* = 7.4 Hz, 2H), 1.70 – 1.56 (m, 4H), 1.47 (dt, *J* = 14.6, 7.3 Hz, 2H), 1.39 – 1.32 (m, 4H), 0.67 (d, *J* = 7.2 Hz, 3H). ^{13}C NMR (101 MHz, MeOD) δ 172.95, 168.56, 142.71, 135.56, 131.79, 131.41, 129.72, 128.75, 122.79, 54.80, 52.42, 42.62, 36.62, 33.65, 30.36, 29.88, 29.77, 29.12, 26.55, 19.51. IR (cm^{-1}): 3179, 2927, 2859, 1662, 1456, 1199, 698. MS(ESI+): Calc for $[C_{22}H_{30}N_4O_3S+H]^+$ 431.212; Found 431.029

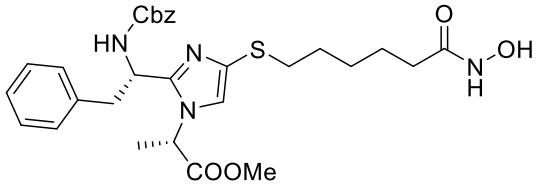

3-38

Methyl (*S*)-2-(2-((*S*)-1-(((benzyloxy)carbonyl)amino)-2-phenylethyl)-4-((6-(hydroxyamino)-6-oxohexyl)thio)-1*H*-imidazol-1-yl)propanoate

To intermediate **3-16** (250 mg, 0.29 mmol, 1 eq) in DCM (1 mL) was added DTT (352 mg, 2.28 mmol, 8 eq). The mixture was stirred 16 h at room temperature. Compound **3-33** (144 mg, 0.68 mmol, 2.4 eq) and Et_3N (190 µL, 1.43 mmol, 5 eq) were added and the reaction mixture was stirred 16 h at room temperature. The reaction mixture was diluted with DCM (10 mL) and

washed with a saturated solution of $NaHCO_3$ (2 x 10 mL), then brine (10 mL). Organic layer was then dried over $MgSO_4$, filtered and evaporated. The residue was purified by reverse flash chromatography (gradient H_2O/MeCN 0.05% TFA) to afford the desired compound (90 mg, 56%). ^{1}H NMR (400 MHz, $CDCl_3$) δ 10.00 (br, 1H), 8.15 (d, *J* = 7.9 Hz, 1H), 7.33 – 7.27 (m, 5H), 7.25 – 7.21 (m, 3H), 7.09 – 7.02 (m, 3H), 5.19 – 5.10 (m, 1H), 5.08, 4.97 (ABq, *J* = 12.5 Hz, 2H), 4.85 (q, *J* = 6.8 Hz, 1H), 3.72 (s, 3H), 3.45 – 3.33 (m, 2H), 2.86 (t, *J* = 6.8 Hz, 2H), 2.12 (t, *J* = 6.2 Hz, 2H), 1.65 – 1.55 (m, 2H), 1.55 – 1.46 (m, 2H), 1.45 – 1.34 (m, 2H), 1.17 (d, *J* = 7.2 Hz, 3H). ^{13}C NMR (101 MHz, $CDCl_3$) δ 168.72, 162.26, 156.55, 149.42, 136.25, 135.20, 129.30, 129.06, 128.56, 128.18, 127.86, 127.52, 122.07, 67.24, 55.14, 53.72, 49.00, 39.63, 35.55, 32.07, 28.53, 27.04, 24.56, 17.54. IR (cm^{-1}): 3193, 3061, 2928, 1670, 1453, 1230. MS(ESI+): Calc for $[C_{29}H_{36}N_4O_6S+H]^+$ 569.243; Found 569.350

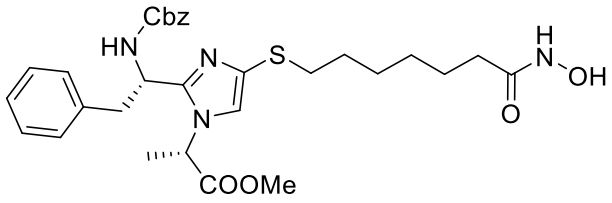

3-39

Methyl (*S*)-2-(2-((*S*)-1-(((benzyloxy)carbonyl)amino)-2-phenylethyl)-4-((7-(hydroxyamino)-7-oxoheptyl)thio)-1*H*-imidazol-1-yl)propanoate

TCEP.HCl (196.10 mg, 0.68 mmol, 3 eq) was added in Milli-Q water (6 mL). Then aqueous NaOH (1M) was added until pH = 5. The solution was then added to intermediate **3-16** (200 mg, 0.23 mmol, 1 eq) in a mixture of $CHCl_3$ (2 mL) and MeOH (6 mL) and the reaction mixture was stirred at room temperature for 16 h. Volatiles were evaporated and the aqueous was extracted with $CHCl_3$ (2 x 10 mL). Combined organic layer was dried over $MgSO_4$, filtered and evaporated. The crude was dissolved in dry $CHCl_3$ (4 mL) under nitrogen atmosphere. Linker **3-34** (204 mg, 0.91 mmol, 4 eq) and DIPEA (159 µL, 0.91 mmol, 4 eq) were added. The reaction mixture was stirred at room temperature for 16 h. The solvent was evaporated and the residue purified by flash chromatography (gradient DCM/MeOH) to afford the desired product (63 mg, 18%). ^{1}H NMR (400 MHz, $CDCl_3$) δ 7.36 – 7.29 (m, 5H), 7.21 – 7.14 (m, 3H), 7.01 (d, *J* = 7.0 Hz, 2H), 6.84 (s, 1H), 6.00 (d, *J* = 8.5 Hz, 1H), 5.10, 5.05 (ABq, *J* = 12.4 Hz, 2H), 4.96 (td, *J* = 9.2, 5.7 Hz, 1H), 4.41 (q, *J* = 7.1 Hz, 1H), 3.60 (s, 3H), 3.30 (dd, *J* = 12.6, 5.4 Hz, 1H), 3.19 (dd, *J* = 12.4, 10.2 Hz, 1H), 2.88 – 2.73 (m, 2H), 2.28 (t, *J* = 7.5 Hz, 2H), 1.65 – 1.57 (m, 2H), 1.49 – 1.38 (m, 3H), 1.38 – 1.29 (m, 3H), 1.10 (d, *J* = 7.2 Hz, 3H). ^{13}C NMR (101 MHz, $CDCl_3$) δ 171.70, 170.33, 156.03, 148.81, 136.90, 136.58, 132.05, 129.39, 128.59, 128.47, 127.97, 127.78, 126.93, 120.30, 66.70,

53.16, 52.97, 48.85, 41.69, 35.74, 33.95, 32.86, 28.80, 28.23, 24.99, 17.79. IR (cm^{-1}) 3318, 2934, 1663, 1190, 1135. MS (ESI+): Calc for $[C_{30}H_{38}N_4O_6S+H]^+$ 583.2590; Found 583.2650

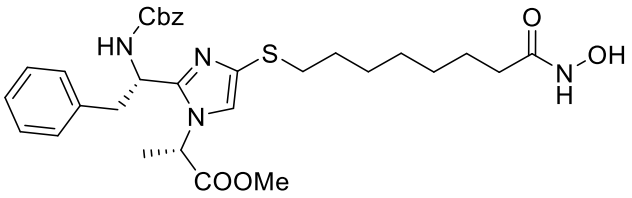

3-40

Methyl (*S*)-2-(2-((*S*)-1-(((benzyloxy)carbonyl)amino)-2-phenylethyl)-4-((8-(hydroxyamino)-8-oxooctyl)thio)-1*H*-imidazol-1-yl)propanoate

To intermediate **3-16** (250 mg, 0.29 mmol, 1 eq) in DCM (1 mL) was added DTT (352 mg, 2.28 mmol, 8 eq). The mixture was stirred 16 h at room temperature. Compound **3-35** (144 mg, 0.68 mmol, 2.4 eq) and Et_3N (190 µL, 1.43 mmol, 5 eq) were added and the reaction mixture was stirred 16 h at room temperature. The reaction mixture was diluted with DCM (10 mL) and washed with a saturated solution of $NaHCO_3$ (2 x 10 mL), then brine (10 mL). Organic layer was then dried over $MgSO_4$, filtered and evaporated. The residue was purified by reverse flash chromatography (gradient H_2O/MeCN 0.05% TFA) to afford the desired compound (135 mg, 79%). ^{1}H NMR (400 MHz, $CDCl_3$) δ 8.22 (d, *J* = 8.0 Hz, 1H), 7.34 – 7.27 (m, 5H), 7.24 – 7.19 (m, 3H), 7.09 – 7.02 (m, 2H), 6.98 (s, 1H), 5.17 – 5.10 (m, 1H), 5.08, 4.98 (ABq, *J* = 12.8 Hz, 2H), 4.82 (q, *J* = 7.2 Hz, 1H), 3.70 (s, 3H), 3.46 – 3.31 (m, 2H), 2.90 (t, *J* = 7.2 Hz, 2H), 2.17 – 2.04 (m, 2H), 1.62 – 1.49 (m, 4H), 1.41 – 1.32 (m, 2H), 1.32 – 1.22 (m, 4H), 1.12 (d, *J* = 7.1 Hz, 3H). ^{13}C NMR (101 MHz, $CDCl_3$) δ 171.56, 168.70, 156.46, 149.28, 136.34, 135.44, 129.16, 129.07, 128.50, 128.25, 128.08, 127.79, 127.71, 121.28, 67.07, 54.84, 53.53, 48.92, 39.86, 35.50, 32.55, 28.97, 28.52, 28.27, 27.84, 25.12, 17.58. IR (cm^{-1}): 3228, 2929, 2856, 1662, 1455, 1198. MS (ESI+) Calc for $[C_{31}H_{40}N_4O_6S+H]^+$ 597.275; Found 597.876

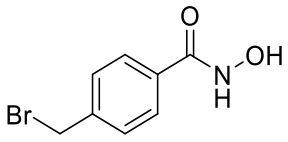

3-41

4-(Bromomethyl)-*N*-hydroxybenzamide

Under argon atmosphere, $SOCl_2$ (10 mL, 137.85 mmol, 10 eq) was added to α-Bromo-p-toluic acid (3.0 g, 13.95 mmol, 1 eq) and the mixture was heated at reflux for 4.5 h. Excess of $SOCl_2$ was then removed *in vaccuo*. Toluene (20 mL) was added to the residue followed by evaporation

to afford the acid chloride (3.26 g). The acid chloride was then dissolved in Et_2O (100 mL) and added dropwise to a solution of NH_2OH. HCl (2.13 g, 30.69 mmol, 2.2 eq) in NaOH (2 M, 15 mL) at 0 °C. The reaction mixture was stirred 30min at room temperature. The solution was then acidified with HCl (2 M) until pH = 2 leading to a precipitate which was filtered and washed with H_2O (20 mL) to afford the desired compound (2.88 g, 90 % yield). ^{1}H NMR (400 MHz, DMSO) δ 11.26 (br, 1H), 7.74 (d, *J* = 8.4 Hz, 2H), 7.52 (d, *J* = 8.3 Hz, 2H), 4.73 (s, 2H). ^{13}C NMR (101 MHz, DMSO) δ 163.79, 141.08, 132.63, 129.31, 127.32, 33.58. IR (cm^{-1}): 3341, 3050, 2685, 1644, 1534, 1466. MS (ESI+) Calc for $[C_8H_8BrNO_2+H]^+$ 229.981; Found 231.455

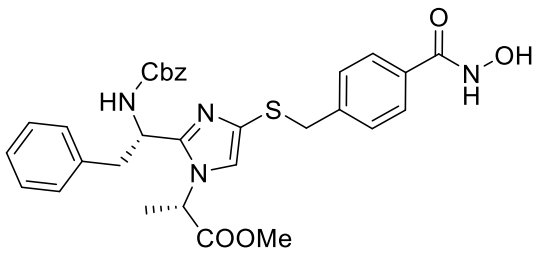

3-42

Methyl (*S*)-2-(2-((*S*)-1-(((benzyloxy)carbonyl)amino)-2-phenylethyl)-4-((4-(hydroxycarbamoyl)benzyl)thio)-1*H*-imidazol-1-yl)propanoate

To intermediate **3-16** (250 mg, 0.29 mmol, 1 eq) in dry DCM (4 mL) under argon atmosphere were added DTT (352 mg, 2.28 mmol, 8 eq) and Et_3N (159 µL, 1.14 mmol, 4 eq). The mixture was stirred 16 h at room temperature. Compound **3-41** (656 mg, 2.85 mmol, 10 eq) was added and the reaction mixture was stirred 16 h at room temperature. The reaction mixture was diluted with DCM (10 mL) and washed with a saturated solution of $NaHCO_3$ (2 x 10 mL), then brine (10 mL). Organic layer was then dried over $MgSO_4$, filtered and evaporated. The residue was purified by reverse flash chromatography (gradient H_2O/MeCN 0.05% TFA) to afford the desired compound (80 mg, 24%). ^{1}H NMR (400 MHz, $CDCl_3$) δ 8.11 (br, 1H), 7.42 – 7.28 (m, 7H), 7.20 – 7.16 (m, 3H), 7.04 (d, *J* = 8.0 Hz, 2H), 6.99 – 6.94 (m, 2H), 6.81 (s, 1H), 5.21 (d, *J* = 12.4 Hz, 1H), 5.04 (d, *J* = 12.4 Hz, 1H), 5.02 – 4.94 (m, 1H), 4.73 (q, *J* = 7.2 Hz, 1H), 4.04, 3.94 (ABq, *J* = 12.7 Hz, 2H), 3.76 (s, 3H), 3.26 (d, *J* = 8.5 Hz, 2H), 1.06 (d, *J* = 7.3 Hz, 3H). ^{13}C NMR (101 MHz, $CDCl_3$) δ 173.82, 168.69, 156.55, 149.72, 140.18, 136.39, 135.21, 131.04, 129.28, 129.20, 128.98, 128.62, 128.27, 128.07, 127.83, 127.66, 125.69, 123.76, 67.30, 54.97, 53.76, 48.85, 40.39, 39.57, 17.57. IR (cm^{-1}): 3209, 2926, 1662, 1456, 1197, 1135. MS (ESI+) Calc for $[C_{31}H_{32}N_4O_6S+H]^+$ 589.212; Found 589.750

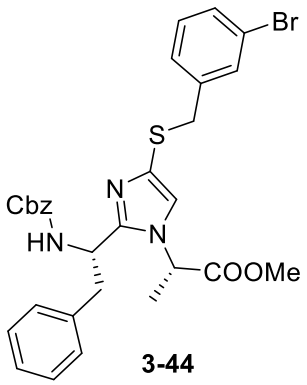

3-44

Methyl (*S*)-2-(2-((*S*)-1-(((benzyloxy)carbonyl)amino)-2-phenylethyl)-4-((3-bromobenzyl)thio)-1*H*-imidazol-1-yl)propanoate

To a mixture of **3-16** (150 mg, 0.17 mmol, 1 eq) in dry DCM (4 mL) under argon atmosphere were added DTT (211 mg, 0.86 mmol, 8 eq) and Et_3N (116 μL, 0.86 mmol, 5 eq). The reaction mixture was stirred for 16 h at room temperature. To the mixture was added 3-bromobenzyl bromide (103 mg, 0.41 mmol, 2.4 eq) the reaction mixture was stirred at room temperature for 5 h. The reaction mixture was then diluted with DCM (10 mL) and washed with an aqueous solution 5% $NaHSO_4$ (3 x 10 mL), then a saturated solution of $NaHCO_3$ (2 x 10 mL) and then brine (10 mL). The organic layer was dried over $MgSO_4$, filtered and evaporated. The crude material was purified by flash chromatography on silica (gradient Hexane/EtOAc) to afford the desired product (133mg, 64%). ^{1}H NMR (400 MHz, $CDCl_3$) δ 7.37 – 7.27 (m, 7H), 7.23 – 7.16 (m, 3H), 7.11 – 7.01 (m, 4H), 6.63 (s, 1H), 5.66 (d, *J* = 8.6 Hz, 1H), 5.11, 5.07 (ABq, *J* = 12.4 Hz, 2H), 4.95 (td, *J* = 9.3, 5.5 Hz, 1H), 4.35 (q, *J* = 7.3 Hz, 1H), 3.95, 3.88 (ABq, *J* = 13.2 Hz, 2H), 3.58 (s, 3H), 3.33 (dd, *J* = 12.8, 5.3 Hz, 1H), 3.20 (dd, *J* = 12.8, 9.9 Hz, 1H), 1.06 (d, *J* = 7.2 Hz, 3H). ^{13}C NMR (101 MHz, $CDCl_3$) δ 170.14, 155.64, 148.51, 141.04, 136.93, 136.47, 132.03, 130.91, 130.06, 129.91, 129.53, 128.79, 128.65, 128.25, 128.08, 127.78, 127.09, 122.25, 121.24, 67.00, 53.57, 53.13, 49.13, 42.48, 39.65, 17.65. IR (cm^{-1}): 3312, 3029, 2921, 1741, 1713, 1217. MS (ESI+) Calc for $[C_{30}H_{30}N_3O_4SBr+H]^+$ 608.1219; Found: 608.1215

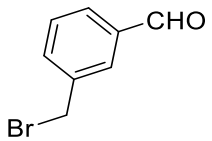

3-63

3-(Bromomethyl)benzaldehyde

To a solution of α–Bromo–m–tolunitrile (1.00 g, 5.1 mmol) in dry toluene (10 mL) under argon atmosphere and cooled in an ice–bath was added dropwise DIBAL–H (1.0 M solution in hexane, 6.63 ml, 6.63 mmol). The reaction mixture was stirred for 2 h in an ice-bath. After completion,

chloroform (15 mL) and 10% HCl (35 ml) were added. Stirring was kept for an additional hour at room temperature. The layers were separated and the organic layer was washed with distilled water (35 mL), brine (30 mL), dried over $MgSO_4$ and filtered. Evaporation afforded the desired compound (886 mg, 87%). ^{1}H NMR (400 MHz, $CDCl_3$) δ 10.02 (s, 1H), 7.90 (t, *J* = 1.5 Hz, 1H), 7.82 (dt, *J* = 7.6, 1.4 Hz, 1H), 7.70 – 7.63 (m, 1H), 7.53 (t, *J* = 7.6 Hz, 1H), 4.54 (s, 2H). ^{13}C NMR (101 MHz, $CDCl_3$) δ 191.73, 139.04, 136.95, 134.98, 129.95, 129.81, 129.68, 32.17. Consistent with reported analysis.[418]

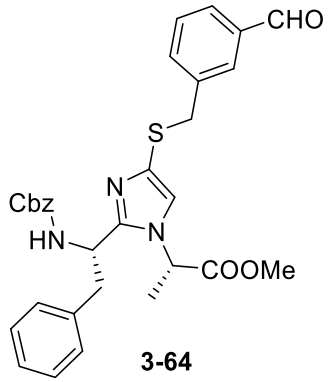

3-64

Methyl (*S*)-2-(2-((*S*)-1-(((benzyloxy)carbonyl)amino)-2-phenylethyl)-4-((3-formylbenzyl)thio)-1*H*-imidazol-1-yl)propanoate

To a mixture of **3-16** (200 mg, 0.23 mmol, 1 eq) in dry DCM (1.75 mL) under argon atmosphere were added DTT (141 mg, 0.91 mmol, 4 eq) and Et_3N (79.5 μL, 0.57 mmol, 2.5 eq). The reaction mixture was stirred for 16 h at room temperature. To the mixture was added **3-63** (90 mg, 0.46 mmol, 2 eq) and the reaction mixture was stirred at room temperature for 5 h. The reaction mixture was then diluted with DCM (10 mL) and washed with an aqueous solution 5% $NaHSO_4$ (3 x 10 mL), then a saturated solution of $NaHCO_3$ (2 x 10 mL) and then brine (10 mL). The organic layer was dried over $MgSO_4$, filtered and evaporated. The crude material was purified by flash chromatography on silica (gradient Hexane/EtOAc) to afford the desired product (137 mg, 54%). ^{1}H NMR (400 MHz, $CDCl_3$) δ 9.89 (s, 1H), 7.74 – 7.66 (m, 1H), 7.58 (s, 1H), 7.44 – 7.27 (m, 7H), 7.23 – 7.15 (m, 3H), 7.06 – 6.99 (m, 2H), 6.62 (s, 1H), 5.67 (d, *J* = 8.6 Hz, 1H), 5.11, 5.07 (ABq, *J* = 12.4 Hz, 2H), 4.94 (td, *J* = 9.2, 5.5 Hz, 1H), 4.35 (q, *J* = 7.2 Hz, 1H), 4.03 (s, 2H), 3.58 (s, 3H), 3.32 (dd, *J* = 12.9, 5.5 Hz, 1H), 3.20 (dd, *J* = 12.8, 9.8 Hz, 1H), 1.04 (d, *J* = 7.2 Hz, 3H). ^{13}C NMR (101 MHz, $CDCl_3$) δ 192.34, 170.11, 155.61, 148.52, 139.91, 136.92, 136.55, 136.44, 135.11, 130.73, 130.47, 129.50, 129.00, 128.69, 128.60, 128.20, 128.09, 128.01, 127.01, 121.28, 66.93, 53.05, 52.94, 49.08, 42.27, 39.64, 17.60. IR (cm^{-1}): 3311, 3030, 1703, 1525, 1247. MS (ESI+) Calc for $[C_{31}H_{31}N_3O_5S+H]^+$ 558.2063; Found: 558.2173

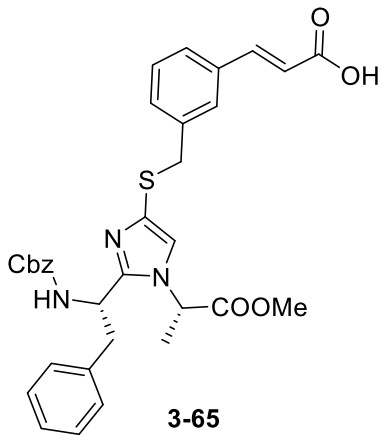

3-65

(*E*)-3-(3-(((2-((*S*)-1-(((Benzyloxy)carbonyl)amino)-2-phenylethyl)-1-((*S*)-1-methoxy-1-oxopropan-2-yl)-1*H*-imidazol-4-yl)thio)methyl)phenyl)acrylic acid

To a mixture of **3-64** (264 mg, 0.47 mmol) in pyridine (2 mL) under argon atmosphere was added malonic acid (148 mg, 1.42 mmol, 3 eq) and piperidine (23 µL, 0.24 mmol, 0.5 eq). The reaction mixture was stirred for 2 h at 100 °C. After completion, the reaction mixture was cooled down to room temperature and a solution of HCl (1M, 20 mL) was added. The aqueous was extracted with EtOAc (2 x 20 mL). Organic layer was dried over $MgSO_4$, filtered and evaporated. The crude product was purified by flash chromatography on silica (gradient DCM/MeOH (2% AcOH)) to afford the desired compound (274 mg, 97%). ^{1}H NMR (400 MHz, $CDCl_3$) δ 7.67 (d, *J* = 16.0 Hz, 1H), 7.57 (s, 1H), 7.39 – 7.29 (m, 6H), 7.20 – 7.08 (m, 4H), 7.02 – 6.92 (m, 3H), 6.86 (s, 1H), 6.51 (d, *J* = 15.9 Hz, 1H), 5.12 (s, 2H), 5.01 (td, *J* = 9.7, 5.9 Hz, 1H), 4.57 (q, *J* = 7.0 Hz, 1H), 4.00, 3.96 (ABq, *J* = 12.3 Hz, 2H), 3.65 (s, 3H), 3.26 (dd, *J* = 12.8, 5.5 Hz, 1H), 3.23 – 3.14 (m, 1H), 1.07 (d, *J* = 7.2 Hz, 3H). ^{13}C NMR (101 MHz, $CDCl_3$) δ 171.57, 169.97, 156.14, 149.30, 144.12, 138.53, 136.84, 136.71, 135.09, 130.65, 129.39, 128.69, 128.49, 127.97, 127.83, 127.00, 121.43, 120.47, 66.71, 53.33, 53.00, 48.84, 41.89, 40.73, 17.66. IR (cm^{-1}): 3260, 2926, 1700, 1635, 1216. MS (ESI+) Calc for $[C_{33}H_{33}N_3O_6S+H]^+$ 600.2168; Found: 600.2155

4.2 Aspartic acid –based scaffold

4.2.i Solution phase synthesis

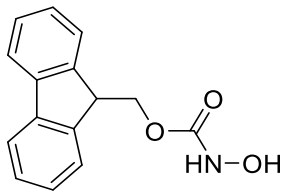

3-72

(9*H*-Fluoren-9-yl)methyl hydroxycarbamate

To a solution of hydroxylamine hydrochloride (208 mg, 3.0 mmol, 1 eq) in EtOAc (20 mL) was added a solution of $NaHCO_3$ (554 mg, 6.6 mmol, 2.2 eq) in H_2O (10 mL). The mixture was cooled to 4 °C in an ice-bath and Fmoc-Cl (775 mg, 3 mmol, 1 eq) dissolved in EtOAc (2 mL) was then added dropwise. The biphasic mixture was let to warm up to room temperature and vigorously stirred for a further 4 h. The reaction mixture was then separated and the organic layer was washed with a saturated solution of $KHSO_4$ (3 x 30 ml) and brine (30 mL). The organic layer was then dried over $MgSO_4$, filtered and evaporated *in vacuo*. The residue was triturated with hexane, and the desired compound was then recovered by filtration (731 mg, 86 %). ^{1}H NMR (400 MHz, $CDCl_3$) δ 7.78 (d, *J* = 6.1 Hz, 2H), 7.59 (d, *J* = 7.1 Hz, 2H), 7.42 (t, *J* = 6.7 Hz, 2H), 7.32 (t, *J* = 8.6 Hz, 2H), 4.52 (d, *J* = 7.0 Hz, 2H), 4.26 (t, *J* = 6.4 Hz, 1H). ^{13}C NMR (101 MHz, $CDCl_3$) δ 158.79, 143.50, 141.48, 128.04, 127.30, 125.16, 120.23, 68.01, 47.09. Consistent with reported analysis.[426]

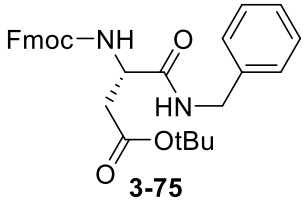

3-75

tert-Butyl (*S*)-3-((((9H-fluoren-9-yl)methoxy)carbonyl)amino)-4-(benzylamino)-4-oxobutanoate

To a solution of Fmoc-L-Asp(OtBu)-OH (5.0 g, 12.15 mmol, 1 eq), in anhydrous DCM (50 mL) under argon atmosphere were added HATU (5.08 g, 13.37 mmol, 1.1 eq), DIPEA (8.5 mL, 48.61 mmol, 4 eq) and benzylamine (1.5 mL, 13.37 mmol, 1.1 eq). The reaction mixture was then stirred at room temperature for 4 h. The reaction was quenched by addition of a saturated solution of NH_4Cl (50 mL). The layers were separated and the aqueous extracted with DCM (20 mL). The organic layer was dried over $MgSO_4$, filtered and concentrated *in vacuo*. The residue was purified by flash chromatography (gradient Hex/EtOAc) to afford the desired compound (5.98 g, 98 %). ^{1}H NMR (400 MHz, $CDCl_3$) δ 7.75 (dd, *J* = 7.6, 3.7 Hz, 2H), 7.57 (d, *J* = 7.4 Hz, 2H), 7.44 – 7.35 (m, 2H), 7.33 – 7.26 (m, 5H), 7.26 – 7.23 (m, 2H), 6.77 (br, 1H), 5.97 (d, *J* = 7.5 Hz, 1H), 4.60 – 4.50 (m, 1H), 4.50 – 4.38 (m, 4H), 4.20 (t, *J* = 6.8 Hz, 1H), 2.97 (dd, *J* = 16.6, 2.9 Hz, 1H), 2.62 (dd, *J* = 17.1, 6.4 Hz, 1H), 1.43 (s, 9H). ^{13}C NMR (101 MHz, $CDCl_3$) δ 171.49, 170.45, 156.18, 143.81, 141.47, 138.00, 128.83, 127.93, 127.67, 127.24, 125.15, 120.20, 82.12, 67.29, 47.31, 43.73, 43.60, 37.59, 28.17. IR (cm^{-1}): 3299, 2975, 1719, 1657, 1539, 1115. MS (ESI+) Calc for $[C_{30}H_{32}N_2O_5+Na]^+$ 523.221; Found: 523.741

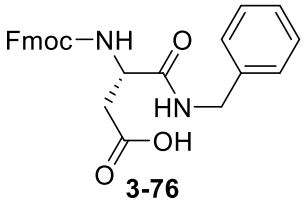

3-76

(*S*)-3-((((9*H*-fluoren-9-yl)methoxy)carbonyl)amino)-4-(benzylamino)-4-oxobutanoic acid

To **3-75** (1.0 g, 2.0 mmol, 1 eq) in DCM (4 mL) was added TFA (1 mL, 12.98 mmol, 6.5 eq) and the reaction mixture was stirred at room temperature for 2 h. The volatiles were evaporated and Et_2O (10 mL) was added. The solvent was removed *in vacuo* and the residue was triturated in hexane. The mixture was filtered to afford the desired compound (860 mg, 97 %). ^{1}H NMR (400 MHz, MeOD) δ 7.79 (dd, *J* = 7.6, 0.7 Hz, 2H), 7.65 (d, *J* = 7.5 Hz, 2H), 7.38 (t, *J* = 7.4 Hz, 2H), 7.30 (ddd, *J* = 7.5, 2.5, 1.2 Hz, 2H), 7.28 – 7.24 (m, 4H), 7.23 – 7.17 (m, 1H), 4.55 (t, *J* = 6.6 Hz, 1H), 4.44 – 4.32 (m, 4H), 4.21 (t, *J* = 6.9 Hz, 1H), 2.86 (dd, *J* = 16.6, 5.8 Hz, 1H), 2.71 (dd, *J* = 16.7, 7.6 Hz, 1H).^{13}C NMR (101 MHz, MeOD) δ 173.97, 173.39, 158.34, 145.21, 142.56, 139.73, 129.47, 128.78, 128.32, 128.16, 126.23, 120.91, 68.15, 53.12, 44.11, 38.87, 37.07. IR (cm^{-1}): 3287, 3139, 1695, 1655, 1542. MS (ESI+) Calc for $[C_{26}H_{24}N_2O_5+H]^+$ 445.176; Found: 445.677

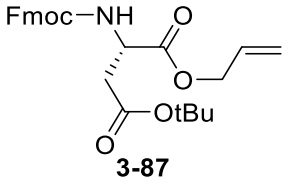

3-87

1-Allyl 4-(tert-butyl) (((9*H*-fluoren-9-yl)methoxy)carbonyl)-L-aspartate

Fmoc-L-Asp(OtBu)-OH (15 g, 36.46 mmol, 1 eq) was added to allyl bromide (31.5 mL, 364.56 mmol, 10 eq) under an argon atmosphere. Then DIPEA (12.7 mL, 72.91 mmol, 2 eq) was added to the mixture. The reaction mixture was heated under reflux and stirred for 1 h resulting in a cloudy yellow solution. After cooling, the solution was poured into EtOAc (200 mL). The diisopropylethylammonium hydrobromide precipitate was filtered off and the filtrate was washed with HCl (1 M, 50 mL), then $NaHCO_3$ (0.5 M, 50 mL), and brine (50 mL). The combined organic layers were dried with $MgSO_4$, filtered and concentrated *in vacuo*. The resulting solution was purified by flash chromatography on silica (gradient Hexane/EtOAc) to afford the desired compound (16.02 g, 97%). ^{1}H NMR (400 MHz, $CDCl_3$) δ 7.77 (d, *J* = 7.5 Hz, 2H), 7.61 (dd, *J* = 7.0, 4.6 Hz, 2H), 7.41 (t, *J* = 7.5 Hz, 2H), 7.32 (td, *J* = 7.5, 1.0 Hz, 2H), 5.98 – 5.87 (m, 1H), 5.85 (d, *J* = 8.8 Hz, 1H), 5.34 (dd, *J* = 17.2, 1.1 Hz, 1H), 5.25 (dd, *J* = 10.4, 1.2 Hz, 1H), 4.71 – 4.60 (m, 3H), 4.43 (dd, *J* = 10.4, 7.3 Hz, 1H), 4.35 (dd, *J* = 10.3, 7.5 Hz, 1H), 4.26 (t, *J* = 7.2 Hz, 1H), 2.98 (dd, *J* = 16.9, 4.6 Hz, 1H), 2.80 (dd, *J* = 16.9, 4.5 Hz, 1H), 1.46 (s, 9H). ^{13}C NMR (101 MHz, $CDCl_3$) δ 170.74, 170.11, 156.09,

144.01, 143.83, 141.40, 131.61, 127.82, 127.18, 125.29, 125.24, 120.09, 118.90, 81.98, 67.38, 66.40, 50.71, 47.20, 37.89, 28.14. IR (cm^{-1}): 3410, 2982, 2950, 1745, 1720, 1507. MS (ESI+) Calc for $[C_{26}H_{29}NO_6+Na]^+$ 474.189; Found: 474.718

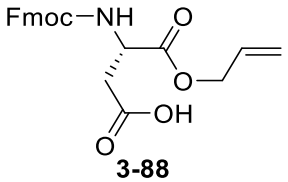

3-88

(*S*)-3-((((9*H*-fluoren-9-yl)methoxy)carbonyl)amino)-4-(allyloxy)-4-oxobutanoic acid

Compound **3-87** (15.95 g, 35.33 mmol, 1 eq) was dissolved in DCM (30 mL), then TFA (30 mL, 353.25 mmol, 10 eq) was added and the mixture was stirred at room temperature for 1 h. The mixture was then concentrated *in vacuo* and the residue washed with Et_2O (30 mL). The residual solid was filtered, washed with Et_2O (2 x 10 mL), and dried to afford the desired compound (11.10 g, 79%). ^{1}H NMR (400 MHz, $CDCl_3$) δ 7.76 (d, *J* = 7.5 Hz, 2H), 7.60 (d, *J* = 7.4 Hz, 2H), 7.40 (t, *J* = 7.4 Hz, 2H), 7.31 (td, *J* = 7.4, 1.0 Hz, 2H), 5.95 – 5.84 (m, 1H), 5.82 (d, *J* = 8.4 Hz, 1H), 5.33 (d, *J* = 17.1 Hz, 1H), 5.26 (d, *J* = 10.5 Hz, 1H), 4.75 – 4.62 (m, 3H), 4.44 (dd, *J* = 10.4, 7.4 Hz, 1H), 4.41 – 4.35 (m, 1H), 4.24 (t, *J* = 6.9 Hz, 1H), 3.13 (dd, *J* = 17.5, 4.4 Hz, 1H), 2.96 (dd, *J* = 17.5, 4.4 Hz, 1H). ^{13}C NMR (101 MHz, $CDCl_3$) δ 175.82, 170.38, 156.20, 143.78, 141.45, 131.41, 127.91, 127.24, 125.25, 120.16, 119.24, 67.54, 66.76, 50.39, 47.22, 36.48. IR (cm^{-1}): 3322, 2960, 1685, 1535, 1274. MS (ESI+) Calc for $[C_{22}H_{21}NO_6+H]^+$ 396.137; Found: 396.521

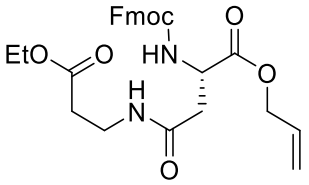

3-89

Allyl N^2-(((9*H*-fluoren-9-yl)methoxy)carbonyl)-N^4-(3-ethoxy-3-oxopropyl)-L-asparaginate

To a solution of **4-88** (5.90 g, 14.92 mmol, 1 eq), in dry DCM (100 mL) under an argon atmosphere were added β-alanine ethyl ester hydrochloride (2.52 g, 16.41 mmol, 1.1 eq), HATU (6.24 g, 16.41 mmol, 1.1 eq) and DIPEA (10.4 mL, 59.68 mmol, 4 eq). The reaction mixture was then stirred at room temperature for 4 h. The reaction was quenched by addition of a saturated solution of NH_4Cl (50 mL). The layers were separated and the aqueous extracted with DCM (20 mL). The organic layer was dried over anhydrous $MgSO_4$ and concentrated in vacuo. The residue was purified by flash chromatography on silica (gradient Hexane/EtOAc) to afford the desired

compound (6.0 g, 81 %). ^{1}H NMR (400 MHz, $CDCl_3$) δ 7.76 (d, *J* = 7.5 Hz, 2H), 7.61 (dd, *J* = 7.2, 3.5 Hz, 2H), 7.40 (t, *J* = 7.4 Hz, 2H), 7.31 (t, *J* = 7.4 Hz, 2H), 6.18 (br, 1H), 6.11 (d, *J* = 8.7 Hz, 1H), 5.97 – 5.82 (m, 1H), 5.33 (d, *J* = 17.1 Hz, 1H), 5.24 (dd, *J* = 10.4, 0.9 Hz, 1H), 4.67 (d, *J* = 5.4 Hz, 2H), 4.65 – 4.57 (m, 1H), 4.43 (dd, *J* = 10.2, 7.2 Hz, 1H), 4.31 (dd, *J* = 10.3, 7.6 Hz, 1H), 4.23 (t, *J* = 7.0 Hz, 1H), 4.15 (q, *J* = 7.1 Hz, 2H), 3.51 (dd, *J* = 11.2, 5.2 Hz, 2H), 2.95 (dd, *J* = 15.8, 4.3 Hz, 1H), 2.72 (dd, *J* = 15.8, 4.3 Hz, 1H), 2.51 (t, *J* = 5.9 Hz, 2H), 1.26 (t, *J* = 7.1 Hz, 3H). ^{13}C NMR (101 MHz, $CDCl_3$) δ 172.63, 170.91, 169.82, 156.28, 143.97, 143.84, 141.35, 131.70, 127.78, 127.15, 125.31, 125.25, 120.04, 118.69, 67.32, 66.35, 60.90, 50.99, 47.17, 37.75, 34.98, 33.97, 14.23. IR (cm^{-1}): 3311, 2952, 1727, 1689, 1541, 1206. MS (ESI+) Calc for $[C_{27}H_{30}N_2O_7+H]^+$ 495.213; Found: 495.700

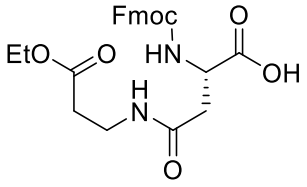

3-90

***N*^{2}-(((9*H*-fluoren-9-yl)methoxy)carbonyl)-*N*^{4}-(3-ethoxy-3-oxopropyl)-L-asparagine**

Phenylsilane (0.75 mL, 6.07 mmol, 1 eq) and $Pd(PPh_3)_4$ (350 mg, 0.30 mmol, 0.05 eq) were added to a solution of **3-89** (3.0 g, 6.07 mmol, 1 eq) in dry DCM (20 mL) under argon atmosphere. The reaction mixture was stirred at room temperature for 16 h. The resulting mixture was filtered through Celite. The filtrate was evaporated and then purified by flash chromatography on silica (gradient DCM/MeOH) to afford the desired compound (1.59 g, 58.0 %). ^{1}H NMR (400 MHz, $CDCl_3$) δ 7.74 (d, *J* = 7.5 Hz, 2H), 7.58 (dd, *J* = 7.2, 3.0 Hz, 2H), 7.38 (t, *J* = 7.4 Hz, 2H), 7.29 (t, *J* = 7.4 Hz, 2H), 6.92 – 6.85 (m, 1H), 6.25 (d, *J* = 6.5 Hz, 1H), 4.55 – 4.48 (m, 1H), 4.40 – 4.28 (m, 2H), 4.19 (t, *J* = 7.1 Hz, 1H), 4.11 (q, *J* = 7.1 Hz, 2H), 3.55 – 3.45 (m, 2H), 2.93 (dd, *J* = 15.8, 2.9 Hz, 1H), 2.75 (dd, *J* = 15.8, 7.3 Hz, 1H), 2.51 (t, *J* = 5.8 Hz, 2H), 1.22 (t, *J* = 7.1 Hz, 3H). ^{13}C NMR (101 MHz, $CDCl_3$) δ 172.82, 172.67, 171.65, 156.29, 143.88, 143.76, 141.39, 127.88, 127.23, 125.28, 120.11, 67.46, 61.15, 50.66, 47.15, 37.84, 35.46, 33.73, 14.22. IR (cm^{-1}): 3313, 2942, 1727, 1694, 1644, 1538, 1183. MS (ESI+) Calc for $[C_{24}H_{26}N_2O_7+H]^+$ 455.182; Found: 455.668

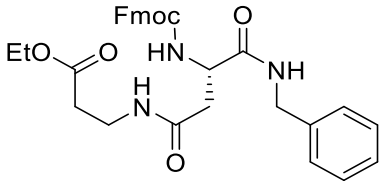

3-91

Ethyl (*S*)-3-(3-((((9*H*-fluoren-9-yl)methoxy)carbonyl)amino)-4-(benzylamino)-4-oxobutanamido)propanoate

To a solution of **3-90** (300 mg, 0.66 mmol, 1 eq) in DCM (10 mL) were added EDC.HCl (152 mg, 0.792 mmol, 1.2 eq) and HOBt.H_2O (121 mg, 0.792 mmol, 1.2 eq). The mixture was stirred in an ice-bath for 30min. Then, benzylamine (72 μL, 0.726 mmol, 1.1 eq) and DIPEA (126 μL, 0.726 mmol, 1.1 eq) were added to the reaction mixture which was then stirred at room temperature for 16 h. The resulting solution was diluted with DCM (30 mL), then washed with a solution of HCl (0.5 M, 30 mL), then NaOH (0.5 M, 30 mL) and distilled water (30 mL). The combined organic layers were dried with $MgSO_4$, filtered, concentrated and purified by flash chromatography on silica (gradient of Hexane/EtOAc) to afford the desired compound (275 mg, 76.6 %). ^{1}H NMR (400 MHz, $CDCl_3$) δ 7.75 (dd, *J* = 7.5, 3.8 Hz, 2H), 7.57 (d, *J* = 7.5 Hz, 2H), 7.39 (dd, *J* = 12.5, 7.3 Hz, 2H), 7.33 – 7.25 (m, 7H), 6.49 (d, *J* = 6.4 Hz, 1H), 6.38 (br, 1H), 4.47 – 4.37 (m, 3H), 4.22 – 4.09 (m, 3H), 3.49 (q, *J* = 6.0 Hz, 2H), 2.92 (d, *J* = 15.0 Hz, 1H), 2.56 (d, *J* = 6.3 Hz, 1H), 2.52 – 2.47 (m, 2H), 1.27 (t, *J* = 7.1 Hz, 3H). ^{13}C NMR (101 MHz, $CDCl_3$) δ 172.47, 171.10, 170.79, 156.38, 143.84, 143.79, 141.43, 138.03, 132.27, 132.17, 128.78, 128.58, 127.87, 127.54, 127.21, 125.19, 120.13, 67.29, 60.97, 51.78, 47.26, 43.64, 37.88, 35.09, 33.97, 14.28. IR (cm^{-1}): 3286, 2920, 2850, 1732, 1687, 1654, 1533. MS (ESI+) Calc for $[C_{31}H_{33}N_3O_6+H]^+$ 544.245; Found: 544.723

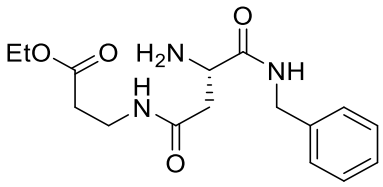

3-92

Ethyl (*S*)-3-(3-amino-4-(benzylamino)-4-oxobutanamido)propanoate

Compound **3-91** (0.240 g, 0.441 mmol, 1 eq) was dissolved in DCM (4 mL) and diethylamine (1 mL, 9.65 mmol, 22 eq) was added. The mixture was stirred at room temperature for 16 h. Then the reaction mixture was diluted DCM (10 mL) and washed with a solution of HCl (1 M, 3 x 5 mL). To the aqueous layer was added NaOH (2 M) until pH = 10 and the solution was extracted

with DCM (3 x 20 mL). The organic layer was dried with $MgSO_4$, filtered, and concentrated *in vacuo*. The residue was purified by flash chromatography on silica (gradient DCM/MeOH) to afford the desired compound (79 mg, 44 %). ^{1}H NMR (400 MHz, $CDCl_3$) δ 7.78 (s, 1H), 7.36 – 7.25 (m, 5H), 6.41 (br, 1H), 4.44 (d, *J* = 6.0 Hz, 2H), 4.16 (q, *J* = 7.1 Hz, 2H), 3.72 (dd, *J* = 7.3, 4.4 Hz, 1H), 3.56 – 3.42 (m, 2H), 2.68 (dd, *J* = 14.9, 4.4 Hz, 1H), 2.56 (dd, *J* = 14.9, 7.3 Hz, 1H), 2.49 (t, *J* = 6.1 Hz, 2H), 1.27 (t, *J* = 7.1 Hz, 3H). ^{13}C NMR (101 MHz, $CDCl_3$) δ 174.01, 172.28, 171.25, 138.32, 128.69, 127.60, 127.42, 60.76, 52.68, 43.27, 40.80, 34.97, 34.13, 14.23. IR (cm^{-1}): 3288, 2919, 2850, 1723, 1630, 1548. MS (ESI+) Calc for $[C_{16}H_{23}N_3O_4+H]^+$ 322.177; Found: 322.704

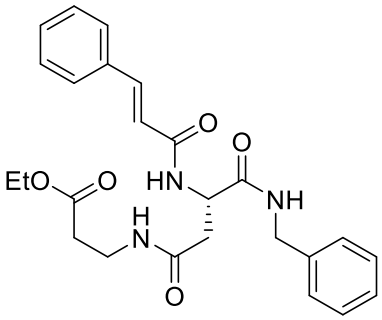

3-93

Ethyl (*S*)-3-(4-(benzylamino)-3-cinnamamido-4-oxobutanamido)propanoate

Compound **3-92** (70 mg, 0.218 mmol, 1 eq) was dissolved in dry DCM (5 mL) under argon atmosphere. Cinnamoyl chloride (36.3 mg, 0.218 mmol, 1 eq) and Et_3N (154 μL, 1.11 mmol, 5 eq) were added and the mixture was then stirred at room temperature for 1 h. Next, the mixture was quenched with H_2O (20 mL) and extracted with DCM (3 x 20 mL). The combined organic layer was washed with brine (20 mL), dried with $MgSO_4$, filtered, and concentrated in vacuo. The residue was purified by flash chromatography on silica (gradient DCM/MeOH) to afford the desired compound (26 mg, 26.4 %). ^{1}H NMR (400 MHz, $CDCl_3$) δ 7.63 (d, *J* = 15.7 Hz, 1H), 7.54 – 7.47 (m, 3H), 7.42 – 7.35 (m, 3H), 7.34 – 7.27 (m, 2H), 7.25 – 7.21 (m, 2H), 6.48 (d, *J* = 15.7 Hz, 1H), 4.89 (td, *J* = 6.8, 3.1 Hz, 2H), 4.45 (d, *J* = 5.9 Hz, 2H), 4.16 (q, *J* = 7.1 Hz, 2H), 3.58 – 3.48 (m, 2H), 2.94 (dd, *J* = 15.2, 3.2 Hz, 1H), 2.57 – 2.48 (m, 3H), 1.27 (t, *J* = 7.1 Hz, 3H). ^{13}C NMR (101 MHz, DMSO) δ 171.34, 170.90, 169.36, 164.87, 139.43, 139.04, 134.92, 129.57, 129.00, 128.21, 127.60, 127.00, 126.67, 122.14, 59.98, 50.20, 42.16, 37.73, 34.74, 33.80, 14.09. IR (cm^{-1}): 3283, 2919, 2850, 1732, 1651, 1538, 1255. MS (ESI+) Calc for $[C_{25}H_{29}N_3O_5+H]^+$ 452.219; Found: 452.738

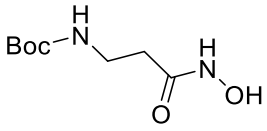

3-95

tert-Butyl (3-(hydroxyamino)-3-oxopropyl)carbamate

To a solution of Boc-β-Ala-OH (9.10 g, 48.1 mmol, 1 eq) in dry THF (120 mL) under argon atmosphere was added CDI (7.8 g, 48.1 mmol, 1 eq). The solution was stirred 30 min at room temperature and then 30 min at reflux. After cooling to room temperature, hydroxylamine hydrochloride (3.34 g, 48.1 mmol, 1 eq) was added and the reaction mixture was stirred 16 h. The reaction mixture was filtered and the filtrate was evaporated. The residue was dissolved in phosphate buffer (30 mL, pH = 6.2) and the aqueous was extracted with EtOAc (3 x 30 mL). The combined organic layer was dried with $MgSO_4$, filtered and evaporated *in vacuo* to afford the desired compound (9.75 g, 99%) which was used in next step without further purification. ^{1}H NMR (400 MHz, D_2O) δ 7.88 (s, 1H), 7.16 (s, 1H), 3.32 (t, *J* = 6.3 Hz, 2H), 2.31 (t, *J* = 6.4 Hz, 2H), 1.41 (s, 9H). ^{13}C NMR (101 MHz, D_2O) δ 170.59, 157.99, 81.09, 36.38, 32.86, 27.58. Consistent with reported analysis.[429]

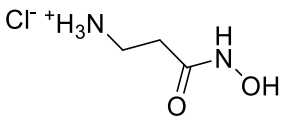

3-96

3-(Hydroxyamino)-3-oxopropan-1-aminium chloride

To a solution of acetyl chloride (27 mL, 383.9 mmol, 8 eq) in EtOAc (140 mL) was slowly added EtOH (22.4 mL, 383.9 mmol, 8 eq). The exothermic reaction mixture was then stirred at room temperature for 30 min. The solution was then added to **3-95** (9.7 g, 47.5 mmol, 1 eq) and the reaction mixture was stirred at room temperature for 16 h. The mixture was then filtered and the solid washed with EtOAc (3 x 20 mL) to afford the desired product (6.54 g, 98 %). ^{1}H NMR (400 MHz, D_2O) δ 8.67 (s, 1H), 7.45 (s, 1H), 3.26 (t, *J* = 6.5 Hz, 2H), 2.57 (t, *J* = 6.8 Hz, 2H). ^{13}C NMR (101 MHz, D_2O) δ 168.96, 35.60, 29.11. IR (cm^{-1}): 2941, 2829, 1723, 1626. MS (ESI+) Calc for $[C_3H_8N_2O_2+H]^+$ 105.066; Found: 105.610

4.2.ii Solid phase synthesis[426,517]

Swelling resin

Dry 2-chlorotrityl chloride resin (1 g, loading 1.3 mmol/g) was placed in a SPPS reactor with a sintered filter and covered with three-times the bead volume using dry DCM. The resin was shaken in an orbital shaker for 30 min.

Resin loading

To the swelled resin was added a solution of Fmoc-hydroxylamine **3-72** (2 mmol, 1.5 eq) and DIPEA (3.25 mmol, 2.5 eq) in DCM (2 mL). The reactor was then shaken for 48 h. Unreacted chloride sites were then capped by addition of MeOH (1 mL), and the shaking was kept for an additional 15 min. The solvent was then removed by filtration, and the resin washed with DCM (5 x 1 min), DCM/MeOH 1:1 (5 x 1 min) and MeOH (2 x 1 min). The resin was then dried *in vacuo*.

Fmoc deprotection and coupling

The resin was swollen in DMF (2 mL) and stirred for 15 min. Then removal of the Fmoc group was achieved using 20% piperidine in DMF over 10 min followed by washing with DMF. The deprotection step was repeated to ensure completion. The resin was filtered and washed several times with DMF (5 x 1 min) to remove any residual piperidine. Then a solution of Fmoc-amino acid (3 eq), HOBt (3 eq), HBTU (3 eq) and DIPEA (6 eq) in DCM (2 mL) was added, and the reaction mixture was shaken for 2 h. The resin was filtered, washed with DMF, and the coupling step was repeated. Following washing with DMF, capping was performed by adding a solution of Ac_2O/pyridine 1:9 (vol/vol) and a 20 min shaking. The resin was then filtered and washed with DMF (5 x 1 min).

Coupling of cinnamoyl chloride

The resin was swollen in DMF, and the Fmoc deprotection procedure was applied. Then a solution of cinnamoyl chloride (3.9 mmol, 3 eq) and DIPEA (5.2 mmol, 4 eq) in DMF was added, and the reaction mixture was shaken 8 h. The resin was filtered, washed with DMF, and the coupling was repeated, then washed with DMF (5 x 1 min).

Cleavage from the resin

The resin was washed with DCM (2 x 1 min) and swollen for 15 min. Resin cleavage were achieved by treating the resin with a cleavage cocktail composed by TFA:DCM:TIPS 95:2.5:2.5 for 3 h with constant agitation. The TFA solution containing the crude peptide was filtered off, and the resin washed with neat TFA (2 mL). The TFA contained in the crude was removed by

rotary evaporation, and the residue precipitated in Et_2O. The crude material was then purified by flash chromatography on a reverse phase (gradient H_2O/MeCN 0.05% TFA).

4.3 Triazole-based scaffold

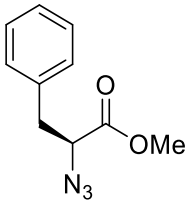

3-116

Methyl (*S*)-2-azido-3-phenylpropanoate

To a solution of NaN_3 (211 mg, 3.25 mmol, 1.4 eq) in dry MeCN (4 mL) under an argon atmosphere and at 0 °C was added dropwise Tf_2O (468 µL, 2.78 mmol, 1.2 eq). The reaction mixture was stirred at 0 °C for 3 h. In another flask, L-Phenylalanine methyl ester hydrochloride (500 mg, 2.32 mmol, 1 eq), $CuSO_4$ (4 mg, 0.02 mmol, 0.01 eq), and Et_3N (0.65 mL, 4.64 mmol, 2 eq) were dissolved in a mixture MeCN/H_2O (4 mL, 3:1). The reaction mixture was stirred at 0 °C and the TfN_3 solution previously prepared was added. The reaction mixture was then stirred at room temperature for 16 h. The volatiles were evaporated *in vacuo* and the residue was dissolved in EtOAc (20 mL). The organic was washed with H_2O (3 x 10 mL), brine (10 mL), dried with $MgSO_4$, filtered and evaporated. The residue was then purified by flash chromatography on silica (gradient Hexane/EtOAc) to afford the desired compound (240 mg, 50%). ^{1}H NMR (400 MHz, $CDCl_3$) δ 7.36 – 7.27 (m, 3H), 7.25 – 7.21 (m, 2H), 4.07 (dd, *J* = 8.7, 5.4 Hz, 1H), 3.78 (s, 3H), 3.18 (dd, *J* = 14.0, 5.4 Hz, 1H), 3.01 (dd, *J* = 14.0, 8.8 Hz, 1H). ^{13}C NMR (101 MHz, $CDCl_3$) δ 170.55, 136.06, 129.32, 128.85, 127.43, 63.43, 52.80, 37.81. IR(cm^{-1}): 3032, 2107, 1738. MS (ESI+) Calc for $[C_{10}H_{11}N_3O_2+H]^+$ 206.0930, Found: 206.1157

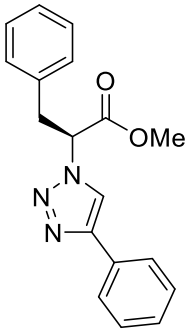

3-117

Methyl (*S*)-3-phenyl-2-(4-phenyl-1*H*-1,2,3-triazol-1-yl)propanoate

To a solution of **3-116** (260 mg, 1.27 mmol, 1 eq) in a mixture H_2O/tBuOH (4.5 mL, 2:1) were added an aqueous solution of sodium ascorbate (1 M, 130 μL, 0.13 mmol, 0.1 eq), an aqueous solution of $CuSO_4.5H_2O$ (0.3 M, 42 μL, 0.01 mmol, 0.01 eq), and phenylacetylene (139 μL, 1.27 mmol, 1 eq). The reaction mixture was stirred at room temperature for 16 h. The mixture was diluted with H_2O (15 mL) and cooled to 0 °C leading to the formation of a precipitate which was recovered by filtration. The solid was washed with cold H_2O (10 mL) and dried *in vacuo* giving the desired compound (380 mg, 98%). ^{1}H NMR (400 MHz, $CDCl_3$) δ 7.82 (s, 1H), 7.82 – 7.78 (m, 2H), 7.45 – 7.39 (m, 2H), 7.35 – 7.30 (m, 1H), 7.26 – 7.21 (m, 3H), 7.09 – 7.04 (m, 2H), 5.63 (dd, *J* = 8.1, 6.7 Hz, 1H), 3.77 (s, 3H), 3.56 (dd, *J* = 11.9, 4.4 Hz, 1H), 3.51 (dd, *J* = 12.0, 6.1 Hz, 1H). ^{13}C NMR (101 MHz, $CDCl_3$) δ 168.86, 147.87, 134.85, 130.55, 129.09, 128.98, 128.95, 128.36, 127.75, 125.89, 119.75, 64.18, 53.23, 39.08. IR (cm^{-1}): 3084, 1757, 1434, 1266, 1199. MS (ESI+) Calc for $[C_{18}H_{17}N_3O_2+H]^+$ 308.1399, Found: 308.1350

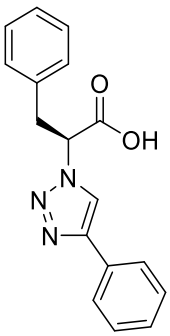

3-118

(*S*)-3-Phenyl-2-(4-phenyl-1*H*-1,2,3-triazol-1-yl)propanoic acid

Compound **3-117** (380 mg, 1.23 mmol, 1 eq) was dissolved in a solution of HCl (6 M, 10 mL). The reaction mixture was stirred at 70 °C for 16 h then extracted with DCM (3 x 15 mL). The organic was dried with $MgSO_4$, filtered and evaporated *in vacuo* to afford the desired compound (350 mg, 97%). ^{1}H NMR (400 MHz, $CDCl_3$) δ 7.78 – 7.63 (m, 2H), 7.44 – 7.37 (m, 2H), 7.35 –

7.26 (m, 2H), 7.23 – 7.19 (m, 3H), 7.09 – 7.03 (m, 2H), 5.76 – 5.61 (m, 1H), 3.66 – 3.49 (m, 2H). ^{13}C NMR (101 MHz, $CDCl_3$) δ 170.39, 147.46, 134.90, 129.85, 129.21, 129.06, 128.97, 128.64, 127.72, 126.13, 120.98, 64.64, 38.95. IR (cm^{-1}): 3424, 3136, 3032, 2927, 2113, 1725, 1234. MS (ESI+) Calc for $[C_{17}H_{15}N_3O_2+H]^+$ 294.1243; Found: 294.1334

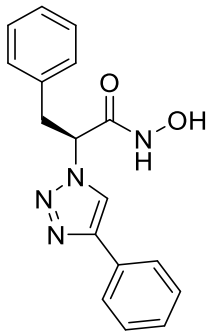

3-119

(*S*)-*N*-hydroxy-3-phenyl-2-(4-phenyl-1*H*-1,2,3-triazol-1-yl)propanamide

To a solution of **3-118** (330 mg, 1.12 mmol, 1 eq) in dry THF (10 mL) and under argon atmosphere was added CDI (274 mg, 1.69 mmol, 1.5 eq) and the reaction mixture was stirred at room temperature for 3 h. Then $NH_2OH.HCl$ (156 mg, 2.24 mmol, 2 eq) was added and the reaction mixture was stirred at room temperature for 2 days. The reaction was quenched by addition of a solution of 5% $KHSO_4$ (10 mL) and the mixture was extracted with EtOAc (3 x 15 mL). The combine organic layer was then washed with brine (10 mL), dried with $MgSO_4$, filtered and evaporated *in vacuo*. The residue was purified by flash chromatography on reverse phase (gradient H_2O/MeCN 0.05% TFA) to afford the desired compound (104 mg, 30 %). ^{1}H NMR (400 MHz, MeOD) δ 8.56 (s, 1H), 7.86 – 7.74 (m, 2H), 7.48 – 7.40 (m, 2H), 7.39 – 7.32 (m, 1H), 7.29 – 7.13 (m, 5H), 5.43 (t, *J* = 8.0 Hz, 1H), 3.58 (dd, *J* = 13.7, 7.7 Hz, 1H), 3.47 (dd, *J* = 13.7, 8.2 Hz, 1H). ^{13}C NMR (101 MHz, MeOD) δ 166.41, 148.85, 136.63, 131.54, 130.20, 129.97, 129.71, 129.41, 128.34, 126.66, 121.42, 64.14, 39.26. IR (cm^{-1}): 3283, 3085, 3032, 1756, 1680, 1435, 1266. MS (ESI+) Calc for $[C_{17}H_{16}N_4O_2+H]^+$ 309.135; Found: 309.640

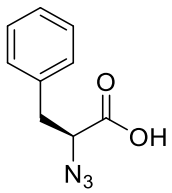

3-120

(*S*)-2-Azido-3-phenylpropanoic acid

Method A:

To a solution of NaN_3 (275 mg, 4.24 mmol, 1.4 eq) in dry MeCN (5 mL) under an argon atmosphere and at 0 °C was added dropwise Tf_2O (611 µL, 3.63 mmol, 1.2 eq). The reaction mixture was stirred at 0 °C for 3 h. In another flask, L-Phenylalanine (500 mg, 3.03 mmol, 1 eq), $CuSO_4$ (5 mg, 0.03 mmol, 0.01 eq), and Et_3N (844 µL, 6.05 mmol, 2 eq) were dissolved in MeCN (5 mL). The reaction mixture was stirred at 0 °C and the TfN_3 solution previously prepared was added. The reaction mixture was then stirred at room temperature for 16 h. The volatiles were evaporated *in vacuo* and the residue was dissolved in H_2O (20 mL). The aqueous was acidified with HCl (1 M) and extracted with DCM (3 x 15mL). The combine organic layer was dried with $MgSO_4$, filtered and concentrated *in vacuo*. The residue was dissolved in a solution of $NaHCO_3$ (2 M, 15 mL) and the aqueous was washed with Et_2O (2 x 10 mL). The aqueous was then acidified with HCl (2 M) and extracted with DCM (3 x 10 mL). The combined organic layer was dried with $MgSO_4$, filtered and evaporated. To afford the desired compound (460 mg, 79%). ^{1}H NMR (400 MHz, $CDCl_3$) δ 7.39 – 7.27 (m, 5H), 4.16 (dd, *J* = 8.9, 5.0 Hz, 1H), 3.24 (dd, *J* = 14.1, 5.0 Hz, 1H), 3.05 (dd, *J* = 14.1, 8.9 Hz, 1H). ^{13}C NMR (101 MHz, $CDCl_3$) δ 174.43, 135.79, 129.38, 128.92, 127.57, 63.19, 37.69. IR (cm^{-1}): 3032, 2111, 1731, 1614, 1140. MS (ESI-) Calc for $[C_9H_9N_3O_2\text{-}H]^-$ 190.0617; Found: 190.0640

Method B:

A solution of NaN_3 (275 mg, 4.24 mmol; 1.4 eq) in dry MeCN (5 mL) under an argon atmosphere was cooled at 0 °C with an ice-bath. Then Tf_2O (611 µL, 3.63 mmol, 1.2 eq) was added dropwise. The reaction mixture was stirred at 0 °C for 2 h and was then added to a solution of L-Phenylalanine (500 mg, 3.03 mmol, 1 eq), K_2CO_3 (1.129 g, 8.17 mmol, 2.7 eq) and $CuSO_4.5H_2O$ (8 mg, 0.03 mmol, 0.01 eq) in a MeOH/H_2O co-solvent (12 mL, 5:1) at 0 °C. The reaction mixture was then stirred for 16 h at room temperature. The volatiles were evaporated *in vacuo* and the residue was dissolved in H_2O (20 mL). The aqueous was acidified with HCl (1 M) and extracted with DCM (3 x 15mL). The combine organic layer was dried with $MgSO_4$, filtered and concentrated *in vacuo*. The residue was dissolved in a solution of $NaHCO_3$ (2 M, 15 mL) and the aqueous was washed with Et_2O (2 x 10 mL). The aqueous was then acidified with HCl (2 M) and

extracted with DCM (3 x 10 mL). The combined organic layer was dried with $MgSO_4$, filtered and evaporated. To afford the desired compound (503 mg, 87%).

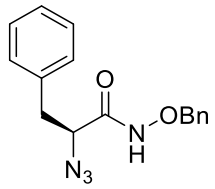

3-121

(*S*)-2-Azido-*N*-(benzyloxy)-3-phenylpropanamide

CDI (534 mg, 3.30 mmol, 1.5 eq) was added to a solution of **3-120** (420 mg, 2.20 mmol, 1 eq) in dry THF (8 mL) under an argon atmosphere. Additionally, dry DMF (1 mL) was added for better dissolution of the starting materials. The reaction mixture was stirred for 1 h at room temperature. Powdered hydroxylamine hydrochloride (700 mg, 4.39 mmol, 2 eq) was added to the mixture, which was then stirred for 16 h at room temperature. THF was removed by evaporation. The crude mixture was then diluted with an aqueous solution of 5% $NaHSO_4$ (30 mL) and extracted with EtOAc (2 x 30mL).The combined organic phases were washed with cold H_2O (30 mL), brine (30 mL), then dried with $MgSO_4$, filtered and evaporated *in vacuo*. The residue was purified by flash chromatography on silica (gradient Hexane/EtOAc) to afford the desired product (463 mg, 71%). ^{1}H NMR (400 MHz, $CDCl_3$) δ 8.60 (s, 1H), 7.44 – 7.23 (m, 10H), 4.84, 4.78 (ABq, J = 11.2 Hz, 2H), 4.16 – 4.06 (m, 1H), 3.31 (dd, J = 14.0, 4.8 Hz, 1H), 3.05 (dd, J = 14.0, 7.6 Hz, 1H). ^{13}C NMR (101 MHz, $CDCl_3$) δ 165.96, 135.67, 134.74, 129.71, 129.50, 129.09, 128.88, 128.77, 127.54, 78.66, 63.95, 38.26. IR (cm^{-1}): 3168, 2922, 2100, 1662, 1454. MS (ESI+) Calc for $[C_{16}H_{16}N_4O_2+H]^+$ 297.135; Found: 297.709

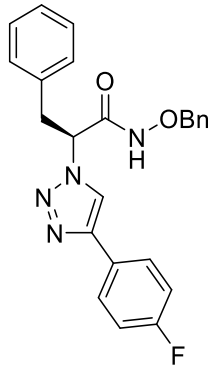

3-122

(*S*)-*N*-(benzyloxy)-2-(4-(4-fluorophenyl)-1*H*-1,2,3-triazol-1-yl)-3-phenylpropanamide

To a solution of **3-121** (100 mg, 0.34 mmol, 1 eq) in a mixture H_2O/tBuOH (1 mL, 1:1) were added an aqueous solution of sodium ascorbate (1 M, 34 μL, 0.03 mmol, 0.1 eq), an aqueous solution of $CuSO_4.5H_2O$ (0.3 M, 11 μL, 0.003 mmol, 0.01 eq), and 4-fluorophenylacetylene (39 μL, 0.34 mmol, 1 eq). The reaction mixture was stirred at room temperature for 16 h. The mixture was diluted with H_2O (15 mL) and extracted with DCM (3 x 15 mL). The combined organic phases were washed with brine (15 mL), then dried with $MgSO_4$, filtered and evaporated *in vacuo*. The residue was purified by flash chromatography on silica (gradient Hexane/EtOAc) to afford the desired product (91 mg, 65%). ^{1}H NMR (400 MHz, $CDCl_3$) δ 10.96 (s, 1H), 8.31 (s, 1H), 7.83 – 7.72 (m, 2H), 7.33 – 7.23 (m, 6H), 7.23 – 7.18 (m, 4H), 7.15 (t, *J* = 8.6 Hz, 2H), 5.74 (t, *J* = 7.9 Hz, 1H), 4.84 (d, *J* = 10.9 Hz, 1H), 4.73 (d, *J* = 10.9 Hz, 1H), 3.63 (dd, *J* = 13.6, 8.3 Hz, 1H), 3.43 (dd, *J* = 13.6, 7.6 Hz, 1H). ^{13}C NMR (101 MHz, $CDCl_3$) δ 164.76, 162.92 (d, *J* = 248.0 Hz), 147.24, 134.84, 134.49, 129.45, 129.23, 128.98, 128.59, 127.70, 127.63 (d, *J* = 8.2 Hz), 126.31 (d, *J* = 3.2 Hz), 119.42, 116.03 (d, *J* = 21.9 Hz), 78.57, 63.18, 39.46. IR (cm^{-1}): 3251, 3032, 2926, 1692. MS (ESI+) Calc for $[C_{24}H_{21}FN_4O_2+H]^+$ 417.1727; Found: 417.1842

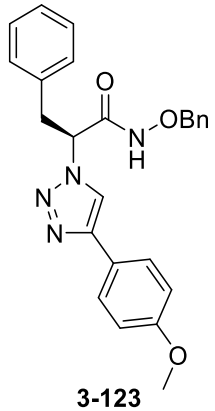

3-123

(*S*)-*N*-(benzyloxy)-2-(4-(4-methoxyphenyl)-1*H*-1,2,3-triazol-1-yl)-3-phenylpropanamide

To a solution of **3-121** (100 mg, 0.34 mmol, 1 eq) in a mixture H_2O/tBuOH (1 mL, 1:1) were added an aqueous solution of sodium ascorbate (1 M, 34 μL, 0.03 mmol, 0.1 eq), an aqueous solution of $CuSO_4.5H_2O$ (0.3 M, 11 μL, 0.003 mmol, 0.01 eq), and 4-methoxyphenylacetylene (44 μL, 0.34 mmol, 1 eq). The reaction mixture was stirred at room temperature for 16 h. The mixture was diluted with H_2O (15 mL) and extracted with DCM (3 x 15 mL). The combined organic phases were washed with brine (15 mL), then dried with $MgSO_4$, filtered and evaporated *in vacuo*. The residue was purified by flash chromatography on silica (gradient Hexane/EtOAc) to afford the desired product (110 mg, 76%). ^{1}H NMR (400 MHz, $CDCl_3$) δ 10.63 (s, 1H), 8.08 (s, 1H), 7.66 (d, *J* = 8.8 Hz, 2H), 7.25 – 7.06 (m, 10H), 6.92 (d, *J* = 8.8 Hz, 2H), 5.57 (t, *J* = 7.9 Hz, 1H), 4.78, 4.68 (ABq, *J* = 10.9 Hz, 2H), 3.83 (s, 3H), 3.54 (dd, *J* = 13.6, 8.1 Hz, 1H), 3.34 (dd, *J* = 13.7, 7.7 Hz, 1H). ^{13}C NMR (101 MHz, $CDCl_3$) δ 164.76, 164.16, 161.69, 147.24, 134.84, 134.49, 129.45, 129.23, 128.98, 128.59, 127.70, 127.67, 127.59, 126.32, 126.29, 119.42, 116.14, 115.92, 78.57, 63.18, 39.46. IR (cm^{-1}): 3269, 2929, 1693, 1250. MS (ESI+) Calc for $[C_{25}H_{24}N_4O_3+H]^+$ 429.1927; Found: 429.1969

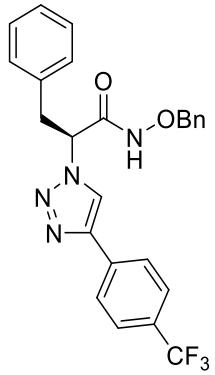

3-124

(*S*)-*N*-(Benzyloxy)-3-phenyl-2-(4-(4-(trifluoromethyl)phenyl)-1*H*-1,2,3-triazol-1-yl)propanamide

To a solution of **3-121** (250 mg, 0.84 mmol, 1 eq) in a mixture H_2O/tBuOH (2 mL, 1:1) were added an aqueous solution of sodium ascorbate (1 M, 84 µL, 0.08 mmol, 0.1 eq), an aqueous solution of $CuSO_4.5H_2O$ (0.3 M, 28 µL, 0.008 mmol, 0.01 eq), and 4-(trifluoromethyl)phenylacetylene (138 µL, 0.84 mmol, 1 eq). The reaction mixture was stirred at room temperature for 16 h. The mixture was diluted with H_2O (15 mL) and extracted with DCM (3 x 15 mL). The combined organic phases were washed with brine (15 mL), then dried with $MgSO_4$, filtered and evaporated *in vacuo*. The residue was purified by flash chromatography on silica (gradient Hexane/EtOAc) to afford the desired product (250 mg, 64%). ^{1}H NMR (400 MHz, $CDCl_3$) δ 9.20 (d, *J* = 3.6 Hz, 1H), 8.09 (s, 1H), 7.89 (d, *J* = 8.0 Hz, 2H), 7.68 (d, *J* = 8.2 Hz, 2H), 7.33 – 7.26 (m, 6H), 7.19 – 7.11 (m, 4H), 5.26 (td, *J* = 7.8, 3.1 Hz, 1H), 4.84 (d, *J* = 11.2 Hz, 1H), 4.71 (d, *J* = 11.2 Hz, 1H), 3.60 (dd, *J* = 13.5, 8.3 Hz, 1H), 3.35 (dd, *J* = 13.5, 7.5 Hz, 1H). ^{13}C NMR (101 MHz, MeOD) δ 166.13, 147.40, 136.43, 136.32, 135.45, 130.71 (q, *J* = 32.3 Hz), 130.48, 130.33, 129.81, 129.74, 129.45, 128.49, 127.06, 126.91 (q, *J* = 3.7 Hz), 125.16 (q, *J* = 271.7 Hz), 122.49, 79.11, 63.94, 39.18. IR (cm^{-1}): 3140, 2967, 1662, 1456, 1324. MS (ESI+) Calc for $[C_{25}H_{21}F_3N_4O_2+H]^+$ 467.169; Found: 467.658

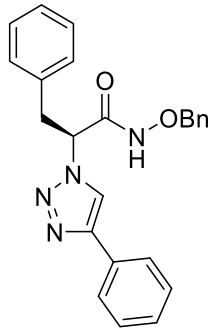

3-125

(*S*)-*N*-(benzyloxy)-3-phenyl-2-(4-phenyl-1*H*-1,2,3-triazol-1-yl)propanamide

To a solution of **3-121** (150 mg, 0.51 mmol, 1 eq) in a mixture H_2O/tBuOH (2 mL, 1:1) were added an aqueous solution of sodium ascorbate (1 M, 51 µL, 0.05 mmol, 0.1 eq), an aqueous solution of $CuSO_4.5H_2O$ (0.3 M, 17 µL, 0.005 mmol, 0.01 eq), and phenylacetylene (56 µL, 0.51 mmol, 1 eq). The reaction mixture was stirred at room temperature for 16 h. The mixture was diluted with H_2O (15 mL) and extracted with DCM (3 x 15 mL). The combined organic phases were washed with brine (15 mL), then dried with $MgSO_4$, filtered and evaporated *in vacuo*. The residue was purified by flash chromatography on silica (gradient Hexane/EtOAc) to afford the desired product (158 mg, 78%). ^{1}H NMR (400 MHz, $CDCl_3$) δ 9.52 (s, 1H), 7.99 (s, 1H), 7.77 (d, *J* = 7.2 Hz, 2H), 7.42 (t, *J* = 7.4 Hz, 2H), 7.39 – 7.31 (m, 2H), 7.26 – 7.22 (m, 5H), 7.21 – 7.15 (m, 2H), 7.14 – 7.08 (m, 2H), 5.40 – 5.21 (m, 1H), 4.83 (d, *J* = 11.0 Hz, 1H), 4.72 (d, *J* = 11.0 Hz, 1H), 3.58 (dd, *J* = 13.5, 7.6 Hz, 1H), 3.36 (dd, *J* = 13.6, 7.5 Hz, 1H). ^{13}C NMR (101 MHz, DMSO) δ 164.14, 146.21, 135.83, 135.43, 130.66, 129.08, 129.02, 128.92, 128.43, 128.41, 128.33, 127.91, 126.95, 125.13, 120.88, 77.05, 61.79, 37.09. IR (cm^{-1}): 3267, 3086, 2900, 1700. MS (ESI+) Calc for $[C_{24}H_{22}N_4O_2+H]^+$ 399.182; Found: 399.651

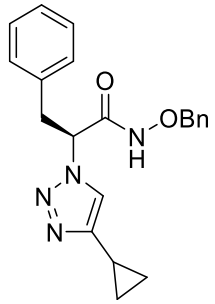

3-126

(*S*)-*N*-(Benzyloxy)-2-(4-cyclopropyl-1*H*-1,2,3-triazol-1-yl)-3-phenylpropanamide

To a solution of **3-121** (58 mg, 0.20 mmol, 1 eq) in a mixture H_2O/tBuOH (1 mL, 1:1) were added an aqueous solution of sodium ascorbate (1 M, 20 µL, 0.02 mmol, 0.1 eq), an aqueous solution of $CuSO_4.5H_2O$ (0.3 M, 7 µL, 0.002 mmol, 0.01 eq), and cyclopropylacetylene (167 µL, 0.20 mmol, 1 eq). The reaction mixture was stirred at room temperature for 16 h. The mixture was diluted with H_2O (15 mL) and extracted with DCM (3 x 15 mL). The combined organic phases were washed with brine (15 mL), then dried with $MgSO_4$, filtered and evaporated *in vacuo*. The residue was purified by flash chromatography on silica (gradient Hexane/EtOAc) to afford the desired product (42 mg, 59%) . ^{1}H NMR (400 MHz, $CDCl_3$) δ 9.65 (s, 1H), 7.42 (s, 1H), 7.33 – 7.27 (m, 3H), 7.25 – 7.16 (m, 5H), 7.13 – 7.01 (m, 2H), 5.27 – 5.12 (m, 1H), 4.81 (d, *J* = 11.0 Hz, 1H), 4.70 (d, *J* = 11.0 Hz, 1H), 3.50 (dd, *J* = 13.5, 7.8 Hz, 1H), 3.26 (dd, *J* = 13.6, 7.8 Hz, 1H), 1.93 – 1.80 (m, 1H), 0.96 – 0.87 (m, 2H), 0.78 – 0.70 (m, 2H). ^{13}C NMR (101 MHz, $CDCl_3$) δ 164.81, 150.48, 135.04, 134.74, 129.41, 129.20, 128.80, 128.50, 127.46, 119.68, 78.39, 62.83, 39.33, 7.95, 7.89, 6.71. IR (cm^{-1}): 3139, 2918, 2850, 1695, 1030. MS (ESI+) Calc for $[C_{21}H_{22}N_4O_2+H]^+$ 363.182; Found: 363.816

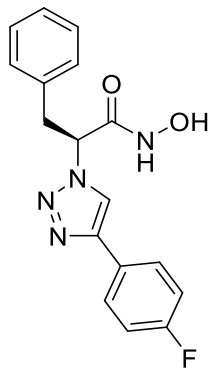

3-127

(*S*)-2-(4-(4-fluorophenyl)-1*H*-1,2,3-triazol-1-yl)-*N*-hydroxy-3-phenylpropanamide

To a solution of **3-122** (60 mg, 0.14 mmol, 1.0 eq) in dry THF (1.2 mL) under an argon atmosphere and at -78 °C was added boron trichloride (1 M solution in DCM, 1.0 mL, 1.01 mmol, 7.0 eq). The reaction mixture was warm-up to room temperature and stirred for 2 h. The reaction was quenched by slow addition of a solution of $NaHCO_3$ (2 M, 20 mL) and the mixture was extracted with DCM (3 x 20 mL). The combined organic phases were then washed with brine (15 mL), dried with $MgSO_4$, filtered and evaporated *in vacuo*. The resulting crude mixture was purified by flash chromatography on reverse phase (gradient H_2O/MeCN 0.05% TFA) to afford the desired compound (25 mg, 53%). ^{1}H NMR (400 MHz, MeOD) δ 8.55 (s, 1H), 7.97 – 7.69 (m, 2H), 7.33 – 7.08 (m, 8H), 5.43 (t, *J* = 8.0 Hz, 1H), 3.57 (dd, *J* = 13.7, 7.7 Hz, 1H), 3.46 (dd, *J* = 13.7, 8.3 Hz, 1H). ^{13}C NMR (101 MHz, MeOD) δ 166.41, 164.17 (d, *J* = 246.2 Hz), 147.96, 136.62, 130.20, 129.73, 128.65 (d, *J* = 8.2 Hz), 128.36, 128.03 (d, *J* = 3.3 Hz), 121.32, 116.78 (d, *J* = 22.1 Hz), 64.16, 39.28. IR (cm^{-1}): 3139, 2896, 1672, 1496. MS (ESI+) Calc for $[C_{17}H_{15}FN_4O_2+H]^+$ 327.126; Found: 327.637

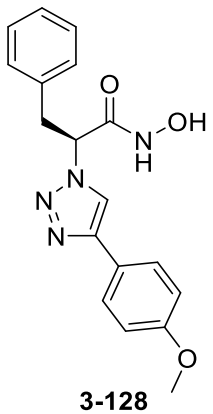

3-128

(*S*)-*N*-hydroxy-2-(4-(4-methoxyphenyl)-1*H*-1,2,3-triazol-1-yl)-3-phenylpropanamide

To a solution of **3-123** (60 mg, 0.14 mmol, 1.0 eq) in dry THF (1.2 mL) under an argon atmosphere and at -78 °C was added boron trichloride (1 M solution in DCM, 0.98 mL, 0.98 mmol, 7.0 eq). The reaction mixture was warm-up to room temperature and stirred for 2h. The reaction was quenched by slow addition of a solution of $NaHCO_3$ (2 M, 20 mL) and the mixture was extracted with DCM (3 x 20 mL). The combined organic phases were then washed with brine (15 mL), dried with $MgSO_4$, filtered and evaporated *in vacuo*. The resulting crude mixture was purified by flash chromatography on reverse phase (gradient H_2O/MeCN 0.05% TFA) to afford the desired compound (25 mg, 53%). ^{1}H NMR (400 MHz, MeOD) δ 8.44 (s, 1H), 7.72 (d, *J* = 8.5 Hz, 2H), 7.29 – 7.13 (m, 5H), 6.98 (d, *J* = 8.6 Hz, 2H), 5.42 (t, *J* = 7.9 Hz, 1H), 3.81 (s, 3H), 3.56 (dd, *J* = 13.7, 7.6 Hz, 1H), 3.45 (dd, *J* = 13.6, 8.2 Hz, 1H). ^{13}C NMR (101 MHz, MeOD) δ 166.36, 161.33, 148.79, 136.63, 130.19, 129.69, 128.31, 128.02, 124.04, 120.52, 115.34, 64.08, 55.76, 39.25. IR (cm^{-1}): 3248, 2939, 2859, 1695, 1500. MS (ESI+) Calc for $[C_{18}H_{18}N_4O_3+H]^+$ 339.146; Found: 339.634

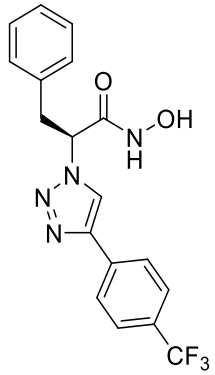

3-129

(*S*)-*N*-hydroxy-3-phenyl-2-(4-(4-(trifluoromethyl)phenyl)-1*H*-1,2,3-triazol-1-yl)propanamide

To a solution of **3-124** (100 mg, 0.21 mmol, 1.0 eq) in dry THF (2 mL) under an argon atmosphere and at -78 °C was added boron trichloride (1 M solution in DCM, 1.5 mL, 1.5 mmol, 7.0 eq). The reaction mixture was warm-up to room temperature and stirred for 2 h. The reaction was quenched by slow addition of a solution of $NaHCO_3$ (2 M, 20 mL) and the mixture was extracted with DCM (3 x 20 mL). The combined organic phases were then washed with brine (15 mL), dried with $MgSO_4$, filtered and evaporated *in vacuo*. The resulting crude mixture was purified by flash chromatography on reverse phase (gradient H_2O/MeCN 0.05% TFA) to afford the desired compound (56.5 mg, 58%). ^{1}H NMR (400 MHz, MeOD) δ 8.73 (s, 1H), 8.03 (d, *J* = 8.1 Hz, 2H), 7.74 (d, *J* = 8.2 Hz, 2H), 7.35 – 7.16 (m, 5H), 5.46 (t, *J* = 8.0 Hz, 1H), 3.59 (dd, *J* = 13.7, 7.6 Hz, 1H), 3.48 (dd, *J* = 13.8, 8.3 Hz, 1H). ^{13}C NMR (101 MHz, MeOD) δ 166.34, 147.35, 136.55, 135.46 (d, *J* = 1.1 Hz), 131.01 (q, *J* = 32.4 Hz), 130.20, 129.73, 128.37, 127.03, 126.90 (q, *J* = 4.0 Hz), 125.61 (q, *J* = 271.7 Hz), 122.58, 64.18, 39.27. IR (cm^{-1}):3345, 2478, 2218, 2072, 1684, 1327. MS (ESI+) Calc for $[C_{18}H_{15}F_3N_4O_2+H]^+$ 377.1225; Found: 377.1471

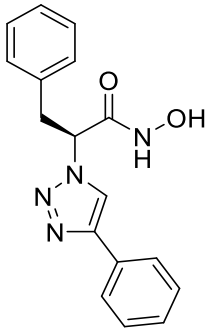

3-119

(*S*)-*N*-hydroxy-3-phenyl-2-(4-phenyl-1*H*-1,2,3-triazol-1-yl)propanamide

To a solution of **3-125** (140 mg, 0.35 mmol, 1.0 eq) in dry THF (2.5 mL) under an argon atmosphere and at -78 °C was added boron trichloride (1 M solution in DCM, 2.46 mL, 2.46 mmol, 7.0 eq). The reaction mixture was warm-up to room temperature and stirred for 2 h. The reaction was quenched by slow addition of a solution of $NaHCO_3$ (2 M, 20 mL) and the mixture was extracted with DCM (3 x 20 mL). The combined organic phases were then washed with brine (15 mL), dried with $MgSO_4$, filtered and evaporated *in vacuo*. The resulting crude mixture was purified by flash chromatography on a reverse phase (gradient H_2O/MeCN 0.05% TFA) to afford the desired compound (50 mg, 46%).

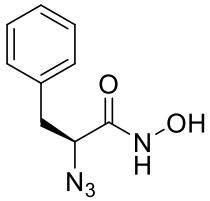

3-133

(*S*)-2-Azido-*N*-hydroxy-3-phenylpropanamide

To a solution of **3-121** (205 mg, 0.69 mmol, 1.0 eq) in dry DCM (6.5 mL) under an argon atmosphere and at -78 °C was added boron trichloride (1 M solution in DCM, 2.08 mL, 2.08 mmol, 3.0 eq). The reaction mixture was then stirred for 2 h at -78 °C. The reaction was quenched by slow addition of a solution of $NaHCO_3$ (2 M, 20 mL) and the mixture was extracted with DCM (3 x 20 mL). The combined organic phases were then washed with brine (15 mL), dried with $MgSO_4$, filtered and evaporated *in vacuo* to afford the desired compound (127 mg, 89%). ^{1}H NMR (400 MHz, D_2O) δ 7.54 – 7.27 (m, 5H), 4.24 (t, *J* = 7.1 Hz, 1H), 3.18 (dd, *J* = 13.8, 7.1 Hz, 1H), 3.13 (dd, *J* = 13.8, 7.3 Hz, 1H). ^{13}C NMR (101 MHz, D_2O) δ 168.15, 135.74, 129.42, 128.83, 127.39, 62.21, 37.12. IR (cm^{-1}): 3171, 3030, 2923, 2100, 1657.

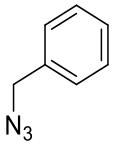

3-139

(Azidomethyl)benzene

To a solution of benzyl bromide (297 μL, 2.5 mmol, 1 eq) in a mixture of H_2O/Acetone (50 mL, 1:4) was added NaN_3 (325 mg, 5 mmol, 2 eq). The reaction mixture was then stirred at room temperature for 16 h. DCM (50 mL) was added, and the layers were separated. The aqueous was extracted with DCM (3 x 10 mL), and the combined organic phases were dried with $MgSO_4$, filtered and evaporated to afford the desired compound (285 mg, 86%). ^{1}H NMR (400 MHz, $CDCl_3$) δ 7.45 – 7.30 (m, 5H), 4.35 (s, 2H). ^{13}C NMR (101 MHz, $CDCl_3$) δ 135.48, 128.94, 128.41, 128.32, 54.89. Consistent with reported analysis.[518]

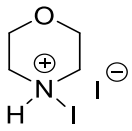

3-144

***N*-iodomorpholine hydroiodide**

To a solution of iodine (1.16 g, 4.57 mmol, 1 eq) in MeOH (23 mL) was added dropwise morpholine (400 μL, 4.57 mmol, 1 eq) leading to the formation of an orange precipitate. The reaction mixture was stirred 1 h at room temperature in the dark, and the precipitate was recovered by filtration, washed with cold MeOH (2 x 10 mL), and dried *in vacuo* to afford the desired product (1.37 g, 88%).

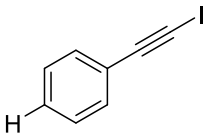

3-145

(Iodoethynyl)benzene

Phenylacetylene (500 μL, 4.55 mmol, 1 eq) was dissolved in THF (15 mL) and CuI (43.4 mg, 0.23 mmol, 0.05 eq) and **3-144** (1.71 g, 5.01 mmol, 1.1 eq) were added. The reaction mixture was stirred at room temperature 1 h after which a white precipitate had formed. The mixture was filtered on a pad of neutral alumina and washed with DCM (3 x 25 mL). The filtrate was evaporated to afford the desired compound (1.02 g, 98%). ^{1}H NMR (400 MHz, $CDCl_3$) δ 7.46 –

7.41 (m, 2H), 7.35 – 7.29 (m, 3H). ^{13}C NMR (101 MHz, $CDCl_3$) δ 132.47, 128.95, 128.38, 123.53, 94.27, 6.22. Consistent with reported analysis.[463]

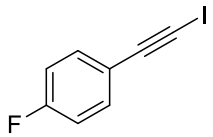

3-146

1-Fluoro-4-(iodoethynyl)benzene

To a solution of 4-fluorophenylacetylene (150 μL, 1.31 mmol, 1 eq) in THF (5 mL) were added CuI (12.5 mg, 0.07 mmol, 0.05 eq) and **3-144** (490.8 mg, 1.44 mmol, 1.1 eq). The reaction mixture was stirred at room temperature 1 h after which a white precipitate had formed. The mixture was filtered on a pad of neutral alumina and washed with DCM (3 x 25 mL). The filtrate was evaporated to afford the desired compound (225 mg, 70%). ^{1}H NMR (400 MHz, $CDCl_3$) δ 7.44 – 7.38 (m, 2H), 7.00 (t, *J* = 8.8 Hz, 2H). ^{13}C NMR (101 MHz, $CDCl_3$) δ 162.92 (d, *J* = 250.3 Hz), 134.41 (d, *J* = 8.5 Hz), 119.63 (d, *J* = 3.5 Hz), 115.70 (d, *J* = 22.2 Hz), 93.14 (s), 6.12 (d, *J* = 1.8 Hz). IR (cm^{-1}): 1599, 1503, 1229,1156. Consistent with reported analysis.[519]

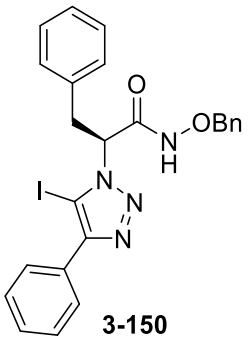

3-150

(*S*)-*N*-(Benzyloxy)-2-(5-iodo-4-phenyl-1*H*-1,2,3-triazol-1-yl)-3-phenylpropanamide

To a solution of **3-121** (150 mg, 0.51 mmol, 1 eq) in THF (2.5 mL) were added **3-145** (115 mg, 0.51 mmol, 1 eq), Et_3N (141 μL, 1.01 mmol, 2 eq) and CuI (5 mg, 0.03 mmol, 0.05 eq). The reaction mixture was stirred for 16 h and then the solvent was evaporated. The residue was purified by flash chromatography (gradient Hexane/EtOAC) to afford the desired compound (170 mg, 64%). ^{1}H NMR (400 MHz, $CDCl_3$) δ 7.79 (d, *J* = 6.9 Hz, 2H), 7.49 – 7.40 (m, 3H), 7.37 – 7.30 (m, 4H), 7.22 – 7.14 (m, 3H), 7.00 – 6.94 (m, 2H), 5.35 (dd, *J* = 10.9, 4.5 Hz, 1H), 4.94 (s, 2H), 3.70 (dd, *J* = 14.1, 3.7 Hz, 1H), 3.55 (dd, *J* = 13.7, 11.4 Hz, 1H). ^{13}C NMR (101 MHz, $CDCl_3$) δ 164.48, 134.96, 134.87, 134.50, 129.51, 129.47, 129.24, 129.17, 129.12, 129.04, 128.96, 128.82, 128.75, 128.70, 128.59, 127.67, 125.90, 78.60, 65.87, 39.83. IR (cm^{-1}): 2971, 1739, 1682, 1366. MS (ESI+) Calc for $[C_{24}H_{21}IN_4O_2+H]^+$ 525.079 ; Found: 525.606

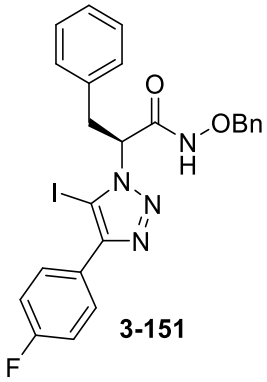

3-151

(*S*)-*N*-(benzyloxy)-2-(4-(4-fluorophenyl)-5-iodo-1*H*-1,2,3-triazol-1-yl)-3-phenylpropanamide

To a solution of **3-121** (300 mg, 1.01 mmol, 1 eq) in THF (15 mL) were added **3-146** (249 mg, 1.01 mmol, 1 eq), Et_3N (282 µL, 2.02 mmol, 2 eq) and CuI (10 mg, 0.05 mmol, 0.05 eq). The reaction mixture was stirred for 16 h and then the solvent was evaporated. The residue was purified by flash chromatography (gradient Hexane/EtOAC) to afford the desired compound (180 mg, 34%).^{1}H NMR (400 MHz, $CDCl_3$) δ 8.48 (s, 1H), 7.50 – 7.38 (m, 2H), 7.38 – 7.26 (m, 10H), 7.00 (t, *J* = 8.8 Hz, 2H), 4.86, 4.79 (ABq, *J* = 11.2 Hz, 2H), 4.13 (t, *J* = 7.1 Hz, 1H), 3.33 (dd, *J* = 13.9, 4.5 Hz, 1H), 3.06 (dd, *J* = 14.0, 7.7 Hz, 1H). ^{13}C NMR (101 MHz, $CDCl_3$) δ 166.07, 162.82 (d, *J* = 250.4 Hz), 135.67, 134.72, 134.33 (d, *J* = 8.5 Hz), 129.62, 129.44, 128.99, 128.81, 128.68, 127.44, 125.89, 119.57 (d, *J* = 3.6 Hz), 115.62 (d, *J* = 22.2 Hz), 93.05, 78.56, 63.52, 38.09. IR (cm^{-1}): 3176, 2970, 1674, 1496, 1225. MS (ESI+) Calc for $[C_{24}H_{20}IFN_4O_2+H]^+$ 543.0693; Found: 543.0698

4.4 Hydantoin-based scaffold

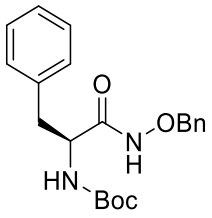

3-168

tert-Butyl (*S*)-(1-((benzyloxy)amino)-1-oxo-3-phenylpropan-2-yl)carbamate

CDI (458 mg, 2.83 mmol, 1.5 eq) was added to a solution of Boc-L-Phe-OH (420 mg, 2.20 mmol, 1 eq) in dry THF (4 mL) under an argon atmosphere. The reaction mixture was stirred for 1 h at room temperature. Then $NH_2OBn.HCl$ (602 mg, 3.77 mmol, 2 eq) was added to the mixture, which was then stirred for 16 h at room temperature. THF was removed by evaporation. The crude

mixture was then diluted with an aqueous solution of 5% $KHSO_4$ (15 mL) and extracted with EtOAc (3 x 10 mL).The combined organic phases were washed brine (20 mL), then dried with $MgSO_4$, filtered and evaporated *in vacuo*. The residue was purified by flash chromatography on silica (gradient Hexane/EtOAc) to afford the desired product (603 mg, 86%). ^{1}H NMR (400 MHz, $CDCl_3$) δ 8.42 (br, 1H), 7.38 – 7.16 (m, 10H), 5.02 (br, 1H), 4.81 (d, *J* = 11.1 Hz, 1H), 4.69 (d, *J* = 10.7 Hz, 1H), 4.16 (q, *J* = 7.4 Hz, 1H), 3.16 – 2.96 (m, 2H), 1.39 (s, 9H). ^{13}C NMR (101 MHz, $CDCl_3$) δ 168.87, 155.57, 136.43, 135.06, 129.51, 129.33, 128.79, 128.74, 128.59, 127.08, 80.53, 78.38, 53.65, 38.50, 28.38. IR (cm^{-1}): 3336, 3248, 2992, 1663, 1521, 1168. MS (ESI+) Calc for $[C_{21}H_{26}N_2O_4+Na]^+$ 393.1790; Found: 393.1891

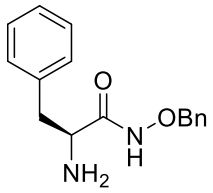

3-169

(*S*)-2-Amino-*N*-(benzyloxy)-3-phenylpropanamide

To a solution of **3-168** (540 mg, 1.46 mmol, 1 eq) in dry DCM (5 mL) under an argon atmosphere and at 0 °C was added TFA (1.12 mL, 14.58 mmol, 10 eq). The reaction mixture was then stirred at room temperature for 3 h. The reaction was quenched by addition of a solution of $NaHCO_3$ (1 M, 20 mL). The layers were separated and the organic was washed with brine (10 mL), dried with $MgSO_4$, filtered and evaporated in vacuo to afford the desired compound (390 mg, 99%). ^{1}H NMR (400 MHz, $CDCl_3$) δ 7.40 – 7.08 (m, 10H), 4.84 (s, 2H), 3.70 – 3.45 (m, 1H), 3.17 (dd, *J* = 13.4, 3.4 Hz, 1H), 2.77 (dd, *J* = 13.4, 8.3 Hz, 1H). ^{13}C NMR (101 MHz, $CDCl_3$) δ 167.34, 134.72, 133.38, 130.19, 129.58, 129.43, 129.18, 128.67, 127.83, 79.44, 56.32, 37.90. IR (cm^{-1}): 3031, 1661, 1454, 1203.

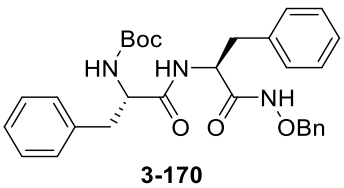

3-170

tert-Butyl ((*S*)-1-(((*S*)-1-((benzyloxy)amino)-1-oxo-3-phenylpropan-2-yl)amino)-1-oxo-3-phenylpropan-2-yl) carbamate

To a solution of Boc-L-Phe-OH (100 mg, 0.38 mmol, 1 eq) in dry DMF (2 mL) at 0 °C and under argon atmosphere were added EDC (79 mg, 0.41 mmol, 1.1 eq), HOBt.H_2O (63 mg, 0.41 mmol, 1.1 eq) and NMM (137 µL, 1.25 mmol, 3.3 eq). The reaction mixture was stirred 10 min at 0 °C

and **3-169** (102 mg, 0.38 mmol, 1 eq) was added. The reaction mixture was then stirred at room temperature for 16 h. The reaction mixture was diluted with EtOAc (20 mL) and washed with a 5% aqueous solution of $KHSO_4$ (20 mL), a saturated solution of $NaHCO_3$ (20 mL) and then brine (20 mL). The organic layer was then dried with $MgSO_4$, filtered and evaporated in vacuo. The residue was purified by flash chromatography on silica (gradient Hexane/EtOAC) to afford the desired compound (123 mg, 63%). ^{1}H NMR (400 MHz, $CDCl_3$) δ 8.95 (s, 1H), 7.35 – 7.27 (m, 7H), 7.25 – 7.21 (m, 3H), 7.18 – 7.09 (m, 3H), 7.09 – 6.99 (m, 2H), 4.80 (d, *J* = 10.7 Hz, 1H), 4.71 (d, *J* = 10.8 Hz, 1H), 4.62 – 4.52 (m, 1H), 4.23 (q, *J* = 6.1 Hz, 1H), 3.21 – 2.87 (m, 4H), 1.33 (s, 9H). ^{13}C NMR (101 MHz, $CDCl_3$) δ 171.70, 167.83, 155.75, 136.43, 136.08, 135.13, 129.54, 129.40, 129.30, 128.74, 128.69, 128.50, 127.11, 127.08, 80.48, 78.27, 55.92, 52.03, 38.25, 38.01, 28.34. IR (cm^{-1}): 3290, 2978, 1689, 1649, 1524. MS (ESI+) Calc for $[C_{30}H_{35}N_3O_5+H]^+$ 518.2655; Found: 518.2728

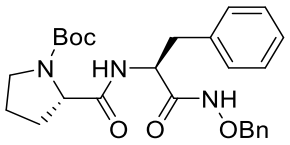

3-171

tert-Butyl (*S*)-2-(((*S*)-1-((benzyloxy)amino)-1-oxo-3-phenylpropan-2-yl)carbamoyl)pyrrolidine-1-carboxylate

To a solution of Boc-L-Pro-OH (96 mg, 0.44 mmol, 1.2 eq) in dry DCM (3 mL) at 0 °C and under argon atmosphere were added HBTU (168 mg, 0.44 mmol, 1.2 eq), DIPEA (226 µL, 1.29 mmol, 3.5 eq) **3-169** (100 mg, 0.38 mmol, 1 eq) was added. The reaction mixture was then stirred at room temperature for 16 h. The reaction mixture was diluted with DCM (20 mL) and washed with a 5% aqueous solution of $KHSO_4$ (20 mL), a saturated solution of $NaHCO_3$ (20 mL) and then brine (20 mL). The organic layer was then dried with $MgSO_4$, filtered and evaporated in vacuo. The residue was purified by flash chromatography on silica (gradient Hexane/EtOAC) to afford the desired compound (60 mg, 35%). ^{1}H NMR (400 MHz, $CDCl_3$) δ 9.50 (s, 1H), 7.41 – 7.26 (m, 8H), 7.16 (d, *J* = 6.6 Hz, 2H), 4.86 (d, *J* = 10.9 Hz, 1H), 4.80 (d, *J* = 10.6 Hz, 1H), 4.74 – 4.64 (m, 1H), 4.11 (dd, *J* = 8.3, 4.0 Hz, 1H), 3.35 – 3.20 (m, 3H), 3.18 – 3.00 (m, 1H), 2.13 – 1.96 (m, 2H), 1.85 – 1.70 (m, 2H), 1.35 (s, 9H). ^{13}C NMR (101 MHz, $CDCl_3$) δ 172.07, 167.97, 155.89, 136.27, 135.24, 129.50, 129.41, 128.81, 128.71, 128.56, 127.24, 81.24, 78.40, 60.88, 51.74, 47.28, 37.16, 29.30, 28.41, 24.64. IR (cm^{-1}): 3245, 2978, 1688, 1647, 1520, 1367. MS (ESI-) Calc for $[C_{26}H_{33}N_3O_5-H]^-$ 466.2342; Found: 466.2466

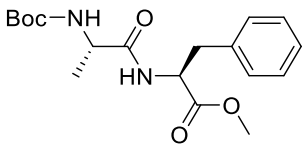

3-174

Methyl (tert-butoxycarbonyl)-L-alanyl-L-phenylalaninate

To a solution of Boc-L-Ala-OH (300 mg, 1.59 mmol, 1 eq) in dry DCM (5 mL) at 0 °C and under argon atmosphere were added HBTU (722 mg, 1.90 mmol, 1.2 eq), L-phenylalanine methyl ester hydrochloride (410 mg, 1.90 mmol, 1.2 eq) and DIPEA (967 μL, 5.55 mmol, 3.5 eq). Then, the reaction mixture was stirred at room temperature for 16 h. The reaction mixture was diluted with EtOAc (20 mL) and washed with a 5% aqueous solution of $KHSO_4$ (20 mL), a saturated solution of $NaHCO_3$ (20 mL) and then brine (20 mL). The organic layer was then dried with $MgSO_4$, filtered and evaporated *in vacuo*. The residue was purified by flash chromatography on silica (gradient Hexane/EtOAC) to afford the desired compound (378 mg, 68%). ^{1}H NMR (400 MHz, $CDCl_3$) δ 7.31 – 7.20 (m, 3H), 7.13 – 7.04 (m, 2H), 6.51 (d, *J* = 7.6 Hz, 1H), 4.84 (dt, *J* = 7.7, 5.9 Hz, 1H), 4.18 – 4.07 (m, 1H), 3.71 (s, 3H), 3.16 (dd, *J* = 13.9, 5.8 Hz, 1H), 3.08 (dd, *J* = 13.8, 6.0 Hz, 1H), 1.43 (s, 9H), 1.31 (d, *J* = 7.1 Hz, 3H). ^{13}C NMR (101 MHz, $CDCl_3$) δ 172.07, 167.97, 155.89, 136.27, 135.24, 129.50, 129.41, 128.81, 128.71, 128.56, 127.24, 81.24, 78.40, 60.88, 51.74, 47.28, 37.16, 29.30, 28.41, 24.64. IR (cm^{-1}): 3317, 2979, 1742, 1663, 1498, 1164. MS (ESI+) Calc for $[C_{18}H_{26}N_2O_5+Na]^+$ 373.174; Found: 373.195

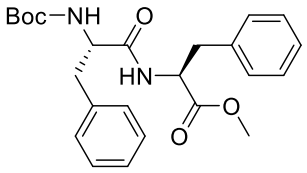

3-175

Methyl (tert-butoxycarbonyl)-L-phenylalanyl-L-phenylalaninate

To a solution of Boc-L-Phe-OH (1.0 g, 3.77 mmol, 1 eq) in dry DCM (38 mL) at 0 °C and under argon atmosphere were added HATU (1.58 g, 4.15 mmol, 1.1 eq), L-phenylalanine methyl ester hydrochloride (894 mg, 4.15 mmol, 1.1 eq) and DIPEA (2.63 mL, 15.08 mmol, 4 eq). The reaction mixture was then stirred at room temperature for 4 h. The reaction mixture was washed with a saturated solution of NH_4Cl (30 mL) and then brine (20 mL). The organic layer was then dried with $MgSO_4$, filtered and evaporated *in vacuo*. The residue was purified by flash chromatography on silica (gradient Hexane/EtOAC) to afford the desired compound (1.05 g, 65%). ^{1}H NMR (400 MHz, $CDCl_3$) δ 7.31 – 7.26 (m, 3H), 7.26 – 7.16 (m, 5H), 7.01 – 6.94 (m, 2H), 6.27 (d, *J* = 6.5

Hz, 1H), 4.94 (br, 1H), 4.78 (q, *J* = 6.1 Hz, 1H), 4.37 – 4.28 (m, 1H), 3.67 (s, 3H), 3.15 – 2.96 (m, 4H), 1.40 (s, 9H). ^{13}C NMR (101 MHz, $CDCl_3$) δ 171.49, 170.92, 155.42, 136.62, 135.76, 129.50, 129.36, 128.81, 128.69, 127.26, 127.12, 80.35, 55.78, 53.41, 52.41, 38.41, 38.10, 28.37. IR (cm^{-1}): 3287, 1696, 1653, 1533. MS (ESI+) Calc for $[C_{24}H_{30}N_2O_5+Na]^+$ 449.205; Found: 449.740

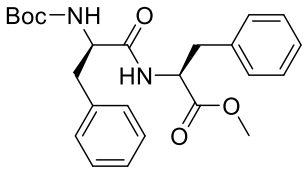

3-176

Methyl (tert-butoxycarbonyl)-D-phenylalanyl-L-phenylalaninate

To a solution of Boc-D-Phe-OH (1.0 g, 3.77 mmol, 1 eq) in dry DCM (38 mL) at 0 °C and under an argon atmosphere were added HATU (1.58 g, 4.15 mmol, 1.1 eq), L-phenylalanine methyl ester hydrochloride (894 mg, 4.15 mmol, 1.1 eq) and DIPEA (2.63 mL, 15.08 mmol, 4 eq). The reaction mixture was then stirred at room temperature for 4 h. The reaction mixture was washed with a saturated solution of NH_4Cl (30 mL) and then brine (20 mL). The organic layer was then dried with $MgSO_4$, filtered and evaporated *in vacuo*. The residue was purified by flash chromatography on silica (gradient Hexane/EtOAC) to afford the desired compound (1.53 g, 95%). ^{1}H NMR (400 MHz, $CDCl_3$) δ 7.35 – 7.22 (m, 6H), 7.22 – 7.16 (m, 2H), 7.02 – 6.94 (m, 2H), 6.48 (d, *J* = 6.9 Hz, 1H), 5.07 – 4.98 (m, 1H), 4.87 (q, *J* = 5.9 Hz, 1H), 4.47 – 4.35 (m, 1H), 3.70 (s, 3H), 3.15 – 2.95 (m, 4H), 1.42 (s, 9H). ^{13}C NMR (101 MHz, $CDCl_3$) δ 171.63, 170.98, 155.41, 136.73, 135.68, 129.44, 129.27, 128.74, 128.70, 127.24, 127.04, 80.24, 55.80, 53.15, 52.35, 38.48, 37.99, 28.33. IR (cm^{-1}): 3288, 1732, 1661, 1520. MS (ESI+) Calc for $[C_{24}H_{30}N_2O_5+Na]^+$ 449.205; Found: 449.740

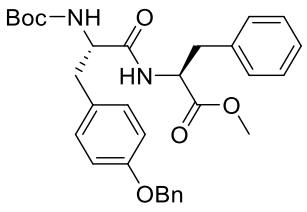

3-177

Methyl ((*S*)-3-(4-(benzyloxy)phenyl)-2-((tert-butoxycarbonyl)amino)propanoyl)-L-phenylalaninate

To a solution of Boc-L-Tyr(OBn)-OH (1.0 g, 2.69 mmol, 1 eq) in dry DCM (27 mL) under argon atmosphere and at 0 °C were added HATU (1.13 g, 2.96 mmol, 1.1 eq), L-phenylalanine methyl

ester hydrochloride (639 mg, 2.96 mmol, 1.1 eq) and DIPEA (1.87 mL, 10.77 mmol, 4 eq). The reaction mixture was then stirred at room temperature for 4 h. The reaction mixture was washed with a saturated solution of NH_4Cl (30 mL) and then brine (20 mL). The organic layer was then dried with $MgSO_4$, filtered and evaporated in vacuo. The residue was purified by flash chromatography on silica (gradient Hexane/EtOAC) to afford the desired compound (1.17 g, 82%). ^{1}H NMR (400 MHz, $CDCl_3$) δ 7.43 – 7.28 (m, 5H), 7.25 – 7.19 (m, 3H), 7.12 – 7.01 (m, 2H), 6.97 – 6.91 (m, 2H), 6.91 – 6.85 (m, 2H), 6.34 (d, *J* = 7.6 Hz, 1H), 5.03 (s, 2H), 4.90 (br, 1H), 4.83 (q, *J* = 5.8 Hz, 1H), 4.36 – 4.22 (m, 1H), 3.67 (s, 3H), 3.07 – 2.89 (m, 4H), 1.39 (s, 9H). ^{13}C NMR (101 MHz, $CDCl_3$) δ 171.63, 171.06, 157.96, 155.41, 137.09, 135.69, 130.49, 129.28, 128.91, 128.71, 128.68, 128.05, 127.53, 127.26, 115.11, 80.23, 70.11, 55.90, 53.14, 52.36, 38.00, 37.60, 28.36. IR (cm^{-1}): 3333, 3025, 1732, 1662, 1510, 1246. MS (ESI+) Calc for $[C_{31}H_{36}N_2O_6+Na]^+$ 555.247; Found: 555.780

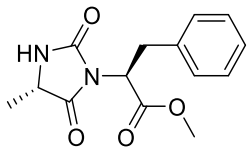

3-178

Methyl (*S*)-2-((*S*)-4-methyl-2,5-dioxoimidazolidin-1-yl)-3-phenylpropanoate

To a solution of **3-174** (370 mg, 1.06 mmol, 1 eq) in dry DCM (5 mL) at 0 °C and under argon atmosphere were added pyridine (256 μL, 3.17 mmol, 3 eq) and Tf_2O (266 μL, 1.58 mmol, 1.5 eq) dropwise. The reaction mixture was kept stirring at 0 °C for 10 min then let to warm up to room temperature and stirred 3 h. The reaction was quenched by addition of a solution of $NaHCO_3$ (2 M, 2 mL) and the reaction mixture was diluted with EtOAc (30 mL). The organic layer was then washed with a saturated solution of $NaHCO_3$ (3 x 15 mL), then brine (15 mL). The organic layer was dried with $MgSO_4$, filtered and evaporated in vacuo. The residue was purified by flash chromatography on silica (gradient Hexane/EtOAc) to afford the desired compound (157 mg, 54%). ^{1}H NMR (400 MHz, $CDCl_3$) δ 7.30 – 7.26 (m, 1H), 7.25 – 7.24 (m, 1H), 7.22 – 7.16 (m, 3H), 5.53 (br, 1H), 4.95 (t, *J* = 8.6 Hz, 1H), 3.95 (qd, *J* = 6.9, 1.1 Hz, 1H), 3.80 (s, 3H), 3.48 (d, *J* = 8.7 Hz, 2H), 1.13 (d, *J* = 6.9 Hz, 3H). ^{13}C NMR (101 MHz, $CDCl_3$) δ 173.94, 169.19, 156.12, 136.58, 129.19, 128.70, 127.10, 53.28, 53.04, 52.79, 34.23, 17.67. IR (cm^{-1}): 3381, 2962, 1741, 1709. MS (ESI+) Calc for $[C_{14}H_{16}N_2O_4+H]^+$ 277.1188; Found: 277.1247

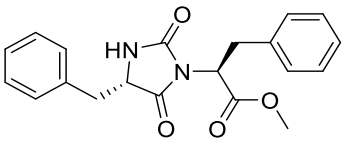

3-179

Methyl (*S*)-2-((*S*)-4-benzyl-2,5-dioxoimidazolidin-1-yl)-3-phenylpropanoate

To a solution of **3-175** (211 mg, 1.06 mmol, 1 eq) in dry DCM (3 mL) at 0 °C and under argon atmosphere were added pyridine (120 µL, 1.48 mmol, 3 eq) and Tf_2O (125 µL, 0.74 mmol, 1.5 eq) dropwise. The reaction mixture was kept stirring at 0 °C for 10 min then let to warm-up to room temperature and stirred 3 h. The reaction was quenched by addition of a solution of $NaHCO_3$ (2 M, 2 mL), the reaction mixture was concentrated in vacuo and then diluted with EtOAc (30 mL). The organic layer was then washed with a saturated solution of $NaHCO_3$ (3 x 15 mL), then brine (15 mL). The organic layer was dried with $MgSO_4$, filtered and evaporated in vacuo. The residue was purified by flash chromatography on silica (gradient Hexane/EtOAc) to afford the desired compound (128 mg, 73%). ^{1}H NMR (400 MHz, $CDCl_3$) δ 7.36 – 7.26 (m, 5H), 7.26 – 7.19 (m, 3H), 7.14 – 7.05 (m, 2H), 5.08 (br, 1H), 4.98 (dd, *J* = 10.2, 7.0 Hz, 1H), 4.06 (ddd, *J* = 10.7, 3.7, 1.2 Hz, 1H), 3.79 (s, 3H), 3.54 – 3.43 (m, 2H), 3.07 (dd, *J* = 13.9, 3.6 Hz, 1H), 2.14 (dd, *J* = 13.9, 10.8 Hz, 1H). ^{13}C NMR (101 MHz, $CDCl_3$) δ 172.41, 169.10, 155.65, 136.63, 135.81, 129.30, 129.20, 129.07, 128.76, 127.61, 127.18, 58.32, 53.28, 53.06, 38.35, 34.27. IR (cm^{-1}): 3296, 2912, 1760, 1708, 1425. MS (ESI+) Calc for $[C_{20}H_{20}N_2O_4+H]^+$ 353.150; Found: 353.144

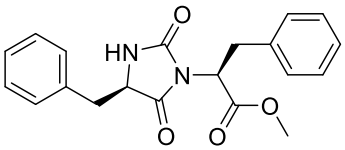

3-180

Methyl (*S*)-2-((*R*)-4-benzyl-2,5-dioxoimidazolidin-1-yl)-3-phenylpropanoate

To a solution of **3-176** (1.45 g, 3.40 mmol, 1 eq) in dry DCM (34 mL) at 0 °C and under argon atmosphere were added pyridine (825 µL, 10.20 mmol, 3 eq) and Tf_2O (858 µL, 5.10 mmol, 1.5 eq) dropwise. The reaction mixture was kept stirring at 0 °C for 10 min then let to warm-up to room temperature and stirred 3 h. The reaction was quenched by addition of a solution of $NaHCO_3$ (2 M, 2 mL), the reaction mixture was concentrated in vacuo and then diluted with EtOAc (30 mL). The organic layer was then washed with a saturated solution of $NaHCO_3$ (3 x 15 mL), then brine (15 mL). The organic layer was dried with $MgSO_4$, filtered and evaporated in vacuo. The residue was purified by flash chromatography on silica (gradient Hexane/EtOAc) to afford the

desired compound (1.15 g, 95%). ^{1}H NMR (400 MHz, $CDCl_3$) δ 7.31 – 7.17 (m, 6H), 7.16 – 7.06 (m, 4H), 5.64 (s, 1H), 4.90 (dd, *J* = 11.3, 5.5 Hz, 1H), 4.02 (ddd, *J* = 9.6, 3.7, 1.1 Hz, 1H), 3.73 (s, 3H), 3.47 (dd, *J* = 14.3, 5.5 Hz, 1H), 3.39 (dd, *J* = 14.2, 11.4 Hz, 1H), 3.16 (dd, *J* = 13.9, 3.7 Hz, 1H), 2.51 (dd, *J* = 13.9, 9.6 Hz, 1H). ^{13}C NMR (101 MHz, $CDCl_3$) δ 172.41, 169.10, 155.65, 136.63, 135.81, 129.30, 129.20, 129.07, 128.76, 127.61, 127.18, 58.32, 53.28, 53.06, 38.35, 34.27. IR (cm^{-1}): 3270, 2920, 1763, 1701, 1431. MS (ESI+) Calc for $[C_{20}H_{20}N_2O_4+H]^+$ 353.150 ; Found: 353.758

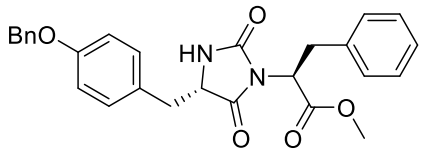

3-181

Methyl (*S*)-2-((*S*)-4-(4-(benzyloxy)benzyl)-2,5-dioxoimidazolidin-1-yl)-3-phenylpropanoate

To a solution of **3-177** (1.1 g, 2.07 mmol, 1 eq) in dry DCM (20 mL) at 0 °C and under argon atmosphere were added pyridine (501 µL, 6.20 mmol, 3 eq) and Tf_2O (521 µL, 3.10 mmol, 1.5 eq) dropwise. The reaction mixture was kept stirring at 0 °C for 10 min then let to warm-up to room temperature and stirred 3 h. The reaction was quenched by addition of a solution of $NaHCO_3$ (2 M, 2 mL) and the reaction mixture was diluted with EtOAc (30 mL). The organic layer was then washed with a saturated solution of $NaHCO_3$ (3 x 15 mL), then brine (15 mL). The organic layer was dried with $MgSO_4$, filtered and evaporated *in vacuo*. The residue was purified by flash chromatography on silica (gradient Hexane/EtOAc) to afford the desired compound (734 mg, 78%). ^{1}H NMR (400 MHz, $CDCl_3$) δ 7.42 – 7.28 (m, 5H), 7.28 – 7.16 (m, 3H), 7.16 – 7.10 (m, 2H), 7.01 (d, *J* = 8.6 Hz, 2H), 6.89 (d, *J* = 8.6 Hz, 2H), 5.47 (s, 1H), 5.02 (s, 2H), 4.90 (dd, *J* = 11.3, 5.6 Hz, 1H), 3.98 (ddd, *J* = 9.6, 3.6, 0.8 Hz, 1H), 3.74 (s, 3H), 3.48 (dd, *J* = 14.3, 5.5 Hz, 1H), 3.41 (dd, *J* = 14.2, 11.3 Hz, 1H), 3.10 (dd, *J* = 14.0, 3.7 Hz, 1H), 2.46 (dd, *J* = 14.0, 9.6 Hz, 1H). ^{13}C NMR (101 MHz, $CDCl_3$) δ 172.39, 169.10, 158.24, 156.03, 136.93, 136.67, 130.33, 129.17, 128.74, 128.67, 128.16, 127.71, 127.55, 127.12, 115.40, 70.15, 58.26, 53.46, 52.99, 37.24, 34.11. IR (cm^{-1}): 3270, 2920, 1763, 1701, 1431. MS (ESI+) Calc for $[C_{27}H_{26}N_2O_5+H]^+$ 458.184; Found: 458.186

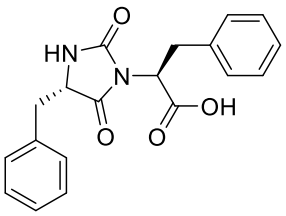

3-184

(*S*)-2-((*S*)-4-benzyl-2,5-dioxoimidazolidin-1-yl)-3-phenylpropanoic acid

To a solution of **3-179** (130 mg, 0.37 mmol, 1 eq) in 1,4-dioxane (7 mL) was added a solution of HCl (6 M, 5 mL) and the reaction mixture was stirred at 80 °C for 16 h. The 1,4-dioxane was evaporated and the reaction mixture was extracted with DCM (3 x 10 mL). The combined organic layers were dried $MgSO_4$, filtered and evaporated *in vacuo* to afford the desired compound (110 mg, 88%). ^{1}H NMR (400 MHz, $CDCl_3$) δ 7.33 – 7.27 (m, 4H), 7.25 – 7.18 (m, 4H), 7.10 (d, *J* = 6.9 Hz, 2H), 5.49 (s, 1H), 4.97 (dd, *J* = 10.8, 6.3 Hz, 1H), 4.07 (dd, *J* = 10.4, 3.3 Hz, 1H), 3.79 (s, 3H), 3.52 – 3.39 (m, 2H), 3.05 (dd, *J* = 13.8, 3.4 Hz, 1H), 2.17 (dd, *J* = 13.8, 10.5 Hz, 1H). ^{13}C NMR (101 MHz, MeOD) δ 174.99, 171.83, 158.21, 138.58, 136.89, 130.54, 130.04, 129.57, 129.50, 128.08, 127.76, 59.08, 54.62, 38.56, 35.00. IR (cm^{-1}): 3325, 3027, 2973, 1748, 1652, 1430 MS(ESI-) Calc for $[C_{19}H_{18}N_2O_4\text{-}H]^-$ 337.1188; Found: 337.1163

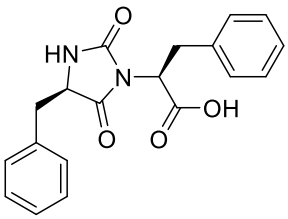

3-185

(*S*)-2-((*R*)-4-benzyl-2,5-dioxoimidazolidin-1-yl)-3-phenylpropanoic acid

To a solution of **3-180** (967 mg, 2.74 mmol, 1 eq) in 1,4-dioxane (8 mL) was added a solution of HCl (6 M, 10 mL) and the reaction mixture was stirred at 80 °C for 16 h. The 1,4-dioxane was evaporated and the reaction mixture was extracted with DCM (3 x 10 mL). The combined organic layers were dried $MgSO_4$, filtered and evaporated in vacuo to afford the desired compound (910 mg, 98%). ^{1}H NMR (400 MHz, $CDCl_3$) δ 7.32 – 7.22 (m, 6H), 7.18 – 7.10 (m, 4H), 6.01 (s, 1H), 4.96 (dd, *J* = 10.8, 6.1 Hz, 1H), 4.05 (ddd, *J* = 9.7, 3.7, 0.9 Hz, 1H), 3.50 – 3.39 (m, 2H), 3.19 (dd, *J* = 13.9, 3.6 Hz, 1H), 2.53 (dd, *J* = 13.9, 9.8 Hz, 1H). ^{13}C NMR (101 MHz, MeOD) δ 174.99, 171.83, 158.21, 138.58, 136.89, 130.54, 130.04, 129.57, 129.50, 128.08, 127.76, 59.08, 54.62, 38.56, 35.00. IR (cm^{-1}): 3325, 3030, 2971, 1746, 1684, 1433. MS (ESI+) Calc for $[C_{19}H_{18}N_2O_4\text{+}H]^+$ 339.134 ; Found: 339.634

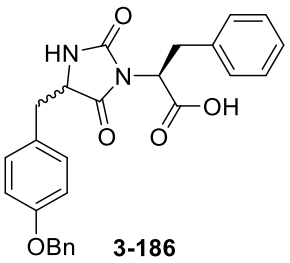

3-186

(2*S*)-2-(4-(4-(benzyloxy)benzyl)-2,5-dioxoimidazolidin-1-yl)-3-phenylpropanoic acid

To a solution of **3-181** (680 mg, 1.48 mmol, 1 eq) in 1,4-dioxane (5 mL) was added a solution of HCl (6 M, 5 mL) and the reaction mixture was stirred at 80 °C for 16 h. The 1,4-dioxane was evaporated and the reaction mixture was extracted with DCM (3 x 10 mL). The combined organic layers were dried $MgSO_4$, filtered and evaporated *in vacuo* to afford the desired compound as a mixture of two diastereoisomers in a 2:1 ratio (910 mg, 98%).

Major isomer: ^{1}H NMR (400 MHz, $CDCl_3$) δ 7.44 – 7.20 (m, 8H), 7.18 – 7.11 (m, 2H), 7.01 (d, *J* = 8.7 Hz, 2H), 6.89 (d, *J* = 8.7 Hz, 2H), 6.41 (s, 1H), 5.78 (s, 1H), 5.02 (s, 2H), 4.99 – 4.89 (m, 1H), 4.01 (dd, *J* = 9.6, 3.8 Hz, 1H), 3.51 – 3.39 (m, 2H), 3.11 (dd, *J* = 14.0, 3.7 Hz, 1H), 2.48 (dd, *J* = 14.1, 9.5 Hz, 1H). ^{13}C NMR (101 MHz, $CDCl_3$) δ 172.71, 172.41, 158.18, 157.16, 136.93, 136.48, 130.42, 129.10, 128.73, 128.16, 127.58, 127.20, 115.40, 70.15, 58.50, 53.44, 37.05, 33.96.

Minor isomer: ^{1}H NMR (400 MHz, $CDCl_3$) δ 77.44 – 7.20 (m, 8H), 7.18 – 7.11 (m, 2H), 6.92 (d, *J* = 8.5 Hz, 2H), 6.64 (d, *J* = 8.5 Hz, 2H), 6.41 (s, 1H), 5.78 (s, 1H), 5.02 (s, 2H), 4.99 – 4.89 (m, 1H), 4.05 (dd, *J* = 6.4, 4.3 Hz, 1H), 3.51 – 3.39 (m, 2H), 2.99 (dd, *J* = 14.2, 4.1 Hz, 1H), 2.76 (dd, *J* = 14.2, 6.7 Hz, 1H). ^{13}C NMR (101 MHz, $CDCl_3$) δ 172.92, 172.41, 157.81, 157.16, 136.93, 136.48, 130.86, 129.03, 128.73, 128.16, 127.58, 127.20, 115.84, 70.15, 58.42, 53.37, 36.47, 34.14.

IR (cm^{-1}): 2971, 1739, 1365, 1217. MS (ESI+) Calc for $[C_{26}H_{24}N_2O_5+H]^+$ 445.1763 ; Found: 445.1708

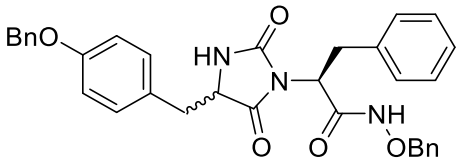

3-187

(2*S*)-*N*-(benzyloxy)-2-(4-(4-(benzyloxy)benzyl)-2,5-dioxoimidazolidin-1-yl)-3-phenylpropanamide

To a solution of **3-186** (480 mg, 1.48 mmol, 1 eq) in dry THF (7 mL) under an argon atmosphere was added CDI (360 mg, 2.22 mmol, 1.5 eq). The reaction mixture was stirred at room temperature for 2 h. Then $NH_2OBn.HCl$ (473 mg, 2.96 mmol, 2 eq) was added to the mixture, which was then stirred for 16 h at room temperature. THF was removed by evaporation. The crude mixture was then diluted with an aqueous solution of 5% $KHSO_4$ (15 mL) and extracted with EtOAc (3 x 10 mL).The combined organic phases were washed brine (20 mL), then dried with $MgSO_4$, filtered and evaporated *in vacuo*. The residue was purified by flash chromatography on silica (gradient Hexane/EtOAc) to afford the desired product as a mixture of two diastereoisomers in a 1:1 ratio (220 mg, 27%).

Isomer 1: ^{1}H NMR (400 MHz, MeOD) δ 7.45 – 7.16 (m, 14H), 7.14 – 7.08 (m, 1H), 7.02 (d, *J* = 8.7 Hz, 2H), 6.89 (d, *J* = 3.7 Hz, 2H), 5.01 (s, 2H), 4.82 – 4.73 (m, 3H), 4.11 – 4.04 (m, 1H), 3.40 – 3.32 (m, 1H), 3.29 – 3.17 (m, 1H), 2.74 (dd, *J* = 13.9, 4.4 Hz, 1H), 2.25 (dd, *J* = 14.1, 8.4 Hz, 1H). ^{13}C NMR (101 MHz, MeOD) δ 175.16, 167.90,159.31, 157.94, 138.71, 138.09, 136.73, 131.46, 130.58, 130.21, 129.68, 129.59, 129.46, 129.27, 128.82, 128.51,127.95, 116.03, 79.12, 70.91, 59.63, 54.07, 38.06, 34.95.

Isomer 2: ^{1}H NMR (400 MHz, MeOD) δ 7.45 – 7.16 (m, 14H), 7.14 – 7.08 (m, 1H), 7.06 (d, *J* = 8.6 Hz, 2H), 6.91 (d, *J* = 3.6 Hz, 2H), 5.01 (s, 2H), 4.82 – 4.73 (m, 2H), 4.70 (dd, *J* = 10.8, 5.6 Hz, 1H), 4.11 – 4.04 (m, 1H), 3.40 – 3.32 (m, 1H), 3.29 – 3.17 (m, 1H), 2.96 (dd, *J* = 14.1, 4.2 Hz, 1H), 2.59 (dd, *J* = 14.1, 7.5 Hz, 1H). ^{13}C NMR (101 MHz, MeOD) δ 175.05, 167.90,159.43, 158.09, 138.71, 138.09, 136.73, 131.68, 130.58, 130.39, 129.68, 129.59, 129.46, 129.06, 128.82, 128.51,127.95, 116.03, 79.12, 70.91, 59.29, 54.61, 37.60, 34.84.

IR (cm^{-1}): 3242, 2940, 1703, 1511, 1422. MS (ESI+) Calc for $[C_{33}H_{31}N_3O_5+H]^+$ 550.2342; Found: 550.2236

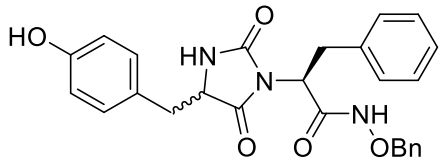

3-188

(2*S*)-*N*-(benzyloxy)-2-(4-(4-hydroxybenzyl)-2,5-dioxoimidazolidin-1-yl)-3-phenylpropanamide

Isolated with **3-187** as a mixture of diasteroisomers in a 1:1 ratio (26 mg, 4%).

Isomer 1: ^{1}H NMR (400 MHz, MeOD) δ 7.44 – 7.39 (m, 2H), 7.39 – 7.33 (m, 3H), 7.25 – 7.20 (m, 3H), 7.07 (d, *J* = 6.7 Hz, 2H), 6.92 (d, *J* = 8.6 Hz, 2H), 6.70 – 6.66 (m, 2H), 4.84 – 4.76 (m, 3H),4.09 – 4.01 (m, 1H), 3.41 – 3.32 (m, 1H), 3.29 – 3.17 (m, 1H), 2.71 (dd, *J* = 14.0, 4.4 Hz, 1H), 2.16 (dd, *J* = 14.0, 8.6 Hz, 1H). ^{13}C NMR (101 MHz, MeOD) δ 175.24, 168.02, 157.97, 157.55, 138.09, 136.75, 131.39, 130.59, 130.23, 129.68, 129.59, 129.45, 127.95, 127.79, 116.38, 79.14, 59.82, 54.05, 38.17, 34.95.

Isomer 2: ^{1}H NMR (400 MHz, MeOD) δ 7.44 – 7.39 (m, 2H), 7.39 – 7.33 (m, 3H), 7.32 – 7.25 (m, 3H), 7.18 (d, *J* = 7.0 Hz, 2H), 6.96 (d, *J* = 8.5 Hz, 2H), 6.73 – 6.70 (m, 2H), 4.84 – 4.76 (m, 2H), 4.70 (dd, *J* = 10.8, 5.6 Hz, 1H), 4.09 – 4.01 (m, 1H), 3.41 – 3.32 (m, 1H), 3.29 – 3.17 (m, 1H), 2.93 (dd, *J* = 14.1, 4.2 Hz, 1H), 2.53 (dd, *J* = 14.1, 7.6 Hz, 1H). ^{13}C NMR (101 MHz, MeOD) δ 175.13, 168.02, 158.11, 157.68, 138.09, 136.75, 131.64, 130.59, 130.39, 129.68, 129.59, 129.45, 127.95, 127.53, 116.38, 79.14, 59.44, 54.64, 37.67, 34.81.

IR (cm^{-1}): 3230, 2937, 1704, 1666, 1515, 1424. MS (ESI+) Calc for $[C_{26}H_{25}N_3O_5+H]^+$ 460.1872; Found: 460.1949

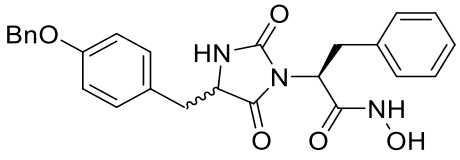

3-189

(2*S*)-2-(4-(4-(benzyloxy)benzyl)-2,5-dioxoimidazolidin-1-yl)-*N*-hydroxy-3-phenylpropanamide

To a solution of **3-187** (200 mg, 0.36 mmol, 1 eq) in dry THF (10 mL) under an argon atmosphere ant at -78 °C was added dropwise a solution of BCl_3 (1 M, 2 mL, 2 mmol, 5.5 eq). The reaction mixture was let to warm-up to 0 °C and stirred for 4 h. The reaction was then quenched by addition of MeOH (3 mL) and the reaction mixture was evaporated in vacuo. The residue was purified by

flash chromatography on reverse phase (gradient H_2O/MeCN 0.05% TFA) to afford the desired compound as a mixture of diastereoisomoers in a 1:1 ratio (47 mg, 35%).

Isomer 1: ^{1}H NMR (400 MHz, MeOD) δ 7.40 – 7.37 (m, 2H), 7.36 – 7.31 (m, 2H), 7.30 – 7.26 (m, 2H), 7.24 – 7.17 (m, 3H), 7.10 – 7.07 (m, 1H), 7.06 – 6.99 (m, 2H), 6.90 (d, *J* = 8.3 Hz, 2H), 5.01 (s, 2H), 4.83 – 4.80 (m, 1H), 4.11 – 4.05 (m, 1H), 3.44 – 3.36 (m, 1H), 3.34 – 3.26 (m, 1H),2.72 (dd, *J* = 14.0, 4.3 Hz, 1H), 2.17 (dd, *J* = 14.0, 8.6 Hz, 1H). ^{13}C NMR (101 MHz, MeOD) δ 175.32, 168.01, 159.29, 158.04, 138.69, 138.18, 131.38, 130.17, 129.58, 129.46, 128.83, 128.52, 127.93, 116.03, 70.92, 59.67, 54.12, 38.14, 34.93.

Isomer 2: ^{1}H NMR (400 MHz, MeOD) δ 7.40 – 7.37 (m, 2H), 7.36 – 7.31 (m, 2H), 7.30 – 7.26 (m, 2H), 7.24 – 7.17 (m, 3H), 7.10 – 7.07 (m, 1H), 7.06 – 6.99 (m, 2H), 6.90 (d, *J* = 8.3 Hz, 2H), 5.02 (s, 2H), 4.76 (dd, *J* = 11.1, 5.4 Hz, 1H), 4.11 – 4.05 (m, 1H), 3.44 – 3.36 (m, 1H), 3.34 – 3.26 (m, 1H), 2.95 (dd, *J* = 14.0, 4.0 Hz, 1H), 2.52 (dd, *J* = 14.1, 7.8 Hz, 1H). ^{13}C NMR (101 MHz, MeOD) δ 175.18, 167.89, 159.41, 158.20, 138.69, 138.18, 131.58, 130.35, 129.58, 129.16, 128.83, 128.52, 127.93, 116.03, 70.92, 59.31, 54.65, 37.71, 34.73.

IR (cm^{-1}): 3282, 3039, 2885, 1700, 1515, 1423. MS (ESI-) Calc for $[C_{26}H_{25}N_3O_5\text{-}H]^-$ 458,1715; Found: 458.1635

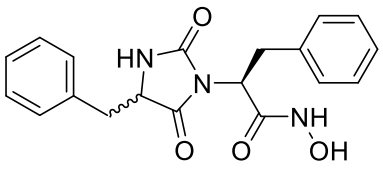

3-190

(*S*)-2-(4-benzyl-2,5-dioxoimidazolidin-1-yl)-*N*-hydroxy-3-phenylpropanamide

To a solution of **3-185** (840 mg, 2.48 mmol, 1 eq) in dry THF (10 mL) under an argon atmosphere was added CDI (403 mg, 2.48 mmol, 1 eq). The reaction mixture was stirred at room temperature for 1 h. Then NH_2OTBDMS (366 mg, 2.48 mmol, 1 eq) was added to the mixture which was then stirred for 16 h at room temperature. THF was removed by evaporation. The crude mixture was then diluted with phosphate buffer (10 mL, pH = 6.2) and extracted with EtOAc (3 x 10 mL). The combined organic phases were washed brine (20 mL), then dried with $MgSO_4$, filtered and evaporated *in vacuo*. The residue was purified by reverse flash chromatography (gradient H_2O/MeCN (0.05% TFA) to afford the desired product as a mixture of two diastereisomers in a 1:1 ratio (17 mg, 2 %).

Isomer 1: ^{1}H NMR (400 MHz, MeOD) δ 7.37 – 7.17 (m, 7H), 7.17 – 7.04 (m, 3H), 4.88 – 4.82 (m, 1H), 4.13 (dd, *J* = 6.1, 2.9 Hz, 1H), 3.47 – 3.32 (m, 2H), 2.78 (dd, *J* = 13.9, 4.5 Hz, 1H), 2.17

(dd, *J* = 13.9, 9.1 Hz, 1H). ^{13}C NMR (101 MHz, MeOD) δ 175.41, 168.01, 158.02, 138.02, 137.20, 130.36, 130.18, 129.66, 129.58, 128.13, 127.99, 59.52, 54.07, 39.00, 34.88.

Isomer 2: ^{1}H NMR (400 MHz, MeOD) δ 7.37 – 7.17 (m, 7H), 7.17 – 7.04 (m, 3H), 4.78 (dd, *J* = 11.2, 5.6 Hz, 1H), 4.10 (dd, *J* = 5.5, 3.0 Hz, 1H), 3.47 – 3.32 (m, 2H), 3.02 (dd, *J* = 13.9, 4.2 Hz, 1H), 2.51 (dd, *J* = 14.0, 8.4 Hz, 1H). ^{13}C NMR (101 MHz, MeOD) δ 175.29, 167.87, 158.20, 138.02, 137.05, 130.43, 130.27, 129.66, 129.58, 128.13, 127.99, 59.15, 54.60, 38.62, 34.68.

IR (cm^{-1}): 3294, 3026, 1768, 1699, 1423. MS(ESI-) Calc for $[C_{19}H_{19}N_3O_4\text{-}H]^-$ 352.1297; Found: 352.1274

4.5 Praziquantel – HDACi hybrid

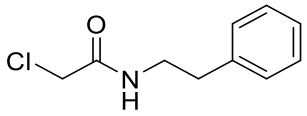

3-193

2-Chloro-*N*-phenethylacetamide

To a solution of phenethylamine (6.0 mL, 47.6 mmol, 1 eq) in dry DCM (82 mL) under argon atmosphere was added $NaHCO_3$ (4.0 g, 47.6 mmol, 1 eq). The mixture was cooled to 0 °C and chloroacetyl chloride (4.6 mL, 57.1 mmol, 1.2 equiv.) was added. The reaction mixture was stirred at room temperature for 4 h, and H_2O (60 mL) was slowly added. The layers were separated and the aqueous phase was extracted with DCM (4 x 50 mL). The organic layers were combined, washed with an aqueous solution of HCl (10 %, 50 mL), dried with $MgSO_4$, filtered, and concentrated *in vacuo* to afford the desired compound (8.05 g, 86 % yield). ^{1}H NMR (400 MHz, $CDCl_3$) δ 7.39 – 7.18 (m, 5H), 6.63 (br, 1H), 4.04 (s, 2H), 3.58 (dd, *J* = 13.0, 7.0 Hz, 2H), 2.86 (t, *J* = 7.0 Hz, 2H). ^{13}C NMR (101 MHz, $CDCl_3$) δ 166.12, 138.41, 128.89, 128.87, 126.88, 42.77, 41.12, 35.59. IR (cm^{-1}): 3338, 2929, 2861, 1736, 1644, 1540. MS (ESI+) Calc for $[C_{10}H_{12}NOCl+H]^+$ 198,0685; Found: 198.0712

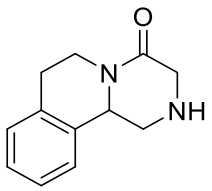

3-195

1,2,3,6,7,11*b*-hexahydro-4*H*-pyrazino[2,1-*a*]isoquinolin-4-one

To a mixture of **3-193** (7.94 g, 40.2 mmol, 1 eq) in dry toluene (105 mL) under argon atmosphere was added dimethoxyethylamine (8.8 mL, 80.3 mmol, 2 eq). The reaction mixture was stirred at reflux for 2 h. The reaction mixture was cooled down with an ice bath and the newly formed precipitate was filtered and washed with cold toluene. After evaporation of the solvent, the oil residue was dissolved in DCM (20 mL), cooled to 0 °C and a solution of HCl in Et_2O (1 M, 50 mL, 1.25 eq) was added. The mixture was then filtered, washed with iced Et_2O (50 mL) then iced hexane (30 mL). The brown solid was dissolved in concentrated H_2SO_4 (10 mL) at 0 °C. The reaction mixture was then stirred for 3 h at room temperature. The mixture was poured on 50 mL of ice and a solution of NaOH (20 %) was added until pH = 12. The aqueous was then extracted with DCM (3 x 30mL). Organic layer was dried over $MgSO_4$, filtered and evaporated to give the desired compound (3.35 g, 41%). ^{1}H NMR (400 MHz, $CDCl_3$) δ 7.31 – 7.16 (m, 4H), 4.91 (ddd, *J* = 12.5, 4.7, 2.3 Hz, 1H), 4.84 (dd, *J* = 9.9, 4.4 Hz, 1H), 3.78 (dd, *J* = 13.1, 4.5 Hz, 1H), 3.71, 3.57 (ABq, *J* = 17.2 Hz, 2H), 3.09 – 2.75 (m, 4H). ^{13}C NMR (101 MHz, $CDCl_3$) δ 167.41, 135.08, 134.35, 129.51, 127.14, 126.74, 124.82, 57.00, 50.19, 49.95, 38.91, 28.95. IR (cm^{-1}): 3315, 2937, 1634, 1440, 1102. MS (ESI+) Calc for $[C_{12}H_{14}N_2O+H]^+$ 203.118; Found: 203.593

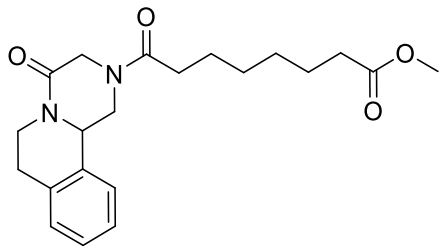

3-202

Methyl 8-oxo-8-(4-oxo-1,3,4,6,7,11*b*-hexahydro-2*H*-pyrazino[2,1-*a*]isoquinolin-2-yl)octanoate

To a solution of **3-195** (370 mg, 1.83 mmol, 1 eq) in dry THF (6 mL) under argon atmosphere was added DIPEA (637 µL, 3.66 mmol, 2 eq). The mixture was cooled to 0 °C and methyl 8-chloro-8-oxooctanoate (312 µL, 2.20 mmol, 1 eq) was added. The reaction mixture was stirred at

room temperature for 4 h. THF was evaporated and H_2O (15 mL) was added to the residue. The aqueous phase was extracted with DCM (3 x 15 mL). The organic layers were combined, dried with $MgSO_4$, filtered, and concentrated *in vacuo*. The residue was purified by flash chromatography on silica (gradient DCM/MeOH) to afford the desired compound as a mixture of enantiomere (606 mg, 88%). ^{1}H NMR (400 MHz, $CDCl_3$) δ 7.29 – 7.13 (m, 4H), 5.11 (dd, *J* = 13.4, 3.8 Hz, 0.7H), 4.90 – 4.82 (m, 0.3H), 4.81 – 4.70 (m, 2H), 4.36 (d, *J* = 17.4 Hz, 0.7H), 4.33 – 4.26 (m, 0.3H), 4.03 (d, *J* = 17.4 Hz, 0.7H), 3.86 (d, *J* = 18.5 Hz, 0.3H), 3.64 (s, 3H), 3.28 – 3.19 (m, 0.3H), 2.99 – 2.72 (m, 3.7H), 2.49 – 2.23 (m, 4H), 1.71 – 1.55 (m, 4H), 1.41 – 1.28 (m, 4H).

Major isomer: ^{13}C NMR (101 MHz, MeOD) δ 174.17, 171.65, 164.27, 134.82, 132.74, 129.34, 127.52, 127.02, 125.54, 54.97, 51.52, 49.09, 45.09, 39.10, 34.00, 33.23, 29.01, 28.91, 28.75, 24.78, 24.72.

Minor isomer: ^{13}C NMR (101 MHz, MeOD) δ 174.17, 171.14, 165.47, 135.52, 132.12, 129.69, 127.74, 127.02, 125.27, 55.57, 51.52, 49.72, 46.22, 38.70, 34.00, 33.05, 29.01, 28.91, 28.75, 24.78, 24.72.

IR (cm^{-1}): 2934, 2860, 1731, 1630, 1420, 1196. MS (ESI+) Calc for $[C_{21}H_{28}N_2O_4+H]^+$ 373.213; Found: 373.741

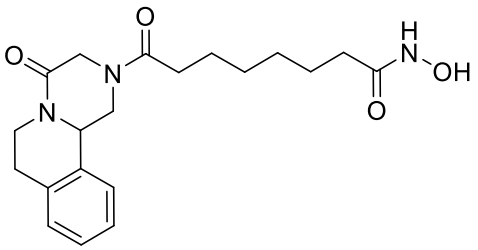

3-191

***N*-Hydroxy-8-oxo-8-(4-oxo-1,3,4,6,7,11*b*-hexahydro-2*H*-pyrazino[2,1-*a*]isoquinolin-2-yl)octanamide**

To **3-202** (560 mg, 1.50 mmol, 1 eq) in 50% aq. NH_2OH/THF/MeOH (0.31 mL, 0.5:1:1) was added KCN (5 mg, 0.08 mmol, 0.05eq). The reaction mixture was stirred at room temperature for 24 h. The volatiles were evaporated *in vacuo* and the residue was purified by flash chromatography on reverse phase (gradient H_2O/MeCN 0.05% TFA) to afford the desired compound as a mixture of enantiomeres (108 mg, 19%). ^{1}H NMR (400 MHz, $CDCl_3$) δ 7.30 – 7.12 (m, 4H), 5.07 (dd, *J* = 13.2, 3.1 Hz, 0.7H), 4.89 (d, *J* = 9.7 Hz, 0.3H), 4.83 – 4.63 (m, 2H), 4.42 (d, *J* = 17.4 Hz, 0.7H), 4.32 (d, *J* = 11.9 Hz, 0.3H), 4.07 (d, *J* = 17.5 Hz,

0.7H), 3.88 (d, *J* = 18.3 Hz, 0.3H), 3.24 (t, *J* = 12.0 Hz, 0.3H), 3.02 – 2.67 (m, 3.7H), 2.49 – 2.27 (m, 2H), 2.22 – 2.06 (m, 2H), 1.72 – 1.52 (m, 4H), 1.39 – 1.24 (m, 4H).

Major isomer: ^{13}C NMR (101 MHz, MeOD) δ 172.48, 171.75, 164.94, 134.76, 132.54, 129.33, 127.63, 127.12, 125.60, 54.93, 48.98, 45.16, 39.36, 33.01, 32.56, 28.70, 28.51, 28.35, 25.07, 24.53.

Minor isomer: ^{13}C NMR (101 MHz, MeOD) δ 172.48, 172.23, 165.91, 135.32, 131.90, 129.59, 127.84, 127.12, 125.47, 55.39, 49.61, 46.17, 38.99, 32.90, 32.56, 28.70, 28.51, 28.35, 25.07, 24.53.

IR (cm^{-1}): 3191, 2927, 1734, 1621, 1430, 1366, 1217. MS (ESI+) Calc for $[C_{20}H_{27}N_3O_4+H]^+$ 374.207; Found: 374.673

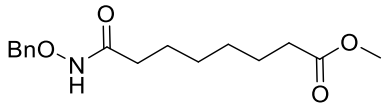

3-203

Methyl 8-((benzyloxy)amino)-8-oxooctanoate

To a solution of $NH_2OBn.HCl$ (289.6 mg, 1.81 mmol, 1.5 eq) in dry THF (6 mL) under argon atmosphere was added DIPEA (632 μL, 3.63 mmol, 3 eq). The reaction mixture was cooled down to 0 °C in an ice-bath and methyl 8-chloro-8-oxooctanoate (172 μL, 1.21 mmol, 1 eq) was added. The reaction mixture was then stirred at room temperature for 16 h. THF was evaporated, H_2O (20 mL) was added to the residue and the aqueous was extracted with DCM (3 x 20 mL). The combined organic layer was dried with $MgSO_4$, filtered and evaporated *in vacuo*. The residue was purified by flash chromatography on silica (gradient DCM/MeOH) to afford the desired compound (293 mg, 83%). ^{1}H NMR (400 MHz, $CDCl_3$) δ 8.53 (br, 1H), 7.43 – 7.29 (m, 5H), 4.88 (s, 2H), 3.63 (s, 3H), 2.26 (t, *J* = 7.5 Hz, 2H), 2.10 – 1.95 (m, 2H), 1.66 – 1.50 (m, 4H), 1.36 – 1.23 (m, 4H). ^{13}C NMR (101 MHz, $CDCl_3$) δ 174.32, 171.05, 135.57, 129.27, 128.76, 128.66, 78.19, 51.57, 34.00, 33.16, 28.75, 25.17, 24.75. IR (cm^{-1}): 3191, 2935, 2860, 1735, 1652, 1455, 1199, 1172. MS (ESI+) Calc for $[C_{16}H_{23}NO_4+H]^+$ 294.1705; Found: 294.1814

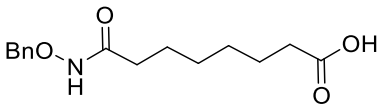

3-204

8-((Benzyloxy)amino)-8-oxooctanoic acid

To a solution of **3-203** (227 mg, 0.77 mmol, 1 eq) in THF (3 mL) at 0 °C was added dropwise an aqueous solution of LiOH (1 M, 14 mL, 3 mmol, 3.9 eq). The reaction mixture was left to warm up to room temperature and the mixture was stirred for 16 h. A solution of HCl (1 M) was added until pH = 2 and the reaction mixture was then extracted with Et_2O (3 x 10 mL). The combined organic layers were dried with $MgSO_4$, filtered and evaporated *in vacuo* to afford the desired compound (191 mg, 88%). ^{1}H NMR (400 MHz, $CDCl_3$) δ 8.05 (br, 1H), 7.43 – 7.32 (m, 5H), 4.91 (s, 2H), 2.33 (t, *J* = 7.4 Hz, 2H), 2.15 – 1.89 (m, 2H), 1.68 – 1.52 (m, 4H), 1.37 – 1.26 (m, 4H). ^{13}C NMR (101 MHz, $CDCl_3$) δ 179.14, 171.20, 135.44, 129.33, 128.82, 128.71, 78.25, 34.05, 33.12, 28.69, 25.18, 24.57. IR (cm^{-1}): 3237, 2936, 2860, 1690, 1653, 1498, 1192. MS (ESI+) Calc for $[C_{15}H_{21}NO_4+H]^+$ 280.1549; Found: 280.1606

4.6 4-amino-2-hydroxybutanoic acid-based scaffold

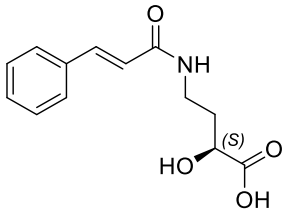

3-205

(*S*)-4-Cinnamamido-2-hydroxybutanoic acid

To a solution of (*S*)-4-amino-2-hydroxybutanoic acid (250 mg, 2.10 mmol, 1 eq) in aqueous NaOH (1 M, 2.1 mL) was added cinnamoyl chloride (350 mg, 2.10 mmol, 1 eq) The reaction mixture was stirred at room temperature for 16 h. A solution of HCl (2 M) was then added until pH = 1 and the mixture was extracted with EtOAc (3 x 10 mL). The combined organic layer was dried with $MgSO_4$, filtered and evaporated *in vacuo*. The residue was purified by flash chromatography on reverse phase (H_2O/MeCN 0.05% TFA) to afford the desired compound (282 mg, 54%). ^{1}H NMR (400 MHz, MeOD) δ 7.58 – 7.54 (m, 2H), 7.53 (d, *J* = 15.9 Hz, 1H), 7.43 – 7.31 (m, 3H), 6.60 (d, *J* = 15.8 Hz, 1H), 4.20 (dd, *J* = 8.6, 4.1 Hz, 1H), 3.53 – 3.40 (m, 2H), 2.13 – 2.00 (m, 1H), 1.95 – 1.82 (m, 1H). ^{13}C NMR (101 MHz, MeOD) δ 177.52, 168.83, 141.77, 136.26, 130.81, 129.93, 128.82, 121.75, 69.40, 37.13, 34.91. IR (cm^{-1}): 3301, 2924, 1725, 1652, 1579, 1564, 1450, 1220. MS (ESI+) Calc for $[C_{13}H_{15}NO_4+H]^+$ 250.108; Found: 250.719

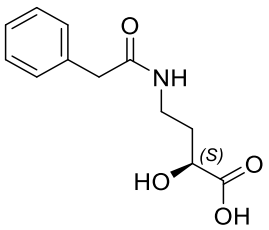

3-206

(*S*)-2-Hydroxy-4-(2-phenylacetamido)butanoic acid

To a solution of (*S*)-4-amino-2-hydroxybutanoic acid (250 mg, 2.10 mmol, 1 eq) in aqueous NaOH (1 M, 2.1 mL) was added phenylacetyl chloride (324 mg, 2.10 mmol, 1 eq) The reaction mixture was stirred at room temperature for 16 h. A solution of HCl (2 M) was then added until pH = 1, and the mixture was extracted with EtOAc (3 x 10 mL). The combined organic layer was dried with $MgSO_4$, filtered and evaporated *in vacuo*. The residue was purified by flash chromatography on reverse phase (H_2O/MeCN 0.05% TFA) to afford the desired compound (273 mg, 55%). ^{1}H NMR (400 MHz, MeOD) δ 7.39 – 7.26 (m, 4H), 7.25 – 7.20 (m, 1H), 4.12 (dd, *J* = 8.7, 4.0 Hz, 1H), 3.50 (s, 2H), 3.38 – 3.31 (m, 2H), 2.07 – 1.87 (m, 1H), 1.87 – 1.69 (m, 1H). ^{13}C NMR (101 MHz, MeOD) δ 177.46, 174.28, 136.87, 130.06, 129.57, 127.88, 69.37, 43.86, 37.16, 34.75. IR (cm^{-1}): 3292, 3063, 2948, 1737, 1694, 1634, 1548. MS (ESI+) Calc for $[C_{12}H_{15}NO_4+H]^+$ 238.108; Found: 238.723

4.7 SETD8 inhibitors

The following compound are not fully characterized because of a limited access to the analytical instrument at the University of Salerno. During my mission, the mass spectrometry was not available due to issues with the spectrometer. In addition, they were experiencing technical problems with NMR spectrometers and the access was restricted and scheduled, thus limiting the number of experiments. The priority was given to the final compounds that were going to be tested.

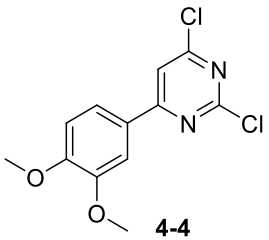

4-4

2,4-Dichloro-6-(3,4-dimethoxyphenyl)pyrimidine

In a microwave vessel, 2,4,6-trichloropyrimidine (376 µL, 3.27 mmol, 1 eq) was added to a mixture of dioxane/H_2O (33 mL, 2/1). Cs_2O_3 (3.197 g, 9.81 mmol, 3 eq), Pd(dppf)Cl_2.DCM

complex (267 mg, 0.33 mmol, 0.1 eq) and 3,4-dimethoxyphenyl boronic acid (655 mg, 3.6 mmol, 1.1 eq) were then added to the solution. The reaction mixture was stirred under microwave irradiation (80 °C, 300 W, 30 min). After completion the reaction mixture was diluted with EtOAc (100 mL) and separated. The aqueous was back extracted with EtOAc (2 x 10 mL) and the combined organic layers were washed with brined (30 mL), dried over Na_2SO_4, filtered and evaporated. The crude was purified by flash chromatography on silica (gradient Hexane/EtOAc with 40% DCM as additive) to afford the desired compound (720 mg, 77 %). ^{1}H NMR (400 MHz, $CDCl_3$) δ 7.67 (dd, *J* = 6.0, 2.0 Hz, 1H), 7.64 (d, *J* = 2.1 Hz, 1H), 7.60 (s, 1H), 6.97 (d, *J* = 8.4 Hz, 1H), 4.00 (s, 3H), 3.97 (s, 3H).

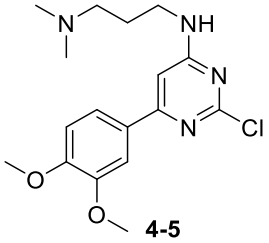

4-5

***N*^{1}-(2-Chloro-6-(3,4-dimethoxyphenyl)pyrimidin-4-yl)-*N*^{3},*N*^{3}-dimethylpropane-1,3-diamine**

In a microwave vessel, **4-4** (300 mg, 1.05 mmol, 1 eq) was dissolved in THF (3 mL). Then 3-dimethylamino-1-propylamine (397 μL, 3.16 mmol, 3 eq) was added to the solution and the reaction mixture was carried under microwave irradiation (80 °C, 200 W, 30 min). THF was evaporated and the residue was purified by flash chromatography on aluminium oxide (gradient Hexane/EtOAc and 2% additive MeOH) and the isomer **4-5** was isolated (110 mg, 30%). ^{1}H NMR (400 MHz, $CDCl_3$) δ 7.58 (s, 1H), 7.51 (d, *J* = 8.3 Hz, 1H), 6.91 (d, *J* = 8.4 Hz, 1H), 6.51 (s, 1H), 4.72 (s, 1H), 3.98 (s, 3H), 3.93 (s, 3H), 3.56 – 3.41 (m, 2H), 2.44 (t, *J* = 6.0 Hz, 2H), 2.26 (s, 6H), 1.80 – 1.74 (m, 2H).

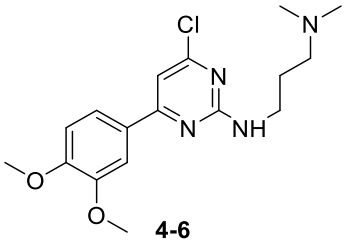

4-6

***N*^{1}-(4-Chloro-6-(3,4-dimethoxyphenyl)pyrimidin-2-yl)-*N*^{3},*N*^{3}-dimethylpropane-1,3-diamine**

Compound **4-6** was isolated with **4-5**. (124 mg, 34%). ^{1}H NMR (400 MHz, $CDCl_3$) δ 7.66 – 7.52 (m, 2H), 6.93 (d, *J* = 8.4 Hz, 1H), 6.91 (s, 1H), 5.89 (s, 1H), 3.97 (s, 3H), 3.94 (s, 3H), 3.61 – 3.54 (m, 2H), 2.41 (t, *J* = 6.8 Hz, 2H), 2.25 (s, 6H), 1.85 – 1.77 (m, 2H).

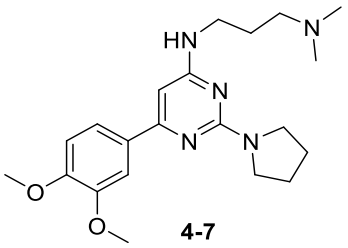

4-7

***N*^{1}-(6-(3,4-Dimethoxyphenyl)-2-(pyrrolidin-1-yl)pyrimidin-4-yl)-*N*^{3},*N*^{3}-dimethylpropane-1,3-diamine**

In a microwave vessel, **4-5** (90 mg, 0.26 mmol, 1 eq) was dissolved in THF (0.8 mL). Pyrrolidine (107 µL, 1.29 mmol, 5 eq) was added to the solution and the reaction was carried under microwave irradiation (120 °C, 300 W, 30 min). THF was evaporated and the residue purified by flash chromatography on silica (gradient DCM/MeOH/ 2% NH_3) to afford the desired product (44 mg, 44%). ^{1}H NMR (400 MHz, $CDCl_3$) δ 7.60 (d, *J* = 1.3 Hz, 1H), 7.49 (dd, *J* = 8.4, 1.5 Hz, 1H), 6.90 (d, *J* = 8.4 Hz, 1H), 6.02 (s, 1H), 3.97 (s, 3H), 3.92 (s, 3H), 3.55 – 3.47 (m, 6H), 2.42 – 2.37 (m, 2H), 2.24 (s, 6H), 2.02 – 1.95 (m, 4H), 1.86 – 1.77 (m, 2H).

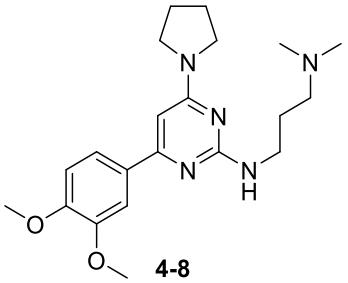

4-8

***N*^{1}-(4-(3,4-Dimethoxyphenyl)-6-(pyrrolidin-1-yl)pyrimidin-2-yl)-*N*^{3},*N*^{3}-dimethylpropane-1,3-diamine**

In a microwave vessel, **4-6** (90 mg, 0.26 mmol, 1 eq) was dissolved in THF (1 mL). Pyrrolidine (107 µL, 1.29 mmol, 5 eq) was added to the solution and the reaction was carried under microwave irradiation (120 °C, 300 W, 30 min). THF was evaporated and the residue purified by flash chromatography on silica (gradient DCM/MeOH/ 2 % NH_3) to afford the desired product (67 mg, 68%). ^{1}H NMR (400 MHz, $CDCl_3$) δ 7.67 (s, 1H), 7.55 (d, *J* = 8.4 Hz, 1H), 6.90 (d, *J* = 8.4 Hz, 1H), 6.05 (s, 1H), 5.23 (br, 1H), 3.96 (s, 3H), 3.92 (s, 3H), 3.66 – 3.60 (m, 4H), 3.45 (dd, *J* = 11.8, 5.9 Hz, 2H), 2.45 (t, *J* = 6.8 Hz, 2H), 2.29 (s, 6H), 1.98 – 1.92 (m, 4H), 1.82 (p, *J* = 6.7 Hz, 2H).

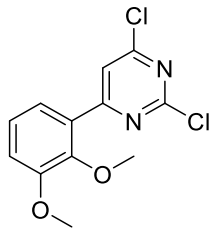

4-10

2,4-Dichloro-6-(2,3-dimethoxyphenyl)pyrimidine

In a microwave vessel, 2,4,6-trichloropyrimidine (376 µL, 3.27 mmol, 1 eq) was added to a mixture of dioxane/H_2O (33 mL, 2/1). Cs_2CO_3 (3.197 g, 9.81 mmol, 3 eq), Pd(dppf)Cl_2•DCM complex (267 mg, 0.33 mmol, 0.1 eq) and 2,3-dimethoxyphenyl boronic acid (595 mg, 3.27 mmol, 1 eq) were then added to the solution. The reaction mixture was stirred in microwave (80 °C, 300 W, 30 min). After completion, the reaction mixture was diluted with EtOAc (30 mL) and separated. The aqueous was back extracted with EtOAc (10 mL) and the combined organic layers were washed with brine (20 mL), dried over Na_2SO_4, filtered and evaporated. The crude was purified by flash chromatography on silica (gradient Hexane/EtOAc with 40% DCM as additive) to afford the desired compound (680 mg, 73 %). ^{1}H NMR (400 MHz, $CDCl_3$) δ 8.00 (s, 1H), 7.56 (dd, *J* = 7.9, 1.5 Hz, 1H), 7.19 (t, *J* = 8.0 Hz, 1H), 7.09 (dd, *J* = 8.2, 1.3 Hz, 1H), 3.93 (s, 3H), 3.82 (s, 3H).

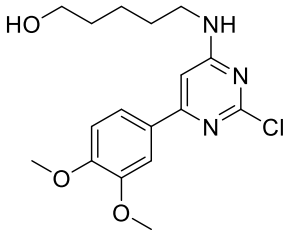

4-11

5-((2-Chloro-6-(3,4-dimethoxyphenyl)pyrimidin-4-yl)amino)pentan-1-ol

In a microwave vessel, **4-4** (450 mg, 1.58 mmol, 1 eq) was dissolved in THF (4.5 mL). To the mixture was added 5-amino-1-pentanol (489 mg, 4.73 mmol, 3 eq) and the reaction was carried under microwave irradiation (80 °C, 300 W, 30 min). THF was evaporated, and the residue purified by flash chromatography on silica (gradient DCM/MeOH/ 2% NH_3) to afford the desired compound (256 mg, 46 %). ^{1}H NMR (400 MHz, $CDCl_3$) δ 7.56 (d, *J* = 1.2 Hz, 1H), 7.49 (dd, *J* = 8.4, 1.4 Hz, 1H), 6.90 (d, *J* = 8.4 Hz, 1H), 6.51 (s, 1H), 5.32 (br, 1H), 3.96 (s, 3H), 3.92 (s, 3H), 3.66 (t, *J* = 6.3 Hz, 2H), 3.43 – 3.29 (m, 2H), 1.69 – 1.59 (m, 4H), 1.53 – 1.45 (m, 2H).

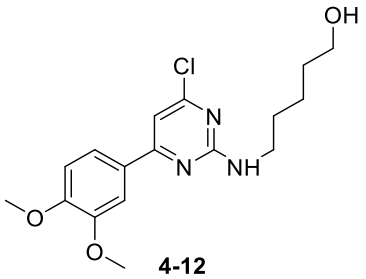

4-12

5-((4-Chloro-6-(3,4-dimethoxyphenyl)pyrimidin-2-yl)amino)pentan-1-ol

Compound **4-12** was isolated with **4-11** (218 mg, 39 %). ^{1}H NMR (400 MHz, $CDCl_3$) δ 7.66 – 7.54 (m, 2H), 6.94 (d, *J* = 7.4 Hz, 1H), 6.93 (s, 1H), 5.27 (br, 1H), 3.97 (s, 3H), 3.94 (s, 3H), 3.67 (t, *J* = 6.1 Hz, 2H), 3.56 – 3.48 (m, 2H), 1.73 – 1.59 (m, 4H), 1.54 – 1.46 (m, 2H).

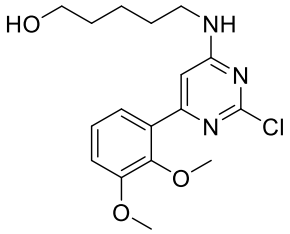

4-13

5-((2-Chloro-6-(2,3-dimethoxyphenyl)pyrimidin-4-yl)amino)pentan-1-ol

In a microwave vessel, **4-10** (190 mg, 0.67 mmol, 1 eq) was dissolved in THF (2 mL). Then 5-amino-1-pentanol (206 mg, 2.0 mmol, 3 eq) was added to the solution and the reaction was carried under microwave irradiation (80 °C, 300 W, 30 min). THF was evaporated. The residue was purified by flash chromatography on silica (gradient Hexane/EtOAc/ 1% MeOH additive) to afford the desired compound (147 mg, 63%). ^{1}H NMR (400 MHz, $CDCl_3$) δ 7.45 (dd, *J* = 7.9, 1.4 Hz, 1H), 7.14 (t, *J* = 8.0 Hz, 1H), 7.00 (dd, *J* = 8.1, 1.1 Hz, 1H), 6.94 (s, 1H), 5.30 (br, 1H), 3.91 (s, 3H), 3.74 (s, 3H), 3.67 (t, *J* = 5.8 Hz, 2H), 3.40 – 3.30 (m, 2H), 1.72 – 1.61 (m, 4H), 1.53 – 1.43 (m, 2H).

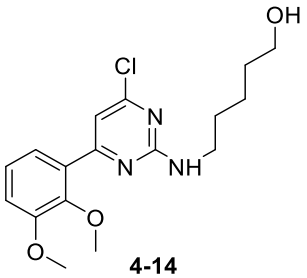

4-14

5-((4-Chloro-6-(3,4-dimethoxyphenyl)pyrimidin-2-yl)amino)pentan-1-ol

Compound **4-14** was isolated with **4-13** (56 mg, 24 %). ^{1}H NMR (400 MHz, $CDCl_3$) δ 7.39 (br, 1H), 7.20 – 7.10 (m, 2H), 7.01 (d, *J* = 7.9 Hz, 1H), 5.28 (br, 1H), 3.91 (s, 3H), 3.79 (s, 3H), 3.66 (t, *J* = 5.6 Hz, 2H), 3.49 (q, *J* = 6.6 Hz, 2H), 1.71 – 1.61 (m, 4H), 1.52 – 1.41 (m, 2H).

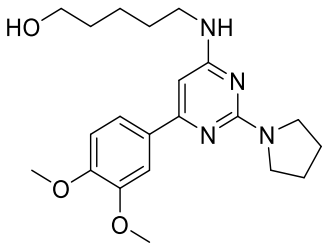

4-15

5-((6-(3,4-Dimethoxyphenyl)-2-(pyrrolidin-1-yl)pyrimidin-4-yl)amino)pentan-1-ol

In a microwave vessel, **4-11** (240 mg, 0.68 mmol, 1 eq) was dissolved in THF (2.4 mL). Pyrrolidine (285 μL, 3.41 mmol, 5 eq) was added to the solution and the reaction was carried under microwave irradiation (120 °C, 300 W, 30 min). THF was evaporated and the residue purified by flash chromatography on silica (gradient Hexane/EtOAc/ 1% MeOH additive) to afford the desired product (178 mg, 68 %). ^{1}H NMR (400 MHz, $CDCl_3$) δ 7.67 (d, *J* = 1.4 Hz, 1H), 7.54 (dd, *J* = 8.3, 1.6 Hz, 1H), 6.90 (d, *J* = 8.4 Hz, 1H), 6.02 (s, 1H), 4.64 (br, 1H), 3.96 (s, 3H), 3.92 (s, 3H), 3.69 – 3.61 (m, 6H), 3.37 (q, *J* = 6.4 Hz, 2H), 1.99 – 1.93 (m, 4H), 1.70 – 1.61 (m, 4H), 1.53 – 1.47 (m, 2H).

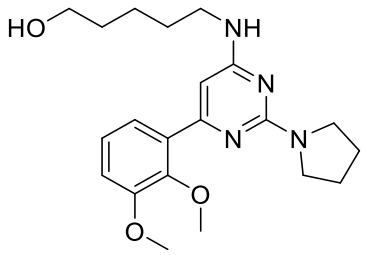

4-16

5-((6-(2,3-Dimethoxyphenyl)-2-(pyrrolidin-1-yl)pyrimidin-4-yl)amino)pentan-1-ol

In a microwave vessel, **4-13** (275 mg, 0.78 mmol, 1 eq) was dissolved in THF (1.2 mL). Pyrrolidine (326 μL, 3.91 mmol, 5 eq) was added to the solution and the reaction was carried under microwave irradiation (120 °C, 300 W, 30 min). THF was evaporated and the residue purified by flash chromatography on silica (gradient Hexane/EtOAc/ 1% MeOH additive) to afford the desired compound (264 mg, 87 %). ^{1}H NMR (400 MHz, $CDCl_3$) δ 7.43 (dd, *J* = 7.9, 1.5 Hz, 1H), 7.10 (t, *J* = 8.0 Hz, 1H), 6.94 (dd, *J* = 8.1, 1.4 Hz, 1H), 6.28 (s, 1H), 4.69 (br, 1H), 3.89 (s, 3H), 3.77 (s, 3H), 3.65 (t, *J* = 6.5 Hz, 2H), 3.62 – 3.56 (m, 4H), 3.32 (q, *J* = 6.1 Hz, 2H), 1.96 – 1.91 (m, 4H), 1.67 – 1.58 (m, 4H), 1.50 – 1.43 (m, 2H).

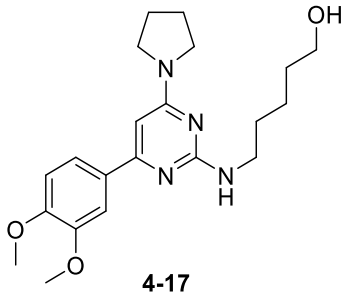

4-17

5-((4-(3,4-Dimethoxyphenyl)-6-(pyrrolidin-1-yl)pyrimidin-2-yl)amino)pentan-1-ol

In a microwave vessel, **4-12** (35 mg, 0.10 mmol, 1 eq) was dissolved in THF (0.5 mL). Pyrrolidine (40 μL, 0.50 mmol, 5 eq) was added to the solution and the reaction was carried under microwave irradiation (120 °C, 300 W, 30 min). THF was evaporated and the residue purified by flash chromatography on silica (gradient Hexane/EtOAc/ 2% MeOH additive) to afford the desired product as a yellowish oil (37 mg, 96 %). ^{1}H NMR (400 MHz, $CDCl_3$) δ 7.60 (d, *J* = 1.5 Hz, 1H), 7.49 (dd, *J* = 8.4, 1.7 Hz, 1H), 6.90 (d, *J* = 8.4 Hz, 1H), 6.03 (s, 1H), 4.86 (br, 1H), 3.97 (s, 3H), 3.92 (s, 3H), 3.65 (t, *J* = 6.5 Hz, 2H), 3.56 – 3.44 (m, 6H), 2.03 – 1.94 (m, 4H), 1.71 – 1.60 (m, 4H), 1.53 – 1.44 (m, 2H).

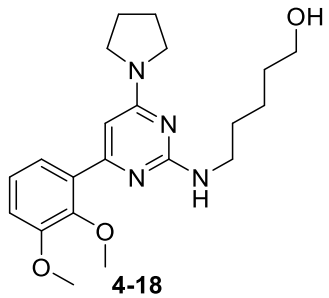

4-18

5-((4-(2,3-Dimethoxyphenyl)-6-(pyrrolidin-1-yl)pyrimidin-2-yl)amino)pentan-1-ol

In a microwave vessel, **4-14** (120 mg, 0.34 mmol, 1 eq) was dissolved in THF (1.2 mL). Pyrrolidine (142 μL, 1.71 mmol, 5 eq) was added to the solution and the reaction was carried under microwave irradiation (120 °C, 300 W, 30 min). THF was evaporated and the residue purified by flash chromatography on silica (gradient Hexane/EtOAc/ 1% MeOH additive) to afford the desired compound (117 mg, 89 %). ^{1}H NMR (400 MHz, $CDCl_3$) δ 7.32 (d, *J* = 7.7 Hz, 1H), 7.10 (t, *J* = 8.0 Hz, 1H), 6.93 (dd, *J* = 8.1, 1.4 Hz, 1H), 6.26 (s, 1H), 4.84 (br, 1H), 3.89 (s, 3H), 3.74 (s, 3H), 3.65 (t, *J* = 6.5 Hz, 2H), 3.56 – 3.34 (m, 6H), 2.01 – 1.91 (m, 4H), 1.69 – 1.58 (m, 4H), 1.52 – 1.44 (m, 2H).

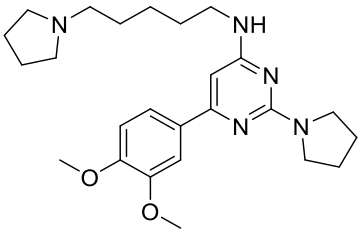

4-29

6-(3,4-Dimethoxyphenyl)-2-(pyrrolidin-1-yl)-*N*-(5-(pyrrolidin-1-yl)pentyl)pyrimidin-4-amine

To a solution of **4-15** (80 mg, 0.21 mmol, 1 eq) in dry DCM (1 mL) and dry $CHCl_3$ (0.5 mL) at 0 °C and under N_2 atmosphere were added Et_3N (35 μL, 0.25 mmol, 1.2 eq) and MsCl (18 μL, 0.23 mmol, 1.1 eq). The mixture was stirred at 0 °C for 3 h. The mixture was diluted in $CHCl_3$ (15 mL) and washed with a saturated solution of $NaHCO_3$ (2 x 5 mL). The organic layer was dried over Na_2SO_4, filtrated and evaporated to afford a yellowish oil residue. The residue was dissolved in THF (1 mL) and pyrrolidine (173 μL, 2.07 mmol, 10 eq) was added. The reaction mixture was sealed and stirred at 80 °C for 16 h. The solvent was evaporated and the residue was purified by flash chromatography on silica (gradient DCM/ MeOH/ 2% NH_3) to afford the desired compound (46 mg, 51%). ^{1}H NMR (400 MHz, $CDCl_3$) δ 7.67 (s, 1H), 7.54 (dd, *J* = 8.4, 1.3 Hz, 1H), 6.90 (d, *J* = 8.4 Hz, 1H), 6.02 (s, 1H), 4.67 (br, 1H), 3.96 (s, 3H), 3.92 (s, 3H), 3.65 – 3.60 (m, 4H), 3.36

(q, *J* = 6.5 Hz, 2H), 2.60 – 2.52 (m, 4H), 2.51 – 2.45 (m, 2H), 1.98 – 1.93 (m, 4H), 1.83 – 1.78 (m, 4H), 1.69 – 1.57 (m, 4H), 1.49 – 1.40 (m, 2H). ^{13}C NMR (101 MHz, $CDCl_3$, DEPTQ) δ 164.00, 163.03, 160.84, 150.32, 148.85, 132.15, 119.51, 110.79, 110.10, 56.41, 55.96, 55.89, 54.22, 46.41, 41.31, 29.56, 28.54, 25.59, 25.07, 23.42.

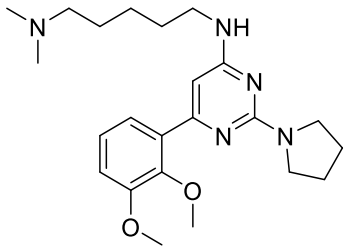

4-30

N^1-(6-(2,3-Dimethoxyphenyl)-2-(pyrrolidin-1-yl)pyrimidin-4-yl)-N^5,N^5-dimethylpentane-1,5-diamine

To a solution of **4-16** (80 mg, 0.21 mmol, 1 eq) in dry DCM (1 mL) and $CHCl_3$ (0.5 mL) at 0 °C were added Et_3N (34.6 µL, 0.25 mmol, 1.2 eq) and MsCl (17.6 µL, 0.23 mmol, 1.1 eq). The mixture was stirred at 0 °C for 3 h. The mixture was diluted in $CHCl_3$ (15 mL) and washed with a saturated solution of $NaHCO_3$ (2 x 5 mL). The organic layer was dried over Na_2SO_4, filtrated and evaporated to afford a yellowish oil residue. The residue was dissolved in THF (1 mL) and dimethylamine (2 M in THF, 1.55 mL, 3.10 mmol, 15 eq) was added. The reaction was then carried under microwave irradiation (120 °C, 300 W, 1 h). The solvent was evaporated, and the residue was purified by flash chromatography on silica (gradient DCM/ MeOH/ 2 % NH_3) to afford the desired compound (17 mg, 20%). ^{1}H NMR (400 MHz, $CDCl_3$) δ 7.43 (dd, *J* = 7.9, 1.4 Hz, 1H), 7.10 (t, *J* = 8.0 Hz, 1H), 6.93 (dd, *J* = 8.1, 1.3 Hz, 1H), 6.28 (s, 1H), 4.71 (br, 1H), 3.89 (s, 3H), 3.77 (s, 3H), 3.62 – 3.57 (m, 4H), 3.36 – 3.25 (m, 2H), 2.29 – 2.24 (m, 2H), 2.22 (s, 6H), 1.94 (t, *J* = 6.6 Hz, 4H), 1.67 – 1.57 (m, 2H), 1.55 – 1.46 (m, 2H), 1.46 – 1.35 (m, 2H). ^{13}C NMR (101 MHz, $CDCl_3$, DEPTQ) δ 163.74, 160.74, 153.21, 147.78, 134.43, 124.18, 122.47, 112.90, 61.29, 59.63, 56.14, 46.61, 45.36, 41.48, 29.65, 27.26, 25.71, 24.94.

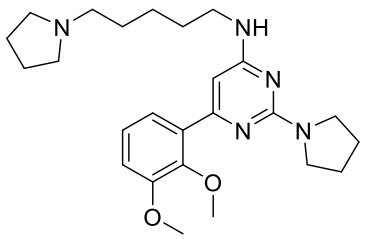

4-31

6-(2,3-Dimethoxyphenyl)-2-(pyrrolidin-1-yl)-*N*-(5-(pyrrolidin-1-yl)pentyl)pyrimidin-4-amine

To a solution of **4-16** (80 mg, 0.21 mmol, 1 eq) in dry DCM (1 mL) and dry $CHCl_3$ (0.5 mL) under N_2 atmosphere at 0 °C were added Et_3N (35 µL, 0.25 mmol, 1.2 eq) and MsCl (18 µL, 0.23 mmol, 1.1 eq). The mixture was stirred at 0 °C for 3 h. The mixture was diluted in $CHCl_3$ (15 mL) and washed with a saturated solution of $NaHCO_3$ (2 x 5 mL). The organic layer was dried over Na_2SO_4, filtrated and evaporated to afford an oil residue. The residue was dissolved in THF (1 mL) and pyrrolidine (173 µL, 2.07 mmol, 10 eq) was added. The reaction was carried under microwave irradiation (120 °C, 300 W, 45 min). The solvent was evaporated and the residue was purified by flash chromatography on silica (gradient DCM/ MeOH/ 2% NH_3) to afford the desired compound (56 mg, 62 %). ^{1}H NMR (400 MHz, $CDCl_3$) δ 7.43 (dd, *J* = 7.9, 1.3 Hz, 1H), 7.10 (t, *J* = 8.0 Hz, 1H), 6.93 (dd, *J* = 8.1, 1.1 Hz, 1H), 6.27 (s, 1H), 4.69 (br, 1H), 3.89 (s, 3H), 3.77 (s, 3H), 3.60 (t, *J* = 6.4 Hz, 4H), 3.36 – 3.25 (m, 2H), 2.60 – 2.52 (m, 4H), 2.51 – 2.45 (m, 2H), 1.96 – 1.91 (m, 4H), 1.83 – 1.77 (m, 4H), 1.69 – 1.55 (m, 4H), 1.46 – 1.38 (m, 2H). ^{13}C NMR (101 MHz, $CDCl_3$, DEPTQ) δ 163.65, 160.60, 153.13, 147.64, 134.30, 124.12, 122.36, 112.85, 61.24, 56.05, 53.99, 46.56, 41.16, 29.34, 27.45, 25.63, 24.79, 23.42.

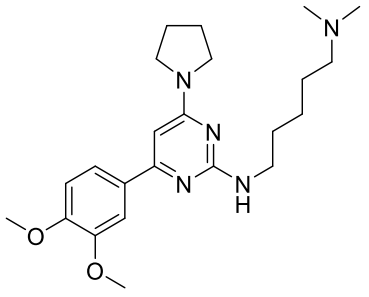

4-32

***N*^{1}-(4-(3,4-dimethoxyphenyl)-6-(pyrrolidin-1-yl)pyrimidin-2-yl)-*N*^{5},*N*^{5}-dimethylpentane-1,5-diamine**

To a solution of **4-17** (60 mg, 0.16 mmol, 1 eq) in dry DCM (1 mL) and dry $CHCl_3$ (0.5 mL) at 0 °C were added Et_3N (26 µL, 0.19 mmol, 1.2 eq) and MsCl (18 µL, 0.23 mmol, 1.1 eq). The mixture was stirred at 0 °C for 3 h. The mixture was diluted in $CHCl_3$ (15 mL) and washed with

a saturated solution of $NaHCO_3$ (2 x 5 mL). The organic layer was dried over Na_2SO_4, filtrated and evaporated to afford an oil. The residue was dissolved in THF (1 mL) and dimethylamine (2 M in MeOH, 1.55 mL, 3.10 mmol, 20 eq) was added. The reaction mixture was stirred at 80 °C for 16 h. The solvent was evaporated and the residue was purified by flash chromatography on silica (gradient DCM/ MeOH/ 2% NH_3) to afford the desired compound (28 mg, 44%). ^{1}H NMR (400 MHz, $CDCl_3$) δ 7.61 (s, 1H), 7.49 (d, *J* = 8.3 Hz, 1H), 6.90 (d, *J* = 8.4 Hz, 1H), 6.02 (s, 1H), 4.91 (br, 1H), 3.97 (s, 3H), 3.92 (s, 3H), 3.60 – 3.41 (m, 6H), 2.30 – 2.23 (m, 2H), 2.21 (s, 6H), 2.04-1.91 (m, 4H), 1.66 – 1.61 (m, 2H), 1.56 – 1.48 (m, 2H), 1.48 – 1.38 (m, 2H).

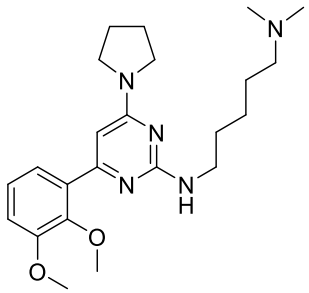

4-33

***N*^{1}-(4-(2,3-Dimethoxyphenyl)-6-(pyrrolidin-1-yl)pyrimidin-2-yl)-*N*^{5},*N*^{5}-dimethylpentane-1,5-diamine**

To a solution of **4-18** (50 mg, 0.13 mmol, 1 eq) in dry DCM (0.8 mL) and dry $CHCl_3$ (0.4 mL) at 0 °C were added Et_3N (22 μL, 0.16 mmol, 1.2 eq) and MsCl (11 μL, 0.14 mmol, 1.1 eq). The mixture was stirred at 0 °C for 3 h. The mixture was diluted in $CHCl_3$ (15 mL) and washed with a saturated solution of $NaHCO_3$ (2 x 5 mL). The organic layer was dried over Na_2SO_4, filtrated and evaporated to afford an oil residue. The residue was dissolved in THF (1 mL) and dimethylamine (2 M in MeOH, 1.55 mL, 3.10 mmol, 24 eq) was added. The reaction mixture was sealed and stirred at 80 °C for 16 h. The solvent was evaporated and the residue was purified by flash chromatography on silica (gradient DCM/ MeOH/ 2% NH_3) to afford the desired compound (10 mg, 19%). ^{1}H NMR (400 MHz, $CDCl_3$) δ 7.32 (d, *J* = 7.7 Hz, 1H), 7.10 (t, *J* = 8.0 Hz, 1H), 6.93 (d, *J* = 8.1 Hz, 1H), 6.26 (s, 1H), 4.88 (br, 1H), 3.88 (s, 3H), 3.74 (s, 3H), 3.58 – 3.35 (m, 6H), 2.30 – 2.23 (m, 2H), 2.21 (s, 6H), 2.01 – 1.91 (m, 4H), 1.67 – 1.59 (m, 2H), 1.55 – 1.46 (m, 2H), 1.45 – 1.36 (m, 2H).

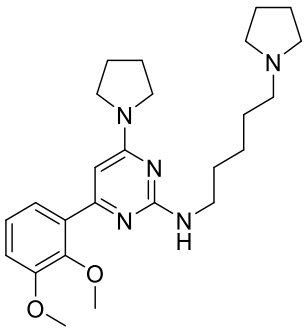

4-34

4-(2,3-Dimethoxyphenyl)-6-(pyrrolidin-1-yl)-*N*-(5-(pyrrolidin-1-yl)pentyl)pyrimidin-2-amine

To a solution of **4-18** (25 mg, 0.06 mmol, 1 eq) and in dry DCM (0.22 mL) at -78 °C were added pyridine (16 µL, 0.19 mmol, 3 eq) and TsCl (37 mg, 0.19 mmol, 3 eq). The mixture was stirred at -78 °C for 3 h and pyrrolidine (108 µL, 1.29 mmol, 20 eq) was added. The reaction mixture was stirred at -78 °C and let to warm up to room temperature over 16 h. The solvent was evaporated and the residue was purified by flash chromatography on silica (gradient DCM/ MeOH/ 2% NH_3) to afford the desired compound (6 mg, 21%). ^{1}H NMR (400 MHz, $CDCl_3$) δ 7.32 (d, *J* = 7.6 Hz, 1H), 7.10 (t, *J* = 8.0 Hz, 1H), 6.93 (dd, *J* = 8.1, 1.2 Hz, 1H), 6.26 (s, 1H), 4.97 (br, 1H), 3.89 (s, 3H), 3.75 (s, 3H), 3.57 – 3.33 (m, 6H), 2.62 – 2.53 (m, 4H), 2.53 – 2.46 (m, 2H), 2.00 – 1.92 (m, 4H), 1.84 – 1.78 (m, 4H), 1.69 – 1.56 (m, 4H), 1.48 – 1.38 (m, 2H). ^{13}C NMR (101 MHz, $CDCl_3$, DEPTQ) δ 162.18, 161.47, 153.15, 147.54, 124.23, 122.26, 112.92, 94.68, 61.32, 56.64, 56.14, 54.30, 46.34, 41.47, 30.00, 28.63, 25.43, 25.27, 23.56.

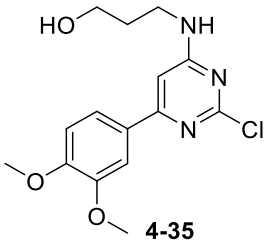

4-35

3-((2-Chloro-6-(3,4-dimethoxyphenyl)pyrimidin-4-yl)amino)propan-1-ol

In a microwave vessel, **4-4** (250 mg, 0.88 mmol, 1 eq) was dissolved in THF (2.5 mL). To the mixture was added 3-amino-1-propanol (201 µL, 2.63 mmol, 3 eq) and the reaction was carried under microwave irradiation (80 °C, 300 W, 30 min). THF was evaporated and the residue purified by flash chromatography on silica (gradient DCM/MeOH/ 2% NH_3) to afford the desired compound (132 mg, 46 %). ^{1}H NMR (400 MHz, $CDCl_3$) δ 7.57 (d, *J* = 1.5 Hz, 1H), 7.51 (dd, *J* = 8.4, 1.6 Hz, 1H), 6.91 (d, *J* = 8.4 Hz, 1H), 6.57 (s, 1H), 5.47 (br, 1H), 3.98 (s, 3H), 3.93 (s, 3H), 3.80 – 3.70 (m, 2H), 3.65 – 3.53 (m, *J* = 4.4 Hz, 2H), 1.89 – 1.80 (m, 2H).

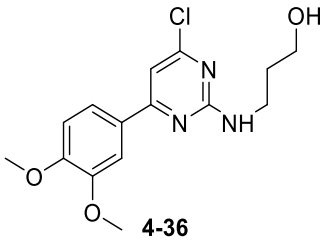

4-36

3-((4-Chloro-6-(3,4-dimethoxyphenyl)pyrimidin-2-yl)amino)propan-1-ol

Compound **4-36** was isolated with **4-35** (106 mg, 36 %). ^{1}H NMR (400 MHz, $CDCl_3$) δ 7.59 – 7.52 (m, 2H), 6.94 (s, 1H), 6.94 (d, *J* = 8.6 Hz, 1H), 5.48 (br, 1H), 3.97 (s, 3H), 3.94 (s, 3H), 3.75 – 3.64 (m, 4H), 1.86 – 1.77 (m, 2H).

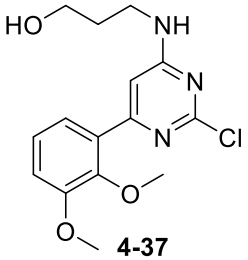

4-37

3-((2-Chloro-6-(2,3-dimethoxyphenyl)pyrimidin-4-yl)amino)propan-1-ol

In a microwave vessel, **4-10** (225 mg, 0.79 mmol, 1 eq) was dissolved in THF (2.5 mL). Then 3-amino-1-propanol (181 μL, 2.37 mmol, 3 eq) was added to the solution and the reaction was carried under microwave irradiation (80 °C, 300 W, 30 min). THF evaporated and the residue was purified by flash chromatography on silica (gradient Hexane/EtOAc, 1% MeOH,) to afford the desired compound (172 mg, 67%). ^{1}H NMR (400 MHz, $CDCl_3$) δ 7.44 (dd, *J* = 7.9, 1.2 Hz, 1H), 7.14 (t, *J* = 8.0 Hz, 1H), 7.00 (dd, *J* = 8.1, 1.0 Hz, 1H), 6.94 (s, 1H), 5.54 (br, 1H), 3.90 (s, 3H), 3.78 – 3.71 (m, 5H), 3.67 – 3.44 (m, 2H), 1.89 – 1.78 (m, 2H).

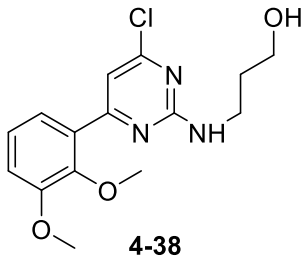

4-38

3-((4-Chloro-6-(2,3-dimethoxyphenyl)pyrimidin-2-yl)amino)propan-1-ol

Compound **4-38** was isolated with **4-37** (62 mg, 24%). ^{1}H NMR (400 MHz, $CDCl_3$) δ 7.35 (d, *J* = 7.5 Hz, 1H), 7.16 (s, 1H), 7.13 (d, *J* = 8.0 Hz, 1H), 7.02 (d, *J* = 8.1 Hz, 1H), 5.55 (br, 1H), 3.90 (s, 3H), 3.78 (s, 3H), 3.70 – 3.59 (m, 4H), 1.87 – 1.75 (m, 2H).

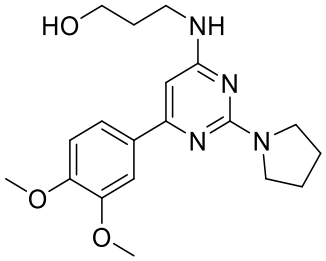

4-39

3-((6-(3,4-Dimethoxyphenyl)-2-(pyrrolidin-1-yl)pyrimidin-4-yl)amino)propan-1-ol

In a microwave vessel, **4-35** (120 mg, 0.37 mmol, 1 eq) was dissolved in THF (1.2 mL). Pyrrolidine (155 μL, 1.85 mmol, 5 eq) was added to the solution and the reaction was carried under microwave irradiation (120 °C, 300 W, 30 min). THF was evaporated and the residue purified by flash chromatography on silica (gradient Hexane/EtOAc/ 1% MeOH additive) to afford the desired compound (101 mg, 76 %). ^{1}H NMR (400 MHz, $CDCl_3$) δ 7.65 (d, *J* = 1.5 Hz, 1H), 7.53 (dd, *J* = 8.4, 1.7 Hz, 1H), 6.90 (d, *J* = 8.4 Hz, 1H), 6.03 (s, 1H), 4.61 (br, 1H), 3.96 (s, 3H), 3.92 (s, 3H), 3.73 – 3.57 (m, 8H), 1.99 – 1.91 (m, 4H), 1.80 – 1.70 (m, 2H).

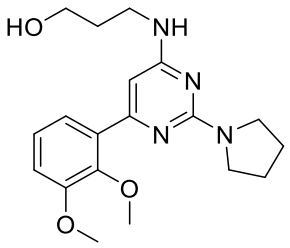

4-40

3-((6-(2,3-Dimethoxyphenyl)-2-(pyrrolidin-1-yl)pyrimidin-4-yl)amino)propan-1-ol

In a microwave vessel, **4-37** (160 mg, 0.49 mmol, 1 eq) was dissolved in THF (1.6 mL). Pyrrolidine (206 μL, 0.77 mmol, 5 eq) was added to the solution and the reaction was carried under microwave irradiation (120 °C, 300 W, 30 min). THF was evaporated and the residue purified by flash chromatography on silica (gradient Hexane/EtOAc/1% MeOH additive) to afford the desired compound (140 mg, 79 %)**.** ^{1}H NMR (400 MHz, $CDCl_3$) δ 7.44 (d, *J* = 7.8 Hz, 1H), 7.10 (t, *J* = 8.0 Hz, 1H), 6.94 (d, *J* = 8.1 Hz, 1H), 6.28 (s, 1H), 4.62 (br, 1H), 3.89 (s, 3H), 3.77 (s, 3H), 3.69 – 3.59 (m, 8H), 1.99 – 1.89 (m, 4H), 1.79 – 1.68 (m, 2H).

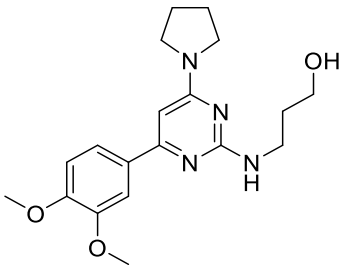

4-41

3-((4-(3,4-Dimethoxyphenyl)-6-(pyrrolidin-1-yl)pyrimidin-2-yl)amino)propan-1-ol

In a microwave vessel, **4-36** (85 mg, 0.26 mmol, 1 eq) was dissolved in THF (1 mL). Pyrrolidine (110 μL, 1.31 mmol, 5 eq) was added to the solution and the reaction was carried under microwave irradiation (120 °C, 300 W, 30 min). THF was evaporated and the residue purified by flash chromatography on silica (gradient Hexane/EtOAc/ 1% MeOH additive) to afford the desired compound (32 mg, 34 %). ^{1}H NMR (400 MHz, $CDCl_3$) δ 7.51 (s, 1H), 7.47 (dd, *J* = 8.4, 2.0 Hz, 1H), 6.91 (d, *J* = 8.4 Hz, 1H), 6.03 (s, 1H), 4.98 (s, 1H), 3.96 (s, 3H), 3.91 (s, 3H), 3.68 (q, *J* = 6.9 Hz, 2H), 3.65 – 3.60 (m, 2H), 3.52 (br, 2H), 2.04 – 1.94 (m, 4H), 1.75 – 1.68 (m, 2H), 1.68 – 1.57 (m, 2H).

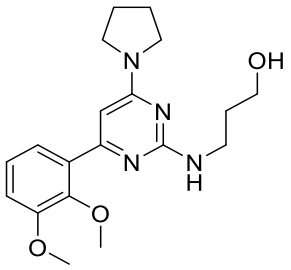

4-42

3-((4-(2,3-Dimethoxyphenyl)-6-(pyrrolidin-1-yl)pyrimidin-2-yl)amino)propan-1-ol

In a microwave vessel, **4-38** (58 mg, 0.18 mmol, 1 eq) was dissolved in THF (0.5 mL). Pyrrolidine (75 μL, 0.90 mmol, 5 eq) was added to the solution and the reaction was carried under microwave irradiation (120 °C, 300 W, 30 min). THF was evaporated and the residue purified by flash chromatography on silica (gradient Hexane/EtOAc/ 1% MeOH additive) to afford the desired compound (60 mg, 93 %). ^{1}H NMR (400 MHz, $CDCl_3$) δ 7.44 (d, *J* = 7.9 Hz, 1H), 7.10 (t, *J* = 8.0 Hz, 1H), 6.94 (d, *J* = 8.0 Hz, 1H), 6.28 (s, 1H), 4.61 (br, 1H), 3.89 (s, 3H), 3.78 (s, 3H), 3.69 – 3.59 (m, 8H), 2.00 – 1.87 (m, 4H), 1.80 – 1.69 (m, 2H).

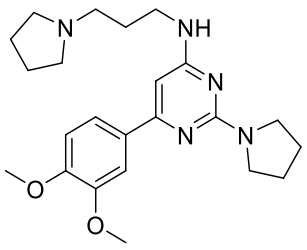

4-43

6-(3,4-Dimethoxyphenyl)-2-(pyrrolidin-1-yl)-*N*-(3-(pyrrolidin-1-yl)propyl)pyrimidin-4-amine

To a solution of **4-39** (40 mg, 0.11 mmol, 1 eq) in dry DCM (0.7 mL) and dry $CHCl_3$ (0.3 mL) under N_2 atmosphere at 0 °C were added Et_3N (19 μL, 0.13 mmol, 1.2 eq) and MsCl (10 μL, 0.12 mmol, 1.1 eq). The mixture was stirred at 0 °C for 3 h. The mixture was diluted in $CHCl_3$ (15 mL) and washed with a saturated solution of $NaHCO_3$ (2 x 5 mL). The organic layer was dried over Na_2SO_4, filtrated and evaporated. The residue was dissolved in THF (1 mL) and pyrrolidine (93 μL, 1.12 mmol, 10 eq) was added. The reaction mixture was stirred at 80 °C for 16 h. The solvent was evaporated and the residue was purified by flash chromatography on silica (gradient DCM/ MeOH/ 2% NH_3) to afford the desired compound (28 mg, 61 %). ^{1}H NMR (400 MHz, $CDCl_3$) δ 7.67 (d, *J* = 1.6 Hz, 1H), 7.54 (dd, *J* = 8.4, 1.7 Hz, 1H), 6.90 (d, *J* = 8.4 Hz, 1H), 6.03 (s, 1H), 5.31 (s, 1H), 3.96 (s, 3H), 3.92 (s, 3H), 3.66 – 3.57 (m, 4H), 3.51 – 3.41 (m, 2H), 2.62 (t, *J* = 6.9 Hz, 2H), 2.59 – 2.51 (m, 4H), 1.97 – 1.92 (m, 4H), 1.89 – 1.78 (m, 6H). ^{13}C NMR (101 MHz, $CDCl_3$, DEPTQ) δ 164.11,

162.94, 160.98, 150.42, 148.97, 132.27, 119.63, 110.91, 110.21, 88.22, 56.09, 56.02, 54.39, 54.16, 46.53, 40.09, 28.19, 25.73, 23.60.

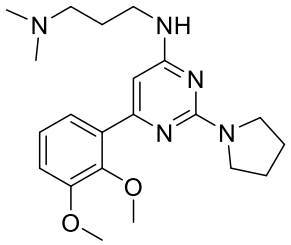

4-44

N^1-(6-(2,3-dimethoxyphenyl)-2-(pyrrolidin-1-yl)pyrimidin-4-yl)-N^3,N^3-dimethylpropane-1,3-diamine

To a solution of **4-40** (60 mg, 0.17 mmol, 1 eq) in dry DCM (1 mL) and dry $CHCl_3$ (0.5 mL) under N_2 atmosphere at 0 °C were added Et_3N (28 µL, 0.20 mmol, 1.2 eq) and MsCl (10 µL, 0.12 mmol, 1.1 eq). The mixture was stirred at 0 °C for 3h. The mixture was diluted in $CHCl_3$ (15 mL) and washed with a saturated solution of $NaHCO_3$ (2 x 5 mL). The organic layer was dried over Na_2SO_4, filtrated and evaporated. To the residue was added dimethylamine (2 M in THF, 1.65 mL, 3.3 mmol, 20 eq). The reaction mixture was stirred at 80 °C for 16 h. The solvent was evaporated and the residue was purified by flash chromatography on silica (gradient DCM/ MeOH/ 2% NH_3) to afford the desired compound (29 mg, 45 %). ^{1}H NMR (400 MHz, $CDCl_3$) δ 7.42 (dd, *J* = 7.9, 1.4 Hz, 1H), 7.10 (t, *J* = 8.0 Hz, 1H), 6.93 (dd, *J* = 8.1, 1.3 Hz, 1H), 6.27 (s, 1H), 5.22 (s, 1H), 3.89 (s, 3H), 3.77 (s, 3H), 3.66 – 3.55 (m, 4H), 3.48 – 3.34 (m, 2H), 2.38 (t, *J* = 6.9 Hz, 2H), 2.23 (s, 6H), 1.96 – 1.91 (m, 4H), 1.81 – 1.72 (m, 2H). ^{13}C NMR (101 MHz, $CDCl_3$, DEPTQ) δ 163.78, 160.91, 153.24, 147.82, 134.57, 124.17, 122.51, 112.86, 61.30, 58.13, 56.16, 46.62, 45.67, 40.42, 27.39, 25.74.

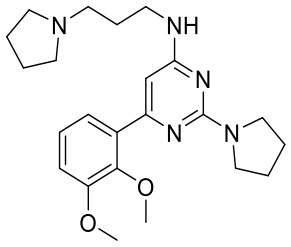

4-45

6-(2,3-Dimethoxyphenyl)-2-(pyrrolidin-1-yl)-*N*-(3-(pyrrolidin-1-yl)propyl)pyrimidin-4-amine

To a solution of **4-40** (60 mg, 0.17 mmol, 1 eq) in dry DCM (1 mL) and dry $CHCl_3$ (0.5 mL) under N_2 atmosphere at 0 °C were added Et_3N (28 µL, 0.20 mmol, 1.2 eq) and MsCl (14 µL, 0.18

mmol, 1.1 eq). The mixture was stirred at 0 °C for 3 h. The mixture was diluted in $CHCl_3$ (15 mL) and washed with a saturated solution of $NaHCO_3$ (2 x 5 mL). The organic layer was dried over Na_2SO_4, filtrated and evaporated. The residue was dissolved in THF (1 mL) and pyrrolidine (140 µL, 1.67 mmol, 10 eq) was added. The reaction mixture was stirred at 80 °C for 16 h. The solvent was evaporated and the residue was purified by flash chromatography on silica (gradient DCM/ MeOH/ 2% NH_3) to afford the desired compound (46 mg, 67 %). ^{1}H NMR (400 MHz, $CDCl_3$) δ 7.42 (dd, *J* = 7.9, 1.4 Hz, 1H), 7.10 (t, *J* = 8.0 Hz, 1H), 6.93 (dd, *J* = 8.1, 1.1 Hz, 1H), 6.26 (s, 1H), 5.36 (br, 1H), 3.89 (s, 3H), 3.77 (s, 3H), 3.63 – 3.56 (m, 4H), 3.50 – 3.37 (m, 2H), 2.66 – 2.50 (m, 6H), 1.96 – 1.90 (m, 4H), 1.86 – 1.77 (m, 6H). ^{13}C NMR (101 MHz, $CDCl_3$, DEPTQ) δ 163.60, 160.68, 153.14, 147.66, 134.39, 124.08, 122.39, 112.84, 92.57, 61.24, 56.08, 54.21, 53.99, 46.56, 27.69, 25.64, 23.49.

Bibliography

1. Aristotle. *On The Generation Of Animals - 350 BC*.

2. Ganesan, A. Epigenetics: The first 25 centuries. *Philos. Trans. R. Soc. B Biol. Sci.* **373**, 2–5 (2018).

3. Gayon, J. From Mendel to epigenetics: History of genetics. *C. R. Biol.* **339**, 225–230 (2016).

4. Avery, O. T., MacLeod, C. M. & Mccarty, M. Studies on the chemical nature of the substance inducing transformation of pneumococcal types: Induction of transformation by a desoxyribonucleic acid fraction isolated from pneumococcus type III. *J. Exp. Med.* **79**, 137–158 (1944).

5. Watson, J. & Crick, F. Molecular structure of nucleic acids. *Nature.* **171**, 737–738 (1953).

6. Crick, F. Central dogma of molecular biology. *Nature* **227**, 561–563 (1970).

7. Waddington, C. H. The epigenotype. 1942. *Int. J. Epidemiol.* **41**, 10–13 (2012).

8. Goldberg, A. D., Allis, C. D. & Bernstein, E. Epigenetics: A Landscape Takes Shape. *Cell* **128**, 635–638 (2007).

9. Portela, A. & Esteller, M. Epigenetic modifications and human disease. *Nat. Biotechnol.* **28**, 1057–1068 (2010).

10. *Epigenetics in Human Disease*. (Elsevier, 2012). doi:10.1016/C2011-0-69819-9

11. Zoghbi, H. Y. & Beadet, A. L. Epigenetics and Human Disease. *Cold Spring Harb Perspect Biol* **8**, a019497 (2016).

12. Kossel, A. Ueber die chemische Beschaffenheit des Zellkerns. *Munchen Med. Wochenschrift* **58**, 65–69 (1911).

13. Olins, A. L. & Olins, D. E. Spheroid Chromatin Units. *Science (80-.).* **183**, 330–332 (1974).

14. Kornberg, R. D. & Thomas, J. O. Chromatin Structure : Oligomers of the Histones. *Science (80-.).* **184**, 865–868 (1973).

15. Kornberg, R. D. Chromatin Structure : A Repeating Unit of Histones and DNA. *Science (80-.).* **184**, 868–871 (1974).

16. Oudet, P., Gross-Bellard, M. & Chambon, P. Electron Microscopic and Biochemical

Evidence that Chromatin Structure Is a Repeating Unit. *Cell* **4**, 281–300 (1975).

17. Richmond, T. J., Finch, J. T., Rushton, B., Rhodes, D. & Klug, A. Structure of the nucleosome core particle at 7 Å resolution. *Nature* **311**, 532–537 (1984).

18. Luger, K., Mäder, A. W., Richmond, R. K., Sargent, D. F. & Richmond, T. J. Crystal structure of the nucleosome core particle at 2.8 Å resolution. *Nature* **389**, 251–260 (1997).

19. Stryer, L. *Biochemistry (4th edition)*. (W.H. Freeman & Company, 1995).

20. Heitz, E. Das heterochromatin der Moose. *Jahrb Wiss Bot.* **69**, 762–818 (1928).

21. Passarge, E. Emil Heitz and the concept of heterochromatin: longitudinal chromosome differentiation was recognized fifty years ago. *Am. J. Hum. Genet.* **31**, 106–115 (1979).

22. Arrowsmith, C. H., Bountra, C., Fish, P. V, Lee, K. & Schapira, M. Epigenetic protein families: a new frontier for drug discovery. *Nat. Rev. Drug Discov.* **11**, 384–400 (2012).

23. Hotchkiss, R. D. The quantitative separation of purines, pyrimidines and nucleosides by paper chromatography. *J .biol. chem.* **175**, 315–332 (1948).

24. Vanyushin, B. F., Tkacheva, S. G. & Belozersky, A. N. Rare bases in animal DNA. *Nature* **225**, 948–949 (1970).

25. Holliday, R. & Pugh, J. E. DNA modification mechanisms and gene activity during development. *Science (80-.).* **187**, 226–232 (1975).

26. Razin, A. & Riggs, A. D. DNA methylation and gene function. *Science* **210**, 604–610 (1980).

27. Cooper, D. N. & Krawczak, M. Cytosine methylation and the fate of CpG dinucleotides in vertebrate genomes. *Hum. Genet.* **83**, 181–188 (1989).

28. Bird, A. The essentials of DNA methylation. *Cell* **70**, 5–8 (1992).

29. Goll, M. G. *et al.* Methylation of tRNAAsp by the DNA methyltransferase homolog Dnmt2. *Science (80-.).* **311**, 395–398 (2006).

30. Robertson, K. D. *et al.* The human DNA methyltransferases (DNMTs) 1, 3a and 3b: Coordinate mRNA expression in normal tissues and overexpression in tumors. *Nucleic Acids Res.* **27**, 2291–2298 (1999).

31. Hirasawa, R. *et al.* Maternal and zygotic Dnmt1 are necessary and sufficient for the maintenance of DNA methylation imprints during preimplantation development. *Genes*

Dev. **22**, 1607–1616 (2008).

32. Okano, M., Xie, S. & Li, E. Cloning and characterization of a family of novel mammalian DNA (cytosine-5) methyltransferases. *Nat. Genet.* **19**, 219–220 (1998).

33. Okano, M., Bell, D. W., Haber, D. A. & Li, E. DNA methyltransferases Dnmt3a and Dnmt3b are essential for de novo methylation and mammalian development. *Cell* **99**, 247–257 (1999).

34. Li, E. Chromatin modification and epigenetic reprogramming in mammalian development. *Nat. Rev. Genet.* **3**, 662–673 (2002).

35. Gowher, H., Liebert, K., Hermann, A., Xu, G. & Jeltsch, A. Mechanism of stimulation of catalytic activity of Dnmt3A and Dnmt3B DNA-(cytosine-C5)-methyltransferases by Dnmt3L. *J. Biol. Chem.* **280**, 13341–13348 (2005).

36. Vertino, P. M., Yen, R. W., Gao, J. & Baylin, S. B. De novo methylation of CpG island sequences in human fibroblasts overexpressing DNA (cytosine-5-)-methyltransferase. *Mol. Cell. Biol.* **16**, 4555–4565 (1996).

37. Egger, G. *et al.* Identification of DNMT1 (DNA methyltransferase 1) hypomorphs in somatic knockouts suggests an essential role for DNMT1 in cell survival. *Proc. Natl. Acad. Sci.* **103**, 14080–14085 (2006).

38. Chen, T., Ueda, Y., Dodge, J. E., Wang, Z. & Li, E. Establishment and Maintenance of Genomic Methylation Patterns in Mouse Embryonic Stem Cells by Dnmt3a and Establishment and Maintenance of Genomic Methylation Patterns in Mouse Embryonic Stem Cells by Dnmt3a and Dnmt3b. *Mol. Cell. Biol.* **23**, 5594–5605 (2003).

39. Riggs, A. D. & Xiong, Z. Methylation and epigenetic fidelity. *Proc. Natl. Acad. Sci.* **101**, 4–5 (2004).

40. Rhee, I. *et al.* CpG methylation is maintained in human cancer cells lacking DNMT1. *Nature* **404**, 1003–1007 (2000).

41. Smith, Z. D. & Meissner, A. DNA methylation: Roles in mammalian development. *Nat. Rev. Genet.* **14**, 204–220 (2013).

42. Lyko, F. The DNA methyltransferase family: A versatile toolkit for epigenetic regulation. *Nat. Rev. Genet.* **19**, 81–92 (2018).

43. Li, E., Beard, C. & Jaenisch, R. Role for DNA methylation in genomic imprinting. *Nature* **366**, 362–365 (1993).

44. Al-Mahdawi, S., Anjomani Virmouni, S. & Pook, M. A. DNA Methylation in Neurodegenerative Diseases. in *Epigenetic Biomarkers and Diagnostics* (ed. García-Giménez, J. L.) 401–415 (Elsevier, 2015). doi:10.1016/B978-0-12-801899-6.00020-6

45. Robertson, K. D. DNA methylation and human disease. *Nat. Rev. Genet.* **6**, 597–610 (2005).

46. Kulis, M. & Esteller, M. DNA Methylation and Cancer. *Adv. Genet.* **70**, 27–56 (2010).

47. Allfrey, G., Faulkner, R. & Mirsky, A. E. Acetylation and methylation of histones and their possible role in the regulation of RNA synthesis. *Proc. Natl. Acad. Sci. U. S. A.* **315**, 786–794 (1964).

48. Fischer, E. H., Graves, D. J., Snyder Crittenden, E. R. & Krebs, E. G. Structure of the Site Phosphorylated Phosphorylase b to a Reaction. *J. Biol. Chem.* **234**, 1698–1705 (1959).

49. Phillips, D. M. P. The Presence of Acetyl Groups in Histones. *Biochem. J.* **87**, 258–263 (1963).

50. Verdin, E. & Ott, M. 50 years of protein acetylation: From gene regulation to epigenetics, metabolism and beyond. *Nat. Rev. Mol. Cell Biol.* **16**, 258–264 (2015).

51. Marmorstein, R. & Trievel, R. C. Histone modifying enzymes: Structures, mechanisms, and specificities. *Biochim. Biophys. Acta* **1789**, 58–68 (2009).

52. Liu, W. R., Wang, Y. & Wan, W. Synthesis of proteins with defined posttranslational modifications using the genetic noncanonical amino acid incorporation approach. *Mol. Biosyst.* **7**, 38–47 (2011).

53. Falkenberg, K. J. & Johnstone, R. W. Histone deacetylases and their inhibitors in cancer, neurological diseases and immune disorders. *Nat. Rev. Drug Discov.* **13**, 673–691 (2014).

54. Brownell, J. E. *et al.* Tetrahymena Histone Acetyltransferase A : A Homolog to Yeast Gcn5p Linking Histone Acetylation to Gene Activation. *Cell* **84**, 843–851 (1996).

55. Glozak, M. A., Sengupta, N., Zhang, X. & Seto, E. Acetylation and deacetylation of non-histone proteins. *Gene* **363**, 15–23 (2005).

56. Rea, S. *et al.* Regulation of chromatin structure by site-specific histone H3 methyltransferases. *Nature* **406**, 593–599 (2000).

57. Kwon, T. *et al.* Mechanism of histone lysine methyl transfer revealed by the structure of SET7/9-AdoMet. *EMBO J.* **22**, 292–303 (2003).

58. Bernstein, B. E. *et al.* A Bivalent Chromatin Structure Marks Key Developmental Genes in Embryonic Stem Cells. *Cell* **125**, 315–326 (2006).

59. Morera, L., Lübbert, M. & Jung, M. Targeting histone methyltransferases and demethylases in clinical trials for cancer therapy. *Clin. Epigenetics* **8**, 1–16 (2016).

60. Black, J. C., Rechem, C. Van & Whetstine, J. R. Review Histone Lysine Methylation Dynamics : Establishment , Regulation , and Biological Impact. *Mol. Cell* **48**, 491–507 (2012).

61. Klose, R. J. & Zhang, Y. Regulation of histone methylation by demethylimination and demethylation. *Nat. Rev. Mol. Cell Biol.* **8**, 307–318 (2007).

62. Yun, M., Wu, J., Workman, J. L. & Li, B. Readers of histone modifications. *Cell Res.* **21**, 564–578 (2011).

63. Tamkun, J. W. *et al.* brahma : A Regulator of Drosophila Homeotic Genes Structurally Related to the Yeast Transcriptional Activator SNF2BWl2. *Cell* **68**, 561–572 (1992).

64. Haynes, S. R. *et al.* The bromodomain: a conserved sequence found in human,Drosophilaand yeast proteins. *Nucleic Acids Res.* **20**, 2603 (1992).

65. Dhalluin, C. *et al.* Structure and ligand of a histone acetyltransferase bromodomain. *Nature* **399**, 491–496 (1999).

66. Dawson, M. A. *et al.* Inhibition of BET recruitment to chromatin as an effective treatment for MLL-fusion leukaemia. *Nature* **478**, 529–533 (2011).

67. Filippakopoulos, P. & Knapp, S. Targeting bromodomains: epigenetic readers of lysine acetylation. *Nat. Rev. Drug Discov.* **13**, 337–356 (2014).

68. Filippakopoulos, P. *et al.* Selective inhibition of BET bromodomains. *Nature* **468**, 1067–1073 (2010).

69. Doroshow, D. B., Eder, J. P. & Lorusso, P. M. BET inhibitors : a novel epigenetic approach. *Ann. Oncol.* **2**, 1776–1787 (2017).

70. Bannister, A. J., Schneider, R. & Kouzarides, T. Histone Methylation : Dynamic or Static ? *Cell* **109**, 801–806 (2002).

71. Shi, Y. *et al.* Histone Demethylation Mediated by the Nuclear Amine Oxidase Homolog LSD1. *Cell* **119**, 941–953 (2004).

72. Hauser, A. *et al.* Discovery of histone demethylase inhibitors. in *Epigenetic Technological*

Applications (ed. Zheng, Y. G.) 397–424 (Elsevier, 2015). doi:10.1016/B978-0-12-801080-8.00018-1

73. Ciccone, D. N. *et al.* KDM1B is a histone H3K4 demethylase required to establish maternal genomic imprints. *Nature* **461**, 415–419 (2009).

74. Tsukada, Y. *et al.* Histone demethylation by a family of JmjC domain-containing proteins. *Nature* **439**, 811–816 (2006).

75. Thinnes, C. C. *et al.* Targeting histone lysine demethylases — Progress , challenges , and the future. *Biochim. Biophys. Acta* **1839**, 1416–1432 (2014).

76. Maes, T. *et al.* KDM1 histone lysine demethylases as targets for treatments of oncological and neurodegenerative disease. *Epigenomics* **7**, 609–626 (2015).

77. Pedersen, M. T. & Helin, K. Histone demethylases in development and disease. *Trends Cell Biol.* **20**, 662–671 (2010).

78. McAllister, T. E. *et al.* Recent Progress in Histone Demethylase Inhibitors. *J. Med. Chem.* **59**, 1308–1329 (2016).

79. Suzuki, T. *et al.* Identification of the KDM2/7 Histone Lysine Demethylase Subfamily Inhibitor and its Antiproliferative Activity. *J. Med. Chem.* **56**, 7222–7231 (2013).

80. Maes, T., Carceller, E., Salas, J., Ortega, A. & Buesa, C. Advances in the development of histone lysine demethylase inhibitors. *Curr. Opin. Pharmacol.* **23**, 52–60 (2015).

81. Inoue, A. & Fujimoto, D. Enzymatic deacetylation of histone. *Biochem. Biophys. Res. Commun.* **36**, 146–150 (1969).

82. Taunton, J., Hassig, C. A. & Schreiber, S. L. A Mammalian Histone Deacetylase Related to the Yeast Transcriptional Regulator Rpd3p. *Science (80-.).* **272**, 408–411 (1996).

83. Seto, E. & Yoshida, M. Erasers of Histone Acetylation : The Histone Deacetylase Enzymes. *Cold Spring Harb. Perspect. Biol.* **6**, a018713 (2014).

84. Sauve, A. A. Sirtuin Chemical Mechanisms. *Biochem. Biophys Acta.* **1804**, 1591–1603 (2010).

85. Karagiannis, T. C. & Ververis, K. Potential of chromatin modifying compounds for the treatment of Alzheimer's disease. *Pathobiol. Aging Age-related Dis.* **2**, 14980 (2012).

86. Vaziri, H. *et al.* hSIR2(SIRT1) functions as an NAD-dependent p53 deacetylase. *Cell* **107**, 149–159 (2001).

87. Milne, J. C. & Denu, J. M. The Sirtuin family: therapeutic targets to treat diseases of aging. *Curr. Opin. Chem. Biol.* **12**, 11–17 (2008).

88. Milne, J. C. *et al.* Small molecule activators of SIRT1 as therapeutics for the treatment of type 2 diabetes. *Nature* **450**, 712–716 (2007).

89. Cencioni, C. *et al.* Sirtuin function in aging heart and vessels. *Journal of Molecular and Cellular Cardiology* **83**, 55–61 (2015).

90. Rizzi, L. & Roriz-Cruz, M. Sirtuin 1 and Alzheimer's disease: An up-to-date review. *Neuropeptides* **71**, 54–60 (2018).

91. Zhou, Z., Ma, T., Zhu, Q., Xu, Y. & Zha, X. Recent advances in inhibitors of sirtuin1/2 : an update and perspective. *Future Med. Chem.* **10**, 907–934 (2018).

92. Finnin, M. S. *et al.* Structures of a histone deacetylase homologue bound to the TSA and SAHA inhibitors. *Nature* **401**, 188–193 (1999).

93. Yang, X. J. & Seto, E. Collaborative spirit of histone deacetylases in regulating chromatin structure and gene expression. *Curr. Opin. Genet. Dev.* **13**, 143–153 (2003).

94. Dokmanovic, M., Clarke, C. & Marks, P. A. Histone Deacetylase Inhibitors: Overview and Perspectives. *Mol. Cancer Res.* **5**, 981–989 (2007).

95. Mai, A., Rotili, D., Valente, S. & Kazantsev, A. Histone Deacetylase Inhibitors and Neurodegenerative Disorders: Holding the Promise. *Curr. Pharm. Des.* **15**, 3940–3957 (2009).

96. Hubbert, C., Guardiola, A. & Shao, R. HDAC6 is microtubule-associated deacetylase. *Nature* **417**, 455–458 (2002).

97. Kawaguchi, Y. *et al.* The deacetylase HDAC6 regulates aggresome formation and cell viability in response to misfolded protein stress. *Cell* **115**, 727–738 (2003).

98. Tran, A. D.-A. *et al.* HDAC6 deacetylation of tubulin modulates dynamics of cellular adhesions. *J. Cell Sci.* **120**, 1469–1479 (2007).

99. Yanginlar, C. & Logie, C. HDAC11 is a regulator of diverse immune functions. *Biochimica et Biophysica Acta - Gene Regulatory Mechanisms* **1861**, 54–59 (2018).

100. Yoshida, M., Horinouchi, S. & Beppu, T. Trichostatin A and trapoxin: novel chemical probes for the role of histone acetylation in chromatin structure and function. *BioEssays* **17**, 423–430 (1995).

101. Richon, V. M. *et al.* Second generation hybrid polar compounds are potent inducers of transformed cell differentiation. *Proc. Natl. Acad. Sci.* **93**, 5705–5708 (1996).

102. Richon, V. M. *et al.* A class of hybrid polar inducers of transformed cell differentiation inhibits histone deacetylases. *Proc. Natl. Acad. Sci.* **95**, 3003–3007 (1998).

103. Qin, H., Li, H. & Liu, F. Selective histone deacetylase small molecule inhibitors: recent progress and perspectives. *Expert Opin. Ther. Pat.* **27**, 621–636 (2017).

104. Roche, J. & Bertrand, P. Inside HDACs with more selective HDAC inhibitors. *Eur. J. Med. Chem.* **121**, 451–483 (2016).

105. Zhang, L., Zhang, J., Jiang, Q., Zhang, L. & Song, W. Zinc binding groups for histone deacetylase inhibitors. *J. Enzyme Inhib. Med. Chem.* **33**, 714–721 (2018).

106. Milite, C. *et al.* The emerging role of lysine methyltransferase SETD8 in human diseases. *Clin. Epigenetics* **8**, 102–117 (2016).

107. Patnaik, D. *et al.* Substrate specificity and kinetic mechanism of mammalian G9a histone H3 methyltransferase. *J. Biol. Chem.* **279**, 53248–53258 (2004).

108. Chin, H. G., Patnaik, D., Estève, P. O., Jacobsen, S. E. & Pradhan, S. Catalytic properties and kinetic mechanism of human recombinant Lys-9 histone H3 methyltransferase SUV39H1: Participation of the chromodomain in enzymatic catalysis. *Biochemistry* **45**, 3272–3284 (2006).

109. Wu, S. & Rice, J. C. A new regulator of the cell cycle: The PR-Set7 histone methyltransferase. *Cell Cycle* **10**, 68–72 (2011).

110. Jørgensen, S., Schotta, G. & Sørensen, C. S. Histone H4 Lysine 20 methylation: Key player in epigenetic regulation of genomic integrity. *Nucleic Acids Res.* **41**, 2797–2806 (2013).

111. Nishioka, K. *et al.* PR-Set7 Is a Nucleosome-Specific Methyltransferase that Modifies Lysine 20 of Histone H4 and Is Associated with Silent Chromatin. *Mol. Cell* **9**, 1201–1213 (2002).

112. Girish, T. S., McGinty, R. K. & Tan, S. Multivalent Interactions by the Set8 Histone Methyltransferase With Its Nucleosome Substrate. *J. Mol. Biol.* **428**, 1531–1543 (2016).

113. Bartel, D. P. MicroRNAs: Target Recognition and Regulatory Functions. *Cell* **136**, 215–233 (2009).

114. Behm-Ansmant, I., Rehwhinkel, J. & Izaurralde, E. MicroRNAs Silence Gene Expression by Repressing Protein Expression and/or by Promoting mRNA Decay. *Cold Spring Harb. Symp. Quant. Biol.* **71**, 523–530 (2006).

115. Song, F. *et al.* An miR-502-binding site single-nucleotide polymorphism in the 3′-untranslated region of the SET8 gene is associated with early age of breast cancer onset. *Clin. Cancer Res.* **15**, 6292–6300 (2009).

116. Wang, C., Guo, Z., Wu, C., Li, Y. & Kang, S. A polymorphism at the miR-502 binding site in the 3' untranslated region of the SET8 gene is associated with the risk of epithelial ovarian cancer. *Cancer Genet.* **205**, 373–376 (2012).

117. Ding, C., Li, R., Peng, J., Li, S. & Guo, Z. A polymorphism at the miR-502 binding site in the 3′ untranslated region of the SET8 gene is associated with the outcome of small-cell lung cancer. *Exp. Ther. Med.* **3**, 689–692 (2012).

118. Guo, Z. *et al.* A polymorphism at the miR-502 binding site in the 3'-untranslated region of the histone methyltransferase SET8 is associated with hepatocellular carcinoma outcome. *Int. J. Cancer* **131**, 1318–22 (2012).

119. Takawa, M. *et al.* Histone lysine methyltransferase setd8 promotes carcinogenesis by deregulating PCNA expression. *Cancer Res.* **72**, 3217–3227 (2012).

120. Zhang, J. *et al.* MicroRNA-127-3p inhibits proliferation and invasion by targeting SETD8 in human osteosarcoma cells. *Biochem. Biophys. Res. Commun.* **469**, 1006–1011 (2016).

121. Ma, Z. Downregulation of SETD8 by miR-382 is involved in glioma progression. *Pathol. Res. Pract.* **214**, 356–360 (2018).

122. Chen, T. *et al.* miR-382 inhibits tumor progression by targeting SETD8 in non-small cell lung cancer. *Biomed. Pharmacother.* **86**, 248–253 (2017).

123. Yu, N. *et al.* MicroRNA-7 suppresses the invasive potential of breast cancer cells and sensitizes cells to DNA damages by targeting histone methyltransferase SET8. *J. Biol. Chem.* **288**, 19633–19642 (2013).

124. Jackson, S. P. & Bartek, J. The DNA-damage response in human biology and disease. *Nature* **461**, 1071–1078 (2009).

125. Taverna, S. D., Li, H., Ruthenburg, A. J., Allis, C. D. & Patel, D. J. How chromatin-binding modules interpret histone modifications: Lessons from professional pocket pickers. *Nat. Struct. Mol. Biol.* **14**, 1025–1040 (2007).

126. Paulsen, R. D. *et al.* Processes and Pathways that Mediate Genome Stability. *Mol. Cell* **35**, 228–239 (2009).

127. Oda, H. *et al.* Monomethylation of Histone H4-Lysine 20 Is Involved in Chromosome Structure and Stability and Is Essential for Mouse Development. *Mol. Cell. Biol.* **29**, 2278–2295 (2009).

128. Beck, D. B., Oda, H., Shen, S. S. & Reinberg, D. PR-Set7 and H4K20me1: at the crossroads of genome integrity, cell cycle, chromosome condensation, and transcription. *Genes Dev.* **26**, 325–337 (2012).

129. Botuyan, M. V. *et al.* Structural Basis for the Methylation State-Specific Recognition of Histone H4-K20 by 53BP1 and Crb2 in DNA Repair. *Cell* **127**, 1361–1373 (2006).

130. Dulev, S., Tkach, J., Lin, S. & Batada, N. N. SET8 methyltransferase activity during the DNA double-strand break response is required for recruitment of 53BP1. *EMBO Rep.* **15**, 1163–1174 (2014).

131. Laptenko, O. & Prives, C. Transcriptional regulation by p53: One protein, many possibilities. *Cell Death Differ.* **13**, 951–961 (2006).

132. Toledo, F. & Wahl, G. M. Regulating the p53 pathway: In vitro hypotheses, in vivo veritas. *Nat. Rev. Cancer* **6**, 909–923 (2006).

133. Shi, X. *et al.* Modulation of p53 Function by SET8-Mediated Methylation at Lysine 382. *Mol. Cell* **27**, 636–646 (2007).

134. Veschi, V. *et al.* Epigenetic siRNA and Chemical Screens Identify SETD8 Inhibition as a Therapeutic Strategy for p53 Activation in High-Risk Neuroblastoma. *Cancer Cell* **31**, 50–63 (2017).

135. Karaczyn, A. *et al.* Two novel human NUMB isoforms provide a potential link between development and cancer. *Neural Dev.* **5**, 31–46 (2010).

136. Pece, S., Confalonieri, S., R. Romano, P. & Di Fiore, P. P. NUMB-ing down cancer by more than just a NOTCH. *Biochim. Biophys. Acta - Rev. Cancer* **1815**, 26–43 (2011).

137. Dhami, G. K. *et al.* Dynamic Methylation of Numb by Set8 Regulates Its Binding to p53 and Apoptosis. *Mol. Cell* **50**, 565–576 (2013).

138. Wu, C. *et al.* BioGPS: an extensible and customizable portal for querying and organizing gene annotation resources. *Genome Biol.* **10**, R130-R130.8 (2009).

139. Malik, J., Getman, M. & Steiner, L. A. Histone Methyltransferase Setd8 Represses Gata2 Expression and Regulates Erythroid Maturation. *Mol. Cell. Biol.* **35**, 2059–2072 (2015).

140. Chen, K. *et al.* Resolving the distinct stages in erythroid differentiation based on dynamic changes in membrane protein expression during erythropoiesis. *Proc. Natl. Acad. Sci.* **106**, 17413–17418 (2009).

141. Malik, J., Lillis, J. A., Couch, T., Getman, M. & Steiner, L. A. The Methyltransferase Setd8 Is Essential for Erythroblast Survival and Maturation. *Cell Rep.* **21**, 2376–2383 (2017).

142. DeVilbiss, A., Boyer, M. & Bresnick, E. Establishing a hematopoietic genetic network through locus-specific integration of chromatin regulators. *Proc. Natl. Acad. Sci. U. S. A.* **110**, E3398–E3407 (2013).

143. DeVilbiss, A. W. *et al.* Epigenetic Determinants of Erythropoiesis: Role of the Histone Methyltransferase SetD8 in Promoting Erythroid Cell Maturation and Survival. *Mol. Cell. Biol.* **35**, 2073–2087 (2015).

144. Wakabayashi, K. -i. *et al.* The Peroxisome Proliferator-Activated Receptor /Retinoid X Receptor Heterodimer Targets the Histone Modification Enzyme PR-Set7/Setd8 Gene and Regulates Adipogenesis through a Positive Feedback Loop. *Mol. Cell. Biol.* **29**, 3544–3555 (2009).

145. Okamura, M., Inagaki, T., Tanaka, T. & Sakai, J. Role of histone methylation and demethylation in adipogenesis and obesity. *Organogenesis* **6**, 24–32 (2010).

146. Zhao, X. *et al.* Neuronal PPAR Deficiency Increases Susceptibility to Brain Damage after Cerebral Ischemia. *J. Neurosci.* **29**, 6186–6195 (2009).

147. Ke, X. *et al.* IUGR disrupts the PPARγ-Setd8-H4K20me1 and Wnt signaling pathways in the juvenile rat hippocampus. *Int. J. Dev. Neurosci.* **38**, 59–67 (2014).

148. Moreno, S., Farioli-vecchioli, S. & Cerù, M. P. Immunolocalization of peroxisome proliferator-activated receptors and retinoid X receptors in the adult rat CNS. *Neuroscience* **123**, 131–145 (2004).

149. Agarwal, S., Yadav, A. & Chaturvedi, R. K. Peroxisome proliferator-activated receptors (PPARs) as therapeutic target in neurodegenerative disorders. *Biochem. Biophys. Res. Commun.* **483**, 1166–1177 (2017).

150. Logan, C. Y. & Nusse, R. The Wnt signaling pathway in development and disease. *Annu.*

Rev. Cell Dev. Biol. **20**, 781–810 (2004).

151. Clevers, H. Wnt/β-Catenin Signaling in Development and Disease. *Cell* **127**, 469–480 (2006).

152. Li, Z., Nie, F., Wang, S. & Li, L. Histone H4 Lys 20 monomethylation by histone methylase SET8 mediates Wnt target gene activation. *Proc. Natl. Acad. Sci.* **108**, 3116–3123 (2011).

153. Driskell, I. *et al.* The histone methyltransferase Setd8 acts in concert with c-Myc and is required to maintain skin. *EMBO J.* **31**, 616–629 (2012).

154. Truong, A. B., Kretz, M., Ridky, T. W., Kimmel, R. & Khavari, P. A. p63 regulates proliferation and differentiation of developmentally mature keratinocytes. *Genes Dev.* **20**, 3185–3197 (2006).

155. Reinberg, D., Trojer, P. & Sbardella, G. Selective inhibitors for transferases. 1–33 (2007). doi:WO2007149782

156. Milite, C. *et al.* Progress in the Development of Lysine Methyltransferase SETD8 Inhibitors. *ChemMedChem* **11**, 1680–1685 (2016).

157. Castellano, S., Milite, C., Campiglia, P. & Sbardella, G. Highly efficient synthesis and chemical separation of 5-amino- and 7-amino-4-hydroxy-2-naphthoic acids. *Tetrahedron Lett.* **48**, 4653–4655 (2007).

158. Cheng, D. *et al.* Small Molecule Regulators of Protein Arginine Methyltransferases. *J. Biol. Chem.* **279**, 23892–23899 (2004).

159. Ragno, R. *et al.* Small Molecule Inhibitors of Histone Arginine Methyltransferases: Homology Modeling, Molecular Docking, Binding Mode Analysis, and Biological Evaluations. *J. Med. Chem.* **50**, 1241–1253 (2007).

160. Kodama, T. *et al.* Pr-SET7 inhibitor. (2011). doi:WO2011010715

161. Valente, S. *et al.* Identification of PR-SET7 and EZH2 selective inhibitors inducing cell death in human leukemia U937 cells. *Biochimie* **94**, 2308–2313 (2012).

162. Mai, A. *et al.* Epigenetic Multiple Ligands: Mixed Histone/Protein Methyltransferase, Acetyltransferase, and Class III Deacetylase (Sirtuin) Inhibitors. *J. Med. Chem.* **51**, 2279–2290 (2008).

163. Williams, D. E. *et al.* Nahuoic Acid A Produced by a Streptomyces sp. Isolated From a

Marine Sediment Is a Selective SAM-Competitive Inhibitor of the Histone Methyltransferase SETD8. *Org. Lett.* **15**, 414–417 (2013).

164. Williams, D. E. *et al.* Structures of Nahuoic Acids B-E Produced in Culture by a Streptomyces sp. Isolated from a Marine Sediment and Evidence for the Inhibition of the Histone Methyl Transferase SETD8 in Human Cancer Cells by Nahuoic Acid A. *J. Org. Chem.* **81**, 1324–1332 (2016).

165. Liu, F. *et al.* Discovery of a 2,4-Diamino-7-aminoalkoxyquinazoline as a Potent and Selective Inhibitor of Histone Lysine Methyltransferase G9a. *J. Med. Chem.* **52**, 7950–7953 (2009).

166. Ma, A. *et al.* Discovery of a selective, substrate-competitive inhibitor of the lysine methyltransferase SETD8. *J. Med. Chem.* **57**, 6822–6833 (2014).

167. Ma, A. *et al.* Structure-activity relationship studies of SETD8 inhibitors. *Med. Chem. Commun.* **5**, 1892–1898 (2014).

168. Butler, K. V. *et al.* Structure-Based Design of a Covalent Inhibitor of the SET Domain-Containing Protein 8 (SETD8) Lysine Methyltransferase. *J. Med. Chem.* **59**, 9881–9889 (2016).

169. Ibanez, G. *et al.* A High Throughput Scintillation Proximity Imaging Assay for Protein Methyltransferases. *Comb. Chem. High Throughput Screen.* **15**, 359–371 (2012).

170. Blum, G. *et al.* Small-Molecule Inhibitors of SETD8 with Cellular Activity. *ACS Chem. Biol.* **9**, 2471–2478 (2014).

171. Luo, M., Sanchez, G. I., Blum, G. J. & Yang, L. Naphtaquinone methyltransferase inhibitors and uses thereof. (2015). doi:WO2015172076A1

172. Judge, R. a. *et al.* Turning a Substrate Peptide into a Potent Inhibitor for the Histone Methyltransferase SETD8. *ACS Med. Chem. Lett.* **7**, 1102–1106 (2016).

173. Dokmanovic, M., Clarke, C. & Marks, P. A. Histone Deacetylase Inhibitors: Overview and Perspectives. *Mol. Cancer Res.* **5**, 981–989 (2007).

174. Ropero, S. & Esteller, M. The role of histone deacetylases (HDACs) in human cancer. *Mol. Oncol.* **1**, 19–25 (2007).

175. Newbold, A., Falkenberg, K. J., Prince, H. M. & Johnstone, R. W. How do tumor cells respond to HDAC inhibition? *FEBS J.* **283**, 4032–4046 (2016).

176. Bolden, J. E., Peart, M. J. & Johnstone, R. W. Anticancer activities of histone deacetylase inhibitors. *Nat. Rev. Drug Discov.* **5**, 769–784 (2006).

177. Nebbioso, A. *et al.* Tumor-selective action of HDAC inhibitors involves TRAIL induction in acute myeloid leukemia cells. *Nat. Med.* **11**, 77–84 (2005).

178. Lindemann, R. K. *et al.* Analysis of the apoptotic and therapeutic activities of histone deacetylase inhibitors by using a mouse model of B cell lymphoma. *Proc. Natl. Acad. Sci.* **104**, 8071–8076 (2007).

179. Insinga, A. *et al.* Inhibitors of histone deacetylases induce tumor-selective apoptosis through activation of the death receptor pathway. *Nat. Med.* **11**, 71–76 (2005).

180. Dokmanovic, M. & Marks, P. A. Prospects: Histone deacetylase inhibitors. *J. Cell. Biochem.* **96**, 293–304 (2005).

181. Matthews, G. M., Newbold, A. & Johnstone, R. W. Intrinsic and Extrinsic Apoptotic Pathway Signaling as Determinants of Histone Deacetylase Inhibitor Antitumor Activity. *Adv. Cancer Res.* **116**, 165–197 (2012).

182. Bolden, J. E. *et al.* HDAC inhibitors induce tumor-cell-selective pro-apoptotic transcriptional responses. *Cell Death Dis.* **4**, e519 (2013).

183. Pérez-Perarnau, A. *et al.* Analysis of apoptosis regulatory genes altered by histone deacetylase inhibitors in chronic lymphocytic leukemia cells. *Epigenetics* **6**, 1228–1235 (2011).

184. Cruickshanks, N. *et al.* Histone deacetylase inhibitors restore toxic BH3 domain protein expression in anoikis-resistant mammary and brain cancer stem cells, thereby enhancing the response to anti-ERBB1/ERBB2 therapy. *Cancer Biol. Ther.* **14**, 982–996 (2013).

185. Chen, M.-C. *et al.* Novel histone deacetylase inhibitor MPT0G009 induces cell apoptosis and synergistic anticancer activity with tumor necrosis factor-related apoptosis-inducing ligand against human hepatocellular carcinoma. *Oncotarget* **7**, 402–417 (2016).

186. Inoue, S., Riley, J., Gant, T. W., Dyer, M. J. S. & Cohen, G. M. Apoptosis induced by histone deacetylase inhibitors in leukemic cells is mediated by Bim and Noxa. *Leukemia* **21**, 1773–1782 (2007).

187. Zhang, Y., Adachi, M., Kawamura, R. & Imai, K. Bmf is a possible mediator in histone deacetylase inhibitors FK228 and CBHA-induced apoptosis. *Cell Death Differ.* **13**, 129–140 (2006).

188. Xargay-Torrent, S. *et al.* Vorinostat-Induced Apoptosis in Mantle Cell Lymphoma Is Mediated by Acetylation of Proapoptotic BH3-Only Gene Promoters. *Clin. Cancer Res.* **17**, 3956–3968 (2011).

189. Ramsey, M. R., He, L., Forster, N., Ory, B. & Ellisen, L. W. Physical Association of HDAC1 and HDAC2 with p63 Mediates Transcriptional Repression and Tumor Maintenance in Squamous Cell Carcinoma. *Cancer Res.* **71**, 4373–4379 (2011).

190. Humphreys, K. J., Cobiac, L., Le Leu, R. K., Van der Hoek, M. B. & Michael, M. Z. Histone deacetylase inhibition in colorectal cancer cells reveals competing roles for members of the oncogenic miR-17-92 cluster. *Mol. Carcinog.* **52**, 459–474 (2013).

191. Zhao, Z.-N. *et al.* TSA Suppresses miR-106b-93-25 Cluster Expression through Downregulation of MYC and Inhibits Proliferation and Induces Apoptosis in Human EMC. *PLoS One* **7**, e45133 (2012).

192. Sampath, D. *et al.* Histone deacetylases mediate the silencing of miR-15a, miR-16, and miR-29b in chronic lymphocytic leukemia. *Blood* **119**, 1162–1172 (2012).

193. Zhao, Y. *et al.* Inhibitors of histone deacetylases target the Rb-E2F1 pathway for apoptosis induction through activation of proapoptotic protein Bim. *Proc. Natl. Acad. Sci.* **102**, 16090–16095 (2005).

194. Brochier, C. *et al.* Specific Acetylation of p53 by HDAC Inhibition Prevents DNA Damage-Induced Apoptosis in Neurons. *J. Neurosci.* **33**, 8621–8632 (2013).

195. Waby, J. S. *et al.* Sp1 acetylation is associated with loss of DNA binding at promoters associated with cell cycle arrest and cell death in a colon cell line. *Mol. Cancer* **9**, 275 (2010).

196. McCourt, C. *et al.* Elevation of c-FLIP in Castrate-Resistant Prostate Cancer Antagonizes Therapeutic Response to Androgen Receptor-Targeted Therapy. *Clin. Cancer Res.* **18**, 3822–3833 (2012).

197. Wood, T. E. *et al.* Selective Inhibition of Histone Deacetylases Sensitizes Malignant Cells to Death Receptor Ligands. *Mol. Cancer Ther.* **9**, 246–256 (2010).

198. Lucas, D. M. *et al.* The Novel Deacetylase Inhibitor AR-42 Demonstrates Pre-Clinical Activity in B-Cell Malignancies In Vitro and In Vivo. *PLoS One* **5**, e10941 (2010).

199. Ruefli, A. A. *et al.* The histone deacetylase inhibitor and chemotherapeutic agent suberoylanilide hydroxamic acid (SAHA) induces a cell-death pathway characterized by

cleavage of Bid and production of reactive oxygen species. *Proc. Natl. Acad. Sci.* **98**, 10833–10838 (2001).

200. Ungerstedt, J. S. *et al.* Role of thioredoxin in the response of normal and transformed cells to histone deacetylase inhibitors. *Proc. Natl. Acad. Sci.* **102**, 673–678 (2005).

201. Rosato, R. R., Almenara, J. A. & Grant, S. The histone deacetylase inhibitor MS-275 promotes differentiation or apoptosis in human leukemia cells through a process regulated by generation of reactive oxygen species and induction of p21CIP1/WAF1. *Cancer Res.* **63**, 3637–3645 (2003).

202. Rosato, R. R., Almenara, J. A., Dai, Y. & Grant, S. Simultaneous activation of the intrinsic and extrinsic pathways by histone deacetylase (HDAC) inhibitors and tumor necrosis factor-related apoptosis-inducing ligand (TRAIL) synergistically induces mitochondrial damage and apoptosis in human leukemia cells. *Mol. Cancer Ther.* **2**, 1273–1284 (2003).

203. Robert, C. & Rassool, F. V. HDAC Inhibitors: Roles of DNA damage and Repair. *Adv. Cancer Res.* **116**, 87–129 (2012).

204. Wiegmans, A. P., Yap, P.-Y., Ward, A., Lim, Y. C. & Khanna, K. K. Differences in Expression of Key DNA Damage Repair Genes after Epigenetic-Induced BRCAness Dictate Synthetic Lethality with PARP1 Inhibition. *Mol. Cancer Ther.* **14**, 2321–2331 (2015).

205. Adimoolam, S. *et al.* HDAC inhibitor PCI-24781 decreases RAD51 expression and inhibits homologous recombination. *Proc. Natl. Acad. Sci.* **104**, 19482–19487 (2007).

206. Lee, J.-H., Choy, M. L., Ngo, L., Foster, S. S. & Marks, P. A. Histone deacetylase inhibitor induces DNA damage, which normal but not transformed cells can repair. *Proc. Natl. Acad. Sci.* **107**, 14639–14644 (2010).

207. Petruccelli, L. A. *et al.* Vorinostat Induces Reactive Oxygen Species and DNA Damage in Acute Myeloid Leukemia Cells. *PLoS One* **6**, e20987 (2011).

208. Conti, C. *et al.* Inhibition of Histone Deacetylase in Cancer Cells Slows Down Replication Forks, Activates Dormant Origins, and Induces DNA Damage. *Cancer Res.* **70**, 4470–4480 (2010).

209. Lindemann, R. K., Gabrielli, B. & Johnstone, R. W. Histone-Deacetylase Inhibitors for the Treatment of Cancer. *Cell Cycle* **3**, 777–786 (2004).

210. Glaser, K. B. *et al.* Gene expression profiling of multiple histone deacetylase (HDAC)

inhibitors: defining a common gene set produced by HDAC inhibition in T24 and MDA carcinoma cell lines. *Mol. Cancer Ther.* **2**, 151–63 (2003).

211. Qiu, L. *et al.* Histone Deacetylase Inhibitors Trigger a G2 Checkpoint in Normal Cells That Is Defective in Tumor Cells. *Mol. Biol. Cell* **11**, 2069–2083 (2000).

212. Ablain, J. & de The, H. Revisiting the differentiation paradigm in acute promyelocytic leukemia. *Blood* **117**, 5795–5802 (2011).

213. Minucci, S., Nervi, C., Coco, F. Lo & Pelicci, P. G. Histone deacetylases: a common molecular target for differentiation treatment of acute myeloid leukemias? *Oncogene* **20**, 3110–3115 (2001).

214. Lin, R. J. *et al.* Role of the histone deacetylase complex in acute promyelocytic leukaemia. *Nature* **391**, 811–814 (1998).

215. Cimino, G. *et al.* Sequential valproic acid/all-trans retinoic acid treatment reprograms differentiation in refractory and high-risk acute myeloid leukemia. *Cancer Res.* **66**, 8903–8911 (2006).

216. Bots, M. *et al.* Differentiation therapy for the treatment of t(8;21) acute myeloid leukemia using histone deacetylase inhibitors. *Blood* **123**, 1341–1352 (2014).

217. Schwartz, B. E. *et al.* Differentiation of NUT Midline Carcinoma by Epigenomic Reprogramming. *Cancer Res.* **71**, 2686–2696 (2011).

218. Hrzenjak, A. *et al.* Valproate inhibition of histone deacetylase 2 affects differentiation and decreases proliferation of endometrial stromal sarcoma cells. *Mol. Cancer Ther.* **5**, 2203–2210 (2006).

219. Yamashita, Y. ichi *et al.* Histone deacetylase inhibitor trichostatin a induces cell-cycle arrest/apoptosis and hepatocyte differentiation in human hepatoma cells. *Int. J. Cancer* **103**, 572–576 (2003).

220. Platta, C. S., Greenblatt, D. Y., Kunnimalaiyaan, M. & Chen, H. The HDAC Inhibitor Trichostatin A Inhibits Growth of Small Cell Lung Cancer Cells. *J. Surg. Res.* **142**, 219–226 (2007).

221. Munster, P. N. *et al.* The histone deacetylase inhibitor suberoylanilide hydroxamic acid induces differentiation of human breast cancer cells. *Cancer Res.* **61**, 8492–8497 (2001).

222. Romanov, V. S. *et al.* p21Waf1is required for cellular senescence but not for cell cycle arrest induced by the HDAC inhibitor sodium butyrate. *Cell Cycle* **9**, 3945–3955 (2010).

223. Cho, J.-H., Dimri, M. & Dimri, G. P. MicroRNA-31 Is a Transcriptional Target of Histone Deacetylase Inhibitors and a Regulator of Cellular Senescence. *J. Biol. Chem.* **290**, 10555–10567 (2015).

224. Shao, Y., Gao, Z., Marks, P. A. & Jiang, X. Apoptotic and autophagic cell death induced by histone deacetylase inhibitors. *Proc. Natl. Acad. Sci.* **101**, 18030–18035 (2004).

225. Robert, T. *et al.* HDACs link the DNA damage response, processing of double-strand breaks and autophagy. *Nature* **471**, 74–79 (2011).

226. Lee, Y. J. *et al.* Molecular Mechanism of SAHA on Regulation of Autophagic Cell Death in Tamoxifen-Resistant MCF-7 Breast Cancer Cells. *Int. J. Med. Sci.* **9**, 881–893 (2012).

227. Liu, Y.-L. *et al.* Autophagy potentiates the anti-cancer effects of the histone deacetylase inhibitors in hepatocellular carcinoma. *Autophagy* **6**, 1057–1065 (2010).

228. Gammoh, N., Marks, P. A. & Jiang, X. Curbing autophagy and histone deacetylases to kill cancer cells. *Autophagy* **8**, 1521–1522 (2012).

229. Dupéré-Richer, D. *et al.* Vorinostat-induced autophagy switches from a death-promoting to a cytoprotective signal to drive acquired resistance. *Cell Death Dis.* **4**, 1–11 (2013).

230. Zhang, J. *et al.* Histone deacetylase inhibitors induce autophagy through FOXO1-dependent pathways. *Autophagy* **11**, 629–642 (2015).

231. Carew, J. S. *et al.* Autophagy inhibition enhances vorinostat-induced apoptosis via ubiquitinated protein accumulation. *J. Cell. Mol. Med.* **14**, 2448–2459 (2010).

232. Magner, W. J. *et al.* Activation of MHC Class I, II, and CD40 Gene Expression by Histone Deacetylase Inhibitors. *J. Immunol.* **165**, 7017–7024 (2000).

233. Setiadi, A. F. *et al.* Epigenetic Enhancement of Antigen Processing and Presentation Promotes Immune Recognition of Tumors. *Cancer Res.* **68**, 9601–9607 (2008).

234. Manning, J. *et al.* Induction of MHC class I molecule cell surface expression and epigenetic activation of antigen-processing machinery components in a murine model for human papilloma virus 16-associated tumours. *Immunology* **123**, 218–227 (2007).

235. Armeanu, S. *et al.* Natural killer cell-mediated lysis of hepatoma cells via specific induction of NKG2D ligands by the histone deacetylase inhibitor sodium valproate. *Cancer Res.* **65**, 6321–6329 (2005).

236. Skov, S. *et al.* Cancer cells become susceptible to natural killer cell killing after exposure

to histone deacetylase inhibitors due to glycogen synthase kinase-3-dependent expression of MHC class I-related chain A and B. *Cancer Res.* **65**, 11136–11145 (2005).

237. López-Soto, A., Folgueras, A. R., Seto, E. & Gonzalez, S. HDAC3 represses the expression of NKG2D ligands ULBPs in epithelial tumour cells: potential implications for the immunosurveillance of cancer. *Oncogene* **28**, 2370–2382 (2009).

238. Christiansen, A. J. *et al.* Eradication of solid tumors using histone deacetylase inhibitors combined with immune-stimulating antibodies. *Proc. Natl. Acad. Sci.* **108**, 4141–4146 (2011).

239. Woods, D. M. *et al.* The antimelanoma activity of the histone deacetylase inhibitor panobinostat (LBH589) is mediated by direct tumor cytotoxicity and increased tumor immunogenicity. *Melanoma Res.* **23**, 341–348 (2013).

240. West, A. C. *et al.* An Intact Immune System Is Required for the Anticancer Activities of Histone Deacetylase Inhibitors. *Cancer Res.* **73**, 7265–7276 (2013).

241. Fiegler, N. *et al.* Downregulation of the activating NKp30 ligand B7-H6 by HDAC inhibitors impairs tumor cell recognition by NK cells. *Blood* **122**, 684–693 (2013).

242. Rouaux, C. *et al.* Critical loss of CBP/p300 histone acetylase activity by caspase-6 during neurodegeneration. *EMBO J.* **22**, 6537–6549 (2003).

243. Kontopoulos, E., Parvin, J. D. & Feany, M. B. α-synuclein acts in the nucleus to inhibit histone acetylation and promote neurotoxicity. *Hum. Mol. Genet.* **15**, 3012–3023 (2006).

244. Sadri-Vakili, G. *et al.* Histones associated with downregulated genes are hypo-acetylated in Huntington's disease models. *Hum. Mol. Genet.* **16**, 1293–1306 (2007).

245. Steffan, J. S. *et al.* Histone deacetylase inhibitors arrest polyglutamine-dependent neurodegeneration in Drosophila. *Nature* **413**, 739–743 (2001).

246. Bates, E. A., Victor, M., Jones, A. K., Shi, Y. & Hart, A. C. Differential Contributions of Caenorhabditis elegans Histone Deacetylases to Huntingtin Polyglutamine Toxicity. *J. Neurosci.* **26**, 2830–2838 (2006).

247. Veterans, B. *et al.* Histone Deacetylase Inhibition by Sodium Butyrate Chemotherapy Ameliorates the Neurodegenerative Phenotype in Huntington ' s Disease Mice. *J. Neurosci.* **23**, 9418–9427 (2003).

248. Hockly, E. *et al.* Suberoylanilide hydroxamic acid, a histone deacetylase inhibitor, ameliorates motor deficits in a mouse model of Huntington's disease. *Proc. Natl. Acad.*

Sci. **100**, 2041–2046 (2003).

249. Dompierre, J. P. *et al.* Histone Deacetylase 6 Inhibition Compensates for the Transport Deficit in Huntington's Disease by Increasing Tubulin Acetylation. *J. Neurosci.* **27**, 3571–3583 (2007).

250. Southwood, C. M., Peppi, M., Dryden, S., Tainsky, M. A. & Gow, A. Microtubule Deacetylases, SirT2 and HDAC6, in the Nervous System. *Neurochem. Res.* **32**, 187–195 (2007).

251. Giralt, A. *et al.* Long-term memory deficits in Huntington's disease are associated with reduced CBP histone acetylase activity. *Hum. Mol. Genet.* **21**, 1203–1216 (2012).

252. Saft, C., Lauter, T., Kraus, P. H., Przuntek, H. & Andrich, J. E. Dose-dependent improvement of myoclonic hyperkinesia due to valproic acid in eight Huntington's Disease patients: A case series. *BMC Neurol.* **6**, 1–6 (2006).

253. Grove, V. E., Quintanilla, J. & DeVaney, G. T. Improvement of Huntington's Disease with Olanzapine and Valproate. *N. Engl. J. Med.* **343**, 973–974 (2000).

254. Unti, E., Mazzucchi, S., Kiferle, L., Bonuccelli, U. & Ceravolo, R. Q09 Valproic Acid for the treatment of aggressiveness in Huntington's disease: 1-year follow-up. *J. Neurol. Neurosurg. Psychiatry* **83**, A57 (2012).

255. Sharma, S. & Taliyan, R. Transcriptional dysregulation in Huntington's disease: The role of histone deacetylases. *Pharmacol. Res.* **100**, 157–169 (2015).

256. Tuppo, E. E. & Arias, H. R. The role of inflammation in Alzheimer's disease. *Int. J. Biochem. Cell Biol.* **37**, 289–305 (2005).

257. Guan, J. *et al.* HDAC2 negatively regulates memory formation and synaptic plasticity. *Nature* **459**, 55–60 (2009).

258. Li, G., Jiang, H., Chang, M., Xie, H. & Hu, L. HDAC6 α-tubulin deacetylase: A potential therapeutic target in neurodegenerative diseases. *J. Neurol. Sci.* **304**, 1–8 (2011).

259. Ding, H., Dolan, P. J. & Johnson, G. V. W. Histone deacetylase 6 interacts with the microtubule-associated protein tau. *J. Neurochem.* **106**, 2119–2130 (2008).

260. Perez, M. *et al.* Tau - An inhibitor of deacetylase HDAC6 function. *J. Neurochem.* **109**, 1756–1766 (2009).

261. Hanger, D. P., Anderton, B. H. & Noble, W. Tau phosphorylation: the therapeutic

challenge for neurodegenerative disease. *Trends Mol. Med.* **15**, 112–119 (2009).

262. Chen, S., Owens, G. C., Makarenkova, H. & Edelman, D. B. HDAC6 Regulates Mitochondrial Transport in Hippocampal Neurons. *PLoS One* **5**, e10848 (2010).

263. Qing, H. *et al.* Valproic acid inhibits Aβ production, neuritic plaque formation, and behavioral deficits in Alzheimer's disease mouse models. *J. Exp. Med.* **205**, 2781–2789 (2008).

264. Kilgore, M. *et al.* Inhibitors of Class 1 Histone Deacetylases Reverse Contextual Memory Deficits in a Mouse Model of Alzheimer's Disease. *Neuropsychopharmacology* **35**, 870–880 (2010).

265. Ricobaraza, A. *et al.* Phenylbutyrate Ameliorates Cognitive Deficit and Reduces Tau Pathology in an Alzheimer's Disease Mouse Model. *Neuropsychopharmacology* **34**, 1721–1732 (2009).

266. Yao, Z. *et al.* Phenylbutyric acid prevents rats from electroconvulsion-induced memory deficit with alterations of memory-related proteins and tau hyperphosphorylation. *Neuroscience* **168**, 405–415 (2010).

267. Wiley, J. C., Pettan-Brewer, C. & Ladiges, W. C. Phenylbutyric acid reduces amyloid plaques and rescues cognitive behavior in AD transgenic mice. *Aging Cell* **10**, 418–428 (2011).

268. Wiley, J. C. *et al.* Phenylbutyric Acid Rescues Endoplasmic Reticulum Stress-Induced Suppression of APP Proteolysis and Prevents Apoptosis in Neuronal Cells. *PLoS One* **5**, e9135 (2010).

269. Ryu, H. *et al.* Sodium phenylbutyrate prolongs survival and regulates expression of anti-apoptotic genes in transgenic amyotrophic lateral sclerosis mice. *J. Neurochem.* **93**, 1087–1098 (2005).

270. Rivieccio, M. A. *et al.* HDAC6 is a target for protection and regeneration following injury in the nervous system. *Proc. Natl. Acad. Sci.* **106**, 19599–19604 (2009).

271. Salminen, A., Tapiola, T., Korhonen, P. & Suuronen, T. Neuronal apoptosis induced by histone deacetylase inhibitors. *Mol. Brain Res.* **61**, 203–206 (1998).

272. McNaught, K. S. P., Shashidharan, P., Perl, D. P., Jenner, P. & Olanow, C. W. Aggresome-related biogenesis of Lewy bodies. *Eur. J. Neurosci.* **16**, 2136–2148 (2002).

273. Spillantini, M. G. *et al.* α-Synuclein in Lewy bodies. *Nature* **388**, 839–840 (1997).

274. Irizarry, M. C. *et al.* Nigral and Cortical Lewy Bodies and Dystrophic Nigral Neurites in Parkinson's Disease and Cortical Lewy Body Disease Contain α-synuclein Immunoreactivity. *J. Neuropathol. Exp. Neurol.* **57**, 334–337 (1998).

275. Olzmann, J. A. *et al.* Parkin-mediated K63-linked polyubiquitination targets misfolded DJ-1 to aggresomes via binding to HDAC6. *J. Cell Biol.* **178**, 1025–1038 (2007).

276. Harrison, I. F. & Dexter, D. T. Epigenetic targeting of histone deacetylase: Therapeutic potential in Parkinson's disease? *Pharmacol. Ther.* **140**, 34–52 (2013).

277. Collins, L. M. *et al.* Class-IIa Histone Deacetylase Inhibition Promotes the Growth of Neural Processes and Protects Them Against Neurotoxic Insult. *Mol. Neurobiol.* **51**, 1432–1442 (2015).

278. Cummings, J. L., Morstorf, T. & Zhong, K. Alzheimer's disease drug-development pipeline: few candidates, frequent failures. *Alzheimers. Res. Ther.* **6**, 37 (2014).

279. Didonna, A. & Opal, P. The promise and perils of HDAC inhibitors in neurodegeneration. *Ann. Clin. Transl. Neurol.* **2**, 79–101 (2015).

280. Dirice, E. *et al.* Isoform-selective inhibitor of histone deacetylase 3 (HDAC3) limits pancreatic islet infiltration and protects female nonobese diabetic mice from diabetes. *J. Biol. Chem.* **292**, 17598–17608 (2017).

281. Ferrari, A. *et al.* Attenuation of diet-induced obesity and induction of white fat browning with a chemical inhibitor of histone deacetylases. *Int. J. Obes.* **41**, 289–298 (2017).

282. Ooi, J. Y. Y. *et al.* HDAC inhibition attenuates cardiac hypertrophy by acetylation and deacetylation of target genes. *Epigenetics* **10**, 418–430 (2015).

283. Qin, L. *et al.* Social deficits in Shank3-deficient mouse models of autism are rescued by histone deacetylase (HDAC) inhibition. *Nat. Neurosci.* **21**, 564–575 (2018).

284. Warnault, V., Darcq, E., Levine, A., Barak, S. & Ron, D. Chromatin remodeling - a novel strategy to control excessive alcohol drinking. *Transl. Psychiatry* **3**, e231 (2013).

285. Bourguet, E., Ozdarska, K., Moroy, G., Jeanblanc, J. & Naassila, M. Class I HDAC Inhibitors: Potential New Epigenetic Therapeutics for Alcohol Use Disorder (AUD). *J. Med. Chem.* **61**, 1745–1766 (2018).

286. Conforti, F. *et al.* The histone deacetylase inhibitor, romidepsin, as a potential treatment for pulmonary fibrosis. *Oncotarget* **8**, 48737–48754 (2017).

287. Choi, S. Y. *et al*. Tubastatin A suppresses renal fibrosis via regulation of epigenetic histone modification and Smad3-dependent fibrotic genes. *Vascul. Pharmacol.* **72**, 130–140 (2015).

288. Bodas, M., Mazur, S., Min, T. & Vij, N. Inhibition of histone-deacetylase activity rescues inflammatory cystic fibrosis lung disease by modulating innate and adaptive immune responses. *Respir. Res.* **19**, 2 (2018).

289. A-Paraddise. Available at: http://a-paraddise.cebio.org/content/workpackages. (Accessed: 10th April 2019)

290. *World malaria report 2017. Geneva: World Health Organization* (2017).

291. Sidhu, A. B. S., Verdier-Pinard, D. & Fidock, D. A. Chloroquine Resistance in Plasmodium falciparum Malaria Parasites Conferred by pfcrt Mutations. *Science (80-.).* **298**, 210–213 (2002).

292. Ashley, E. A. *et al.* Spread of Artemisinin Resistance in Plasmodium falciparum Malaria. *N. Engl. J. Med.* **371**, 411–423 (2014).

293. Andrews, K. T., Haque, A. & Jones, M. K. HDAC inhibitors in parasitic diseases. *Immunol. Cell Biol.* **90**, 66–77 (2012).

294. Coleman, B. I. *et al.* A Plasmodium falciparum Histone Deacetylase Regulates Antigenic Variation and Gametocyte Conversion. *Cell Host Microbe* **16**, 177–186 (2014).

295. Darkin-Rattray, S. J. *et al.* Apicidin: A novel antiprotozoal agent that inhibits parasite histone deacetylase. *Proc. Natl. Acad. Sci.* **93**, 13143–13147 (1996).

296. Joshi, M. B. *et al.* Molecular cloning and nuclear localization of a histone deacetylase homologue in Plasmodium falciparum. *Mol. Biochem. Parasitol.* **99**, 11–19 (1999).

297. Andrews, K. T. *et al.* Potent antimalarial activity of histone deacetylase inhibitor analogues. *Antimicrob. Agents Chemother.* **52**, 1454–1461 (2008).

298. Patel, V. *et al.* Identification and Characterization of Small Molecule Inhibitors of a Class I Histone Deacetylase from Plasmodium falciparum. *J. Med. Chem.* **52**, 2185–2187 (2009).

299. Andrews, K., Tran, T. N. & Fairlie, D. P. Towards Histone Deacetylase Inhibitors as New Antimalarial Drugs. *Curr. Pharm. Des.* **18**, 3467–3479 (2012).

300. Hailu, G. S. *et al.* Lysine Deacetylase Inhibitors in Parasites: Past, Present, and Future

Perspectives. *J. Med. Chem.* **60**, 4780–4804 (2017).

301. Vos, T. *et al.* Global, regional, and national incidence, prevalence, and years lived with disability for 310 diseases and injuries, 1990–2015: a systematic analysis for the Global Burden of Disease Study 2015. *Lancet* **388**, 1545–1602 (2016).

302. Wang, H. *et al.* Global, regional, and national life expectancy, all-cause mortality, and cause-specific mortality for 249 causes of death, 1980–2015: a systematic analysis for the Global Burden of Disease Study 2015. *Lancet* **388**, 1459–1544 (2016).

303. Saxena, A. *et al.* Analysis of the Leishmania donovani transcriptome reveals an ordered progression of transient and permanent changes in gene expression during differentiation. *Mol. Biochem. Parasitol.* **152**, 53–65 (2007).

304. Guerrant, W. *et al.* A Structure-Activity Relationship Study of the Antimalarial and Antileishmanial Activities of Nonpeptide Macrocyclic Histone Deacetylase Inhibitors. *ChemMedChem* **5**, 1232–1235 (2010).

305. Patil, V. *et al.* Antimalarial and antileishmanial activities of histone deacetylase inhibitors with triazole-linked cap group. *Bioorganic Med. Chem.* **18**, 415–425 (2010).

306. Sodji, Q. *et al.* The antileishmanial activity of isoforms 6- and 8-selective histone deacetylase inhibitors. *Bioorg. Med. Chem. Lett.* **24**, 4826–4830 (2014).

307. Ingram, A. K. & Horn, D. Histone deacetylases in Trypanosoma brucei: two are essential and another is required for normal cell cycle progression. *Mol. Microbiol.* **45**, 89–97 (2002).

308. Mandava, V. *et al.* Histone modifications in Trypanosoma brucei. *Mol. Biochem. Parasitol.* **156**, 41–50 (2007).

309. Pays, E. Regulation of antigen gene expression in. *Trends Parasitol.* **21**, 517–520 (2005).

310. Wang, Q.-P., Kawahara, T. & Horn, D. Histone deacetylases play distinct roles in telomeric VSG expression site silencing in African trypanosomes. *Mol. Microbiol.* **77**, 1237–1245 (2010).

311. Engel, J. A. *et al.* Profiling the anti-protozoal activity of anti-cancer HDAC inhibitors against Plasmodium and Trypanosoma parasites. *Int. J. Parasitol. Drugs Drug Resist.* **5**, 117–126 (2015).

312. Kelly, J. M. *et al.* Inhibitors of human histone deacetylase with potent activity against the African trypanosome Trypanosoma brucei. *Bioorg. Med. Chem. Lett.* **22**, 1886–1890

(2012).

313. Carrillo, A. K., Guiguemde, W. A. & Guy, R. K. Evaluation of histone deacetylase inhibitors (HDACi) as therapeutic leads for human African trypanosomiasis (HAT). *Bioorg. Med. Chem.* **23**, 5151–5155 (2015).

314. El-Sayed, N. M. *et al.* The Genome Sequence of Trypanosoma cruzi, Etiologic Agent of Chagas Disease. *Science (80-.).* **309**, 409–415 (2005).

315. INSERM. A-PARADDISE Report Summary. *Project ID: 602080* 1–21 (2017). Available at: https://cordis.europa.eu/project/rcn/109335/reporting/en. (Accessed: 20th April 2019)

316. King, C. H. Toward the Elimination of Schistosomiasis. *N. Engl. J. Med.* **360**, 106–109 (2009).

317. World Health Organization. *Schistosomiasis - Progress report 2001-2011 and strategic plan 2012-2020*. (WHO Library, 2013).

318. Fallon, P. G. Schistosome resistance to praziquantel. *Drug Resist. Updat.* **1**, 236–241 (1998).

319. Seto, E. Y. W., Wong, B. K., Lu, D. & Zhong, B. Human Schistosomiasis Resistance to Praziquantel in China: Should We Be Worried? *Am. J. Trop. Med. Hyg.* **85**, 74–82 (2011).

320. Ismail, M. *et al.* Resistance to praziquantel: direct evidence from Schistosoma mansoni isolated from Egyptian villagers. *Am. J. Trop. Med. Hyg.* **60**, 932–935 (1999).

321. Oger, F. *et al.* The class I histone deacetylases of the platyhelminth parasite Schistosoma mansoni. *Biochem. Biophys. Res. Commun.* **377**, 1079–1084 (2008).

322. Marek, M. *et al.* Structural Basis for the Inhibition of Histone Deacetylase 8 (HDAC8), a Key Epigenetic Player in the Blood Fluke Schistosoma mansoni. *PLoS Pathog.* **9**, e1003645 (2013).

323. Dubois, F. *et al.* Histone deacetylase inhibitors induce apoptosis, histone hyperacetylation and up-regulation of gene transcription in Schistosoma mansoni. *Mol. Biochem. Parasitol.* **168**, 7–15 (2009).

324. Kannan, S. *et al.* Discovery of inhibitors of Schistosoma mansoni HDAC8 by combining homology modeling, virtual screening, and in vitro validation. *J. Chem. Inf. Model.* **54**, 3005–3019 (2014).

325. Heimburg, T. *et al.* Structure-Based Design and Synthesis of Novel Inhibitors Targeting

HDAC8 from Schistosoma mansoni for the Treatment of Schistosomiasis. *J. Med. Chem.* **59**, 2423–2435 (2016).

326. Utzinger, J., Keiser, J., Shuhua, X., Tanner, M. & Singer, B. H. Combination Chemotherapy of Schistosomiasis in Laboratory Studies and Clinical Trials. *Antimicrob. Agents Chemother.* **47**, 1487–1495 (2003).

327. Yoshida, M., Kijima, M., Akita, M. & Beppu, T. Potent and Specific Inhibition of Mammalian Histone Deacetylase Both in Vivo and in Vitro by Trichostatin A. *J. Biol. Chem.* **265**, 17174–17179 (1990).

328. Marks, P. A. & Breslow, R. Dimethyl sulfoxide to vorinostat: development of this histone deacetylase inhibitor as an anticancer drug. *Nat. Biotechnol.* **25**, 84–90 (2007).

329. Finn, P. W. & Carstensten, E. The discovery and development of Belinostat. in *Successful Drug Discovery; volume 2* (eds. Fischer, J. & Childers, W. E.) 31–57 (2017).

330. Atadja, P. & Perez, L. Discovery and Development of Farydak (NVP-LBH589, Panobinostat) as an anticancer agent. in *Successful Drug Discovery; volume 2* (eds. Fischer, J. & Childers, W. E.) 59–88 (2017).

331. Novotny-Diermayr, V. *et al.* SB939, a Novel Potent and Orally Active Histone Deacetylase Inhibitor with High Tumor Exposure and Efficacy in Mouse Models of Colorectal Cancer. *Mol. Cancer Ther.* **9**, 642–652 (2010).

332. Mandl-Weber, S. *et al.* The novel inhibitor of histone deacetylase resminostat (RAS2410) inhibits proliferation and induces apoptosis in multiple myeloma (MM) cells. *Br. J. Haematol.* **149**, 518–528 (2010).

333. Leoni, F. *et al.* The Histone Deacetylase Inhibitor ITF2357 Reduces Production of Pro-Inflammatory Cytokines In Vitro and Systemic Inflammation In Vivo. *Mol. Med.* **11**, 1–15 (2005).

334. Buggy, J. J. *et al.* CRA-024781: a novel synthetic inhibitor of histone deacetylase enzymes with antitumor activity in vitro and in vivo. *Mol. Cancer Ther.* **5**, 1309–1317 (2006).

335. Arts, J. *et al.* JNJ-26481585, a Novel 'Second-Generation' Oral Histone Deacetylase Inhibitor, Shows Broad-Spectrum Preclinical Antitumoral Activity. *Clin. Cancer Res.* **15**, 6841–6851 (2009).

336. Moffat, D. *et al.* Discovery of 2-(6-{[(6-Fluoroquinolin-2-yl)methyl] amino}bicyclo[3.1.0]hex-3-yl)- *N* -hydroxypyrimidine-5-carboxamide (CHR-3996), a

Class I Selective Orally Active Histone Deacetylase Inhibitor. *J. Med. Chem.* **53**, 8663–8678 (2010).

337. Butler, K. V. *et al.* Rational Design and Simple Chemistry Yield a Superior, Neuroprotective HDAC6 Inhibitor, Tubastatin A. *J. Am. Chem. Soc.* **132**, 10842–10846 (2010).

338. Kalin, J. H., Butler, K. V., Akimova, T., Hancock, W. W. & Kozikowski, A. P. Second-Generation Histone Deacetylase 6 Inhibitors Enhance the Immunosuppressive Effects of Foxp3+ T-Regulatory Cells. *J. Med. Chem.* **55**, 639–651 (2012).

339. Cossio Mora, F. P. *et al.* Histone deacetylase inhibitors based on derivatives of tricycle polyhydroacridine and analogs possessing fused saturated five-and seven-member rings. (2014). doi:WO2014180984

340. Lin, X. *et al.* Design and Synthesis of Orally Bioavailable Aminopyrrolidinone Histone Deacetylase 6 Inhibitors. *J. Med. Chem.* **58**, 2809–2820 (2015).

341. Abeywickrama, C., Bradner, J. E. & Ponnala, S. Selective inhibitors for histone deacetylase 6 and method thereof. (2015). doi:US2015197497A1

342. De Vreese, R. *et al.* Synthesis of Potent and Selective HDAC6 Inhibitors Bearing a Cyclohexane- or Cycloheptane-Annulated 1,5-Benzothiazepine Scaffold. *Chem. Eur. J.* **23**, 128–136 (2017).

343. Balasubramanian, S. *et al.* A novel histone deacetylase 8 (HDAC8)-specific inhibitor PCI-34051 induces apoptosis in T-cell lymphomas. *Leukemia* **22**, 1026–1034 (2008).

344. Suzuki, T. *et al.* Rapid discovery of highly potent and selective inhibitors of histone deacetylase 8 using click chemistry to generate candidate libraries. *J. Med. Chem.* **55**, 9562–9575 (2012).

345. Ingham, O. J. *et al.* Development of a Potent and Selective HDAC8 Inhibitor. *ACS Med. Chem. Lett.* **7**, 929–932 (2016).

346. Shen, S. & Kozikowski, A. P. Why Hydroxamates May Not Be the Best Histone Deacetylase Inhibitors-What Some May Have Forgotten or Would Rather Forget? *ChemMedChem* **11**, 15–21 (2016).

347. Knipstein, J. & Gore, L. Entinostat for treatment of solid tumors and hematologic malignancies. *Expert Opin. Investig. Drugs* **20**, 1455–1467 (2011).

348. Saito, A. *et al.* A synthetic inhibitor of histone deacetylase, MS-27-275, with marked in

vivo antitumor activity against human tumors. *Proc. Natl. Acad. Sci.* **96**, 4592–4597 (1999).

349. Zhou, N. *et al.* Discovery of *N* -(2-Aminophenyl)-4-[(4-pyridin-3-ylpyrimidin-2-ylamino)methyl]benzamide (MGCD0103), an Orally Active Histone Deacetylase Inhibitor. *J. Med. Chem.* **51**, 4072–4075 (2008).

350. Garcia-Manero, G. *et al.* Clinical activity and safety of the histone deacetylase inhibitor MGCD0103: Results of a phase I study in patients with leukemia or myelodysplastic syndromes (MDS). *J. Clin. Oncol.* **24**, 6500 (2006).

351. Siu, L. L. *et al.* Phase I study of MGCD0103 given as a three-times-per-week oral dose in patients with advanced solid tumors. *J. Clin. Oncol.* **26**, 1940–1947 (2008).

352. Lu, X. P. *et al.* Discovery and development of HDAC subtype selective inhibitor chidamide: Potential immunomodulatory activity against cancers. in *Successful Drug Discovery; volume 2* (eds. Fischer, J. & Childers, W.) 89–116 (2017).

353. Qiao, Z. *et al.* Chidamide, a novel histone deacetylase inhibitor, synergistically enhances gemcitabine cytotoxicity in pancreatic cancer cells. *Biochem. Biophys. Res. Commun.* **434**, 95–101 (2013).

354. Ning, Z. Q. *et al.* Chidamide (CS055/HBI-8000): A new histone deacetylase inhibitor of the benzamide class with antitumor activity and the ability to enhance immune cell-mediated tumor cell cytotoxicity. *Cancer Chemother. Pharmacol.* **69**, 901–909 (2012).

355. Hildmann, C. *et al.* Substrate and inhibitor specificity of class 1 and class 2 histone deacetylases. *J. Biotechnol.* **124**, 258–270 (2006).

356. Witter, D. J. *et al.* Optimization of biaryl Selective HDAC1&2 Inhibitors (SHI-1:2). *Bioorg. Med. Chem. Lett.* **18**, 726–731 (2008).

357. McClure, J. J. *et al.* Comparison of the Deacylase and Deacetylase Activity of Zinc-Dependent HDACs. *ACS Chem. Biol.* **12**, 1644–1655 (2017).

358. Chen, B. *et al.* Chemistry and biology of mercaptoacetamides as novel histone deacetylase inhibitors. *Bioorg. Med. Chem. Lett.* **15**, 1389–1392 (2005).

359. Kozikowski, A. P. *et al.* Functional Differences in Epigenetic ModulatorsSuperiority of Mercaptoacetamide-Based Histone Deacetylase Inhibitors Relative to Hydroxamates in Cortical Neuron Neuroprotection Studies. *J. Med. Chem.* **50**, 3054–3061 (2007).

360. Kalin, J. H., Zhang, H., Gaudrel-Grosay, S., Vistoli, G. & Kozikowski, A. P. Chiral

Mercaptoacetamides Display Enantioselective Inhibition of Histone Deacetylase6 and Exhibit Neuroprotection in Cortical Neuron Models of Oxidative Stress. *ChemMedChem* **7**, 425–439 (2012).

361. Gu, W., Nusinzon, I., Smith, R. D., Horvath, C. M. & Silverman, R. B. Carbonyl- and sulfur-containing analogs of suberoylanilide hydroxamic acid: Potent inhibition of histone deacetylases. *Bioorganic Med. Chem.* **14**, 3320–3329 (2006).

362. Nakajima, H., Kim, Y. B., Terano, H., Yoshida, M. & Horinouchi, S. FR901228, a Potent Antitumor Antibiotic, Is a Novel Histone Deacetylase Inhibitor. *Exp. Cell Res.* **241**, 126–133 (1998).

363. Taori, K., Paul, V. J. & Luesch, H. Structure and activity of largazole, a potent antiproliferative agent from the Floridian marine cyanobacterium Symploca sp. *J. Am. Chem. Soc.* **130**, 1806–1807 (2008).

364. Ying, Y., Taori, K., Kim, H., Hong, J. & Luesch, H. Total Synthesis and Molecular Target of Largazole, a Histone Deacetylase Inhibitor. *J. Am. Chem. Soc.* **130**, 8455–8459 (2008).

365. Wang, C. *et al.* Thailandepsins: Bacterial Products with Potent Histone Deacetylase Inhibitory Activities and Broad-Spectrum Antiproliferative Activities. *J. Nat. Prod.* **74**, 2031–2038 (2011).

366. Furumai, R. *et al.* FK228 (Depsipeptide) as a Natural Prodrug That Inhibits Class I Histone Deacetylases. *Cancer Res.* **62**, 4916–4921 (2002).

367. Ganesan, A. Macrocyclic inhibitors of zinc-dependent histone deacetylases (HDACs). in *Macrocycles in Drug Discovery* (ed. Levin, J.) 109–140 (2014).

368. Ganesan, A. Romidepsin and the zinc-binding thiol family of natural product HDAC inhibitors. in *Successful Drug Discovery; volume 2* (eds. Fischer, J. & Childers, W. E.) 13–30 (2016).

369. Souto, J. A. *et al.* Synthesis and Biological Characterization of the Histone Deacetylase Inhibitor Largazole and C7- Modified Analogues. *J. Med. Chem.* **53**, 4654–4667 (2010).

370. Yao, Y. *et al.* Discovery of Novel Class i Histone Deacetylase Inhibitors with Promising in Vitro and in Vivo Antitumor Activities. *J. Med. Chem.* **58**, 7672–7680 (2015).

371. Almaliti, J. *et al.* Largazole Analogues Embodying Radical Changes in the Depsipeptide Ring: Development of a More Selective and Highly Potent Analogue. *J. Med. Chem.* **59**, 10642–10660 (2016).

372. Benelkebir, H. *et al.* Total synthesis of largazole and analogues: HDAC inhibition, antiproliferative activity and metabolic stability. *Bioorganic Med. Chem.* **19**, 3650–3658 (2011).

373. de Lera, A. R. & Ganesan, A. Epigenetic polypharmacology: from combination therapy to multitargeted drugs. *Clin. Epigenetics* **8**, 1–21 (2016).

374. Morphy, R., Kay, C. & Rankovic, Z. From magic bullets to designed multiple ligands. *Drug Discov. Today* **9**, 641–651 (2004).

375. Ganesan, A. Multitarget Drugs: an Epigenetic Epiphany. *ChemMedChem* **11**, 1227–1241 (2016).

376. Mahboobi, S. *et al.* Design of Chimeric Histone Deacetylase- and Tyrosine Kinase-Inhibitors: A Series of Imatinib Hybrides as Potent Inhibitors of Wild-Type and Mutant BCR-ABL, PDGF-Rβ, and Histone Deacetylases †. *J. Med. Chem.* **52**, 2265–2279 (2009).

377. Cai, X. *et al.* Discovery of 7-(4-(3-Ethynylphenylamino)-7-methoxyquinazolin-6-yloxy)-N -hydroxyheptanamide (CUDC-101) as a Potent Multi-Acting HDAC, EGFR, and HER2 Inhibitor for the Treatment of Cancer. *J. Med. Chem.* **53**, 2000–2009 (2010).

378. Galloway, T. J. *et al.* A phase I study of CUDC-101, a multitarget inhibitor of HDACs, EGFR, and HER2, in combination with chemoradiation in patients with head and neck squamous cell carcinoma. *Clin. Cancer Res.* **21**, 1566–1573 (2015).

379. Beckers, T. *et al.* Chimerically designed HDAC- and tyrosine kinase inhibitors. A series of erlotinib hybrids as dual-selective inhibitors of EGFR, HER2 and histone deacetylases. *Medchemcomm* **3**, 829–835 (2012).

380. Zuo, M., Zheng, Y.-W., Lu, S.-M., Li, Y. & Zhang, S.-Q. Synthesis and biological evaluation of N-aryl salicylamides with a hydroxamic acid moiety at 5-position as novel HDAC–EGFR dual inhibitors. *Bioorg. Med. Chem.* **20**, 4405–4412 (2012).

381. Zhang, X., Su, M., Chen, Y., Li, J. & Lu, W. The Design and Synthesis of a New Class of RTK/HDAC Dual-Targeted Inhibitors. *Molecules* **18**, 6491–6503 (2013).

382. Qian, C. *et al.* Cancer network disruption by a single molecule inhibitor targeting both histone deacetylase activity and phosphatidylinositol 3-kinase signaling. *Clin. Cancer Res.* **18**, 4104–4113 (2012).

383. Chen, L. *et al.* Dual inhibitors of inosine monophosphate dehydrogenase and histone deacetylase based on a cinnamic hydroxamic acid core structure. *Bioorg. Med. Chem.* **18**,

5950–5964 (2010).

384. Chen, J.-B. *et al.* Design and Synthesis of Dual-Action Inhibitors Targeting Histone Deacetylases and 3-Hydroxy-3-methylglutaryl Coenzyme A Reductase for Cancer Treatment. *J. Med. Chem.* **56**, 3645–3655 (2013).

385. Fischer, J. *et al.* Synthetically accessible non-secosteroidal hybrid molecules combining vitamin D receptor agonism and histone deacetylase inhibition. *Chem. Biol.* **19**, 963–971 (2012).

386. Chen, G. L. *et al.* Discovery of a small molecular compound simultaneously targeting RXR and HADC: Design, synthesis, molecular docking and bioassay. *Bioorganic Med. Chem. Lett.* **23**, 3891–3895 (2013).

387. Atkinson, S. J. *et al.* The structure based design of dual HDAC/BET inhibitors as novel epigenetic probes. *Medchemcomm* **5**, 342–351 (2014).

388. Stenzel, K. *et al.* Isophthalic Acid-Based HDAC Inhibitors as Potent Inhibitors of HDAC8 from Schistosoma mansoni. *Arch. Pharm. (Weinheim).* **350**, 1–10 (2017).

389. Simoben, C. *et al.* A Novel Class of Schistosoma mansoni Histone Deacetylase 8 (HDAC8) Inhibitors Identified by Structure-Based Virtual Screening and In Vitro Testing. *Molecules* **23**, 566 (2018).

390. Chakrabarti, A. *et al.* HDAC8: A multifaceted target for therapeutic interventions. *Trends Pharmacol. Sci.* **36**, 481–492 (2015).

391. Lipinski, C. A. Lead- and drug-like compounds: The rule-of-five revolution. *Drug Discov. Today Technol.* **1**, 337–341 (2004).

392. Martins, M. B. & Carvalho, I. Diketopiperazines: biological activity and synthesis. *Tetrahedron* **63**, 9923–9932 (2007).

393. Borthwick, A. D. 2,5-diketopiperazines: Synthesis, reactions, medicinal chemistry, and bioactive natural products. *Chem. Rev.* **112**, 3641–3716 (2012).

394. Wang, H. & Ganesan, A. The *N* -Acyliminium Pictet−Spengler Condensation as a Multicomponent Combinatorial Reaction on Solid Phase and Its Application to the Synthesis of Demethoxyfumitremorgin C Analogues. *Org. Lett.* **1**, 1647–1649 (1999).

395. Bonnet, D. & Ganesan, A. Solid-Phase Synthesis of Tetrahydro-β-carbolinehydantoins via the N-Acyliminium Pictet-Spengler Reaction and Cyclative Cleavage. *J. Comb. Chem.* **4**, 546–548 (2002).

396. Bonnet, D. *et al*. Combinatorial aid for underprivileged scaffolds: Solution and solid-phase strategies for a rapid and efficient access to novel aza-diketopiperazines (aza-DKP). *ACS Comb. Sci.* **14**, 323–334 (2012).

397. Petit, S., Fruit, C. & Bischoff, L. New family of peptidomimetics based on the imidazole motif. *Org. Lett.* **12**, 4928–4931 (2010).

398. Holler, T. P., Ruan, F., Spaltenstein, A. & Hopkins, P. B. Total synthesis of marine mercaptohistidines: ovothiols A, B, and C. *J. Org. Chem.* **54**, 4570–4575 (1989).

399. Lecointre, B. Functionalization of pyridine N-oxide - Peptidomimetics based on the imidazole motif used as Histone Deacetylase inhibitors. (University of Rouen Normandy, 2014).

400. Waghmare, A. A., Hindupur, R. M. & Pati, H. N. Propylphosphonic anhydride (T3P®): An expedient reagent for organic synthesis. *Rev. J. Chem.* **4**, 53–131 (2014).

401. Hiebl, J. *et al.* Large-scale synthesis of hematoregulatory nonapeptide SK and F 107647 by fragment coupling. *J. Pept. Res.* **54**, 54–65 (1999).

402. Ho, C. Y., Strobel, E., Ralbovsky, J. & Galemmo, R. A. Improved Solution and Solid phase preparation of hydroxamic acids from ester. *J. Org. Chem* **70**, 4873–4875 (2005).

403. Botta, C. B. *et al.* Oxime amides as a novel zinc binding group in histone deacetylase inhibitors: Synthesis, biological activity, and computational evaluation. *J. Med. Chem.* **54**, 2165–2182 (2011).

404. Usachova, N., Leitis, G., Jirgensons, A. & Kalvinsh, I. Synthesis of Hydroxamic Acids by Activation of Carboxylic Acids with *N* , *N* ′-Carbonyldiimidazole: Exploring the Efficiency of the Method. *Synth. Commun.* **40**, 927–935 (2010).

405. Amitai, G. *et al.* Novel bifunctional hybrid small molecule scavengers for mitigating nerve agents toxicity. *Chem. Biol. Interact.* **259**, 187–204 (2016).

406. Konya, K. G., Paul, T., Lin, S., Lusztyk, J. & Ingold, K. U. Laser flash photolysis studies on the first superoxide thermal source. First direct measurements of the rates of solvent-assisted 1,2-hydrogen atom shifts and a proposed new mechanism for this unusual rearrangement. *J. Am. Chem. Soc.* **122**, 7518–7527 (2000).

407. Reisch, H. A., Leeming, P. & Raje, P. S. Methods of synthesis of certain hydroxamic acid compounds. (2008). doi:WO2009/040517

408. Lee, H. Y. *et al.* Azaindolylsulfonamides, with a more selective inhibitory effect on

histone deacetylase 6 activity, exhibit antitumor activity in colorectal cancer HCT116 cells. *J. Med. Chem.* **57**, 4009–4022 (2014).

409. Lee, H. Y. *et al.* 3-Aroylindoles display antitumor activity in vitro and in vivo: Effects of N1-substituents on biological activity. *Eur. J. Med. Chem.* **125**, 1268–1278 (2017).

410. Fitton, P. & Rick, E. A. The addition of aryl halides to tetrakis(triphenylphosphine)palladium(0). *J. Organomet. Chem.* **28**, 287–291 (1971).

411. de Meijere, A. & Meyer, F. E. Fine Feathers Make Fine Birds: The Heck Reaction in Modern Garb. *Angew. Chemie Int. Ed. English* **33**, 2379–2411 (1995).

412. Hassan, M. E., Greenfield, A. A. & Liu, K. Substituted-3-sulfonylindazole derivatives as 5-hydroxytryptamine-6 ligands. doi:US20070037802A1

413. Olesen, P. H. Novel compounds for the treatment of obesity. doi:WO2005051900A1

414. Bléger, D. *et al.* Janus-like 3D tectons: Self-assembled 2D arrays of functional units at a defined distance from the substrate. *Angew. Chemie - Int. Ed.* **50**, 6562–6566 (2011).

415. Epple, R. *et al.* 1,3,5-Trisubstituted aryls as highly selective PPARδ agonists. *Bioorganic Med. Chem. Lett.* **16**, 2969–2973 (2006).

416. Xu, F. *et al.* Substituted 5,6,11,12-tetradehydrodibenzo[a, e]cyclooctenes: Syntheses, properties, and DFT studies of substituted sondheimer-wong diynes. *J. Org. Chem.* **79**, 11592–11608 (2014).

417. Lennox, A. J. J. & Lloyd-Jones, G. C. Selection of boron reagents for Suzuki-Miyaura coupling. *Chem. Soc. Rev.* **43**, 412–443 (2014).

418. Simpson, M. G., Pittelkow, M., Watson, S. P. & Sanders, J. K. M. Dynamic combinatorial chemistry with hydrazones: Libraries incorporating heterocyclic and steroidal motifs. *Org. Biomol. Chem.* **8**, 1181–1187 (2010).

419. Franzmann, P., Trosien, S., Schubert, M. & Waldvogel, S. R. Modular Approach to 9-Monosubstituted Fluorene Derivatives Using Mo ^{V} Reagents. *Org. Lett.* **18**, 1182–1185 (2016).

420. Hanessian, S., Moitessier, N. & Viau, M. N-Aryl Sulfonyl Homocysteine Hydroxamate Inhibitors of Matrix Metalloproteinases: Further Probing of the S1,S1′, and S2′ Pockets. *J. Med. Chem.* **44**, 3066–3073 (2001).

421. Belvedere, S. *et al.* Aminosuberoyl hydroxamic acids (ASHAs): A potent new class of

HDAC inhibitors. *Bioorganic Med. Chem. Lett.* **17**, 3969–3971 (2007).

422. Wilson, D. M., Silverman, L. N., Bergauer, M. & Keshari, K. R. Solid phase synthesis of hydroxamate peptides for histone deacetylase inhibition. *Tetrahedron Lett.* **54**, 151–153 (2013).

423. Dose, A. *et al.* Interrogating substrate selectivity and composition of endogenous histone deacetylase complexes with chemical probes. *Angew. Chemie - Int. Ed.* **55**, 1192–1195 (2016).

424. Wheatley, N. C. *et al.* Antimalarial histone deacetylase inhibitors containing cinnamate or NSAID components. *Bioorganic Med. Chem. Lett.* **20**, 7080–7084 (2010).

425. Glenn, M. P. *et al.* Antiproliferative and phenotype-transforming antitumor agents derived from cysteine. *J. Med. Chem.* **47**, 2984–2994 (2004).

426. Mellor, S. L., McGuire, C. & Chan, W. C. N-Fmoc-aminooxy-2-chlorotrityl polystyrene resin: A facile solid-phase methodology for the synthesis of hydroxamic acids. *Tetrahedron Lett.* **38**, 3311–3314 (1997).

427. Guibé, F. Allylic protecting groups and their use in a complex environment Part II: Allylic protecting groups and their removal through catalytic palladium π-allyl methodology. *Tetrahedron* **54**, 2967–3042 (1998).

428. CHANG, C.-D. *et al.* PREPARATION AND PROPERTIES OF Nα-9-FLUORENYLMETHYLOXYCARBONYLAMINO ACIDS BEARING TERT.-BUTYL SIDE CHAIN PROTECTION. *Int. J. Pept. Protein Res.* **15**, 59–66 (2009).

429. Kohn, H. *et al.* Compositions having antimycrobial activity including a hydroxamate or a hydroxamate and a hydroxylamine. (2005). doi:WO2005020973A2

430. Rostovtsev, V. V., Green, L. G., Fokin, V. V. & Sharpless, K. B. A stepwise huisgen cycloaddition process: Copper(I)-catalyzed regioselective 'ligation' of azides and terminal alkynes. *Angew. Chemie - Int. Ed.* **41**, 2596–2599 (2002).

431. Huisgen, R. 1,3-dipolar cycloadditions. *Proc. Chem. Soc. Chem. Soc.* (1961).

432. Worrell, B. T., Malik, J. a. & Fokin, V. V. Direct Evidence of Direct Evidence of a Dinuclear Copper Intermediate in Cu(I)-Catalyzed Azide-Alkyne Cycloadditionsa Dinuclear. *Science (80-.).* **340**, 457–460 (2013).

433. Jin, L., Tolentino, D. R., Melaimi, M. & Bertrand, G. Isolation of bis(copper) key intermediates in Cu-catalyzed azide-alkyne "click reaction". *Sci. Adv.* **1**, e1500304 (2015).

434. Guerrant, W. *et al*. Dual-acting histone deacetylase-topoisomerase i inhibitors. *Bioorganic Med. Chem. Lett.* **23**, 3283–3287 (2013).

435. Guerrant, W., Patil, V., Canzoneri, J. C. & Oyelere, A. K. Dual targeting of histone deacetylase and topoisomerase II with novel bifunctional inhibitors. *J. Med. Chem.* **55**, 1465–1477 (2012).

436. Rajulu, G. G. *et al.* New Hydroxamic Acid Derivatives of Fluoroquinolones: Synthesis and Evaluation of Antibacterial and Anticancer Properties. *Chem. Pharm. Bull.* **62**, 168–175 (2014).

437. Raji, I. *et al.* Bifunctional conjugates with potent inhibitory activity towards cyclooxygenase and histone deacetylase. *Bioorganic Med. Chem.* **25**, 1202–1218 (2017).

438. Purwin, M. *et al*. Design and synthesis of novel dual-target agents for HDAC1 and CK2 inhibition. *RSC Adv.* **6**, 66595–66608 (2016).

439. Gryder, B. E. *et al.* Histone deacetylase inhibitors equipped with estrogen receptor modulation activity. *J. Med. Chem.* **56**, 5782–5796 (2013).

440. Hou, J. *et al*. Discovery and extensive in vitro evaluations of NK-HDAC-1: A chiral histone deacetylase inhibitor as a promising lead. *J. Med. Chem.* **55**, 3066–3075 (2012).

441. Shen, J. *et al*. Histone Deacetylase Inhibitors through Click Chemistry. *J. Med. Chem.* **51**, 7417–7427 (2008).

442. Hou, J. *et al.* Structure-based optimization of click-based histone deacetylase inhibitors. *Eur. J. Med. Chem.* **46**, 3190–3200 (2011).

443. Sun, Q. *et al.* Design, synthesis, and biological evaluation of novel histone deacetylase 1 inhibitors through click chemistry. *Bioorganic Med. Chem. Lett.* **23**, 3295–3299 (2013).

444. Suzuki, T. *et al*. Identification of Highly Selective and Potent Histone Deacetylase 3 Inhibitors Using Click Chemistry-Based Combinatorial Fragment Assembly. *PLoS One* **8**, 1–12 (2013).

445. Suzuki, T. *et al.* An unexpected example of protein-templated click chemistry. *Angew. Chemie - Int. Ed.* **49**, 6817–6820 (2010).

446. Suzuki, T. *et al*. Design, Synthesis, and Biological Activity of NCC149 Derivatives as Histone Deacetylase 8-Selective Inhibitors. *ChemMedChem* **9**, 657–664 (2014).

447. Beeler, A. B., Porco, J. A., Ingham, O. J. & Bradner, J. E. Selective histone deacetylase 8

inhibitors. (2014). doi:WO2014116962A1

448. Cavender, C. J. & Shiner, V. J. Trifluoromethanesulfonyl Azide. Its Reaction with Alkyl Amines to Form Alkyl Azides. *J. Org. Chem.* **37**, 3567–3569 (1972).

449. Fischer, N. *et al.* Sensitivities of some imidazole-1-sulfonyl azide salts. *J. Org. Chem.* **77**, 1760–1764 (2012).

450. Alper, P. B., Hung, S. C. & Wong, C. H. Metal catalyzed diazo transfer for the synthesis of azides from amines. *Tetrahedron Lett.* **37**, 6029–6032 (1996).

451. Nyffeler, P. T., Liang, C. H., Koeller, K. M. & Wong, C. H. The chemistry of amine-azide interconversion: Catalytic diazotransfer and regioselective azide reduction. *J. Am. Chem. Soc.* **124**, 10773–10778 (2002).

452. Pandiakumar, A. K., Sarma, S. P. & Samuelson, A. G. Mechanistic studies on the diazo transfer reaction. *Tetrahedron Lett.* **55**, 2917–2920 (2014).

453. Yan, R.-B., Yang, F., Wu, Y., Zhang, L.-H. & Ye, X.-S. An efficient and improved procedure for preparation of triflyl azide and application in catalytic diazotransfer reaction. *Tetrahedron Lett.* **46**, 8993–8995 (2005).

454. Oueis, E., Jaspars, M., Westwood, N. J. & Naismith, J. H. Enzymatic Macrocyclization of 1,2,3-Triazole Peptide Mimetics. *Angew. Chemie - Int. Ed.* **55**, 5842–5845 (2016).

455. Huang, F. chih *et al.* Differential Effects of a Series of Hydroxamic Acid Derivatives on 5-Lipoxygenase and Cyclooxygenase from Neutrophils and 12-Lipoxygenase from Platelets and Their in Vivo Effects on Inflammation and Anaphylaxis. *J. Med. Chem.* **32**, 1836–1842 (1989).

456. Bantscheff, M. *et al.* Chemoproteomics profiling of HDAC inhibitors reveals selective targeting of HDAC complexes. *Nat. Biotechnol.* **29**, 255–268 (2011).

457. Sousa, C. & Silva, P. J. BBr 3 -Assisted Cleavage of Most Ethers Does Not Follow the Commonly Assumed Mechanism. *European J. Org. Chem.* **2013**, 5195–5199 (2013).

458. Kosak, T. M., Conrad, H. A., Korich, A. L. & Lord, R. L. Ether Cleavage Re-Investigated: Elucidating the Mechanism of BBr3-Facilitated Demethylation of Aryl Methyl Ethers. *European J. Org. Chem.* **2015**, 7460–7467 (2015).

459. Ackermann, L., Potukuchi, H. K., Landsberg, D. & Vicente, R. Copper-Catalyzed "Click" Reaction/Direct Arylation Sequence: Modular Syntheses of 1,2,3-Triazoles. *Org. Lett.* **10**, 3081–3084 (2008).

460. Chuprakov, S., Chernyak, N., Dudnik, A. S. & Gevorgyan, V. Direct Pd-catalyzed arylation of 1,2,3-triazoles. *Org. Lett.* **9**, 2333–2336 (2007).

461. Wei, F. *et al.* Cu/Pd-Catalyzed, Three-Component Click Reaction of Azide, Alkyne, and Aryl Halide: One-Pot Strategy toward Trisubstituted Triazoles. *Org. Lett.* **17**, 2860–2863 (2015).

462. Berry, M. T., Castrejon, D. & Hein, J. E. Oxidative esterification of aldehydes using mesoionic 1,2,3-triazolyl carbene organocatalysts. *Org. Lett.* **16**, 3676–3679 (2014).

463. Hein, J. E., Tripp, J. C., Krasnova, L. B., Sharpless, K. B. & Fokin, V. V. Copper(I)-catalyzed cycloaddition of organic azides and 1-iodoalkynes. *Angew. Chemie - Int. Ed.* **48**, 8018–8021 (2009).

464. Dheer, D. *et al.* β-CD/CuI catalyzed regioselective synthesis of iodo substituted 1,2,3-triazoles, imidazo[1,2-a]-pyridines and benzoimidazo[2,1-b]thiazoles in water and their functionalization. *Tetrahedron* **73**, 4295–4306 (2017).

465. Goyard, D. *et al.* Efficient atropodiastereoselective access to 5,5′-bis-1,2,3- triazoles: Studies on 1-glucosylated 5-halogeno 1,2,3-triazoles and their 5-substituted derivatives as glycogen phosphorylase inhibitors. *Chem. - A Eur. J.* **20**, 5423–5432 (2014).

466. Deobald, A. *et al.* Synthesis of Arylseleno-1,2,3-triazoles via Copper-Catalyzed 1,3-Dipolar Cycloaddition of Azido Arylselenides with Alkynes. *Synthesis (Stuttg).* **2011**, 2397–2406 (2011).

467. Ingham, O. J. *et al.* Development of a Potent and Selective HDAC8 Inhibitor. *ACS Med. Chem. Lett.* **7**, 929–932 (2016).

468. Fu, D., Zhang, J. & Cao, S. Copper-mediated trifluoromethylation of 5-iodotriazole with (trifluoromethyl)trimethylsilane promoted by silver carbonate. *J. Fluor. Chem.* **156**, 170–176 (2013).

469. Deng, J., Wu, Y.-M. & Chen, Q.-Y. Cross-Coupling Reaction of Iodo-1,2,3-triazoles Catalyzed by Palladium. *Synthesis (Stuttg).* **2005**, 2730–2738 (2005).

470. Jurricek, M., Stout, K., Kouwer, P. H. J. & Rowan, A. E. Fusing triazoles: Toward extending aromaticity. *Org. Lett.* **13**, 3494–3497 (2011).

471. Langmuir, I. Isomorphism, isosterism and covalence. *J. Am. Chem. Soc.* **41**, 1543–1559 (1919).

472. Friedman, H. L. Influence of isosteric replacements upon biological activity. in

Symposium on Chemical-Biological correlation Sciences, N. A. o 295 (Washington DC, 1951).

473. Duan, J., Decicco, C., Wasserman, Z. & Maduskuie, T. P. J. Novel lactam metalloprotease inhibitors. (1999). doi:WO9918074A1

474. Chollet, a M. *et al.* General synthesis of alpha-substituted 3-bisaryloxy propionic acid derivatives as specific MMP inhibitors. *Bioorg. Med. Chem. Lett.* **11**, 295–9 (2001).

475. Janser, P., Neumann, U., Miltz, W., Feifel, R. & Buhl, T. A cassette-dosing approach for improvement of oral bioavailability of dual TACE/MMP inhibitors. *Bioorganic Med. Chem. Lett.* **16**, 2632–2636 (2006).

476. O'Brien, P. M. *et al.* Structure-activity relationships and pharmacokinetic analysis for a series of potent, systemically available biphenylsulfonamide matrix metalloproteinase inhibitors. *J. Med. Chem.* **43**, 156–166 (2000).

477. Konnert, L., Lamaty, F., Martinez, J. & Colacino, E. Recent Advances in the Synthesis of Hydantoins: The State of the Art of a Valuable Scaffold. *Chem. Rev.* **117**, 13757–13809 (2017).

478. Urech, F. Ueber Lacturaminsaure und Lactylharnstoff. *Justus Liebigs Ann. Chem.* **165**, 99–103 (1873).

479. Bucherer, H. T. & Lieb, V. A. Über die Bildung substituierter Hydantoine aus Aldehyden und Ketonen. Synthese von Hydantoinen. *J. für Prakt. Chemie* **141**, 5–43 (1934).

480. Liu, H., Yang, Z. & Pan, Z. Synthesis of Highly Substituted Imidazolidine-2,4-dione (Hydantoin) through Tf_2O-Mediated Dual Activation of Boc-Protected Dipeptidyl Compounds. *Org. Lett.* **16**, 5902–5905 (2014).

481. Laurent, S. A.-L. *et al.* Synthesis of "Trioxaquantel"® Derivatives as Potential New Antischistosomal Drugs. *European J. Org. Chem.* **2008**, 895–913 (2008).

482. Pictet, A. & Spengler, T. Uber die Bildung von Isochinolin-derivaten durch Einwirkung von Methylal auf Phenyl-athylamin, Phenyl-alanin und Tyrosin. *Berichte der Dtsch. Chem. Gesellschaft* **44**, 2030–2036 (1911).

483. Baldwin, B. J. E. Rules for ring closure. *J. Chem. Soc., Chem. Commun.* 734–736 (1976).

484. Yokoyama, A., Ohwada, T. & Shudo, K. Prototype Pictet-Spengler reactions catalyzed by superacids. Involvement of dicationic superelectrophiles. *J. Org. Chem.* **64**, 611–617 (1999).

485. Maryanoff, B. E., Zhang, H. C., Cohen, J. H., Turchi, I. J. & Maryanoff, C. A. Cyclizations of *N*-acyliminium ions. *Chem. Rev.* **104**, 1431–1628 (2004).

486. Senger, J. *et al.* Synthesis and Biological Investigation of Oxazole Hydroxamates as Highly Selective Histone Deacetylase 6 (HDAC6) Inhibitors. *J. Med. Chem.* **59**, 1545–1555 (2016).

487. Crouch, S. P. M., Kozlowski, R., Slater, K. J. & Fletcher, J. The use of ATP bioluminescence as a measure of cell proliferation and cytotoxicity. *J. Immunol. Methods* **160**, 81–88 (1993).

488. Promega. CellTiter-Glo® Luminescent Assay Chemistry. Available at: https://www.promega.co.uk/products/cell-health-assays/cell-viability-and-cytotoxicity-assays/celltiter_glo-luminescent-cell-viability-assay/?catNum=G7570&cs=y. (Accessed: 20th April 2019)

489. Santo, L. *et al.* Preclinical activity, pharmacodynamic, and pharmacokinetic properties of a selective HDAC6 inhibitor, ACY-1215, in combination with bortezomib in multiple myeloma. *Blood* **119**, 2579–2589 (2012).

490. Kalinsky, K. *et al.* Phase IB trial of ACY-1215 (Ricolinostat) combined with nab-paclitaxel in metastatic breast cancer. *J. Clin. Oncol.* **36**, 1058–1058 (2018).

491. Lecointre, B. *et al.* Isoform-selective HDAC1/6/8 inhibitors with an imidazo-ketopiperazine cap containing stereochemical diversity. *Philos. Trans. R. Soc. B Biol. Sci.* **373**, 1–7 (2018).

492. Sugimoto, B. K. *et al.* Frequent Mutations in the p53 Gene in Human Myeloid Leukemia Cell Lines. *Blood* **79**, 2378–2383 (1992).

493. Yu, Z. *et al.* Antiproliferative and apoptotic activities of sequence-specific histone acetyltransferase inhibitors. *Eur. J. Med. Chem.* **138**, 320–327 (2017).

494. Gopalakrishnapillai, A., Kolb, E. A., McCahan, S. M. & Barwe, S. P. Epigenetic drug combination induces remission in mouse xenograft models of pediatric acute myeloid leukemia. *Leuk. Res.* **58**, 91–97 (2017).

495. Howard, J. A. K., Hoy, V. J., O'Hagan, D. & Smith, G. T. How good is Fluorine as a Hydrogen Bond Acceptor. *Tetrahedron* **52**, 12613–12622 (1996).

496. Dalvit, C. & Vulpetti, A. Weak Intermolecular Hydrogen Bonds with Fluorine: Detection and Implications for Enzymatic/Chemical Reactions, Chemical Properties, and

Ligand/Protein Fluorine NMR Screening. *Chem. - A Eur. J.* **22**, 7592–7601 (2016).

497. Schomaker, J. M. & Delia, T. J. Arylation of halogenated pyrimidines via a Suzuki coupling reaction. *J. Org. Chem.* **66**, 7125–7128 (2001).

498. Cocuzza, A. J., Chidester, D. R., Culp, S., Fitzgerald, L. & Gilligan, P. Use of the Suzuki reaction for the synthesis of aryl-substituted heterocycles as corticotropin-releasing hormone (CRH) antagonists. *Bioorg. Med. Chem. Lett.* **9**, 1063–1066 (1999).

499. Luthin, D. R. *et al.* Characterization of mono- and diaminopyrimidine derivatives as novel, nonpeptide gonadotropin releasing hormone (GnRH) receptor antagonists. *Bioorg Med Chem Lett* **12**, 3635–3639 (2002).

500. Montebugnoli, D. *et al.* Traceless solid-phase synthesis of 2,4,6-chlorodiamino and triaminopyrimidines. *Tetrahedron* **59**, 7147–7156 (2003).

501. Peng, Z. H., Journet, M. & Humphrey, G. A highly regioselective amination of 6-aryl-2,4-dichloropyrimidine. *Org. Lett.* **8**, 395–398 (2006).

502. Mitsunobu, O., Yamada, M. & Mukaiyama, T. Preparation of Esters of Phosphoric Acid by the Reaction of Trivalent Phosphorus Compounds with Diethyl Azodicarboxylate in the Presence of Alcohols. *Bull. Chem. Soc. Jpn.* **40**, 935–939 (1967).

503. Fletcher, S. The Mitsunobu reaction in the 21st century. *Org. Chem. Front.* **2**, 739–752 (2015).

504. Fukuyama, T., Jow, C. K. & Cheung, M. 2- and 4-Nitrobenzenesulfonamides: Exceptionally versatile means for preparation of secondary amines and protection of amines. *Tetrahedron Lett.* **36**, 6373–6374 (1995).

505. Laclef, S. *et al.* Scalable asymmetric synthesis of a key fragment of Bcl-2/Bcl-$_{xL}$ inhibitors. *RSC Adv.* **4**, 39817 (2014).

506. Huang, H. & Kang, J. Y. Mitsunobu Reaction Using Basic Amines as Pronucleophiles. *J. Org. Chem.* **82**, 6604–6614 (2017).

507. PerkinElmer. Alpha reagent. Available at: http://www.perkinelmer.com/fr/category/alpha-reagents. (Accessed: 20th April 2019)

508. Fulmer, G. R. *et al.* NMR Chemical Shifts of Trace Impurities: Common Laboratory Solvents, Organics, and Gases in Deuterated Solvents Relevant to the Organometallic Chemist. *Organometallics* **29**, 2176–2179 (2010).

509. Borrello, M. T. *et al.* Fluorinated tranylcypromine analogues as inhibitors of lysine-specific demethylase 1 (LSD1, KDM1A). *Bioorg. Med. Chem. Lett.* **27**, 2099–2101 (2017).

510. Molecular Operating Environment (MOE), 2014.09; Chemical Computing Group Inc., 1010 Sherbooke St. West, Suite #910, Montreal, QC, Canada, H3A 2R7, 2014.

511. Schrödinger Release 2014-2: LigPrep, Schrödinger, LLC, New York, NY, 2014.

512. Berman, H. M. *et al.* The Protein Data Bank. *Nucleic Acids Res.* **28**, 235–242 (2000).

513. Schrödinger Release 2014-2: Schrödinger Suite 2014-2 Protein Preparation Wizard; Epik version 2.8, Schrödinger, LLC, New York, NY, 2014; Impact version 6.3, Schrödinger, LLC, New York, NY, 2014; Prime version 3.6, Schrödinger, LLC, New York, NY, 2014.

514. Small-Molecule Drug Discovery Suite 2014-2: Glide, version 9.8, Schrödinger, LLC, New York, NY, 2014.

515. Wutz, D. *et al.* Photochromic histone deacetylase inhibitors based on dithienylethenes and fulgimides. *Org. Biomol. Chem.* **15**, 4882–4896 (2017).

516. Ebner, S., Jaun, B., Goenrich, M., Thauer, R. K. & Harmer, J. Binding of coenzyme B induces a major conformational change in the active site of methyl-coenzyme M reductase. *J. Am. Chem. Soc.* **132**, 567–575 (2010).

517. Chatterjee, J., Laufer, B. & Kessler, H. Synthesis of N-methylated cyclic peptides. *Nat. Protoc.* **7**, 432–444 (2012).

518. Alonso, F., Moglie, Y., Radivoy, G. & Yus, M. Unsupported Copper Nanoparticles in the 1,3-Dipolar Cycloaddition of Terminal Alkynes and Azides. *European J. Org. Chem.* **2010**, 1875–1884 (2010).

519. Liu, Y., Huang, D., Huang, J. & Maruoka, K. Hypervalent Iodine Mediated Chemoselective Iodination of Alkynes. *J. Org. Chem.* **82**, 11865–11871 (2017).

Appendix

^{1}H NMR and ^{13}C NMR spectra of **3-186**

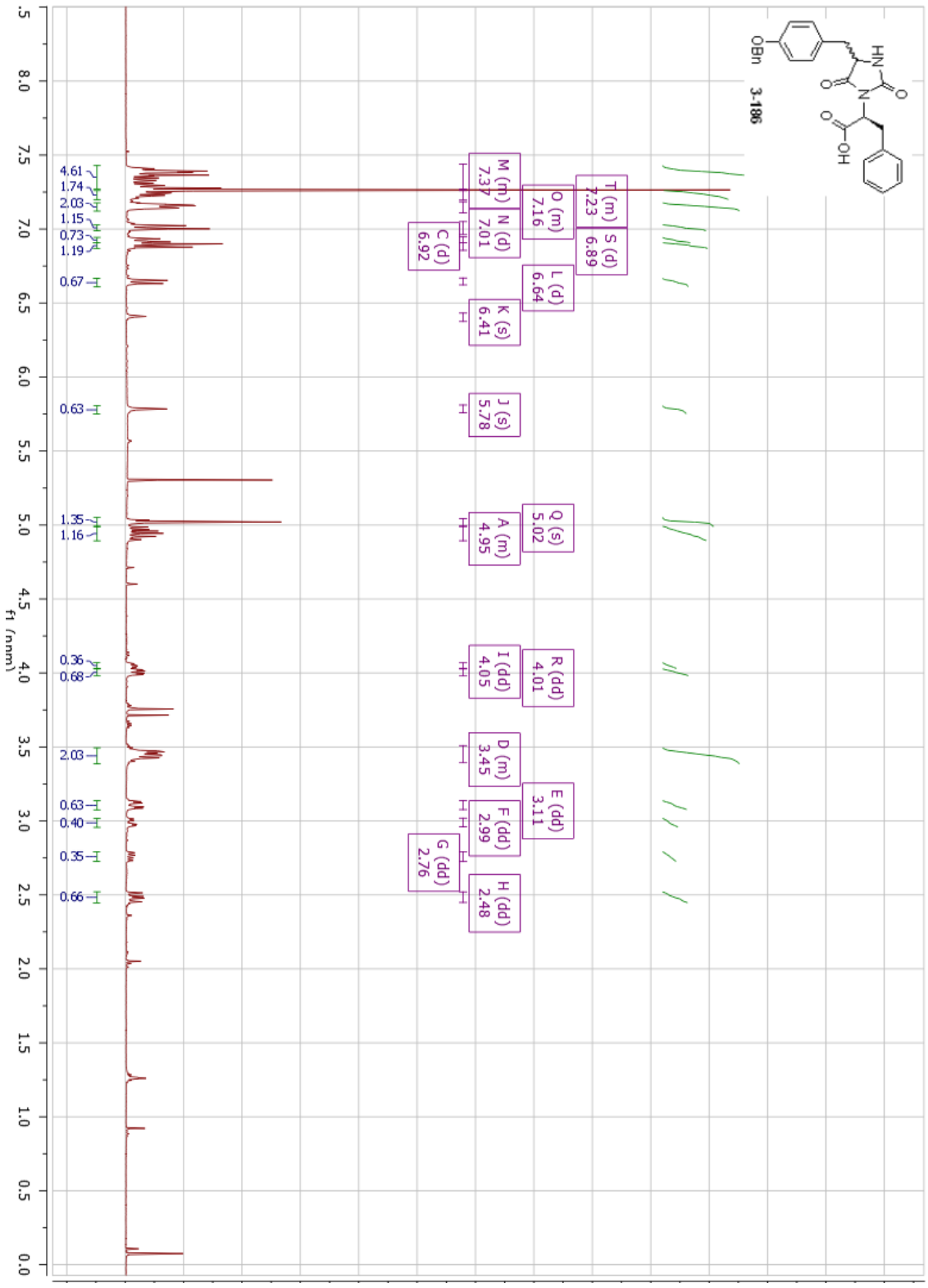

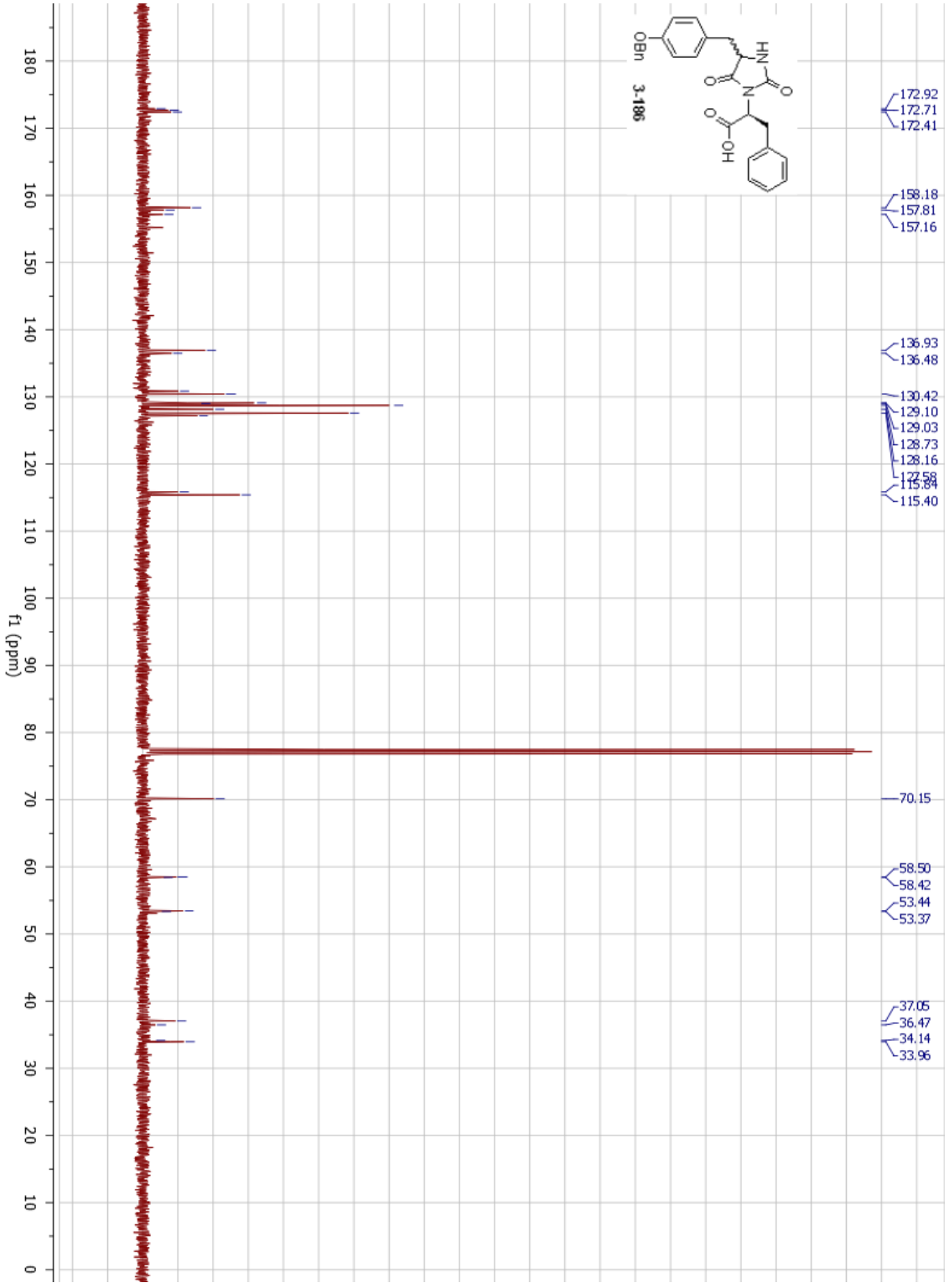
OBn
3-186
HN
O
O
N
O
OH
172.92
172.71
172.41
158.18
157.81
157.16
136.93
136.48
130.42
129.10
129.03
128.73
128.16
127.58
115.84
115.40
70.15
58.50
58.42
53.44
53.37
37.05
36.47
34.14
33.96
f1 (ppm)
180
170
160
150
140
130
120
110
100
90
80
70
60
50
40
30
20
10
0

^{1}H NMR and ^{13}C NMR spectra of **3-187**

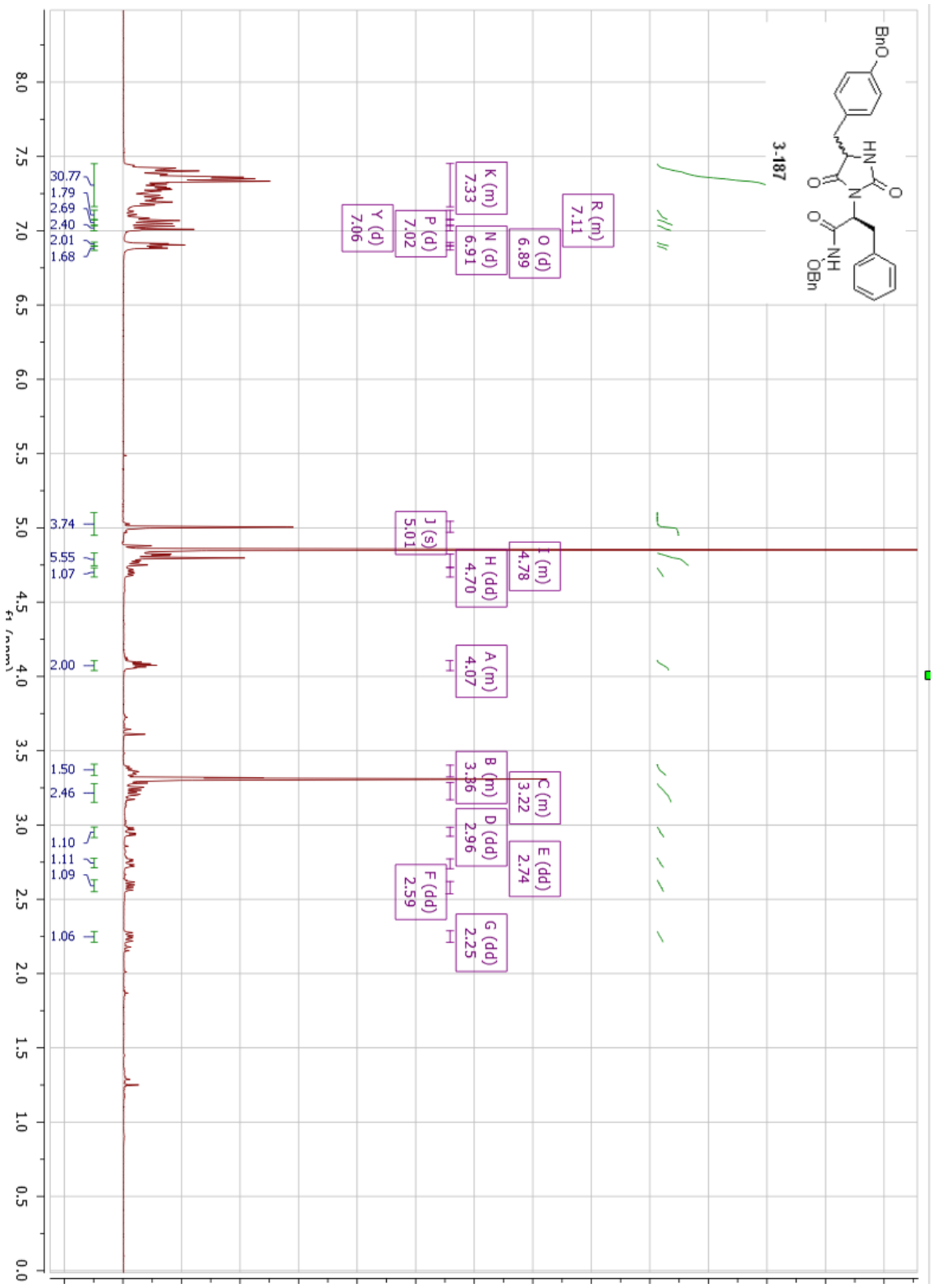

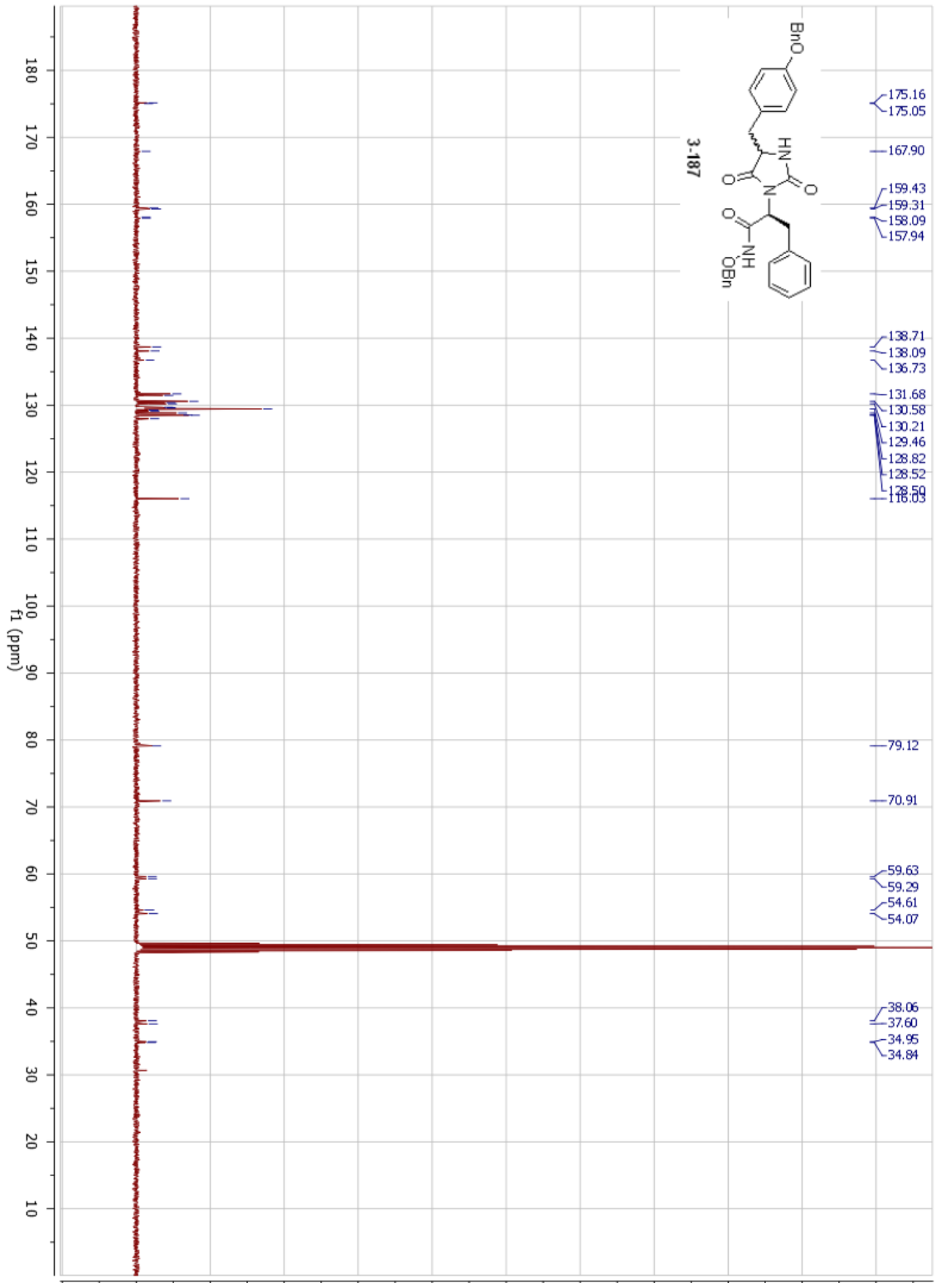
3-187
BnO
HN
O
O
N
O
NH
OBn
175.16
175.05
167.90
159.43
159.31
158.09
157.94
138.71
138.09
136.73
131.68
130.58
130.21
129.46
128.82
128.52
128.50
116.03
79.12
70.91
59.63
59.29
54.61
54.07
38.06
37.60
34.95
34.84
f1 (ppm)

COSY, HSQC and HMBC spectra of **3-187**

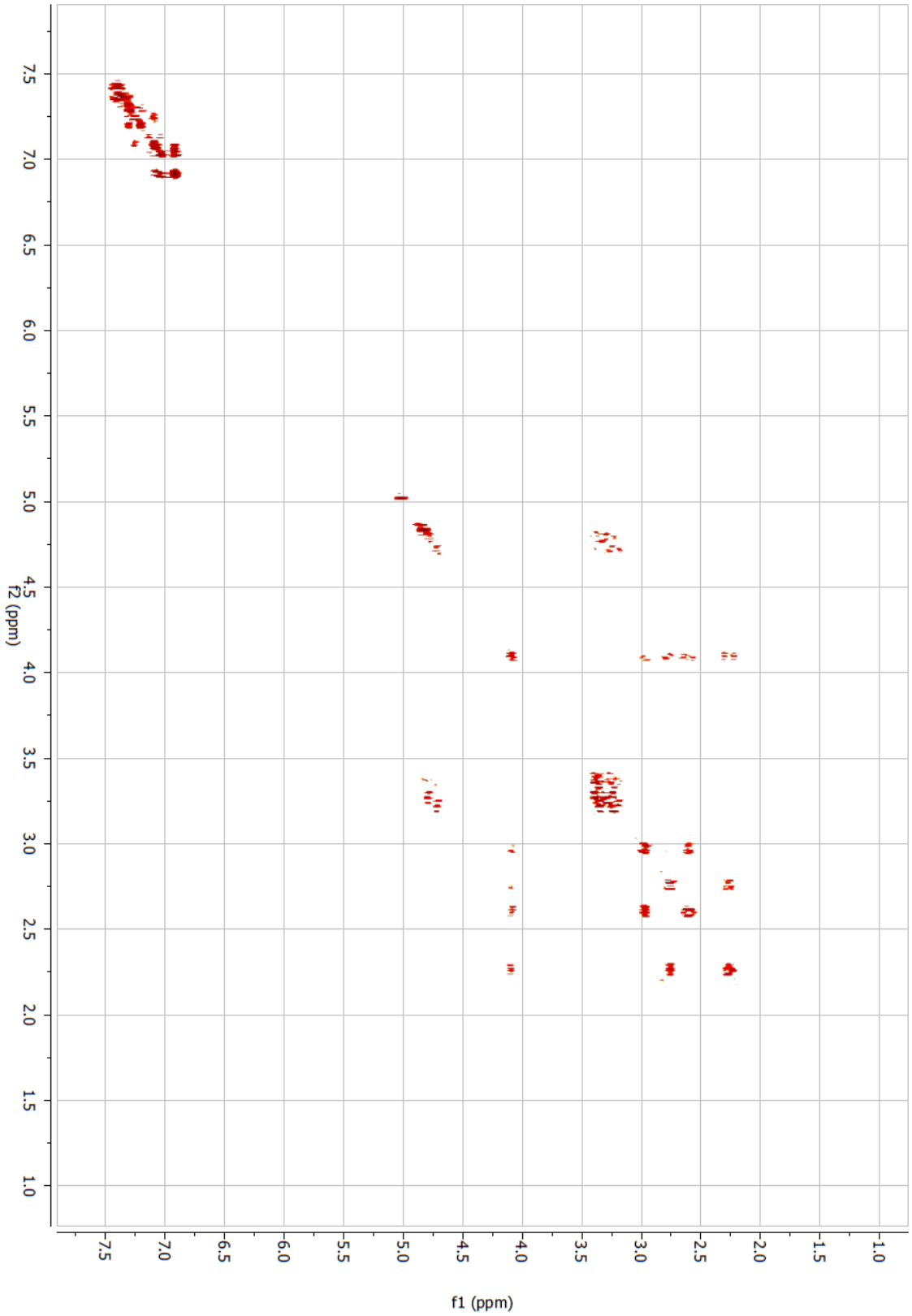

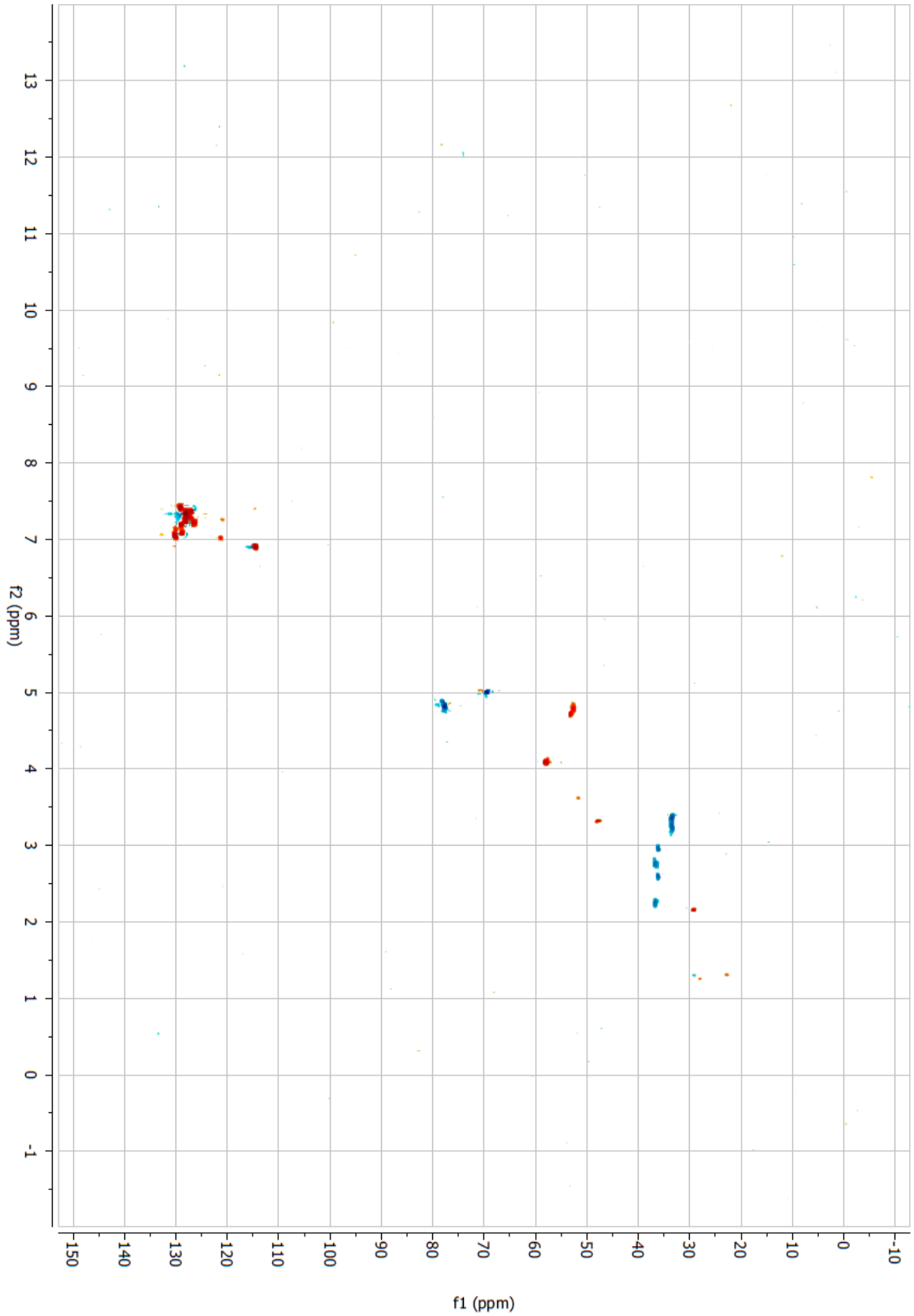
f2 (ppm)
13
12
11
10
9
8
7
6
5
4
3
2
1
0
-1
f1 (ppm)
150
140
130
120
110
100
90
80
70
60
50
40
30
20
10
0
-10

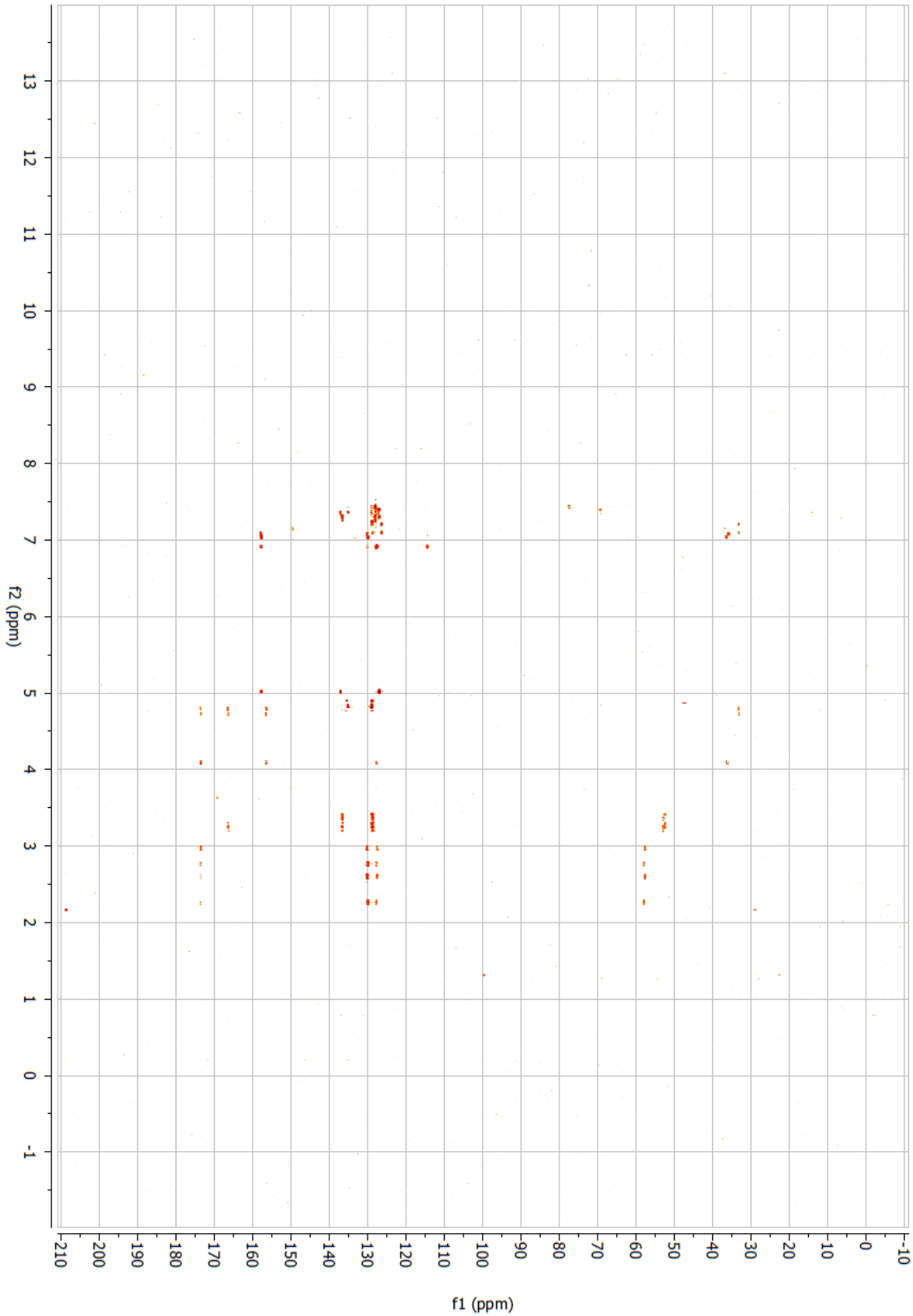
f2 (ppm)
13
12
11
10
9
8
7
6
5
4
3
2
1
0
-1
f1 (ppm)
210
200
190
180
170
160
150
140
130
120
110
100
90
80
70
60
50
40
30
20
10
0
-10

^{1}H NMR and ^{13}C NMR spectra of **3-188**

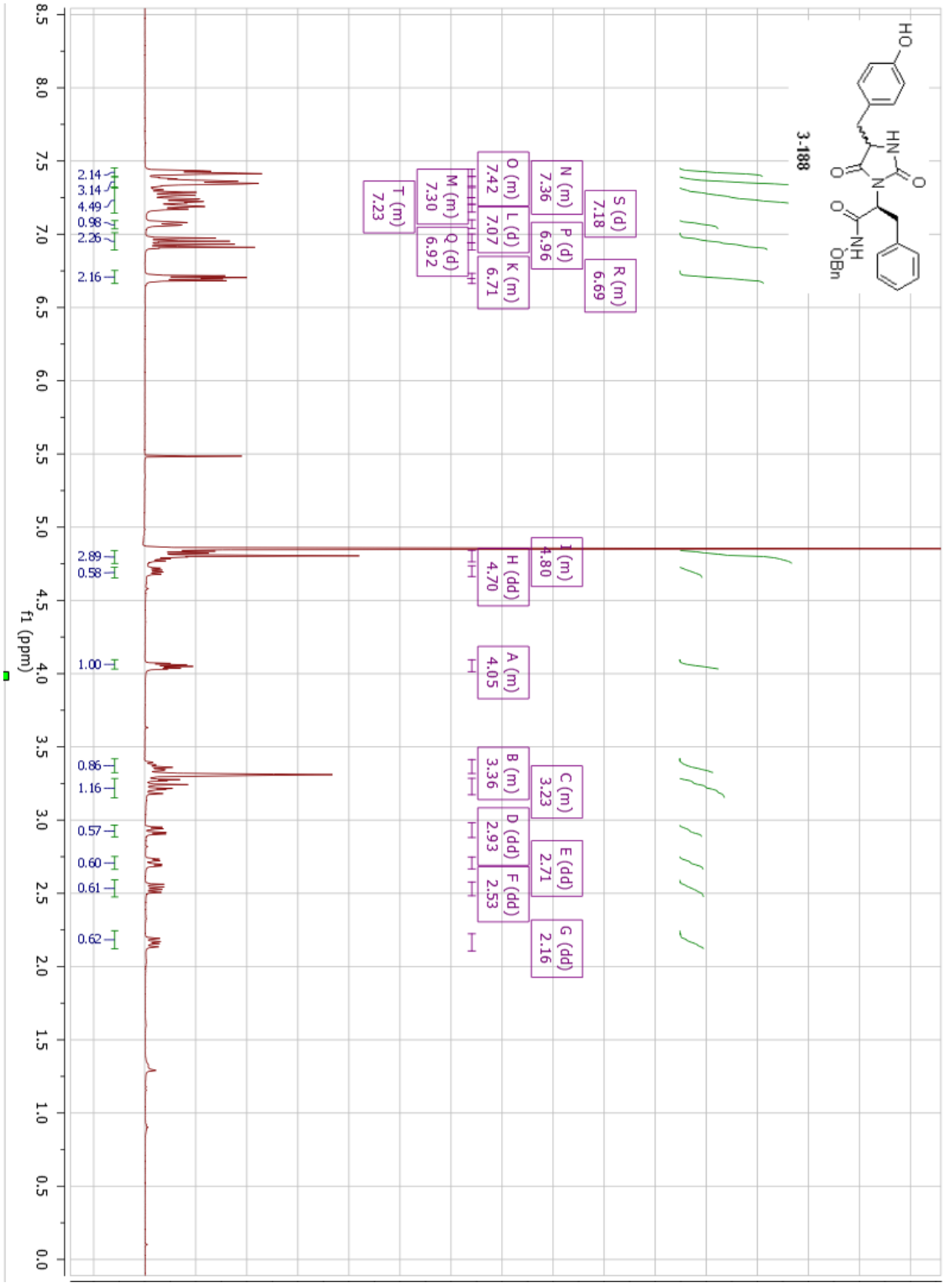

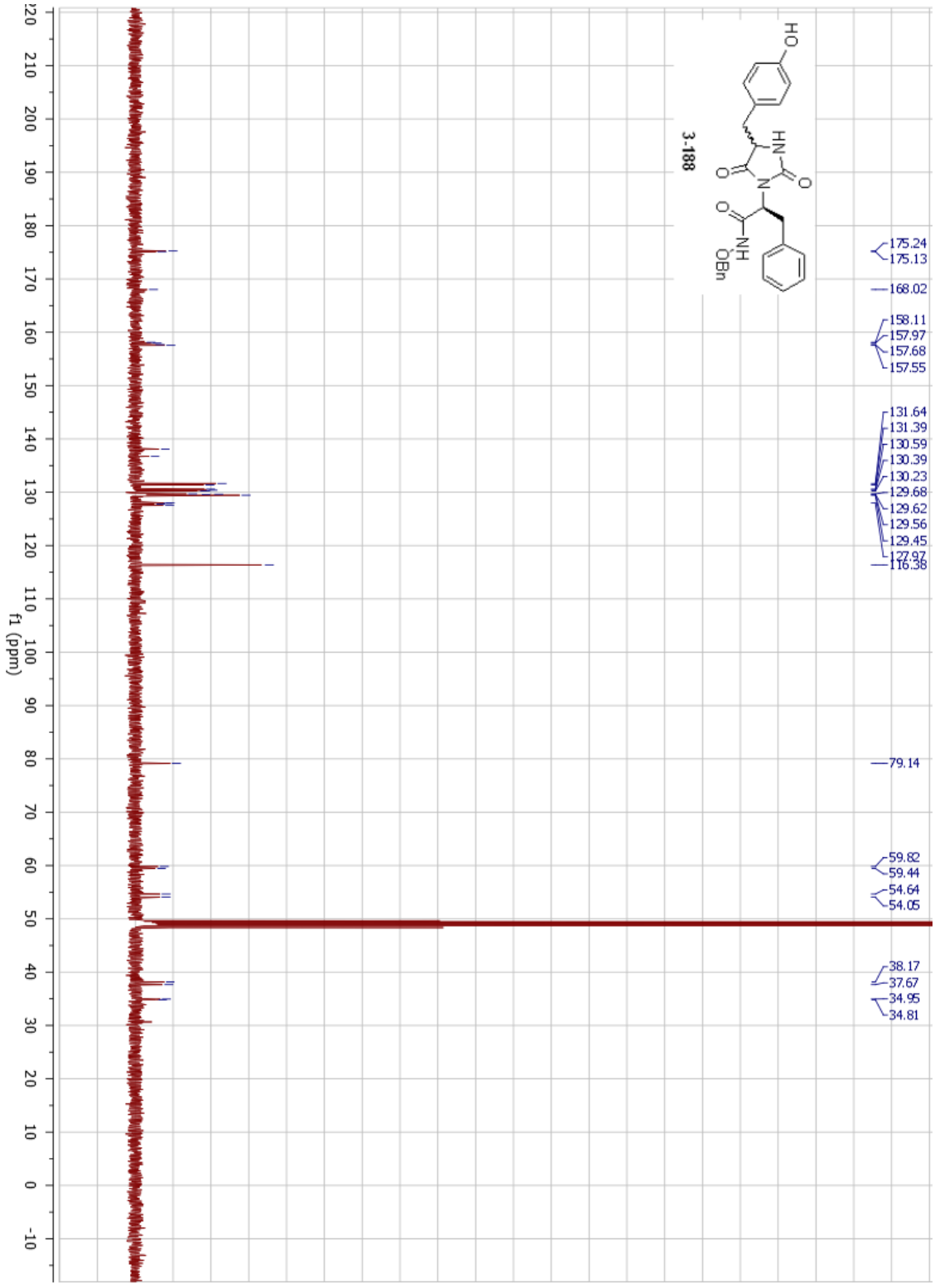
3-188
HO
HN
O
O
N
O
NH
OBn
175.24
175.13
168.02
158.11
157.97
157.68
157.55
131.64
131.39
130.59
130.39
130.23
129.68
129.62
129.56
129.45
127.97
116.38
79.14
59.82
59.44
54.64
54.05
38.17
37.67
34.95
34.81
f1 (ppm)

COSY, HSQC and HMBC spectra of **3-188**

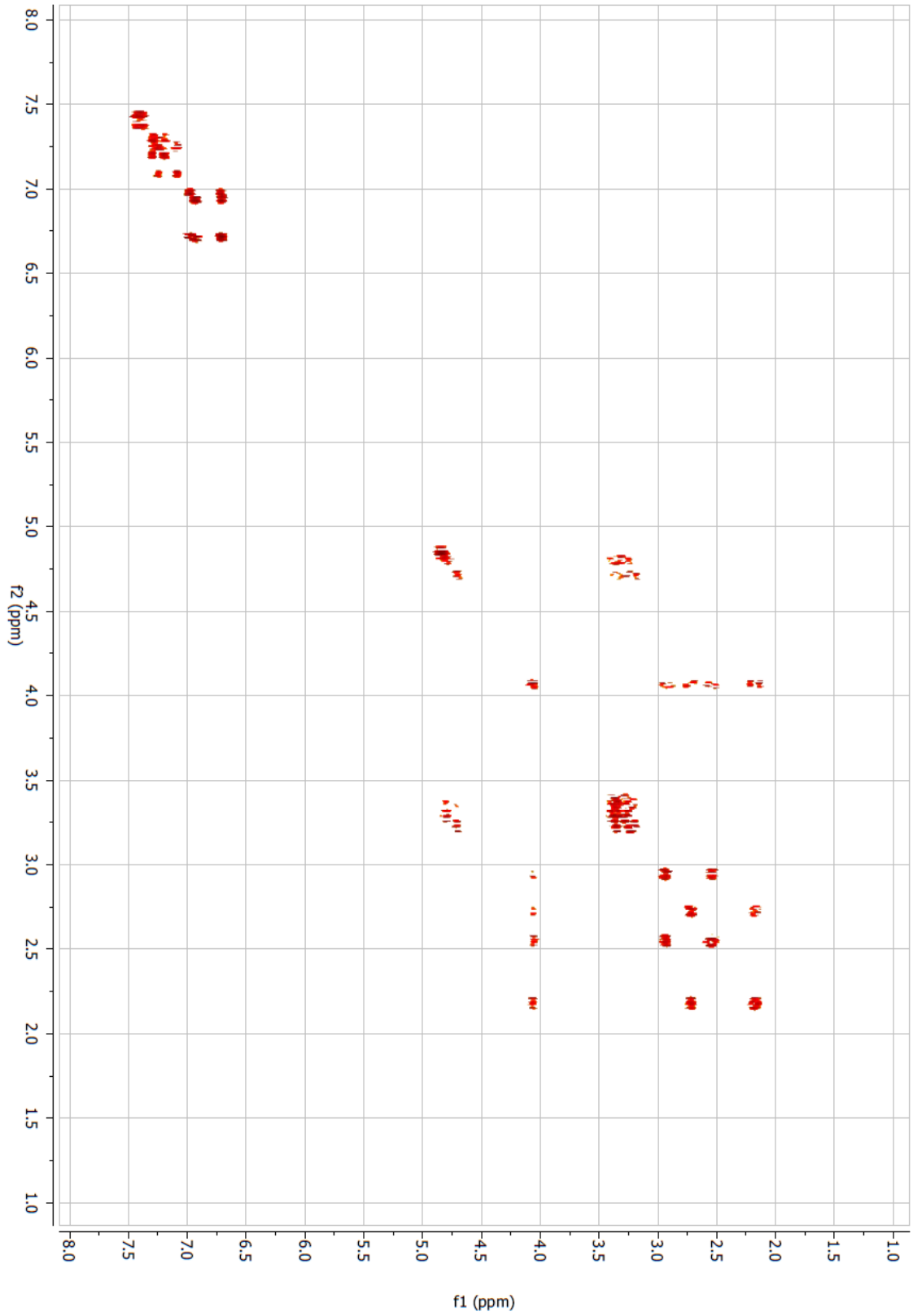

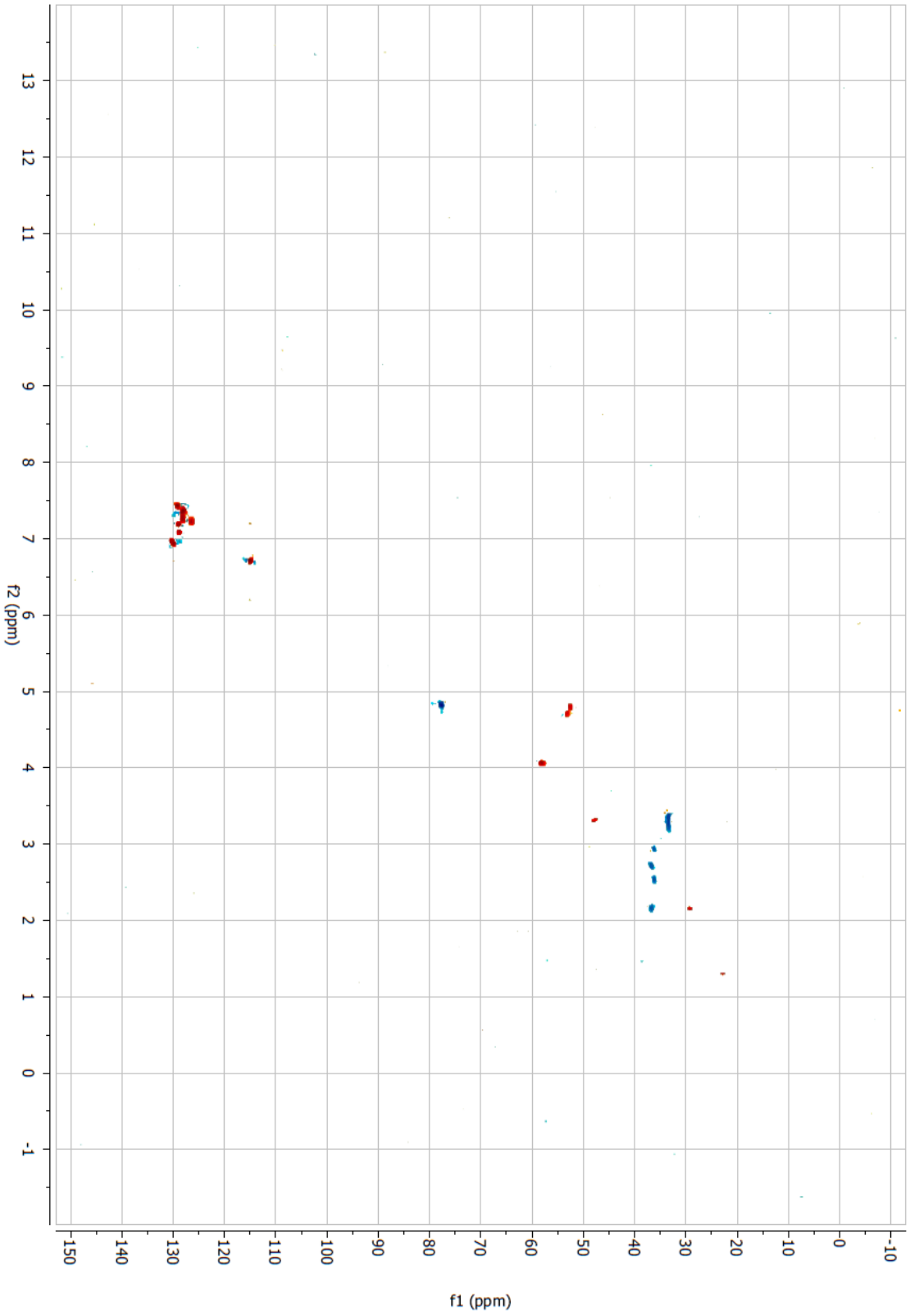
f2 (ppm)
13
12
11
10
9
8
7
6
5
4
3
2
1
0
-1
f1 (ppm)
150
140
130
120
110
100
90
80
70
60
50
40
30
20
10
0
-10

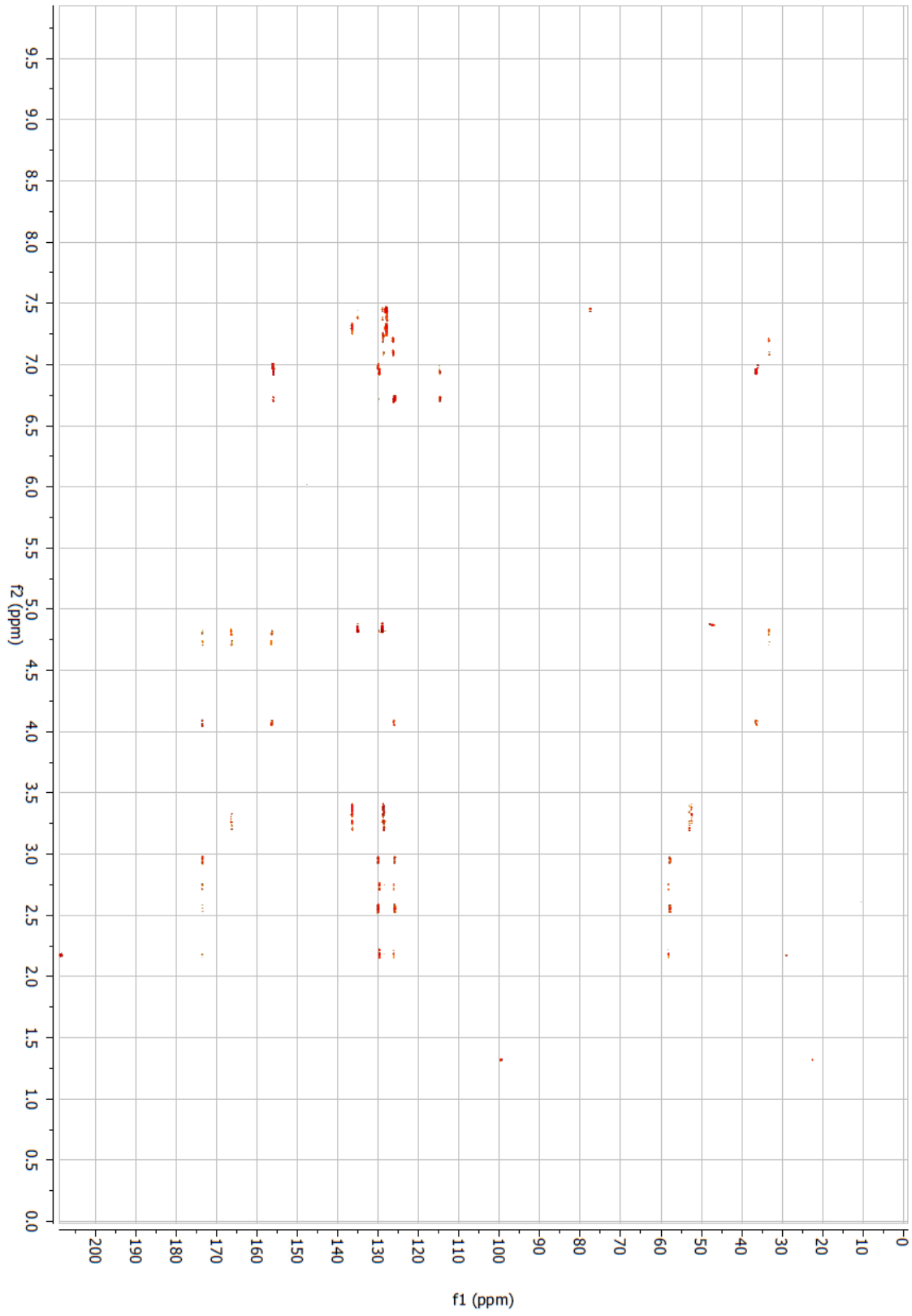
f2 (ppm)
9.5
9.0
8.5
8.0
7.5
7.0
6.5
6.0
5.5
5.0
4.5
4.0
3.5
3.0
2.5
2.0
1.5
1.0
0.5
0.0
f1 (ppm)
200
190
180
170
160
150
140
130
120
110
100
90
80
70
60
50
40
30
20
10
0

^{1}H NMR spectrum of **4-5**

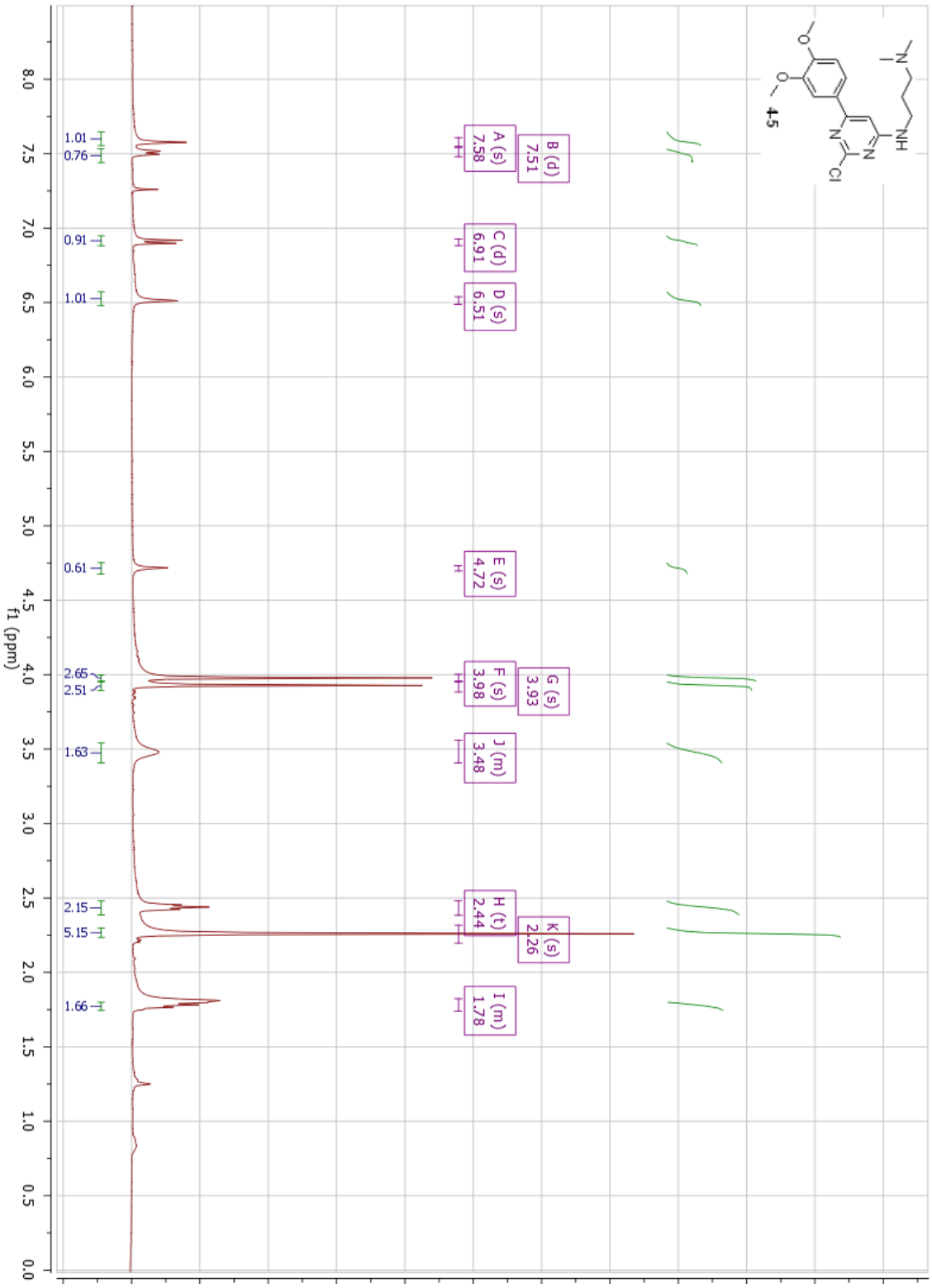

^{1}H NMR spectrum of **4-6**